DESIGN, INSTALLATION AND ASSESSMENT OF A NOVEL VARIABLE COMPRESSION RATIO MECHANISM FOR MULTIFUEL SPARK IGNITION ENGINE

A Thesis
Submitted in Partial Fulfillment of the Requirements for
the Award of the Degree of

DOCTOR OF PHILOSOPHY

By

ASHISH JAGANNATH CHAUDHARI

CENTRE FOR ENERGY
INDIAN INSTITUTE OF TECHNOLOGY GUWAHATI
GUWAHATI, INDIA

JUNE, 2017

Dedicated to my Parents....

Mrs. Sunita Jagannath Chaudhari

and

Mr. Jagannath Dula Chaudhari

whose endless faith and blessings always
inspired me to move forward

Declaration

I hereby certify that the work compiled in this dissertation is the outcome of the research work, performed by myself, else stated, under the guidance of Professor Niranjan Sahoo and Associate Professor Vinayak Kulkarni.

Any part of this work has not earlier been submitted for the award of any degree, diploma, associate-ship, fellowship or its equivalent to any University or Institution.

Ashish Jagannath Chaudhari
Registration No. 126151006
Centre for Energy
Indian Institute of Technology Guwahati

Certificate

It is certified that the work contained in the thesis entitled Design, installation and assessment of a novel variable compression ratio mechanism for multifuel spark ignition engine, by Ashish Jagannath Chaudhari (Registration No. 126151006), a student of the Centre for Energy, Indian Institute of Technology Guwahati, India, for the award of the degree of Doctor of Philosophy has been carried out under our supervision and this work has not been submitted elsewhere.

Prof. Niranjan Sahoo
Professor
Department of Mechanical Engineering
Indian Institute of Technology Guwahati
Guwahati – 781039, India

Dr. Vinayak Kulkarni
Associate Professor
Department of Mechanical Engineering
Indian Institute of Technology Guwahati
Guwahati – 781039, India

Abstract

Spark ignition (SI) engines are the most versatile in the arena of internal combustion engines. The most common fuel for SI engines is petrol which is obtained from fossil fuels. But it faces a deep concern of depleting reserves due to its consumption at faster rate worldwide. The emissions of harmful gases through exhaust of those spark ignition engines do impact the ecology, human being and environment. Considering this energy crises and pollution problems, investigations are centered on different performance improvement techniques for the petrol or spark ignition (SI) engines. Attachment for variable compression ratio (VCR) is one such prominent method which helps to decrease the specific fuel consumption of the engine. With higher compression ratio, same combustion temperature can be reached with lesser fuel attaining more power output. In such situations, there is need of self-adjusting variable compression ratio technology for the fuel in use and as per the load on engine. Different researchers worked on variable compression ratio in commercial spark ignition engines. The major contributions are tilting block arrangement, oval piston, modified connecting rod, crank shaft modification etc. But the VCR engine is still a dream to the major automobile manufacturers. Alongside, alternative fuels can be assessed in the commercial engines with VCR attachment for their performance with variable CR in addition to reduction in concentration of toxic components of combustion products. Liquefied petroleum gas (LPG) is a favorite alternative to petrol in a SI engine even though it is a renewable fuel. The remarkable properties such as higher octane number and lower auto ignition temperature, greater flame velocity and wider flammability limit make the LPG a better SI engine fuel. Raw Biogas from non-fossil carboneous sources like urban refuse, cattle dung, and agricultural wastes can be utilized as fuel for spark ignition engine. As a fuel, biogas has extremely low energy density on volume basis, low flame velocity and not so wide flammability limits on account of its high CO_2 content. The self-ignition temperature is high for biogas and hence it resists auto ignition which sometimes resist undesirable knock also. But the advantages of those fuels cannot be fully exploited when they are used in petrol engines.

In view of the literature based findings, present investigations are centered on developing a novel variable compression ratio attachment for a generic SI engines so as to facilitate the run time variation of CR. The conventional SI engine has a fixed spark plug location that has been decided considering the fuel properties such as heating value of the petrol, method of flow around and inside the cylinder chamber, flame velocity and flame kernel developed by combustion of petrol fuel. This spark plug location may be different if the fuel supplied to the engine is different. So the objective is to locate spark plug at optimum place inside combustion chamber along with increment or decrement of CR. The breakthrough concept is the VCR mechanism consisting of variable displacement secondary piston protruding in and out of engine combustion chamber. This secondary piston design is versatile in terms of accommodating spark plug concentric to the secondary piston. The engine with this attachment is most advanced engine accommodating any fuel attaining best performance under the conditions such as high load, low load, change of octane fuel etc. Detailed

experimentations on this VCR based SI engine are carried out using variety of fuels viz. petrol, kerosene, LPG and raw biogas. The operating variables considered for these investigations are compression ratio, ignition timing, EGR rate and spark plug location. This novel VCR mechanism is implemented in HONDA GK100 engine and tested for petrol and kerosene fuels. This implementation in a small size engine led the insight for further extension of such implementation in large size engines. The baseline study with a tilting block based VCR mechanism (Make: Apex) in SI engine using petrol, LPG and raw biogas fuels are carried out for understanding the usability of the mechanism and for arriving at appropriate spark timing for different fuels at different CRs. Effect of EGR treatment influencing CR and spark timing is explored herein. Based on effective outcome of novel VCR mechanism on HONDA engine, implementation of in-house VCR mechanism in the Kirloskar make SI engine and its testing with petrol, LPG and raw biogas fuels has been undertaken for study. Comparative study of two VCR approaches in terms of performance, combustion and emissions is further analyzed. Effect of VCR with variable SP location is further analyzed for optimum configuration for a particular engine and fuel. Computational study using development and testing of a MATLAB SIMULINK based IC engine simulator is a vital step towards minute comparison of experimental results. These simulations are thought for getting the combustion details in the experiments with HONDA GK100 engine.

Initial tests on HONDA engine are conducted with the VCR attachment, for the compression ratio range 4.8 to 5.5(small engine), using petrol and kerosene as fuels. It was found that the combustion becomes smoother with drastic decrement in vibrations while working with novel VCR attachment on the engine. Optimum CR is noted to be 5.02 for petrol and 5.27 for kerosene. This experience is found to be helpful in incorporating the proposed VCR attachment in the large size APEX engine. While varying compression ratio, there is a scope to alter the protrusion length of secondary piston from 2 mm to 10 mm inside combustion chamber. It is possible to alter the VCR mechanism or use both the mechanisms simultaneously as per the requirement. Additional intake system is designed and incorporated herein to have provision of testing gaseous fuels, specifically bio gas. This system facilitates uniform supply of biogas to the engine cylinder at constant intake pressure. While performing experiments on large size VCR test rig as per objectives, the pressure-crank angle data for complete 10 cycles has been recorded. Thus it gives better understanding of cycle-by-cycle variations of combustion pressure as well as the combustion duration. Experiments for the effect of ignition timing on engine performance in case of raw biogas and LPG fuels have shown the maximum brake torque(MBT) is at 45 ^{0} bTDC and 26 ^{0} bTDC respectively. Presently considered higher heating value fuel, LPG, is expected to combust in less time after spark ignition which in turn maximizes the compression stroke and thereby attains maximum pressure at the end of compression stroke. On the other side, raw biogas, takes more time to initiate combustion which ultimately leads to lower pressure at the end of compression stroke. The percentage of carbon dioxide content in biogas is also a factor which extends the ignition timing. In these studies it is found that optimum ignition timing remains same even at part throttle condition. Experiments are then performed with the tilting block VCR mechanism for the individual optimum spark timing, stoichiometric air/fuel ratio and 90% wide open throttle (WOT) with petrol, LPG and biogas fuels for different compression ratios. The brake thermal

efficiency (BTE) is found to be 24.06 % for LPG and 24 % for raw biogas at CR10 which is 31 % for petrol. The exhaust gas emission is noted to be maximum in case of LPG and minimum in case of bio gas for any compression ratio under consideration. The NO_x emission is seen to have raising trend for all the fuels with increase in compression ratio. The fuels are tested with optimized CR and spark timing for various EGR rate from 10 % (very low) to 40 % (very heavy). In presence of EGR, there is compromise in efficiency with substantial reduction in NO_x. Similar trials are also performed using the novel VCR mechanism where same compression ratios are achieved by simultaneously operating both the VCR mechanisms. In these experiments with novel VCR mechanism, it has been noticed that it is possible to change the compression ratio smoothly in analogue manner during the running state of the engine. However the established mechanism (APEX engine) has the limitations since it can change the compression ratio only after stopping the engine and in the discrete manner. Thus presently designed attachment of variable compression is found to have an edge over the established one.

Detailed experiments are then carried out for bio gas and LPG fuel with the simultaneous use of both VCR mechanisms highlighting an objective of optimum spark plug location for fixed compression ratios. The performance parameter BTE shows noticeable improvement with initial change in SP location from SP1 (original) to SP2 (protrusion by 2 mm) for all CR with biogas and SP1 to SP4 (protrusion by 10 mm) for LPG fuel under consideration at a particular compression ratio. So SP2 and SP4 locations are noted to be an optimum for biogas fuel since it is associated with maximum BTE. Major reason for higher value of NO_x is the higher net heat release rate (NHRR) which results in high peak temperature at the end of combustion. Therefore such higher NO_x is the major concern for operating the engine with this location of spark plug. Measured cylinder pressure has indicted that the combustion duration is lower for this optimum location which would be due to faster flame initiation, development and propagation inside the combustion chamber. In addition to this, SP2 location doesn't cause crevices around the periphery of secondary piston which is quite obvious for SP3 and SP4 positions where protrusion length is 5 mm and 10 mm respectively. The effect of compression ratio combined with spark plug location analysis is focused towards further improvement in efficiency. The novelty of research footprints is the moulding of the spark ignition engine according to the available fuel for the best performance. Such method of moulding has been analyzed here in thesis for HONDA and Kirloskar engine which could be easily followed for any other engine as per their technical specifications. With this CR 10.48 and SP2 is an optimum combination if engine working at speed 1430 rpm for biogas fuel as well as well as CR10.48 with SP3 (5 mm protrusion)for LPG fuel. If the speed varies the new combination is found optimum and this is how continuous variation in CR and SP location can be found to be an efficient tool for best performance of the engine. During further experiments, it has been noted that, if EGR rate is a part of intake charge, then also there is effect on optimum CR and corresponding spark location was found.

Keywords: *spark ignition, variable compression ratio, ignition timing, variable spark plug location, exhaust gas recirculation rate, flame speed, flame kernel, Emission*

Acknowledgements

PhD is although a small part of life; still it teaches us how to live the life in a large scale. It is equally a magnificent and a prodigious training. Apart from acquiring some knowledge about a tiny, part of scientific fraternity, PhD also teaches one, how to talk, to work in a group, to know people and also to make one understandable to others. In this regard, I have also interacted with a number of personalities, without the support of whom, I may not come this far.

Firstly, I will take this opportunity to express my earnest gratitude to my honorific supervisors, Prof. Niranjan Sahoo and Dr. Vinayak Kulkarni, Department of Mechanical Engineering, Indian Institute of Technology Guwahati, India, for accepting me as their PhD student. They have provided me the complete freedom in my research and allowed me to work in my own way. They always have listened to my ideas with patience and constantly motivated to accomplish my goal. I have learnt from them, how to work with enthusiasm, energy, and life, yet remain composed and grounded. It is hard to express my gratitude with only a few words to these two personalities. The best way to express my thanks to them will probably be to follow the lessons I have leant from them throughout my life.

My sincere acknowledgement goes to Prof. Pinakeswar Mahanta, Prof. A.K. Ghoshal, Prof. Pranab Goswami and Prof. V.S.Mohalkar former and present Heads of Centre for Energy. I thank them for their encouragement, guidance, and support from the initial to the final stages of my PhD work. I am also indebted to the members of Doctoral Committee Prof. Kaustubha Mohanti, Prof. K. Pakshirajan and Dr. Vaibhav V. Goud for their precious suggestions about critical issues related to my work. I will also drive thank to Dr. C. Somayaji, Dr. Hrishikesh Gadgil for their immense support during the course work.

I would like to thank Prof. Pankaj Kalita, Dr. L. Barbora , Mr. Debarshi Barua , Mr. Dinesh Huzuri and Mr.Paragjyoti Sharma of Centre for Energy as well as Mr. R. Saikia, Mr. S. Sarma, Mr. N. Borah of Department of Mechanical Engineering for their enthusiastic support for various apparatus purchase and laboratory necessitates.

I owe to my senior Dr.Biplab Debnath and Dr. Bhoskarjyoti Borah to introduce me to the fascinating field of Internal Combustion Engine and Alternative Fuels. Accompanying them in the laboratory and helping them during their experimental works have bestowed me with valuable knowhow and search the objectives of my work. I am also thankful to my colleagues,

Mr. Santosh Hotta and Mr. Menelick, who have provided me technical assistance during experimentation and helped me to gather data. I am fortunate enough to get ample support from the technicians Mr. J. Saikia, Mr. M. Sarma, Mr. D. Khaklary, Mr. D. Chetri, Mr. M.K. Baishya, and Mr. C. Banikya, directly or indirectly, to build the experimental setup. Thankful to Mr.Swapan and QIP cell team for supporting me in fulfilling the academic needs.

I am very much thankful for providing state of the art manufacturing support by Mr. V.V.Mujumdar, IAR,Pune and Mr. Bitupan and Mr.Dharmendra , MSME Machine Tool, Amingaon during development of novel VCR mechanism.

I am also thankful to Dr. Jnyana Ranjan Pati , Mr. R.C.Mishra, Dr. Gajanan Shelke, Mr. Sumit Agarwal and many other individuals with whom I have come into contact during my stay in IIT Guwahati. The friendship and unforgettable attachments shared with them has made my life pleasant.

I am very much grateful towards my parent institute Vidyavardhini's College of Engineering and Technology, Vasai for sponsoring me to pursue PhD under QIP scheme. Special thanks to Honorable President Shri Pratapbhai Khokani, Honorable Chairman Shri Arunsheth Vartak, Honorable Ex-principal Prof. M.N.Bhawe, Honorable Principal, Prof. A.V.Bhonsale, our HOD Mr. U.V.Asolekar, Dr.R.D.Jilte, Mr. V.D.Patel and Mr. Dipak Chaudhari for their continuous support during the period made me to reach this milestone.

I am blessed to be the son of my parents, with whom I was unable to spend at least 1 month continuous for last 6 years. Their love and support without any complaint or regret has enabled me to complete this Ph.D. I owe to both of them, whatever I achieve in life. I feel proud of my wife Varsha and my sweet little daughter Diya who provided me sharing and caring support all along without any complaint. I express my gratitude to my parents-in-law and in-laws who have aided and encouraged me throughout this endeavor.

Last but not the least; I am indebted to SRI SWAMI SAMARTHA for keeping me capable to counter the tests of life and making my life beautiful. May everyone's life be anointed and blooms with YOUR blessings.

June 2017

Guwahati, India ***Ashish Jagannath Chaudhari***

Contents

Nomenclature

Notations

A	Area (mm^2)
BP	Brake Power (kW)
r	Crank radius (mm)
d_o	Diameter of the Orifice (m)
R	Dynamometer Arm Radius (m)
W	Dynamometer Load (N)
Q	Energy (kJ)
D	Engine Cylinder Diameter (m)
L	Engine Stroke Length (m)
R'	Gas Constant (kJ/kg-K)
$\dot{m}_a$	Mass Flow Rate of Air (kg/s)
n	Number of Revolutions per Cycle
p	Pressure (bar)
N	Revolutions per Minute (rpm)
C_p	Specific Heat (kJ/kg-K)
T	Temperature (K)
V	Volume (cc)
VE	Volumetric Efficiency

Greek symbols

θ	Crank Angle (degree)
η	Efficiency
ρ	Density of Fluid, kg/m^3
μ	Dynamic Viscosity, Ns/m^2
γ	Ratio of Specific Heats
λ	Stoichiometric Air Fuel Ratio
k	Polytrophic process constant

Subscripts

10%MFB	10% mass fraction burned
90%MFB	90% mass fraction burned
a	Air
amb	Ambient Condition
C	Clearance volume
EGR	Exhaust gas recirculation
EVO	Exhaust valve open
fuel	Fuel
IVC	Intake Valve open
d	Swept volume
w	Water

Abbreviations

aTDC	After Top Dead Centre (degree)
bTDC	Before Top Dead Centre (degree)
BSFC	Brake Specific Fuel Consumption (kg/kW-h)
BTE	Brake Thermal Efficiency
CO_2	Carbon Dixoxide(%)
CO	Carbon Monoxide (ppm)
COV	Coefficient of variance
CNG	Compressed Natural Gas
CI	Compression Ignition
CR	Compression Ratio
CA	Crank Angle (degree)
EGR	Exhaust Gas Recirculation
EGT	Exhaust Gas Temperature (ºC)
EVC	Exhaust valve closed
EVO	Exhaust valve open
HC	Hydrocarbon (ppm)
ID	Ignition Delay (degree)
IT	Ignition Timing (degree)
IMEP	Indicated mean effective pressure
IP	Indicated Power
IP	Indicated Power (kW)
IVO	Inlet valve open
IC	Internal Combustion
LPG	Liquefied petroleum gas
LHV	Lower Heating Value (kJ/kg)
MFB	Mass fraction burned
MGT	Mean Gas Temperature
NHRR	Net Heat Release Rate (J/deg.CA)
NO	Nitric Oxide (ppm)
NO_X	Oxides of Nitrogen (ppm)
PCP	Peak Cylinder Pressure (bar)
PFI	Port fuel injection
RON	Research Octane Rating
rpm	Revolution Per Minute
SI	Spark Ignition
VCR	Variable Compression Ratio
VSPL	Variable spark plug location

List of Figures

List of Tables

LIST OF PUBLICATIONS

Journals:

1. Chaudhari A., Kulkarni V. and Sahoo N. (2013), "A Simulation Models for Spark Ignition Engine: A Comparative Performance study," *Energy Procedia*, Vol. (54), pp. 330-341

2. Chaudhari, A., Kulkarni, V., and Sahoo, N. (2015), "Effect of Variable Compression Ratio and Intake Charge Dilution on Fuel Efficiency and Emission for a Spark Ignition Engine," *SAE Technical Paper* 2015-01-0772, doi:10.4271/2015-01-0772.

3. Chaudhari A., Kulkarni V. and Sahoo N. (2016), "The combined impact of variable compression ratio and re-circulated exhaust gas on the performance of a biogas fuelled spark ignition engine," *Energy and Environment*, Vol. (*), pp. **(Under Review)

4. Chaudhari A., Kulkarni V. and Sahoo N. (2017), "Structural Exertion Requirement for Best Performance of Raw Biogas as Potential Fuel in Spark Ignition," *Energy Engineering*, Vol. (*), pp. **(Under Review)

5. Chaudhari A., Kulkarni V. and Sahoo N. (2017), "Effect of Variable Compression Ratio using an Innovative Mechanism on Multi Fuelled Spark Ignition Engine," Sadhana Academy Proceeding in Engineering Science, Vol.(*),pp.**(Under Review)

Conferences:

1. Chaudhari A., Kulkarni V. and Sahoo N. (2013), "Spark ignition engine with gasoline and alternative fuel: A comparative performance study," 22nd National and 11th *ISHMT-ASME Heat and Mass Transfer Conference*, Dec 28-31, 2013, IIT Kharagpur, India.

2. Chaudhari A., Garg U., Kulkarni V. and Sahoo N. (2013), "A Simulation Models for Spark Ignition Engine: A Comparative Performance study," 4th *International Conference on Advances in Energy Research*, Dec10-12, 2013, IIT Bombay, India.

3. Chaudhari A., Kulkarni V. and Sahoo N. (2014), "Performance Assessment of Octane Fuels on a Variable Compression Ratio Spark Ignition Engine," Proceedings of ICTACEM 2014 *International Conference on Theoretical, Applied, Computational and Experimental Mechanics* December 29 – 31, 2014, IIT Kharagpur, India

4. Chaudhari A., Kulkarni V. and Sahoo N. (2016), "Raw Biogas as a future fuel for I.C.Engines: A socio-economic development route for farmers in INDIA," *International conference of Emerging Trends in Agricultural Engineering*-2016, IIT Kharagpur, India, Dec 27.-30, 2016.

5. Chaudhari A., Kulkarni V. and Sahoo N. (2017), "Different Gaseous Fuels under Variable Compression Ratio and Spark Location in Spark Ignition Engine: The Comparative Performance Study," *International Conference on Theoretical, Applied, Computational and Experimental Mechanics*, December 28 – 30, 2017, IIT Kharagpur, India.

CHAPTER 1

Introduction

OVERVIEW

Internal combustions (IC) engines have become integral part of many engineering systems or sub-systems. Use of alternative fuels for the IC engines is a topic of investigation for many researchers. Possible alternative fuels for the conventional gasoline, in case of spark ignition engines, are discussed in this chapter. It is then followed by the performance enhancement of an engine while running on a particular fuel through various techniques like variable compression ratio (VCR) attachment, spark timing adjustment and location of spark plug. Further this chapter deals with the emission issues of the IC engines and associated remedies. As an outcome of the present requirements, objectives are set for the present studies. This chapter ends with the organization of the thesis.

1.1 MOTIVATION

The world is moving towards an energy crisis because of the depleting reserve of fossil fuels.

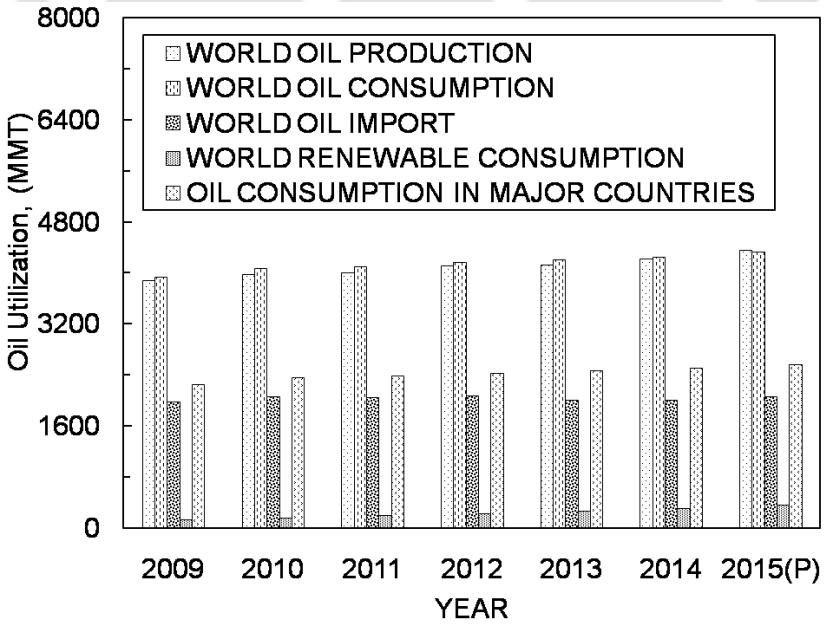

Fig.1.1 World energy scenario (Ref- BP statistical Review of World Energy, 2016)

The rapid rise in the use of fossil fuel in addition to improvements in the standard of living is favoring this depletion. The world population has been increasing steadily over the last 5

decades, and this trend is expected to continue. As a result, total energy consumption has grown by about 36% over the last 15 years.

Energy consumption is expected to increase further in the future, as world population is expected to grow by 2 billion in the next 30 years (Korakianitis et al., 2011).World Energy outlook, 2014 published in its report that energy demand globally will grow by 37% by the year 2040. The world energy scenario as shown in Fig.1.1 justifies the rise in oil consumption rate worldwide since year 2009. The major energy contributors such as petroleum products comprises of gasoline, LPG, CNG, kerosene etc have their demand rising for energy from 3949 MMT to 4331 MMT over period of year 2009 to 2015.

The footprints of crisis of world energy demand reflect over Indian scenario as well where the rise in energy demand shows increment from 38.04 MT to 58.72 MT over tenure of year 2009 to 2015 for gasoline, LPG and such petroleum fuels. Other fuels such as diesel also shows the increment of 25% during the same period reported by Power and Natural Gas Report, 2016 as plotted in Fig.1.2.

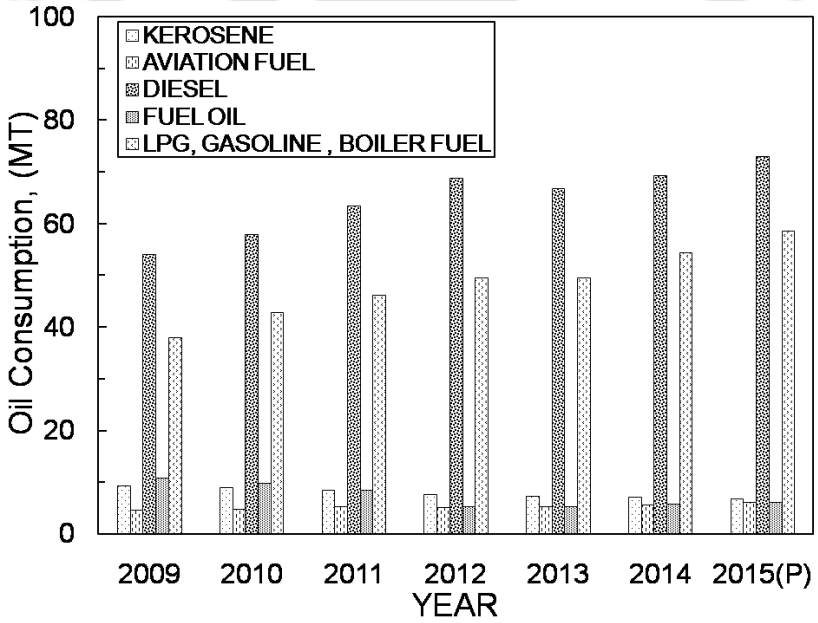

Fig.1.2 Indian energy scenario (Ref- Power and Natural Gas Report,2016)

The internal combustion engines are mostly used for the automobiles in transportation purpose. The gasoline engines are maximum used by the city populations owing cars, bikes, mopeds etc. The crisis for petroleum products raises the price of gasoline per liter day by day. Looking at the vertical rise in demand of energy, it is difficult to fulfill it by the non renewable sources of energy such as petrol, diesel, LPG, coal etc.

The crude oil is the raw material for petrol and from it, various derivatives are extracted. The finer and refined the derivative, better is the quality and efficiency of the fuel. So the extraction results in so many varieties of fuels with dfferent Octane ratings. Back to the year 2000, there was leaded petrol which had 0.15 gms of lead per liter. Lead had distinct advantages which helped the engine to enjoy a long and durable life. But the presence of lead in petrol meant more emission of CO (carbon monoxide) which is the reason why the

government introduced compulsory use of unleaded petrol in year 2000. The unleaded petrol is much 'greener' petrol and the emission of CO is much less and with honeycomb catalytic converters in the exhausts of cars and bikes, the pollution levels reduce to certain extent. In India, companies like BPCL, IOCL, HPCL, IBP red and Shell etc supply with varieties of petrol fuel to power vehicles (Table 1.1).

Table 1.1 Petrol Types and Quality in INDIA(Ref: company manual)

Sr No	Name of company	Type of petrol	RON	Price@May2014
01	Bharat Petroleum CL	Normal unleaded	91	76.10
		speed93	93+additives	83.58
		speed97	97+additives	97.06
02	Indian Oil CL	Normal unleaded	91	76.10
		Xtra Premium	91+additives	
03	Hindustan Petroleum CL	Normal unleaded	91	
		Power	91+additives	
04	Shell	Normal unleaded	95	85.64
		Super unleaded with fuel economy	98+additives	93.55
05	Essar Oil	Punch	>91+additives	74.80
06	Chennai Petroleum CL	0.25% SulphurNon-metro		79.55
		0.05% sulphur Metro		
		Xtra premium grade		
07	NRL	Normal unleaded	91	74.78

There are higher grade petrols available in the market for bikes and vehicles such as Power from HPCL, xtra premium from IOCL over regular petrol supplied by those companies. Those higher grade petrols have higher Octane rating and so cost more. These Octane ratings reflect the quality, purity, refinement, efficiency and heat bearing capacity of petrol. Hence there are different grades of petrol for different uses ranging from bikes to spacecrafts. The specifications of the petrol/gasoline in India are listed in Table 1.2.

Higher octane fuel may not only be a waste of money (Fig.1.3) but may harm the vehicle, as well (Sudsanguan and Chanchaowna, 1999; Chanchaowna, 1999 and Chicurel, 1996). However sticking to one brand of fuel is always good for the engine. It is beneficial for the vehicle to use the recommended fuel grade by the manufacturer. Both BSIII and BSIV petrol having minimum RON rating of 91RON covers every nook and corner from Leah to Kanyakumari of INDIA.

Besides, increasing fossil fuel price based upon type of petrol being used, emission of greenhouse gases and the security and diversity of energy are tending the scientists to turn their attention to find out alternative sources of fuel and most economic consumption of fuel in engine with minimum pollution (Arbab et al., 2013). Hook and Tang, 2006 reported the positive implication of fossil fuel depletion worldwide. According to authors, the diminution

of these sources will set a limit to mankind's ability to damage the environment to certain extent by harmful exhaust gas emissions.

Table 1.2 Indian gasoline specification by auto industry in India.
(Ref: Society of Indian Automobile Manufacturer)

Sr No	Characteristics	Unit	BHARAT STAGE II	BHARAT STAGE III	BHARAT STAGE IV
01	Colour, Visual		As decided by Refiners / Marketers		
02	Density,15^{0}C		710-770	720-775	720-775
03	Distillation				
a	Recovery upto 70^{O}C (E 70)	% volume	10-45	10-45	10-45
b	Recovery upto 100^{O}C (E 100) percent by volume	% volume	40-70	40-70	40-70
c	Recovery upto 150^{O}C (E 150) percent by volume, Min	% volume	-	75 min	75 min
d	Recovery upto 180^{O}C (E 180) percent by volume, Min	% volume	90	-	-
e	Final boiling point ,Max	^{0}C	210	210	210
f	Residue max	% volume	2	2	2
04	Research Octane Number (RON),min		88	91	91
05	Anti knock index (AKI)/MON, min		84 (AKI)	81(MON)	81(MON)
06	Sulphur, total max	% mass	0.05	150 mg/kg	50 mg/kg
07	Lead content (Pb),max	g/l	0.013	0.05	0.05
08	Vapor pressure max	kPa	35-60	60	60
09	Benzene content	% volume	-	1	1
a	Metros		3		
b	For the rest		5		
10	Olefin content, Max	% volume	-	21	21
11	Aromatic content, Max	% volume	-	42	35

The pollution level in cities continuously rises due to exhaust from vehicles which are very harmful for city lives and environment. Air pollution is a major environmental risk to health. By reducing air pollution levels, we can help countries reduce the global burden of disease from respiratory infections, heart disease, and lung cancer.

In other words, the fossil fuel reserves and the anthropogenic climate change issues are interrelated and need to be treated with optimum solution (Hook and Tang, 2006). The WHO had prepared Air Quality Guideline (AQG) in year 2005 for the control of pollution in cities due to vehicles.

Renewable technology can become a pillar of producing a low carbon energy sources which is rapidly gaining popularity for the green energy. According to the predictions made by World Energy Outlook, the renewable fuels account for almost half of the total increase in energy generation by targeted year 2040.

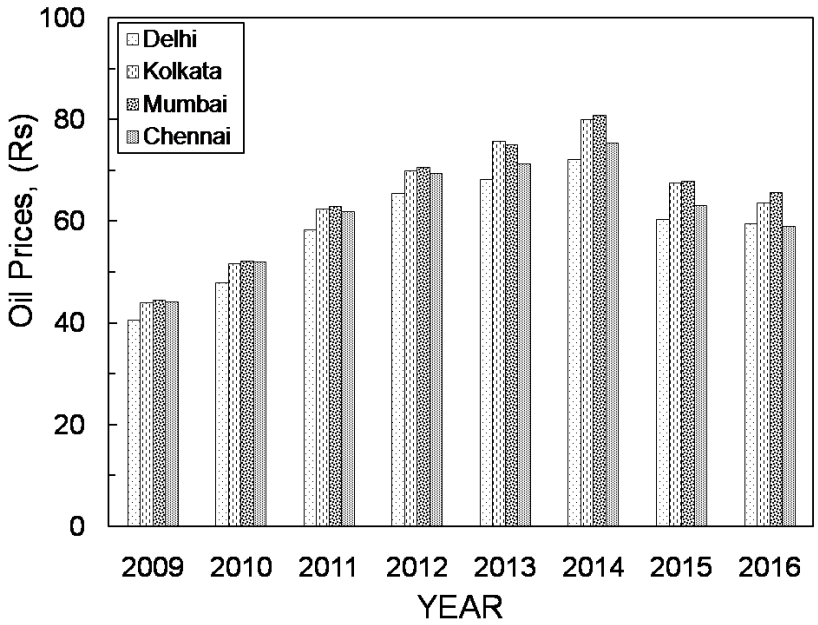

Fig.1.3 Oil Prices in INDIA (Ref- Power and Natural Gas Report, 2016)

The most harmful gas NO_x should be 40 µg/ m^3 annual mean as per AQG- 2005.

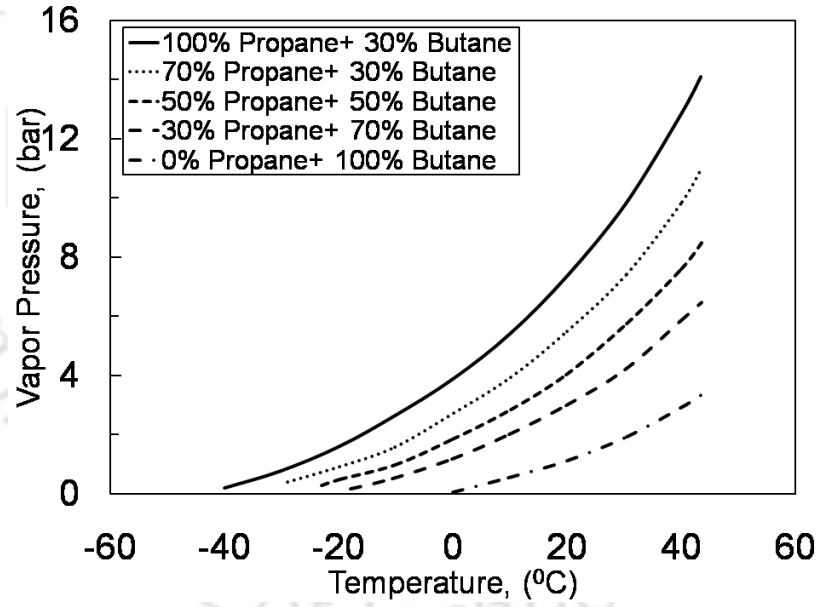

Fig.1.4 Vapor pressure for different composition of LPG gas

1.2 ALTERNATIVE OCTANE FUELS

Gaseous fuels in general are promising alternative fuels due to their economical costs, high octane numbers, high calorific values and lower polluting exhaust emissions. LPG, although a non-renewable fuel can be widely used as an alternative fuel by name called AutoLPG gas for automobiles due to its efficient combustion characteristics and low emissions.

This fuel can be liquefied at low pressures, in the range 0.7–0.8 MPa, and low atmospheric temperatures, which facilitates its use. It is common to distribute a mixture of propane (C_3H_8) and butane (C_4H_{10}) for combustion purposes in household cooking. Propane is more suited to

colder environments since it evaporates at - 44 ^{o}F (-42 ^{o}C) at atmospheric pressure. Butane evaporates at 33 ^{o}F (0.6 ^{o}C) at atmospheric pressure. From the Fig.1.4, the vapor pressure keeps on increasing with increase in temperature of LPG gas with varying composition of constituent gases.

LPG can be produced from natural gas and crude oil. Although this fuel mainly consists of propane and butane, it may also include different hydrocarbons such as iso-butane and n-butane in various proportions. Its higher octane number 110, greater flame velocity and wider flammability limits make LPG a better spark-ignition engine fuel than gasoline. LPG is a powerful alternative to gasoline, but the advantages of LPG cannot be fully exploited when it is used in gasoline engines with well-developed techniques of conversion application. For example, LPG-fuelled cars, having fuel systems converted from those of gasoline engines, can't take advantage of higher octane number of LPG because of no change in structural components of engine. Only those which are manufactured specifically for LPG use can have higher compression ratios and can achieve higher thermal efficiencies with LPG (Erkus et al., 2013). Auto LPG gas is now a days available on fuel pumps is different than that of the LPG gas for food in terms of RON.

Biogas a non-fossil carboneous sources derived from urban refuse, cattle dung, and agricultural wastes (Table 1.2) can be utilized as fuel for internal combustion engine both spark ignition engine as well as compression ignition engines (Borjesson,1991). It is attractive source of energy for rural areas particularly in developing countries. It is produced from anaerobic digestion of cow dung and other animal and plant waste in absence of oxygen (Table 1.3). It consist mainly two-third (by volume) of Methane (CH_4) and rest is mostly Carbon Dioxide (CO_2), traces of Hydrogen Sulfide (H_2S) with 5-10% water vapor. As a fuel biogas has extremely low energy density on volume basis, low flame velocity and not so wide flammability limits on account of its high CO_2 content.

The self ignition temperature is in the range of 645–850^{0}C which is very high and hence it resist the auto ignition. This is a desirable feature in spark ignition engine as it reduces the chance of knock (Porpatham et al., 2007). The rate of flame spread is low, with the maximum of only 0.25 m/s, about 1/3 of which is the methane.

Table 1.3 Biogas yield and methane content from different feedstock (Subramanian et al., 2013)

Feed stock	Gas yields m^3/kg	Methane(%)
Cattle dung	0.297	55
Pig	0.40	65
Poultry	0.45	70
Straw	0.341	51
Grass sillage	0.576	52
Municipal solid waste	0.308	60
Jatropha curcas seedcake	0.640	66.5
Pongamia pinnata seedcake	0.738	62.5

The characteristics such as low burning velocity, high exhaust temperature, anti-detonation performance, and very high octane value illustrate that this could be an excellent fuel in spark ignition engine in its raw form. In order to enhance the efficiency of biogas based SI engine, there are different methods that were successfully implemented by researchers such as CH_4 enrichment, or preheating of intake charge with exhaust gas (Yingiian et al.2014). Biogas also needs small amount of air for combustion per unit mass of fuel as compared to other hydrocarbon fuels.

Table 1.4 Sample chromatography at different sites nearby IIT Guwahati

Sr No	Name of gas	Site			
		Auhnihati (2.5 km) (3 m^3)	Jalukbari (10 km) (6 m^3)	MaligaonGoshala (15 km) (20 m^3)	Kukumara (25 km) (3 m^3)
01	CH_4	51.6	64.4	50.2	62.9
02	CO_2	47.9	45.2	49.5	46.8
03	O_2	.1	0.2	0.1	0.1
04	H_2S	580	665	335	170

Around ,IIT Guwahati, Guwahati, Assam, INDIA, some biogas production plants were located and the biogas produced from cow dung is collected and tested on site using portable gas chromatography GFM406 (Make: Gas Data, UK) instrument. The Table 1.4 gives the outcomes based on average of three repeated tests for each constituent. Table 1.5 represents the properties of the fuels under consideration from liquid to gaseous fuels.

1.3 PERFORMANCE IMPROVEMENT METHODS

The spark ignition engine with different octane fuels needs to be utilized to their optimum performance. In order to achieve this it becomes necessary to rethink about the structural alterations during running of the vehicle as per load and acceleration on the engine. The attempt has been made in this thesis towards some performance improvement techniques as detailed herein.

Table 1.5 A comparison of some physical properties of engine fuels

Properties	**LPG**	**Biogas**	**Petrol**
Molecular formula	C_3H_8	CH_4+CO_2	C_8H_{18}
Density at 15^0C	507	1.1	730
Lower heating value, MJ/kg	46.10	25	44.0
Heat of vaporization, MJ/kg	0.426	0.5	0.33
Stoichiometric A/F ratio	15.7	9.5:1	14.7
Research octane number	112	110	91

1.3.1 Variable compression ratio

The technique of variable compression ratio is quite old since 1920 where Harry Ricardo developed an engine with varying compression ratio. He paid attention towards the variation of clearance volume inside combustion chamber. In doing the work, Ricardo forms the Octane rating system for the fuel which still being used. But the VCR engine development was not successful due to mechanical complex manufacturing and difficulty of controlling all of the parameters. The advantages of the increase in compression ratio, increases the power output and efficiency. This is due to higher pressure intern higher temperature of compressed fuel- air causing complete combustion of fuel air mixture in cylinder. The compression ratio may vary for different octane fuels, different load conditions and different speed as represented in Table 1.6 reported by different researchers based on their exhaustive experimentations. So it is a challenge to find the optimum compression ratio which gives maximum power, efficiency, lower bsfc and lower emission.

Table 1.6 compression ratio with varying the octane rating of gasoline.

Octane Rating	72	81	87	92	96	100	104	108
Compression ratio	5:1	6:1	7:1	8:1	9:1	10:1	11:1	12:1

There is a maximum compression ratio limit beyond which the knock may occur (Crookes, 2006). The renewable fuels and non-renewable fuels discussed above such as petrol of different brands, the xtra premium petrol, power petrol and such various grades, gaseous fuel such as LPG, raw biogas consist of various different compositions of hydrocarbon , different additives. This fact suggests that there is different engine combustion environment for maximum performance with each. The variable compression ratio is one of the technique whereby the CR can be optimized for each different fuel in the same SI engine (Cerri et al., 2013). The advantage of this is the high specific power out put accompanied by good reliability and longer engine life.

The optimum CR for different liquid and gaseous fuels reported by authors is as tabulated in Table1.7. It is very clear from this discussion is that, the compression ratio variation is important in spark ignition engine with variation in fuel being supplied to the engine. For the spark ignition engine, the compression ratio is made fixed at a particular optimum location as per the fuel that is supplied to the engine. From this, one must ensure that the fuel performance is optimum. However when engine operates, there are certain other parameters which needs to be accommodated for optimizing the compression ratio. Those parameters are load on the engine and ultimately the speed of engine. From literature, it was observed that with the lower load higher compression ratio should be maintained and vice-a-versa during higher load condition. The high peak pressure problems occur at high load, so need to reduce the CR whereas during part load or cold starting condition high CR is recommended.

Table 1.7 The optimum CR for variety of fuels and engines reported by researchers.

Sr No	Type of Engine	Fuel used	Optimum CR	Reference
01	12.78 kW Ricardo E6 petrol engine@3000 rpm	Simulated biogas	13:1	Crookes,2006
02	3.5 kW diesel converted to petrol engine@1500 rpm	Raw biogas	13:1	Porpatham,2007
03	3.5 kW diesel converted to petrol engine@1500 rpm	Simulate biogas	12:1	Chandra et al.,2012
		Methane	13:1	
		Raw biogas	13:1	
04	58.88 kW, 4 cylinnder,4-stroke, 1.4 ltr SI engine@1200-2300 rpm	91 RON Gasoline	8:1	Sayin, 2010
		93 RON gasoline	8:1	
		95.5 RON gasoline	8:1	
05	12.78 kW Ricardo E6 petrol engine@3000 rpm	Power gas($CO+H_2$)	8:1	Mustafi et al.,2006
06	191 kW ,6cylinder SI engine@2300 rpm	Biogas with hydrogen	10.5:1	Park et al.,2011
07	107 kW, 4-stroke, 5 cylinder FIAT engine@6100 rpm	LPG	10	Masi, 2012

The method of continuous variation of CR adjusting the clearance volume and swept volume of combustion chamber will definitely achieve the maximum performance from the engine. Many researchers worked in this regards but still the vehicle with VCR implemented technology is a dream.

1.3.2 Optimum Ignition timing or spark timing

The ignition timing of the fuel-air mixture is important for the best performance of the engine. The ignition timing is assumed to be the spark timing of the spark plug. This spark timing may be advanced or delayed of crank angle before TDC. During combustion for much advanced spark timing the cylinder pressure increases substantially before compression stroke complete and hence useful compression work reduces. Much delayed spark timing reduces the peak pressure for expansion stroke so expansion work reduces. Due to this, the optimum spark timing is very important. The spark timing optimization should be focused for some important parameters such as type of fuel, its octane rating, its heating value.

Depending upon the phase of fuel whether liquid or gaseous the ignition timing may be optimized. Even the octane rating matters a lot for optimizing the spark timing. Higher octane fuels needs to settle the ignition timing to avoid knock causing vibrations and shocks. In this regards, the engine control management advances or retarded the ignition timing based on the signal provided by knock sensors fixed at different places inside combustion chamber. The

quality of fuel also becomes an important parameter for optimum spark timing to have homogeneous combustion of charge with maximum efficiency.

Table 1.8 Indian emission standards for four wheelers
(Emission Standards, 2017)

Standard	Reference	Date	Region
India 2000	Euro 1	2000	Nation wide
Bharat stage II	Euro 2	2001	NCR*, Mumbai, Kolkata, Chennai
		April, 2003	NCR*, 11 Cities$
		April, 2005	Nation wide
Bharat stage III	Euro 3	April, 2005	NCR*, 13 Cities$
		April, 2010	Nation wide
Bharat stage IV	Euro 4	April, 2010	NCR*, 13 Cities$
		April,2017	Nation wide
Bharat stage V	Euro5	To be skipped	
Bharat stage VI	Euro6	April,2020(proposed)	Entire country

* National Capital Region (Delhi)
$ Mumbai, Kolkata, Chennai, Bangaluru, Hyderabad, Ahmedabad, Pune, Surat, Kanpur, Lucknow, Solapur, Jamshedpur and Agra

1.3.3 Optimum spark plug location

The spark ignition engine which are generally designed and developed under impression of the fuel being used is petrol. The properties of petrol fuel are known and accordingly the spark plug is located inside combustion chamber. This location of spark plug is optimum from the point of view of combustion chamber design, petrol fuel in regards to the flame kernel development and faster flame travel towards opposite corner of combustion chamber. In the conventional engine, if the fuel other than petrol is used for combustion, then the issue of combustion duration arises as well as corresponding mass fraction burned as a function of crank angle displaced. Flame speed of the fuel air mixture inside combustion chamber depends largly on compression ratio, ignition timing as well as ignition location and that will be different for different fuels.

Many researchers worked in this area of optimizing the spark plug location for variety of fuels. The engine performance will be maximum if all three parameters CR, I.T. and ignition location are adjusted at the optimum magnitude for the particular fuel (Yamin and Badran, 2000).

The research of varying the spark plug location from centroidal axis towards wall of cylinder were attempted as well as some researchers are working on laser based spark ignition which can be concentrated at position inside combustion chamber as per fuel in use, load condition and CR (Pal and Agarwal, 2016).

Table 1.9 Emission standards for city cars, 3-wheel and 2-wheel petrol vehicles, g/kWh (Emission Standards, 2012)

		Year of assessment						
		1991	**1996**	**1998**	**2000**	**2005$**	**2010$**	**2010$$**
Reference		-	-	-	**EURO1**	**EURO2**	**EURO3**	**EURO4**
Emission(Gross vehicle weight≤3500 kg),g/km	CO	14.3-27.1	8.68-12.4	4.34-6.20	2.72-6.90	2.2-5.0	2.3 4.17 5.22	1.0 1.81 2.27
	HC	2.0-2.9	-	-	-	-	0.20 0.25 0.29	0.1 0.13 0.16
	$HC+NO_x$	-	3.00-4.36	1.50-2.18	0.97-1.70	0.5-0.7	-	-
	NO_x	-	-	-	-	-	0.15 0.18 0.21	0.08 0.10 0.11
Emission for 3-wheel petrol vehicles, g/km	CO	12-30	6.75	-	4.0	2.25	1.25	-
	HC	8-12	-	-	-	-	-	-
	$HC+ NO_x$	12-30	5.50		2.00	2.00	1.25	-
Emission for 2-wheel petrol vehicles, g/km	CO	12-30	5.5	-	2.0	1.5	1.0	-
	HC	8-12	-	-	-	-	-	-
	$HC+ NO_x$	-	3.60	-	2.22	1.5	1.0	-

+ for catalytic converter fitted vehicles
$ Mumbai, Kolkata, Chennai, Bangaluru, Hyderabad, Ahmedabad, Pune, Surat, Kanpur, Lucknow,Solapur, Jamshedpur and Agra

1.4 EMISSION CONTROL NORMS AND METHODS

Emission norms came into force with Idle Emission Norms in 1984. Mass Emission Norms were introduced in 1991 for petrol vehicles and in 1992 for diesel vehicle.

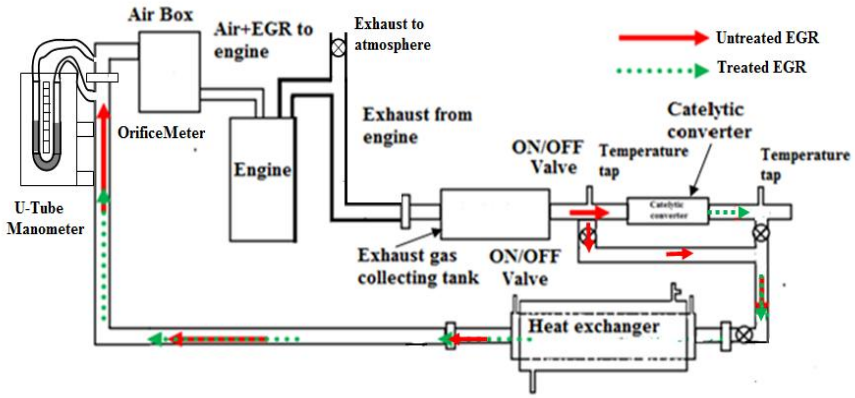

Fig.1.5 Exhaust Gas Recirculation System with catalytic converter (Cooled and uncooled)

Following the EURO norms, the BHARAT STAGE (BS) norms are developed, according to the atmospheric conditions in INDIA, the BS Norms are updated narrowing the gap with that of EURO norms. In the following year 2005, BS-II or EURO-II equivalent norms are in force throughout the country and BS-III or EURO-III norms in selected thirteen cities. The structure of European standards as applied for Indian climatic conditions is tabulated in Table 1.8. Table 1.9 shows the emission level norms for CO, HC, NO_x and HC+NO_x for passenger cars, three wheelers as well as for two wheeler vehicles in INDIA.

1.4.1 Exhaust gas recirculation

The EGR is an attractive means of improving the fuel economy of S.I. engines, as it offers the benefits of charge dilution (lower pumping and cooling losses) retaining the stoichiometric air fuel mixture at intake (Neame et al., 1995) . The EGR uses the exhaust gases recirculated to the intake manifold for combustion in engine (Fig 1.5). The percentage of excess air is reduced by introducing the exhaust gas in intake manifold. The EGR rate refers to the volume fraction of exhaust gases found at the intake as a percentage of the total inlet charge. The temperature of the combustion gets reduced due to exhaust gas recirculated and due to reduced temperature, the emission like NO_x is also reduced which is very harmful gas for living organisms on earth. The EGR is suitable for high speed engine with part load applications. The schematic diagram of EGR circulation to the spark ignition engine is as shown in Fig.1.5 where dark arrow path (Red color) represents the untreated EGR Rate supplied to the cylinder. The other dotted arrow (Green color) represent the treated EGR (catalytically treated EGR) Rate supply path to the cylinder. In addition to this the cooled EGR or uncooled EGR also can be accommodated in this set up. The method of measurement of EGR rate is elaborated in (Eq-C-19-21) the mass of the inducted charge decreases. This causes an overall increase in cylinder temperatures. Also the ignition delay as well as flame structure found changed with introduction of EGR. In-cylinder wear rate increased on account of exhaust gases present inside combustion chamber during combustion.

1.5 SUMMARY

The demand for internal combustion (IC) engines has grown over the years because of its ability to provide safe and reliable power. However, the IC engines are generally designed for a known fuel and hence their performance with any other fuel remains below the optimum value for that fuel. In addition to this, IC engines with alternative fuels produce adverse impact on environment and human health in terms of emissions. In order to improve the efficiency with less harmful emissions and also to meet the growing energy demand with alternate fuels, some techniques such as continuous variation in compression ratio and exhaust gas recirculation have been reviewed. It is understood that there is scope for improvement of efficiency, specifically in case of spark ignition (SI) engine, with suitable VCR method. The VCR method with adjustable spark plug location is thought for present studies. Thus there would an optimum spark plug location for a given fuel which would fetch the best performance of the engine. Hence the literature related to different VCR and emission control techniques are reviewed in detail in chapter 2.

CHAPTER 2

Literature Review

Over view

Various researchers have proposed different performance enhancement methods for a given SI engine. Proposition of an efficient VCR attachment being one of the objectives of present studies, initial sections of this chapter are dedicated to different VCR mechanisms and use of those VCR based SI engine for different alternative fuels. These outcomes are mainly compiled under three categories viz. performance analysis, combustion analysis and emission analysis. Further, understandings through the use of computational techniques and simulations are also mentioned. Thus present chapter provides detailed review of the literature and their shortcomings to make a platform for proposed objectives.

2.1 INTRODUCTON

Internal combustion engines have been a driving force for the vehicles and energy production worldwide. The engines found applications such as transportation may be by road, rail or sea as well as electricity production with intervention of electrical generator. Initially water based steam engine is a basic reciprocating engine which was known to be external combustion engine was developed 150 years back. Until year 1860, the developments were taken place and Mr. J. J. E. lenoir developed the first internal combustion engine which is spark ignited up to six horsepower capacity. Continuous research and understanding the shortcomings in the present engine, Mr. Nicolaus A. Otto proposed the engine cycle consisting of four piston stroke. His prototype engine first ran in year 1876. There was enormous reduction in weight and volume of engine based on Otto cycle. Commercially around 50000 of these engines had been sold in Europe and United States. In order to control knock, the compression ratio was set to less than four in those engines. Accordingly numerous patents were published in this regards. For the available fuels the carburetor and ignition system developments made the high speed gasoline engines in the late 1880. In all these innovations, fuels play a major impact on engine design and development. The engines utilizing the conventional fuels such as petrol and diesel becomes absolute because they are fossil fuels which are non renewable. There reserves are depleting day by day. So, it is important to work on some parallel source of hydrocarbon fuels by which the internal combustion engine remain working and serve the mankind. But the engines made to run on conventional fuel such as petrol and diesel becomes absolute if these sources are consumed completely. So, it could be the time to think about the parallel sources by use of which this internal combustion engines keep functioning and helpful for society and atmosphere. To utilize those resources to long periods, there must be

some performance improvement techniques such as variable compression ratio; variable spark plug location needs to be explored. In this regards, this chapter discusses about the research so far carried out by different peoples in the area of development of variable compression ratio engine where different mechanisms incorporated and tried to improve the performance of the engine. These variable compression ratio engine performance for petrol fuels as well as other liquid and gaseous fuels become utmost important to harness maximum efficiency with minimum consumption of fuels. Some renewable and non-renewable gaseous fuel applications in spark ignition engine has been explored by many authors. Further the work done so far in area of variable spark plug location which would be varying with load, speed, type of fuel etc are discussed here in details.

2.2 VARIOUS PROPOSALS OF VCR MECHANISM

The compression ratio can be changed through modifications from the head side or the piston side. Dated back from 1920 several mechanisms for VCR have been developed and several key conclusions have been drawn from experiments. With the need for improvement in performance of engines, researches in VCR have also grown in recent years. Although the exhaustive listing of all the concepts of VCR mechanisms cannot be made the general ideas behind all those mechanisms are presented as below:

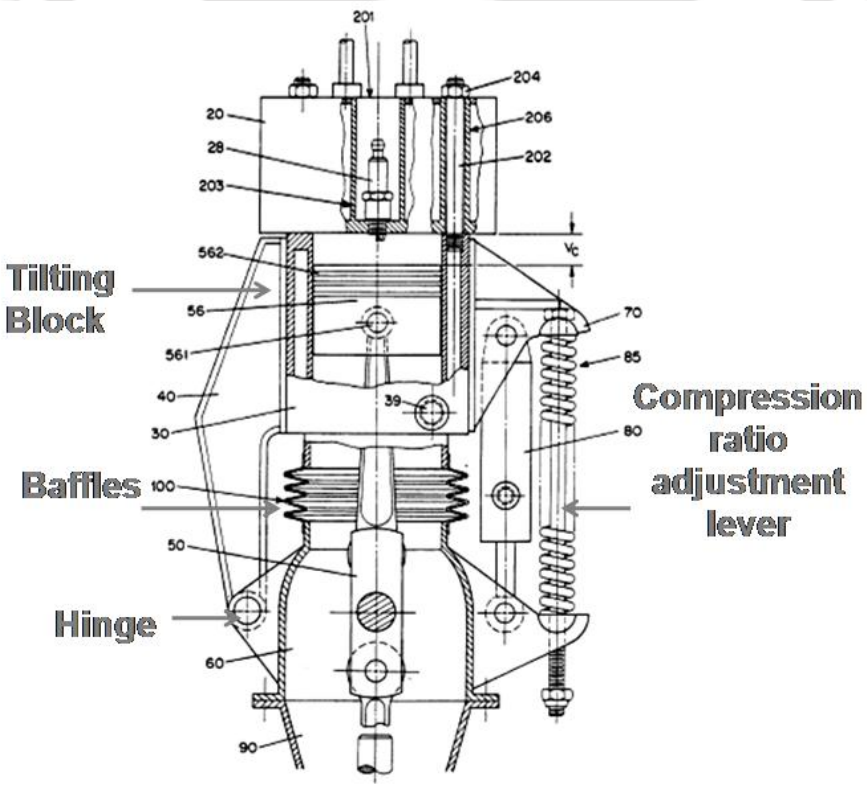

Fig. 2.1 Tilting Block mechanism by SAAB Auto (Larsen, 1991)

Modification in cylinder head - One concept is of moving head by SAAB (a premium car manufacturer) as shown in Fig. 2.1. By combining cylinder head and liners into a semi mono block construction which pivots with respect to the remainder of the engine, SAAB has enabled a tilting motion to adjust the effective height of the piston crown at TDC (Larsen,

1991). However, the method is manual and could be utilized for stationary engines. The lower fixed portion of engine accommodates the crank case comprised of connecting rod, crank shaft, lubricating oil, gear box and other auxiliaries. The upper half movable part consists of liner, cam shaft, and cylinder head. This method enables the tilting motion to increase the clearance volume, thereby reducing CR. The compression ratio from 8-14 could be possible with this method.

Modification in piston- Assanis et al., 2005 ; Brevick, 2003 developed a model (Fig. 2.2) called as Pressure-reactive-piston. The pressure reactive piston assembly consists of a piston crown and a separate piston skirt and a set of spring contained between them.

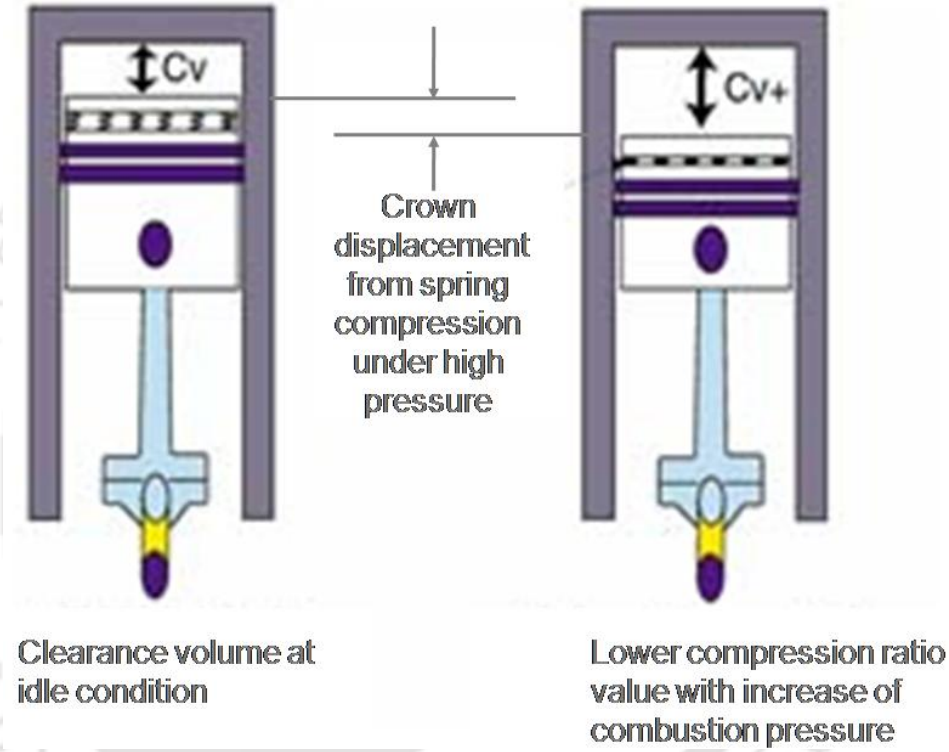

Fig.2.2 Pressure Reactive Piston (Assanis et al., 2005)

The piston crown deflects in response to the cylinder pressure. As the piston crown deflects, the cylinder clearance volume increases, lowering the effective compression ratio and reducing peak cylinder pressure. Since the system is passively controlled by cylinder pressure, it can accommodate rapid changes in engine operation as per load and speed.

Ma et al. came up with concept of combustion chamber with auxiliary chamber in which during low compression ratio, the auxiliary chamber constantly connected to combustion chamber and during high compression ratio, the auxiliary chamber is isolated through a one-way valve (Ma et al., 1992). Fig. 2.3 shows the patent for compression adjustment using a secondary piston or valve developed by Ford auto. The device is presented primarily as a means of controlling knock as its dormant state is the high CR condition. It is suggested that the piston could be maintained at an intermediate position, corresponding to the optimum CR for a particular condition, however this would require a finite length bore in which the piston could travel which raises further questions of sealing, packaging and durability.

Wittek et al. developed a two stage variable compression ratio engine with eccentric piston pin whereby the variation of CR reduces the fuel consumption of high boosted gasoline engine. The FEV, North America is currently testing this VCR mechanism in on road vehicles where almost 50 engines were developed with two stage variable compression ratio technique (Automotive Engineering Report, 2016).

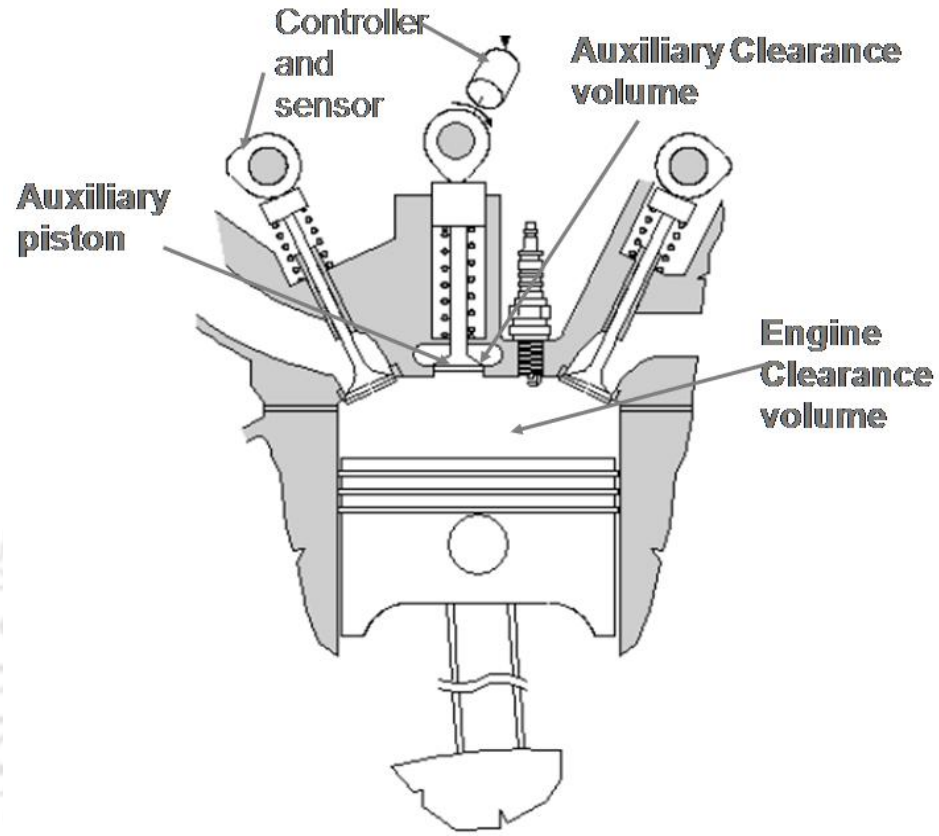

Fig.2.3 Auxiliary clearance volume accompanied through auxiliary piston by Ford Auto (Ma et al., 1992)

The connecting rod is modified having rotating eccentric small eye at piston pin. The two hydraulic cylinders accompanied with piston are attached on the connecting rod such that if one is emptied, then another gets filled locking the piston at particular position. This transition of CR takes 0.2 to 0.6 sec. and CR variation 11:1 to 15:1 could be achieved. The system is completely passive and CR adjustment depends upon load, available fuel and its quality (Wittek et al.,2009).

Cowans, 2003 developed an internal combustion engine using variable compression ratio and variable fuel supply. The author coordinated the relationship of compression ratio and fuel feed to the engine.

They developed a two part variable compression ratio cylinder having inner and outer sleeves wherein relative movement between the sleeves alter the volume of combustion chamber and hence vary the CR. The cylinder pressure inside combustion chamber automatically varies

the position of inner and outer sleeves to regulate combustion chamber volume of the internal combustion engine.

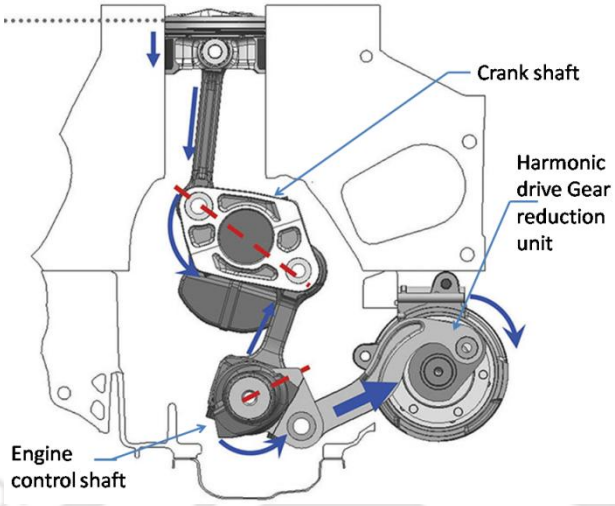

Fig.2.4 Multi-link technology for VCR developed by Nissan

Nissan VC-turbo engine introduces the VCR technology in the form of multi-link connecting rod. It consist of harmonic drive reduction gear which rotates according to the required compression ratio at any given moment. This operates the connecting control shaft at base of the engine as shown in Fig. 2.4. Thus it allows the multi-link mechanism to move the connecting rods to alter the piston stroke position for all cylinders at same time.

2.3 INVESTIGATIONS WITH VARIABLE COMPRESSION RATIO ENGINE

Variable compression ratio is the method by which the compression ratio could be altered to a range of values so that the fuel can be used with high efficiency during the loading conditions on high and lower side (Filip and Assanis , 2000; Wirbeleit et al., 1990; Freudenstein and Maki, 1981; Pierce, 1914; Welsh and Riley, 1971). The following are the advantages of variable compression ratio as discussed by literature (Boretti et al., 2011).

i. The fuel efficiency could be increased due to complete combustion of fuel-air charge.

ii. Engine can be used with alternative fuels having higher research octane rating attaining maximum efficiency by adjusting at higher compression ratio.

iii. The emissions such as CO and HC could be reduced with the optimum compression ratio for the particular fuel.

Certain disadvantages are also there which restrict its application in the commercial engine yet.

i. The engine structure may not able to sustain the pressure with increase in compression ratio. So there is a limit for the increase of CR for particular engine.

ii. Due to complete combustion, the temperature of combustion is increased which increases the harmful emission NO_x in atmosphere. However there are techniques by which this could be reduced to certain extent.

iii. The user may not able to calculate the optimum compression ratio, which may damage the engine.

2.3.1 Liquid fuels in VCR engines

The disadvantages listed above could be reduced and concept if applied in the spark ignition engine, then it is definitely helpful for the fossil fuels to reduce their consumption. Alongside Variable compression ratio Engine (VCR) is one promising technology with increasing focus towards practical implementation in the existing engines or new engines to enhance the efficiency of the engine. The compression ratio of an engine is a value that represents the ratio of the volume of its combustion chamber from its largest capacity to its smallest capacity (Heywood, 1988). With higher compression ratio same combustion temperature can be reached with lesser fuel, while giving a longer expansion cycle, lowering the exhaust temperature and creating more mechanical power output. But petrol engines have a limit on the maximum pressure during the compression stroke, after which the fuel/air mixture detonates rather than burns which is called knocking. So higher compression ratios may cause knocking (Sayin , 2012).To achieve higher power outputs at the same speed, more fuel air mixture must be burnt but this would result in detonation unless the compression ratio was decreased. However, increase in power is possible. The effect of lowering the CR is that under light loading, the engine can lack power and torque. So higher loads require lower CR to be more efficient and vice versa. Thus all IC engines have a fixed compression ratio with optimal value to prevent knocking. This prevents the engine to perform with highest efficiency all the time as the load is varying. Variable compression ratio technology allows adjusting the compression ratio of an internal combustion engine to suit the requirement of the load and increase fuel efficiency. When the compression ratio is increased comparatively higher gas temperature is produced during the latter part of the expansion stroke. Thus producing higher oxidation of hydrocarbons in the cylinder increasing the emission of exhaust hydrocarbons. But the effect of compression ratio on NO emissions is small.

Caris and Nelson,(1959) conducted experiments on a series of eight-cylinder 5.3 dm^3 displacement engines at a throttle of 2000 rev/min using gasoline fuel. The experimental results showed that the mechanical efficiency and the volumetric efficiency essentially remained constant over the full compression range. Both indicated fuel conversion efficiency and MEP showed a maximum at compression ratio. But for higher compression ratios the efficiency and MEP decreased slightly. This trend was explained as being due to increase in surface/volume ratio and slower combustion and is also due to increasing importance of crevice volumes. The heat losses to the combustion chamber decreased as the compression ratio are increased.

Kerley and Thurston, (1962) studied the effect of compression ratio on fuel conversion efficiency. They studied the variation of ratio of fuel conversion efficiency at given

compression ratio divided by the efficiency at CR8 and found some results that are good till CR < 14. Over the compression ratio range that are accessible by SI engines with available fuels (r < 12) he found that the fuel conversion efficiency increases to about 3% per unit of compression ratio increase.

Abdel and Osman, (1997) studied the effect of varying the compression ratio on the engine performance with different ethanol-gasoline fuel blends using a variable compression ratio engine. The results obtained show that ethanol addition up to 10% improved the indicated power at CR 10. When the ethanol addition increased beyond 20% as the CR increases, the indicated power increases. For each fuel blend, there is an optimum compression ratio that gives maximum indicated power. In this study, the optimum compression ratios were found to be 8, 10, 12 for 10%, 20% and 30% ethanol and above respectively.

Maher et.al., (2010) made an analytical model of spark ignition engine operating on hydrogen fuel and then studied the effects of varying compression ratio, equivalence ratio and engine speed on the performance of engine against experimental data of engine. In summary

1. Highest power occurred at a compression ratio of 11:1 and with further increase, the power reduced due to unstable combustion.
2. The optimum spark timing decreased as compression ratio is increased.
3. The indicated thermal efficiency increased with compression ratio, reaching maximum between 10:1 and 11:1.
4. The specific fuel consumption decreased with increase in compression ratio until 11:1 and after 11:1 specific fuel consumption increased.
5. The NO_x emissions increased with compression ratio for all equivalence ratios less than 0.8 due to high combustion temperature with abundance of oxygen and decreased with compression ratio for all equivalence ratios over 0.8 due to decreasing amount of oxygen.

Yuh and Tohru, (2010) conducted research to observe the effect of higher compression ratios in 2 stroke engines. The results showed that actual fuel consumption was improved by 1-3 % for each unit rise in compression ratio range 6.6 to 13.6. It was concluded that the rate of improvement was smaller when compared to the theoretical values and the difference was mainly due to increased mechanical and cooling losses. Power output was also increased, but the maximum compression ratio was limited due to knock and increase in thermal load.

The author studied the theoretical behavior of combustion in Otto cycle for variable compression ratio as plotted in Fig. 2.5. According to the author, the efficiency of the engine keeps on increasing with compression ratio. However there is certain CR which gives maximum work and found reduced for other CRs.

Srinivas et al.,(2010) tests on variable compression ratio mechanism for a 2 stroke petrol engine concluded that with increase on compression ratio specific fuel consumption reduced,

brake thermal efficiency and mechanical efficiency increased. It was also possible with their design for the driver to operate the engine at compression ratio of his choice based on the terrain he is driving.

Aina et al.,(2012) conducted research on a 4 stroke spark ignition variable compression ratio engine having a maximum compression ratio of 9. Although there were differences in theoretical and experimental engine performance characteristics due to mechanical and cooling losses in the engine. The conclusion was that an increase in the compression ratio increases the brake power, brake thermal efficiency, brake mean effective pressure and reduction in specific fuel consumption which means that higher compression ratios makes it possible to improve the performance characteristics of spark ignition engines.

Researcher (Ozcan and Yamin, 2007; Adams et al., 1987) reported the modification in the SI engine in terms of variable compression ratio to find the best performance and least emissions conditions. Li et al., (2010) study the effect of injection timing and ignition timing of methanol in direct injection stratified charge spark ignition engine and found the optimum timings to get complete combustion, maximum cylinder pressure and temperature. Author explained the methodology of experimentation with all measuring devices clearly in this paper.

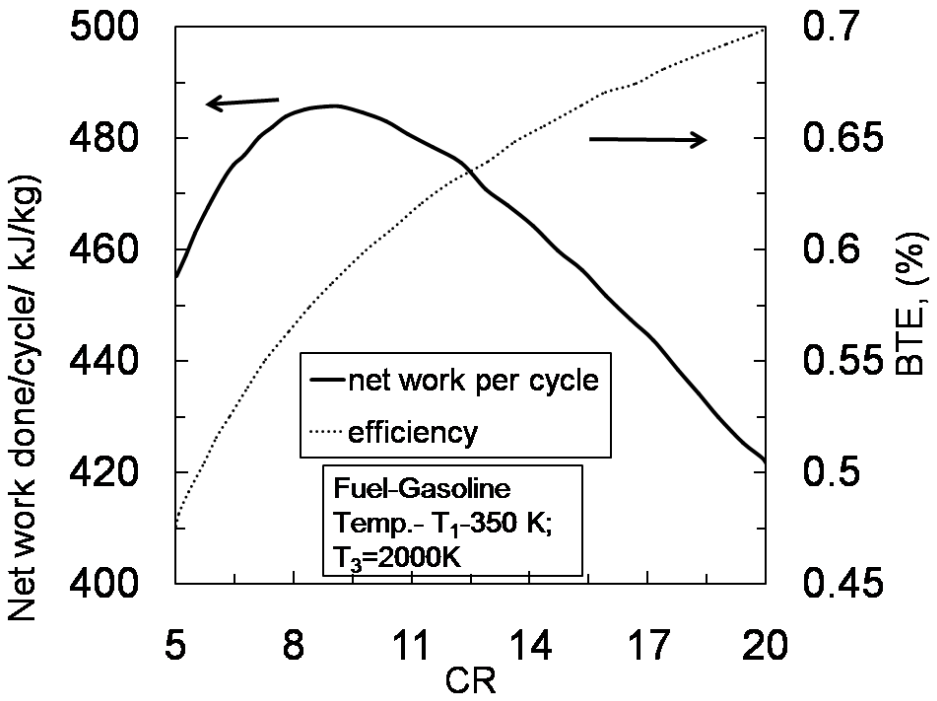

Fig.2.5 Net work done/cycle and efficiency variation with compression ratio(Klein,1991)

Turkoz et al., (2013) investigated experimentally the best ignition timing in an 4-stroke, 4-cylinder SI engine. The author experimented E85 (15% Gasoline + 85% ethanol) ethanol fuel blends by altering the timing angle with respect to gasoline use. The output performance parameters of interest were power, efficiency and energy distribution of engine. The ignition timing was successively delayed in 2^0 increments up to 6^0 (denoted as -2, -4, -6, respectively) and then successively advanced by 2^0 up to 6^0 (denoted as +2, +4, +6, respectively) with

respect to that ignition advance values used with gasoline (called the ‘‘original advance values’’) at full load operation within 2000 to 4000 rpm at increment of 500 rpm The best performance like brake torque and brake power were obtained with + 4^0 crank advances at 3500 rpm which results in better overall efficiency.

2.3.2 Findings with gaseous Fuel

Gaseous fuels are categorized as renewable (raw biogas, producer gas etc) and non renewable (Liquefied Petroleum Gas(LPG),Natural gas, Compressed Natural Gas(CNG) etc). The fuel dependent modifications of the existing engine are necessary to flow gaseous fuels from intake port to the combustion chamber as per load and speed on the engine. Gaseous fuels like LPG and CNG fuel supply systems are quite standardized and commercially successful since years. Many authors worked using LPG and CNG fuels in SI engine such as Gumus, 2011; Choi et al., 2002; Masi, 2012; Ibrahim and Bari, 2009; Murillo et al., 2005. Gaseous fuel filling stations are available on highways which cost less than petrol per kg (IOCL Report, 2017). The emissions from the gaseous fuels are cleaner and there will be less maintenance of the engine by use of gaseous fuel. However the use of gaseous fuels in the conventional petrol engine are found to be underutilized. In order to improve the performance of the engine with the gaseous fuels, the experimentations are carried out by those authors and analyzed the outcomes as discussed here forth.

2.3.2.1 Effect of load

a. Combustion

The correlation between the % brake load and specific gas consumption for operation of engine on CNG, methane enriched biogas and raw biogas was studied by Chandra et al., (2011). It was seen that specific gas consumption on raw biogas is comparatively very high at all working brake loads of engine in comparison to that of CNG and enriched biogas due to reason of higher % of natural gas and methane which improves heating and had reduced the gas consumption rate. The relative air fuel ratio variation for all three fuels with % brake load was studied by author and found that engine running on CNG and methane enriched biogas is supplied with lean air-fuel ratio for 30^0 and 40^0 ignition advance but at 35 ^{0} bTDC the air-fuel ratio is rich ($\lambda < 1.0$). But relative air-fuel ratio for raw biogas was observed to be rich at all three selected ignition advance.

b. Efficiency

The performance results of 5.9 kW stationary diesel engine which was converted to spark ignition mode and run on compressed natural gas, methane enriched biogas and biogas produced from biomethanation of jatropha and pongamia oil seedcake was studied by Chandra et al., (2011). The CR 12.65 was kept constant but the results were plotted for 30 ^{0}, 35 ^{0} and 40 ^{0} ignition advance of TDC. The author found that the brake power developed by the engine increases with increase in brake load for the selected fuels at all three selected ignition advances. The maximum brake power obtained when operated on CNG at ignition advance of 30 ^{0}, 35 ^{0}, 40 ^{0} bTDC and it is 3.548, 3.914, 3.763 kW and with maximum brake

load development of 59.7 %, 68.2 % and 67.9 % respectively. In case of raw biogas the power produced from engine was almost similar at ignition advance of 35 ^{0}and 40 ^{0} bTDC, the best performance was at 35 ^{0}. Due to conversion from CI to SI there is 13 to 30 % drop in power was observed by the author. The methane enriched biogas shows 1.43 times more power output than raw biogas; this gives clear cut advantage of use of methane enriched biogas in engine operation for better output over raw biogas. The maximum brake thermal efficiency of engine on CNG was 22.2 % at brake load of 59.5 %, for enriched biogas 26.2 % at brake load of 59 % at 35 ^{0} bTDC and for raw biogas it is 23.3 % at 35 ^{0} and 40 ^{0} bTDC. The raw biogas as supplied from biogas plant with pressure about 100 mm of water column which results in lower volumetric efficiency so the supply of right mixture of air and fuel is of utmost importance for performance of spark ignition engine.

c. Emission

Ceper et al., (2009) investigated the effect of brake load on emissions like HC, CO, CO_2 for varying excess air ratio for the CH_4 and H_2 mixture blend in spark ignition engine. He reported that for the different percent of H_2 in mixture the emissions are reduced with increase in excess air ratio for 65% load and full load on engine.

2.3.2.2 Effect of speed

a. Combustion

The effect of speed on cylinder pressure and temperature of combustion were studied by Ozcan and Jehad, (2008) for LPG fuel. They found that with the increase in speed the cylinder pressure and temperature in cylinder during combustion increases for a particular stroke length.

b. Efficiency

Ozcan and Jehad, (2008) studied the performance of engine for LPG fuel in terms of speed. They found that brake power increases (7-54% at low speed and 7-57% at high speed) as the engine speed increases for a particular stroke length. Also the volumetric efficiency increases with increase in speed at a particular stroke length. The brake mean effective pressure (bmep), brake specific fuel consumption (bsfc) reduces up to 2000 rpm. But due to less volume during which pressure will act, the work done on piston will be less and hence the brake mean effective pressure decreases and bsfc increases with further increase in speed for a particular stroke length.

The performance parameters like brake specific fuel consumption as a function of engine operating speed for the baseline fuels like gasoline, natural gas and powergas (CO + H_2) were studied by Mustafi et al., (2006). He found that the bsfc for natural gas is almost constant but for gasoline and power gas, bsfc shows mild increase with increase in speed. For particular operating speed the powergas requires very high specific fuel consumption (2.7 times of gasoline and 3.4 times of natural gas) compared to other fuels. The stoichiometric air-fuel ratio for power gas was about 4.25:1 which was much lower than natural gas (15.5:1) and

(14.6:1) gasoline since it contains CO and H_2. The optimum spark timing MBT was found for powergas to be about 4 ^{0} bTDC, 24 - 30 ^{0} bTDC for natural gas, for gasoline (12-18) ^{0} bTDC at compression ratio of 8:1 which shows very rapid combustion process of powergas. The brake torque in every case gradually declined as engine speed increases from 1000-2000 rpm. For the particular operating speed the brake torque decreased significantly in case of powergas operation compared with other fuels. Also volumetric efficiency normally reduced for gaseous fuel compared to liquid fuels. The decrement in volumetric efficiency is more for powergas and due to this its torque output also decreases.

c. Emission

The effect of speed on the exhaust gas like NO_x and HC emission was observed by Ozcan and Jehad, (2008) for LPG fuel. With increase in speed the NO_x emission also increase due to increase (0.65-2% at low speed) in combustion gas temperature. HC emission decreased with increase in speed for a particular stroke length.

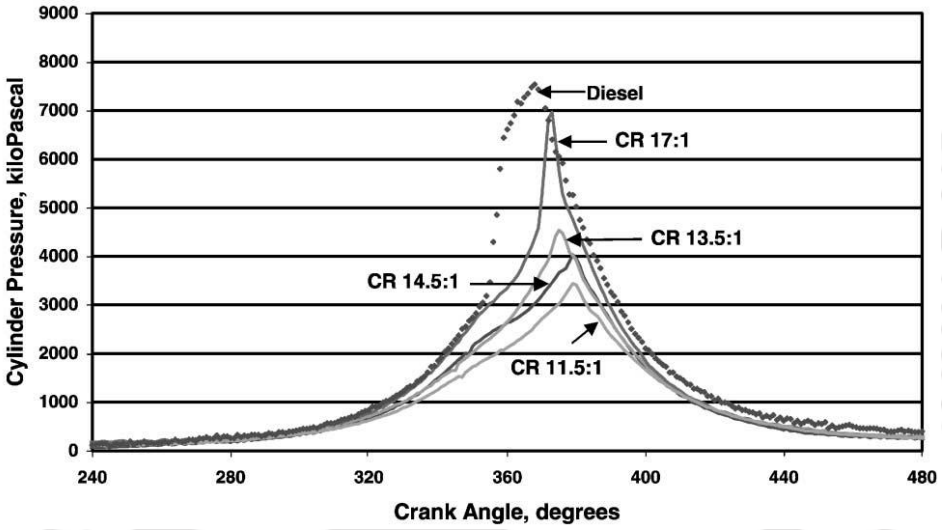

Fig.2.6 Cylinder pressure variation with crank angle for producer gas fuel(Sridhar et al.,2001)

2.3.2.3 Effect of ignition timing

Sridhar et al., (2001); Turkoz et al., (2013); Li et al., (2010); Lee et al.,(2010) studied the effect of variable ignition timing concept and its implications on engine combustion, performance and emissions.

a. Combustion

Sridhar et al., (2001) studied the producer gas with some percentage of hydrogen fuel in CI converted to SI engine at varying compression ratio. The calorific value of producer gas used is 4.65 ± 0.15 MJ Nm^{-3}. The cylinder pressure reaches upto 70 bar using producer gas while engine operating at CR17. The peak pressure occurred between 18-19 ^{0} aTDC for all the CRs considered as shown in Fig. 2.6. The coefficient of variance of IMEP at all CR and ignition timings lying between 3-3.5 % showing lower variation. Since the maximum flame speed was strong function of hydrogen content in gas, MBT will differ based on actual composition

of fuel. The spark timing had a considerable influence on the combustion characteristics and therefore on the engine performance and combustion products. A spark timing that was too advanced causes the cylinder pressure to increase substantially and rapidly before the end of compression stroke. The pressure rise due to spark before compression stroke reduces the work of compression and decreased the net useful work (Turkoz et al., 2013). In contrast the too delayed spark timing resulted in lower peak pressure occurring very late in expansion process. This reduced the work transfer from the expanding gases to the piston.

For this, the optimum spark timing was very important. Lee et al.,(2010) reported the effect of EGR on optimum spark timing of gas spark ignition engine with different fuels like natural gas, model biogas, model biogas + 5 % hydrogen.

The optimum spark timings were advanced as the recirculated exhaust gas percentage is increased. For biogas engine generator, the optimum spark timing with the maximum generating efficiency advanced from 16 ^{0} to 22 ^{0} bTDC as EGR rate increased from 0 % to 15 %. Also at optimum spark timing, above 15 % EGR rate the Korean Industrial NO_x Regulation (< 50 ppm) were satisfied.

b. Efficiency

Li et al., (2010) found that the BSFC was minimized at an injection timing of 39 ^{0} bTDC and an ignition timing of 18 ^{0} bTDC, so these were optimal timings under 1600 rpm speed and full load working conditions. Optimal injection timing and ignition timing clearly increased as the engine speed increases.

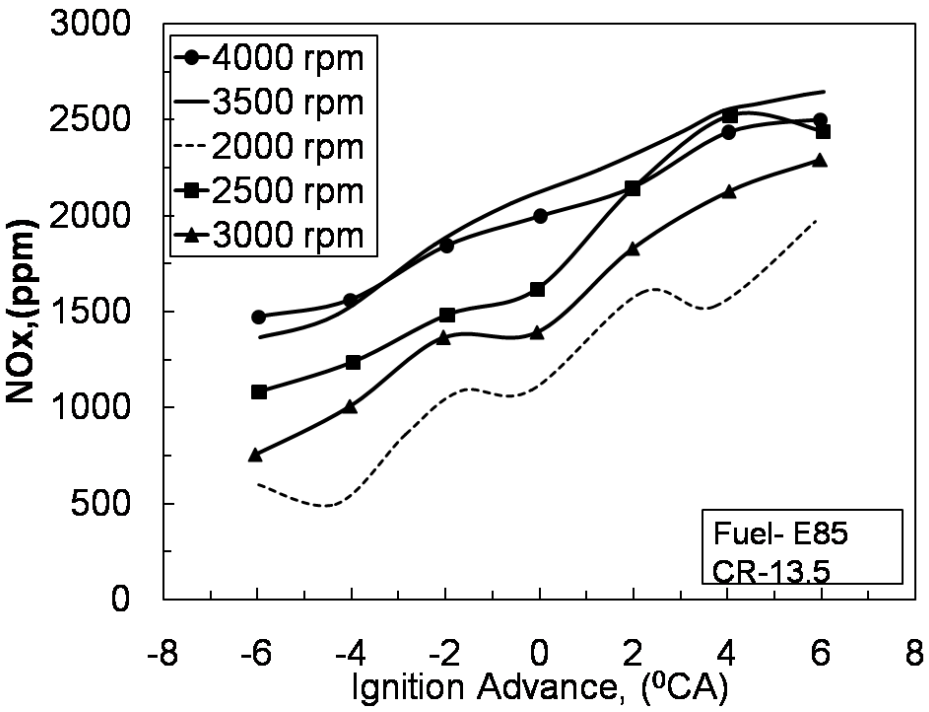

Fig.2.7 NOx variation with ignition advance for different speed (Turkoz et al., 2003)

This was consistent with the spark-ignition engine and compression–ignition engine, and was helpful for controlling the two parameters affecting the combustion process. Optimal and non

optimal bsfc decreased with increasing BMEP because as BMEP rises, injection quantity per cycle increases.

c. Emission

NO emissions with ignition advance for different CR was plotted by Turkoz et al., 2003 reported that the higher CR gives higher NO_x for 12-35 ^{0} bTDC. Increase in hydrocarbon emissions with advanced spark timing mainly caused by two different mechanisms: first, increased pressure in combustion space at the same piston position resulted with greater mass of hydrocarbons trapped in the piston crevices, and the second, lower exhaust temperature allowed for less oxidation of the hydrocarbons released from the crevices during expansion stroke. This was observed at 3000, 3500 and 4000 rpm engine speeds for 4^0 advanced ignition as shown in Fig.2.7. Delayed ignition caused delayed completion of the combustion process, and the average combustion temperature was lower in this case. The highest NO_x emissions are measured at 3500 and 4000 rpm. Sridhar et al., (2001) reported the NO variation with ignition timing for various values of CR for powergas in spark ignition engine. He followed the Swiss Norms of emission which are more stringent. The NO level reduced with the retardation of ignition timing and this feature was observed for all CRs. The NO level was observed to be maximum at the highest compression ratio with advanced ignition timings, whereas for the MBT range of 6–20 ^{0} bTDC, the NO was roughly about the same in almost all the cases. He found that NO was higher at MBT and 13.5 compression ratio. It is a well-known fact that NO generation is strongly dependent on the temperature and also residence time in the combustion chamber. With the flame speed of the gas mixture being high, the ignition setting is retarded whereby the residence time in the high temperature combustion chamber is automatically reduced. Therefore, the low NO levels at retarded ignition setting is an expected and consistent behavior.

2.3.2.4 Effect of engine compression ratio

It is well acknowledged fact that it is desirable to operate an internal combustion engine at the highest possible CR so as to attain highest overall efficiencies. But the gain in efficiency beyond a certain CR can be expected to be marginal (Fig.2.1) due to other influencing factors such as heat loss and friction. The limitation of CR in SI engine comes from knock sensitivity of the fuel. It was experimentally investigated that upper limit of compression ratio for SI engine operation is 17:1 beyond which there is fall in efficiency for iso-octane fuel doped with anti-knock agents Sridhar et al., (2001).

a. Combustion

For the CR changes from 8:1 to 15:1 the maximum cylinder pressure increased from 2.63 to 8.51 MPa and detonation started to occur. This phenomenon reduced the operating efficiency and durability of an engine so author Huang and Crookes, (1998) gave the upper limit of CR to be 13:1 for simulated biogas as fuel (Fig. 2.8).

Pressure- crank angle results are plotted which showed smooth pressure variation during the entire combustion process without any sign of knock.

The study of engine combustion chamber and design for producer gas is a work to be done ahead. The fuel-air equivalence ratio was 1.00-1.06 at which maximum power was derived with exception of 0.86 at CR 13.5:1 Sridhar et al.,(2001). Li and Karim, (2005); Park et al., 2011 reported that the effect of changes in compression ratio on the oil consumption was in comparison relatively poor in case of hydrogen with methane mixture .

b. Efficiency

The author Huang and Crooks, (1998) studied the effect of change in compression ratio on engine performance at a fixed engine speed of 2000 r/min with RAFR and CO_2 fraction in biogas fuel. He found after experimentation that both brake thermal efficiency and brake mean effective pressure increased steadily with compression ratio upto critical value of 13:1. The same results were in agreement with those of Nayeloff (1981).The cylinder pressure increased sharply due to detonation above 15:1.

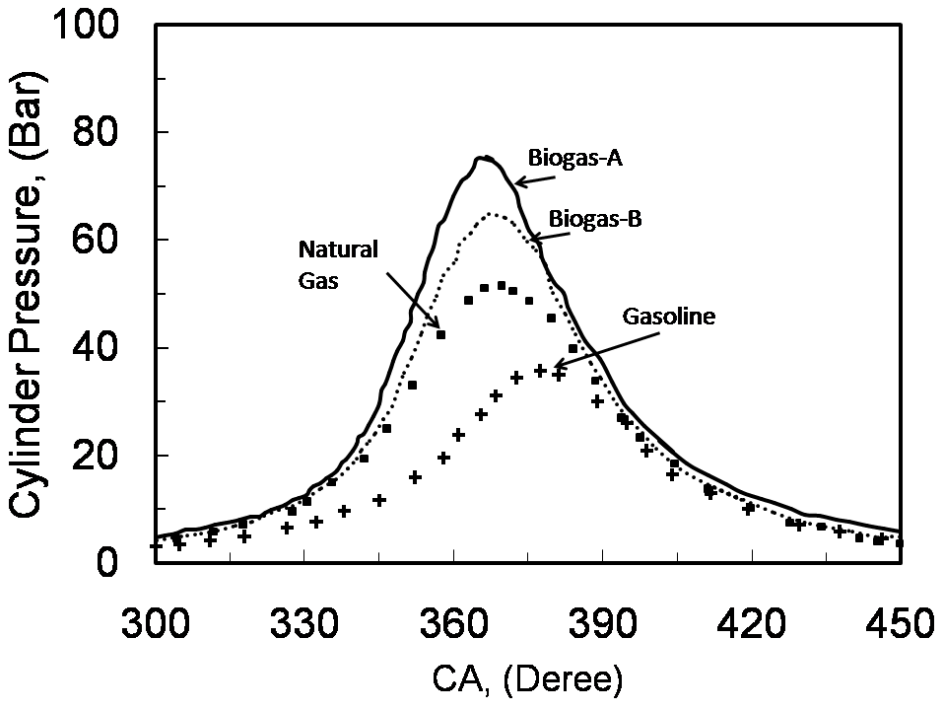

Fig.2.8 Cylinder pressure variation with CA for different fuels. (Huang and Crookes, 1998)

Sridhar et al., (2001) used the producer gas in reciprocating engines at high compression ratio from 17:1 to 12:1. The experimentation was done to evaluate the brake power, overall efficiency. This researcher did systematic study on engine behavior using producer gas fuel. The availability of standard and proven gasification system which could generate gas of consistent quality and on continuous basis for engine application. This engine was tested with different compression ratios and arrived at an optimum CR for maximum brake power. Engine works smoothly without knock at high CR 17:1 delivering 20 kW shaft power with overall efficiency 21 % compared to 24 kW shaft power and 31 % efficiency in diesel mode. With lowering CR useful power and efficiency decreases. To achieve MBT, for produce gas engine it is required to retard the ignition timing. Author suggested increasing the quantity of hydrogen in fuel for ideal cycle operation.

Table 2.1 Producer gas Engine output at MBT (Sridhar et al., 2001)

CR	IGN, bTDC	PHI	H_2/CO	Max. Power(kWe)
17:1	6	1.05	1.01	17.5
14.5:1	10	1.04	1.00	16.4
13.5:1	13	0.86	1.08	16.2
11.5;1	16	1.00	1.06	15.3

When author tested powergas with higher compression ratio of 11:1, the brake torque was improved compared to other fuels (Mustafi et al., 2001).

Zheng et al., (2009) did an experimental study on the natural-gas direct-injection spark ignition engine and its performance was studied by varying the compression ratio. The results showed that the compression ratio has a large influence on the engine performance. The brake thermal efficiency increased with increase in CR at low and medium loads but for high load engine the trend followed only up to CR 12.

c. Emission

Raising the compression ratio had the effect of increasing in cylinder temperature, NOx and HC. So if compression ratio was increased to 13:1 the emissions can be reduced by dilution of CO_2 or N_2, suggested by Crookes (2006).The variation of exhaust gas for variable compression ratio engine with fixed RAFR and CO_2 fraction in biogas were plotted by Huang and Crookes, (1998). Higher the compression ratio greater was the NO_x. HC and CO emission were less noticeably affected by change in compression ratio. Above CR 13:1 all emissions start increasing. Zheng et al., (2009) perform experimental study on the natural-gas shows the emission analysis where the author found that decrease in CO and increase in NO_x with increasing CR. The HC showed a decreasing trend and then an increasing trend with increasing CR. Based on the comprehensive evaluation of performance and emissions, CR of 12 is suggested as an optimum value for engine.

2.3.2.5 Effect of type of fuel

The performance, combustion and emission in spark ignition engine using gaseous fuel have been extensively studied (Choi et al., 2003; Morganti et al., 2013; Gumus, 2011, Hyun et al.) and analyzed. The author Raslavicous et al., 2014 suggest the LPG as medium term option in the transition to sustainable fuels and transport along with cooking. The LPG gas having characteristics such as clean, relatively low in cost, low carbon to hydrogen ratio and at present abundant energy source to provide affordable fuel efficient transportation. Auto ignition and non auto ignition test have been performed by author Morganthi et al., 2014 for different constituents of LPG such as pure propane (C_3H_8), propylene, n-butane and iso-butane and experimentally analyzed the research and motor octane rating of different LPG compositions. Similarly there are some renewable fuels like raw biogas having properties exactly opposite to that of LPG as fuel. Borjesson, 1997 suggest that biogas is more advantageous than use of biofuels or biodiesels in engine. Aaroya et al., 2001 catalytically

decomposed the biogas to form syngas which could be more advantageous for testing in the engine. Huang and crookes,1998; Igoni et al., 2008 and Park et al., 2011 uses the simulated biogas with varying percentage of CO_2 or added with H_2 in the fuel and study the performance of the engine.

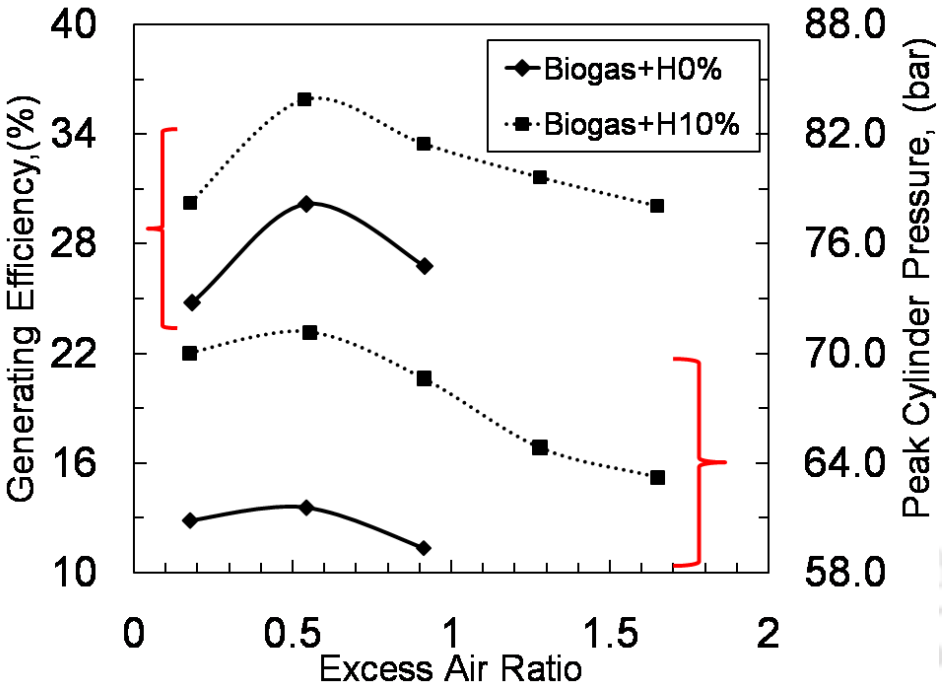

Fig.2.9 Generating Efficiency and Peak cylinder pressure variation with excess air ratio (Jeong et al., 2009)

a. Combustion

Lot of research has been carried out by different authors such as Ceviz and Yaksel, 2006 who studied the effect of LPG fuel combustion on cycle-by-cycle variations with respect to gasoline engine in lean operating conditions. The advantage of this is the scope for rise in thermal efficiency and decrease in exhaust emissions. According to author, the cyclic variations are the results of random fluctuations, excess air ratio, and flow field due to turbulent nature of flow in cylinder. The author reported that the gaseous fuel reduces cyclic variation if runs at lean operating limits. Li et al., 2007 also have the same opinion in terms of lean operating limit of LPG fueled engine which directly influence cylinder pressure, engine speed and NO emissions of first firing cycle during cold start. To improve the combustion stability of biogas for lowest energy density fuel (80% inert gas N_2 dilution), H_2 addition test were carried out by Park et al., (2011) in a stoichiometric excess air ratio. An increase of H_2 concentration in fuel blend enhanced combustion characteristics so that combustion duration was shortened. The excess air ratio of biogas-hydrogen blend was analyzed by Jeong et al., (2009) for the highest pressure and temperature in cylinder. He found that at EAR 1.2 where maximum thermal efficiency was observed, the cylinder pressure and temperature also maximum at that point which increases flame propagation speed and also increase tendency for knock consequently help lean combustion of fuel. The generating efficiency as well as peak cylinder pressure at same excess air ratio as shown in Fig. 2.9.

The author Turnheer et al., (2009) tested spark ignition engine with five types of fuels like gasoline, methane, methane + 5 % hydrogen, Methane + 10 % hydrogen, Methane + 15 % hydrogen. The authors found out optimum spark timing experimentally for all the fuels with reference to MBT keeping the parameters like speed 2000 rpm, BMEP at 2 bar to be constant. They used WEG; a zero dimensional two zone thermodynamic model for heat release analysis. The addition of hydrogen with methane allowed for retarding the optimum spark timing at about 4- 5 ^{0} CA for 15 % H_2 compared to pure methane. Similar outcomes were also reported by Sridhar et al., 2001; Jeong et al., 2009.

The combustion duration gets shortened with addition of hydrogen specifically during flame development angle ($\Delta\Theta_{0-5\%}$) by more than 15% for 15% hydrogen with methane. Gasoline shows shortest centre of combustion angle ($\Delta\Theta_{5-50\%}$). The centre of combustion was located in 367^0 CA (7^0 after TDC). Addition of hydrogen decreases combustion losses but increases wall heat loss. The fuel conversion efficiency was also improved by hydrogen addition compared to gasoline and methane alone.

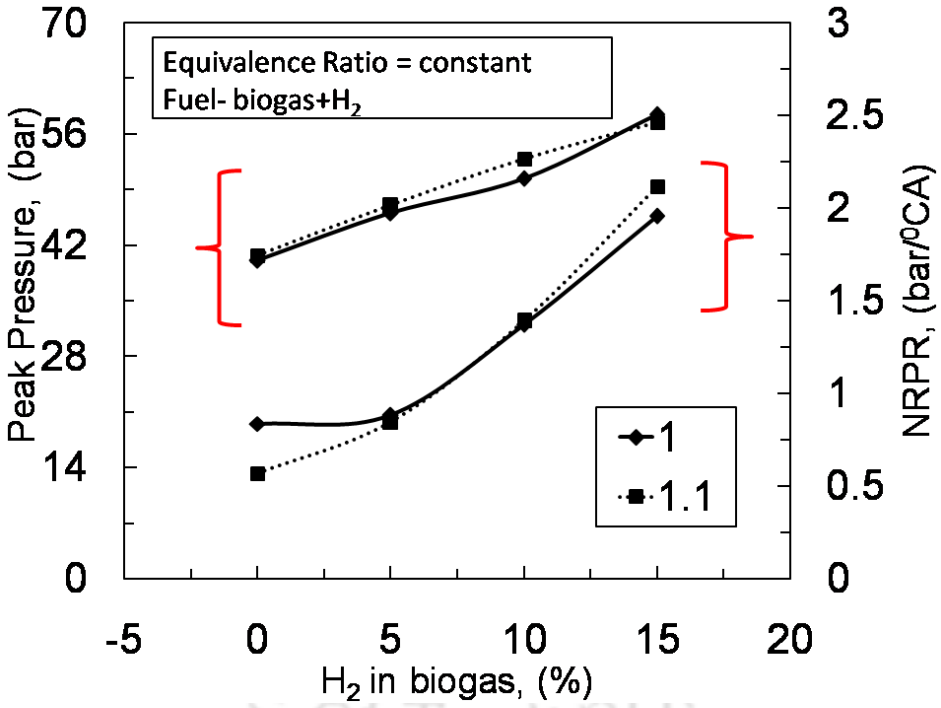

Fig.2.10 Peak pressure and NRPR variation with H_2% at constant equivalence ratio(Porpatham et al., 2007)

Porpatham et al., (2007) reported the effect of hydrogen (5%, 10% and 15% on energy basis) to the biogas and tested in a spark ignition engine at constant speed with different equivalence ratios. Hydrogen addition with biogas extended the lean misfire limit. With neat biogas it was 0.66 whereas with hydrogen fraction of 5, 10, 15 and 20 %, it was extended to 0.63, 0.56 and 0.51. There was drop in COV of IMEP with lean mixture with hydrogen addition. Peak pressure and Maximum Rate of Pressure Rise (MRPR) did not increased with hydrogen addition as the spark timing was retarded to avoid knock (Fig. 2.10).

Choi et al., (2003) reported the effect of hydrogen enrichment (0, 10, and 20 %) with LPG fuel in CI engine converted to work as spark ignition engine. The compression ratio was maintained at 8:1 and found the maximum thermal efficiency and emissions. To maintain the equal heating value the amount of LPG reduced and hydrogen addition increases. The relative air/fuel ratio was increased from 0.8 to 1.3 with increments of 0.1 and ignition timing controlled at MBT. The cylinder pressure curve at bTDC (before top dead center) tends to be little low and the pressure curve at aTDC (after top dead center) tends to be little high because it was thought that the effective compression ratio becomes low as the closing of the inlet valve was accomplished at aTDC.

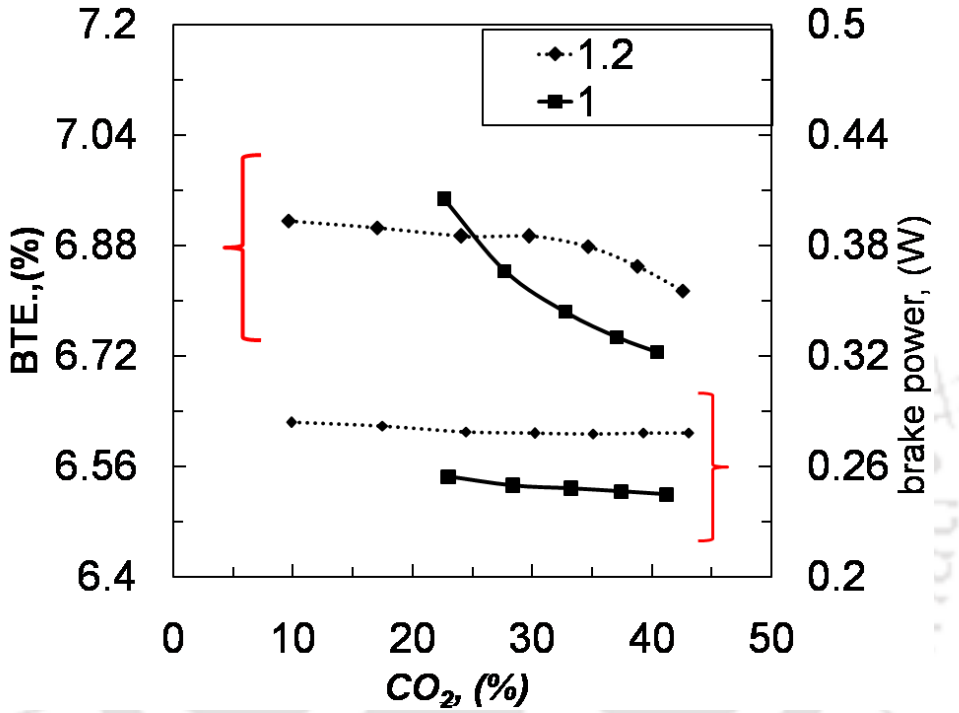

Fig. 2.11 BTE and Brake power variation with CO_2 percentage (Huang and Crooke, 2007).

b. Efficiency

The effect of N_2 dilution from simulated biogas increasing methane concentration was studied by Park et al., (2011). 80% dilution of N_2 (NG: N_2 = 2: 8) required about 2.5 times nitrogen flow rate. Also 80% dilution of N_2 was equivalent to 32 % EGR as suggested by Crookes (2006) also. With the increase in N_2 concentration in biogas from 0 to 80 % the thermal efficiency increased, coefficient of variance show increase from 60 % above of N_2 dilution. Less cooling loss to coolant and thermal dissociation occurred with higher N_2 dilution due to lower combustion temperature. The biogas fuel with different percentage of CO_2 was experimented by author Huang and Crooke, 1998) observing the performance of engine for different equivalence ratios (Fig.2.11).

The author Gumus (2011) had tested LPG with higher percentage 25, 50, 75 and 100 % with gasoline in dual fuel mode at constant speed 3800 rpm and load range 5, 30, 60 and 90 % condition. Author found that the volumetric efficiency decreases with 25 % LPG level. Further this decrement is proportional to the percentage of LPG in mixture. Positive results

obtained for brake thermal efficiency and emissions level as previous. Some authors (Badr et al., 1997; Erkus et al., 2013; Ozcan and Jehad, 2008; Alasfour , 2001 and Yamin, 2007) were used 100% LPG in SI engine with modification in fuel supply system and reported the performance and emissions with that of petrol fuel. The author Badr et al, 1997; Alasfour, 2001 did the parametric study of lean operational limits of Ricardo E6 engine using propane and LPG as fuel in SI engine. The parameters considered were speed, spark timing, compression ratio, intake temperature, intake pressure and relative humidity of intake air. The lean misfire limit is the condition when detectable misfire observed and torque becomes zero. Other author Erkus et al., 2013 analyzed the performance of LPG fueled SI engine using carburetor and injection method of fuel intake at fixed throttle 25 % and 50 % WOT within speed range 2000-4000 rpm. They found that LPG injection and its control scheme produce better engine performance than conventional gasoline and LPG carburetion.

Similar to Park et al., (2011) the generating efficiency of a four stroke spark ignition gas engine generator operating on biogas-hydrogen blend with varying excess air ratio was evaluated. Actual air-fuel ratio to the stoichiometric air-fuel ratio was studied by Jeong et al., (2009) for raw biogas with typical properties is in Table 2.2.

Table 2.2 Properties and major fuel components of raw biogas (Jeong et al., 2009)

Property	**Specification**
Density (dry basis)	1.2kg/m^3
Heat value	5.0 -7.5 kWh/m^3
Ignition point	700^{0}C
Ignition concentration gas content	6-12%

Fuel component	**Specification**
Methane	60±0.5%
Carbon dioxide	40±0.5%
Hydrogen Sulfide	0.2-1 ppm
Siloxane	0-3ppm
Ammonia	0.4-1.1 ppm

Jeong et al., (2009) obtained results for generating efficiency of biogas-hydrogen blend as a function of EAR at engine speed of 1200 rpm and engine load 10 kW with compression ratio of 13:1. The maximum generating efficiency was noted at EAR around 1.2 and the generating efficiency under same EAR improved with increase in hydrogen concentration (0, 5, 10, 15 %) (Fig.2.10). This was due to relatively fast burning speed and work by fuel on piston was maximized when complete combustion of fuel occurred. Low NOx emission was found from EPN (29.26% at 50 ppm) when hydrogen concentration in biogas was 15%. However the cost of hydrogen production and NO_x reduction devices were considered, the optimum operating condition could change. Porpatham et al., (2007) reported the effect of hydrogen addition with biogas on engine power output and efficiency. It was observed that high flame velocity of hydrogen improves the combustion rate and raises the power output. With lean mixture 15% hydrogen was found to be the best. It was also found that with hydrogen upto10% the efficiency was maximum.

Nagalingam et al., (1983) carried out experimentations on an Austalt Fur Verbrennungsmotoren List (AVL) Austria research Engine. This engine is a single cylinder, four strokes, spark ignited research engine having CR11.73: 1. Power output measured on eddy current dynamometer. All experiment was carried out at wide open throttle at constant speed of 1200 rpm and maintaining optimum spark timing. The engine was first operated on natural gas and the combustion air ratio was varied by regulating the amount of gas flow. At each operating point the power output, fuel consumption and emission data was observed. The same observations were made using hydrogen supplemented natural gas for comparison with natural gas. Finally the engine was observed on hydrogen at 1200 rpm. About 23% loss of maximum engine output on hydrogen fuel and 12% loss in brake thermal efficiency as compared with natural gas. The range of combustion air ratio was found higher for hydrogen than natural gas. The optimum spark timing for hydrogen at all combustion air ratio tested was more retarded than natural gas by an average of 20^0 crank angle due to higher combustion speed of hydrogen. The performance of hydrogen supplemented natural gas was found to be in between that of natural gas and hydrogen engine.

Experimental investigations relating to the use of producer gas in a spark ignition engine are reported in the proposed paper by Subrahmanyam et al., (2001). The experimental setup consists of a single cylinder diesel engine converted to operate on a spark ignition engine mode coupled to a swinging field electrical dynamometer. A downdraft closed top charcoal gasifier had been used to generate the producer gas.

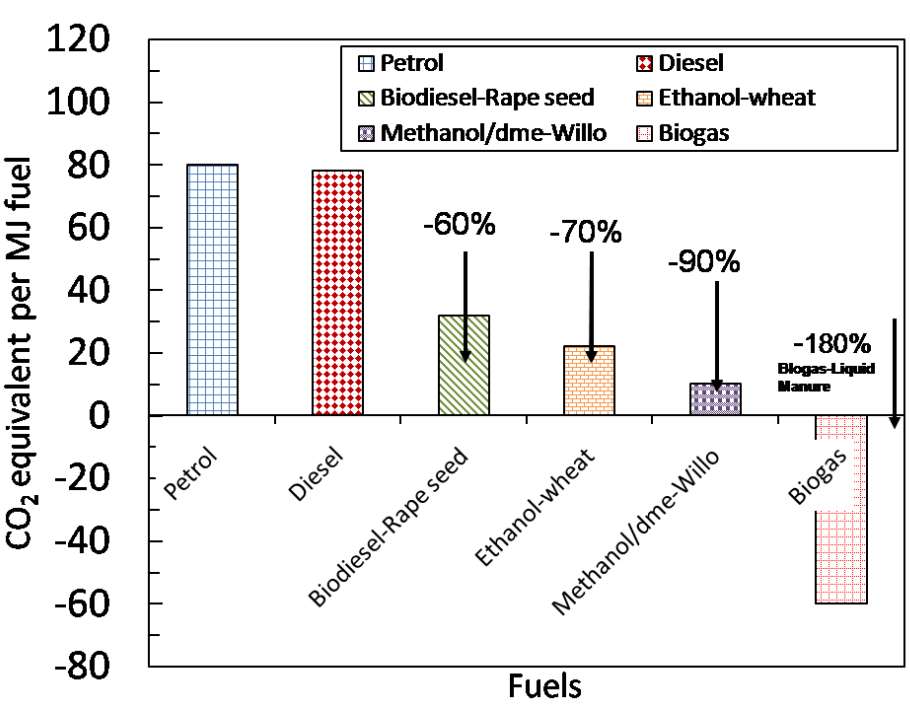

Fig.2.12 CO_2 emission from different fuels along with biogas(Brjesson,2007)

After cooling and cleaning, it was fed to a venturi type gas carburetor, which ensures proper mixing of gas and air before it enters the engine. However initial test using gasoline were performed followed by producer gas tests at different compression ratios. The decrease in efficiency is observed with producer gas than gasoline fuel.

c. Emission

The main driving force to use LPG still remains the low cost for end user, its favorable pollutant emissions (Masi et al., 2012; Choi et al., 2003, Borjesson, 2007) in both steady and transient condition is best analyzed with respect to gasoline fuel. The variation of THC and NOx emissions as a function of N_2 dilution ratio at MBT timing shown by Park et al., (2011). As per author increased inert gas decreases flame propagation velocity, advancing MBT spark timing. Thus NO_x formation was lowered while THC emission increased in biogas.

The variation of CO concentration, NO_x and CO_2 emission for the biogas and hydrogen blends were plotted by Jeong et al., (2009). They stated that CO emission at EAR 1.0 was maximum and decreased with decrease in hydrogen concentration and reduced further for EAR above 1.0. The CO concentration could be extended up to EAR 2.0 but when hydrogen content was 15%. The CO concentration ends for pure biogas was up to EAR1.4 only (Borjeson, 2007) as shown in Fig. 2.12. So lean limit was extended if hydrogen was used with biogas due to larger flame propagation speed. NO_x emission shows the similar behavior as the maximum thermal efficiency for EAR. At EAR 1.2 the maximum NO_x emission was found and increases as the hydrogen concentration increases because higher pressure in cylinder causes higher temperature and ultimately higher NO_x. Further with lean combustion the temperature decreases and NO_x emission decreases. CO_2 values decreases inversely with the excess air ratio because with the lean combustion the oxygen in air was more than enough for combustion. Also CO_2 emission decreased as hydrogen concentration increased at same EAR condition due to combustion of hydrogen instead of Methane in biogas. When operating on powergas ($CO + H_2$) the THC emission were very low at 0 - 20 ppm due to absence of hydrocarbon in the fuel whereas for gasoline THC vary from 90 - 225 ppm and for natural gas 20-106 ppm, the results were plotted by Mustafi et al.,(2006). The author gave the CO_2 concentration which was found highest for powergas operate on among the three fuels. The NO_x emission was found very high for powergas compared to other fuels due to higher temperature and shorter combustion duration. For power gas CO emission was found very much lower than other two fuels under almost similar operating conditions. Porpatham et al.,(2007) found that drastic reduction of HC emission (1530 ppm to 660 ppm) was found with 10 % hydrogen addition in biogas. This was mainly due to improvement in combustion by way of extension of lean limit and increase in combustion rate. There was not any significant increase in NO level since CO_2 act as diluents. Carbon monoxide emissions were less than 1 % by volume and hydrocarbon emissions were negligible throughout the entire load operations at all engines speeds and compression ratios when used producer gas in a spark ignition engine were reported in the proposed paper by Subrahmanyam et al., (2001).

2.3.2.6 Effect of relative air/fuel ratio

a. Combustion

The minimum specific fuel consumption is increased from about 0.07 kg/ MJ by addition of CO_2 above relative air fuel ratio of 1.12 as commented by Crookes, (2006). Porpatham et al.,

(2008) investigated experimentally the influence of reduction in concentration of CO_2 in biogas on combustion in a constant speed spark ignition engine. Using lime water scrubbing method reduced the CO_2 concentration from 41 % to 30 % and 20 %. The peak pressure increased significantly with reduction in CO_2 for a particular equivalence ratio in case of lean mixture. This was due to faster combustion. However at rich mixture the increase in peak pressure with reduction in CO_2 concentration was not significant as the spark timing had to be retarded. The spark timing had to be retarded with reduction of CO_2 for lean to rich equivalence ratio. Li and Karim, (2005) reported the oil consumption rates of a SI H_2 engine increased gradually and almost linearly with increasing the equivalence ratio and hence engine load for non-knocking operation.

b. Efficiency

Crookes, (2006) found the effect of adding CO_2 in natural gas on brake power shows that brake power is relatively unchanged but slightly decreased with the relative air fuel ratio above 1.12. Simulated biogas was tested in spark ignition engine by Huang and Crookes, (1998) where fraction of CO_2 is changed from 0 to 40% by volume for different relative air-fuel ratio and compression ratio. When RAFR is on lean side, there was no significant power deterioration for different fraction of CO_2 but on rich side power decreased by some 3% as CO_2 fraction increased from 20 to 40%. Brake thermal efficiency also reduced with CO_2 fraction due to reduction in flame propagation rate.

Choi et al. (2003**)** reported the effect of hydrogen enrichment (0, 10, and 20 %) with LPG fuel in CI engine converted to work as spark ignition engine. Thermal efficiency as a function of relative air/fuel ratio shows increment with the addition of hydrogen. At λ ~1, thermal efficiency was increased by about 5 % with the addition of 10 ~ 20 % hydrogen. The reason for this increase in thermal efficiency was that the hydrogen fuel burns all at once.

The blend of methane with hydrogen 0, 10, 20 and 30 % by volume was tested by Orhan et al., (2007) experimentally with different equivalence ratio from 0.6 to 1.2. The ignition timing (30 ^{0} bTCD), load, speed (2000 rpm) was kept constant for all fuel fractions and 88 - 92 Nm torque. The brake thermal efficiency variation with equivalence ratio showed efficiency decreased with decrease in equivalence ratio below 0.7. In case of rich mixture (Ø > 1), combustion was not complete due to which there would be decrease in thermal efficiency to a certain level, when equivalence ratio was higher than 0.9. For equivalence ratio between 0.7 to 0.9, the BTE value increased for a particular fuel also with increase in per cent of hydrogen. The highest efficiency noted at 0.85 equivalence ratio. Porpatham et al., (2008) investigated that with reduction in CO_2 concentration from 41 % to 30 % and 20 %, the brake power and brake thermal efficiency was increased from lean to rich equivalence ratio at full throttle and 25 % throttle. This was due to lower heating value increase by reduction of CO_2 in the biogas. Aaroya et al studied the synthetic gases performance and emission for varying equivalence ratio and compared with petrol (Table 2.3). The authors reported that at $\phi = 1$, the gaseous fuel have maximum efficiency upto 28% while other fuels

such as Methane report 30% and petrol 37% efficiency at higher load and minimum speed (Aaroya et al.,2001).

Table- 2.3 Syngas from biogas composition (Aaroya et al., 2001)

Denomination	H_2, (%)	CO, (%)	CH_4, (%)	CO_2, (%),	LHV, (MJ/kg)
Syngas1	23	23	26	28	14.095
Syngas2	40	389	11	10	16.525

c. Emission

The objective to get satisfactory performance and emission can be achieved for relatively low power requirement in rural communities without access to costly fuels was examined by Crookes, (2006). The author uses low technological solution and local bio-fuels like natural gas with varying percent of CO_2 (20, 30, 40 %) in fuel mixture. The effect of adding CO_2 is to reduce specific NO_x values due to reduction in temperature of combustion from 7 g / MJ about 50 % but increases the unburnt HC. The author Huang and Crookes, (1998) and Wang, (1997) were found similar trends of emission for two values of RAFR 0.98 and 1.05. They found that NO_x emission decreased significantly as CO_2 fraction in biogas fuel increased. On other side total unburnt HC emission increased as more CO_2 was introduced relative to natural gas. CO emissions were low when mixture was lean and up to 25% CO_2 fraction but then increased when mixture becomes rich and CO_2 fraction increased.

Choi et al. (2003) reported the effect of hydrogen enrichment (0, 10, and 20%) with LPG fuel in CI engine converted to work as spark ignition engine. The CO emission decreased if the relative air fuel ratio (λ) was increased from 0.8 to 1.3, and the CO emission also decreased as hydrogen was added. For rich relative air-fuel ratios around λ = 0.8, CO emission exhibits a maximum value, and it appears that there was almost zero CO emission above λ = 1.2. Since insufficient supply of air prevents all carbon of the fuel from becoming the perfect combustion gas CO_2causes rise in CO. THC emissions tend to be similar to CO emission at rich mixture conditions as the relative air-fuel ratio was increased from 0.8 to 1.3. The THC emissions decreased, when LPG fuel supply decreases. The NO_x emission were maximum at about λ = 1, and the addition of 20 % hydrogen results in a 40 % increase in the amount of NO_x emission compared to that of pure LPG combustion. This fact result from the fast combustion of hydrogen fuel and the higher maximum temperature and pressure in the cylinder compared to LPG combustion.

Orhan et al., (2007) studied the effect of equivalence ratio on the exhaust emission using different fuels like methane and hydrogen (5, 10, 20, and 30%) blends at constant load and 2000 rpm speed. The variation of brake specific carbon monoxide (BSCO) with equivalence ratio was found, that between 0.6 to 0.85 the BSCO values linearly decreased but increased exponentially between 0.85 to1.2 equivalence ratio. With rise in H_2 percentage, BSCO values decreased for a particular equivalence ratio. During fuel rich mixture due to incomplete combustion there will be rise in BSCO emission. As per authors, 0.92 value was optimum for low emission of CO. CO_2 concentration have a strong relationship with equivalence ratio.

While equivalence ratio increased the CO_2 percentage values increased initially, but found decreased thereafter. For particular equivalence ratio with increase in H_2 percentage, the CO_2 concentration in exhaust emission deceased. The maximum CO_2 percentage is in 0.9 - 0.95 equivalence ratio. The brake specific Nitrogen oxide (BSNO) variation with equivalence ratio showed that the BSNO values increased as equivalence ratio increased also hydrogen percent increased and reached at peak at Ø=0.9. From Ø = 0.9 to 1.2 the BSNO values decreased. Theoretically maximum BSNO should be at stoichiometric equivalence ratio but due to existence of local mixture in-homogeneity in cylinder, shifted the maximum BSNO to Ø=0.9. The maximum temperature in cylinder would be at equivalence ratio on rich side but oxygen supply was also required for complete combustion. BSNO concentration increased with increase in hydrogen fraction in fuel due to increase of peak combustion temperature. The brake specific unburnt hydrocarbon (BSUHC) values decreased with increase in percent of hydrogen addition. The BSUHC values were least at equivalence ratio 0.9 but from 0.9 to 1.2 the BSUHC starts increase. This was due to excess air during lean equivalence ratio.

Porpatham et al., (2008) investigated the reduction in emission of hydrocarbon (HC) particularly with lean mixtures. NO level was raised with reduction in CO_2 from lean to rich equivalence ratio. The NO emission peaks with leaner than stoichiometric mixtures in all cases of throttle position because decrease of CO_2, increases methane concentration leads to faster combustion and higher temperature. The CO level increases with decrease in amount of CO_2 inducted at both 100 % and 25 % throttle and rich equivalence ratio.

Li and Karim, (2005) reported the effect of hydrogen with methane on emission for the variable compression ratio and equivalence ratio. It was found that the carbon bearing species CO and CO_2 present in the exhaust gas in a very small concentration. The addition of some hydrogen to the methane, produces little change in the NO_x emission for mixtures around the stoichiometric region ($0.89 < ER < 1.0$). However, when the operating mixture was gradually leaned, the fuel mixture tends to increase the emission of NO_x concentrations over a wider range of equivalence ratios. The variation of carbon monoxide (CO) is shown by Sridhar et.al. (2001) for powergas operated with compression ratio 11.5 and 17.5:1. The CO levels have been represented in grams per MJ of input energy. The CO increases with increase in PHI. The CO levels were lower at the highest CR, and this could be attributed to higher temperatures, leading to relatively complete combustion.

The exhaust gas emission from the engine at equivalence ratio $\phi = 1$, $\phi = 0.85$, $\phi = 0.7$ was studied by Aaroya et al.,2001. It was found that the specific CO_2 as well as specific CO emissions were higher than gasoline and methane emissions. However they found it to be advantageous in terms of NO_x emission which is minor as compared to gasoline and methane.

2.3.2.7 Effect of bore/stroke ratio

a. Combustion

The effect of bore/ stroke ratio on cylinder pressure and temperature of combustion were studied and plotted for LPG fuel by Ozcan and Jehad, (2008). They found that with the

decrease in stroke length i.e. increasing the bore/ stroke ratio, the cylinder pressure and temperature in cylinder during combustion increased for a particular speed.

b. Efficiency

Ozcan and Jehad, (2008) studied the performance of engine for LPG fuel in terms of bore/ stroke ratio. They found that for the given speed, brake power increases as the engine bore/ stroke ratio decreases. Also with decrease in bore/ stroke ratio the volumetric efficiency increased for a particular speed. Hence more energy would be available to be converted to useful work. The brake specific fuel consumption increased as bore/ stroke ratio decreased. Due to increase in bsfc, the thermal efficiency decreased as bore/ stroke ratio decreased (Fig. 2.13).

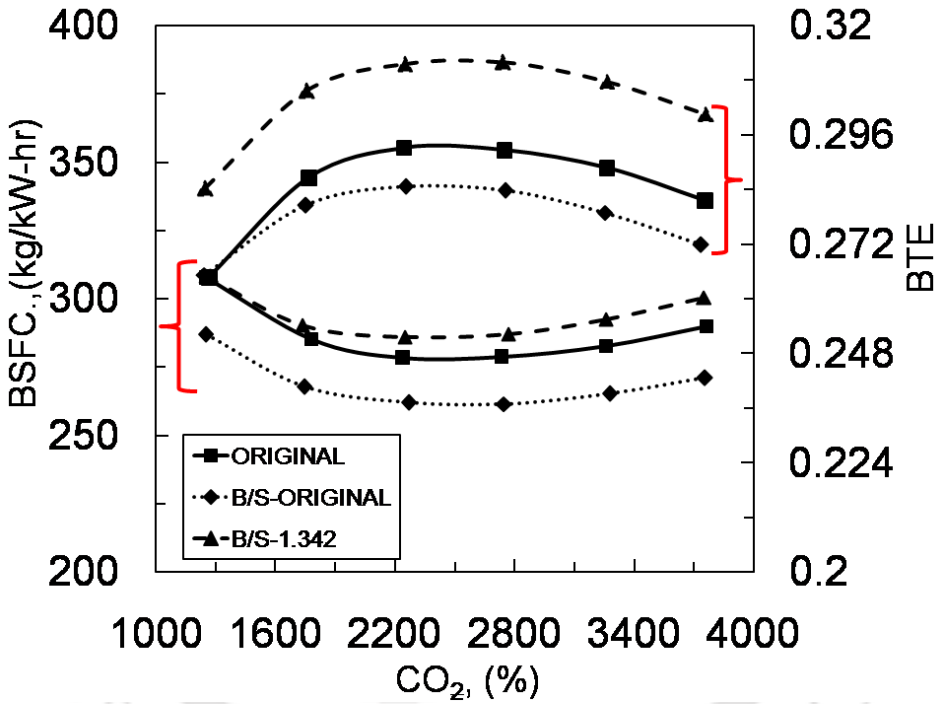

Fig.2.13 (a) BSFC variation with CO_2 for different bore to stroke ratio; (b) BTE variation with CO_2 for different B/S ratio (Ozcan and Jehad, 2008)

The effect of bore/ stroke ratio on friction loss was important because with increase in friction loss the mechanical efficiency decreased. Authors found that with the decrease in bore/ stroke ratio the friction loss increased due to more distance travel by piston and corresponding to that mechanical efficiency decreased. The variable stroke technique was helpful to improve the performance and emission characteristics of LPG fueled spark ignition engine.

c. Emission

Reduction of heat loss and an increment in exhaust gas temperature observed when bore/ stroke ratio increased, noted by Ozcan and Jehad, (2008) for LPG fuel. The wasted heat of exhaust gas could be converted to useful work like electricity generation etc. The NO_x and HC emission of LPG depend very much on bore/ stroke ratio because if the bore/ stroke ratio

increases the NOx emission increases from 2725 ppm at B/ S ratio 0.887 to 2800 ppm at B/ S ratio1.342 operated at speed 1000 rpm . Similarly HC emission from 1900 ppm at B/ S ratio 0.887 to 1930 ppm at B/S ratio 1.342 at same speed 1000 rpm so selection of stroke length is very important.

2.3.2.8 Effect of EGR and Intake air temperature

In this method the exhaust gases from engine were taken and supplied back to the inlet port of engine through manual valve. To reduce the volumetric efficiency of EGR the gas was cooled before supplying to inlet port. Initially engine runs at fixed speed with lean air/ fuel ratio i.e. excess air with equivalence ratio around 0.35, when it runs smooth, the exhaust gas recirculated slowly by manual valve to the inlet port reducing the excess air till the mixture becomes stoichiometric. This is depicted by Xie et al., 2013; Park et al., 2011; Alger et al., 2012; Hu et al., 2009; Lee et al., 2009.

a. Combustion

Xie et al., (2013) study the effect of ignition timing on the spark ignition methanol engine with wide open throttle at 1400 rpm and full load with compression ratio 18.5. The authors found that when the engine runs at 18, 15 and 12^0 bTDC the engine runs smoothly without knock. The authors suggested that the ignition timing could be adjusted to get better performance of engine at variable load especially when variable EGR was supplied. There findings were for lower EGR and higher load; ignition timing should be delayed for avoiding knock whereas higher EGR with lower load, ignition timing should be advanced to maintain good combustion quality and low cycle-by-cycle variations.

b. Efficiency

It can also be seen that both brake thermodynamic efficiency and torque decreased as the EGR percent increased (Hu et al., 2009). The authors found that with lean mixture, torque was 94 N-m decreased to 88 N-m with EGR. Similarly brake thermodynamic efficiency for lean burn is 36 % decreased to 32 % for EGR. This was thought to be due to the reduction in volumetric efficiency brought on by the increase in MAT (Manifold Air Temperature) and the additional work required by the engine to pump the water through the combustion chamber.

Hu et al., (2009) reported that the addition of hydrogen with natural gas would increase the power output at large EGR also. But the effective thermal efficiency was found to be decreasing at small EGR rate while increased with large EGR rate. One reason being the combustion improvement of natural gas hydrogen blend. The other reason was the free radicals produced during combustion processing and the presence of radicals will activate the pre-ignition reaction and leads to the improvement of combustion efficiency.

Xie et al., (2013) studied ignition timing with EGR for spark ignition methanol engine and found that with increasing EGR rate and reducing load, ignition timing needs to be advanced in order to make the fuel economy of engine to optimum. The optimal ignition timing for the

minimum BSFC was constantly changing with the changing of EGR rate. When the EGR rate was between 0 and 0.1, the minimum BSFC was obtained at ignition angle of 18 ^{0} bTDC; when the EGR rate was between 0.1 and 0.2, it is 21 ^{0} bTDC; when the EGR rate was between 0.2 and 0.32, it was 24^0 bTDC. Ignition timing should increase to 33 - 36 ^{0} bTDC to reach minimum fuel consumption.

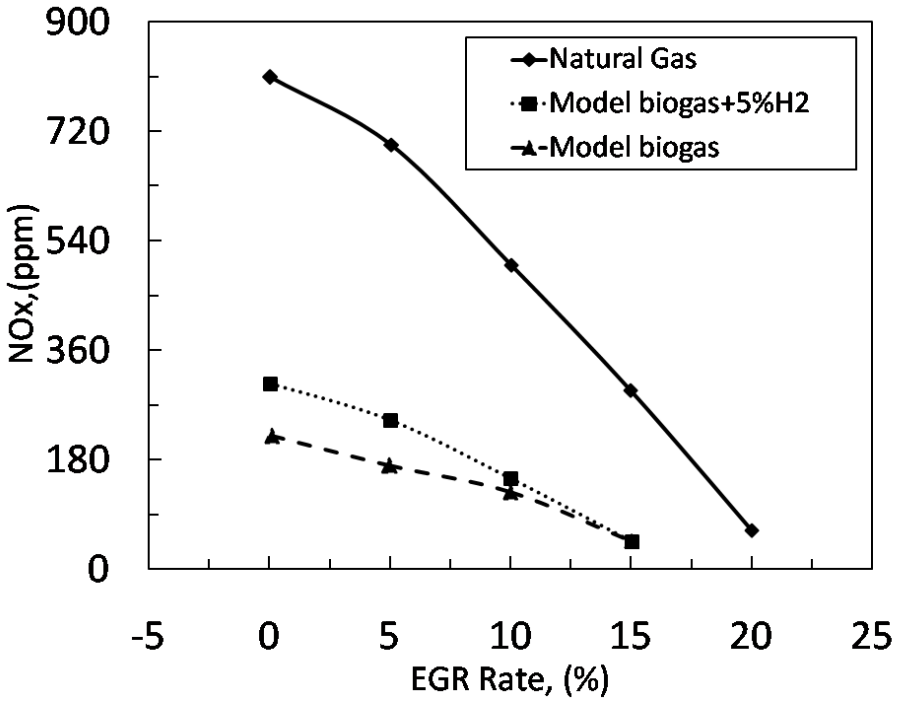

Fig. 2.14 NO_x variation with EGR Rate for different composition of biogas (Lee et al.,2010)

Lee et al., (2010) reported the effect of low pressure exhaust gas recirculation on generating efficiency using different gaseous fuels like natural gas, model biogas +5 % hydrogen and model biogas. The experiment carried out at fixed spark timing and optimum spark timing. Author did experimentation of optimum spark timing for the listed fuels without EGR. Utilizing this optimum spark timing which was 14 ^{0} bTDC for natural gas, 16 ^{0} bTDC for model biogas and 13 ^{0} bTDC for model biogas with 5% hydrogen. The generating efficiency in model biogas engine test had a tendency to decrease from 30.15 % to 29.02 % as EGR rate increased from 0 % to 15 % since incomplete fuel combustion occurred because of CO_2 in mixture. When 5 % hydrogen was added to model biogas, generating efficiency was improved by 1.18 % without application of EGR.

Different methods were considered by different authors to mitigate the exhaust gas emission. One such technique is reported by Tartakovsky et al.,2015 where the gaseous hydrogen rich methanol reforming products were used in direct injection SI engine. This technique has a great potential of emission mitigation as compared with gasoline. The NOx in exhaust was found to be reduced by factor of 7 as a result of lean combustion and lower cylinder temperature.

Another technique of high level EGR for high efficiency engines was discussed by Alger and Mangold, 2009. They experimented the use of high level EGR for reduction in emission and

improvement of efficiency. In this proposal, out of 4 cylinders, exhaust of one of the cylinders was used for recirculation. Hence, that exhaust manifold was directly connected to the intake manifold leading to constant 25% EGR rate. This concept showed large gain in fuel efficiency over the baseline performance and also had significantly reduces the emission from engine.

c. Emission

Author Haffel, (2003) studied the effect of EGR on exhaust gases leaving the hydrogen fueled engine specifically NO_x emission. Author uses the engine at 3000 rpm constant speed with varying fuel supply from 1.63 to 2.72 kg/ h. The maximum equivalence ratio limited in lean burn strategy by NO_x emissions (maximum 0.4). As per author, with the increase of torque the NO_x emission increases. So for zero NO_x emission the EGR gives more torque than lean burn fuel air mixture.

Alger et al., (2012) studied the effect of addition of exhaust gas recirculation on the performance and emission of spark ignition gasoline engine. They reported that EGR improves the fuel consumption of gasoline engine by reducing pumping losses and knock by eliminating enrichment regions. The EGR substantially reduces the emissions of nitrogen oxide (NO_x) and CO. Authors tested 2.4v litre multi-point injection engine and a 1.6 liter gasoline direct injection with high levels of both cooled and uncooled EGR. The results showed that an improvement of 5 and 30 percent in fuel consumption is possible. Emissions like NO_x reduce by 80 % and CO by 30 %.

Xie et al., (2013) studied ignition timing with EGR for spark ignition methanol engine and found that for optimum EGR rate and ignition timing, NO emissions decreased with reduction of engine load. HC and CO emissions deteriorate significantly at lower load due to excessive EGR.

Lee et al., (2010) reported the effect of low pressure exhaust gas recirculation on NO_x emission using different gaseous fuels like natural gas, model biogas + 5 % hydrogen and model biogas as shown in Fig.2.14. The NO_x emission of model biogas generally lower compared to those of natural gas test. In addition, NO_x concentration of exhaust gas decreased from 221 ppm to 38 ppm as recycled exhaust gas increased to 11.8 %. Addition of hydrogen to model biogas increases the NO_x emission in comparison to those generated by model biogas. The NO_x production of hydrogen with model biogas was decreased to the level of model biogas when EGR rate increased to 15 %.

Hu et al., (2009) reported the effect of natural gas hydrogen blend with EGR on the exhaust gas emissions. They found that for a specified hydrogen fraction, the NO fraction decreases with increase in EGR and HC emission increased with increasing of EGR rate. The CO and CO_2 emissions show little variation with EGR but they decrease with increase of hydrogen fraction.

2.3.2.9 Effect of variable spark plug location

Quader (1973) reported the effect of variable spark location on combustion and emissions of gasoline fuelled engine. It was noticed that if spark plug is at center from exhaust and intake valve, it increases emissions of NO_x. But, HC emissions would be lower if spark plug is nearer to the exhaust valve. Alteration in combustion duration and its effect on HC and NO emissions was discussed by Wentworth (1974) for different combustion chamber shapes and spark plug locations in case of SI engine. Witze (1982) presented effect of swirl level and spark location on combustion duration in homogeneous charge engine. As per the author, for lower swirl level ignition point should be located towards center of the chamber while for higher swirl the same should be moved towards wall of the chamber. Han et al.,(2000) discussed about changes in flame propagation with flow direction and its variation at the spark plug. Ducols et al. (1996) explored the combustion model (Multiblock version of Kiva2 code for 4 valve engine) for understanding the effect of fuel, residuals and spark location. Srivastava and Agarwal (2013) reported the effect of variation in spark location using laser ignition for CNG fuel. Shah et al. (2012) investigated combustion behavior during their comparative studies with pre chamber and conventional spark plug location. It was found that there is reduction in combustion duration by 30% with pre chamber spark plug location. Demesoukas et al.,2015 explained about the near wall combustion model especially the flame wall combustion phenomenon of spark ignition engine.

Some authors (Yamin and Badran, 2002; Yamin et al.,2003, Pal and Agarwal, 2015) explored the ignition centre for the particular fuel which according to them keeps on varying as per fuel, load, speed, any intake charge dilution, equivalence ratio. Yamin et al., 2003 developed a computer model of 4-stroke spark ignition engine and tested for optimum compression ratio using LPG fuel. They reported that with higher compression ratio, combustion duration will be reduced because of increase in end-of-compression pressure and temperature. This creates favorable condition for reduced ignition delay and increase in flame speed. In addition to this they were tested different spark plug locations (Ratio of distance between spark plug location from nearest wall to cylinder diameter) radially at four places between centre and periphery wall of cylinder. They found that with change in location from outer wall to centre, the combustion duration found reduced. There is rise in power as location moved towards centre. So optimum location achieved is 0.395 times radius from centre where efficiency is maximum. But to get lower emissions author suggest 0.29 times radius is the optimum position. Pal and Agarwal, 2015 did compare between laser ignition and spark ignition method of combustion initiation. The experimentation has been performed on single cylinder gasoline engine. Author suggests that laser ignition causing central combustion increases the BMEP in start of combustion (10 %). When spark plug mounted at centre over engine head reduces the flame speed to cause complete combustion and thereby reduced power of the engine. So here laser ignition is synonyms to variable spark plug location that to coaxial to certain extent. Another author Aleiferis et al., 2004; Getiel and Tsai, 1983 reported the study related to the flame kernel development and the speed of flame for the spark ignition engine and found that spark plug location and its design is an important factor for efficient combustion to be happened inside combustion chamber. Badawy et al., 2017 carried out the

investigation of flame kernel development with change in spark plug gap using gasoline fuel. The authors reported that the larger gap increases the fast development of flame kernel with higher radius with increment in flame speed.

2.4 COMPUTATIONAL WORK

Some authors modeled the spark ignition engine for LPG as fuel (Bayraktar, 2005; Hyun et al.; Yamin and Badran, 2002). A quasi dimensional model has been developed by Bayraktar, 2005 and predicts the cycle performance, exhaust emissions. The performance parameters such as volumetric efficiency decrement causing brake power and ultimately thermal efficiency to be reduced. But the emissions reduced to a great extent.

Rakopoulos et al., (2009) developed the CFD model which gave the intake manifold and in cylinder geometry affecting the in cylinder flow field and mixing process in Otto engine. The model was tested with three different conditions. First model was applied to simulate the external mixing in intake manifold with tee-mixer injection system. Second was the transient gas flow field in intake manifold and engine cylinder was tested over complete engine cycle. Finally the transient mixing process in intake manifold and spatial and temporal distribution of species concentration inside the cylinder. To validate the model the experimental results from literature are compared with simulation results.

Ibrahim and Bari, (2009) studied the effect of EGR alternative to lean burn strategy for natural gas spark ignition engine. Authors developed the two zone combustion model for four stroke spark ignition natural gas engine to simulate the in-cylinder condition during combustion. Kinetic model based on extended Zeldovich Mechanism was developed in order to predict the NO emissions. The combustion model was validated with experimental data and a good agreement between results was found. Adding recirculated gas decreases the power more rapidly than excess air. But if pressure was raised the power output increased. It was found that dilution with EGR, the NO emissions were extremely lower than excess air emissions. The NO emission was reduced by about 70 % when the inlet charge was diluted at a rate of 20 % using EGR instead of excess air.

Al-Baghdadi (2006) studied the effect of different fuels (gasoline, ethanol, hydrogen) alone or their mixtures on the performance parameters and toxic emissions using a 2-zone simulation model. The incidence of pre-ignition and its relative density and cyclic variation were also considered. They found the effective duration of combustion and associated mass burning rate for various operating conditions and fuels. The mathematical and simulation model had been developed, tested and verified against the experimental data. A good agreement was obtained between the simulation results with experimental results. The hydrogen alone when tested required no major changes in engine. Also it saves oil, environment from toxic pollution, improved the combustion process, reduced the ignition delay, speeds up the flame front propagation, retarded spark timing and reduced combustion duration. When hydrogen was blended CO reduces and NO_x increases, heat release rate increases and exhaust temp. and sfc reduces. Ethanol added with 30% gasoline improves output power, reduces NO_x. Blending of ethanol reduces CO and NO_x emission and peak

temperature. It increases heat release rate and also sfc. Gasoline with ethanol increases pressure of blended fuel to a maximum of 10 %. Also enhances octane number of blended fuels.

Wu et al., (2009) developed the modified heat transfer model for predicting the heat transfer rate value which will be accurate and improved over the other models developed by researchers. In order to improve of the predicted heat transfer rate of different engines, author proposed modified heat transfer model using Stanton Number based on two engines. The author noted the results of instantaneous heat flux, global heat transfer, heat release rate, and cylinder pressure based on the proposed model and compared with the experimental results of three engines and results of previous model. The literature results were closer to measured data. The proposed model was determined as a function of compression ratio, stroke, cylinder volume, and mean piston speed.

Rakopoulos et al., (2005) used a zero-dimensional model to study computationally the generation of irreversibility during combustion between hydrogen and hydrocarbon fuels like natural gas and landfill gas. Author demonstrate the decrease in irreversibility with increase in hydrogen content of fuel reflecting the increase in second law efficiency. Rakopoulos et al., (2008**)** used a previously developed and validated zero-dimensional, multi-zone, thermodynamic combustion model for prediction of engine performance and NO_x emission had been extended to include second law analysis. The model was applied to a multi-cylinder four strokes, turbocharged and after cooled natural gas SI engine running on synthesis gas. Rakopoulos, (1993) presented the simulation model of actual processes occurring during the thermodynamic cycle of real spark ignition engine. The main focus was given on the heat transfer to cylinder wall, spark ignition timings, real valve timing and closing timing .The results obtained from first law analysis of real cycle like pressure indicator diagram, efficiencies were compared favorably with the relevant experimental data obtained from a flexible, variable compression ratio Ricardo engine. The thermodynamic state points found from first law analysis were used to find the availability at each engine crank angle. The results of second law analysis were compared with existing ideal cycle Otto engine results.

Yamin and Dado (2004) developed the simulation model was verified with experimental results and plot the effect on engine performance, combustion and emission under variable bore/ stroke ratio and variable compression ratios. Heat loss for different bore/ stroke ratio was plotted and reported that the heat was wasted more with larger stroke length and lost to cylinder walls so less heat liberated by combustion was available to produce useful work.

The increase of stroke length reduced the compression ratio and causes cylinder temperature at EVO to increase mainly due to lower expansion ratio. The overall effect of these factors together increased overall specific fuel consumption (- 6 to + 4 %). Author found that the engine indicated power increases with increase in stroke length. IMEP decreased due to increasing engines displacement volume due to reduced volumetric efficiency and CR, the CO emission increases by 2.5 -15 % and NO_x by 2-58 % at larger bore/ stroke ratio.

Ismail and Mehta, (2011) reported the estimation of irreversibility associated with various sub-processes occurring during combustion in a hydrogen fuelled spark ignition engine. The author developed a quasi-three dimensional phenomenological combustion model and used for predicting the pressure and temperature histories of a single cylinder four stroke spark ignition engine operating at equivalence ratios of 0.3 - 0.75 in speed range 1500 - 3500 rpm and was simulated using MATLAB. The cylinder contents were divided into three zones, viz. the unburned, freshly burned and previously burned. The six sub processes studied were charge preheating, chemical reaction, pressure equilibration, product mixing, wall heat transfer, piston motion for each sub-process, the availability destruction during combustion and effect of operating conditions are discussed. Author found that the chemical reaction was a major contributor to irreversibility generation and overall availability destruction (50 % and more) followed by pressure equilibration (20 - 40%) and heat loss to walls (10 – 20 %) while charge preheating contribute to (< 2 %), the product mixing and piston motion have insignificant direct influence on availability destruction. Maximum energetic efficiency is obtained at engine speed of 3000 rpm.

Hakan and Jehad,(2008) developed a computer simulation model of a variable stroke length LPG fuelled single cylinder four stroke spark ignition engine. The performance of the engine was simulated at each Bore to stroke ratio keeping maximum CR as 10.The analysis showed that the brake torque and power had increased from 7-54% at low speeds and 7-57 % at high speeds compared to the original engine. The brake specific fuel consumption registered a reduction of 6% to an increase of about 3% at low speed and a reduction of 6% to an increase of about 8% at high speed compared to original engine. On the other hand the pollutants increased from 0.65- 2 %. Larger stroke lengths resulted in reduction of pollutants level about 1.5 % at lower speeds and at lower stroke lengths an increase about 2% occurred.

2.5 ANALYTICAL WORK

Wu et al., (2006**)** developed a heat transfer model using Stanton Number for small scale spark-ignition engines. The results of instantaneous heat flux, global heat transfer and cylinder pressure based on proposed model were compared with experimental results and results of previous models.

Sezer and Bilgin, (2012**)** reported the effect of intake air-fuel mixture properties on the exergy balance of spark ignition engine. The developed model included the compression, combustion and expansion cycle. The variations of exergy variables as a function of air-fuel equivalence ratio, residual gas fraction, and initial charge temperature were studied and plotted. The results showed that increase in air-fuel equivalent ratio causes increase in irreversibility and exergy losses with heat transfer and exhaust gases. Slightly richer mixture above stoichiometric ratio makes no significant contribution to exergy transfer with work transfer. Slightly leaner mixture also gave the best first and second law efficiency. An increase in residual gas fraction decreased the irreversibility and exergy loss. However increasing the residual gas fraction affect the first and second law efficiency positively because of diluting the charge. Increase of initial charge temperature reduces irreversibility and lower exergy output and also reduces the first and second law efficiency.

Li et al.,(2013) reported an in-depth analysis of the effects of cooled EGR on the fuel conversion efficiency of a boosted, spark-ignited, direct-injection, gasoline engines operated at the full, medium and low loads. The EGR reduced the fuel enrichment at high load, the combustion phasing and increase the degree of constant volume heat release at medium and high load. Author reported that 1.1. to 4.1 % improvement in brake thermal efficiency were obtained by the 12 – 17 % EGR at different loads. The fraction of indicated work in the total availability increased with EGR for all the operating loads. The reduction in heat transfer loss due to EGR improved the conversion efficiency at constant air fuel ratio. Replacement of fuel enrichment with EGR was most effective at full load.

2.6 SUMMARY OF LITERATURE AND SCOPE OF WORK

It is noticed that multiple liquid fuels such as petrol, ethanol, methanol etc. are the preferred choices for an SI engine. Alongside, the non-renewable gaseous fuels such as LPG, CNG, methane etc are also been highlighted for their performance in SI engines. Further, some researchers have also tried for exploring the renewable gaseous fuels such as biogas, producer gas etc. while working with the SI engines. But the potential of those renewable fuels is still to be explored as a potential alternative fuels to the conventional fossil fuels. Such investigations are highly desirable for the countries like India with agricultural base. Possibility of huge biogas fuel production and its utilization in fields of stationary engines even for transportation engines can lessen the demand of the conventional fuels. Hence, gaps in the literature are identified and scope for detailed research is mentioned in this section.

- As seen in the literature, VCR technique can improve the performance of an SI engine. However, effectiveness of the same VCR attachment for a multi-fuel engine is still not investigated. Further, there is a need of a VCR technique which can provide change in compression ratio in the running condition of the engine. Thus designed VCR mechanism when mounted on an SI engine can provide optimum engine performance for a given fuel.

- Many researchers have considered LPG as a fuel for their studies. However the use of LPG for varying engine operating parameters like compression ratio (CR), ignition timing (IT), throttle position and exhaust gas recirculation (EGR) rate is seen to be unexplored. Therefore study elaborating the consequences of speed, throttle position, CR, IT, EGR rate needs to be investigated.

- Most of the experimental findings related to biogas as fuel are based on the synthetically made biogas. Therefore research related to raw biogas is still to be explored. Such studies would provide the practical solution for the performance enhancement of an SI engine operating with biogas fuel. Thereafter, optimization of engine parameters namely CR, IT, throttle needs to be explored for biogas fuel.

- Emission control for biogas fuel is still an unattended topic. The exhaust gas emission, especially $NO_{x,}$ should be thought for the raw biogas fuels through EGR technique. Therefore a break even analysis between efficiency and emission needs to be studies for arriving at an conceded EGR rate.

- Many literature based findings concentrate upon optimizing CR for maximum efficiency of the engine. But there is scope for raising the engine performance further while running at the best CR if the spark plug (SP) is located optimally. Axial relocation of the spark plug should therefore be though for various SI engine fuels. In line with this, it is highly essential to find out the better composition of CR and spark plug location with and without EGR treatment for getting best engine performance.

2.7 OBJECTIVES

The motive of this study is not only be focused on replacing petrol with normally available gaseous fuels but also with a variety of alternative fuels that can be produced through CO_2 capturing thus allowing CO_2 neutral economy. This is to be executed by converting petrol engine to gaseous fuel mode. The gaseous fuels selected are from non renewable as well as from renewable group are Liquefied petroleum Gas (LPG) and raw biogas respectively.

The fuel LPG is non-renewable petroleum by product of crude oil distillation. The LPG primarily used in cooking purpose. By developing the fuel supply system for the spark ignition engine, it is very much possible to use LPG in the engine. However as the LPG fuel is having higher octane and higher calorific value as compared to petrol, the heat produced after combustion is also more, causing rise of unwanted greenhouse gas emission called NOx. In order to control this, exhaust gas recirculation (EGR) Rate of varying percentage is considered. So, the optimization of CR and IT in presence of EGR rate becomes important.

The investigation extended further where the LPG gas is replaced with renewable raw biogas in the same application discussed above. This is for the reason that, raw biogas is available in plenty especially in rural areas that to of negligible cost. It is used for cooking purpose but it is also having potential to be used as a fuel in engine by certain modification in fuel supply system.

The fuel supply system using raw biogas is different in the sense that the raw biogas is available at atmospheric pressure and supply of it to the combustion chamber needs the provision of additional infrastructure. In addition to this the higher octane rating with lower heating value needs to optimize the compression ratio as well as ignition timing. Further with rise in CR, to control the rise in temperature EGR rate with varying percentage is also implemented.

The parallel study is to be performed for development of novel VCR mechanism which can minutely alter the compression ratio over fixed optimum compression ratio in order to harness maximum power from the engine. In doing so, it is very well possible that any octane fuel can be utilized efficiently in conventional SI engine with novel mechanism. Initial trial of the developed mechanism is proposed on small 1.3 kW, 97 cc HONDA engine where petrol and kerosene fuels will be implemented. If the performance found improved for those fuels over original working conditions, the plan of demonstrating the novel VCR mechanism on 4.5 kW, 661 cc engine with gaseous fuels LPG and raw biogas will be incorporated. The

detailed study with methods of varying compression ratio, ignition timing as well as EGR rate is to be carried out.

Plan is also to concentrate on the spark plug and its location in conventional petrol engine. If fuel is other than petrol in same petrol engine, then it may possible that spark plug location needs to be altered. This study is to be undertaken where the spark plug will be installed inside auxiliary piston of novel VCR mechanism. This causes the spark plug movement inside out of the combustion chamber with respect to engine head parallel to the centroidal axis of the cylinder. The study of variable spark plug location(VSPL) for LPG as well as raw biogas is undertaken and followed by comparison of the results. Again optimization of compression ratio in presence of VSPL for the fuels becomes important. This kind of study has not been reported in literature.

The original petrol engine performance is hard to achieve by using these fuels by running the engine with standard design and operating parameters. Therefore, in this study following key objectives are planned to be executed.

- Exploration of LPG and raw biogas in VCR petrol engine for a combination of load, CR and EGR to realize its performance, combustion and emission characteristics.
- Optimize the CR, ignition timing and EGR rate of those fuels so that the performance improved close to the petrol fuel with minimum emissions.
- Development of new VCR mechanism such that the alteration in compression ratio could be easily achieved and engine can run to its best performance.
- Initial trials using novel VCR mechanism on small engine with petrol and kerosene are examined.
- Based on the feedback on small engine performance, the necessary modifications to be carried out on novel VCR mechanism and incorporate it on large size VCR engine to evaluate the performance of LPG and raw biogas fuels using combination of tilting VCR and novel VCR mechanisms.
- Development of Variable spark plug location mechanism inbuilt of novel VCR mechanism to examine the effect of VCR, spark timing and spark plug location of the gaseous fuels under study. The similar study also carried out in presence of EGR rate as well.

2.8 ORGANIZATION OF REPORT

The thesis has been organized by focusing the concentration towards the clean and efficient power production from a petrol engine using multi-fuels from liquid to gaseous phase with continuous variation of CR, spark location and spark timing as per fuel, load and speed conditions. **Chapter 1** offers the motivation acquired towards the use of fuels efficiently with minimum emissions. This is followed by the objective of the dissertation. **Chapter 2** presents a brief review of available literature dealing with the different variable compression ratio (VCR) mechanisms; work on variable compression ratio SI engines using liquid fuels thereafter work on variable compression ratio using gaseous fuels. Concentrating more on

gaseous fuels, the study in terms of the effect of load, speed, ignition timing, compression ratio. **Chapter 3** elaborates about the experimental facility such as small HONDA engine set up with rope brake dynamometer measurement system. Similarly the variable CR engine setup and its different measurement and instrumentation devices are explained. The experimental methods adopted for testing of LPG, raw biogas is described. Similarly the exhaust gas analyzer used for emission analysis is discussed. **Chapter 4** emphasis on the details of novel VCR mechanism designed and developed in-house. The method of installation of this novel VCR mechanism on HONDA engine as well as on variable CR engine is presented. Further the operation of novel VCR mechanism and thereby the variation in CR magnitude is tabulated and elaborated as well. The novel technique of variable spark plug location (VSPL) is explained further. The method of operation using VSPL for the different fuels is included. **Chapter 5** explains the performance of different fuels such as petrol and kerosene using novel VCR mechanism on HONDA engine set up. **Chapter 6** shows the outcome of experiments done using fuels LPG and raw biogas in VCR SI engine for various composition of speed, CR, IT, throttle position and EGR rate. The results of the experiments help to optimize the aforementioned design parameters to achieve optimum performance, combustion and emission characteristics of those fuels in SI engine. **Chapter 7** represents the outcomes of novel VCR mechanism on variable CR engine. First the gaseous fuels performance, combustion and emission study with novel variable spark plug location only being discussed. Based on the outcomes of this study, the combined effect of novel VCR along with novel VSPL on the gaseous fuels are analyzed. Further the effect of EGR rate is discussed and optimized the novel CR and novel VSP location for the gaseous fuels under study. **Chapter 8** indulges the computation technique of analyzing the performance and combustion for the fuel under study. The Mathematical MATLAB Simulink software and CFD simulation software are tuned as per the engine and fuel available. The Honda engine will be concentrated for combustion analysis with computational results. **Chapter 9** recaps the key findings of the experiments performed and the future works are proposed.

CHAPTER 3

Experimental Facility

OVERVIEW

This chapter provides details of the SI engine experimental set-ups used for present investigations. One of the engines is the HONDA GK100 model which is a small size engine under discussion over here. An experimental test rig is developed in-house for measurement of power, torque and speed especially for this engine. Commercially available set-up of APEX is described herein. This large size variable compression ratio SI engine and associated measurement systems are elaborated in this chapter. These engines are then used to achieve the aforementioned objectives.

3.1 RESEARCH ENGINE TEST RIG

A single cylinder, air-cooled petrol engine (Make:HONDA; Model GK-100) having rated power of 1.3 kW and 3600 rpm is used to study the performance of the fuel. A transistor type magneto ignition system is used on the engine for supply of spark current to the spark plug installed at the engine head. The schematic diagram of the engine test set up installed is as shown in Fig.3.1.

The main components of the engine test rig are: (i) SI engine, (ii) Rope brake dynamometer, (iii) engine speed measurement, (iv) fuel consumption measurement and (vi) air consumption measurement.

3.1.1 Spark ignition (SI) engine

A single cylinder 4-stroke variable speed spark ignition engine of HONDA (Model GK100) working on petrol is used for study. The schematic diagram of the experimental facility is as shown in Fig.1. The alternative fuel kerosene can be used without any modification in the existing engine i.e. at fixed compression ratio of 4.8. The method of carburetion and the ignition timing will also remain unchanged.

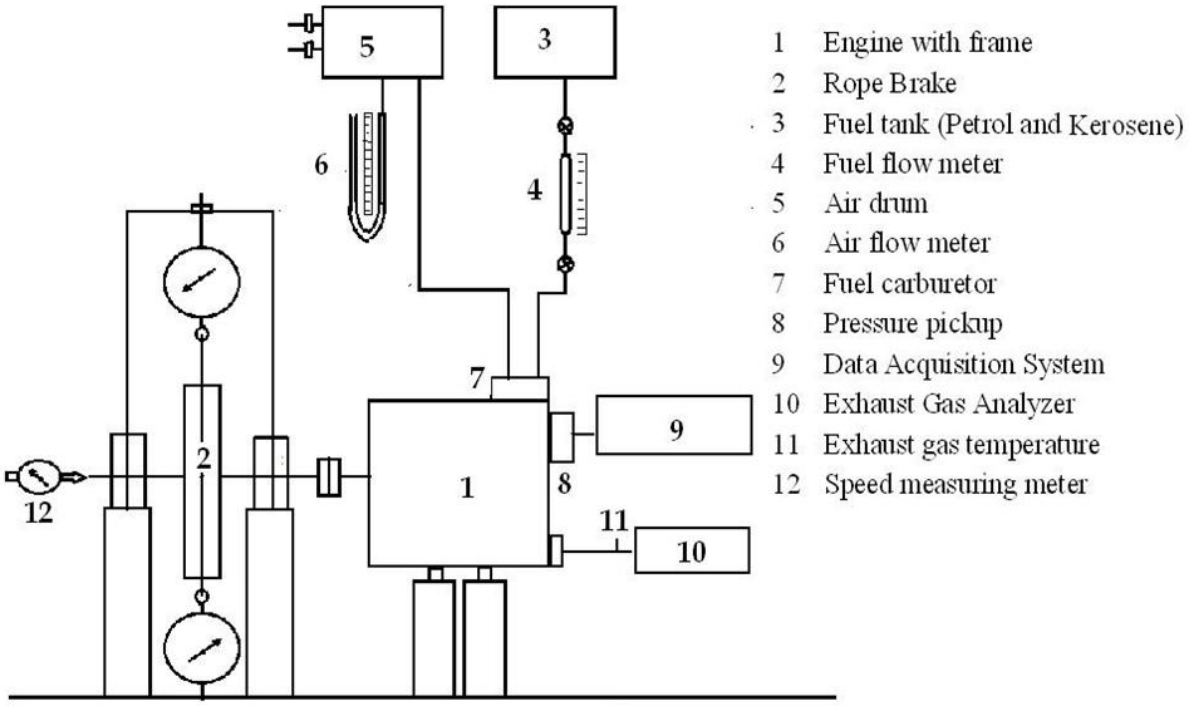

Fig. 3.1 HONDA Engine Experimental Test Facility

The engine combustion chamber as supplied by manufacturer is designed of the form of Ricardo's turbulent head geometry to attain higher engine efficiency. The spark plug is located in the head optimally such that the flame can spread faster over the combustion chamber. The specifications of the engine are tabulated in Table 3.1.

Table 3.1 Specification of spark ignition engine

Make	HONDA GK100
Type	Side valve, 4-stroke,air cooled, horizontal shaft, single cylinder
Displacement	97 cc
Bore × stroke	52×46 mm
Compression ratio	4.8:1
Rated Horse power	1.3 kW@3600 rpm
Max. Torque	0.4 kg. m @3000 rpm
Ignition system	Transistor Type Magneto Ignition

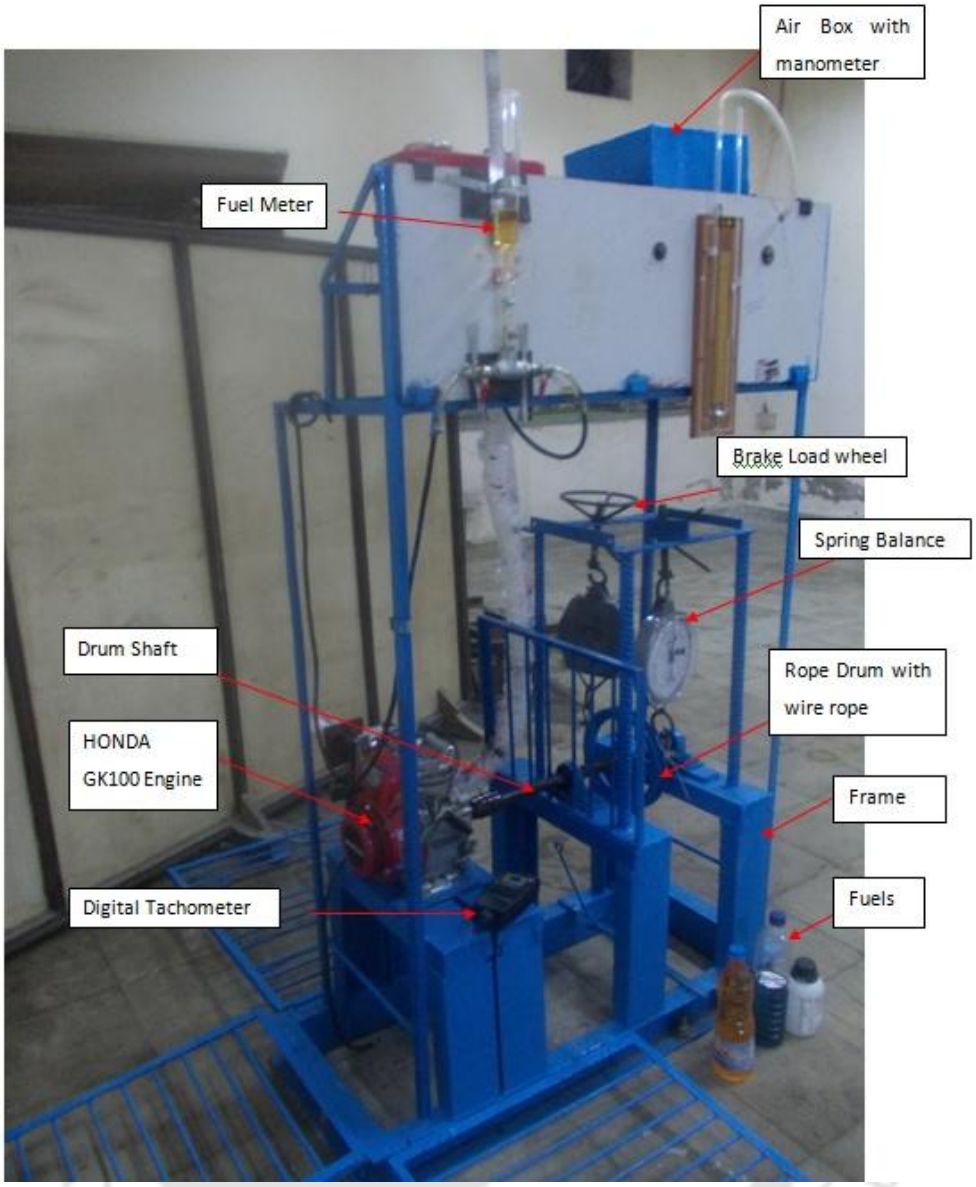

Fig. 3.2 Experimental Set up of Spark Ignition Engine test bench

3.1.2 Engine instrumentations

The experimental set up with all measuring instruments is as displayed in Fig. 3.2**.**Here engine is coupled with the rope drum by means of the universal joint type coupling fixed with key. The rope drum consists of a flywheel mounted on the shaft called driven shaft. The assembly of rope drum and shaft are fixed on to the frame with bearing inside of frame. The rope drum designed for 3Nm torque capacity, is hollow in construction with a rim of 3 mm thickness. Outside diameter of drum is 200 mm. The engine shaft and rope drum shaft are made completely axisymmetric and attached to each other by means of universal coupling which can accommodate eccentricity to certain percentage for smooth torque transmission during rotation at high speed.

Table 3.2 Specification of rope brake dynamometer

Torque capacity	3 Nm
Outside diameter of drum	200 mm
Rim thickness	3mm
Cooling method	Air cooled
Hub diameter	100 mm
Width of drum	30 mm
Rope dimension(OD)	5 mm (7×36)
Material	Steel wire

3.1.2.1 Engine load

The method of brake load on engine shaft is rope brake dynamometer (Singh, 2014) with spring balance type. The specifications of dynamometer are listed in Table 3.2. The steel wire rope 5 mm diameter with cross lay construction moving over the drum is used to apply the brake making angle of lap 180^{0} over the drum. Two spring balances (0-25 kg) hanging on the bracket such that one is fixed to the hanger with no displacement and pointer coinciding with 0 ± 0.2 kg for no-load case. The other one is movable on the hanger with rotary lever such that it moves up and down by rotation of lever to apply or release brake on drum. The wire rope towards the fixed spring balance was subjected to tension (pull force) as rope drum rotates and on the side of the adjustable spring balance there will be slack in rope (push force) while applying brake load. The brake load is the algebraic difference of both the spring balance reading. This is how the brake torque can be assessed using prony brake dynamometer for different set of brake loads.

3.1.2.2 Engine speed measurement

The Honda GK100 is a variable speed engine with throttle valve to vary engine speed manually. Operating the throttle performs the controlling of proper air-fuel mixture supplied to the cylinder through carburetor. The throttle valve can be locked at a particular position represent percentage throttle opening during experimentation. The Enercon make digital panel tachometer with proxy-methyl photo reflective sensor was used for measurement of speed in rpm. This instrument has measurement range of 1-9999 rpm with a sampling time of 1 second. For measurement, a photo reflective tape was mounted on the drum face. With over a distance of 150 mm, the tachometer records the speed in rpm.

3.1.2.3 Air consumption measurement

Air box is manufactured of size 370×370×350 cu. mm inside volume having two openings of 40 mm diameter. Towards inlet side of air box, the orifice having diameter of 25 mm is installed with help of flanges. The U-tube ethanol column manometer is connected to the air

box on one end and other end is open to atmosphere. This records gauge pressure in the air in terms of meter of ethanol. Using the continuity equation, the mass flow rate of air can be calculated by converting the pressure head.

3.1.2.4 Fuel consumption measurement

Fuel flow is measured on volumetric basis with help of fuel measuring tube (Make- Borosil) calibrated in ml of fuel supply (0-50 ml). The tube is open to atmosphere on one side and flow control valve on opposite end. Fuel flow measurement has been carried out with the volume of fuel consumed for the time period of 30 s for the particular load and speed condition.

3.1.3 Procedure of experimentation

- The experimental test bench is initially made to run on petrol fuel for the complete test run. There is no modification made while performing the trials. The test run consist of performance of the engine at constant CR (4.8:1), stoichiometric A/F ratio (14.5:1), load range from 0.3 N to 12 N on the rope drum.

- Once the engine reaches steady state without any substantial knock or misfire, the speed is measured at 0.1 kg load. The other parameters of interest such as air consumption and fuel consumption (for 10 sec) are also recorded. Now the load is applied on the prony brake dynamometer by increasing the tension in the rope by rotating lever of movable spring balance. The net load set is 0.3 kg on the spring balance.

- Due to application of load, the brake is applied on the drum and ultimately on the engine shaft by rope and speed is found to be reduced at constant A/F ratio. Once the steady state is reached, the reading of speed, spring balance, air consumption, fuel consumption for 10 sec is noted.

- By increasing the load on the rope drum stepwise as 0.5, 0.7, 0.9, 1.0, 1.2 kg, the trials are repeated.

- The alternative fuel such as kerosene can also be tested on the engine without any modification in the existing engine setup.

- Further experiments are also performed by incorporating a modified engine head accommodating the novel VCR mechanism.

3.2 LARGE CAPACITY SOPHISTICATED VCR TEST FACILITY

Figure 3.3 and 3.4 shows the schematic diagrams of the experimental setup used for testing gaseous fuel like LPG and raw biogas respectively. The set up consist of a 4.5 kW@1800 rpm, single cylinder, 4-stroke, water cooled, manifold injection VCR petrol engine (Make:Kirloskar India) coupled with eddy current dynamometer (SAJ Make, Model AG10) for loading. The detailed specifications of the engine and corresponding measuring devices are listed in Table B-1(APPENDIX-B). The injection nozzle has three holes of 0.3 mm

diameter with a spray angle of 120°. The engine is having a piston with hemispherical bowl in combustion chamber. Cooling of the engine is accomplished by circulating water through the jackets of the engine block and cylinder head. The VCR can be achieved by use of tilting block method in which the clearance volume can be increased or decreased by tilting the cylinder block from one side, hinged on the opposite side without stopping the engine as discussed in chapter 2. In Petrol mode, fuel injection time, fuel injection angle, ignition angle can be programmed with open ECU at each operating point based on RPM and corresponding throttle position. It helps in optimizing engine performance throughout its operating range. Throttle position sensor and trigger sensors are connected to Open ECU (Make: PE3) which control ignition coil, fuel injector, fuel pump and idle air sensors. The switching of these equipments are carried out with relays. Set up is provided with necessary instruments called as piezo power unit for combustion pressure and crank-angle measurements. These signals are interfaced with computer for pressure crank-angle diagrams. Data logger device (Make: National instruments USB6210) is used to interface for airflow, fuel flow, air temperature, coolant temperature and load measurements. The setup has stand-alone panel box consisting of air box, two fuel tanks for duel fuel test, manometer, fuel measuring unit, transmitters for air and fuel flow measurements, process indicator and hardware interface. Rota meters are provided for water flow rate measurement in engine jacket cooling and exhaust gas calorimeter. A battery, starter and battery charger is provided for engine electric start arrangement.

3.2.1 Engine Instrumentation

3.2.1.1 Braking System

The crank shaft of the engine is coupled with an water cooled eddy-current type dynamometer (Make: Saj Test Plant Pvt. Ltd.). The load on the engine can be varied by manually controlled knob of a potentiometer connected to the eddy-current dynamometer with a digital display unit, which shows the applied load (kg) on the engine. The load applied on dynamometer will be sensed by load cell of strain gauge type (Make: Sensotronics Sanmar Ltd., Model 60001, Type S beam, Universal, Capacity 0-50 kg) with a digital load indicator to display the magnitude of load.

3.2.1.2 Temperature measurement

The K type thermocouples are used to measure the temperature of the exhaust gas at in/out of the calorimeter. Engine jacket water flow in/out temperature, Exhaust gas calorimeter water flow in/out temperature has been measured by PT100 (RTD) sensors. These temperatures are essential to perform the thermodynamic analysis of the engine. All of these are interfaced with computer through NI USB 6210 data logger for automatic data recording.

3.2.1.3 Measurement of fuel consumption

I) Volumetric method: The fuel consumed by an engine is measured by determining the volume flow of the fuel in a given time interval and multiplying it by the specific gravity of

fuel. Generally a glass burette having graduations (in ml) is used for volume flow measurement. Time taken by the engine to consume this volume is measured by stopwatch.

II) Gravimetric method: In this method the time to consume a given weight of the fuel is measured. Differential pressure transmitters working on hydrostatic head principles can be used for fuel consumption measurement. The liquid fuels were supplied to the engine injection pump from the fuel tank under gravity feed. One minute fuel consumption measurements at a particular load were performed on a volumetric basis by using graduated glass burette. This volumetric fuel consumption were converted to gravimetric basis by measuring fuel density.

For measurement of gaseous LPG fuel consumption, the positive displacement diaphragm type of gas meter (Make: Hot Plate Centre, Delhi) with a stand-alone twin chamber measuring unit was used. The specification of the gas meter is as shown in Table 3.4.

The measurement of raw biogas is different than that of the LPG gas measurement. The major reason for this is that the density of raw biogas is variable and may be different per batch per location as well. So it would be difficult to measure the flow rate using diaphragm gas flow meter. Another reason is that the raw biogas is available in the storage balloon at atmospheric pressure and in order to run the SI engine, it needs to raise pressure little higher than atmospheric pressure which may not be sustained by diaphragm flow meter. Considering this, the variable area float type rota-meter (100-0-100 LPM) is selected for the measurement of raw biogas consumption. It is a acrylic variable cross-section (Make-Flotech, India) tube with float inside is connected in pipe system of gas flow with help of flanges. According to the flow rate, the gas consumption is measured in LPM. There is a provision for restricting the mass flow rate of gas to stoichiometric A/F ratio by operating the control valve.

3.2.1.4 Air consumption

The air consumption was measured by using an air box fitted with orifice plate (20 mm diameter) and an U-tube manometer attached across orifice meter. The volume of air consumed for a particular load was found out by measuring the water level difference in mm. The coefficient of discharge of orifice meter is 0.6.The automatic air and fuel flow quantity is evaluated by using air flow transmitter (WIKA Instruments Ltd.) and differential pressure transmitter (Yokogawa Electrical Corporation) which are lined with DAC.

3.2.1.5 P- θ Measurement

Cyclic variation of combustion chamber pressure can be measured using the diaphragm type dynamic piezoelectric pressure transducer with an inbuilt amplifier(PCB Piezotronic Make; Model M111A22) fitted on the cylinder head. Kubler made optical crank angle encoder is incorporated to measure each degree crank rotation with TDC pulse. Thus measured pressure and corresponding crank angle data are acquired into the computer through piezo power unit (Make: Apex innovation, India). The crank angle encoder is having the measurement speed 0-1200 pulse/min.

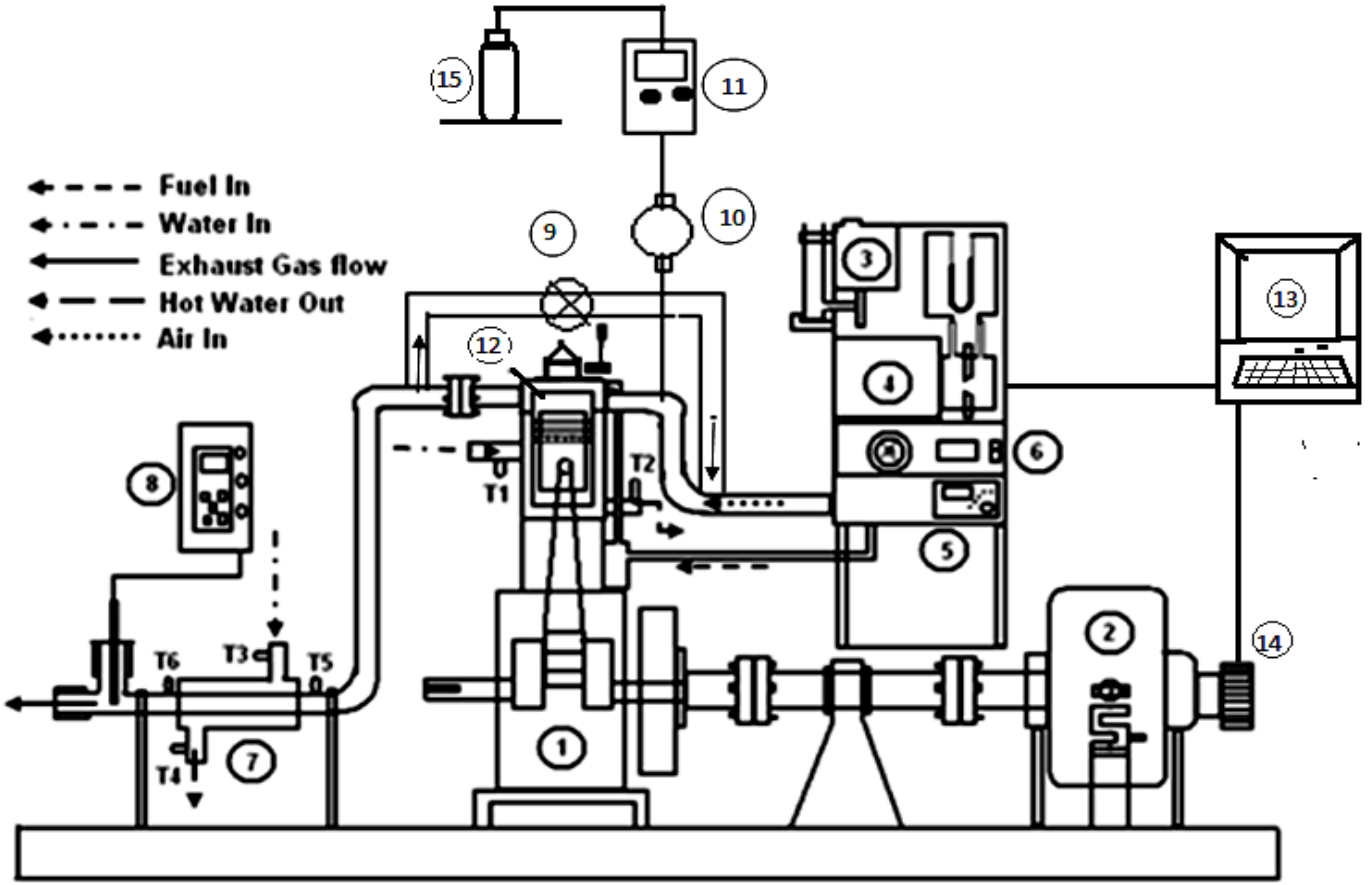

Fig. 3.3. Schematic of experimental set up for LPG fuel

1- VCR Petrol Engine; 2- Eddy current dynamometer; 3- Fuel tank with fuel measuring unit; 4- Air box with orifice meter attached to U-Tube manometer; 5- Six point digital temperature indicator; 6- Potentiometer with load indicator; 7- Exhaust gas calorimeter; 8- Exhaust gas Analyzer with probe inserted in tube; 9- EGR flow rate adjustment valve; 10- LPG Gas Mixer; 11- LPG Gas flow meter;12- Cylinder pressure sensor; 13- Computer for data logging; 14- Crank Angle encoder; 15 - LPG fuel gas tank; T1, T2—T6- Thermocouples for temperature measurement

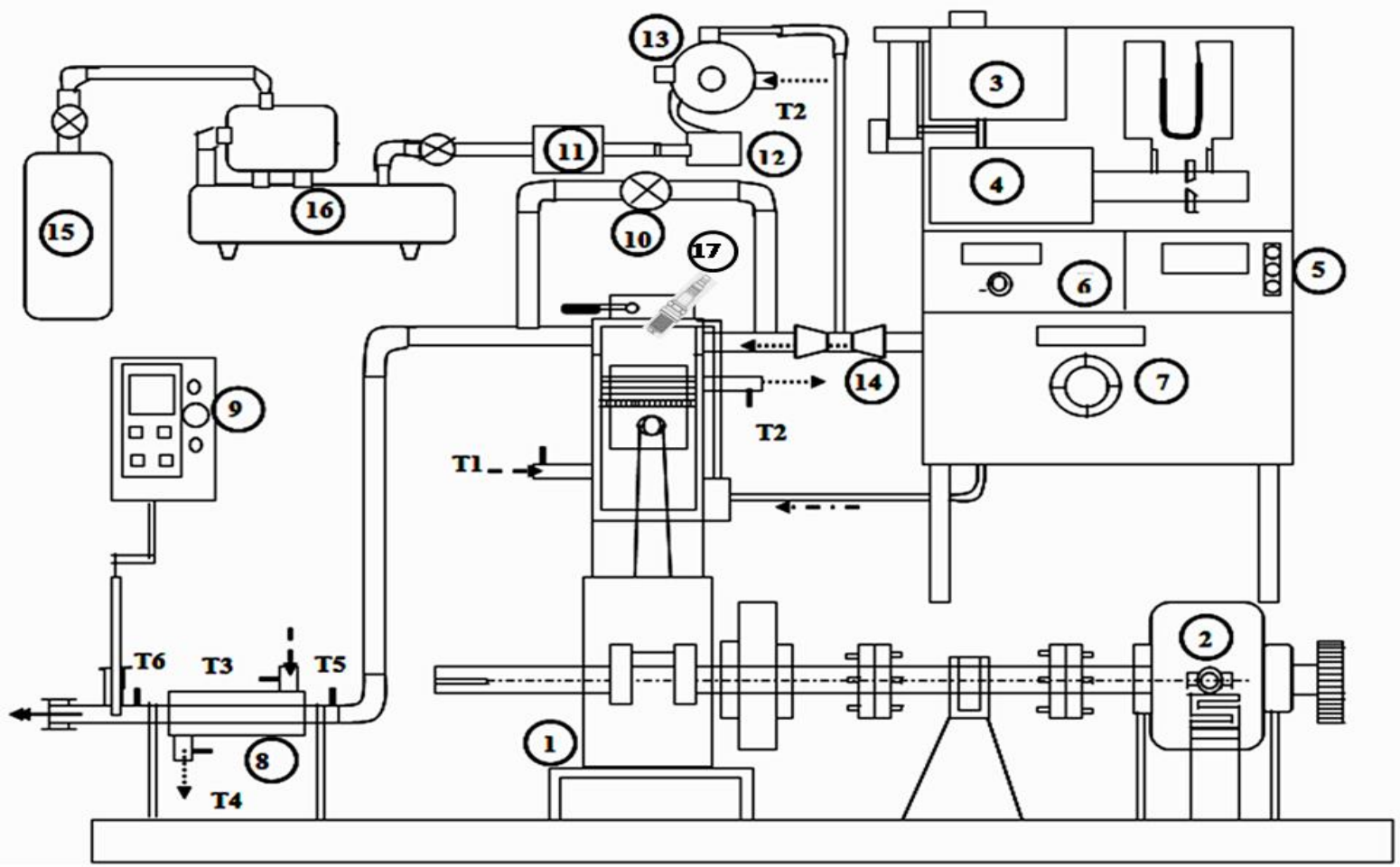

Fig.3.4. Schematic of experimental set up for raw biogas

1- Engine test bench,2- Eddy current dynamometer, 3-fuel tank,4- air tank, 5- piezo power unit, 6- temperature indicator,7- brake load potentiometer with digital display,8- Exhaust gas calorimeter, 9- Exhaust gas analyzer,10- Exhaust gas recirculatoion,11- fuel meter,12- expansion valve,13- diaphragm gas pump,14- venture gas mixer,15- Biogas filled balloon, 16- single stage biogas compressor, 17-spark plug

3.2.1.6 Compression ratio variation control

The VCR petrol engine has provisions for five (5) step CR variation from 6 to 10. This is done by tilting cylinder head with the help of locknut and adjuster arrangement as shown in Fig.3.5.The concept was first introduced by Larsen,1991(SAAB Auto).If the CR adjuster turns clockwise, the CR increases and if turns anticlockwise, CR decreases. The pivot length of the block is a important parameter, whose increment or decrement in length attains the required compression ratio. This means 150.1 mm length between pivot represent CR10, if length becomes 153.3 mm then CR reduces to 9 and further increase in length to 156 mm, CR reduces to 8. This variation of pivot length is not linear but follows polygonal nature. The pointer rotates on scale plotted by above relation to locate the exact CR instantly.

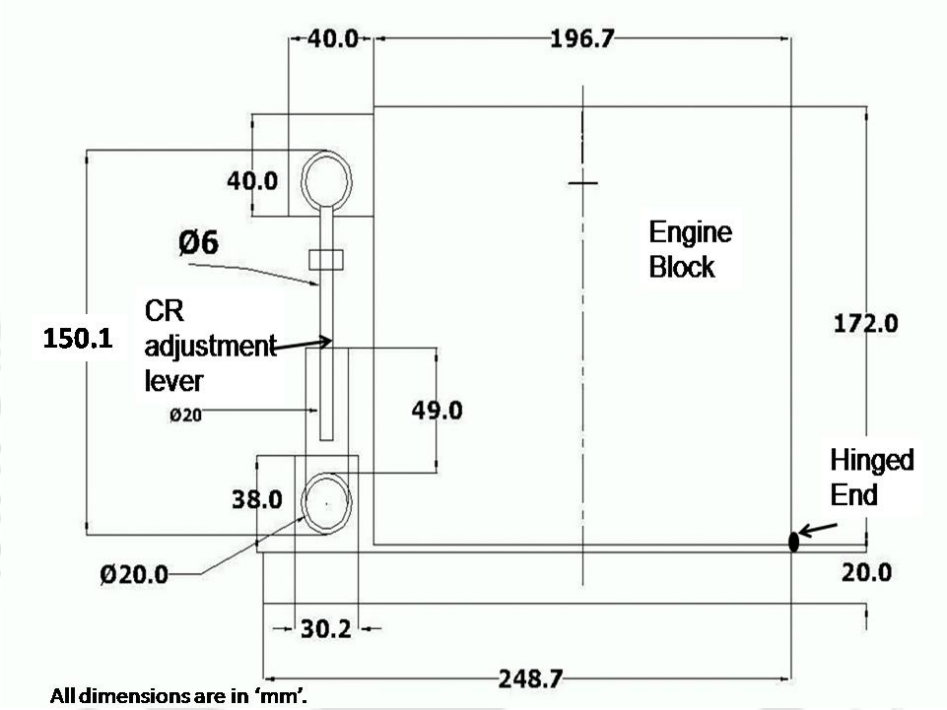

Fig.3.5 Method of tilting block for variable compression ratio with spark plug along the vertical centre line.

The engine compression ratio can be set manually whether engine is in running or stopped condition. However, the engine starting should be done at the standard CR10 and later on changes in CR can be accomplished. There are six (6) socket headed vertical allen bolts fitted on two supporting blocks on the two sides of the cylinder, which needed to be loosen for CR variation. The appropriate value of CR should be entered manually in the software for data acquisition.

3.2.1.7 Exhaust gas measurement

A Testo-350S/M/XL Engine flue gas analyzer is used for measurements of exhaust emissions of liquid and gaseous fuels. The gases O_2, CO, CO_2, NO_X, HC are measured from this flue gas analyzer. The exhaust gas was drawn from the exhaust manifold using the probe for fixed time duration under the specified set of operating conditions. These gas samples are then

analyzed in a flue gas analyzer system for direct reading of CO, CO_2, NO, NO_2, O_2 and hydrocarbon (HC) emissions. The resolution, accuracy, and range of these parameters are shown in the Table B-2(APPENDIX-B).

3.2.1.8 Raw biogas chromatography

Raw biogas produced by method of bio methanation varies in the composition of gases that are greatly influenced by surrounding environment and atmospheric conditions as discussed in chapter 1.The percentage of methane and carbon dioxide in raw biogas obtained through gas chromatography analyzer (GFM406). It is an ATEX accredited hand held gas analyzer configured for biogas. It is light weight, small and robustly constructed with a weather resistant case making it perfect for use on biogas plants. The composition of biogas in terms of CH_4 percentage, CO_2 percentage, oxygen percentage and hydrogen sulphide content in ppm can be directly recorded using 24 character alphanumeric display. The data recorded on GFM406 can be transferred to computer using USB through the Site man 5 software installed in the instrument. The detailed specifications of GFM406 are as shown in Table.B-3(APPENDIX-B). The sample compositions as recorded by GFM406 are shown in Table 1.4 (chapter 1) for different locations around IIT Guwahati.

3.2.1.9 Ignition timing variation

Ignition timing in case of VCR engine can be attained electronically through trigger sensor and microcontroller based electronic control unit(ECU) (Make: PE, USA). The ECU could be configured as per the fuel such as petrol, LPG or raw biogas selected to burn in engine. The provision of computer interface with PE3 monitor software is made so that programming of ECU for the ignition timing, range of throttle position from 0 to 100% and range of speed 900 to 2000 rpm of the engine can be easily optimized. The magnitude of ignition timing bTDC can be configured on ignition table and the ECU sends signal to trigger sensor for initiating the spark at the same crank angle bTDC. This method is versatile in the sense of varying the ignition timing for optimizing MBT for the fuels under study. The throttle position control is manual but the percentage throttle at a particular instance can be easily identified from the ignition table of PE3-monitor software.

3.2.1.10 LPG fuel supply system

Liquefied petroleum gas used for cooking application can be used for optimizing CR, IT and EGR rate. This LPG gas is stored in the form of liquid in a metal bottle at high pressure 6-14 bar (IOCL manual for LPG). As shown in Fig. 3.3, a flexible Surksha rubber hose may be recommended by IS:9573:1998 Type-4 and LERC guidelines connected on one end to pressure regulator of LPG bottle with another end is connected to the mass flow measuring instrument of the type as depicted above. The outlet of mass flow meter is connected to the diaphragm pump on inlet side. The outlet of which is connected to the ‘T’ venture mixer attached at the intake manifold of engine. The diaphragm pump is operated to set the required fuel supply so that stoichiometric A/F ratio will be maintained for each trial.

3.2.1.11 Raw biogas fuel supply system

The biogas used in the study is being produced by anrobic digestion of cow dung and ligno cellular biomass at "Auniati Satara", North Guwahati, Assam. The gas is collected from the site in a neoprene coated rubber fabric balloon of size 0.8 cubic meter and the filled balloons were transported to the laboratory for testing. Before testing the fuel in the engine the composition of the gas has been analyzed onsite using DGAS 406 gas chromatography (GC) system each time. The sample report has been tabulated in Table 1.4 of chapter 1. Biogas stored in balloon is supplied to the compressor through a flexible tube where the pressure built up to 4 bar (gauge). The gas is then passed through filter and regulator unit mass flow controller, where the gas pressure is set to 1.3 bar (gauge). Biogas fuel line leaving the mass flow controller is further connected to biogas fuel metering rota meter for measurement of mass flow rate as explained earlier followed by a diaphragm pump driven with the suction stroke of the engine. Biogas leaving the diaphragm pump is then connected to 'T' venturi mixer where it mixes with air in intake plenum. The diaphragm pump has a provision of flow rate adjustment by operating a valve where the minute setting of the valve only decide the smooth operation of engine using 100% raw biogas fuel.

3.2.2 Experimental Design and Procedure

The experimentation on VCR engine set up follows the plan of testing different fuels such as liquid fuel petrol and gaseous fuels LPG and raw biogas are structured. The performance parameters of interest are the brake torque, brake power, brake thermal efficiency and brake specific fuel consumption, air fuel ratio. The basic correlations used for estimating above parameters are included in APPENDIX-C

3.2.2.1 The baseline test

This particular study consist of two phase. The first phase is optimizing the ignition advance for MBT or finding out the optimum spark advance required for MBT. The second phase of the study consist of optimizing the compression ratio for the particular SI engine used in this experiment, for which the maximum CR is limited to 10 on APEX large engine.

The 'Baseline Test' is performed for setting the foundation for comparison of later experimental works. Here onwards these test are called as E-0 test (means No EGR). The test is performed by running the engine initially with petrol as fuel .The maximum brake torque timing is already set in the ECU software for petrol fuel. Once the engine started, load is applied and by adjusting the throttle to 60%,engine attains particular speed. During this time the water jacket outlet water temperature raises which needs to be observed continuously. As soon as the temperature there becomes 60^0 C (steady state) as explained in section 3.5.1, the set up is ready to switch to the LPG or raw biogas fuels. After achieving the steady state condition the speed of the engine was set to 1450 rpm at WOT condition. The fuel line valve is operated so that the fuel is supplied to the intake manifold. At this point of time there are two fuels ie petrol and LPG or raw biogas burned in combustion chamber. This causes rise in speed of the engine as fuel rich mixture is being supplied to the engine. Later on the switch

used for ON or OFF the petrol injector should be turned OFF which shut down the petrol fuel supply to the engine. As soon as shifting is done from petrol to any fuel LPG or raw biogas, the engine does not function smooth and misfire occurs. For this the diaphragm pump valve needs to operate minutely so that the stoichiometric A/F ratio could be maintained and engine further runs smooth without misfire and capable of varying load on the engine. Now the engine is running on 100% gaseous fuel only. Due to change of fuel from petrol to gaseous, the "Enginesoft" software needs to be configured for particular CR, fuel calorific value, fuel density and the ten number of cycles for recording pressure per degree crank angle (0-1200 pulse/min) for which data has to be recorded. In the first phase, the ignition timing is varied from 28^0 bTDC advance to 33^0, 38^0, 43^0, 45^0 and 47^0 bTDC. Similarly retarded by 26^0 and 24^0 bTDC. For each setting of ignition timing, the speed will be maintained constant at 1430 rpm with increment or decrement of brake load on the dynamometer. This is how the ignition timing is optimized for each fuel for further study evaluating the maximum brake torque.

In second phase, the ignition timing or spark timing is adjusted to optimum magnitude for concerned fuel on PE3 monitor for the speed range 1200-1700 rpm. Set the throttle position to WOT (90% of full throttle) and increase the load on dynamometer so that minimum speed 1200 rpm could be attained by the engine. At this point of time, the data has been logged on the "Enginesoft" software for 30 time interval. The parameters such as load (kg), speed (rpm), temperature of water inlet into the jacket(^{0}C), temperature of water leaving the engine jacket(^{0}C), temperature of water inlet to calorimeter(^{0}C), temperature of water leaving the exhaust gas calorimeter(^{0}C), exhaust gas temperature(^{0}C) before calorimeter and exhaust gas temperature after calorimeter(^{0}C), cylinder pressure (bar) per degree crank angle(^{0}CA) are measured for complete revolution of crank (360^0CA) and for 10 such cycles. Also the fuel consumption reading for 60 s time duration is noted from gas flow meter. The exhaust gas is checked for emission quantification of CO, CO_2, NO_X and HC by utilizing exhaust gas analyzer as discussed in section 4.3.4. The same procedure is repeated while experimentation on part throttle position (50% WOT). The set of data has been collected for CR8, CR9 and CR10. The uneven knock is recorded based on noise and vibration in engine functioning, as the set up doesnot have provision of knock measurement while engine operating.

3.2.2.2 The EGR Test

After completing the E-0 test, the set of data for gaseous fuels with EGR will be recorded. As per the plan the engine will be started as mentioned in previous section. As the gaseous fuels are of completely different properties, the EGR rate 10-40% for LPG fuel and 10-25% for raw biogas is considered for analysis. The engine jacket outlet water temperature found steady for long time, the EGR control valve would be opened and set to specific EGR flow rate. So at the intake plenum, the charge consists of fuel, air and recirculated exhaust gas. The percentage of EGR has been decided by calculating the mass flow rate of exhaust gas through the orifice meter. The pressure gauge attached across the orifice metre records the pressure difference in terms of ' mm' of water. This head can be used to calculate the mass flow rate of EGR. The engine has been allowed to run for 10 minutes to obtain the set speed because with application of EGR the speed of engine reduces slightly based on amount of EGR. Once

the engine runs steady, the throttle position set to WOT and procedure is repeated as done for E-0 test. The load is applied from maximum to minimum in the required speed range 1200-1700 rpm of the engine. Emission performance is recorded by using exhaust gas analyzer. At all load and set speed, the engine is allowed some time to get stability of measuring parameters and then data recording is completed. Similarly the experiment is conducted for other loads. The trials are performed for Variable CR8-CR10 with EGR rate range as depicted above.

Table 3.3 LPG Gas meter Specifications

Parameter	Specification
Made from	Actaris Metering Company
Model	Gallus 2000 G1.6
Gas type	Natural gas, LPG, biogas
Cyclic volume	1.2 dm^3
Operating temperature	-25^0C to $+55^0C$
Storage temperature	-30^0C to $+55^0C$
Max. operating pressure	0.5 bar
Measuring Range	Q_{max}-2.5 m^3/hr Q_{min}-0.016 m^3/hr
Pulse generator	0.01m^3/pulse

Table 3.4 A comparisons of some physical properties of engine fuel

Properties	LPG	Biogas	Petrol	Kerosene
Molecular formula	C_3H_8+ C_4H_{10}	CH_4+CO_2	C_8H_{12}	$C_{12}H_{26}$
Density(gas) at 15^0C, kg/m^3	1.15	1.27(dry)	730	780-850
Lower heating value, MJ/kg	46.10	15.74	44.0	45.636
Heat of vaporization, MJ/kg	0.426	0.5	0.33	--
Stoichiometric A/F ratio	15.7	5.36	14.7	14.12
Research octane number	112	110	91	70-85

3.3 SUMMARY

A sophisticated experimental set-up has been successfully designed and developed for the HONDA engine for power and torque measurement. The APEX engine test rig is commissioned and calibrated for the desired output considering different working parameters. Different measurement systems of both the facilities are critically analysed for their accuracy in measurement. Applicability of the commercial flue gas analyzer is tested and verified in this phase. As an outcome of this, it is possible to conduct experiments for petrol and kerosene fuels in the HONDA engine set-up. In line with this, the APEX engine is capable to work with petrol and gaseous fuels.

CHAPTER 4

Design and Development of VCR Mechanism

OVERVIEW

Internal combustion engines are used from many decades with innovative technologies for improving its performance and earing higher fuel economy. There are variety of SI engine fuels starting from different octane ratings based gasoline, LPG, biogas, CNG, producer gas etc. Across the globe, lot of research is going on to improve the thermal efficiency of these engines so as to get more work with the minimum amount of fuel burnt. One such technique is the variable compression ratio engine (VCR). This method helps to provide higher compression ratio for the higher octane rating of fuels to achieve the maximum brake thermal efficiency and less fuel consumption. In order to achieve this goal, proposal of a novel VCR mechanism put forth in this chapter. It is possible to change the compression ratio of the engine in its running condition if the engine is commissioned with this VCR mechanism. Details of various parts of the mechanism, its working principle and settings are elaborated in different section.

4.1 VARIABLE COMPRESSION RATIO INTERNAL COMBUSTION ENGINE

In general, the variable compression ratio has been obtained by altering the geometric clearance volume of the internal combustion engine. This invention of VCR technology relates to the maximum thermal efficiency and less fuel consumption to be achieved from the different octane fuels on the same internal combustion engine. It is the main objective of the present investigation is incorporating the VCR technique to set the optimum compression ratio for the particular octane fuel. The fuels for spark ignition engines may be from different octane petrol to higher octane gaseous fuels like LPG, raw biogas etc. Another objective of the present investigation in view of the above is to present a technique which will give improved combustion inside the internal combustion engine in terms of power output and fuel consumption. So, the VCR technique should be compatible for both the spark ignition engine and compression ignition engine. In this regard a novel VCR mechanism is proposed. Details of this mechanism are given in following section.

4.1.1 Detailed description of the mechanism

Figure 4.1 depicts the cut away view wherein the variable compression ratio assembly for the present configuration (1) is shown. The construction of the novel VCR mechanism consist of the secondary cylinder (2) attached to the main cylinder head (6) through metric threads of 40 mm height. The secondary piston (5) slides inside the secondary cylinder. The ball screw (3) consist of threads of constant pitch and rotates along the axis of the screw.

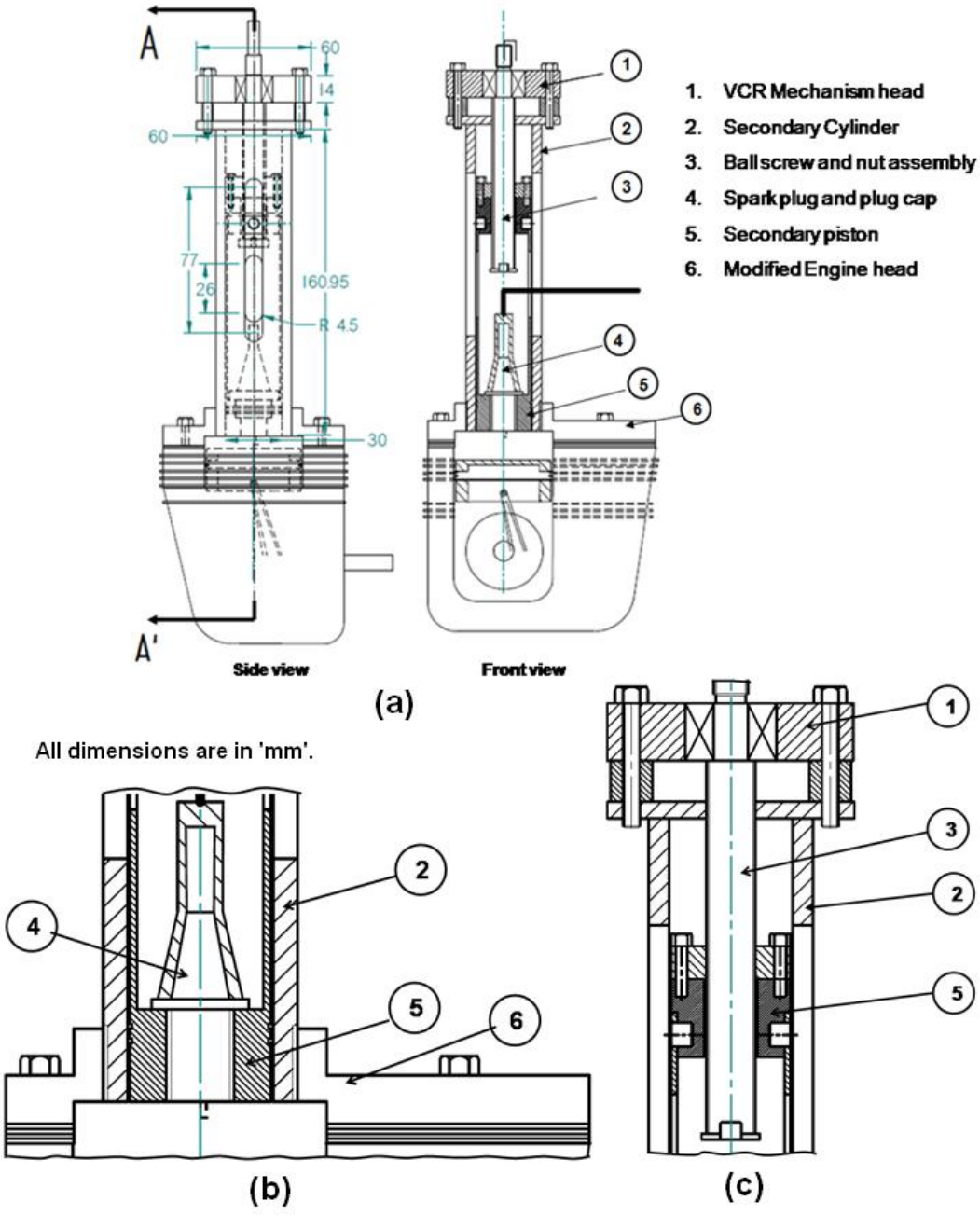

Fig. 4.1 Details of VCR attachment assembled with SI engine: (a) the schematic of VCR mechanism ; (b) the enlarged view of VCR mechanism towards engine cylinder block; (c) the enlarged view of the VCR mechanism showing the secondary piston and ball screw motion transfer

The ball screw nut which glides with small balls over the screw threads gives the linear motion to the nut. The maximum travel of the nut over the ball screw is limited by the screw stopper. Spark plug (4) is fixed inside the secondary piston itself so that it also moves forward and backward along with secondary piston (5). Spacing inside the combustion chamber due to clearance volume is altered by the secondary piston (5). The complete assembly is fixed with ball screw holder (3) with the help of allen bolts. The lock nut locks the ball screw (3) over bearings. The ball screw (3) is made to rotate inside the bearings fixed inside the secondary cylinder head (1). The secondary cylinder head is fixed to the cylinder with help of bolts and nut with gap of 10 mm. The spacer bushes are maintaining the gap between the head and secondary cylinder body for air cooling by natural draught. As there is clearance fit between secondary cylinder and piston, the secondary piston (5) is accompanied with the piston rings for sealing the space between secondary cylinder (2) and piston (5) during the operation. There are two such piston rings mounted on the secondary piston.

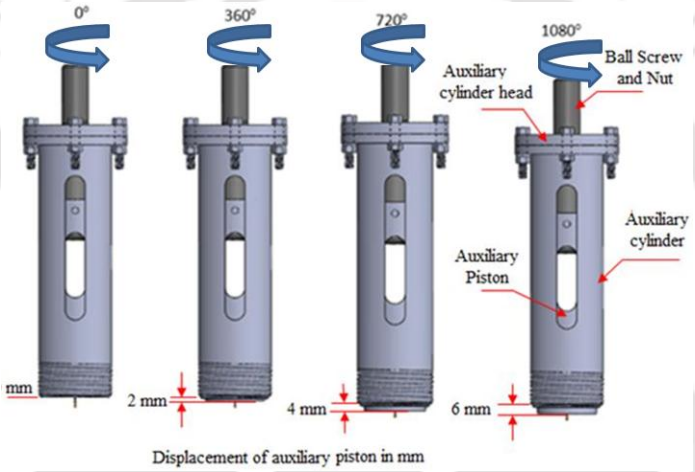

Fig. 4.2 The VCR mechanism operation process

Accuracy of the manufacturing of secondary cylinder (2) and secondary piston (5) as well as depth of piston ring groove on secondary piston are important parameters for the successful functioning of this mechanism. The assembly model of novel VCR mechanism is as shown in Fig.4.2. Spark plug cap with the spark plug cable is attached to the spark plug (4). Space around the spark plug and secondary piston is opened to air by natural draught. The main cylinder head (6) is conventionally fixed to the main cylinder block with help of bolts with gasket sealing. Main piston producing work slides inside combustion chamber. The connecting rod transfer the power generated to the cranks shaft for power production. During the calibration of novel VCR mechanism, as per procedure mentioned in APPENDIX-A, displacement of the secondary piston is measured. Thus measured values for different degrees of anti-clockwise (loading) and clockwise (unloading) rotations are compared with the theoretical estimates. This comparison is shown in Fig.4.3. Loading curve has encouraging match with the theoretical prediction. But, as seen in the figure, actual displacement curve, for same angle of rotation of screw, shows deviation from theoretical by 5%, 7%, 10% respectively at 180^0, 270^0 and 360^0 for the loading case (anticlockwise rotation)

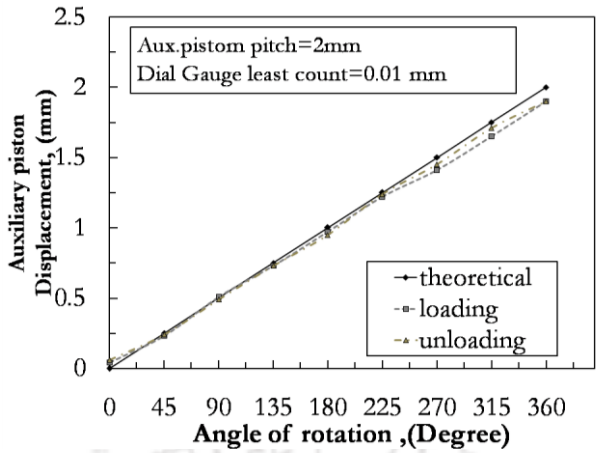

Fig.4.3 Auxiliary piston displacement varying with angle of rotation

VCR mechanism as per procedure mentioned in APPENDIX-A, However with actual displacement for same angle of rotation of screw, the loading (anticlockwise rotation) curve shows the deviation from theoretical by 5%, 7%, 10% respectively at 180^0, 270^0 and 360^0. Compression ratio keeps on rising during this process. However if the compression ratio needs to reduced, then the secondary piston should be retracted back and in this course of action the ball screw rotates in clockwise direction. At zero displacement ($\theta = 0^0$) of auxiliary piston, the actual measurement following return stroke does not coincide and the hysteresis error of 0.12 mm is reported.

4.2 COMPONENTS OF VCR MECHANISM

In this section, the construction of present VCR mechanism is discussed. Additional mechanical components that are added to the head are discussed as follows

4.2.1 Secondary cylinder

Secondary cylinder is a hollow flanged cylinder threaded on the outer surface as shown in Fig 4.4. This is the important body of the mechanism housing all moving and rotating components of the system. The cylinder with complete system has been fixed over the engine head such that the location of the original spark plug is exactly axisymmetric. Threads on the outer surface of the secondary cylinder are precision threads maintaining the precision level to ± 0.001mm. This is important to avoid leakage of compressed gases. Inside surface of the secondary cylinder is also very important from the point of view of any kind of leakage. The surface quality maintained to the precision level of ± 0.001. As the piston rings glide to and fro over the internal surface of the secondary cylinder, quality of machining has to be maintained. To avoid the rotation of the moving piston inside the secondary cylinder, the guide ways are provided from inside of the secondary cylinder which opens towards the flanged portion of cylinder.

The cylinder is made up of Mild Steel with allowable tensile strength to be 380 N/mm^2. Similarly the maximum pressure inside the cylinder is 5 times the radial pressure exerted by the piston rings on the cylinder, so the maximum design pressure considered is 0.15 N/mm^2

when considered in Honda engine having rated power ouput 1.3 kW. Based on this consideration the parameters of design include cylinder wall thickness as defined by Eq-4.1, cylinder flange thickness, height of secondary cylinder, type of threads and maximum height of threaded length over engine cylinder.

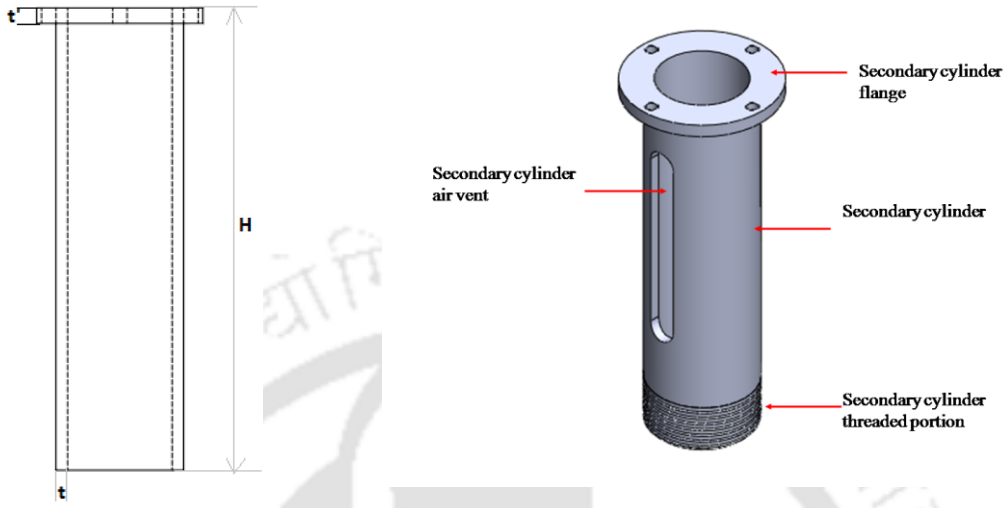

Fig.4.4 Geometry of secondary cylinder

Therefore, Secondary cylinder wall thickness, $$t = \frac{DP_{\max}}{2\sigma_c} \quad \text{(Eq-4.1)}$$

Where, D is diameter of the secondary cylinder; P_{max} is the maximum pressure inside combustion chamber; t is the thickness of the secondary cylinder. The secondary cylinder flange thickness can be approximated as 1.3 to 1.4 times of secondary cylinder wall thickness. The height of secondary cylinder considering all the moving components inside the secondary cylinder. The major heights include the piston height, the ball screw nut height, the connector height.

$$H = h_p + h_b \quad \text{(Eq.4.2)}$$

Where, H is total height of secondary cylinder; h_P is the height of secondary piston and h_b is the height of ball nut. The materials of component used in VCR mechanism gets heated with continuous engine working, it can be controlled using natural draught of air flowing through inside components of the mechanism in case of stationary engines . For this purpose the rectangular notch has been provided on opposite sides of secondary cylinder (size- 90 mm×9mm) as shown in Fig. 4.4. For moving engine either the notches are in direction of moving vehicle or parallel to flow of air from radiator fan so that forced draught can cool the system efficiently. The calculations are performed for large size engine

4.2.2 Secondary Piston

This secondary piston is a component which alters the compression ratio by protruding inside the combustion chamber with displacement of 1 mm or higher. If the secondary piston displaces opposite to the previous motion beyond normal position, then it is considered to

decrease in compression ratio of the engine. The design of the secondary piston is important from the point of view of the maximum pressure carrying element in the complete system. The maximum pressure developed due to combustion of air-fuel mixture is a basis for the selection of secondary piston.

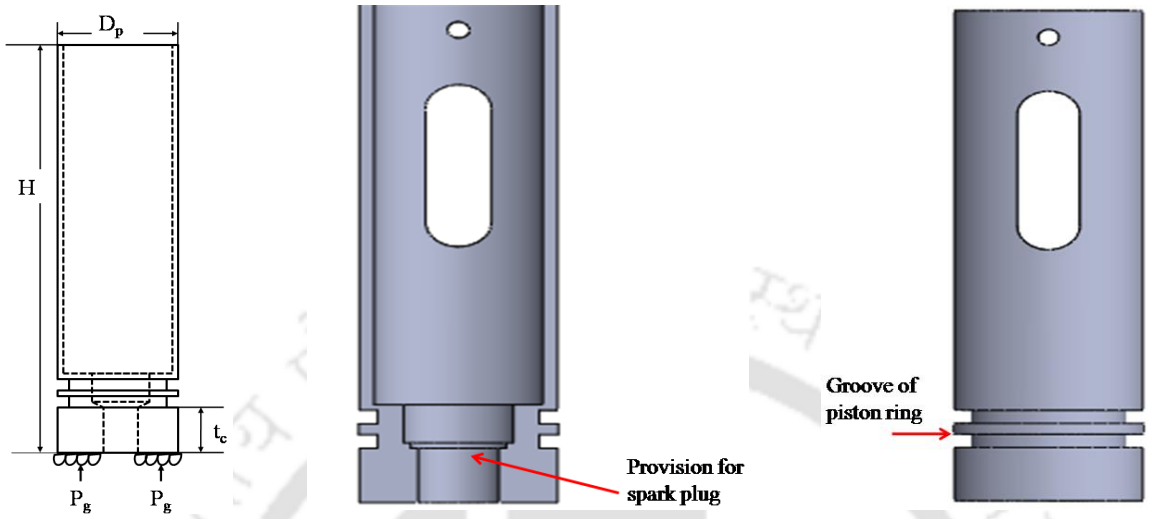

Fig.4.5 Schematic drawing of secondary piston

The secondary piston holds the piston rings that are mounted with due precision on the outer periphery of the piston as shown in Fig. 4.5. These piston ring groove dimensions should be selected such that the rings should freely rotate inside the groove when free and after connecting end to end, the gap between ring and piston should be so minimum that the compressed gases should not escape from that gap.

After inserting the piston rings along with secondary piston inside secondary cylinder, the rings should properly seal the gap between secondary cylinder and piston. In addition to increase or decrease in compression ratio the secondary piston also performs another function of changing spark plug location which may be sometimes reaching towards the combustion centre and sometimes away from combustion centre. This is important for the selection of optimum spark location for the multifuels engine. The spark plug mounting inside the secondary piston is done by precision threads which is also the another location from where there is a chance of exhaust gas escape and loss of compression work inside the combustion chamber. Important dimensions of the secondary piston that needs to be designed are as shown in Fig. 4.5 which include secondary piston diameter (d_p), crown thickness (t_C), secondary piston wall thickness (t_W) and secondary piston height (h_P). The methodology includes spark plug dimensions which decide the diameter of the secondary piston in general. Based on the magnitude of safe stress, the magnitude of diameter of piston has been standardized. It is assumed that, inside the cylinder the maximum gas pressure (P_{max}) is 4 times the indicated mean effective pressure (P_m) $P_{max} = 4P_m$ (Eq.4.3).

So maximum gas pressure is , $P_{max} = \dfrac{P \times n}{V_d \times N}$ (Eq-4.3)

For the given engine the specifications are , P be the power output in watt; n be the Number of revolutions per cycle (for 4 stroke, n=2); V_d be the displacement volume in cubic meter; N is speed of the engine in rps, Therefore,

$$\text{Maximum Force, } F = P_{\max}\left[\frac{\pi}{4}\left(d_p{}^2 - d_{spark}{}^2\right)\right] \qquad \text{(Eq-4.4)}$$

The piston crown transmits the gas pressure force (Eq-4.4) and transfers heat to the piston rings for the dissipation through cylinder wall. The depth of clearance volume with modified engine head is 12 mm in Honda Engine and 13 mm in case of large VCR engine. The secondary piston can be displaced inside combustion chamber upto 10 mm at both set ups. Crown thickness is the distance from the top of the piston to the first ring groove. The piston rings act as a sealing between the secondary piston and secondary cylinder. To avoid release of rings from secondary cylinder, the linear travel of secondary piston is restricted through engine combustion chamber up to a maximum of 10 mm so the crown thickness is chosen to be 12 mm. Weakest portion of secondary piston is at the seat of the gas pressure ring which is subjected to compressive force and failure may occur. Taking mean diameter of that section as 85% of piston diameter (Patil, 2001). The thickness of this section can be calculated (Eq-4.5) and this thickness is known as wall thickness. Let, t_w be wall thickness, then

$$\text{Secondary piston thickness, } \quad t_w = \frac{F}{\pi(0.85)d_p\sigma_{allow}} \qquad \text{(Eq-4.5)}$$

The secondary piston height (Eq-4.6) is the height of the piston depends on the spark plug length (h_{sp}) and length of spark plug cap (h_{cap}), ball screw height inside the secondary piston (h_{screw}), Ball screw nut $(h_{threadd})$. The secondary piston is supported by ball screw and ball nut as seen from Fig.4.1.Using these relations the calculations are performed for small engine as well as large VCR engine.

$$h_P = h_{sp} + h_{cap} + h_{screw} + h_{thread} \qquad \text{(Eq-4.6)}$$

- The secondary cylinder and secondary piston are subjected to temperature gradient which introduces thermal shock. Corrective measures are taken to counter this thermal shock. Those measures are mentioned herewith.
- The choice of material for the secondary cylinder is mild steel which has high yield strength of 360 N/mm^2.
- Use of water jacket cooling for the secondary cylinder.
- The choice of material of secondary piston is aluminium alloy grade 2024 heat treated and aged having yield strength of 351 MPa.

- The design of secondary cylinder and secondary piston is made such that cooling of secondary piston takes place with natural draught of air over complete circumference of piston.
- The secondary piston is provided with piston rings which while sliding inside the secondary cylinder can accommodate certain degree of thermal shock received by the secondary piston.

4.2.3 Ball screw and ball nut

A ball screw is a mechanical linear actuator that translates rotational motion of screw to linear motion of nut with little friction. It has a threaded shaft on which a nut is fixed with balls rolling in between the shaft and traces the path of the nut over the grooves as displayed in Fig.4.6.

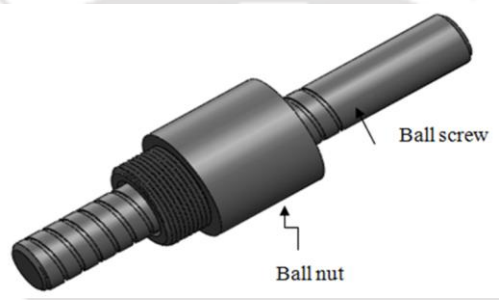

Fig.4.6 The ball screw with ball nut assembly

The nut is called ball nut and it is a flange type that can be fixed to the secondary piston wall and the whole system moves up and down inside the secondary cylinder. The ball screw is accurate to a precision level of ± 1%. The linear displacement of ball nut can be programmed in relation to the rotation of ball screw as shown in Fig. 4.6. The ball screw mechanism is as shown in 4.7. The ball screw design is based on some assumptions such as the material used for ball screw is stainless steel with allowable strength 300 N/mm^2 . The manufacturers catalog by IAR Pune is adopted for selecting the appropriate ball screw. Based on the input data such as maximum force on nut, the maximum static capacity of ball screw can be evaluated by Eq. 7,

Screw static capacity, $C_o = F \times S.F.$ (Eq.4.7)

Assuming the ball screw will work for 4 hrs a day, 5 days a week, 4 weeks a month and for 2 years, the ball screw dynamic capacity can be calculated using (Eq-4.8) ,

$$C_{ao} = \left(X\, F_r + Y\, F_a\right)\left(\frac{60 N_b L_h}{10^6}\right)^{0.33} \quad \text{(Eq.4.8)}$$

Using IAR Pune Catalogue (APPENDIX-B), the ball screw selected is IAR 12 × 2 by considering static and dynamic loading capacities. The ball nut is an IAR flanged nut series 1011 its specifications are given in the table below

Table 4.1 Ball Screw specifications

Engine Make	Nominal diameter d_o	Lead P_h	C_a(N)	C_{ao}(N)	Designation
HONDA	12	2	3000	3400	IAR 12×2
APEX	14	2	3000	3400	IAR 14×2

In this model of ball screw, the nut used is "flanged nut" as shown in Figure below

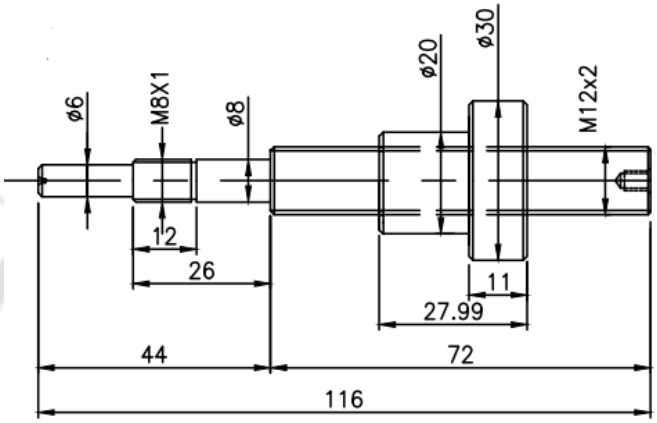

Fig. 4.7 IAR 12×2 ball screw with its dimensions (Honda Engine)

The length of threaded portion of ball screw can be calculated as

$$L_{screw} = h_{screw} + h_{thread} + h_{space} + t_{flange} \quad \text{(Eq-4.9)}$$

Where, L_{screw} is length of threaded shaft of ball screw; h_{screw} length of ball screw inside secondary piston; h_{thread} is the length of ball nut; h_{space} space height for natural draught; L_{screw} is the secondary cylinder flange thickness. Using this methodology, the ball screw and ball nut are selected for Honda engine as well as large VCR engine (APEX).

4.2.4 Secondary cylinder head

Secondary cylinder head is a circular disc (Fig. 4.8) that has ball bearings fixed at centre to support the ball screw and this is fixed to the secondary cylinder with the help of bolts and nuts. The forces exerted on this component are due to gas force by combustion or internal gas pressure as well as force due to self weight of moving system.

So while selecting the thickness of plate, care has been taken to confirm the safety for stress in case of both engine set ups.

4.2.5 Piston rings

The secondary piston (Fig. 4.5) has been designed from the view point of actual piston cylinder of I.C.engine. The main function of the piston ring is to maintain a seal between

secondary cylinder wall and secondary piston and prevent leakage of gas past the secondary piston.

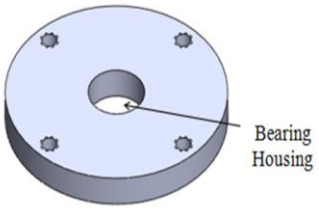

Fig 4.8 Secondary Cylinder Head

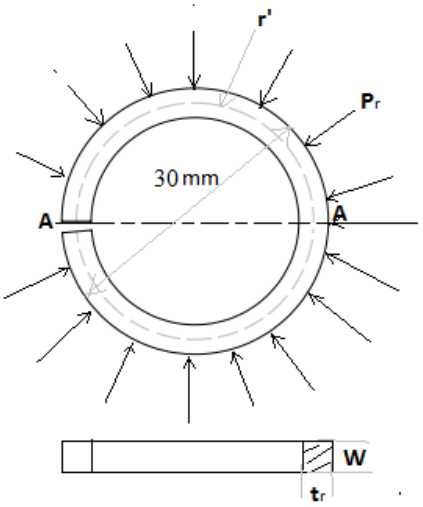

Fig.4.9 Piston ring when fitted in cylinder

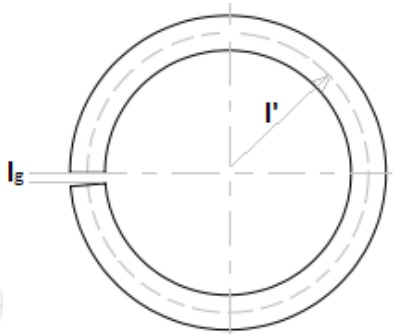

Fig 4.10 Free ring before installation

Piston rings are made of grey cast iron having excellent wear resistance. These rings have to provide radial force against the cylinder to prevent leakage of gas past them. Generally the value of this radial pressure is between 0.025 to 0.042 N/mm^2 (Patil, 2001).

So assuming radial pressure of 0.03 N/mm^2, calculating the piston ring width when fitted in the groove (Fig. 4.9), contact pressure develops a bending moment on the ring at section AA (Hanipah et al.,2015)**.** So, the radial wall thickness (Eq-4.10) of piston ring is

$$t_r = \sqrt{\left(\frac{6 \times P_{rad} \times w \times 2r \times r}{w \times \sigma_{all}}\right)} \qquad \text{(Eq-4.10)}$$

Where,

t_r is the radial wall thickness, R is the radius of the piston ring when fitted in cylinder, r' is the radius of neutral axis after installation, w is the axial thickness of the piston ring.

Therefore the radial thickness of the piston ring is 1mm. The axial thickness of the piston ring is given by $(0.7 \approx 1)$ t_r. Therefore the axial thickness is assumed to be equal to radial thickness which is equal to 1 mm. The free size of ring (Fig. 4.10) signifies that the ring has to exert the radial pressure when fitted in groove.

This is obtained by initial elastic compression of ring in the cylinder bore diameter. Cross section of ring is rectangular and its neutral axis is at the center of radial width. Applying the relation between neutral axis (Eq-4.11) before

compression and after compression, the radius of neutral axis before installation is given by the relation

$$l' = \left[\left(\frac{E \times t_r \times r'}{E \times t_r - (2 \times \sigma_{all} \times r')} \right) \right] \quad \text{(Eq-4.11)}$$

Where, E is the modulus of elasticity of material, So, the circumferential gap (l_g) before installation (Eq-4.12) at neutral axis of the ring cross section is calculated as

$$l_g = 2\pi(l' - r') \quad \text{(Eq-4.12)}$$

With this gap, when the ring is fitted the open ends will meet. However, during operation of engine, rings get heated and if not permitted to expand they will not provide the desired sealing pressure. Hence an additional gap of about 0.5 mm is provided.

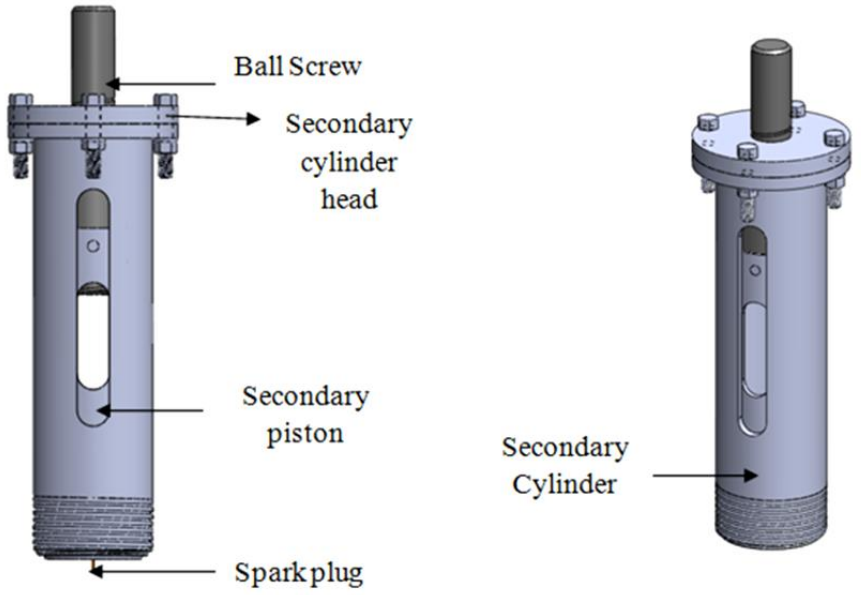

Fig. 4.11 Assembly drawing of VCR mechanism

4.2.6 Stepper motor

A stepper motor is connected to the ball screw with the help of a flexible coupling (Fig. 4.11). A stepper motor is chosen here because the displacement of the secondary piston inside the secondary cylinder is discrete and knowing the pitch, (*P)* of the ball screw implies that the ball nut travels P unit linear distance in 1 revolution of the screw. So if a stepper motor rotates in steps of 90^0 then the secondary piston moves $P/4$ linear distance. Hence the desired length of piston can be travelled inside or outside of engine combustion chamber thereby changing the clearance volume of the engine. With the help of all these components, the completely designed variable compression ratio mechanism and its assembly drawing of the VCR mechanism is as shown in Fig. 4.11 –a and b).

Fig.4.12 Original HONDA engine head

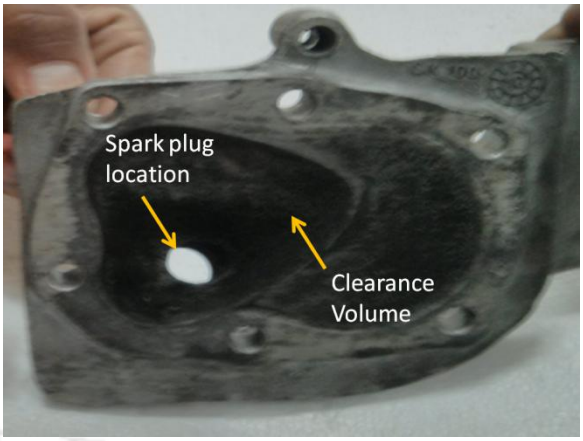

Fig.4.13 The combustion chamber of HONDA engine

4.3 ATTACHMENT OF NOVEL VCR MECHANISM ON THE HONDA ENGINE

The VCR mechanism designed and developed for two different engines having different engine specifications.

Table 4.2 Specifications of Novel VCR mechanism

Sr No	Specification	HONDA Engine (mm)	APEX Engine (mm)
01	Secondary cylinder		
	Outside diameter of the cylinder	38.10	38.10
	Thickness of cylinder	3.5	3.5
	Height of cylinder	150.63	236.92
	Flange diameter	61.10	61.10
02	Secondary Piston		
	Outside diameter of piston	31.10	31.10
	Crown thickness	24.20	15.20
	Piston groove radial depth	2.02	2.02
	Piston groove axial depth	2.02	1.45
	Piston groove gap	2.02	4.33
	Number of rings	2	3
	Total height of piston	150.46	179.80
	Wall thickness of piston	3.5	3.5
03	Ball screw		
	Length of screw	134	134
	Mean diameter of screw	M12	M12
	Pitch	2	2
04	Ball nut		
	Maximum diameter of nut	31	30
	Total length of nut	28	28
05	Ball nut holder		
	Total length	60.03	60.40
	Maximum outside diameter	31	31
06	Secondary cylinder head		
	Diameter of head	61.10	61.30
	Thickness of head	14.20	14.20

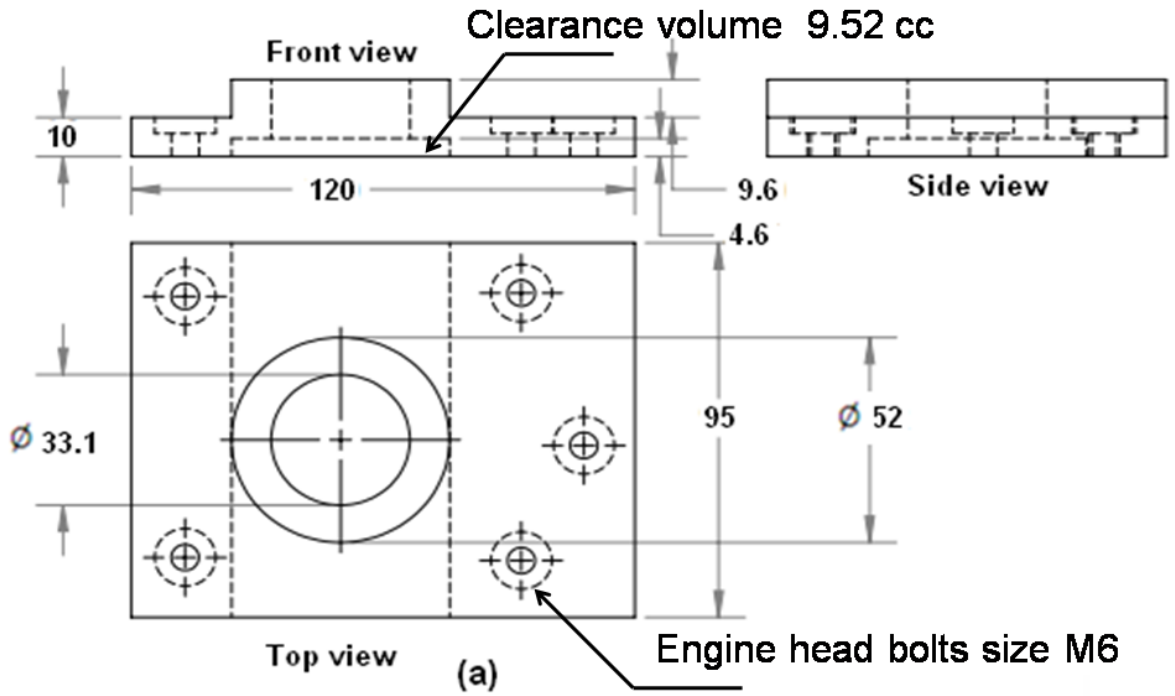

Fig.4.14 New HONDA engine head for Honda engine

So the detailed specification of VCR mechanism for each individual is tabulated in Table 4.2.

In order to convert the constant compression ratio HONDA engine into the variable compression ratio HONDA engine, the novel VCR mechanism needs to be mounted on the engine. The method of mounting of novel VCR mechanism is done by modifying the existing engine head of HONDA engine.

The outside and inside shape of the original engine head is as shown below in Fig.4.12 and Fig 4.13. For the available Honda engine the displacement volume is 97 cc (Table. 3.1) having the fixed compression ratio,4.81 as specified by the manufacturer. If clearance volume is taken as V_c, then

$$CR = 1 + \frac{V_d}{V_c} \qquad \text{(Eq-4.13)}$$

From Eq-13, the clearance volume for the available engine, $V_c = 25.52\ cc$

4.3.1 New engine head

To accommodate the novel VCR mechanism, the existing engine head (Fig. 4.14) of the type Ricardo's turbulent head-side valve combustion chamber (Ricardo,1979) is found to be inappropriate due to its polygonal shape. In addition, the engine head thickness is very less and hence couldnot be suitable for novel VCR attachment. To overcome this issue, a new

engine head is designed and developed as shown in Fig.4.15. The new engine head is designed which follows L-head type combustion chamber geometry to provide sufficient base for attaching the novel VCR mechanism as shown in Fig. 4.14.

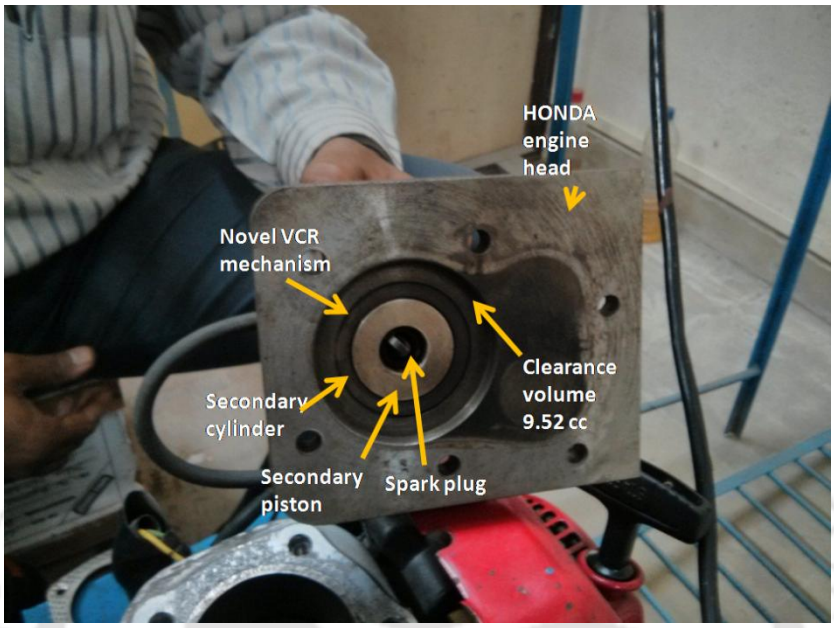

Fig 4.15 Assembly drawing of VCR Mechanism and new engine head

The design would be so precise that required clearance volume of original engine head could be achieved. Similar to the original engine head, the new engine head should takes care of the lift of the inlet and exhaust valves during working of the engine. For the available engine the valve lifts of both inlet and exhaust valves is 3 mm. The gasket used to seal the engine head and cylinder block has a volume of 4 cc and a thickness of 1 mm.

So if four gaskets are inserted between cylinder block and engine head, the clearance volume gets raised to 16 cc (4 x 4 cc). Along with this, there left sufficient space for the valve lift. The remaining 9.52 cc clearance volume is crafted in the new engine head. The design of the new engine head mounted on engine accommodated with novel VCR mechanism is as shown in Fig.4.16. The remaining 9.52 cc clearance volume is crafted in the new engine head. The design of the new engine head mounted on engine accommodated with novel VCR mechanism is shown in Fig.4.16.

The clearance volume on the new engine head consist of 33.1 mm diameter and 4.9 mm depth as shown in Fig. 4.15. The diameter taken here is equal to diameter of cylinder bore. Doing this practice, the compression ratio of the engine is maintained to be constant. The complete assembly of engine head and the variable compression ratio mechanism is shown in Fig. 4.15 and Fig.4.16. The engine head with the above design has been manufactured at MSME Tool Room, Amingaon, Guwahati and then both the new engine head and the VCR mechanism was assembled. To accommodate for the clearance volume, four gaskets are placed between the new engine head and the cylinder block which are fitted with bolts as a assemblage.

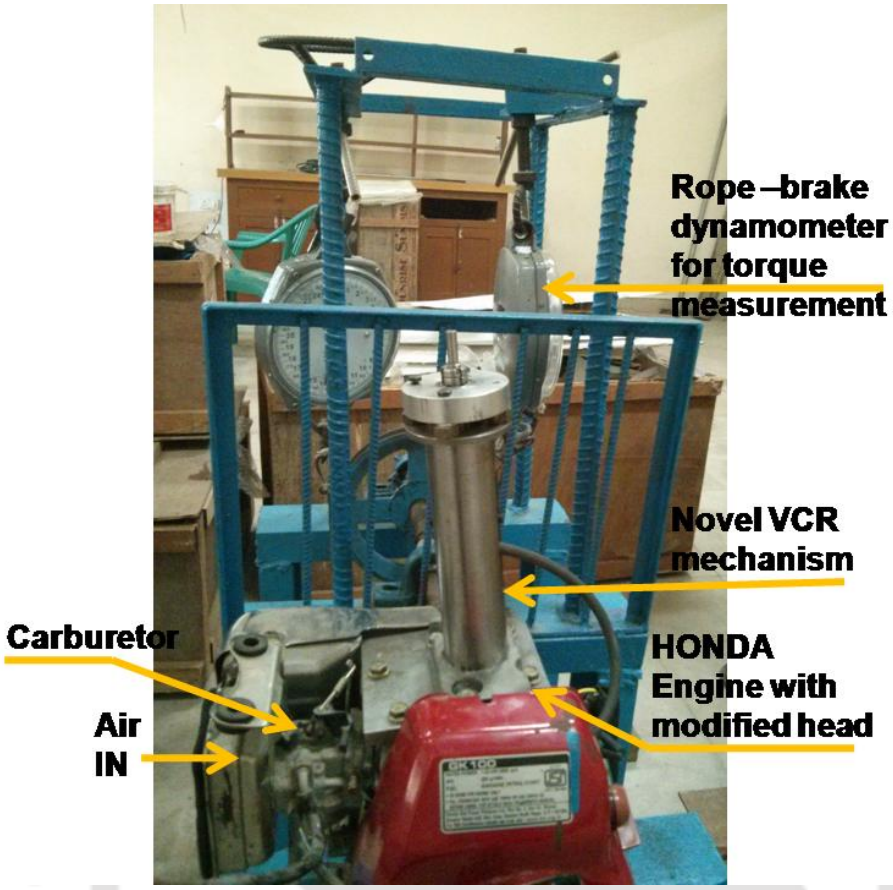

Fig 4.16 Assembly of VCR HONDA engine

The procedure laid in section 4.5 for converting the constant CR engine to variable CR Honda engine as shown in Fig.4.16. The experiments are then performed on the VCR Honda engine with variation of CR by novel mechanism only. The range of CR obtained are CR 4.91, CR 5.02, CR 5.27 and CR 5.4 over fixed CR 4.81. This range represent the minute increment of CR because for the spark ignition engine, it will be beneficial to keep the compression ratio variation with small magnitude for safety of the engine as well as possible knock.

4.4 METHOD OF ATTACHMENT OF NOVEL VCR MECHANISM ON THE LARGE VCR ENGINE

Successful installation of the Novel VCR mechanism on small (1.3 kW) engine is followed by development of VCR mechanism for inline alteration of compression ratio on commercial engine.

The commercial engine is a large VCR SI engine considered for the purpose whose specifications details are elaborated in Chapter 3.

The construction of this engine is different in the sense of valve arrangement. In article 4.5, the engine is Ricardo' s head geometry type of construction because the compression ratio is less and enough space is available to accommodate the valves (Haywood,1988). But the large

VCR engine is having large bore diameter 87.5 mm to carry the high CR. The design of the novel VCR mechanism consist of secondary cylinder, secondary piston, ball screw and nut, cylinder piston rings, secondary cylinder head. Following the Eq.4.1 to Eq.4.12, the design of the novel VCR mechanism is presented. The specifications of the novel VCR mechanism are tabulated in Table 2. This additional secondary mechanism is also integrated with the engine for change in compression ratio.

Fig. 4.17 The procedure of mounting novel VCR mechanism on the engine head following procedure (a) The provision made for mounting VCR mechanism; (b) the drill of 31.8 mm diameter with thread inside over 40 mm depth; (c) the novel VCR mechanism fixed over engine ; (d) the assembly of engine head with novel VCR; (e)the space consumed on the convention engine; (f) the inside structure of the engine head occupying suction, exhaust valve and third is secondary piston arranged very precisely; (g) the secondary piston displacement of 5 mm inside combustion chamber;(h) the secondary piston displacement of 2 mm inside combustion chamber;(i) the secondary piston displacement of 0 mm inside combustion chamber.

This top-up mechanism (Fig.4.17: a- i) consists of secondary cylinder and piston mounted on the engine head. The method of operation of top up mechanism has been discussed in section 4.2. The unique feature of this mechanism is that the spark plug is mounted inside the secondary piston which also moves coaxially with the piston.

As per this technique discussed in article 4.6, the geometric clearance volume (CV) is calculated using Eq.4.14. Any kind of alterations in this geometric CV allows to increase or decrease in compression ratio.

The theoretical compression ratios have been found from

$$V_C' = V_c - \Delta V \; ; \; CR = \frac{V_C' + V_D}{V_C'} \qquad \text{(Eq-4.14)}$$

Where, V_C' is the clearance volume of the cylinder; ΔV is the volume of secondary piston protruded inside clearance volume; V_C is the geometric clearance volume as specified by the manufacturer of the engine; V_D is the swept volume of cylinder, and CR is the compression ratio of the engine

The diameter of secondary piston is 31.10 mm and secondary cylinder diameter is 31.8mm. The possible combinations of CR and secondary piston displacement are coordinated as displayed in Table.4.3.

4.4.1 Simultaneous use of two VCRs

In addition to the tilting block VCR arrangement of large VCR engine, when the top up mechanism (Novel VCR mechanism) is added, the engine becomes versatile and there are range of CR can be attained depending on the secondary piston displacement in or out of combustion chamber. However one important point here is that the increase in CR is limited by the engine structure capacity.

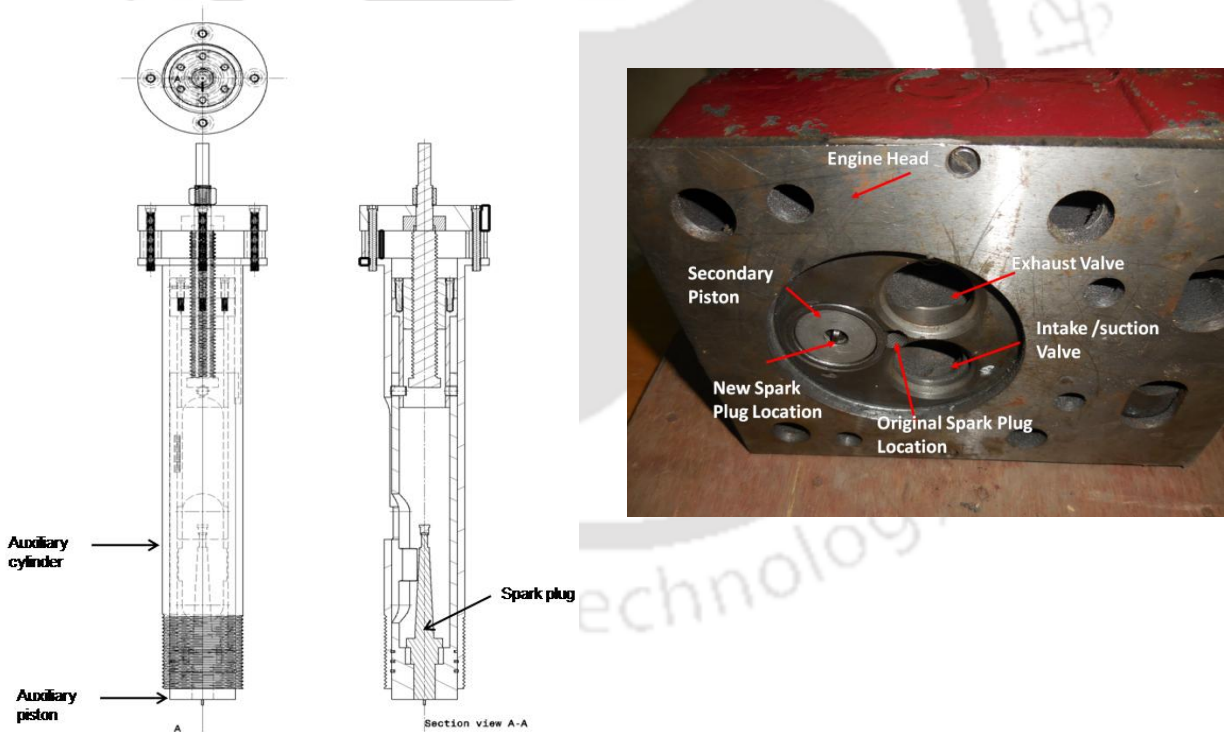

Fig. 4.18 Top up VCR mechanism and its location on engine head

Considering this, as the engine structure is light in weight and subjected to lower pressure comparative to diesel, it is beneficial to vary the compression ratio over minute level, so that there could be no chance of engine gets damaged. The other octane fuels also need a minute increase or decrease in CR over petrol fuel.

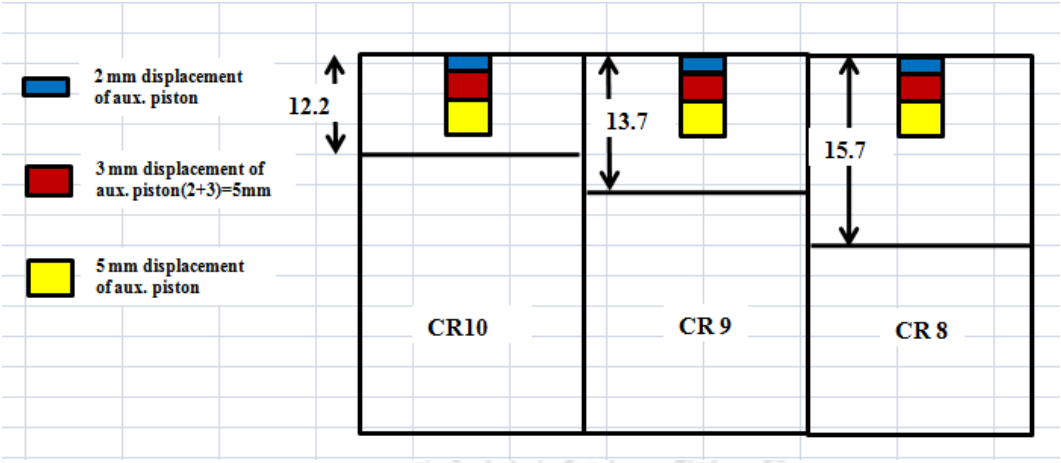

Fig. 4.19 The secondary piston movement in clearance volume of SI engine.

Knowing this fact, the topup mechanism is designed to vary the compression ratio online to a minute level as depicted schematically in Fig. 4.19 and tabulated in Table 4.3. As shown in Fig. 4.19, for CR10, the depth 12.2 mm is available to move the secondary piston inside combustion chamber. Similarly, if CR9 is maintained by tilting block mechanism then the same will be 13.7 mm and for CR8, it will be 15.7 mm. So whatever be the displacement of secondary piston inside combustion chamber, it will reduce the clearance volume by an amount equal to protrusion volume of secondary piston which ultimately causes rise in CR (Eq.4.14).

Table 4.3 The theoretical VCR for novel mechanism

To maintain CR8	Displacement of pivot, mm	To maintain CR9	Displacement of pivot, mm	To maintain CR10	Displacement of pivot, mm	auxiliary piston displacement, mm	Above CR10	Above CR9	Above CR8
7.89	6.8	8.86	4	9.82	1	2	10.18	9.15	8.11
7.73	7.5	8.65	4.2	9.56	1.8	5	10.48	9.38	8.29
7.48	8.8	8.33	5.2	9.16	2.8	10	11.02	9.8	8.6

Table 4.3 shows the change in magnitude of CR with the displacement of secondary piston. The rise in CR of the engine above fixed CR8, the possible increment is CR8.11, CR8.29 and CR8.6 similarly at fixed CR9, the increment is CR9.15, CR9.38 and CR9.8 and finally for fixed CR10, the CR increased to CR10.18, CR10.48 and CR11.02 for displacement of 2 mm, 5mm and 10 mm of secondary piston respectively. It is very interesting to observe the effect of such minute change in compression ratio over performance, combustion and emission analysis.

In order to compare the performance of the engine with top up VCR attachment and that with conventional VCR engine, can be justified only if the working conditions are constant. This includes the fixed compression ratio, fixed ignition timing and air/fuel ratio.

The schematic diagram of original tilting block assembly from Fig.3.5 for large VCR engine is considered. The CR adjustment lever length is 150.1 mm between two pivots represent CR10. If this length increased then CR keeps on reducing. After installation of top up mechanism on this engine block and to keep compression ratio fixed, it needs to coordinate both the tilting block VCR and top-up VCR simultaneously such that the final compression ratio is CR8 or CR9 or CR10 (Fig. 4.20-a).

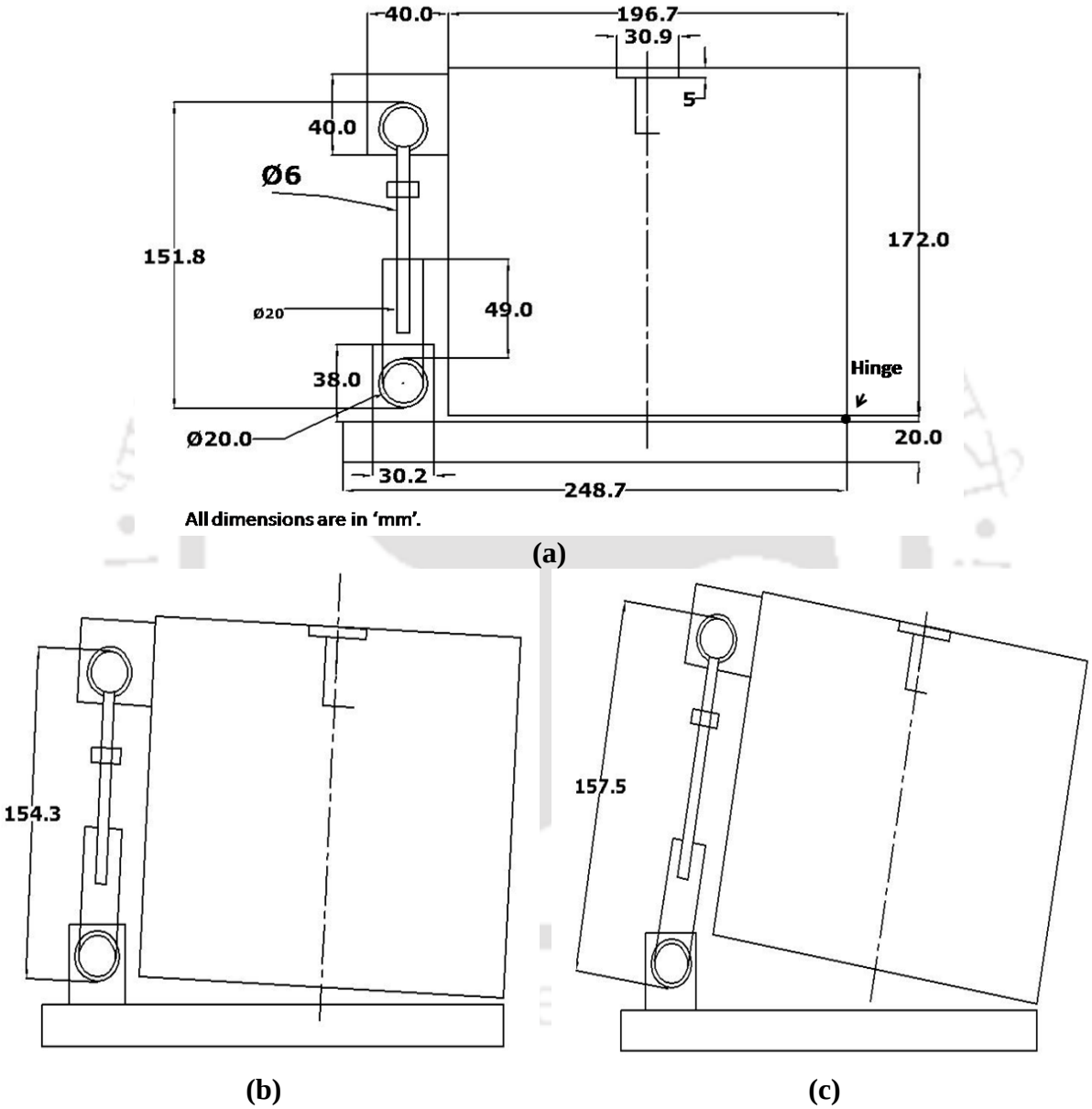

Fig. 4.20 (a) Simultaneous adjustment of tilting and top up VCR for fixed CR10; **(b)** Simultaneous adjustment of tilting and top up VCR for fixed CR9; **(c)** Simultaneous adjustment of tilting and top up VCR for fixed CR8.

The method of simultaneous coordination of two VCR mechanisms can be achieved as demonstrated in Fig. 4.20(a-c). A shown in Fig.4.20, if top up VCR mechanism becomes operational by 5mm protrusion inside combustion chamber, then scenario will be changed and displayed in Fig.4.19.

There is reduction in clearance volume equal to volume occupied by protruded secondary piston inside combustion chamber. In such situation, the pivot distance needs to be increased causing increase of clearance volume and ultimately maintain constant CR. To maintain CR10 with 5mm protrusion length of secondary piston, the pivot distance of 151.8 mm must be adjusted (Table.4.3), Similarly for same protrusion length corresponding length of 154.3 mm and 157.5 mm should be adjusted to operate engine at CR9 and CR8 respectively (Fig.4.20 b-c).

4.5 METHOD OF VARYING SPARK PLUG LOCATION IN LARGE VCR ENGINE

Petrol based spark ignition engine has the spark plug located inside combustion chamber at its optimum location. If the working fuel is changed from petrol to some other such as LPG, raw biogas etc, then the spark plug location may be different as compared with that of petrol fuel. So in order to improve the performance of the engine, the study of optimum spark location for the particular fuel such as raw biogas and LPG becomes important.

Change in compression ratio with alteration in spark plug location for a given setting of tilting block can be understood from Fig. 4.21. The original location of the spark plug is as shown in Fig 4.22-A which is named as SP1. This location, SP1, is exactly midway of both the suction and exhaust valves. While operating the top up VCR mechanism, piston accompanied with

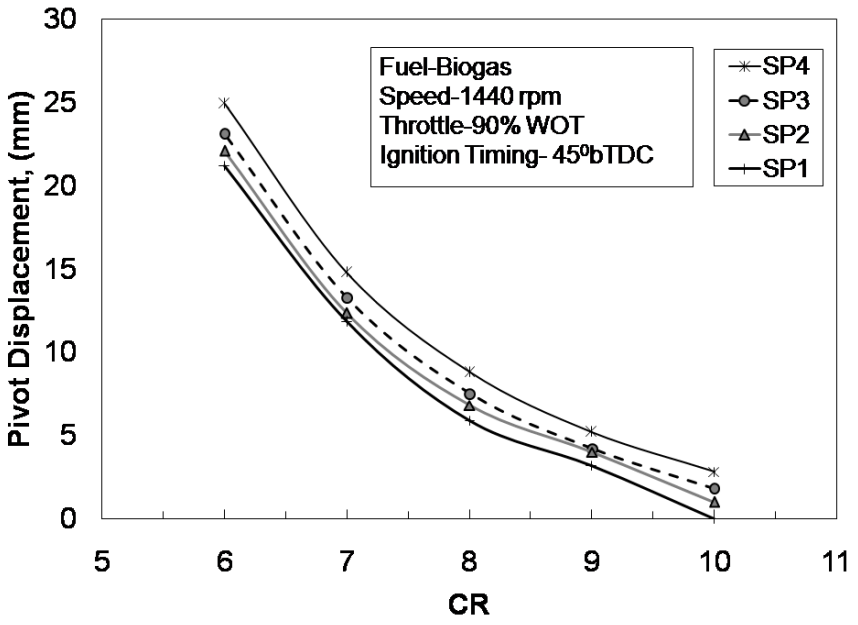

Fig.4.21 Compression Ratio variation with pivot displacement of tilting block VCR mechanism

spark plug protruded in and out of combustion chamber and thus the location of the spark plug changes axially in the clearance volume.

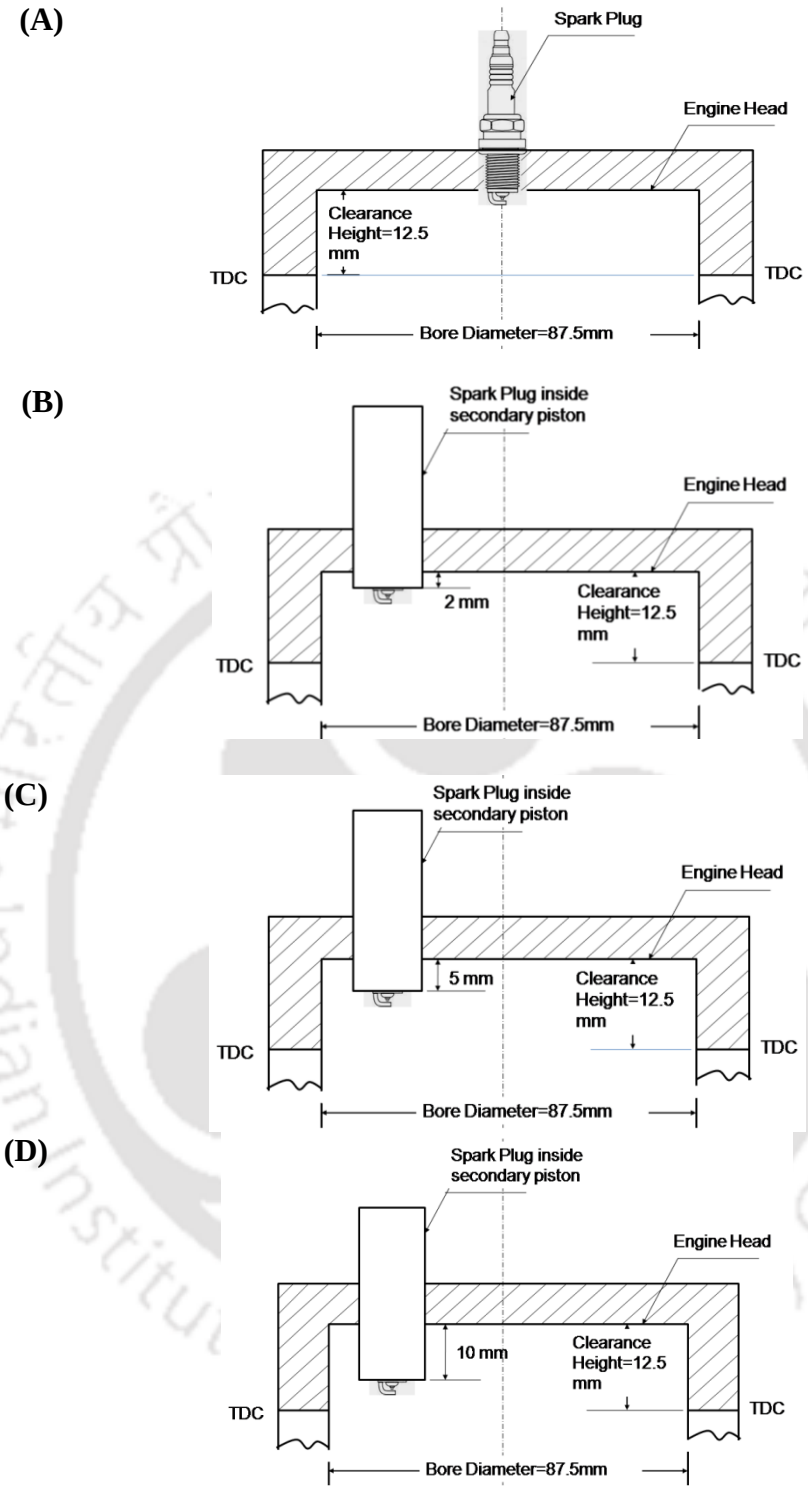

Fig.4.22 Spark plug arrangement in spark ignition engine used, (C) Spark plug at new position with 5mm inside chamber[SP3]; (D) Spark plug at new position with 10 mm inside chamber[SP4].

Some of those locations of the spark plug such as 2mm protrusion inside combustion chamber represent SP2 (Fig 4.22-B), 5mm travel inside considered to be SP3 (Fig 4.22-C) and SP4 assumes to be 10 mm depth of spark plug in clearance volume (Fig 4.22-D) of engine are as shown in Fig.4.22.This top-up VCR mechanism without spark plug can be

considered independently for changing the compression ratio. With spark plug, as per procedure discussed in section 4.7.1, the simultaneous coordination of top up VCR and tilting block VCR is maintained following Table 4.3.

In order to observe the effect of different spark plug location such as 2mm, 5mm and 10mm protrusion, the mechanism has been tested for the fuels LPG and locally available raw biogas.

4.6 Weight to size assessment of novel VCR mechanism

There are two VCR mechanisms being installed and operated on the two different capacity engines. In doing so, space available over the engine head is utilized for installing the mechanism. It should be noted that, it is simple to install the proposed mechanism if the suction and exhaust valves operate from the engine block as in HONDA engine. But in case of APEX engine it was very difficult to accommodate the VCR mechanism on engine head as valves are on engine head itself. In such situation the available space and engine capacity are considered to decide the dimensions and weight of each element of the mechanism. However the total weight of the VCR mechanism is far less in comparison to the complete engine set up. The details of the weight and size of the VCR mechanism designed in present case are given in **Table 4.4**.

Table 4.4 The weight to size penalty assessment for novel VCR mechanism

Sr No	Name of Engine	Weight of VCR mechanism, N	Maximum diameter of mechanism, mm	Maximum height of the mechanism,mm	Weight to size ratio(N/mm)
01	HONDA	12.29	60	216.9	0.204
02	APEX	14.47	61.1	241.5	0.218

4.7 SUMMARY

This chapter describes the method of varying the compression ratio using the novel VCR mechanism. Importance of variable compression ratio for the different octane fuels could be achieved with this proposed method. However the leakage of combustion gas is a major issue which can only be rectified by accurate design and manufacturing of the mechanism components especially the secondary piston with piston ring grooves. This method of VCR is a commercially viable technique and can be easily implemented in any SI/CI engine, although this it's working is mentioned here only for SI engines. Standard component design calculations are considered for obtaining dimensions of each part of this mechanism. Same mechanism in two different sizes is thus designed, fabricated and commissioned successfully for the small size HONDA engine and large size APEX engine. Since, change in compression ratio over here is based on change in spark plug location, all the possible values of compressions ratios are precisely measured for both the engines. Possibility of change in compression ratio in running condition of the engine is also verified along with the different spark plug locations for same compression ratio settings. Thus, presently proposed VCR mechanism which alters compression ratio in a small range is found advantageous to tune to the compression ratio and spark plug location for a given fuel in the given engine.

CHAPTER 5

Novel VCR Mechanism Analysis using Honda Engine

OVERVIEW

In view of efforts undertaken for design and development of the sophisticated VCR engine set-up, present chapter is centered on exploring the possibility of multi-fuel testing capability of the engine equipped with newly designed VCR mechanism. This objective internally demands for change in compression ratio with change in fuel due to difference in octane numbers. These studies would ultimately be useful to suggest the effective compression ratio for different octane rating fuels getting tested in the same engine. The small size HONDA engine, fitted with the new VCR mechanism, has been opted for the proposed experiments with petrol and kerosene fuels. As an outcome of the present experiments, optimum compression ratio for the petrol is noted to be 5.02. Similarly, for the experiments with kerosene, it is found that the compression ratio, 5.27, is more economical than the commercially provided fixed compression ratio (4.8).

5.1 NOVEL VCR RESULTS USING HONDA ENGINE

The Honda engine set up as shown in Fig.3.2 has fixed CR. In order to consume fuels other than petrol such as kerosene in the engine, the properties of fuel becomes important. Based on which it could be analyzed that the engine performs well for the alternative fuel. However, some properties such as lower heating value, auto ignition temperature of fuel are deciding parameters of performance of the engine for the given fuel. The working conditions referred here are fixed for ignition timing, air-fuel ratio and spark plug location under variable load and speed conditions. So the attempt has been made to develop the continuously varying compression ratio top up mechanism (as depicted in chapter 4) to find an optimum CR. Thus objective of this top up mechanism is to optimize the compression ratio of engine to a minute level so that the particular fuel burned in the engine can produce maximum power with lower fuel consumption. To explore the top up mechanism, trials are performed on Honda engine set up as demonstrated in chapter 4. The performance of the engine is evaluated on petrol and kerosene as per the guidelines of Bureau of Indian Standards (IS10000, 1980). The performance parameters (i.e. power, brake specific fuel consumption and brake thermal efficiency) are evaluated according to the experimental matrix Table 5.1 against speed for different compression ratios with the VCR mechanism at fixed throttle position of 52% WOT.

The throttle position has been chosen for the reason of maximum on-road vehicles that are run between 30-60% throttle for best performance and most economic fuel consumption (Sridhar et al., 2001; Yang et al.,2011).The brake power (BP)can be evaluated using the rope brake dynamometer. The brake specific fuel consumption $(BSFC)$has been calculated after measuring the fuel consumed for a particular test. Finally, the brake thermal efficiency (BTE)

Table 5.1 The experimental matrix for fixed CR engine

Engine set up	Throttle position (%)	Fuel	Compression Ratio				
			Original Engine Head	Modified Engine Head with Novel VCR mechanism			
HONDA Engine	52	Petrol	4.8	4.8	5.02	5.4	
				4.9	5.27		
	52	Kerosene	4.8	4.8	4.9	5.27	5.4

of the engine for different loads is being calculated with the knowledge of heating value of the fuel. All the relevant expressions are given in APPENDIX-C

5.1.1 Effect of speed for original engine

The baseline tests are initially performed on the engine at original compression ratio of 4.8 defined by manufacturer of the engine with petrol and kerosene as fuel (Fig. 5.1) at predefined ignition timing settings. These tests are essential to understand the change in engine output parameters owing to proposed modifications in the engine for VCR attachment. Referring to Fig. 5.1(a),for designed compression ratio and given fuel, engine torque is found to be decreasing with increase in speed which is the line of argument with literature (Pulkrabek,2003).

For petrol, when engine is running at throttle position 52% WOT, the maximum torque recorded is 1.58 N-m at speed 1953 rpm whereas the minimum torque obtained is 0.28 N-m at 2191 rpm. The same trend has been noted for kerosene as shown in Fig. 5.1(b). As brake torque is a function of brake load only and with increase in load on the engine the magnitude of torque increases with reduction of speed. Therefore, brake power also varies with the speed in the same way as that of the torque with increase in speed for both the fuels (Fig.5.1-a & Fig.5.1-b).This observation is consistent with the fact that brake power is directly dependent on the torque and speed hence with increase in speed, proportionate decrease of torque take place with overall reduction in power. The variation in torque and power is fuel dependent but the trend has been found to be same for petrol and kerosene. For petrol, the maximum power is obtained as 324 W at 1953 rpm while the minimum power is 64 W at 2191 rpm (Fig.5.1-a). The maximum power recorded for kerosene is 310 W at 2072 rpm lowered to 26 W at 2155 rpm(Fig.5.1-b).

At the fixed compression ratio for a given fuel, the brake thermal efficiency decreases with increase in speed (Fig.5.1-c) and (Fig.5.1-d). At higher engine speeds, more friction losses

are expected and thus, BTE decreases while BSFC increases. This observation is consistent with the literature findings (Sayin et al., 2005). For petrol fuel, the maximum BTE is recorded as 8.3% at 1953 rpm and at the same speed, minimum brake specific fuel consumption of 0.275 kg/kW-hr is logged (Fig.5.1-c). Similarly for kerosene fuel, the maximum BTE is measured as 9 % at 2072 rpm and at the same speed, minimum brake specific fuel consumption of 0.254 kg/kW-hr is noted (Fig.5.1-d).

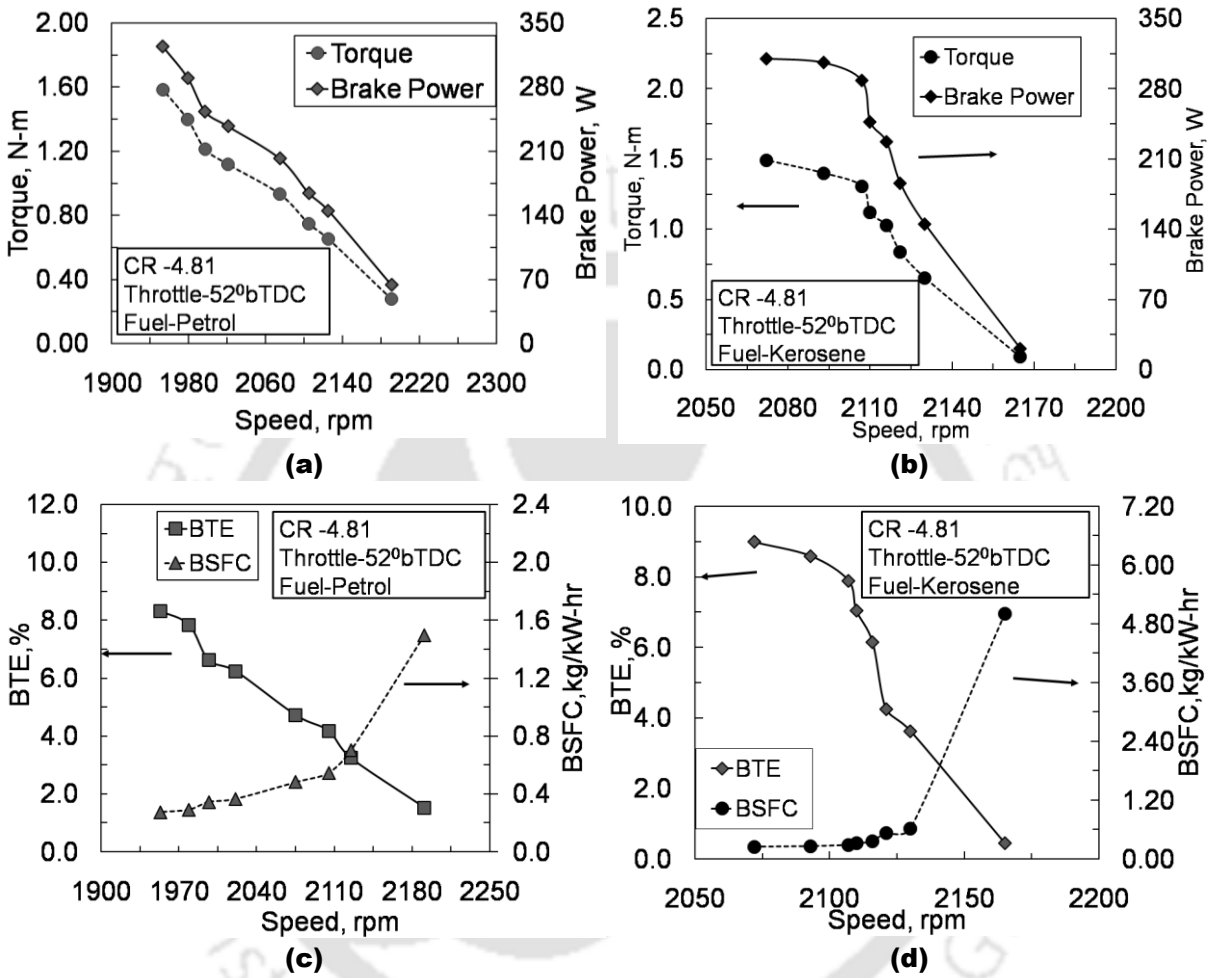

Fig. 5.1 Variation of engine performance parameters with speed with original compression ratio.

5.1.2 Effect of speed on performance parameters with novel VCR mechanism

It is well acknowledged fact that an internal combustion engine can operate at the highest possible CR for attaining the highest overall efficiencies. But, the gain in efficiency beyond a certain CR can be expected to be marginal due to other influencing factors such as heat loss and friction (Martyn, 2002). It has been experimentally investigated that upper limit of compression ratio for SI engine is very specific to a particular engine for which there is fall in efficiency after certain CR for iso-octane fuels (Sridhar et al.,2001). This particular information is evident with this VCR mechanism about the chosen engine. The comparison of engine parameters between original engine and the modified engine attached with the new VCR mechanism at no load condition, compression ratio of 4.8 and fixed throttle position of 52% are given in Table-5.2. For both fuels, it is found that the brake power of the modified engine is same as that of the original engine. However, increment of 1.3% and 9.7 % has been observed in the brake thermal efficiency (BTE) for petrol and kerosene respectively,

with the engine modifications. Similarly, the brake specific fuel consumption (BSFC) for petrol and kerosene with the incurred changes to accommodate the VCR mechanism showed slight decrement of 1.1 % and 9.5%, respectively. The reason for this disparity is the uncertainty in measurement and subsequent machining of the modified engine head. Studies are extended with the base engine setting along with VCR attachment to analyze the engine performance for change in engine speed. Further, the presently designed VCR mechanism has been tested for different compression ratios with minute increment above the original compression ratio (CR) of 4.8. In these experiments, fuel being used is petrol having research Octane number 91 (RON-91) and kerosene (RON-75).

Table 5.2. Performance parameters of the engine with modified cylinder head at no load condition

Fuel	Performance parameter	Original head	New head with VCR mechanism	Deviation (%)
Gasoline	Torque (N-m)	0.28	0.28	0
	Brake power (W)	64	64	0
	BTE (%)	1.52	1.54	1.32
	BSFC(kg/kWhr)	1.5	1.48	1.07
	Fuel consumption (cc/sec)	0.037	0.036	2.77
Kerosene	Torque (N-m)	0.093	0.093	0
	Brake power (W)	21	21	0
	BTE (%)	0.44	0.48	9.7
	BSFC(kg/kWhr)	5.01	4.53	9.54
	Fuel consumption (cc/sec)	0.038	0.034	10

The variations of engine performance parameters with speed (or load) are plotted in Figs. 5.2 and 5.3. During testing, the engine has been set at 52% wide open throttle (WOT) position. At this throttle position, for the knock limited speed of engine (obtained by applying maximum possible load), the data for net brake force, fuel consumption, air consumption, speed have been recorded and the corresponding trends are plotted (Figs. 5.2 and 5.3). In the successive investigations, the set of data has been collected with constant increment of 100 rpm in speed above knock limited speed against release of load on the brake load dynamometer.The torque variation with speed of engine is as shown in Fig. 5.2- a & Fig.5.2-b for various compression ratios with both fuels. The trend of the torque-speed variation is same for all compression ratios as it is the case for the base line tests (Fig. 5.1-a & Fig. 5.1-b). In these figures, torque is found to be reduced with increase in speed (Erkus et al.,2013)at a particular CR. However for a given speed, torque increases initially with increase in compression ratio and then decreases. This limiting CR is 5.02 for the engine speed of 2092 rpm in case of petrol. . If CR increases further to 5.27 then the secondary piston displacement is 4mm inside cylinder. This causes the spark location shifted to 4 mm inside combustion chamber. In this situation, when fuel gets ignited, the flame kernel developed takes more time to spread inside combustion chamber causing combustion delay and accordingly reduced power at output. That is the reason for the fact that the CR can not be further increased beyond 5.02 using novel VCR mechanism.

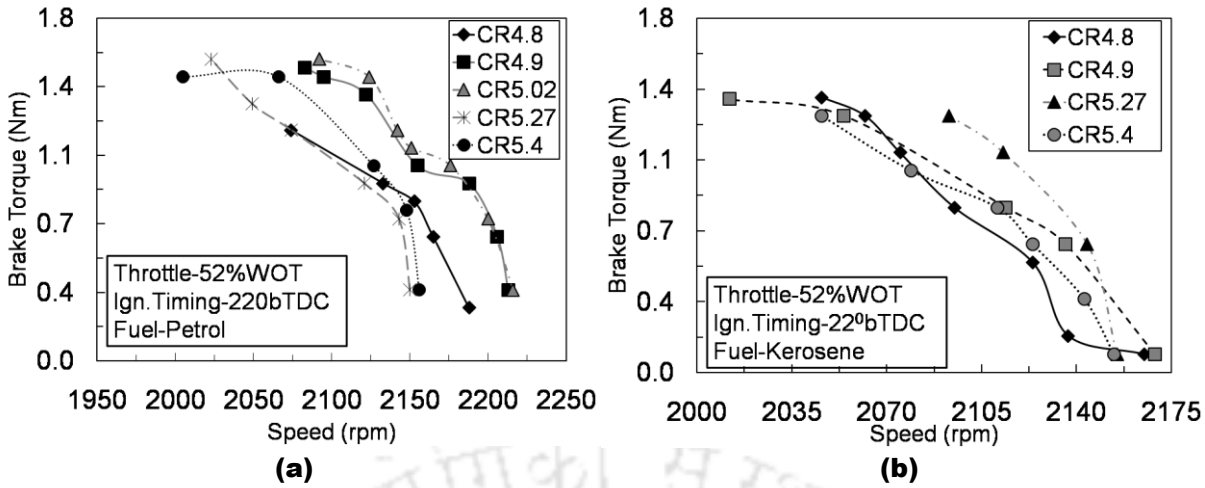

Fig. 5.2: Variation of brake torque with modified head and VCR mechanism for petrol and kerosene

This observation hints for the presence of an optimum CR producing maximum torque at that speed. The maximum torque at CR 5.02 for gasoline is 18% higher than the torque at default CR of 4.8 (Fig.5.2-a). It may be worth noting that the increase in CR increases friction of the engine particularly between piston ring and cylinder wall of engine. So, there is a point at which further rise in compression ratio would not be profitable. This optimum CR is 5.27 for kerosene fuel as evident from Fig. 5.2(b). This observation is consistent with the fact that the lower heating value for kerosene is lower than that of gasoline which in turn hints for the higher optimum CR for kerosene.

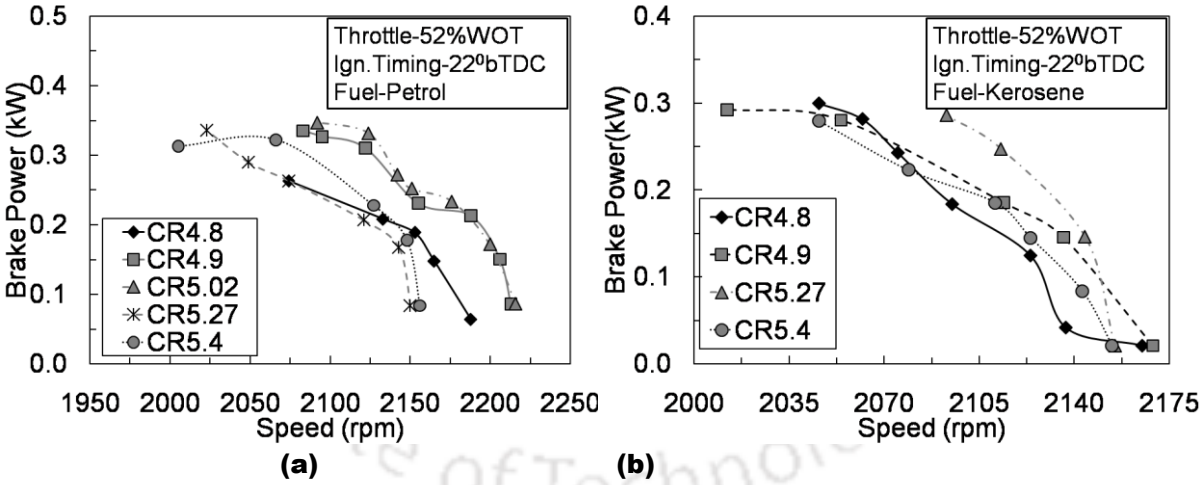

Fig. 5.3: Variation of brake power with modified head and VCR mechanism for petrol and kerosene.

The brake power variation with speed is shown in (Fig. 5.3-a & Fig.5.3-b) for various compression ratios starting from original CR of 4.8 to 5.4 for both fuels. As seen in figure, the brake power for a compression ratio increases initially up to certain speed and then decreases with further increase in speed for both the fuels. This trend has already been encountered in the baseline tests of these fuels. With the present VCR mechanism, at speed of 2124 rpm the brake power at CR 5.02 for petrol fuel is 12.08% higher than that of the brake power corresponding to CR 4.8 and same speed (Fig.5.3-b). With the increase in compression ratio, the cylinder pressure increases and in turn the brake mean effective pressure (BMEP) increases for the given valve opening and spark timing. The expected value of maximum

BMEP is corresponding to optimum condition of petrol is 0.69 bar. Thus, increased BMEP for a given swept volume enhances the efficiency of the engine. This justification is in well agreement with observation of literature reported findings from (Huang and Crookes,1998).Moreover, the power obtained for the compression ratios above the optimum CR of petrol is lower than the base value. The brake power with kerosene as fuel is found maximum at the CR of 5.27 and the percentage increment of 35.67% has been recorded over CR4.8 at speed 2095 rpm (Fig. 5.3-b). This observation is in line with the conclusion from the torque-speed plot for kerosene (Fig. 5.1-b). The reason for lower power with kerosene may be related to its density which is more than that of petrol. Therefore, higher compression ratio over optimum CR 5.27 adds more volume of fuel in to the cylinder which in turn increases the ignition time and results in the reduced power output (Dagaut and Michel,2006).

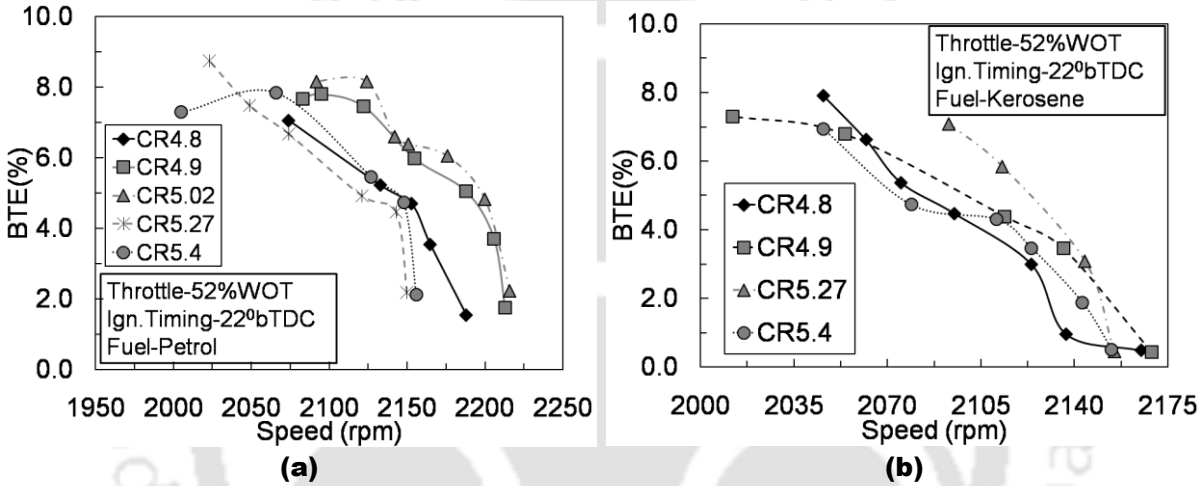

Fig. 5.4: Variation of BTE with modified head and VCR mechanism for petrol and kerosene.

Thus, power output for kerosene gets reduced by 22% in the phase of further rise in compression ratio from 5.27 to 5.4.There is considerable change in brake thermal efficiency (BTE) with the compression ratio(Huang and Crookes,1998)and speed for petrol and kerosene (Fig. 5.4-a & Fig.5.4-b). For any choice of the fuel, BTE is found to be decreased with increase in speed at a particular speed condition. The maximum BTE for petrol is noted at CR 5.02 and it is 19% higher that the BTE of original CR of 4.8 (Fig.5.4-a). This is because of the fact that the increased compression ratio reduces the clearance volume and therefore increases the density of cylinder gases during burning. In turn, the peak pressure, temperatures are increased, thereby reducing the total combustion duration and ignition lag (Abdel and Osman,1997). Hence, the earlier observed optimum CR for gasoline retains its place from the analysis of efficiency as well. For kerosene also, the optimum CR from the perspective of efficiency is 5.27 from the Fig. 5.4-b. In this case, the maximum efficiency is noted to be 7.08% which is about 37% higher than the efficiency corresponding to normal compression ratio of 4.8. The brake specific fuel consumption (BSFC) is plotted for both the fuels (Fig. 5.5-a & Fig.5.5-b). The variation of BSFC with speed is same in either case and follows the same trend as that of the baseline test for a given compression ratio. It has been seen that the BSFC increases with increasing speed of the engine for the particular CR(Chandra et al., 2011).

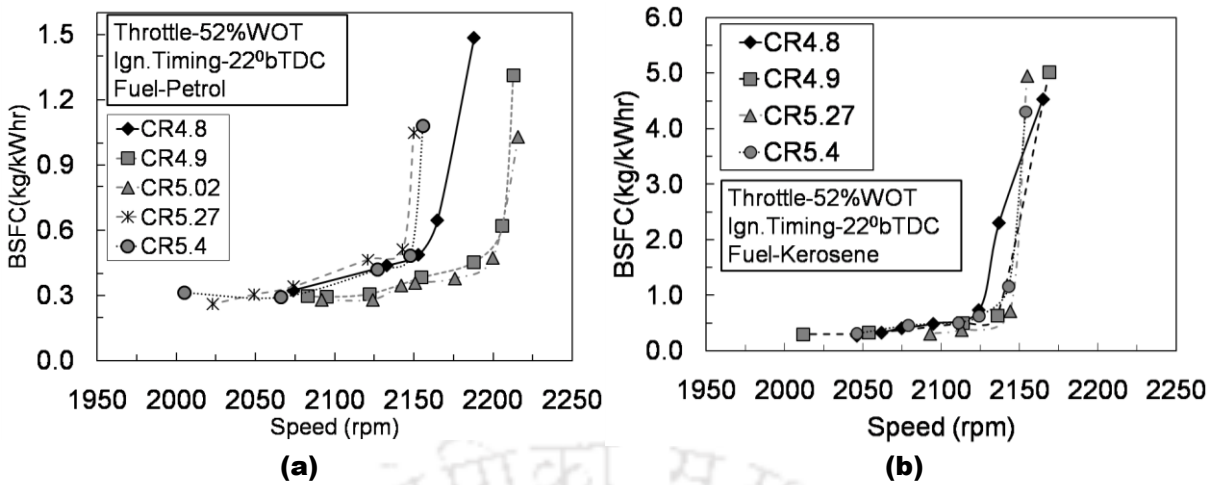

Fig. 5.5: Variation of BSFC with modified head and VCR mechanism for petrol and kerosene.

The heat loss to combustion chamber wall is proportionately greater and combustion efficiency is poor at high speed. Along with this, the friction power increases at a rapid rate with speed, resulting in slower increase in brake power which increases the fuel consumption (Abdel and Osman,1997)**.** Apart from this fact, BSFC for a particular speed decreases with increase in compression ratio for petrol till CR equals to 5.02. At this CR, BSFC of petrol is found to be 17.64% lower with that of CR 4.8 (Fig.5.5-a). However, increase in CR, above the optimum one, tends to increase the BSFC substantially. Similarly for kerosene (Fig.5.5-b) also there is 37% decrement in BSFC when engine run at optimum CR 5.27 with that of CR 4.8. These inferences are aligned with the observations drawn from the efficiency plot. As shown in Fig.5.5a, the increasing trend is low upto 2150 rpm for CR4.9 as well CR5.02. But after 2150 rpm the BSFC shows increment with greater slope. The CR4.9 and CR5.02 could be achieved by 1 mm and 2 mm displacement of secondary piston inside combustion chamber respectively. With increase in CR, the cylinder pressure increases causing more homogeneous and complete combustion of charge. Therefore, BSFC for CR5.02 is found lower than that of CR4.9 over a speed range.

5.2 SUMMARY

A novel VCR mechanism has been successfully designed, developed, fabricated and installed in the HONDA engine. This mechanism is found an appropriate and viable alternative among the present available ones, mainly due to possibility of change in compression ratio in the running condition of the engine. Two fuels viz. petrol and kerosene are used during the experiments for torque and power measurement in a specially designed experimental set-up. Optimum compression ratio is noted to be 5.02 for petrol and 5.27 for kerosene. These compression ratios are consistent with their octane rating and heating values. Thus, it has been revealed that the commercial engine used to operate at lower performance for petrol as well as kerosene fuel without the variable compression mechanism attachment. Therefore, possibility of performance enhancement of the engine for a fuel by altering the compression ratio and also accommodation of different fuels in the same engine have been demonstrated from current investigations. Similar optimum engine operating conditions can be obtained for fuels other than those mentioned here such as gaseous fuel LPG or even some renewable gaseous fuels like biogas with this novel VCR mechanism.

CHAPTER 6

Studies with Alternative SI Engine Fuels

OVERVIEW

The primary objective of the thesis is to understand the performance of petrol engine when it is supplied with alternative gaseous fuels. Possibility of change in compression ratio, ignition timing and exhaust gas recirculation rate are assessed in this chapter while experimenting with the APEX engine and its conventional VCR mechanism. This engine is tested with biogas and LPG fuels separately and the speed is maintained in the range of1200-1740 rpm for the rated power output of 4.5 kW. All the observations from the experiments with either fuel are segregated in three parts viz. performance analysis, combustion analysis and exhaust gas emission analysis. In order to overcome the NO_x emissions, technique of intake charge dilution or exhaust gas recirculation is introduced from low (10%) to very heavy(40%) rates in case of LPG fuel combustion. The raw biogas is a poor heating value fuel therefore EGR rate is varied from 10% to 25%. As an outcome of the experiments for LPG fuel, optimum ignition time is noted to be 26^0bTDC for CR10 while the same for bio-gas is 45^0bTDCfor CR10. Although higher EGR rates indicated higher reduction in NO_x, present studies recommend use of 10% EGR for both the fuels for better economy.

6.1 INTRODUCTION

The applications of gaseous fuels as a substitute for octane petrol fuel has been widely studied by different researchers(Sridhar et al., 2001, Choi et al., 2003, Gumus, 2011).These gaseous fuels includes LPG, methane, syngas, natural gas, simulated biogas, power gas(ozcan and Jehad, 2008; Crookes, 2006;Subrahmanyam et al., 2001). Those gaseous fuels listed above are mostly non renewable but some are renewable. Combustion of those gases in pure form as well as adulterating with some high heating value gaseous fuels such as H_2 are also analyzed by different authors (Porpatham et al., 2006, Park et al., 2011,Hu et al., 2009). As the gaseous fuels have higher octane rating, there is need of higher compression ratio than that for petrol engine. But higher compression ratio has structural limitations in engine. So the gaseous fuels such as LPG and raw biogas should be treated specially so as to get improved efficiency and superiority over petrol fuel.

The review of literature on LPG as well as raw biogas run petrol engine confirms that, the performance, combustion and emission characteristics of LPG and raw biogas run engine under variable compression ratio and ignition timing is not clearly demonstrated. Hence this chapter explores the petrol engine run with LPG as well as raw biogas fuel for a range of

compression ratio and ignition timing. Thus it is dedicated to optimization of engine parameters for fuels other than petrol.

Sophisticated Apex engine test rig is considered for experiments with LPG and raw biogas as detailed in chapter 3. The LPG fuel is tested with compression ratio 8, 9 and 10 with different ignition timings from 24 ^{0}, 26 ^{0}, 28 ^{0},33 ^{0},38 ^{0},43 ^{0} and 46 ^{0} bTDC. The combinations of CR and IT are prepared to check the optimum combination. The variations of load are performed such that the speed varies in range from 1200 rpm to1740 rpm. The optimum petrol fuel run engine specification is at CR10 and IT at 28 ^{0} bTDC and used as a baseline data for testing of gaseous fuels LPG and raw biogas (chaudhari et al., 2015).Experiments are also conducted with 100% raw biogas fuel in the same test rig for optimum spark timing; different CRs at wide open throttle position. The range of CR 8 to CR10 is used which is the optimum range for petrol fuel. Biogas is a non-conventional fuel, but in present studies, it is burnt in the conventional petrol based spark ignition engine. Moreover, combustion of raw biogas is different than that of petrol fuel in spark ignition engine due to difference in their compositions and heating values. Calorific value of raw biogas fuel is very poor as compared to petrol (Ibrahim and Bari,2009; Porpatham,2007, Borah,2015). So, in order to initiate combustion, it is important to create spark in advance by certain crank angle before the compression stroke completes. Therefore, experiments are performed to arrive at an optimum spark timing or maximum brake torque (MBT) timing for different compression ratios (CRs). These set of experiments are carried out at constant engine speed of 1429 rpm for different spark advances viz. 37 ^{0}(323 ^{0} CA), 39 ^{0}(321^0 CA), 41 ^{0}(319 ^{0} CA), 43 ^{0}(317 ^{0} CA), 45 ^{0}(315 ^{0} CA) and 47 ^{0}(313 ^{0} C A) before top dead center (bTDC).

The performance analyses evaluated are brake thermal efficiency (BTE) and brake specific fuel consumption (BSFC). The combustion analyses includes the cylinder pressure variation, peak cylinder pressure (PCP), net heat release rate (NHRR), mass fraction burned (MFB) and mean gas temperature (MGT). All the experiments are performed within 20 ± 3^0 C and atmospheric pressure conditions. The theoretical equations, based on which performance and combustion analysis are used for further estimation and they are included in Appendix-C.

6.2 GASEOUS FUEL OPTIMUM SPARK TIMING ANALYSIS

6.2.1 Performance analysis

The Apex made variable compression ratio spark ignition engine is working with tilting block technique for varying the compression ratio of the engine (chapter 3). This set up undergoes variety of fuels starting from petrol to gaseous fuels like LPG and raw biogas. So during the course of time, the results are plotted for all the above listed fuels under different parameters such as variable compression ratio, variable throttle position, variable ignition timing and variable EGR rate.

6.2.1.1 Effect of ignition timing

It is known that the brake torque is influenced to a great extent with the variation of spark timing for the particular fuel. The effect of spark timing on the LPG fueled spark ignition

engine is as plotted in Fig. 6.1.From the Fig. 6.1 (a) the variation of brake torque with spark timing is shown for varying compression ratio and at constant speed 1430 rpm.

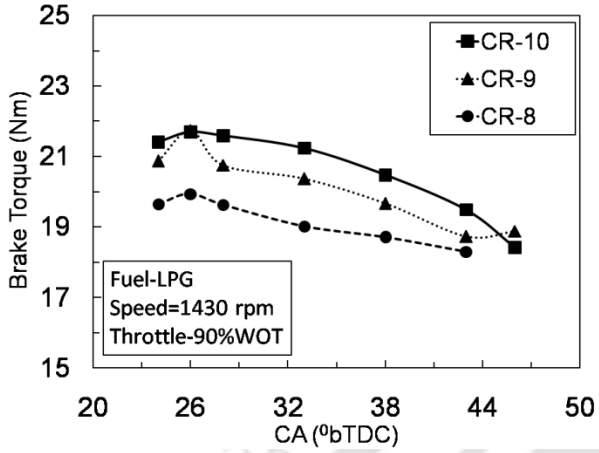

Fig.6.1(a) Brake torque variation with spark timing for LPG fuel

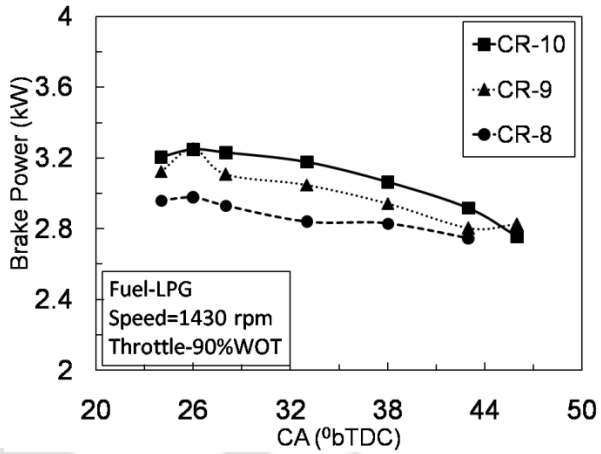

Fig.6.1(b) Brake power variation with spark timing for LPG fuel

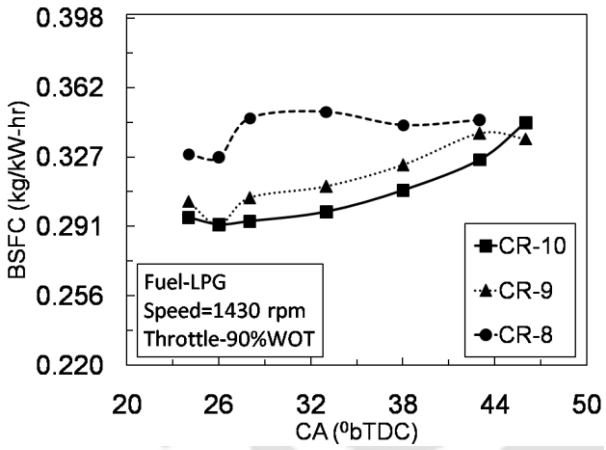

Fig.6.1(c) Brake specific fuel consumption variation with spark timing for LPG fuel

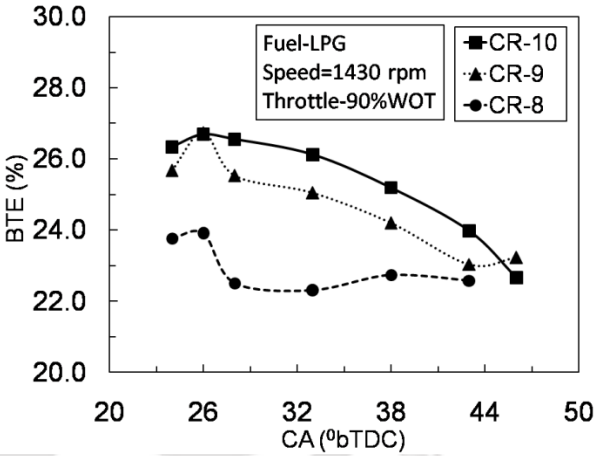

Fig.6.1(d) BTE variation with spark timing for LPG fuel

The brake torque increases initially with 1.33% increment from 24 ^{0} bTDC and continues up to 26 ^{0} bTDC. But thereafter the same is found to be reduced with an decrement of 0.5%, 2.12%, 5.6%, 10.16% and 15.09% at 28 ^{0}, 33 ^{0}, 38 ^{0}, 43 ^{0} and 46 ^{0} bTDC respectively. This reflects the spark timing 26 ^{0} bTDC (334 ^{0} CA) is the optimum spark advance attaining the maximum brake torque. The brake torque in turn influences the brake power which also shows the increment from 24^{0}to 26^{0}bTDC by 1.3%. After 26^{0}bTDC, there is decrement in power for the ignition timings considered as shown in Fig. 6.1(b). As the calorific value of the fuel is higher than that of petrol, the ignition timing is seen to be retarded and comes very close to the TDC. Also the gas needs less time to get ignited as compared to that of petrol fuel where the first phase of ignition is from liquid to vapor and thereafter to the gas. So this transformation needs the spark timing to be advanced with respect to TDC (Bayraktar and Durgun, 2005).

The optimized spark timing achieving maximum brake power could be a cause of rise in BTE. This BTE variation with spark timing is as plotted in Fig. 6.1 (d). Higher BTE of 26.7%

for 26^0bTDC is the outcome of complete combustion of fuel air charge with maximum utilization of power (expansion) stroke at CR10 (Bayraktar and Durgun, 2005).The BSFC variation as shown in Fig. 6.1(c) which is the ratio of mass of fuel burnt to the brake power of the engine found to be decreasing at rate of 1.35% initially up to 26 ^{0} bTDC. But there after it is found increased at rate of 0.68%, 2.39%, 5.80%, 10.42%, 15.30% respectively with 28 ^{0} , 33 ^{0} , 38 ^{0} ,43 ^{0} and 46 ^{0} bTDC crank angle at CR10. If the mass flow rate of fuel remains constant and the spark timing is optimized then higher brake power may be obtained so as to reduce BSFC.

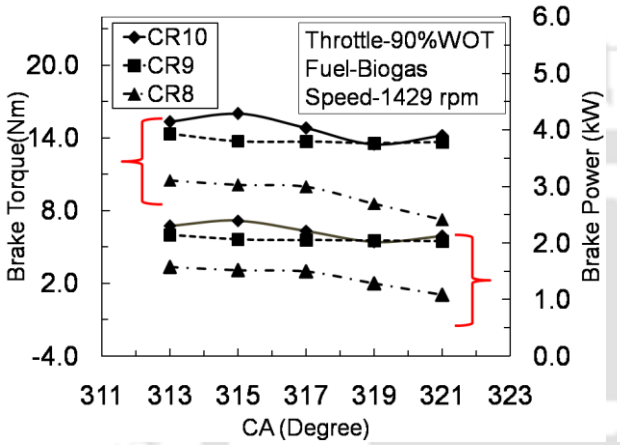

Fig.6.2(a) Brake torque and power variation with spark timing for raw biogas fuel

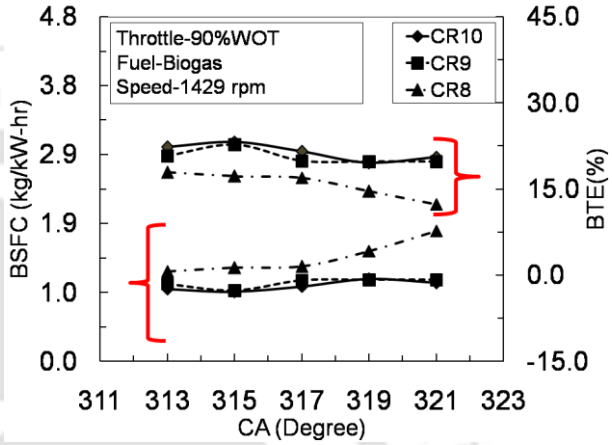

Fig.6.2(b) BSFC and BTE variation with spark timing for raw biogas fuel

As seen in Fig. 6.2(a), brake torque of 16.0 Nm as well as brake power of 2.4 kW are obtained at 45 ^{0} bTDC for CR10 using 100% raw biogas, which seems to be maximum in all ignition timing considered herein. However at other spark timings, there is decrement in brake torque by 4.11%, 7.43%, 15.74% and 11.37% for 47 ^{0}, 43 ^{0},41 ^{0},39 ^{0} bTDC crank angle respectively. As an effect of this, BTE is found to be increased to 23.258% with substantial reduction in the BSFC to 0.968 kg/kW-hr as seen in Fig. 6.2 (b) for CR10 at 45^0 bTDC. In the similar way at other spark timings, the decrement in BTE is reported to be 4.11%, 8%, 16% and 11% for 47 ^{0},43 ^{0},41 ^{0} and 39 ^{0} bTDC respectively. The crank angle for the previously tested LPG fuel is 26 ^{0} bTDC where as for raw biogas the same is advanced to 45^0 bTDC. This has happened due to the fuel heating value intern quality of the fuel. As the raw biogas composed of 52% methane and rest are carbon dioxide and allied gases which are non combustible. This makes the raw biogas to be a very poor fuel in terms of its calorific value by 65% lower than LPG (Park et al., 2011). In addition to this, the auto ignition temperature of the raw biogas is much higher than that of LPG fuel which forces to advance the ignition timing while using raw biogas in the engine (Chandra et al., 2011).

6.2.1.2 Effect of compression ratio

With the variation of compression ratio, there is effect on performance parameters such as brake torque and power for each fuel considered here. The variation of torque with CR at 26^0bTDC shows (Fig. 6.2-a) that the torque increment of 8.06% and 1% could be achieved when CR increases from 8 to 9 and further upto 10. The brake power as well shows increment of 7% and 2% with rising CR from 8 to 9 upto10. The BTE variation with spark

advance resemblances the close relationship with that of brake power variations. With the increment of CR, the BTE is found to be increased (Fig. 6.2-d). At Spark advance of 26^0 bTDC, the BTE increment is 8.07% and 3% respectively for rise in CR8 to CR10. This shows that at optimum spark timing, the increase in CR attains the higher efficiency. The BTE of 23.26% at CR8 is the outcome of this study. With increase in CR, the cylinder pressure increases which cause the homogeneous combustion of charge and in turn generate more heat which gets converted in useful work.

At 26^0 bTDC using LPG fuel, the brake torque is 19.95, 21.70 and 21.74 Nm whereas at 43^0 bTDC, torque is 18.31, 18.73 and 19.50 Nm respectively at CR8, 9 and 10 as shown in Fig. 6.1-a. This reflects the optimum spark timing 26^0 bTDC remains constant for all CR 8, CR9 and CR10 attaining maximum torque (Ozcan and Jehad, 2008). In terms of brake power (Fig. 6.1- b), the LPG fuel power is 2.98, 3.20 and 3.25 kW whereas with increase in spark advance at 43^0 bTDC, it is 2.75, 2.80 and 2.91 kW respectively for CR8, CR9 and CR10 at speed 1430 rpm. This shows increment of 7.71 %,12.5 % and 10.46 % in brake power when engine is running at MBT timing. At 26^0 bTDC, the BTE can be found to be 23.9 %, 26.0 %, 26.7 % whereas with spark advance in rising order at 43^0 bTDC, the BTE is 22.58 %, 23.0%, 23.9% respectively at CR8, CR9 and CR10 as reflected in Fig. 6.1- c. This makes 26^0 bTDC is the MBT timing for maximum efficiency achieving increment of 5.52%, 11.53% and 10.78% respectively for CR8, CR9 and CR10. At 26^0 bTDC, the decrement of 5.22%, 13.60% and 11.04% in BSFC with change in spark timing from 43^0 bTDC to 26^0 bTDC at CR8, CR9 and CR10 respectively for the engine running at speed 1430 rpm and at stoichiometric air fuel ratio.

The raw biogas when burned in spark ignition engine, the compression ratio is vital to attain the maximum efficiency from the fuel. So the effect of compression ratio variation with spark timing on performance parameters are as displayed in Fig. 6.2(a & b). The brake torque (Fig. 6.2-a) at 45^0 bTDC shows increment of 26% and 14% respectively from CR 8 to 9 and further to 10. The brake power (Fig. 6.2-a) is 1.52 kW, 2.07 kW and 2.4 kW showing increment of 26% and 14% from CR8 to CR9 till CR10 respectively.

The effect of higher torque and power at 45^0 bTDC ultimately attains the increment in BTE (Fig. 6.2-b) by 17.26%, 22.77% and 23.25% respectively at CR8 to CR9 upto CR10 when running at 1430 rpm. This is because with higher CR, pressure inside the combustion chamber increases causing the proper mixing of fuel air charge. This intern increases the flame speed and initiates the combustion faster. Due to reduce time of combustion, the heat released in short time gets converted in to work. The BSFC (Fig. 6.2-b) with increase in CR is found to be decreased at particular ignition timing. At 45^0 bTDC, the BSFC recorded is 1.304 kg/kW-hr, 0.988 kg/kW-hr and 0.968 kg/kW-hr showing the decrement from CR 8 to CR9 and further to CR10. With the rise in CR the brake power increases as discussed before for the particular speed 1430 rpm and if the mass of fuel supplied remains constant then there will be decrement in BSFC. That is how the raw biogas fuel in spark ignition engine obtains the maximum power at CR10 and so the lowest BSFC.

The brake torque using raw biogas fuel at 45 ^{0} bTDC optimum spark timing is 10.15 Nm, 13.76 Nm and 16.01 Nm where as at 43 ^{0} bTDC the same is 9.99 Nm, 13.717 Nm and 14.818 Nm for CR8, CR9 and CR10 respectively. With the adjustment of spark at optimum location, there is increment of 1.52%, 0.3% and 7.43% respectively at CR8, CR9 and CR10. The similar trend is followed for the ignition timings considered here with respect to optimum findings. The brake power shows increment of 1.32%, 0.5% and 7.46% for CR8, CR9 and CR10 respectively. The BTE for raw biogas is maximum at 45 ^{0} bTDC by 1.53%, 12.51% and7.43% for all CR8, CR9 and CR10 respectively with respect to 43 ^{0} bTDC spark advance (Fig. 6.2-b). This intern shows the decrement of BSFC towards 45 ^{0} bTDC as compared to 43 ^{0} bTDC spark advance.

The performance analysis outcomes are more supported with the corresponding combustion analysis where the fuel air charge combustion behavior has been studied.

6.2.2 Combustion Analysis

6.2.2.1 Effect of ignition timing

Combustion analysis is important for attaining the optimum spark timing for the LPG and raw biogas fuels. These outcomes will closely justify the performance parameters reveled in the last section 6.2.

According to the performance analysis, 26 ^{0} bTDC and 45 ^{0} bTDC are the optimum spark advance for 100% LPG and raw biogas fuels. To backup those outcomes, the study of cylinder combustion pressure variation with crank angle for different spark advance at CR10 and speed 1430 rpm is as plotted in Fig. 6.3(a) for LPG fuel and in Fig. 6.4(a) for raw biogas. As shown in figure, the peak cylinder pressure is 29.61bar at 15 ^{0} aTDC, 34.16 bar at 7 ^{0} aTDC, 36.83 bar at 5 ^{0} aTDC, 38.39 bar at 1 ^{0} aTDC, 37.07 bar at 2 ^{0} bTDC for 24 ^{0},26 ^{0},28 ^{0}, 43 ^{0} and 46 ^{0} bTDC spark advance respectively when engine running at CR10 with speed 1430 rpm. It is seen that with advancing the spark timing, the peak pressure increases (Heywood,1988, Stone,1999). At the same time the crank angle at which peak pressure occurred also gets close to TDC. As the MBT timing for LPG fuel is 26 ^{0} bTDC, the peak pressure 34.16 bar is the optimum pressure at 7 ^{0} aTDC. The optimum timing of spark ultimately helps to generate more heat from the fuel which can be understood clearly from heat release analysis.

The Net Heat Release Rate (NHRR) which is the heat gets converted to work out of total heat or gross heat produced at the end of spark with crank angle. According to 1st law of thermodynamics, the NHRR analysis has been carried out as detailed in APPENDIX-C. NHRR for LPG fuel at CR10 and speed 1430 rpm is as shown in Fig. 6.3(b).The peak NHRR is observed for 26 ^{0} bTDC and its amount is 32.681 J/^{0}CA at crank angle 2^{0}bTDC as compared to other spark timings. With increase in spark timing bTDC, the peak NHRR keeps on shifting towards the left of TDC (bTDC) (Heywood, 1988, Stone, 1999). In case of 46 ^{0} bTDC, the peak NHRR is 25.47 J/^{0} CA occurred at 21 ^{0} bTDC. This causes the combustion pressure reaches at its peak close to TDC as shown in Fig. 6.2(a). The overall effect is the

loss of work during compression and reduced the conversion of heat energy in to useful work during expansion stroke. In regards to the maximum brake power, from the literature it was noticed that peak NHRR should be before TDC (Heywood, 1988; Taylor, 1999). The same is observed at 26 ^{0} bTDC where the brake power is also found more as shown in Fig. 6.1(b).

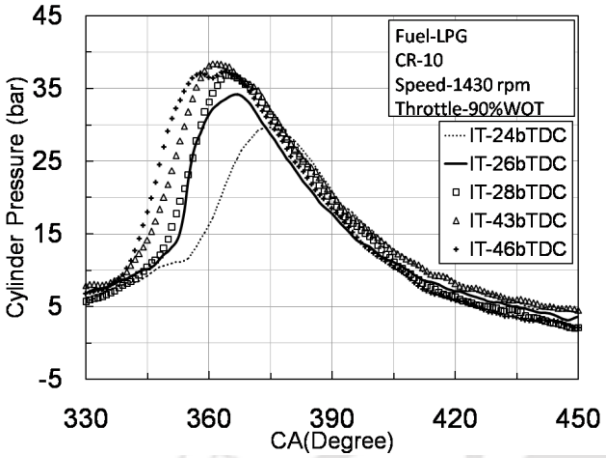

Fig.6.3(a) Cylinder Pressure variation with crank angle for spark timing using LPG fuel

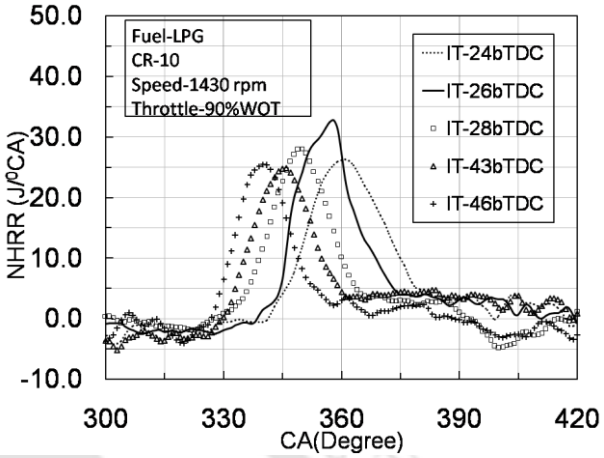

Fig.6.3(b) NHRR variation with crank angle for spark timing using LPG fuel

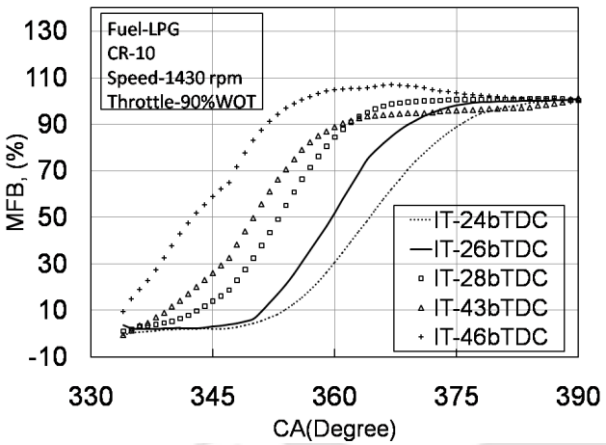

Fig.6.3(c) Percent MFB variation with crank angle for spark timing using LPG fuel

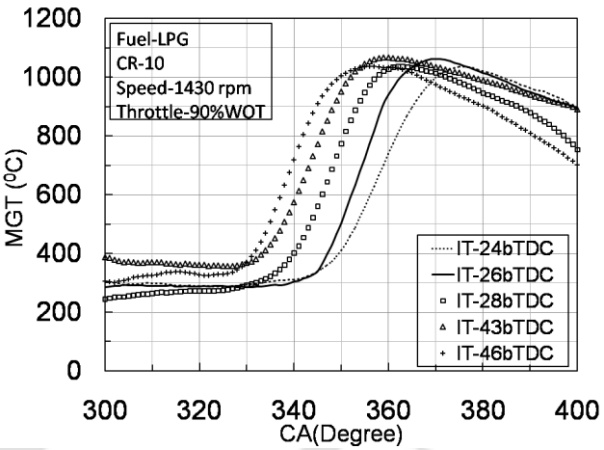

Fig.6.3(d) Mean Gas Temperature (MGT) variation with crank angle for spark timing using LPG fuel

Percentage mass fraction burned (MFB) is a ratio of actual mass burned to the theoretical mass burned which can be calculated by approach as discussed in APPENDIX-C (Stone,1999). Percent MFB as function of crank angle for CR10 and speed 1430 rpm is as shown in Fig. 6.2(c). Percent MFB at TDC is 30.37%, 51.90%, 84.50%, 93.68% and 100% for 24 ^{0}, 26 ^{0}, 28 ^{0}, 43 ^{0} and 46 ^{0} bTDC respectively. As the ignition timing advances to 46^0 bTDC, the combustion initiation gets advanced and that may be the reason, the MFB is 100% at TDC. However at optimum spark location 26^0 bTDC the MFB obtained was 62% at TDC. This shows that with advancing the ignition timing, the magnitude of percentage MFB represent higher consumption of charge. But the spark timings such as 46 ^{0} bTDC could not able to attain the maximum brake torque (Fig. 6.1-a). This means that the necessary compression stroke which generates the compression pressure is less for 46 ^{0} bTDC spark advance. This ultimately reduced the brake power. However for 26 ^{0} bTDC, the percent MFB is 51.90% at TDC which signifies that there should be maximum compression pressure required for combustion of fuel air charge to cause complete combustion. So the crank angle

of 26 ^{0} bTDC is the optimum ignition timing for the LPG fuel in this experimental test set up. The effect of rise in pressure of the engine at CR10 and speed 1430 rpm by different spark advance affects the mean gas temperature (MGT) of the combustion. MGT is the temperature after combustion of fuel air charge inside combustion chamber at the prevailing pressure and volume of chamber. Using the universal gas equation, MGT can be evaluated as explained in APPENDIX-C. This is found to be 1062.42^{0}C at 370 ^{0} CA when spark advance is 26 ^{0} bTDC. During combustion the optimum spark timing is of utmost importance for the flame development and propagation as well as length of flame travel across the combustion chamber and finally the flame termination after reaching the wall (Heywood,1988).The optimum spark location of 26 ^{0} bTDC is again justified in terms of MGT.

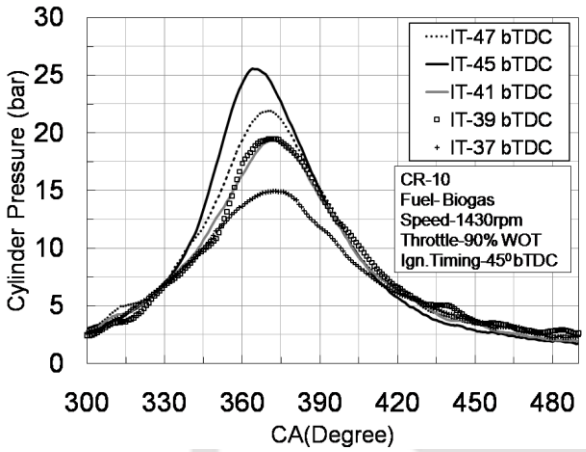

Fig.6.4 (a) Cylinder Pressure variation with crank angle for different spark timing using raw biogas fuel for different CR

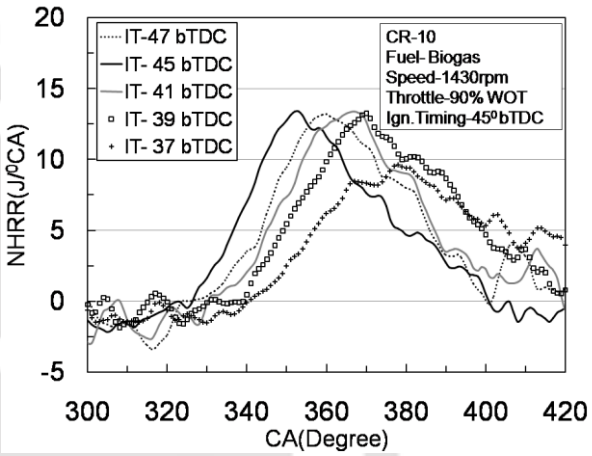

Fig.6.4 (b) NHRR variation with crank angle for different spark timing using raw biogas fuel for different CR

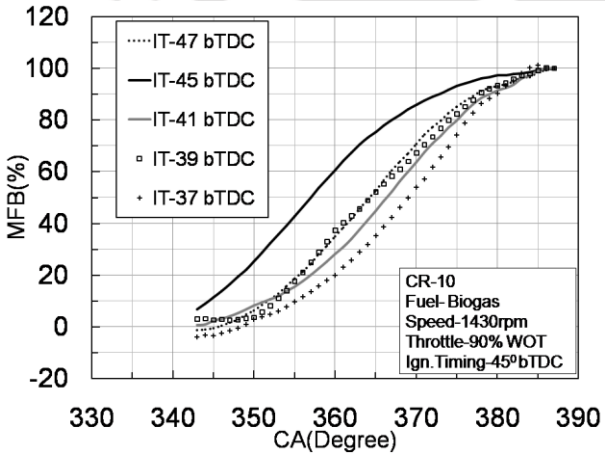

Fig.6.4 (c) Percent Mass Fraction Burned (MFB) variation with crank angle for different spark timing using raw biogas fuel for different CR

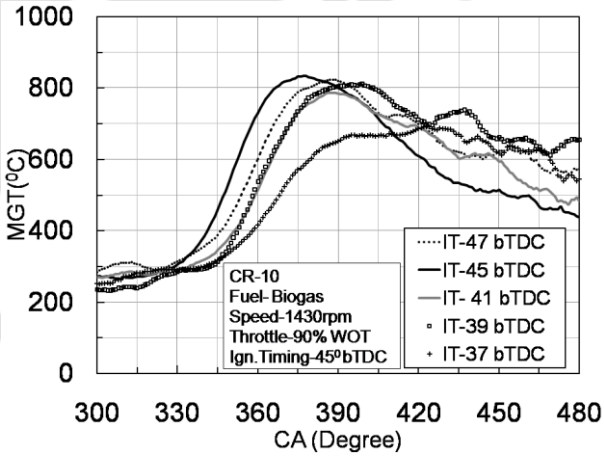

Fig.6.4 (d) Mean Gas Temperature(MGT) variation with crank angle for different spark timing using raw biogas fuel for different CR

6.2.2.2 Effect of compression ratio

With the very poor heating value fuel raw biogas, the optimum spark timing is 45 ^{0} bTDC. The cylinder pressure in case of raw biogas is 25.536 bar observed at4 ^{0} aTDC as represented in Fig. 6.4(a) while engine working at CR10 and speed 1430 rpm with 90% WOT. At the same time the peak cylinder pressure found to be reduced and keep on shifting away from TDC on right side (aTDC) with other spark locations such as 37 ^{0} bTDC, 39 ^{0} bTDC, 41 ^{0}

bTDC , 47 ^{0} bTDC. As the auto ignition temperature of 100% raw biogas is higher, it takes 49 ^{0} CA (angle from spark initiation to the peak pressure) to attain the peak pressure. However it is seen here that with respect to LPG fuel (Fig. 6.3-a), the peak pressure is lowered. There are numerous reasons for this but the major reason from combustion point of view is the reduction in effective compression stroke causing reduced pressure of charge before spark. This is seen clearly in Fig. 6.4(b) where NHRR variation with crank angle is shown for the spark timings considered using raw biogas fuel. Here the optimum spark timing is 45 ^{0} bTDC as NHRR is found to be 13.382 J/^{0} CA which is maximum and occurred at 7 ^{0} bTDC. An increment of 0.5%, 0.1%, 0.9% and 28% is observed with respect to 47 ^{0} bTDC, 41 ^{0} bTDC, 39 ^{0} bTDC, 37 ^{0} bTDC respectively while combustion takes place at optimum spark advance. The contents of raw biogas such as H_2S and water lower the heating value of fuel. In addition, whatever heat is produced is being absorbed by such ingredients lowering the NHRR further (Razbani, 2011).

The mass fraction burned for raw biogas fuel combustion is as plotted in Fig. 6.4(c) for different crank angles. The significance of MFB is the understanding about the speed of combustion inside combustion chamber. Accordingly, at TDC, the percent MFB is 64% at MBT spark timing and shows maximum charge gets burned. However it is seen that before TDC the speed of combustion is faster as compared to that during expansion stroke (aTDC). This is the reason that is why combustion duration is increased to 28 ^{0} CA. At other spark timings, the percent MFB is 23% to 40% and combustion extended till 19 ^{0} aTDC. At 45 ^{0} bTDC, the flame gets enough time to spread across the chamber so that homogeneous combustion may be happened. That is the reason NHRR shows peak value at 45 ^{0} bTDC (Fig. 6.4-b) as well.

Table 6.1 The experimental matrix for multifuels VCR engine

<table>
<tr><th></th><th>Throttle</th><th>EGR0</th><th>EGR10</th><th>EGR20</th><th>EGR30</th><th>EGR40</th></tr>
<tr><td colspan="7">Conventional VCR Mechanism Engine</td></tr>
<tr><td>LPG</td><td>WOT</td><td>CR8,CR9 and CR10 +Untreated EGR</td><td>CR8,CR9 and CR10 +Untreated EGR</td><td>CR8,CR9 and CR10 +Untreated EGR</td><td>CR8,CR9 and CR10 +Untreated EGR</td><td>CR8,CR9 and CR10 +Untreated EGR</td></tr>
<tr><td>LPG</td><td>WOT(IT)</td><td colspan="5">ALL CR (+5,+10,+15,+18,0,-2,-4)</td></tr>
<tr><td colspan="7">Conventional VCR Mechanism Engine</td></tr>
<tr><td rowspan="2">Biogas</td><td>WOT</td><td rowspan="2">CR8,CR9, CR10+Untreated EGR</td><td rowspan="2">CR8,CR9, CR10+Untreated EGR</td><td rowspan="2">CR8,CR9, CR10+Untreated EGR</td><td rowspan="2">CR8,CR9, CR10+Untreated EGR</td><td rowspan="2"></td></tr>
<tr><td>POT</td></tr>
<tr><td>Biogas</td><td>WOT(IT)</td><td colspan="4">ALL CR (+2,0,-2,-4,-6,-8,-10)</td><td></td></tr>
</table>

The mean gas temperature for the 100% raw biogas fuelled engine is as illustrated in Fig. 6.4(d). The MGT is 823 ^{0} C, 833 ^{0} C, 786 ^{0} C, 811 ^{0} C and 669 ^{0} C respectively at 47 ^{0} , 45 ^{0} , 41 ^{0}, 39 ^{0} and 37 ^{0} bTDC. At MBT timing, the MGT found maximum as compared to other spark advances

6.3 GASEOUS FUELS WITH AND WITHOUT EGR

Considering the optimized parameters (IT- 26 ^{0} bTDC spark advance) for using the LPG fuel in petrol based spark ignition (SI) engine, the effect of it in the SI engine on the performance and exhaust emission is experimentally studied. For this purpose, the tilting block technique (Larsen,1991) of varying the compression ratio from CR8 to CR10 of the engine has been implemented and attention has been paid towards the variation of performance and combustion parameters with LPG fuel. The range of CR selected is the optimum range for the petrol fuel in SI engine.

Most undesirable emissions are exhausted by the SI engines in which the primary pollutants from the engine (such as NOx) which when mixed in the atmosphere react with ozone and create the secondary green house gas which is more harmful to human health. Looking at this fact, while optimizing the compression ratio, the emission reduction technique like intake charge dilution with exhaust gas from the engine is studied. This intake charge dilution method is called Exhaust Gas Recirculation (EGR) Rate. The method of evaluation of percentage EGR rate is as depicted in APPENDIX-C. The percentage of EGR is varied from lower 10% to very heavy 40% scale of EGR Rate. In addition to this, EGR treatment methods are incorporated such as two-way catalytic conversion of EGR gas called as treated EGR and if the gas is not conditioned through catalytic converter, then referred as untreated gas.

6.3.1. LPG analysis without EGR

The experimental study has been performed in two parts. In first part VCR engine is run on 100% LPG fuel for base line test. The test is carried out at Wide Open Throttle (WOT) position which is 90% throttle valve opening. The load is varied from maximum to minimum in 0-12 kg range attaining the speed range of 1200 to 1700 rpm of the VCR engine with fixed increment of 50 rpm in speed. The air/fuel equivalence ratio is maintained at $(\lambda = 1 \pm 0.2)$ throughout the experiments. The spark timing set at Maximum Brake Torque (MBT) as discussed in section 6.2. MBT timing has been maintained constant for all the compositions of test using LPG fuel as listed in experiment matrix Table 6.1. The 'baseline test' is performed for setting the foundation for comparison of later experimental works. These tests here onwards called as EGR0 test means 0% EGR test. After completing the EGR0 test, the set of data for LPG fuel with EGR is recorded as EGR10, EGR20, EGR30 and EGR40 rate.

6.3.1.1 Performance Analysis

The experiments using LPG fuel are performed on the engine called as baseline tests. The performance parameters such as brake torque, brake power , BTE and BSFC are evaluated at 90% WOT and 50% WOT conditions.

(A) Effect of Compression ratio

Compression ratio variation effect on the brake torque using LPG gas is plotted in Fig. 6.5(a). It is seen that with the increase in compression ratio at speed 1430 rpm, the torque at CR8 is 19.95 Nm raises to 21.70 Nm at CR9 and further 21.74 Nm at CR10.This depicts the

increment of torque with rise in compression ratio. At speed 1430 rpm, the brake power is found increasing with increase in compression ratio from CR 8 to CR 9 further to CR10. The increment at maximum compression ratio is 8.25% with respect to CR8 at constant speed 1430 rpm. This is particularly happened due to decrement in volumetric efficiency (Erkus et al., 2013) for the gaseous fuel used which intern reduces the brake power.

The LPG gas has higher octane number rating and hence the higher limiting compression ratio. Owing to this, its performance is expected to enhance initially with increase in compression ratio. Compression ratio effect on the brake thermal efficiency (BTE) can be seen from Fig. 6.5(b) wherewith the increase in compression ratio, the maximum BTE at CR8 is 23.94% found increased to 26.69 % when engine run at CR 10. With the rise in compression ratio, the combustion temperature increases performing micro explosions of the fuel particles with raising the cylinder pressure (Debnath et al., 2013). Due to this, the force on the piston increases producing more power (as seen in Fig. 6.5-a) and higher efficiency. The variation in BSFC with CR shows that when speed is 1290 rpm, the BSFC is 326 gm/kW-hr, 303 gm/kW-hr, 299 gm/kW-hr for CR 8,CR 9 and CR 10 respectively. That shows BSFC is decreasing with the increase in compression ratio at a particular speed. The similar finding was reported by Li et al, 2007. The major reason may be with the increase in speed the friction loss takes place which reduces the effective power and thereby increases the fuel consumption. However this friction loss was lowered with rise in compression ratio which results in decrease in fuel consumption at a particular speed and leads to lower BSFC (Debnath et al., 2013).

(B) Effect of speed

It is seen that the brake torque decreases with increase in speed at a specific compression ratio. The corresponding decrement is 31%,28% and 28% respectively for CR8, CR9 and CR10 over speed range 1200-1740 rpm. The equivalence ratio remains constant at (1 ± 0.2) supplied to the engine. So with the increase in load, the speed of engine gets reduced and hence the torque increased. Initial increment in speed is seen to un-alter the power for all the compression ratios.

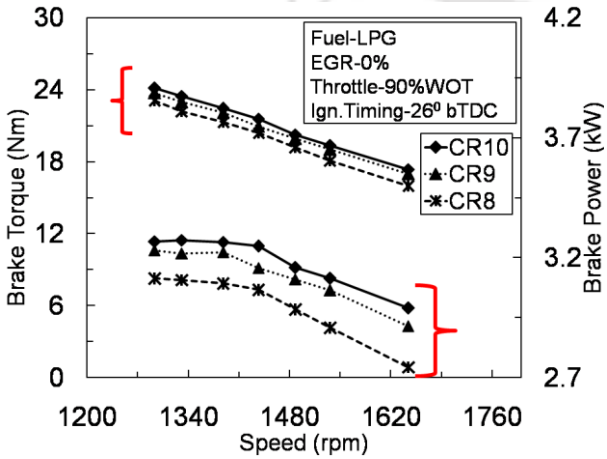

Fig.6.5 (a) Brake torque and Brake power variation with speed for different compression ratio using LPG fuel

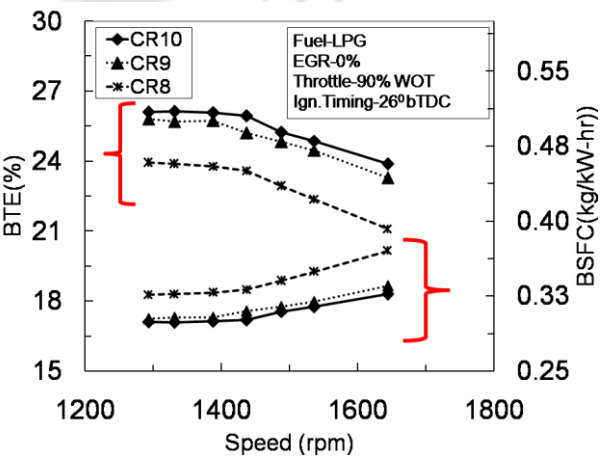

Fig.6.5 (b) BTE and BSFC variation with speed for different compression ratio using LPG fuel

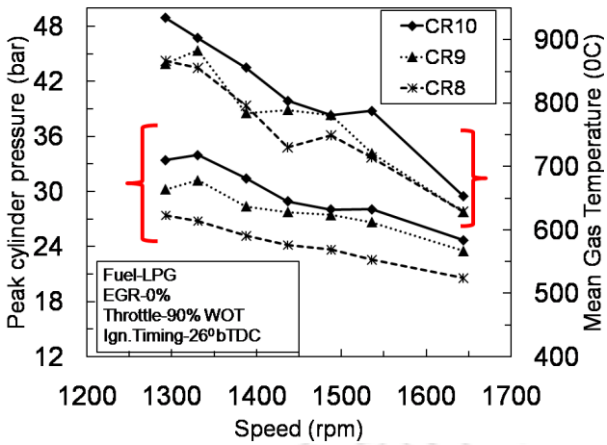

Fig.6.5 (c) Peak cylinder pressure and mean gas temperature variation with speed for different compression ratio using LPG fuel

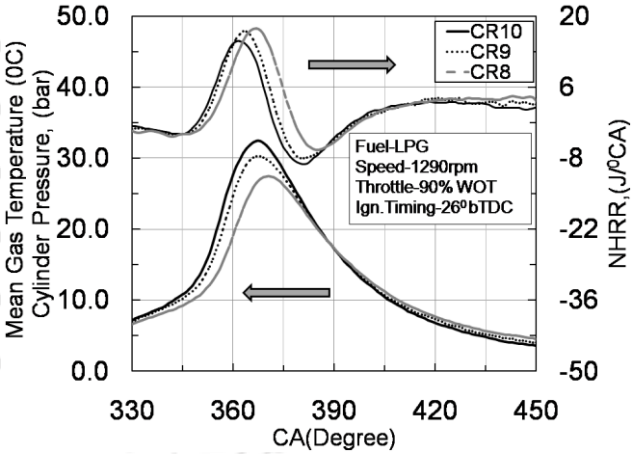

Fig.6.5 (d) Cylinder pressure and Net Heat Release Rate variation with speed for different compression ratio using LPG fuel

However the power decreases with increase in speed with greater slope beyond a limiting speed which corresponds to 1430 rpm in these cases. Power which is proportional to torque and speed follows this trend mainly due to larger decrement in torque for a given speed enhancement (Fig. 6.5-a). BTE found decreases with increase in speed over the range of speed studied herein (Ozcan and Jehad, 2008). At minimum speed the efficiency is higher and with further increase in speed the efficiency decreases showing the decrement of 11.9%, 9.78% and 8.51% as recorded with CR8, CR9 and CR10 respectively from minimum to maximum speed. The brake specific fuel consumption (BSFC) is plotted in Fig. 6.5(b) is found increasing with speed especially during higher speed range. The BSFC variation is less during low speed range for a particular CR. The lowest BSFC was 299 gm/kW-hr for CR 10.

6.3.1.2 Combustion Analysis

The combustion of LPG fuel is smooth as observed during the combustion study based on the optimum spark timing in section 6.2. The behavior of combustion parameters under the conditions of different CR andspeed is detailed below.

(A) Effect of compression ratio

The compression ratio effect can be seen on the combustion behavior inside the engine cylinder. The cylinder pressure variation with crank angle is plotted in Fig. 6.5(c). The parameters such as optimum spark timing, speed range, throttle position, equivalence ratio remains same during all the engine compression ratio study. The effect of compression ratio over cylinder pressure follows the similar nature as discussed before in section 6.2. The peak cylinder pressure varies with CR at particular speed showing increase in cylinder pressure 27.45 bar, 30.24 bar and 33.43 bar at increasing CR from 8, 9 and 10 respectively at speed 1290 rpm. This is because with the increase in CR the cylinder volume reduces which intern increases temperature and pressure of compressed gas. The peak net heat release rate (NHRR) as seen from Fig. 6.5(d) for CR10 and 1290 rpm is 15.09J/ ^{0} CA which found reduced beyond TDC with decrease in CR from 10 to 8 . As a result, the fuel burns with far

more intensity which causes the heat release at TDC to raise further high (Erkus et al., 2013). The mean Gas temperature as shown in Fig. 6.5(c) reported increment with increment in CR. The maximum MGT recorded is 934.70 ^{0} C at CR10, 862.72 ^{0} C at CR9 and 866.41 ^{0} C at CR8 when engine runs at speed 1290 rpm with maximum load on the engine. MGT at CR9 is lower than that at CR8 by 4%. This may be because of uncertainty in measurement of cylinder pressure or temperature during the trials.

(B) Effect of speed

It is found that the peak cylinder pressure is of decreasing nature with increase in speed. This decrement may be because of decrease in load on the engine. Accordingly, the cylinder pressure reports increment of 18% at CR10 with respect to CR8 at 1290 rpm. This trend is more or less similar over range of speed. With the increase in speed the load on engine gets reduced causing the uneven combustion in presence of low compression and temperature results in reduced cylinder pressure (Fig. 6.5-c).The mean gas temperature is the flag of complete combustion by converting the chemical energy to heat energy after combustion. This MGT is of reducing trend with increase in speed for each compression ratio. The corresponding decrement recorded is 27%, 27% and 30% respectively for CR8,CR9 and CR10 respectively over the speed range 1200-1700 rpm.

6.3.1.3 Emission Analysis

(A) Effect of compression ratio

The LPG fuel combustion shows the decrement in CO emission with increase in CR. As shown in Fig. 6.6(a), Carbon Monoxide (CO) emission variation is plotted with speed for different CR. It is seen that the CO decrement of 70% at low speed 1290 rpm and 11% at high speed 1644 rpm correspondingly from CR8 to CR10 with respect to CR8. This may be happened due to the increase in mean gas temperature with increase in CR (Fig. 6.5-c) causing the CO to be oxidized and converted to CO_2 in the exhaust (Debnath et al., 2013). Over the range of speed, the stoichiometric air/fuel ratio is maintained even though some amount of CO is unavoidable due to combustion of fuel (Poraptham et al., 2007). The HC emission as a function of compression ratio can be studied from Fig. 6.6(a). With increase in compression ratio, HC emission found reduced. If the combustion of charge is homogeneous and complete, then there is very less HC emission especially because of some charge in crevices left unburnt. In regards to this, there is decrement of 66% and 32% respectively at minimum speed 1290 rpm and maximum speed 1640 rpm.

The major harmful emission is $NO_{x,}$ whose variation with CR under the constant throttle position 90% WOT, constant ignition timing 26 ^{0} bTDC is plotted in Fig. 6.6(b). From the figure, the NO_x is 243 ppm at CR10 lowered to 235 ppm at CR9 and 95 ppm at CR8 at lowest speed condition. This shows decrement of 3.29% from CR10 to CR9 and further 60% when CR reduces from CR9 to CR8. At maximum speed condition the decrement observed to be 41% and 13.40% from CR10 to CR9 and further to CR8. The reason for decrease in NOx with decrease in compression ratio may be the cylinder pressure shown in Fig. 6.5(d) which

is found reduced with reduced CR causing lower combustion temperature. The CO_2 emission is also dependent upon the compression ratio of engine. For the CR10, the CO_2 is recorded to be 2.62% at CR10, 2.43% at CR9 and 0.72% at CR8 when engine running at maximum load or lower speed condition. The temperature after combustion inside the combustion chamber and stoichiometric combustion of fuel air charge shows rise in CO_2. On the other side at maximum speed condition the CO_2 in exhaust is 3.6%, 1.72% and 1.51% at CR10, CR9 and CR8 respectively.

(B) Effect of speed

The effect of speed on CO emission can be seen in Fig. 6.6 (a). At WOT and CR10, the CO emissions shows increase from 11 ppm to 190 ppm in speed range of 1290 to 1644 rpm . Similarly at CR9, the CO is 30-200 ppm and 37-214 ppm at CR8 respectively.

Sometimes it is necessary to enrich the fuel-air mixture when engine is cold, so CO emissions are much higher during engine warm up period as compared to the maximum loaded or already warmed up engine. Because of exhaust gas temperature, CO oxidation in exhaust pipe gets reduced and causes rise in CO in exhaust (Heywood, 1988; Mahanta et. al,.2006).

The Hydrocarbon (HC) emissions are found increasing with increase in speed. The HC upto 1490 rpm is having positive slope of lesser magnitude but found increased with greater slope after that for CR10. With increase in speed, the combustion should be accelerated with faster flame speed. If the combustion is left incomplete then there is rise in HC emissions. However at maximum load or lowest speed the flame developed in all corners of the engine causing complete combustion. That is why the HC emission is less at low speed condition.

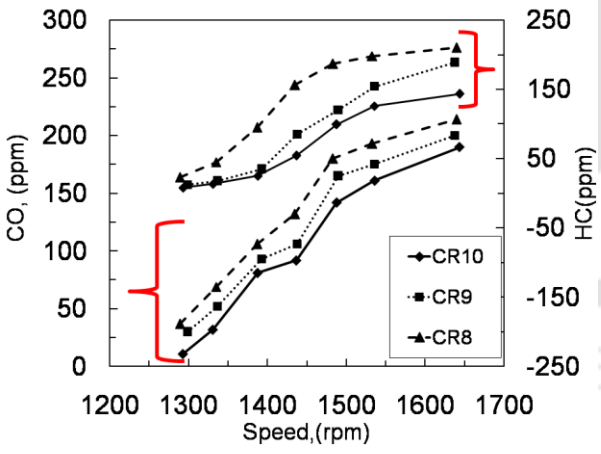

Fig.6.6 (a) CO and UHC variation with speed for different compression ratio using LPG fuel

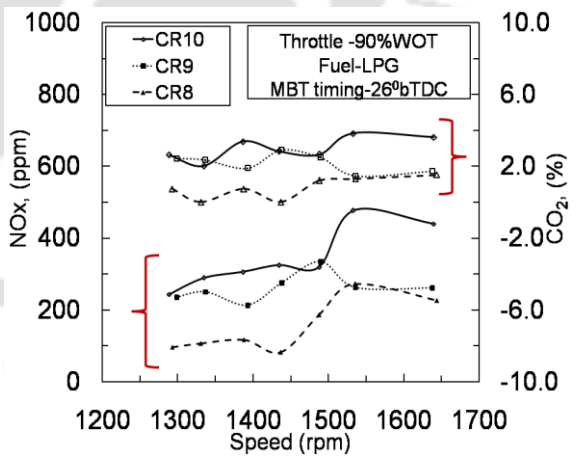

Fig.6.6 (b) NOx and CO_2 variation with speed for different compression ratio using LPG fuel

It is seen that with the increase in speed from 1293 rpm, NOx increases. At CR10, this increment is low upto 1500 rpm but shows substantial rise at further speed. More or less similar trends are observed for CR8 and CR9. The percentage increment of 44.65% at CR10, 9.96% at CR9 and 57.96% at CR8 respectively for minimum to maximum speed range as shown in Fig. 6.6(b). This is happened due to increase in exhaust gas temperature with increase in speed at all CR's.The gaseous fuel has relatively shorter combustion duration and

that is how temperature after combustion would be more causing higher NO_x. Similar observations have been recorded by Mustafi et al., 2006 while working using powergas ($CO+H_2$) in SI engine. The effect of speed on CO_2 emission seems to be minor in the sense that for CR10 the increase from 2.62 % to 3.6 % has been reported. Similarly at CR9,CO_2 emission shows decrement from 2.43 % to 1.72 % and at CR8 the same is 1.72 % to 1.51 % over a complete speed range.

6.3.2 RAW BIOGAS ANALYSIS WITHOUT EGR

6.3.2.1 Performance Analysis

A. Effect of compression ratio

The raw biogas being a lower heating value fuel, need more compression ratio for complete combustion of charge and thereby attaining the maximum brake thermal efficiency. As shown in Fig. 6.7, the BSFC and BTE are the functions of speed as well as compression ratio. Thus BSFC which is a parameter of measurement of fuel consumption is found reduced with increase in CR (Fig. 6.7). At 1430 rpm, BSFC are 1.304 kg/kW-hr, 0.988 kg/kW-hr and 0.968 kg/kW-hr showing increment respectively from CR8 to CR9 and ahead to CR10 respectively.

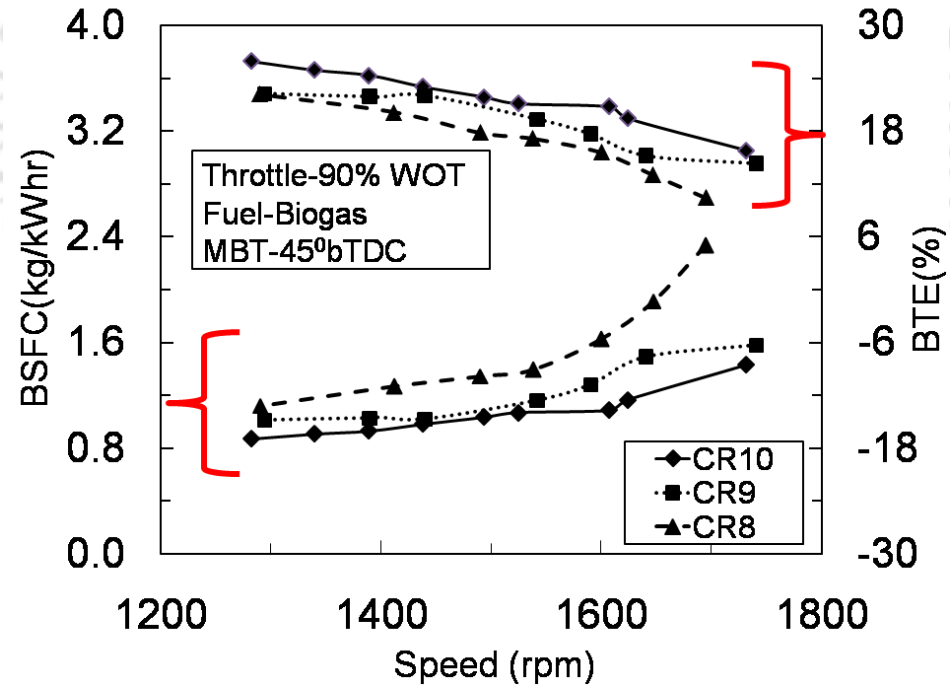

Fig.6.7 BSFC and BTE variation with speed using raw biogas fuel for different CR

With higher CR, the charge inside combustion chamber burns faster with lower combustion duration. The ultimate effect of it is the rise in brake power of the engine. Thereby reduces BSFC for the constant equivalence ratio. The BTE varies with change in compression ratio. Therefore with increase in compression ratio, the BTE is found increased similar to study done using LPG fuel in section 6.2.1. At speed 1430 rpm, the increment in BTE is 19.30% and 2.64% when CR is changed from 8 to 9 further to 10 respectively. For the biogas fuel,

BTE of 25.86% can be achieved with CR10 for 45 ^{0} bTDC spark advance , stoichiometric air fuel ratio and speed 1290 rpm. The calorific value of raw biogas used here is 16000 kJ/kg which is much lower as compared to that of LPG fuel. Even in this scenario, the engine performance is found smooth and attained a good efficiency.

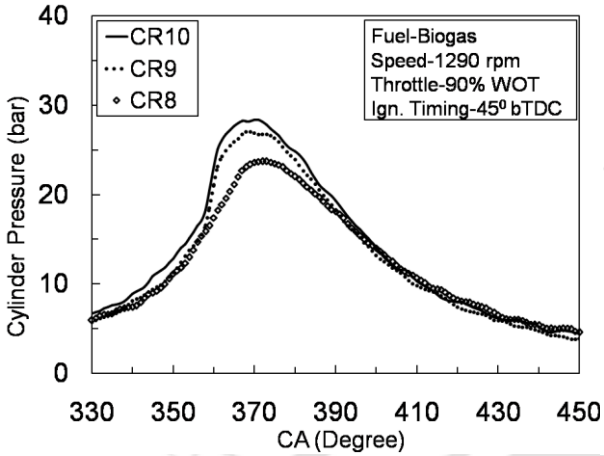

Fig.6.8 (a) Cylinder Pressure variation with crank angle for spark timing using raw biogas fuel for different CR

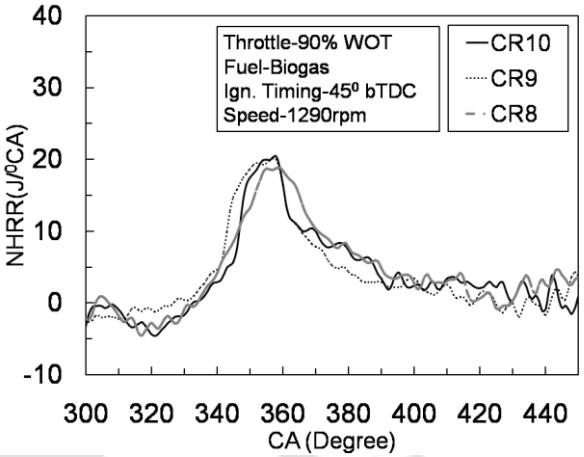

Fig.6.8 (b) NHRR variation with crank angle for spark timing using raw biogas fuel for different CR

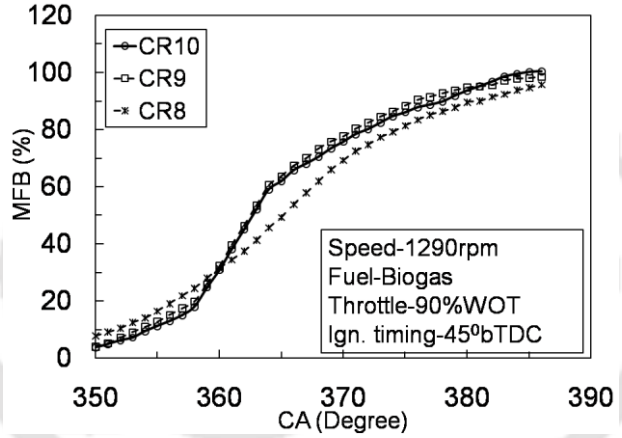

Fig.6.8 (c) Percent MFB variation with crank angle for spark timing usingraw biogas fuel for different CR

B. Effect of speed

Experiments are further carried out for different engine speeds with same engine settings as 90% WOT and spark timing as 45 ^{0} bTDC. The specific fuel consumption as shown in Fig. 6.7(a) keeps on increasing with increase in speed. The mass flow rate of fuel is constant and if the speed is increased, then the combustion may not be proper and hence leaves some charge unburnt. This causes brake power reduction and as such BSFC is being raised with an increment of 52%, 36% and 39% respectively at CR8,CR9 and CR10.As BTE is reciprocal of BSFC, the nature of BTE variation with speed can be expected as in Fig. 6.7(a).

Thus BTE decrement with speed at CR10 is 53% whereas it is 36% and 40% at CR9 and CR8 respectively over speed range of 1290-1731 rpm. Thus present experiments support the use of raw bio gas at higher CR with optimum spark timing at any engine speed (Chandra et al., 2011)

6.3.2.2 Combustion Analysis

A. Effect of compression ratio

Experiments are then conducted to investigate the effect of CR on performance of engine in terms of combustion behavior. Initially experiments are performed with optimum spark timing and for constant engine speed of 1290 rpm.

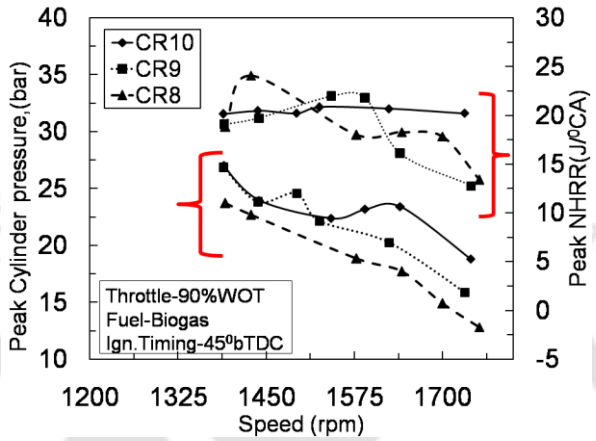

Fig.6.9 (a) Peak cylinder pressure and peak NHRR variation with speed for spark timing usingraw biogas fuel for different CR

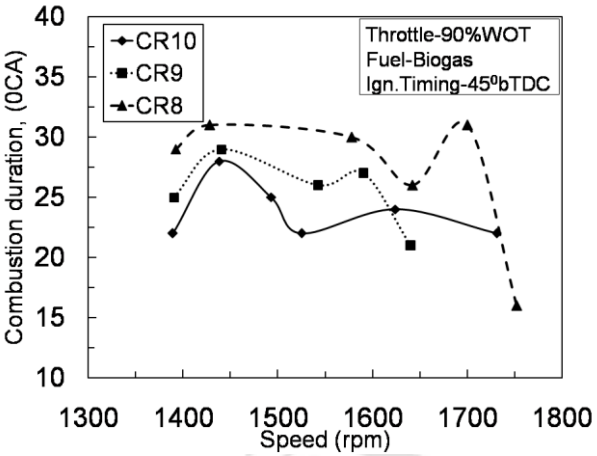

Fig.6.9 (b) Combustion duration variation with speed for spark timing usingraw biogas fuel for different CR

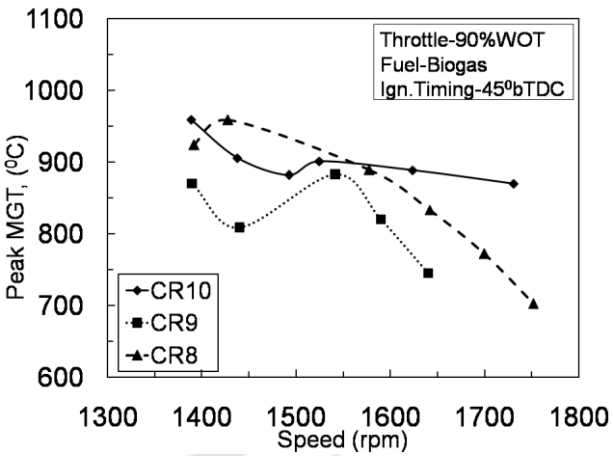

Fig.6.9 (c) Peak MGT variation with speed for spark timing usingraw biogas fuel for different CR

Experimentally obtained cylinder pressure variation as a function of crank angle is plotted in Fig. 6.8(a). With rise in compression ratio, there is rise in peak cylinder pressure (Aaroya et al., 2013). Initial rise in CR from 8 to 9 introduces 14% rise in peak pressure. However, further raise in CR from 9 to 10 brings only 4.9% rise in peak cylinder pressure. Along with this, the crank angle corresponding to peak pressure is found to be towards TDC with increase in CR. As shown in figure, the peak pressure at CR8, CR9 and CR10 are at12 ^{0} aTDC , 8 ^{0} aTDC and 4 ^{0} aTDC respectively. This effect can be further analyzed using net heat release rate (NHHR) and mass fraction burnt (MFB). Figure 6.8(b) gives the variation of NHHR while Fig. 6.8(c) gives percentage MFB for different CRs. With the increase in compression ratio the NHRR is reported to be 18.81 J/ ^{0} CA, 20.13 J/ ^{0} CA and 20.38 J/ ^{0} CA for CR8, CR9 and CR10 respectively. This shows the rise in NHRR with CR. Also, shift in

crank angle of peak NHRR to 1^0 bTDC, 3^0 bTDC and 2^0 bTDC respectively at CR8, CR9 and CR10. On these lines, with increase in CR, there is increase in the percentage MFB (Fontana and Galloni, 2010). Thus, for higher percentage of MFB, higher heat release rate near TDC and maximum value of peak pressure with its shift towards TDC conclusively declare that increment in CR is advantageous for biogas. Biogas being higher octane fuel, it is expected to perform better at higher CR which is indeed supported by present findings (Erkus et al., 2013). This conclusion is mainly based on the fact that higher CR leads to higher pressure of the charge during compression stroke which increases the overall cylinder temperature which in turn helps to complete the combustion close to TDC by burning the maximum charge (Chaudhari et al., 2015).

B. Effect of speed.

The combustion behavior of the biogas fueled spark ignition engine at variable speed can be understood from the Fig. 6.9. Hence engine running conditions corresponds to CR8,CR9 and CR10 with optimum spark timing 45^0 bTDC and 90% WOT.

The peak cylinder pressure variation with speed for CR10 shows decrement with speed from 27.02 bar at 1390 rpm to 18.8 bar at 1740 rpm with over all decrement of 30%. At CR8 and CR9 also the nature follows the same trend with overall decrement of 46% and 41% respectively over full range of speed. The peak cylinder pressure at CR9 and speed 1493 rpm shows higher magnitude of 24.59 bar at 13^0 aTDC than that of peak pressure at CR10 which is 23.82 bar at 9^0 aTDC. This shows delayed combustion at CR9 which is clearly seen in combustion duration plot (Fig. 6.9-b). As shown in Fig. 6.9(b) the combustion duration is higher for all speed steps with CR9 and CR8 as compared to that of CR10. This is happened because the pressure and temperature at end of the compression stroke are reduced with decrease in CR. Owing to this, the flame speed gets reduced after spark and hence the combustion is delayed increasing combustion duration which varies from 20 to 30^0 CA on positive and negative sides of TDC. The engine operating at 1752 rpm speed with CR 8 shows lower combustion duration. This may be due to abnormal combustion causing auto ignition of charge or residual charge of previous cycle at very less CR and with very less load.

The peak NHRR as shown in Fig. 6.9(a) is plotted with speed for varying CR and constant spark advance 45^0 bTDC. The peak NHRR at CR10 does not vary much and falls in range of 20 J/ ^{0} CA to 21J/ ^{0} CA for the complete speed range over 357^0 CA to 368^0 CA. However there are variations in peak NHRR with speed when engine operates at CR9 and CR8. The range of NHRR varies from 20.37J/ ^{0} CA to 12.80 J/ ^{0} CA at CR9 within 357^0 CA to 373^0 CA and 18.81J/ ^{0} CA to 13.39J/ ^{0} CA at CR8 within 359^0 CA to 378^0 CA. This shows that the combustion at CR9 as well as at CR8 is not at all smooth and it is also delayed. This is the main reason for reduction in BTE as mentioned in Fig. 6.7.

The mean gas temperature (MGT) variation with speed shows that the MGT for CR8 is much higher than that of CR9 and CR10. This is happened due to NHRR variations which are the outcomes of cycle to cycle variations of pressure curve for each speed at CR8. However, the

crank angle range is 387 ^{0} CA to 397 ^{0} CA for attaining peak MGT. The peak temperature at speed 1390 rpm is 959.5 ^{0} C at 376 ^{0} CA, 871 ^{0} C at 379 ^{0} CA and 924.5 ^{0} C at 389 ^{0} CA while running at CR10, CR9 and CR8 respectively.

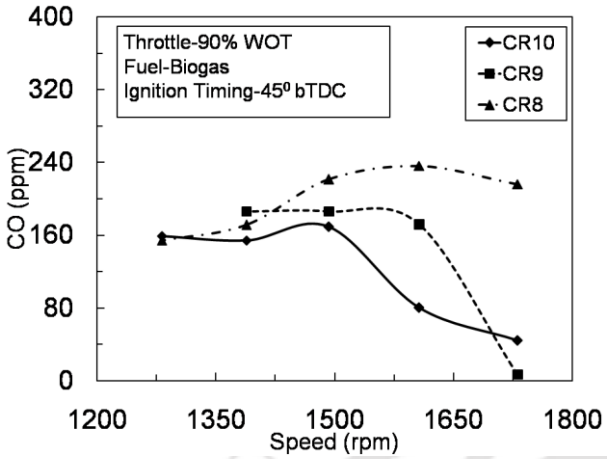

Fig.6.10 (a) CO variation with speed for different compression ratio using raw biogas fuel

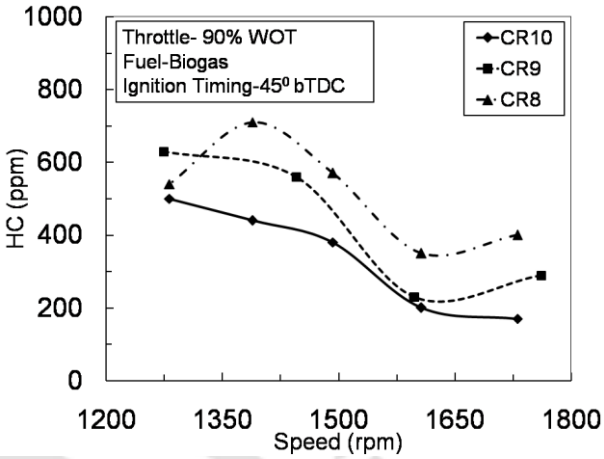

Fig.6.10 (b) HC variation with speed for different compression ratio using raw biogas fuel

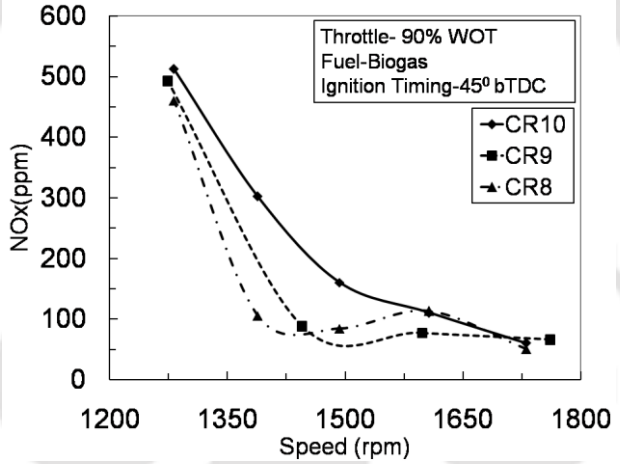

Fig.6.10 (c) NOx variation with speed for different compression ratio using raw biogas fuel

6.3.2.3 Emission Analysis

The harmful emissions such as carbon monoxide (CO), unburnt hydrocarbon (HC), carbon dioxide (CO_2) and Nitrogen Oxides (NOx) are plotted for 100% raw biogas fuel combustion in spark ignition engine as shown in Fig.6.10.

A. Effect of compression ratio

The raw biogas combustion in SI engine also emits the harmful emissions as other fuels such as LPG and petrol do. As the raw biogas is a composition of CH_4 and CO_2, the combustion temperature is lower. At speed 1493 rpm, the increment of 10 % and 30.76 % for CR9 and CR8 with respect to CR10 is reported. Lower calorific value needs higher CR to cause complete combustion. So, CO emission is the outcome of incomplete combustion at lower CR. With the decrease in volumetric efficiency, the charge couldn't get the oxygen for complete combustion and hence some CO doesnot oxidized to CO_2. The unburnt hydrocarbon (HC) emission variation with speed for different CR is as shown in Fig. 6.10(b). It is seen that with decrease in CR, HC emission is increased at a particular speed. This is due

to incomplete combustion in the part of engine cycle in terms of partial burning or even misfire. Also, if the CR is reduced, then combustion is not smooth for poor quality fuel such as raw biogas which leads to higher unburnt HC in exhaust.

NOx emission variation with speed for different CR is plotted in Fig. 6.10(c). The higher combustion temperature is the cause of NO_x increase in exhaust. With higher CR, the combustion temperature reaches high and results in higher NO_x. However the biogas fuel containing 48% CO_2 reduces the NOx as compared to another fuels like LPG or petrol. As shown in Figure, at speed 1496 rpm, the decrement of NOx is 45% and 47.5% for CR9 and CR8 respectively with respect to CR10. At peak speed 1282 rpm, the same is 3.71% and 10.15% respectively for CR9 and CR8 with respect to CR10.

B. Effect of speed

From the Fig. 6.10(a), it is observed that the CO emission increases with speed upto 1493 rpm for all CR under consideration. Thereafter there is decrement till 1731 rpm for all CRs. During high load condition, the fuel rich mixture is supplied to the engine. This is because the engine is initially running on petrol fuel. Once steady state is reached, the engine is switched to biogas fuel. During this time the fuel rich mixture is sucked at intake manifold and accordingly set of data collected beginning with maximum load on the engine. That is the reason, it shows higher CO emission being deficiency of fresh air. However when the engine runs at higher speed above 1496 rpm, the fuel intake charge becomes leaner causing complete combustion in presence of extra oxygen, thereby reducing CO.The range of CO emitted is 44-159 ppm, 7-186 ppm and 154-216 ppm at CR10, CR9 and CR8 respectively. The HC emission also follows the trend of decreasing magnitude with increase in speed. This HC emission is the outcome of unburnt hydrocarbon left inside combustion chamber and carried with exhaust outside. This hydrocarbon emission is more during high load condition for the reason of fuel rich mixture supplied for carrying the load. Sometimes due to wall quenching or crevices the fuel charge remains unburnt and carried with exhaust. From the Fig. 6.10(b), the HC emission is 170-500 ppm, 290-630 ppm and 350-710 ppm respectively for CR10, CR9 and CR8 respectively.

As shown in Fig. 6.10(c), NO_x keeps on decreasing with increase in speed. But here the NOx is higher at high load and reduces towards the minimum load on the engine. It ranges between 60-512 ppm, 66-493ppm and 50-460 ppm for CR10, CR9 and CR8 respectively. High load on the engine increases the fuel consumption inturn increases temperature. This is the reason, the NOx is found to be higher.

6.3.3 Gaseous fuels LPG analysis in presence of EGR

6.3.3.1 Experiments using LPG fuel for optimum spark timing with EGR

The high octane gaseous fuels are utilized in spark ignition engine, the important parameters of conventional petrol engine needs to be readjusted for accommodating the gaseous fuel with the best performance of the conventional engine. In this regard when the petrol based spark ignition engine utilizes LPG gas, then some parameters such as ignition timing,

compression ratio are adjusted to 26 ^{0} bTDC and variable CR from 8 to10 respectively as discussed in section 6.1. However when engine runs with LPG gas the harmful emission such as NO_x is of great concerned. This NO_x is possibly reduced to minimum acceptable limits as stated by Bharat Stage-IV (Table 1.1 from chapter 1) by method of intake fuel air charge dilution also called as exhaust gas recirculation rate. The method of operating EGR system is discussed in chapter 1 with the system designed and developed at IIT Guwahati. The performance study is as detailed below.So, the EGR rate of magnitude low (0 to10%), medium(10 to 20%), heavy (20-30%) and very heavy(above 30%) are experimented with LPG gas fuel in the spark ignition engine

A. Effect of compression ratio

The optimum spark timing for LPG fuel is 26 ^{0} bTDC (334 ^{0} CA) when used in pure form in spark ignition engine. In case if there is some form of additional gas (exhaust gas) supplied with intake charge of LPG and air then there is need of searching for the optimum spark timing. When the exhaust gas composed of mixture containing CO, unburnt HC and NO_x constituents mixed with fresh LPG gas and air, mixture formed has different combustion behavior. This causes the ignition timing to be altered as shown in Fig 6.11(a).

From the figure, it is observed that with increase in EGR rate to 10% the spark timing doesnot found any change to get maximum brake torque and remains at 26 0 bTDC for CR10 while running at 1430 rpm. Even further increase in EGR rate to 20% reported the optimum spark time as 26 0 bTDC at CR10. This means the combustion doesnot have any effect till 20% EGR rate.

However further increase in EGR rate needs to advance the spark timing as charge becomes dilute which further reduces its heating value. At this stage the spark advance of 38 ^{0} bTDC (322^0 CA) for 30% EGR rate and 46 ^{0} bTDC for 40% EGR rate only attain the maximum brake torque.

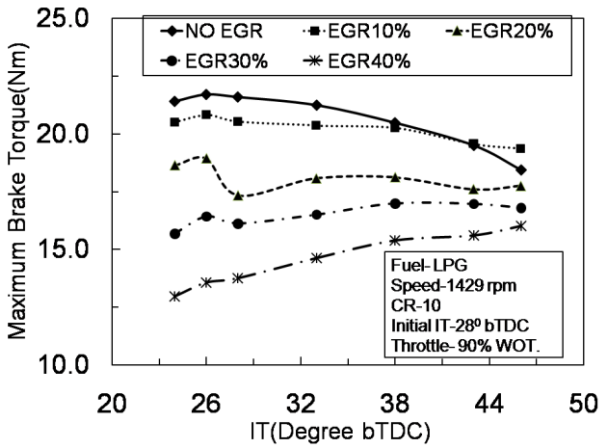

Fig.6.11 (a) Brake torque variation with ignition advance for different EGR rate using LPG fuel

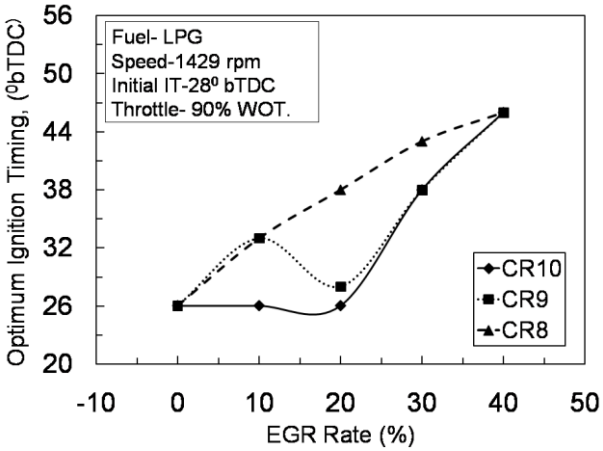

Fig.6.11 (b) Optimum ignition timing variation with EGR rate for different CR using LPG fuel

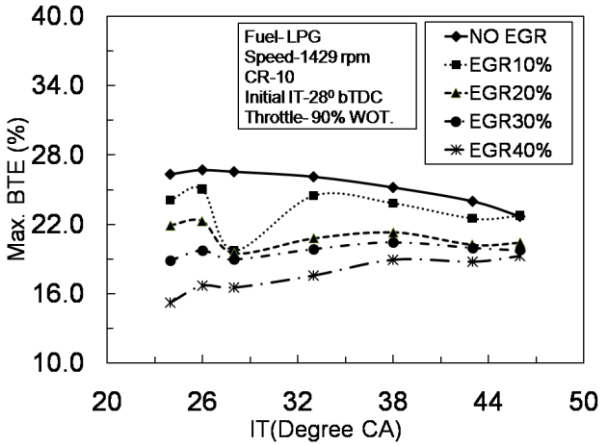

Fig.6.11 (c) BTE variation with ignition advance variation for different EGR rate using LPG fuel

The combustion at EGR 40% is not smooth and knock is observed during the combustion at high load condition. That is the reason measurement of optimum spark timing is crucial. However the spark advance of 46 ^{0} bTDC is the outcome of repeated trials on the engine with LPG at 40% EGR rate for CR10.The similar trend is observed at CR9 and CR8 as well where the spark timing needs to be advanced with increase in EGR rate (Fig.6.11-a).

The spark timings are 26 ^{0}, 33 ^{0}, 28 ^{0}, 38 ^{0}, 46 ^{0} for EGR0, EGR10, EGR20, EGR30 and EGR40 when engine operated at CR9 with speed 1430 rpm. At the same time for CR8 the same are 26 ^{0}, 33 ^{0}, 38 ^{0}, 43 ^{0} and 46 ^{0} bTDC. The optimum spark timing is the outcome of a point where the maximum brake torque is observed. With increase in EGR rate, it is observed that the spark timing needs to be advanced. This may be due to the increase in combustion duration due to which the flame speed gets reduced and combustion duration increases (Hu et al.,2009).

B. Effect of spark advance

The selection of optimum ignition timing is very important for the best performance of the engine. For selecting optimum spark timing the only parameter of concerned is brake torque.

As shown in Fig. 6.11(b), for EGR0, the brake torque varies with spark timing with rising nature from 24 ^{0} bTDC upto 26 ^{0} bTDC reaching its peak value. But then with further increase in spark timing the magnitude falls with negative slope. So the peak represents the maximum brake torque (MBT) and the corresponding spark timing is optimum for EGR0. For EGR0 with operating at CR10 and speed 1430 rpm , the optimum spark timing is 26 ^{0} bTDC attaining the maximum brake torque of 21.702 Nm. The percentage decrement of 1.33%, 0.5%, 2.12%, 5.70%, 10.17%, 15.10% at 24 ^{0},28 ^{0},33 ^{0},38 ^{0},43 ^{0},46 ^{0} bTDC spark advance is observed. As every hydrocarbon fuel has its own calorific value and auto ignition temperature, the combustion process inside cylinder gets influenced by those parameters. This is the reason, the spark timing is retarded for LPG gas as compared to that of petrol where optimum spark timing is 28 ^{0} bTDC (chaudhari et al., 2015) for petrol fuel. When the EGR rate raise to 10% keeping other operating parameters unchanged, the MBT is 20.818 Nm at 26 ^{0} bTDC. There is percentage decrement in range of 1.56%, 1.41%, 2.21%, 2.72%,

6.03% and 7.02% at 24 ^{0}, 28 ^{0}, 33 ^{0}, 38 ^{0}, 43 ^{0}, 46 ^{0} bTDC spark advance are observed. Here also with further increase in EGR rate the maximum brake torque is found reduced to 18.934 Nm and 16.989 Nm respectively for EGR20% and 30%. Further, the optimum spark timing gets reduced to 46 ^{0} bTDC (314 ^{0} CA) attaining torque of 16.007 Nm. Similarly the maximum brake torque of 19.98 Nm, 19.11 Nm, 16.70 Nm and 15.50 Nm at optimum spark 38 ^{0}, 28 ^{0}, 38 ^{0} and 46^0 bTDC for CR9 at speed of 1430 rpm at EGR10, EGR20, EGR30 and EGR40 respectively has been noticed. Similarly the optimum spark advance for CR8 are 26 ^{0}, 28 ^{0}, 33 ^{0}, 38 ^{0}and 46 ^{0} bTDC. The MBT of 18.252 Nm, 17.68 Nm, 16.71 Nm and 14.40 Nm are obtained with the above spark timings at EGR10, EGR20, EGR30 and EGR40 respectively. The BTE variation nature is very close to that of brake torque for the constant speed condition as shown in Fig.6.11(c).The BTE at EGR0 is 26.69% with CR10 at 26 ^{0} bTDC MBT timing. If there is addition of 10% EGR, then BTE found reduced to 25.02 % at 26 ^{0} bTDC MBT timing with decrement of 1.67%. If EGR rate is raised further then BTE is 22.25 %, 20.42 % and 19.24 % respectively at EGR20, EGR30 and EGR40 with respective optimum ignition timing. This means decrement of 4.44 %, 6.27 %, 7.45 % is a compromise for controlling the harmful emission NOx from the engine.

6.3.3.2. Performance Analysis in presence of EGR

Performance analysis executed further which includes the variation of BP, BTHE, BSFC, EGT. The experiment was performed in speed range of 1200-1800 rpm. The variations in CR for LPG fuel will be performed first with wide open throttle and part throttle position. Thereafter the treated EGR and untreated EGR performance test will be performed with EGR from low (0 to10%), medium (10 to 20%), heavy (20-30%) and very heavy (above 30%) . The detailed discussion of the results obtained is analyzed here in this chapter with three broad effects.

A. Effect of compression ratio

The effect of EGR rate with optimum spark timing has been experimented and the results in terms of BTE are plotted as shown in Fig. 6.12(a). As seen in previous section 6.3.3.1 there is a decrement of 1.64 % in efficiency with respect to that obtained with CR 10 without EGR is acceptable, then settings with CR10 and EGR10 can be successfully demonstrated in engine. Similar to this other combinations may be possible where EGR can be introduced without affecting the BTE to certain extent. If engine settings are fixed at CR8, then BTE obtained is 23.9% where no EGR is supplied. Now if EGR 10% is introduced and CR raised to 9, then also BTE remains same 23.9%. But with this arrangement, there is a chance of controlling the NOx produced during combustion.

The brake specific fuel consumption (BSFC) which is a deciding parameter for the brake thermal efficiency is as plotted in Fig. 6.12(b) for optimum spark timing and constant speed of 1430 rpm. The BSFC found to be increased by 2.73%, 20.21%, 30.82% and 39.04% with increase in EGR rate to EGR10, EGR20, EGR30 and EGR40 respectively over EGR0 having BSFC of 299 gm/kW-hr for CR10.The similar trend is observed for other CR9 and CR8 as shown in figure. The dilution of exhaust gas in intake charge reduces the cylinder combustion

temperature which produces less amount of heat to convert in to work. Outcome of this is the drop in brake power which affects the BSFC. There is increment in BSFC with decrease in compression ratio which was discussed in section 6.2.

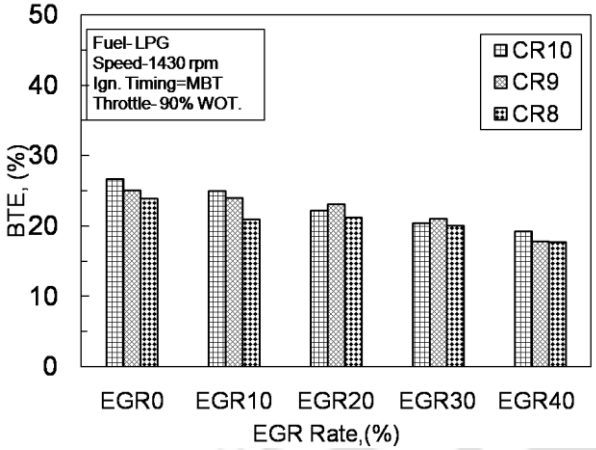

Fig.6.12 (a) BTE variation with EGR Rate for different CR using LPG fuel

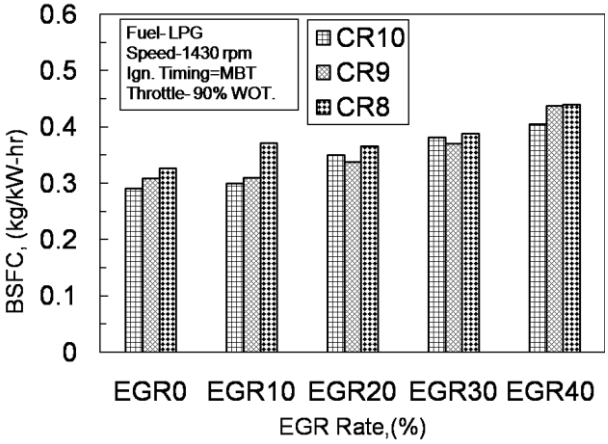

Fig.6.12 (b) Optimum ignition timing variation with EGR rate for different CR using LPG fuel

B. Effect of EGR

Exhaust gas recirculation effect on torque variation can be seen from Fig. 6.12 (a, b and c) when engine running at MBT timing and constant air-fuel ratio.

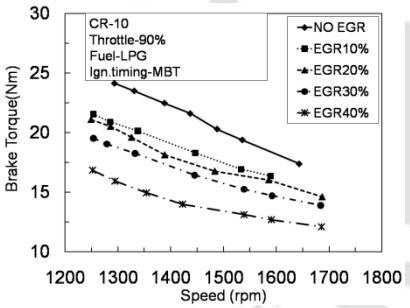

Fig.6.13(a) Brake Torque variation with speed for different EGR rate at CR10

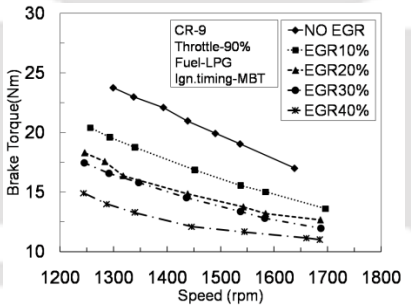

Fig.6.13(b) Brake Torque variation with speed for different EGR rate at CR9

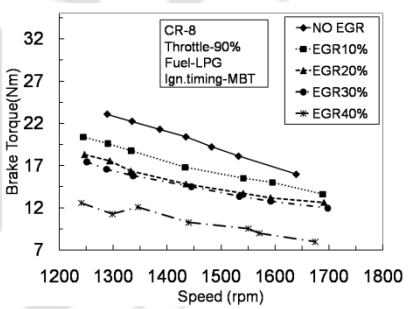

Fig.6.13(c) Brake Torque variation with speed for different EGR rate at CR8

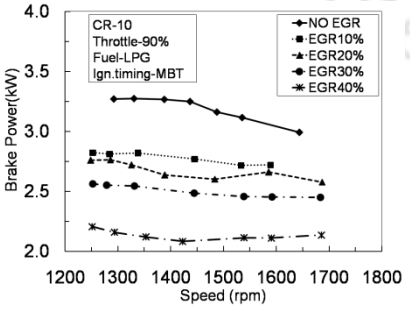

Fig.6.14 (a) Brake Power variation with speed for different EGR rate at CR10

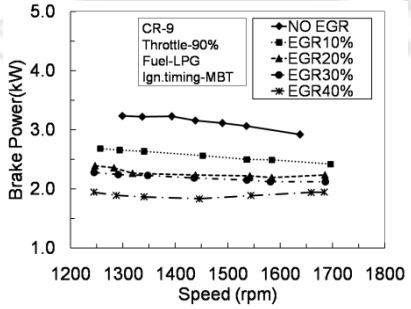

Fig.6.14 (b) Brake Power variation with speed for different EGR rate at CR9

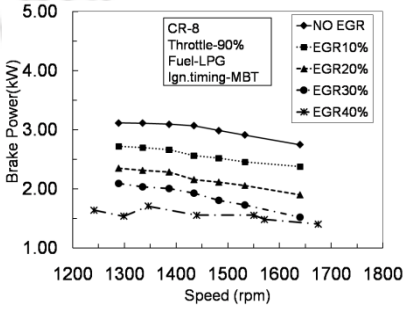

Fig.6.14 (c) Brake Power variation with speed for different EGR rate at CR8

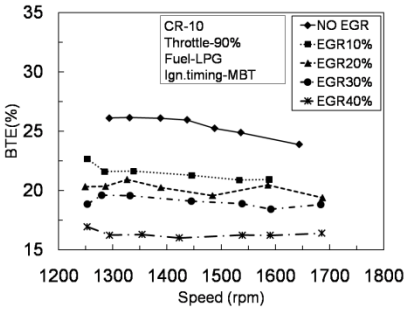

Fig.6.15(a) BTE variation with speed for different EGR rate at CR10

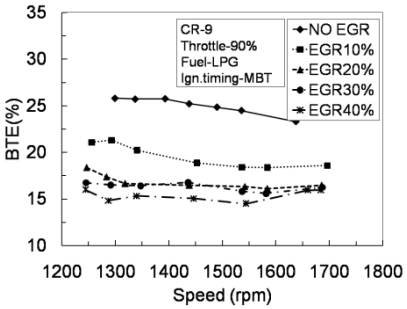

Fig.6.15 (b) BTE variation with speed for different EGR rate at CR9

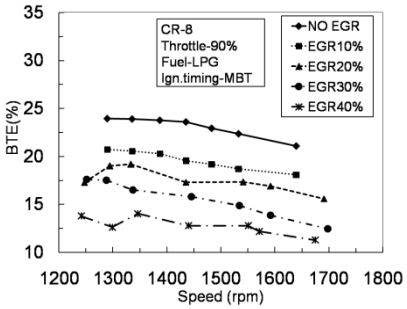

Fig.6.15(c) BTE variation with speed for different EGR rate at CR8

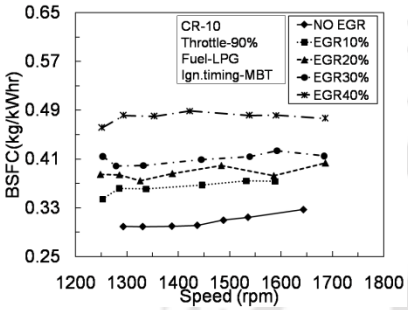

Fig.6.16(a) BSFC variation with speed for different EGR rate at CR10

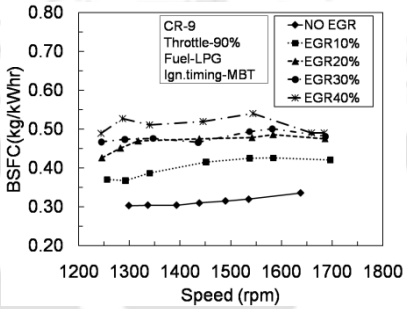

Fig.6.16(b) BSFC variation with speed for different EGR rate at CR9

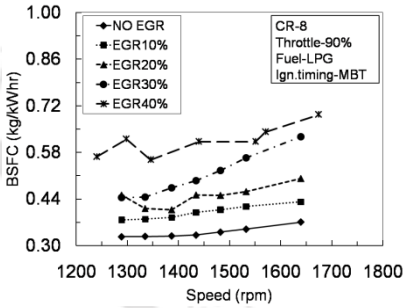

Fig.6.16(c) BSFC variation with speed for different EGR rate at CR8

The torque decrement of 28-30 % is observed with increase in speed from 1293 rpm to 1700 rpm for all EGR 0 to EGR 40 (Fig.6.12-a). The maximum decrement is observed at EGR40. At a particular speed 1293 rpm and CR10, the torque decrement with EGR10, EGR 20, EGR 30 and EGR 40 is 13.2%, 14.9%, 21.37% and 33.08% respectively with respect to EGR 0 (Fig. 6.12-a). With decrease in compression ratio to 9, the torque decrement is 28.45%, 33.23%, 30.85%, 31.34% and 26.26% at EGR0, EGR10, EGR20, EGR30 and EGR40 respectively over a speed range of 1253-1700 rpm (Fig. 6.12-b). Similarly for a constant speed of 1293 rpm, the torque percentage decreases to 17.8, 27.01, 29.85 and 39.54 percent at CR9 with EGR10, EGR20, EGR30 and EGR40 (Fig. 6.12-b). At CR 8 the torque decrement is 30.75%, 35.65%, 40.40%, 46.59% and 22.45% over speed range of 1253-1700 rpm at EGR0, EGR10, EGR20, EGR30 and EGR40 respectively (Fig. 6.12-c). At a constant speed of 1293 rpm the decrement of torque is 14.04, 27.89, 37.76, 48.25 percent at 1293 rpm at EGR10, EGR20, EGR30 and EGR40 respectively (Fig. 6.12-c). This decrement in torque due to rise in EGR at 90% WOT shows that the fuel air mixture strength deteriorates with rise in EGR percentage which results in poor performance in terms of torque over fixed speed range 1200-1700 rpm (Haywood,1988). EGR effect is seen for LPG fuel from lower EGR10 to very heavy EGR40 over brake power as shown in Fig. 6.13 (a,b and c). It is acknowledged that the trend followed by magnitude of power at maximum load is of decreasing order with speed. The brake power shows decrement with increase in EGR rate. At a particular speed of 1293 rpm and CR10, EGR10, EGR20, EGR30 and EGR40 in intake charge, shows power decrement of 14, 16, 22, 33% with respect to EGR0 (Fig. 6.13-a). Similarly at lower CR9 and same speed 1293 rpm, the power decrement was 17, 26, 30, 40% (Fig. 6.13-b) whereas at CR8 the power decrement was 13, 25, 33, 47% with respect to EGR0 (Fig. 6.13-c). Intake

charge mixture dilution rate in terms of EGR introduction leads to decrease in flame propagation speed and amount of air and fuel into the engine cylinder, this consequently results in decrease in brake power with increase of EGR rate (Hu et al.,2009). The VCR and EGR effect on the brake thermal efficiency can be explored from Fig. 6.14 (a,b and c) where the BTE variation with speed for different percentage EGR is shown for CR10, CR9 and CR8. The BTE is decreasing with increasing speed for EGR0 to EGR40. The decrement in BTE is more if EGR percentage is more in the intake charge. At a particular speed of 1293 rpm and CR10 the BTE decrement is 6, 16, 22 and 30% at EGR 10, EGR 20, EGR 30 and EGR 40 dilution of exhaust gas with respect to EGR0 (Fig. 6.14-a). At similar speed and CR9, the BTE shows 11, 23, 29 and 33% decrement at EGR 10 EGR 20, EGR 30 and EGR 40 respectively with respect to EGR0 (Fig. 6.14-b) whereas at CR8 the decrement in BTE is 8, 23, 22 and 39% at speed 1293 rpm with respect to EGR0 (Fig.6.14-c). This decrement in BTE is found higher among all EGR tests from medium to very heavy EGR (EGR 30 and EGR 40). As the EGR increases from 0% to 40%, there will be more dilution of untreated exhaust gas with the fresh air-fuel charge, so the heat supplied by this charge gets reduced due to decrease of lower calorific value of the charge inducted in the engine cylinder. So less heat was released and the power produced gets lower. The ultimate effect of this is the reduction in brake thermal efficiency.

The BSFC variation with speed due to variation in EGR for CR10, 9 and 8 can be studied from Fig. 6.15 (a,b and c). Here, BSFC increases with the increase in speed for the complete speed range at a particular CR combined with EGR 0 or EGR 10 or EGR 20 even at EGR 30 and EGR 40. At 1293 rpm and CR 10, the increment in BSFC from EGR 10, EGR 20, EGR 30 and EGR 40 is 6, 18, 27 and 42 % respectively with respect to EGR0 (Fig. 6.15-a). At similar speed and CR 9 this increment is 13, 30, 42 and 49% with respect to EGR0 (Fig. 6.15-b). Whereas at CR8 this increment at lowest speed 1253 rpm is 8, 30, 48 and 63% with respect to EGR0 (Fig.6.15-c).The higher EGR rate means lower flame development and longer

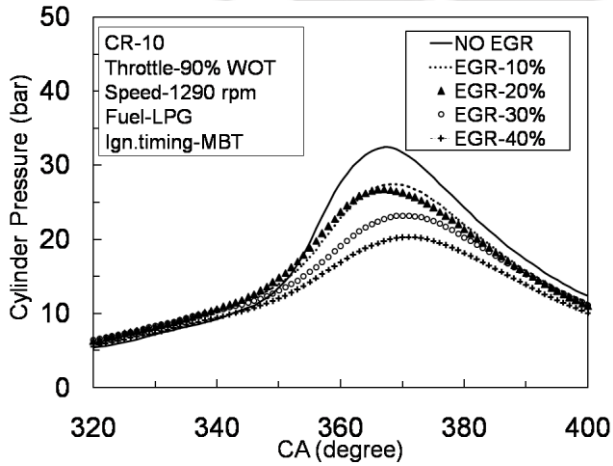

Fig.6.17 (a) Cylinder pressure variation with crank angle for different untreated EGR rate using LPG fuel for 90% WOT

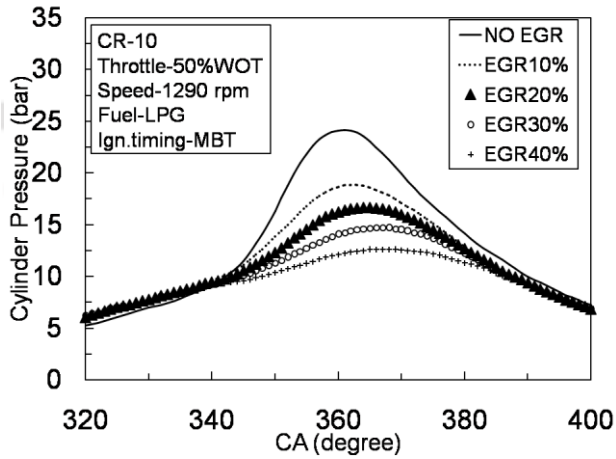

Fig.6.17 (b) Cylinder pressure variation with crank angle for different untreated EGR rate using LPG fuel for 50%throttle

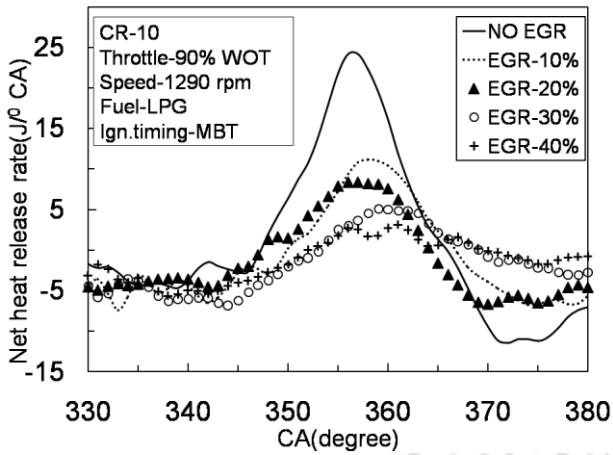

Fig.6.17 (c) NHRR variation with crank angle for different untreated EGR rate using LPG fuel for 90% WOT

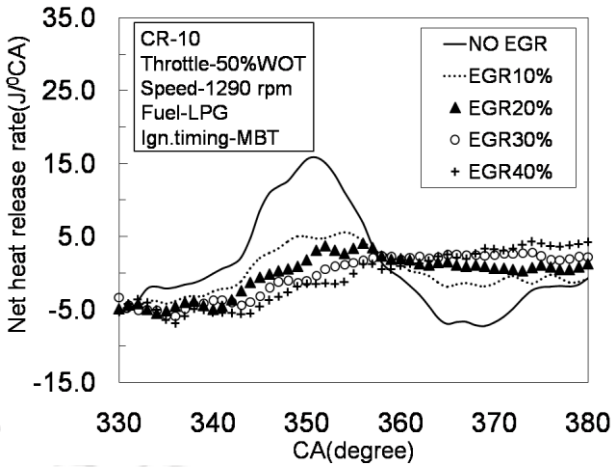

Fig.6.17 (d) Cylinder pressure variation with crank angle for different untreated EGR rate using LPG fuel for 50% WOT

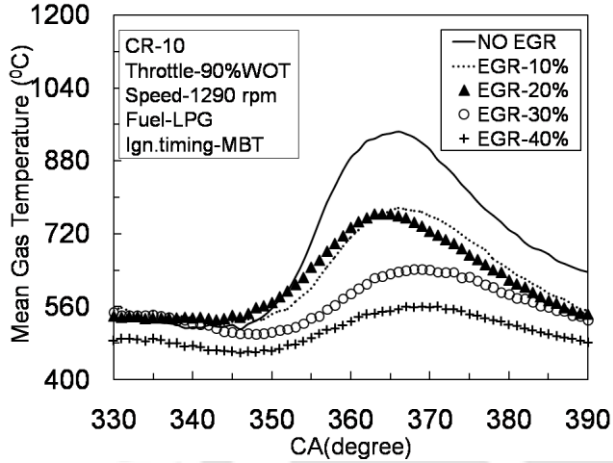

Fig.6.17 (e) MGT variation with crank angle for different untreated EGR rate using LPG fuel for 90% WOT

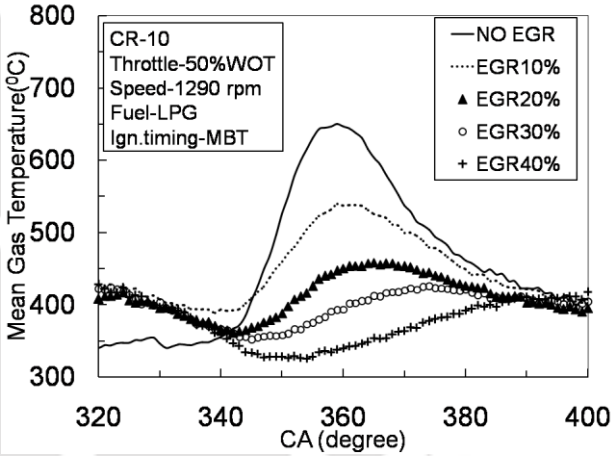

Fig.6.17 (f) MBT variation with crank angle for different untreated EGR rate using LPG fuel for 50% WOT

combustion duration results in slow combustion and thus lower power output. The decrement in power produced for the constant fuel consumption results ultimately in higher BSFC (Fontana and Galloni,2010)

6.3.3.3. Combustion Analysis in presence of EGR

The combustion analysis is also presented herein where the effect of EGR is clearly seen. The combustion parameters include the cylinder pressure, net heat release rate (NHRR),percent mass fraction burned (MFB) and mean gas temperature (MGT) are of primary concerned. Along with this the combustion duration and fuel conversion efficiency are also important for selection of right combination of CR and EGR rate. Based on the evaluation of spark advance in section 6.2.3, the optimum spark advance is used for the analysis.

A-Effect of EGR

As shown in Fig. 6.17 (a- f), the peak pressure decreases with increase in EGR rate at 90% WOT. At CR10 the decrement in cylinder pressure of 15.45 %, 17.92 %, 28.62 % and 37.45 % is observed for EGR 10, EGR 20. EGR 30 and EGR 40 with respect to EGR 0 (Fig. 6.17-a). The cooled EGR which is recirculated back to the engine cylinder dilutes the mixture

composition, thereby reduces the strength of combustion intern temperature after combustion. This is the reason that with increase in EGR the peak pressure decreases (Fig. 6.17-a). The similar nature is observed for CR9 where decrement of 13.41 %, 26.07 %, 33.67 % and 43.01 % for EGR 10, EGR 20, EGR 30 and EGR 40 respectively at 90% WOT. At CR8, the decrement of 19.47 %, 29.2 %, 45.59 % and 53.38 % for EGR 10, EGR 20, EGR 30 and EGR 40 respectively at 90% WOT. It is seen that increase in EGR rate causes the incomplete combustion of charge and the unburnt fuel lost through the exhaust in the form of HC emission. This ultimately affects the performance of the engine. At part throttle condition, the situation is similar to that of 90% WOT (Fig. 6.17-b). During 50% WOT, at CR10 the peak pressure is 24.137 bar at 361 ^{0} CA. This shows that combustion is faster as compared to that of 90 % WOT. The peak pressure at EGR 40 and 50 % WOT is 12.645 bar at 366 ^{0} CA showing decrement of 47 % (Fig. 6.17-b). The NHRR is the parameter by which the effect of EGR could be justified as shown in Fig. 6.17(c). As previous fuel mixture composition is very lean and the residual gases are mixed in the fresh charge when EGR has been supplied, so net heat release gets reduced. At CR10, the maximum NHRR is 24.149 J/ ^{0} CA at 356 ^{0} CA for EGR0 which further reduces to 17.161 J/ ^{0} CA at 357 ^{0} CA, 8.360 J/ ^{0} CA at 356 ^{0} CA, 5.14 J/ ^{0} CA at 358 ^{0} CA and 3.139 J/ ^{0} CA at 361 ^{0} CA respectively for EGR 10, EGR 20, EGR 30 and EGR 40(Fig. 6.17-c). It is seen that upto 10% EGR rate may be acceptable with compromise in BTE from the engine (Fig.6.15-a).At part throttle 50% WOT condition, the peak NHRR is 15.85 J/ ^{0} CA at 351 ^{0} CA for EGR0 and CR10 (Fig. 6.17-d) and (Fig. 6.18-d). For further EGR rate, the peak NHRR found reduces showing decrement of 64% at EGR10 and 73% at EGR40 with respect to EGR0 extending combustion upto crank angle 3740CA. Mean gas temperature as shown in Fig. 6.17(e) is found decreased with increase in EGR rate showing decrement of 40% in peak temperature when EGR increased to 40% at CR10 with respect to EGR0. Similar to this, decrement of temperature by 38% and 31% has been reported when supplied with very heavy EGR 40% when engine runs at CR9 and CR8 respectively.

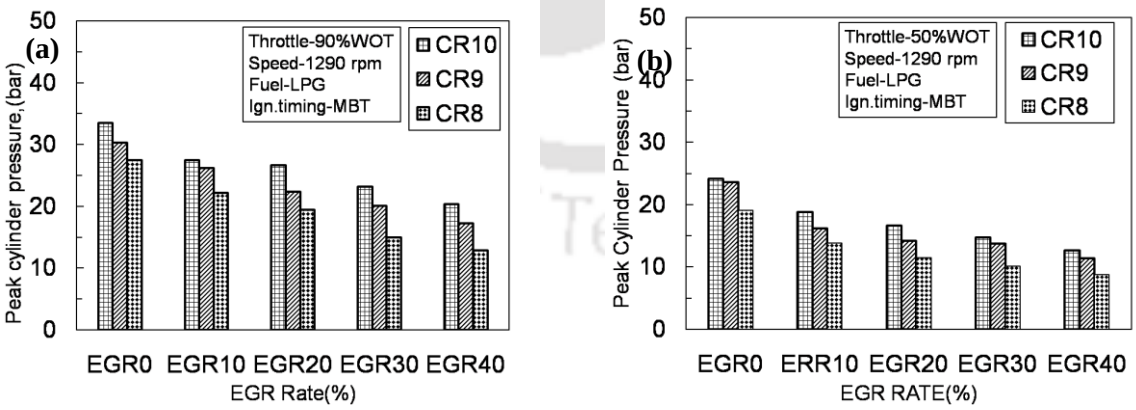

The effect of EGR over engine stability can be evaluated in terms of cycle-by-cycle variation (coefficient of Variance) in indicated work per cycle. Variation of COVIMEP is as shown in Fig.6.18(e) for LPG fuel from very low EGR rate of 10% to very heavy rate of 40%. As seen from the figure the COV initially reduces upto EGR10 for all CR8, CR9 and CR10.

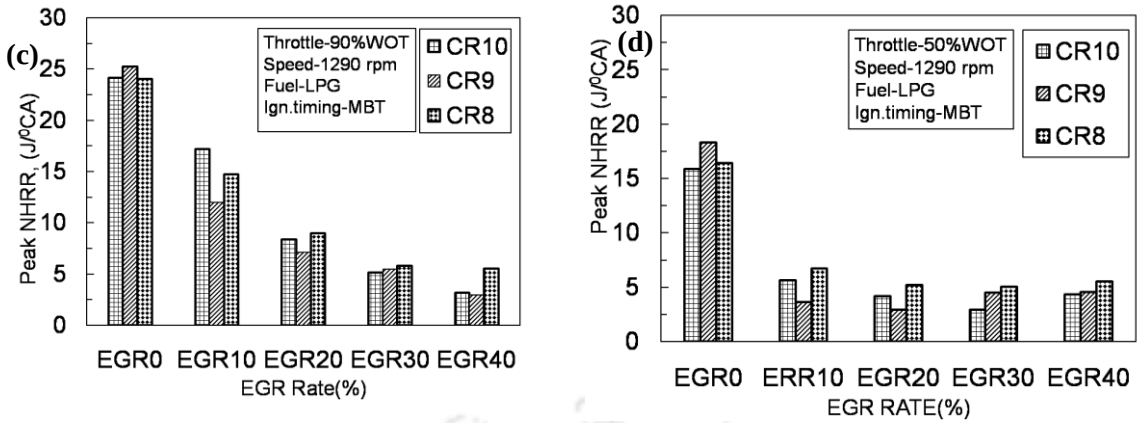

Fig.6.18 Peak cylinder pressure vaiation with EGR rate at (a) 90% throttle;(b) 50% throttle.
Fig.6.18 Peak NHRR variation with EGR rate for at (a) 90% throttle ;(b) 50% throttle.

Thereafter, it shows increment upto EGR40 (Fontana and Galloni, 2010; Debnath et al., 2013). At EGR30, maximum COV is recorded for CR8 and lowest for CR10. This may be attributed to reduction in cylinder pressure with reduction in CR causing more pressure variation.

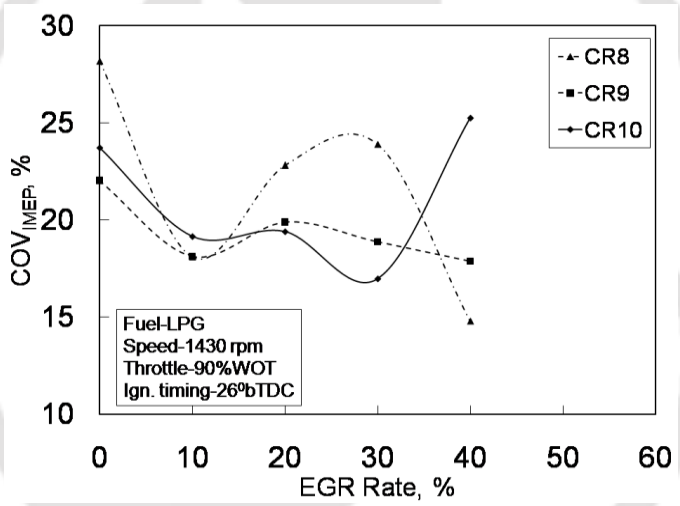

Fig.6.18(e) COV_{IMEP} variation with EGR rate for variable CR

B. Effect of CR

With the variation in compression ratio, the cylinder pressure is found to be improved causing complete combustion. There is increment of 9.23% when CR raised from CR 8 to CR 9 and 38 % when CR increases further to 10 while engine is running at 90 % WOT, EGR 0 and speed 1290 rpm. With the increase in CR, the compressed charge temperature increases and reaches early to auto ignition temperature of volume mixture of fuel, air and EGR as compared to lower CR9 and CR8. Even at EGR 10, the corresponding increment is 16 % from CR 8 to CR 9 and 45 % when CR further increases to CR 10 are observed. If EGR rate is increased further, the percentage increment raises further. Similarly at part throttle condition the increment of 19 % for rise in CR 8 to CR 9 which further shows increment of 1.93 % for CR 9 to CR 10 at EGR 0 running a constant speed 1290 rpm. If the EGR rate is 10 % then the corresponding increment is 14.54 % for CR 8 to CR 9 and 14.23 % when CR increases to CR 10 from CR 9. This means that there in increment in cylinder pressure with rise in CR proportional to the decrease in EGR rate. The possible combinations for attaining

the maximum cylinder pressure and reduced emissions with adaptation of EGR rate as explained in Fig. 6.19.

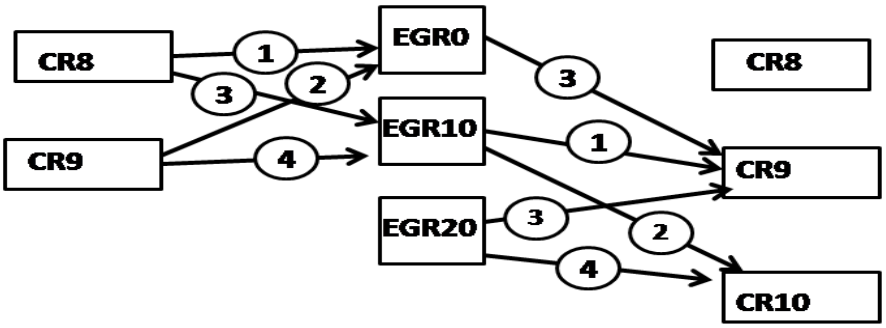

Fig.6.19 Combination Diagram of CR and untreated EGR rate using LPG fuel for 90% and 50% WOT

The NHRR is also affected with variation in CR and EGR rate similar to the cylinder pressure. There is increment of 4.68% with increase from CR 8 to CR 9 which further shows a small decrement of 4.15 % at EGR 0 and speed 1290 rpm. The decrement in NHRR from CR 9 to CR 10 is surprising and combustion phenomenon is responsible for the similar results. There may be certain uncertainties present while measuring cylinder pressure or crank angle which reflects in reduction of NHRR with increase in CR. If EGR rate is increased to 10, then increment of 18.54 % for CR 8 to CR 9 and 30.12 % when CR raises from 9 to 10.

6.3.3.4. Emission Analysis of LPG fuel in presence of EGR

Emission of spark ignition engine with combustion of LPG fuel consist of CO, CO_2, HC and NO_x constituents which are harmful to the environment. So the efforts are made to control these harmful gas emissions by implementing the EGR with varying percentage during combustion of fuel air mixture.

A- **Effect of speed**

Carbon Monoxide (CO) emission is as plotted in Fig. 6.20(a) varying with speed for different EGR rate from 0 % to 40 % with increment of 10 %. It is found that with the increase in speed, the CO raises for EGR 0 with possible increment of 82 % over speed range 1290-1700 rpm working at CR10 and constant air-fuel ratio. The CO emission found more serious with addition of EGR in the intake charge. As shown in figure, if EGR10 is implemented then there is a rise in CO emission showing increment of 60% over speed range. Similarly the increment of 64%, 56% and 56% are obtained when EGR raised to 20 %, 30 % and 40 % respectively. At a particular compression ratio, due to mixing of EGR with gaseous LPG fuel, reduces the actual volume of air supplied with intake charge. This in turn reduces the oxygen required to cause complete combustion. Hence the incomplete combustion takes place which ultimately a major cause of rise on CO. The unburnt HC is a component of emission exhausted through the spark ignition engine. HC emission is outcome of abnormal combustion or the fuel charge left unburned in the crevices such as piston rings, carbon deposits on cylinder walls which gets exhausted causing HC pollution. This emission is severe in spark ignition engine and needs to be controlled to possible extent. At EGR 0, when

engine runs at CR 10 using LPG fuel, the HC emission is found to raise with speed showing the increment of 82 ppm - 144 ppm from 1290-1700 rpm speed range as shown in Fig. 6.20(b).

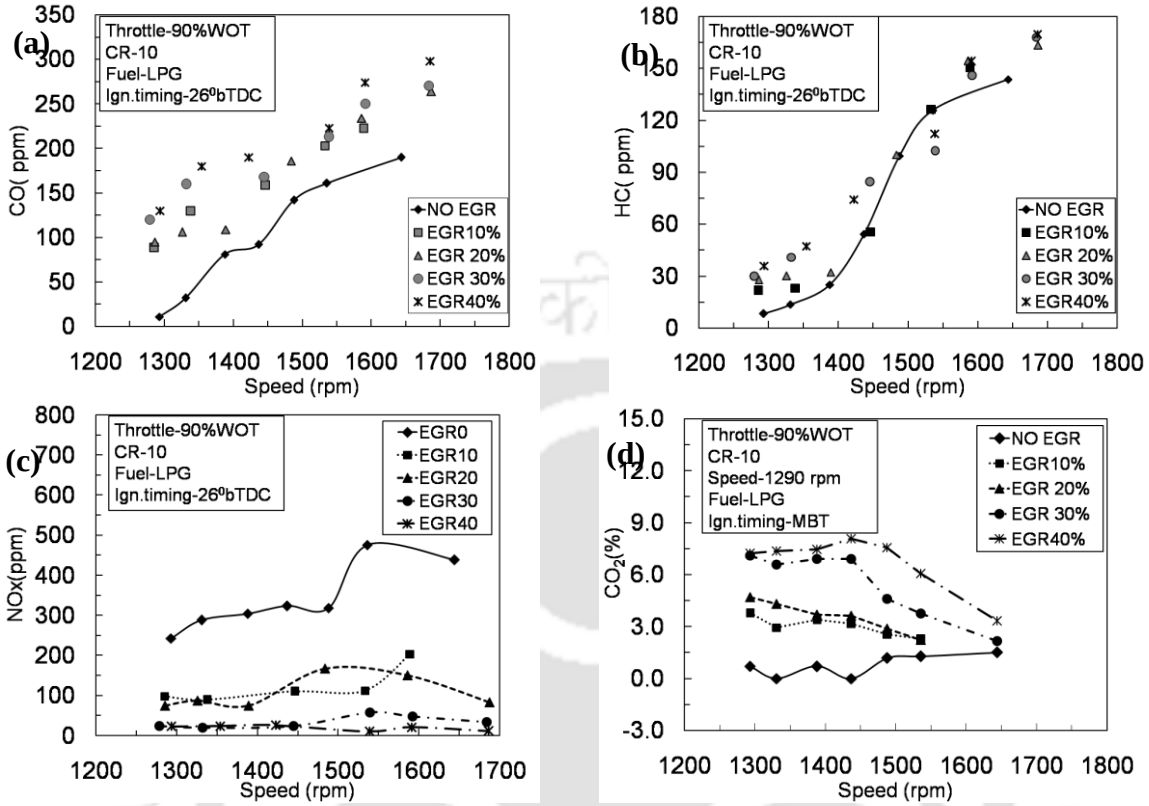

Fig.6.20 (a) CO;(b) HC;(c) NOx;(d) CO_2 variation with speed for different EGR rate at constant CR using LPG fuel at 90% throttle

When the engine runs at low speed or maximum load condition, the cylinder temperature is more and hence it helps to cause the homogeneous combustion without any charge left inside cylinder. However when the combustion is in progress (Fig. 6.18-c) during power stroke, suddenly opening of exhaust valve causes some unburnt charge left outside with exhaust gas which is responsible for HC emission. Due to this, the HC emission is less during low speed. However it is found increased with increase in speed or decreasing the load. With the increase in speed the combustion should be faster, if it is not so, then incomplete combustion takes place and it is responsible for rise in HC emissions. Nitrogen Oxides (NO_x) is another harmful emission which is the outcome of in cylinder combustion temperature. NO_x is very harmful to atmosphere and its control in exhaust gas is more important. The oxygen combined with nitrogen in air forms the Nitrogen oxides and when this further combined with oxygen follows the Zeldowich Mechanism to form NO_x. The NO_x can be successfully reduced to possible extent by a method called as exhaust gas recirculation(EGR). The variation of NO_x with speed for different EGR rate is as shown in Fig. 6.20-c. For EGR0, the NO_x can be found increased with speed showing the increase from 243 ppm to 439 ppm with an increment of 44.64%. Such rise takes place with speed due to rise in temperature of combustion gases with each load cycle. Also at EGR10, the NO_x is found less as compared to that of EGR0 and vary between 99 ppm - 201 ppm from minimum to maximum load showing increment of 52%. Similarly the increment of 9.63% and 2.93% when EGR 20 and EGR 30

being supplied to the engine. At EGR 40, the prominent results are obtained where the decrement of 4.78% is observed. The adulteration of percentage of exhaust gas with fresh intake charge make the charge leaner and lowers the heating capacity to a great extent. This causes the delayed combustion of charge after spark ignition producing less heat and ultimately reduces the combustion temperature inside cylinder. So the NO_x formation is affected and its percentage in exhaust gas decreases.

Carbon dioxide is a green house gas and as far as possible it is beneficial to have exhaust gas composed of CO_2 and water. This means that all the harmful emissions such as CO, HC, NO_x should be converted to CO_2 or water. The CO_2 variation with speed for different EGR rate is as plotted in Fig. 6.20-d. Here CO_2 emission at EGR0 shows the variation from 0.72% to 1.51% over the speed range 1290-1700 rpm while running at CR10. However with increase in EGR rate to 10% the CO_2 percentage in exhaust gas shows decrement of 16% upto 1440 rpm but thereafter the decrement of 27% up to speed 1700 rpm is recorded. This is clearly justified from the CO emission as shown in Fig. 6.20-a. The CO_2 is found less with the excess air ratio because with the lean combustion the oxygen in air is more than enough for combustion (Jeong et al., 2009). Also the combustion temperature is high during higher load condition which cause oxidation of CO to form CO_2 and H. If EGR rate is increased further then CO_2 decrement is 2.46 %, 4.92 % and 3.89 % as observed for EGR 20, EGR 30 and EGR 40 respectively.

B. Effect of EGR

The effect of EGR is clearly seen for the harmful exhaust gases such as CO, HC, NO_x and CO_2 as shown in Fig. 6.21. As seen in Fig. 6.21-a, the CO variation with EGR rate shows that the CO increases with increase in EGR rate for all CRs. There is increment of 3.57 %, 14.60 % and 41.11 % respectively for CR 8, CR 9 and CR 10 when engine operated at speed 1390 rpm. It is observed that there is small increment at lower CR and the increment rate keeps on increasing with increase in CR.

This may be because at lower CR, the CO emission is more due to lower combustion temperature causing incomplete combustion. This remains same even after addition of heavy EGR (40%).

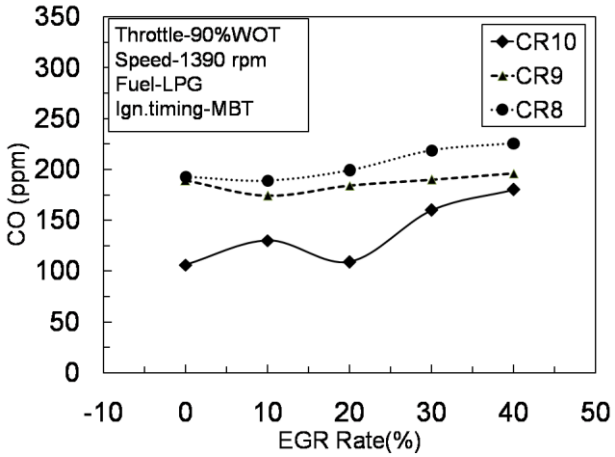

Fig.6.21 (a) CO variation with EGR rate at 1390 rpm

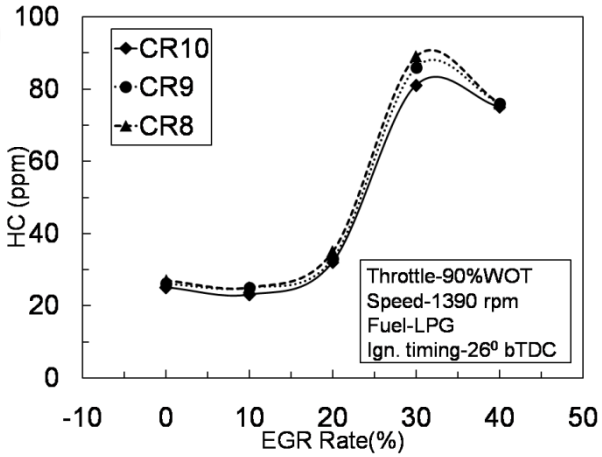

Fig.6.21 (b) HC variation with EGR rate at 1390 rpm

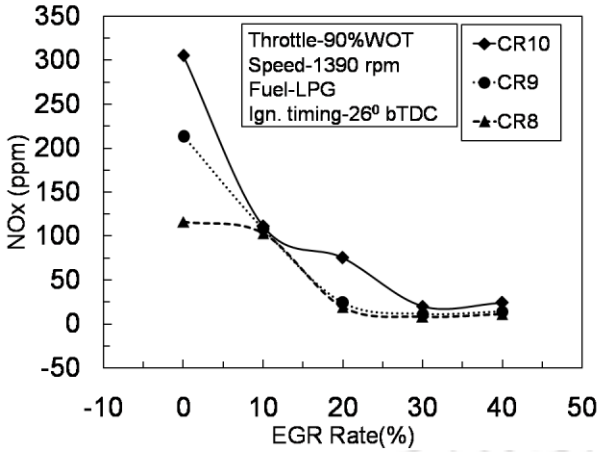

Fig.6.21 (c) NOx variation with EGR rate at 1390 rpm for different CR using LPG fuel at 90% throttle

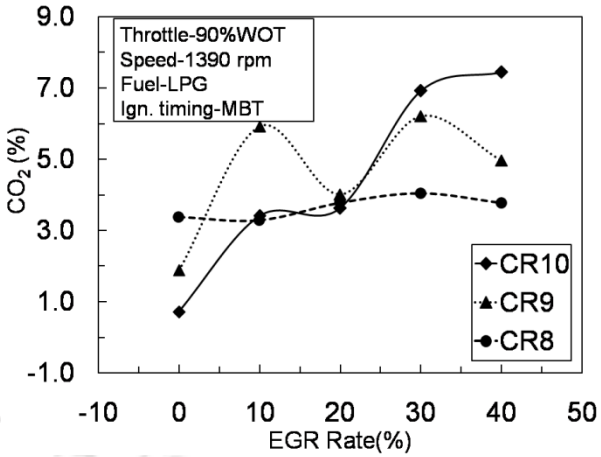

Fig.6.21 (d) CO_2 variation with EGR rate at 1390 rpm for different CR using LPG fuel at 90% throttle

So, overall the magnitude of CO in exhaust is more for all EGR with respect to other EGR rate. However at higher CR (CR10), the combustion temperature is more and with variation of EGR rate, the combustion is greatly influenced causing such a big variation in CO emissions (Fig.6.21-a). Other gas HC is a major constituent, its emission is plotted with EGR rate for different CR as shown in Fig. 6.21-b. The SI engine when operated at CR10 and speed 1390 rpm with 90% throttle, there is decrement of 8.0% from EGR 0 to EGR 10. But thereafter there is sudden increment of 69.33 % from EGR 10 to EGR 40.

In the initial phase when EGR is increased from 0 to 10%, the combustion is found improved causing slight decrease in HC emission. But with further increase in EGR rate, the abnormal combustion happened because of degrade in quality of fuel causing certain amount of charge left unburnt. This ultimately increases the HC emission. At EGR 0, with CR10, the compression pressure is more and hence the post combustion temperature is higher causing homogeneous combustion. Hence HC emission is less. If the compression ratio is changed to 9, the combustion temperature is found reduced and ultimately there is increment of HC emission by 3.84%. If further, CR gets reduced to 8 then HC emission can be found increased by 7.41% with respect to CR10. Even at EGR 40, there is increment of 2.0% for CR10 to CR9 further to CR8.

Oxides of Nitrogen (NO_x) emission is as plotted in Fig. 6.21-c which shows the decrement in NO_x with increase in EGR rate. NO_x emission is combustion temperature dependent and if there is a rise in temperature then there will be more NO_x and vice-a –versa. Accordingly, at CR10, and speed 1390 rpm the NO_x is 305 ppm at EGR0 which reduces to 111 ppm when EGR10 is incorporated in engine. This is happened due to the decrease in combustion temperature on account of reduction in fuel quality in terms of its heating value. Further with increase in EGR rate to 20%, the NO_x is 75 ppm showing decrement of 35% with respect to EGR0. The EGR here is really influenced the combustion pattern and reduces the NO_x emission. With further rise in EGR rate to 30% and 40%, there found a decrement of 93% and 92% respectively with respect to EGR0. This shows the EGR could be effective

technique for lowering down the NOx emission. However there is little compromise in the BTE with addition of EGR.

The carbon dioxide (CO_2) emission due to combustion of LPG fuel in SI engine is as plotted in Fig. 6.21-d. Here, the CO_2 emission found increase with rise in EGR rate. This could be because of EGR composed of CO_2 as one of the constituent which increases with EGR rate. At CR10, the CO_2 shows increment of 90% from EGR 0 to EGR 40 when running at speed 1390 rpm. Similarly the increment of 62% and 11% for CR 9 and CR 8 respectively. The CO_2 emission rate at EGR 0 shows increment of 62% and 78% with rise in CR from 10 to 9 and further to CR8. The trend remains same till EGR 20. Thereafter the nature remains changed and CR10 shows maximum CO_2 emission as compared to that with CR9 and CR8.

6.3.4 Raw biogas fuel performance analysis with EGR

Investigations are continued with the raw bio gas to understand the effect of EGR. These studies are desirable to reduce the pollution in the presence of bio gas fuel. In these set of experiments, EGR rate is varied between 0% - 25% while engine speed is maintained constant.

A. Effect of EGR

Effect of EGR for different CR of the engine on its performance parameters such as BSFC and BTE is as shown in Fig. 6.22 and Fig. 6.23. .Brake specific fuel consumption is having major impact of EGR for any CR. It has been already noticed, in earlier section that, rise in CR leads to decrement in BSFC for a particular speed and load on the engine.

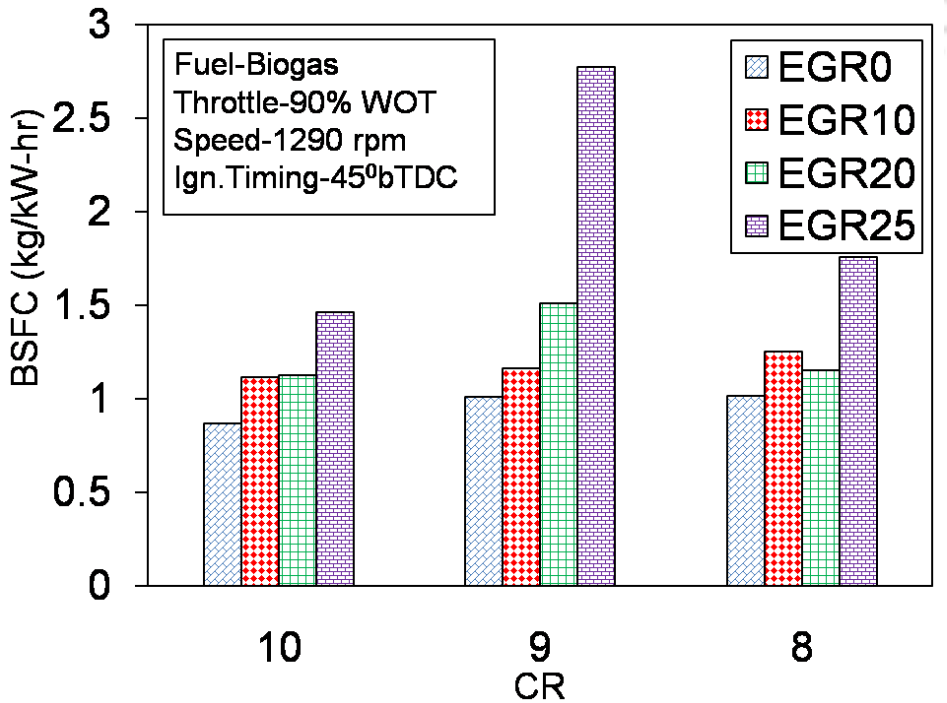

Fig.6.22. Variation of BSFC with CR for different EGR Rate.

But the same fact is found untrue for some EGR rates. For no EGR case, BSFC reduces by 0.4% when CR rises from 8 to 9.

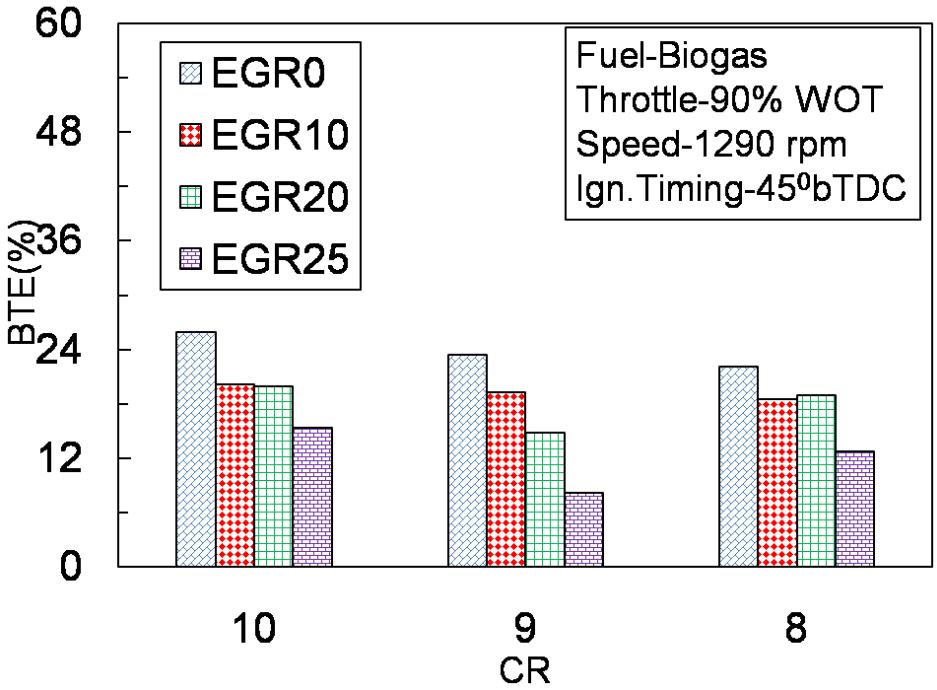

Fig.6.23. Variation of BTE with CR for different EGR Rate.

Further rise in CR to 10 lowers the BSFC by 14%. Similarly along with EGR10, if CR is raised from 8 to 9 and then from 9 to 10, the percent decrement is 7% and 0.4% respectively (Zheng and Huang, 2009). Also at EGR 20, if CR is raised from 8 to 9, there is unexpected rise in BSFC by 24% but further rise from 9 to 10 gives 25 % decrement in BSFC.

However, when EGR25 is supplied to the engine, the combustion is not found to be smooth. Here also, the BSFC increases by 54% while rising CR from 8 to 9, onwards for CR 9 to 10, BSFC shows decrement of 43% (Chandra et al.,2011).

Thus it is evident that, at certain CR the BSFC does not follow the trend for EGR. It could be because the selected compression ratios are low for bio-gas as fuel and it had led to uneven combustion.

The BTE variation with compression ratio is plotted in the Fig. 6.23 for varying EGR rate where the BTE can be found increasing with increase in compression ratio (Huang and Crookes., 1998; Chandra et al., 2011; Porpatham et al., 2010 and Taylor, 1985). If CR is raised from 8 to 9 then percentage increment is 5.5% and 4.25%, for EGR0 and EGR10 cases while there is decrement of 27% and 36% for EGR 20 and EGR 25 respectively. But when CR increases further from 9 to 10, the percent increment is 9.26%, 4.05%, 25% and 47% at EGR 0, EGR 10, EGR 20 and EGR 25 respectively. The BTE is greatly affected due to EGR which increases CO_2 in the intake charge. So it reduces the combustion temperature and hence net heat released gets reduced which affects the thermal efficiency of the engine (Bedoya et al., 2013; Sahoo, 2011).The effects of treated EGR for experimental conditions of

CR 9, 90% WOT and speed 1290 rpm are presented in Fig. 6.24 in terms of cylinder pressure.

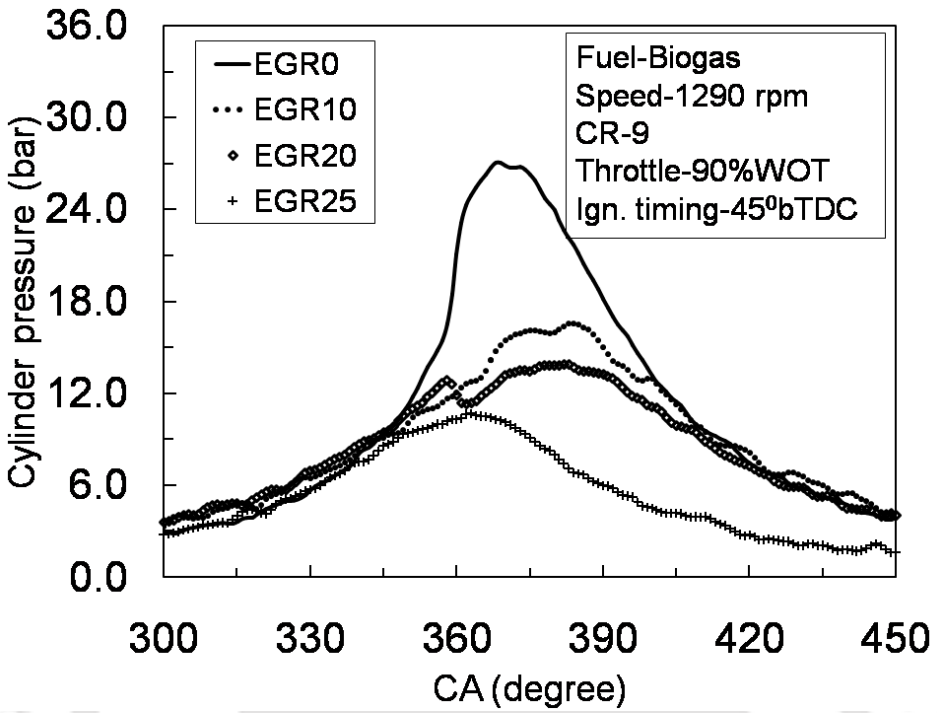

Fig. 6.24. Cylinder pressure variation with crank angle for different EGR

The peak cylinder pressure is clearly seen to be decreased with increase in EGR rate from 0 to 25 %. For no EGR case, the maximum cylinder pressure is measured as 27.018 bar at 369 ^{0} CA. If EGR is kept as 10 then peak pressure decreases and it is 16.578 bar at 387 ^{0} CA.

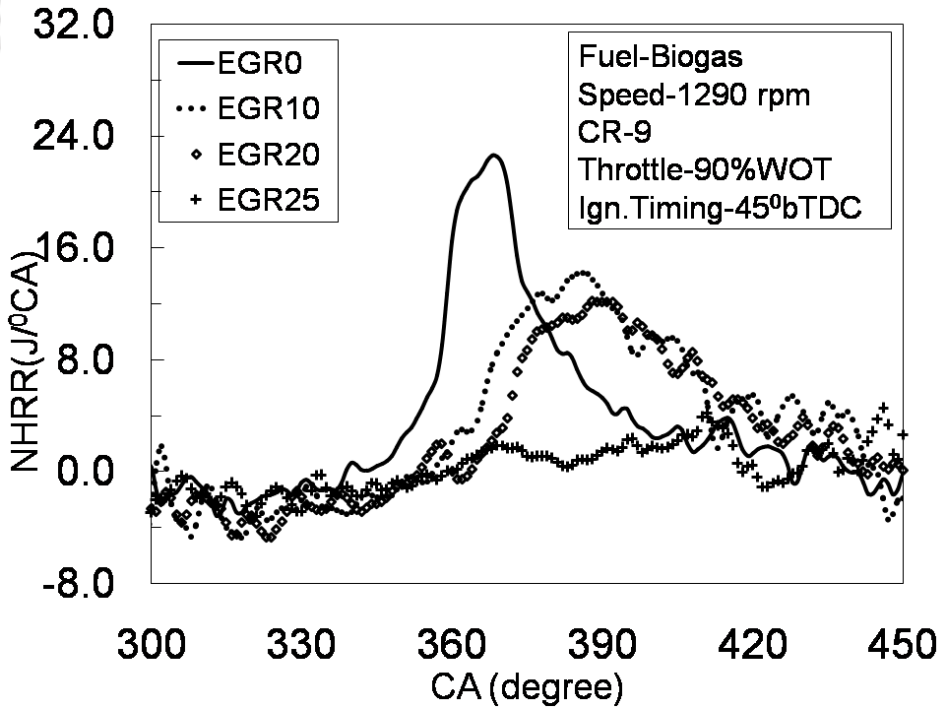

Fig 6.25. Net Heat Release Rate variation with crank angle for different EGR

At EGR20, the cylinder pressure is 13.912 bar at 388 ^{0} CA. It could be seen that cylinder pressure not only reduces with increase in EGR but also the spark advance of peak pressure shifts ahead from the TDC causing delayed combustion. The peak pressure and respective crank angle depend upon the percentage EGR supplied to the engine. This is mainly due to higher auto ignition temperature of biogas and reduction of the effective heating value of the charge due to EGR. These two things lead to lowering the combustion rate and reduction of peak pressure. It is also clear from the figure that, with rise in EGR, the combustion is not smooth and there are pressure pulses (Fontana and Galloni, 2010). Thus higher EGR leads to fluctuations in cylinder pressure along with its delay and lower value.

Variation of net heat release rate (NHRR) with crank angle, for same engine running conditions as those for Fig.6.23, is plotted in Fig.6.24 for different EGR rates. It is evident here that the NHHR depends strongly upon the EGR rate. With EGR0 the NHRR is 22.623J/ ^{0} CA at 368 ^{0} CA which further reduces to 14.233 J/ ^{0} CA at 386 ^{0} CA for EGR10 (Fontana and Galloni, 2010). The EGR20 case shows 12.233J/ ^{0} CA at 387 ^{0} CA which is further reduced with respect to EGR 0 and EGR 10. The NHRR for heavy EGR 25 shows no definite peak having magnitude of 9.549 J/ ^{0} CA over range of crank angle about the TDC position. The calorific value of the intake charge reduces with increase in EGR and there is also reduction of oxygen which in turn leads to prolonged combustion. This is the reason for peak NHRR getting shifted away after TDC with respect to EGR0 case. The important ingredient in EGR is CO_2 which causes the reduced NHRR with rise in its rate. Thus, analysis of the Fig.6.25 is in coherence with that of Fig. 6.24.

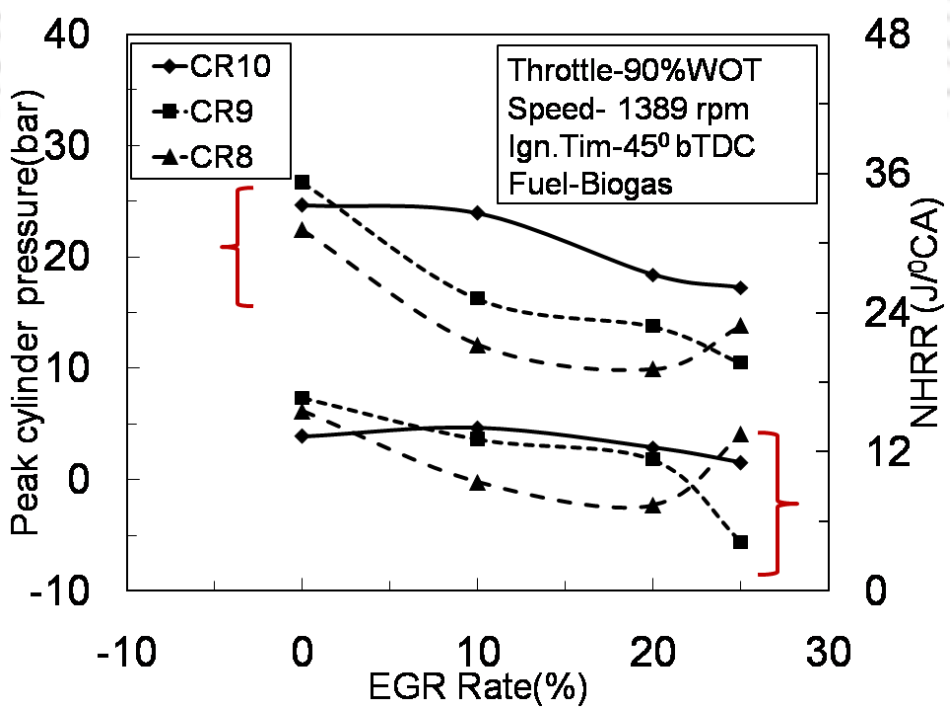

Fig.6.26. Variation of peak cylinder pressure and NHRR with EGR rate.

The variation of peak cylinder pressure with that of EGR rate for different CR as represented in Fig.6.26 shows that with increase in EGR rate the pressure falls which was seen in Fig.6.26

also. At the other end, at a particular EGR rate with decrement of CR, there is decrease in peak pressure. This may be due to the increase in total volume of cylinder causing the lower compression pressure of constant mass of air and fuel inside combustion chamber and ultimately reduced the combustion rate and lowered peak cylinder pressure. At EGR0, the peak cylinder pressure for CR10 is lower than that of pressure at CR9 by 7.61%. This may be happened due to the quality of raw biogas as discussed earlier (Walsh,1988). However at EGR10, there is substantial decrement of 32.19% and 25.55% for CR reduced from 10 to 9 and further to CR8 respectively. This percentage decrement is 25.23% and 27.93% for EGR20 is observed. At maximum EGR rate the combustion is not proper and hence the pressure pulsations are observed showing 39.30 % increment and 24.34 % decrement when engine functions at CR 10 transfer to CR 9 and at last CR 8 respectively.

The peak NHRR variation with EGR rate for varying CR is as plotted in Fig. 6.25. The NHRR as discussed before in Fig. 6.25 influenced to a great extent by EGR rate. The raw biogas fuel itself is a very lower calorific value fuel containing 46% CO_2 in our case. If such fuel is further added with EGR containing CO_2, dilutes the fuel air charge and reduces the heat capacity. At EGR 0, the peak NHRR for CR 10 is lower than that of CR 8 and CR 9. However if EGR rate is increased to EGR 10, then there is decrement of 6.98 % and 28.16 % when CR decreases from CR 10 to CR 9 and further to CR 8. Similar trend is observed at EGR 20 as well. However at EGR 25, there is increment of 62.15% in NHRR from CR 10 to CR 9 and 69.0 % decrement from CR 9 to CR 8. As stated previously the combustion consistency is poor at EGR 25 causing abnormal outcomes.

Mean gas temperature due to heat release can be computed using the plot for NHHR using equation from APPENDIX-C (Stone,1999). This temperature for different EGR and different CR are given in Table 6.1. It is clear from the table that the mean gas temperature increases with increase in CR for any EGR rate.

Table 6.2. Details of combustion for VCR and EGR rate for biogas fuel

CR	Mean Gas temperature (K)				Combustion initiation (MBF10%)			
	EGR0	EGR10	EGR20	EGR25	EGR0	EGR10	EGR20	EGR25
10	902	868	739	879	351	354	348	355
9	859	783	686	520	352	355	356	359
8	836	651	551	432	353	353	364	364

Along with this, mean gas temperature decreases with increase in EGR rate for any CR. The gas temperature variation thus supports the observation from Fig. 6.26.

Percent mass fraction burned (MFB)with respect to crank angle for different EGR rates at 1290 rpm and CR9 is as shown in Fig 6.27. It can be judged from this figure that 90% mass fraction gets consumed from 20 ^{0} bTDC to 10 ^{0} aTDC for EGR0 using raw biogas fuel. At

TDC position, the MFB for pure biogas is 69.76 % which is reduced to 15.474 % when added with 10% EGR in biogas. If the EGR is increased to 20 percent, MFB at the same state is 8.926 %. Further the results of EGR 25 are showing vague results owing to uneven combustion in engine.

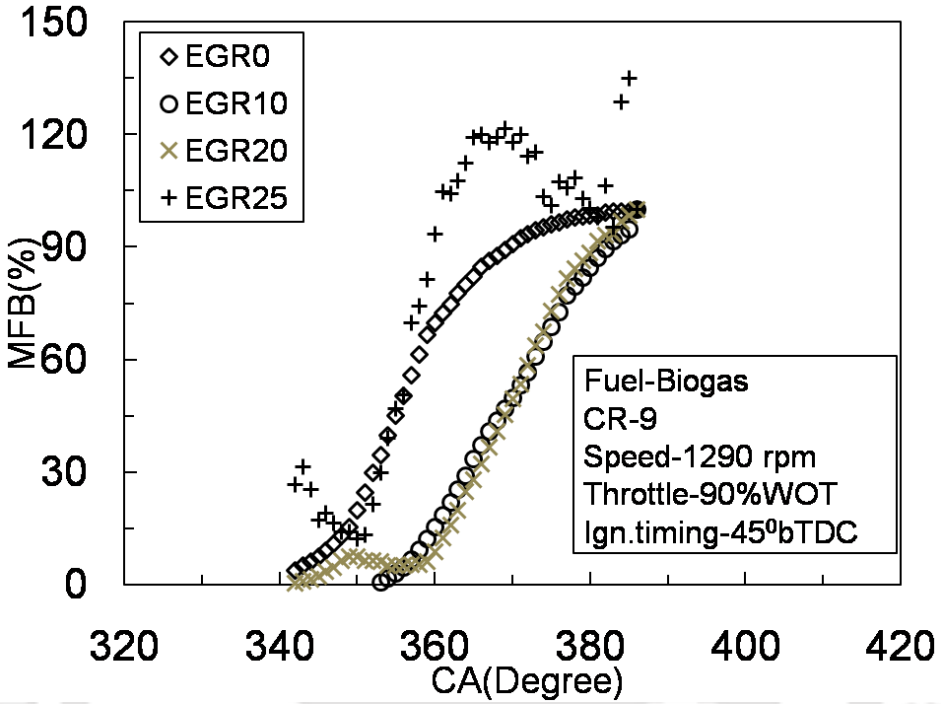

Fig 6.27. Mass Fraction burned with crank angle for different EGR distribution

Thus, with increase in EGR rate, charge burning rate gets reduced and so combustion process extends after TDC leading to increase in the combustion duration.

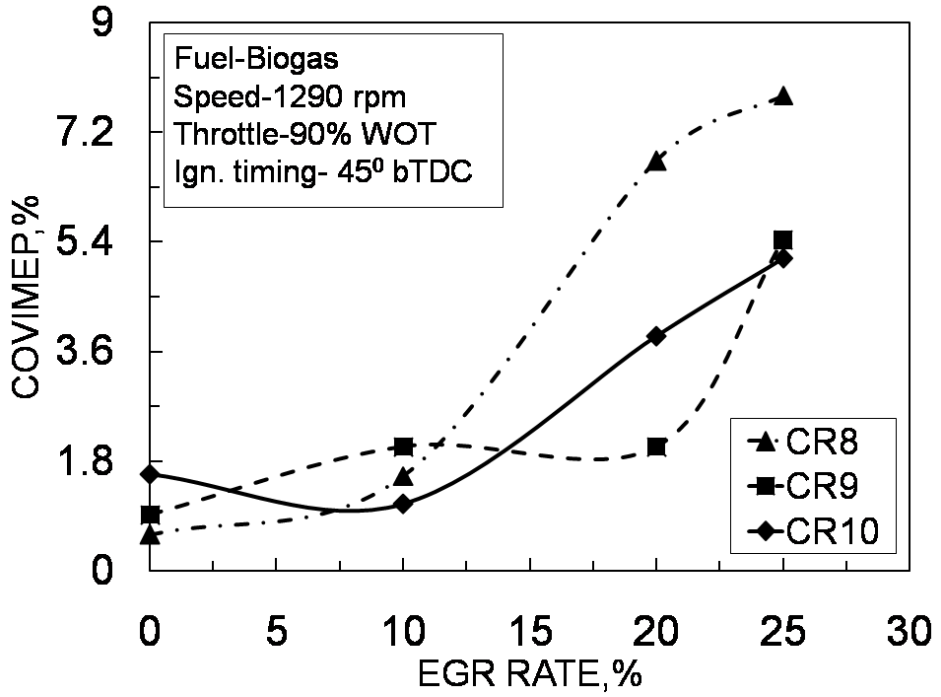

Fig 6.28. Cycle-by-cycle variations for biogas with different EGR and CR

So this figure also asserts the earlier conclusion that the addition of residual gas reduces the overall calorific value of the charge and delays combustion which in turn may lead to incomplete consumption of the charge. Combustion analysis can be further carried out using Table 6.2. Here combustion initiation is expressed as the crank angles required for 10% burning of fuel, and it is calculated from Fig. 6.27. It can be seen here that combustion initiation depends upon the EGR rate for the fixed ignition advance of 45 ^{0} bTDC (315 ^{0} CA). In absence of EGR (EGR 0), the combustion initiation is found to be 351 ^{0} CA at CR10 which rises to 352 ^{0} CA when engine runs at CR 9. Also with CR 8, the ignition delay is further raised to 353 ^{0} CA. The ignition delay increases with decrease in CR for the reason of lower fuel-air homogeneous quiescent mixing in a constant volume chamber at lower compression pressure (Pan et al., 2014). So the time required for initiating flame increases which leads to increase in ignition delay. With addition of EGR, very first observation is that the ignition delay increases for all CR as compared to no EGR case. It is mainly due to the fact that dilution of fuel-air mixture due to EGR further increases the auto ignition temperature of the charge. So, higher the EGR higher will be the ignition delay.

Cycle-by-cycle variation in indicated work per cycle (COV) is presented with respect to EGR rate in Fig. 6.28. As per the figure, the COV keeps on increasing from EGR 0 to EGR25 (Fontana and Galloni, 2010; Debnath et al., 2013). In general, it is expected to have low COV because the engine stability starts to deteriorate if COV exceeds above 5%. At EGR0 the combustion is smooth showing very less variation in cylinder pressure per cycle. Upto EGR10, the curve is smooth and having less slope for all CRs.

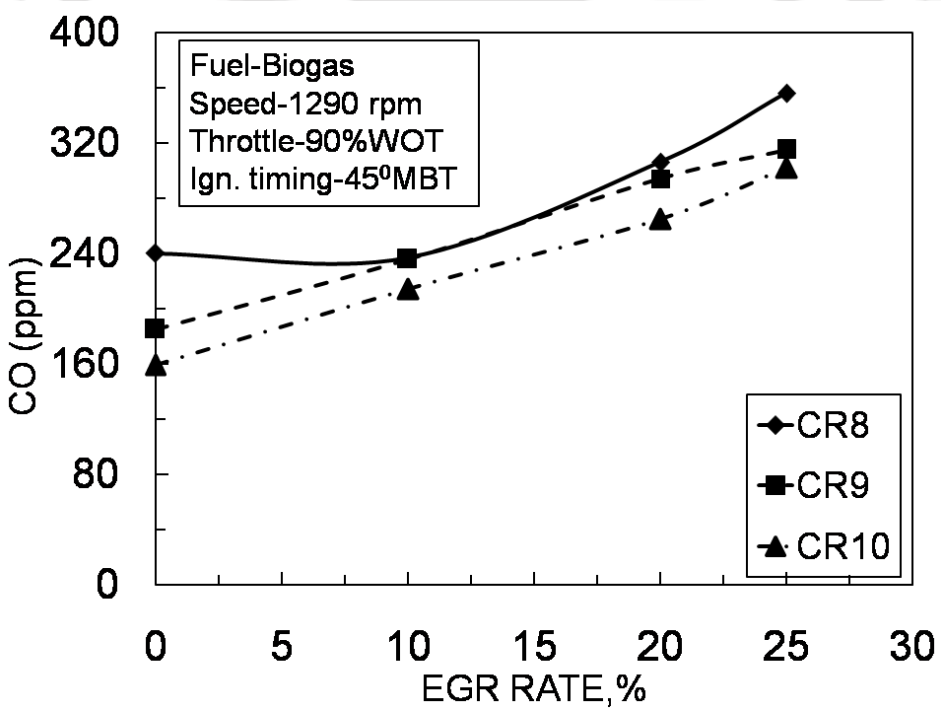

Fig. 6.29 Emission of CO for different EGR rate and CRs.

But when EGR level reaches to 20%, the cycle-by-cycle variations are pulsating which shows abnormal combustion reducing the stability of the engine. When EGR level raises to 25%, the COV crosses the limit for all CRs. Although, fuel type, combustion duration, flame kernel

and noise in pressure transducer are the major reasons of COV variation (Pan et al., 2014), it is evident here that the charge, which has exhaust gas with it, is responsible for the variation of COV.

Major usefulness of EGR is in controlling the emission of exhaust gas. In this regards, here the variations of CO, NO_x and HC with CR and EGR for raw biogas fuel are given in Fig. 6.29 to Fig. 6.31. As seen in the Fig. 6.29, the CO content increases with increase in EGR rate from 0 to 25 for all the CRs. Amount of CO at CR 8 is 216 ppm for EGR0 which rises to 237 ppm, 306 ppm and 356 ppm with EGR 10, EGR 20 and EGR 25 respectively. The similar trend is also followed for higher CR 9 and 10. The reason of raising the CO concentration in exhaust gas is that the fuel-air mixture combined with EGR does not have enough oxygen for converting carbon to carbon dioxide. As a result of it, part of fuel does not burn and the carbon remains in the form of CO. Similar observation was made by Midkiff et al., 2001.

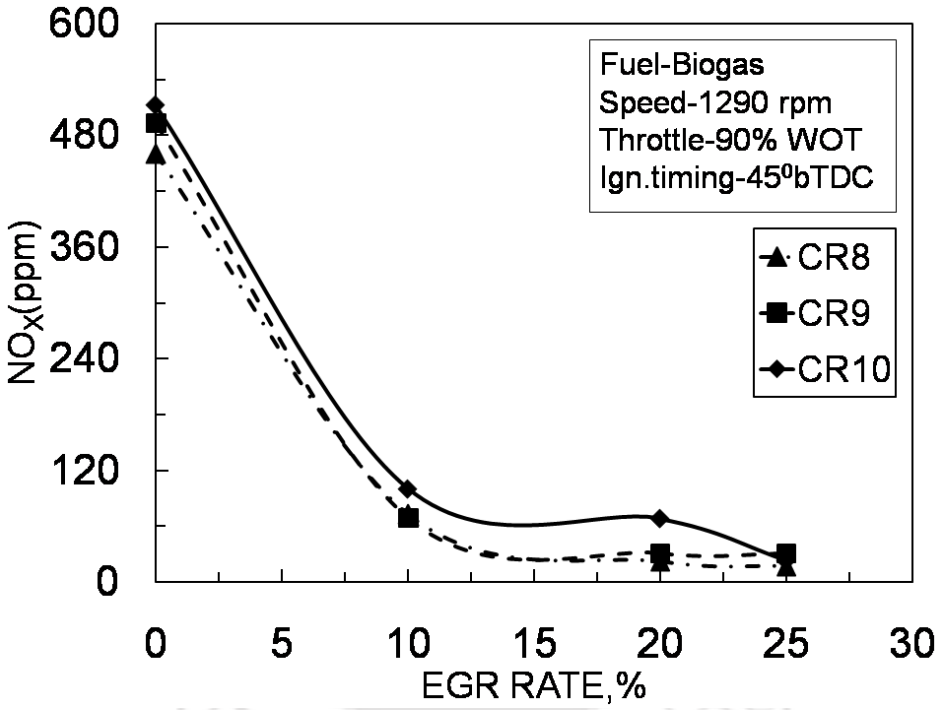

Fig 6.30 Emission of NOx for different EGR rate and CRs.

From the variation of CO with CR, it is evident that rise in CR leads to lower CO concentration in exhaust gas. The percentage decrement of 33.75 % has been observed when CR raises from 8 to 10 at EGR 0. This decrement was 9.70 %, 6.80 % and 15.16 % for rise in EGR rate to 10, 20 and 25% respectively. Lower the CR, lower will be the heat generated in combustion chamber causing reduction in combustion temperature. Similar findings are also reported by author Huang and Crooks, 1998.The variation of nitrogen oxide (NO_x) with EGR Rate is plotted in Fig. 6.30. It is found that the NO_x concentration in exhaust gas is 512 ppm, 493 ppm and 460 ppm at CR10, CR9 and CR8 respectively for no EGR case. This reflects that, NO_x concentration in exhaust gas increases with increase in CR (Huang and Crookes,1998). The reason for this is the increase in combustion temperature with rise in cylinder pressure due to increase of CR. After supply of very light, EGR10, it can be noticed

that the NO_x in exhaust gas decreases drastically to 100 ppm, 69 ppm and 73 ppm at CR10, CR9 and CR8 respectively (Lee et al.2010). There onwards with increase in EGR in stages of 20 and further to 25% continues to decrease the NO_x concentration (Alger et al., 2012).

At EGR 25, the NO_x concentration is 23 ppm, 31 ppm, 17 ppm at CR10, CR9 and CR8 respectively. Thus, having EGR mixed with charge, NO_x emissions seems to be reduced. This is due to reduced heat release and lower combustion temperature. These observations portray usefulness of EGR in reducing the emission of NO_x for biogas based engines.

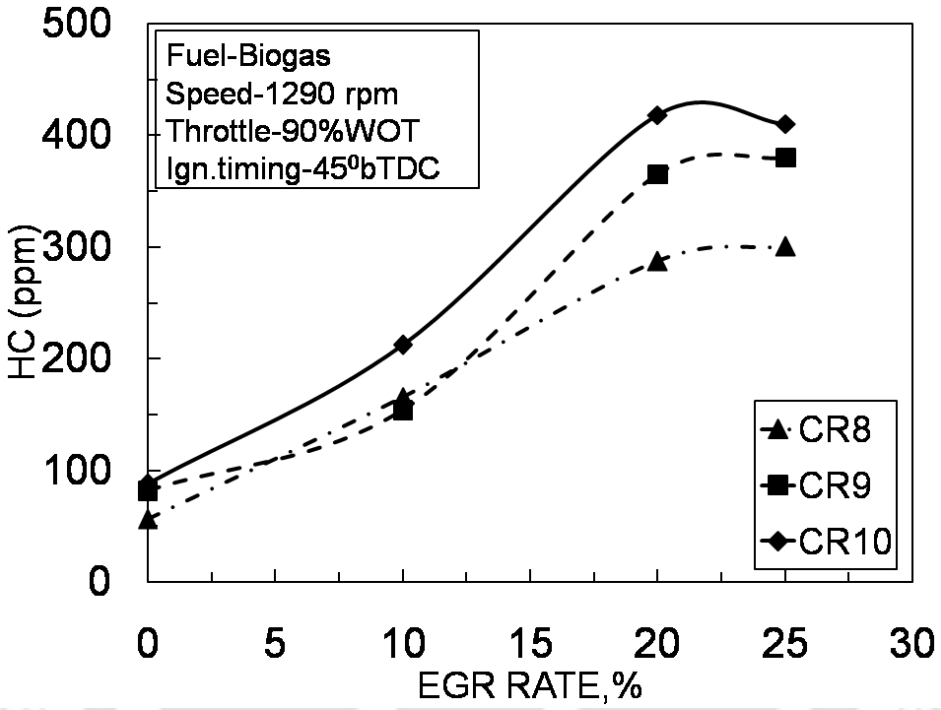

Fig 6.31 Emission of HC for different EGR rate and CRs.

The unburnt hydrocarbon (HC) variation with EGR rate is given in Fig. 6.31. Variation of HC with CR shows that with increase in CR, HC emission is increased (Porpatham et al.,2007). As shown in same figure, the HC concentration increases with increase in EGR rate (Hu et al., 2009; Debnath et al., 2003). At CR10, HC emission is 88 ppm which reaches to 418 ppm at EGR 20. Similar trend is seen for other compression ratio also. Thus, presence of HC is noticed to be higher at higher CR and higher rate of EGR.

B. Effect of speed

The emissions as produced due to combustion of raw biogas in SI engine are here by plotted in Fig. 6.31. The harmful CO emission is plotted with respect to speed for different EGR rate at 90% WOT as shown in Fig. 6.31(a). As seen from the figure, CO emission keeps on reducing with increase in speed which was discussed in Fig. 6.10. It is important to note here is the distribution of CO in presence of EGR rate and CO variation with speed. The trend followed remains the same as that of EGR 0. The CO emission ranges between 137-214 ppm, 173-265 ppm and 226-302 ppm for EGR 10, EGR 20 and EGR 25 respectively in decrease in order. Raw biogas composition containing CO_2 is a very poor fuel from SI engine view point. In addition to that if EGR rate is inducted with intake charge, makes the charge dilute with

more percentage of incombustible constituents in the fuel. This causes the decrease in volumetric efficiency in turn amount of oxygen for complete combustion, thereby showing more CO at each speed with respect to EGR0. At a particular speed of 1282 rpm, the increment in CO is 34.59 % ,66.67 % and 89.92 % for EGR 10, EGR 20 and EGR 25 respectively with respect to EGR 0. Incomplete combustion and absence of oxygen doesnot convert complete CO into CO_2. That is why the CO emission found increased with EGR as shown in Fig.6.32(a). Even at higher speed 1607 rpm, increment of 71.25%, 116% and 182% is recorded for CO emission with respect to EGR 0.

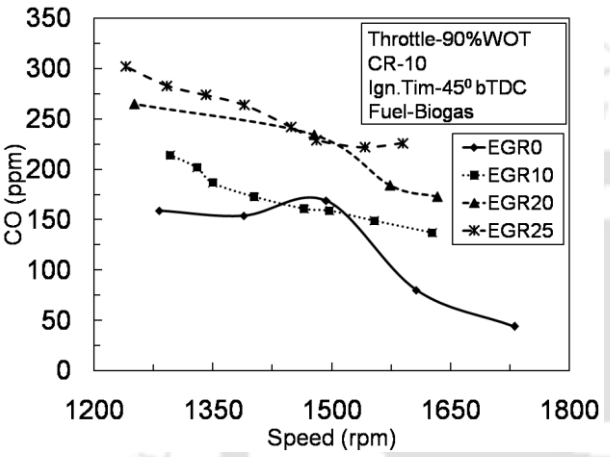

Fig.6.32 (a) CO emission variation with speed for different EGR Rate with biogas fuel

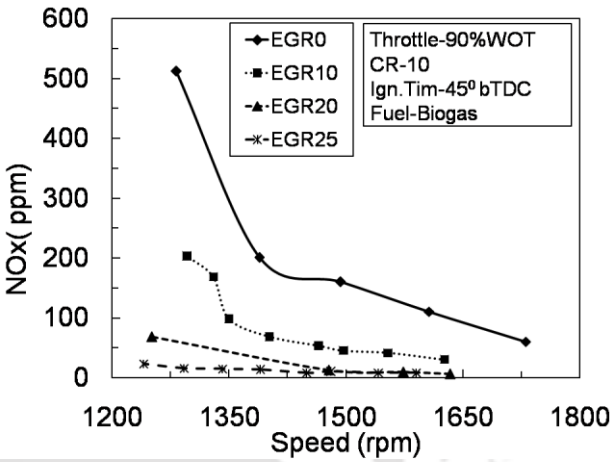

Fig.6.32 (b) NOx emission variation with speed for different EGR Rate with biogas fuel

As shown in Fig.6.32(b), Nitrogen Oxide(NO_x) emission is found decreasing nature with increase in speed for all the EGR rate from 0% to 25% discussed herein. The decrease in NO_x with increase in speed ranges between 512 - 60 ppm, 203 - 30 ppm, 68- 6 ppm and 23- 8 ppm respectively for EGR 0, EGR 10, EGR 20 and EGR 25 respecively. The results are promising interms of reduction of NO_x with addition of EGR in the intake charge. Whtih the increase in EGR rate, the diluted mixture of fuel, air and exhaust recirculated gas makes the charge leaner and thereby reduces maximum temperature reached inside combustion The NOx emission is greatly influenced with EGR rate and shows that with increase in EGR rate, the NOx emission found reduced (Fig.6.32-b). At speed 1282 rpm, the NOx shows decrement of 60.35%, 86.72%, 95.51% for raw biogas combustion with EGR10,EGR20 and EGR25 respectively with respect to EGR0. Even at higher speed say 1607 rpm, the percentage decrement of 72.72 %, 94.5 % and 92.73 % in NOx is observed with respct to EGR0. The exhaust of the engine becomes environmental friendly in respect of NOx emission.

6.3.5 Raw biogas fuel with full and part throttle position

The biogas is used in spark ignition engine and at CR range from 10 to 8 both at 90%WOT and 50% WOT. The throttle valve is manually operated and the throttle position is recognised by throttle sensor. The performance of the engine during part throttle is important from the fuel economy view point. So the effect of speed, load and stoichiometric air fuel ratio on the perfromance of the engine is important to be discussed herein. As shown in Fig.6.34(a) the brake torque variation with speed in range of 1285 to 1731rpm reported magnitude in range of 7 to 16 Nm at WOT and 3 to 8 Nm at part throttle positions.

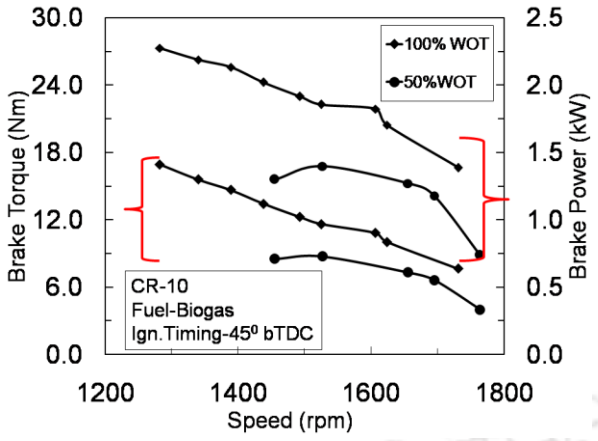

Fig.6.33 (a) Brake Torque and Power variation with speed for different throttle with biogas fuel

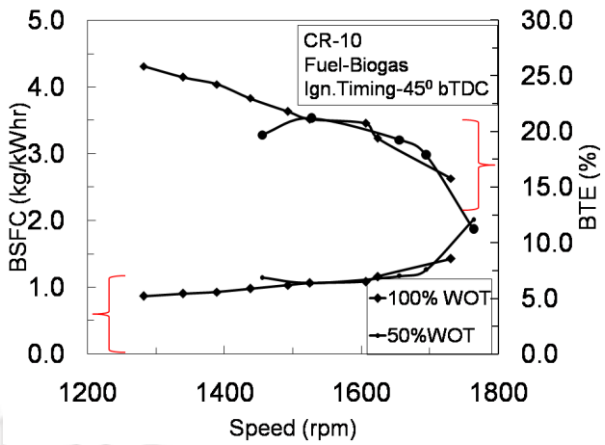

Fig.6.33 (b)) BSFC and BTE variation with speed for different throttle with biogas fuel

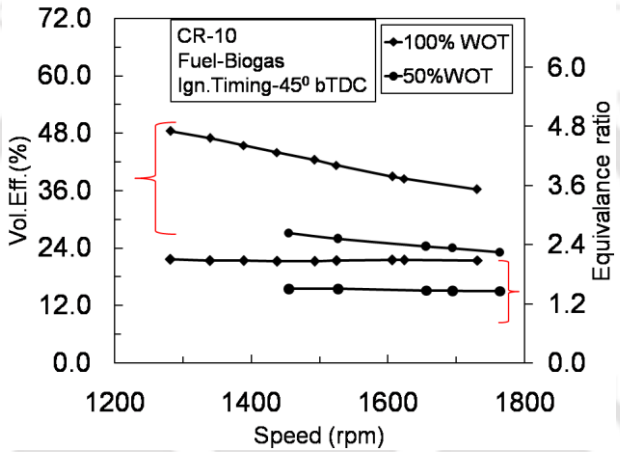

Fig.6.33 (c) Volumetric efficiency and Equivalence ratio variation with speed for different throttle with biogas

The brake power variation with speed is also shown in Fig. 6.34(a) where the brake power is found decreasing with increase in speed. The maximum brake power at CR10 with 90% WOT is 2.27 kW at 1290 rpm . The 64% rise in brake power has been achieved within speed range 1290-1740 rpm. The brake power during part throttle is reduced to 1.30 kW at 1390 rpm with overall increment of 73%. Biogas being a very low grade renewable gas in terms of engine fuel, the brake power obtained is excellent for the experiment test. During 100% throttle, the volumetric efficiency is higher and hence charge has enough oxygen for complete combustion. This leads to the wide load range usage of the engine. On the other side, at 50% throttle, the volumetric efficiency gets reduced and hence it follows poor combustion with unburnt charge left at the exhaust. So the useful load range of the engine gets lowered showing different trends during 100% and 50% throttle position.

The BSFC variation with speed for biogas fuel during WOT and POT is shown in Fig.6.34(b). The BSFC found increasing with increase in speed. The lowest BSFC at 90%WOT is 0.870 kg/kW-hr at low speed condition showing incement with speed and reaches to 1.426 kg/kW-hr at maximum speed. The overall increment in BSFC during WOT is 63.9%. As the mass of fuel supplied to the engine is 1.98 kg/hr which is constant, the only deciding parameter of BSFC variaition is brake power. During part throttle also the BSFC shows the same nature as found during WOT condition and reported the overall rise of 79% in the speed range considered. The BSFC during part throttle is much higher in comparison to

that of WOT. At a particular speed 1390 rpm, BSFC duing 90% WOT is 0.979 kg/kW-hr which is 1.14 kg/kW-hr during part throttle. BTE is a impotant parameter in terms of performance of the engine.

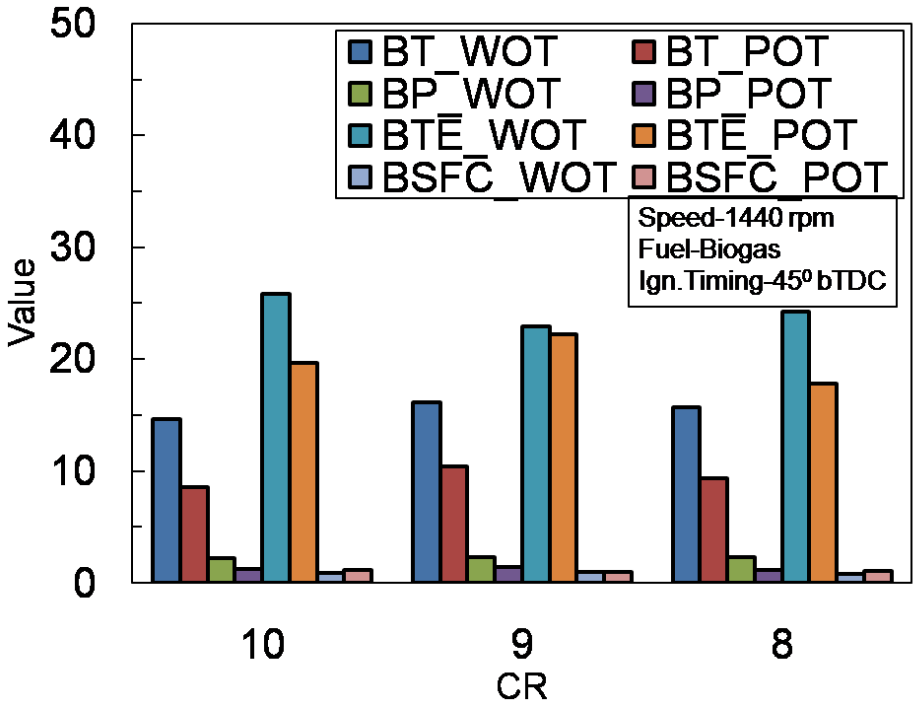

Fig.6.34 Performance variation with CR for different throttle with biogas fuel

The BTE also slopes downward with rise in speed of the engine. At 90% WOT operating at CR10, the maximum BTE achieved is 25.863 % at 1290 rpm which is further reduced to 15.774 % at 1740 rpm. With the rise in brake power on the engine, for the stoichiometric A/F ratio, BTE is directly proportional to brake power. So with increase of brake power represent corrosponding increment of BTE. The overall rise of 64% is found during WOT. Similar trend is followed during part throlttle also where maximum efficiency obtained is 19.70 % at speed 1440 rpm which further reduces to 11.19% at speed 1740 rpm. The quite similar trend is followed for CR9 and CR8 also (Fig.6.34). Volumetric efficiency (Fig. 6.33- c) of the biogas run engine is lying in the range of 36 to 48% at CR10, WOT which is 23-27% during part throttle condition. Similarly at CR 9 also the volumetric efficiency is 34 to 44% from 1370-1740 rpm. Volumetric efficiency depends upon the load and type of fuel used in engine. The gaseous fuel like raw biogas is very low density gas so more volume of biogas needs to be burned at any time to make up the load on the engine. In such a case the intake charge consist of higher percentage of gaseous fuel and remaining is fresh air . So the volumetric efficiency has been found reduced. Also at CR8, WOT the volumetric efficiency is 35% at 1740 rpm and 47% at 1290 rpm.

Equivalance ratio for biogas fueled engine at CR 10 and operating at WOT is 1.1 ± 0.3 for speed range of 1740 rpm to 1290 rpm. It doesnot vary much wth speed. Similarly at POT also the Equivalence ratio is 1.45 to 1.50 . The effect of biogas fuel on the combustion in spark ignition engine is plotted in Fig. 6.33(a). As shown in figure, the combustion initiates earlier than that of petrol fuel because the ignition timing has been advanced to 45 ^{0} bTDC while

using raw biogas fuel. As shown in figure the cylinder pressure is 26.87 bar at 367 ^{0} CA at 1440 rpm with 90% WOT and CR10. While at part throttle condition it was 17.31 bar at 378 ^{0} CA.

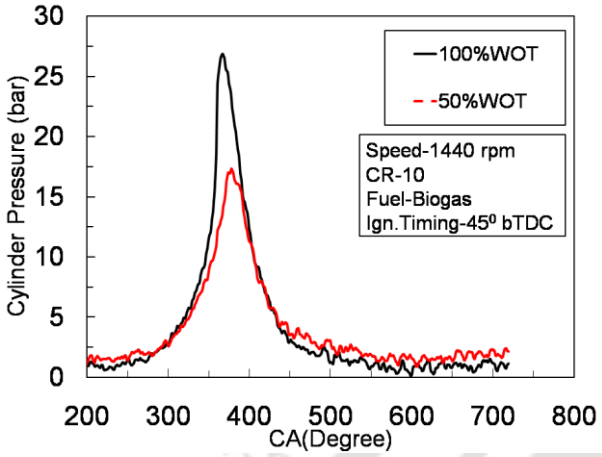

Fig.6.35 (a) Cylinder pressure variation with CA for different throttle with biogas fuel

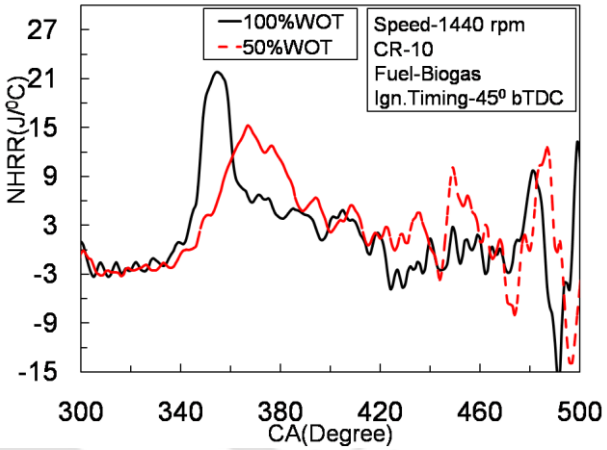

Fig.6.35 (b) NHRR variation with CA for different throttle with biogas fuel

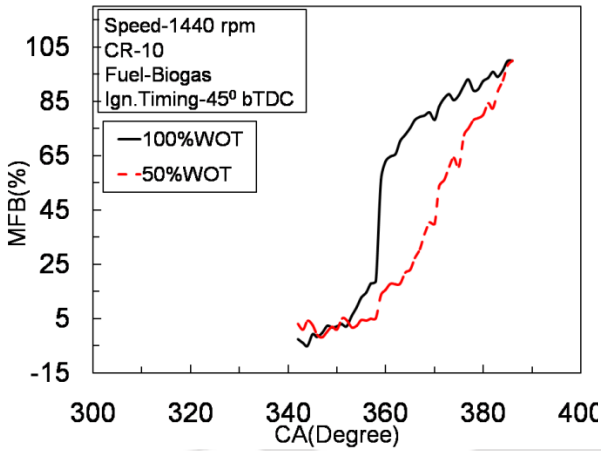

Fig.6.35 (c) Percent MFB variation with CA for different throttle with biogas fuel

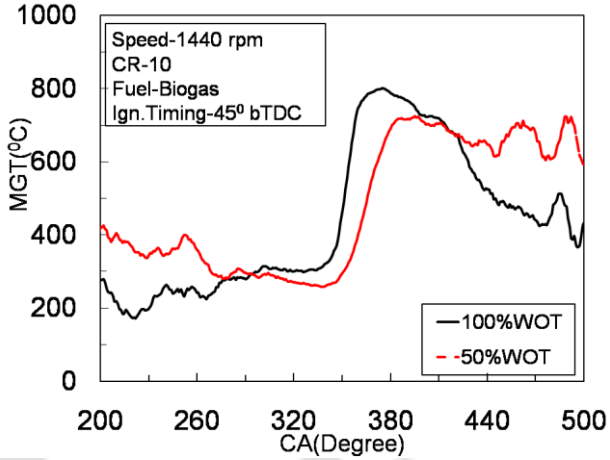

Fig.6.35 (d) Brake Torque and Power variation with CA for different throttle with biogas fuel

This is because the partial closure of throttle valve reduces fuel air mixture supply to the engine. Thereby maximum load carrying capacity gets reduced. Similar trend has been found in the other compression ratio where maximum cylinder pressure is 27.13 bar at 367 ^{0} CA and 21.16 bar at 378 ^{0} CA during WOT and the same at POT are 13.65 bar at 366 ^{0} CA and 13.41 bar at 380 ^{0} CA at CR 9 and CR 8 respectively (Table 6.2). The crank angle at which peak is observed gets delayed aTDC with the decrease in CR.

Net heat release rate (NHRR) as depicted in Fig. 6.35(b) is relation of pressure and actual volume available for combustion of the mixture inside cylinder. The net heat release rate for CR 10 is 21.771 J/ ^{0} CA at 355 ^{0} CA during 90% WOT which is reduced to 15.23 J/ ^{0} CA at 367 ^{0} CA during part throttle condition. At CR 9, it is 23.69 J/ ^{0} CA at 357 ^{0} CA and 13.65 J/ ^{0} CA at 366 ^{0} CA at WOT and POT respectively. Similarly at CR 8, it is 21.354 J/ ^{0} CA at 363 ^{0} CA and 13.41 J/ ^{0} CA at 380 ^{0} CA are obtained. The heat release angle gets shifted towards TDC even aTDC as the fuel combustion takes place.

The mass fraction burned (MFB) for biogas fuel has been plotted at CR10 and speed 1440 rpm as represented in Fig. 6.35(c). During WOT condition, the 62% mass fraction burned while it is 15% during POT. This may be happened due to the volume occupied by intake charge inside combustion chamber before compression is more during WOT causing high compression pressure. When charge is ignited, the flame kernel developed and spread faster across closely packed chamber causing homogeneous combustion. This shows that the combustion is faster during WOT. The combustion duration is smaller and hence the energy released during combustion completely utilized for expansion stroke. With the reduction in compression ratio, the % MFB is 17 % at CR9 and 15% at CR 8 during WOT while it is 20 % at CR 9 and 2 % at CR8 during POT. From the Table 6.3, it is seen that the crank angle at which 10 % mass fraction burned are 354 ^{0},356 ^{0} and 358 ^{0} CA at WOT shows increase in CA to 359 ^{0}, 358 ^{0} and 364 ^{0} CA at POT for CR10,CR9 and CR8 respectively.

Mean gas temperature (MGT) as a function of crank angle has been plotted as shown in Fig. 6.35 (d). The maximum MGT at CR10 and throttle 90% WOT is 800.43 ^{0} C which is found reduced at part throttle to 723.48 ^{0} C. Similarly at CR9, the MGT is 835.19 ^{0} C and 743.67 ^{0} C at WOT and POT respectively. Further at CR 8, the MGT is found to be 908.42 ^{0} C and 794.64 ^{0} C at WOT and POT respectively.

Table 6.3 Combustion parameter variation with CR for different throttle with biogas fuel

CR	Cylinder Pressure, bar		NHRR, J/^{0}CA		%MFB						MGT	
	WOT, bar	POT, bar	WOT, bar	POT, bar	WOT			POT			WOT, ^{0}C	POT, ^{0}C
					10%, ^{0}CA	90%, ^{0}CA	TDC	10%, ^{0}CA	90%, ^{0}CA	TDC		
10	26.875	17.317	21.771	15.23	354	373	62%	359	388	15%	797.39	723.47
9	27.13	17.55	12.05	13.65	356	383	17%	358	380	20%	781.50	743
8	21.16	13.11	21.354	13.41	358	380	15%	364	382	2%	908.42	720.13

6.4 SUMMARY

The conventional VCR mechanism of tilting block method is successfully utilized to check the performance, combustion and emission of the multi-fuel capability engine. Separate intake arrangements are used for LPG and raw biogas fuels. As an outcome these experiments, optimum ignition timing is found to be 26^0 bTDC for LPG and 45^0 bTDC for biogas. The performance of the engine using LPG fuel shows 26.79% BTE at optimum CR10. The lower heating value fuel, raw biogas, shows 23.253% BTE while operating at maximum CR 10. The peak pressure attained by LPG is 34.16bar which is 25.536 bar during raw biogas combustion at CR10 and respective optimum ignition timings. The emissions such as CO and NO_x are of significant magnitude in case of LPG fuel with respect to that of raw biogas fuel. However, HC emission is found higher for raw biogas fuel. Results of these baseline tests for LPG and bio-gas considered as platform for their further improvement using the novel VCR mechanism.

CHAPTER 7

Novel VCR SI Engine using Gaseous Fuels

OVERVIEW

While previous chapter deals with the baseline studies for LPG and biogas using a tilting block type VCR attachment, this chapter concentrates on use of presently proposed VCR technique with the same fuels. In some experiments, both the VCR attachments are used so as to get different spark plug locations for a particular CR. Further CR and spark plug location, both, are alerted to arrive at a better combination for a specific fuel in an SI engine. Therefore present chapter also deals with performance analysis, combustion analysis and emission analysis for all those alterations with and without EGR treatment.

7.1 INTRODUCTION

It is evident that, the gaseous fuels can be efficiently used in conventional spark ignition engine. Along with this, the method of variable compression ratio (VCR) discussed earlier can definitely upgrade the performance of the engine. But the conventional method of tilting block is useful in case of stationary engine and that too with manual intervention to adjust the most optimum CR. However in case of tilting block arrangement; one cannot increase the CR beyond certain final value which is CR10 in our case. So those fuels are not utilized upto mark and thus it increases fuel consumption for producing same power. In order to trace this problem, the research is focused in direction of improving efficiency of the available fuel with increasing the CR over fixed maximum CR of the engine. Here the important point is the engine structural strength which should be capable to accommodate the minute increment in CR (Erkus et al., 2013; Ozcan and Yamin, 2007; Shehata, 2010). The chapter3 elaborates the method of increasing the CR over fixed conventional CR. The method incorporated is novel secondary piston displacement method called as Top-up Mechanism by which the clearance volume of the engine is altered for increasing the compression ratio. Hence this chapter explores the petrol engine modified to run with LPG as well as raw biogas fuel for a range of compression ratio and range of spark locations inside combustion chamber.

7.2 NOVEL VARIABLE SPARK PLUG LOCATION RESULTS

The VCR mechanism without changing original location of spark plug is found prominent for all the gaseous fuels in chapter 6. The novel VCR mechanism called as Top-up Mechanism is designed developed and successfully installed in the conventional VCR engine as described in details in chapter 4. So, to analyze the optimum spark plug location for Apex experimental set up using LPG and raw biogas with the top up mechanism is considered herein. The testing

facility is arranged as per procedure laid down in chapter 4. The corresponding results are discussed in this section.

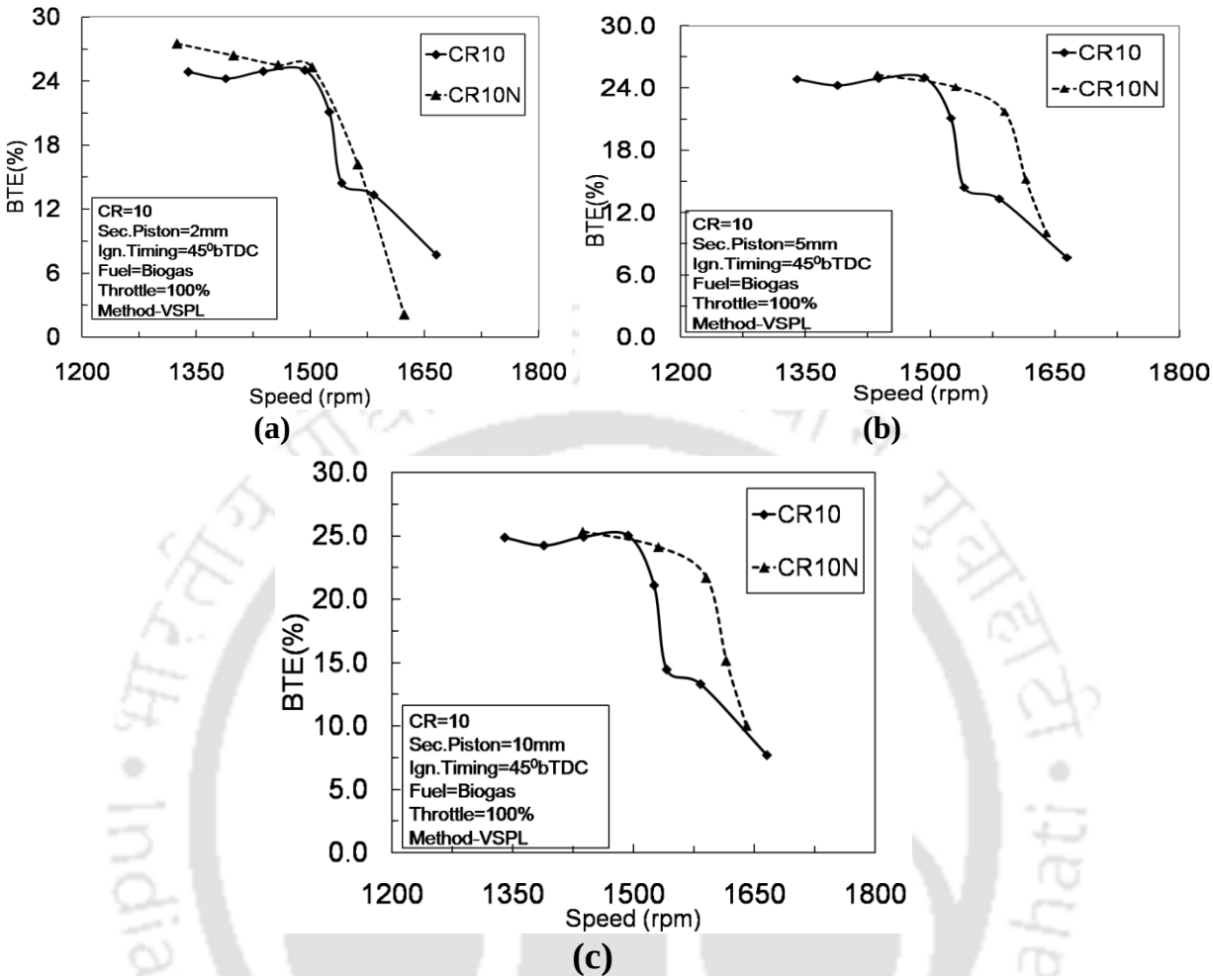

Fig. 7.1 Variation of BTE with speed for different inward displacements of spark plug (a) 2 mm; (b) 5 mm; (c)10 mm. Here CR 10 refers to default setting based CR while CR 10 N refers to use of both VCR mechanisms to attain CR10.

7.2.1 Biogas performance under variable spark location concept.

In order to understand the effect of spark plug location (VSP) in the clearance volume, independently from the compression ratio variation, studies are conducted. In a set of experiments conventional or tilting block VCR mechanism engine is used along with the Top-up VCR Mechanism to achieve compression ratio 10. Three variants of this situation are discussed here where spark plug location is 2 mm, 5 mm and 10 mm from its flush mounting state. Variation of BTE with engine speed for these three cases along with the default flush mounting spark plug case is shown in Fig. 7.1.

Similar observation can be registered here that efficiency decreases with increase in engine speed for all the three cases. From the Fig.7.1 (a), for the spark plug displacement of 2 mm, it can be

Table 7.1. Experiment Matrix for Novel VCR with large VCR engine

Novel VCR Mechanism Engine			
Petrol And LPG And Biogas	50% ,100% (x=2mm)	Increment above normal	CR8.11,CR9.14,CR10.18
		Decrement below normal	CR7.89,CR8.86,CR9.82
	50% ,100% (x=5mm)	Increment above normal	CR8.29,CR9.38,CR10.48
		Decrement below normal	CR7.73,CR8.65,CR9.56
	50% ,100% (x=10mm)	Increment above normal	CR8.6,CR9.8,CR11.02
		Decrement below normal	CR7.48,CR8.33,CR9.16
Novel VCR+ VSP LOCATION Mechanism Engine			
Petrol And LPG And Biogas	50% ,100% (x=0mm)	SP1(CR8,CR9, CR10)	
	50% ,100% (x=2mm)	SP2(CR8,CR9, CR10)	
	50% ,100% (x=5mm)	SP3(CR8,CR9, CR10)	
	50% ,100% (x=10mm)	SP4(CR8,CR9, CR10)	

seen that the BTE remains higher as compared to the default setting of spark plug. Table.7.1 shows the magnitude of BTE for two speeds under study for various spark plug locations. It is evident here that maximum BTE at low speed can be achieved with 2 mm case while for high speed case maximum BTE is associated to 5 mm location. Experiments are then conducted for compression ratios 8 and 9 and analysis of all the results is discussed in following section for specific engine speed.

Table 7.2 The BTE variation for VSP location with speed

VSP location, mm	BTE (CR10)%	
	1390 rpm	1600 rpm
0*	24.900	7.690
2	26.400	2.097
5	25.300	10.00
10	24.100	6.575

*Original location of spark plug.

7.2.1.1 Performance analysis for change in spark plug location

The method of spark plug alteration is discussed in details in chapter 4. In short SP1 represent the original spark plug location, SP2 is the spark plug location with 2mm protrusion of plug inside combustion chamber, SP3 suggest for 5 mm protrusion of plug and SP4 referred for 10 mm protrusion of spark plug. Considering this the analysis is carried out as follows.

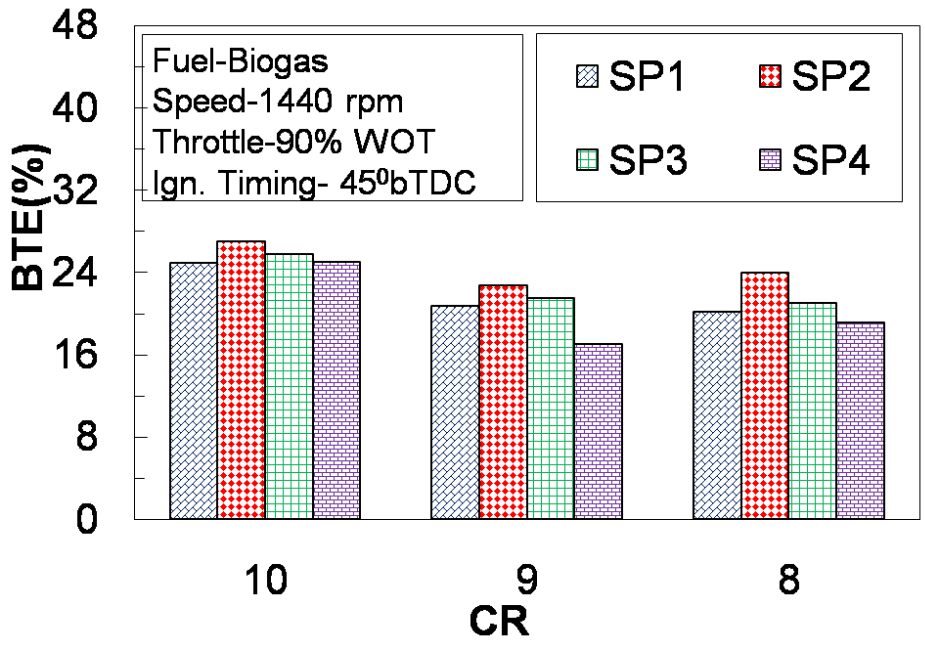

Fig.7.2 BTE variation with compression ratio for different spark plug location

Effect of change in spark plug location on thermal efficiency of the engine is given in Fig. 7.2**.** It can be clearly seen here that the engine efficiency can be further increased by changing spark plug location for same spark timing and fuel-air ratio. Similar alterations in brake specific fuel consumption for different compression ratios and spark plug locations are given in Fig.7.3.

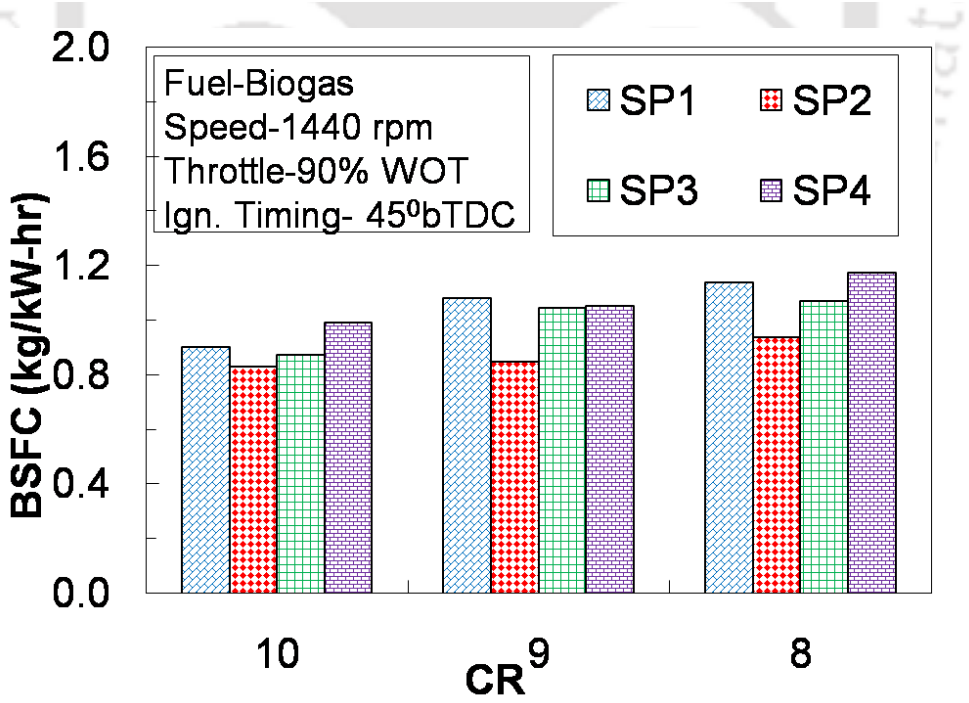

Fig.7.3 BSFC variation with compression ratio for different spark plug location

Initial inward movement of the spark plug from SP1 (default) to SP2 (Fig.4.25 from chapter 4) improves the engine performance in terms of efficiency and brake specific fuel consumption for all compression ratios.

Increase in efficiency is seen to 16 %, 9 % and 8 % for CR 8, CR 9 and CR 10 respectively. While 18 %, 21 % and 8 % decrement in BSFC has been noticed for those compression ratios respectively. However further movement of spark plug degrades the performance by decreasing efficiency and by increasing specific fuel consumption for both spark plug locations SP3 and SP4. Let's consider the case of CR10, here, from the figure, BTE for SP1 is 24.9 % which rises to 26.40 % at position SP2. The BTE at SP3 is 25.3 % which is quite lower than SP2, similarly for SP4 the efficiency decreased to 24.10 % (Shah et al., 2006).

Similarly, for the same CR, BSFC is 0.903 kg/ kW-hr, 0.832 kg/ kW-hr, 0.874 kg/ kW-hr and 0.993 kg/ kW-hr respectively for SP1, SP2, SP3 and SP4. This shows that BSFC at SP2 is lowest among all. Same variation of performance parameters is noticed for all the compression ratios. Hence it is expected that the spark plug location is having relevance with the combustion characteristics of the engine.

7.2.1.2 Combustion Analysis for change in spark plug location

After performance analysis, combustion analysis is carried out to access the effectiveness of spark plug location.

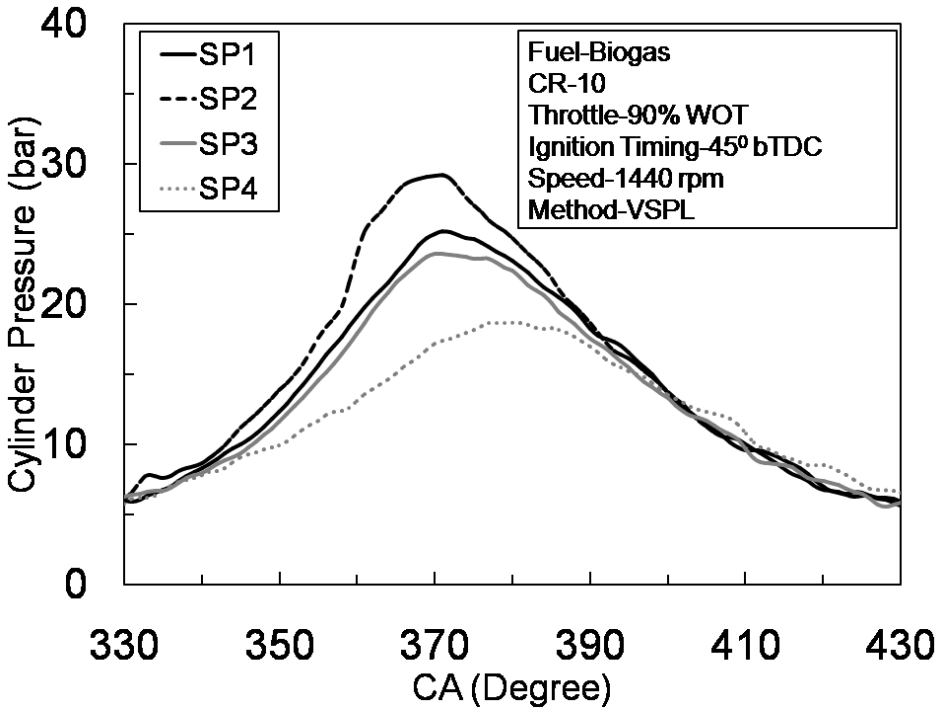

Fig.7.4 Cylinder pressure variation with crank angle for different spark plug location.

The combustion rate due to variable spark plug location can be monitored in terms of combustion chamber pressure variation with respect to crank angle as shown in Fig.7.4. In this figure, compression ratio 10 is considered as representative for discussion. The pressure variation recorded during experiments is smoothened as mentioned in literature (Stone 1999). From the figure it is clear that the peak cylinder pressure is 25.156 bar at 371 ^{0} CA, 29.160 bar at 370 ^{0} CA, 23.556 bar at 370 ^{0} CA and 18.651 bar at 380 ^{0} CA for SP1, SP2, SP3 and SP4 respectively. Higher the cylinder pressure more will be the homogeneous combustion of fuel air mixture in the combustion chamber.

In this regards, the position SP2 is more optimum than other positions for the complete combustion of charge.

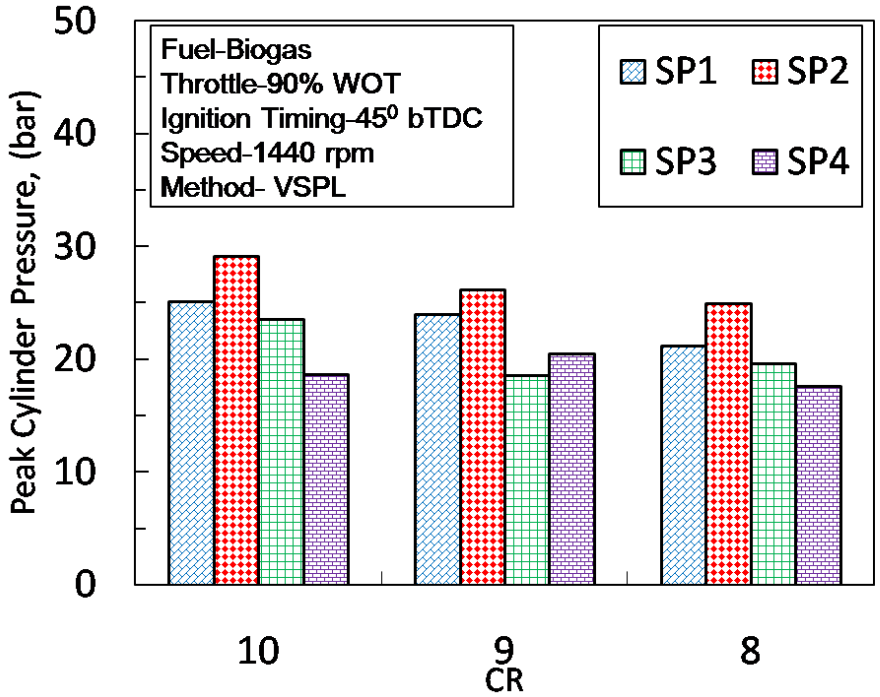

Fig.7.5 Peak cylinder pressure variation with compression ratio for different spark plug location

Same fact is logged for all the compression ratios and it clearly reflects from Fig.7.5. At position SP2, the peak cylinder pressure reaches maximum value of 29.1 bar, 26.12 bar and 24.9 bar for CR 10, CR 9 and CR 8 respectively

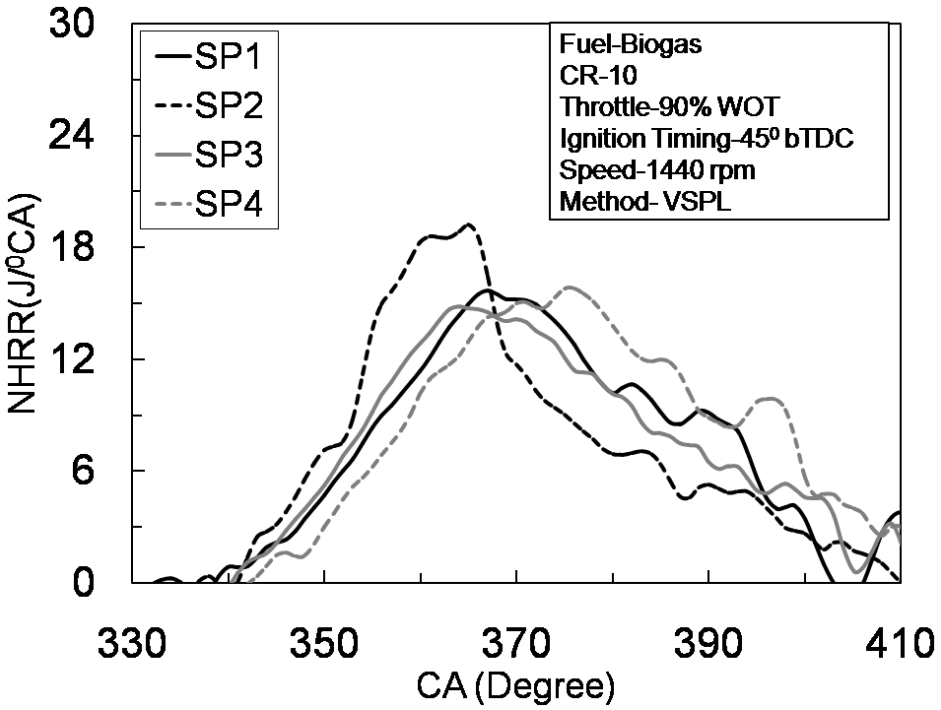

Fig. 7.6 NHRR variation with crank angle for different spark plug location

The performance improvement for excess protrusion by 2 mm has clearly influenced the combustion process. Thus, for the same ignition timing, combustion duration decreases on account of rise in spark plug location. Lesser time required for the flame to travel in the combustion chamber and thus in turn to raise cylinder pressure is expected for such observation (Taylor, 1977). With the increase in extruded length of spark plug, the crank angle at which peak pressure observed seems to be after TDC.

Locations SP3 and SP4 have protrusion length of 5 mm and 10 mm which might lead to crevice flow around the secondary piston which would delay the combustion (Alger, 2005).

The calculated NHRR [Eq-C-13 (APPENDIX-B)] variation with crank angle is plotted in Fig.7.6. The NHRR for raw biogas combustion at CR10, speed 1440 rpm and ignition timing 45^0 bTDC shows 18.43% rise when spark plug occupies new position SP2 over original position SP1

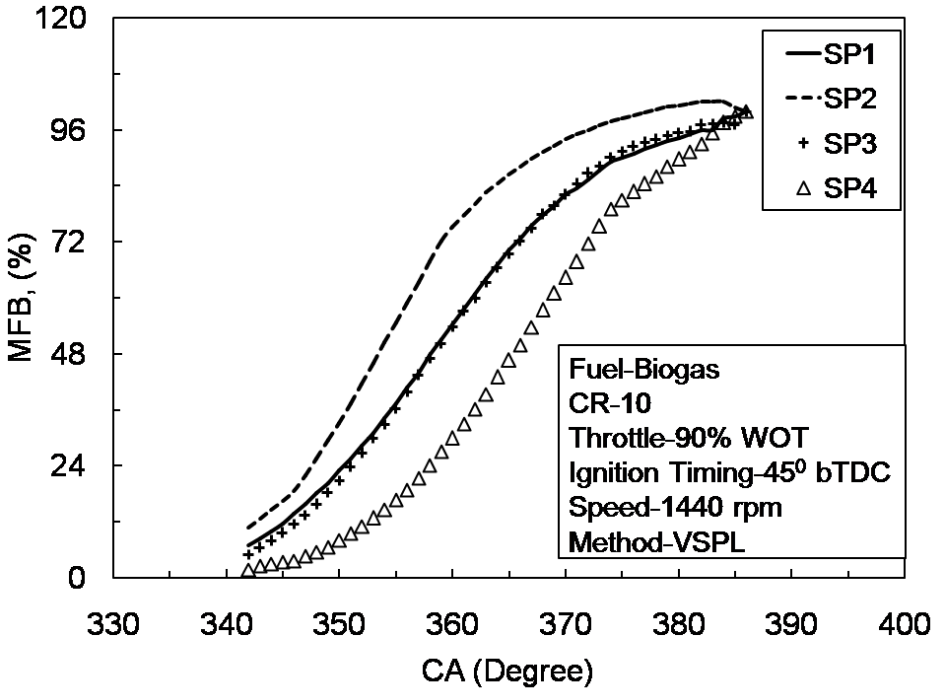

Fig.7.7 Variation of MFB with crank angle for different spark plug location

Here the crank angle at which peak heat release takes place also found advanced for SP2 with respect to original SP1 position. Spark plug at position SP3 and SP4 shows 5.85 % decrement and 0.8 % increment respectively in heat release with respect to SP1.The crank angle at which the peak NHRR observed for SP4 is 377 ^{0} CA showing delayed combustion results and thus reduced power output and efficiency.

Mass fraction burned [Eq-C-14 (APPENDIX-C)] with respect to crank angle for variable spark plug locations is presented in Fig.7.7. As the spark timing is fixed at 45 ^{0} bTDC, the 10% mass is found to be burned at 344 ^{0} CA, 342 ^{0} CA, 345 ^{0} CA and 351 ^{0} CA for SP1, SP2, SP3 and SP4 respectively.

Table 7.3. Crank angle during the combustion phase for different CR and VSP

CR	Beginning of combustion (10% MFB), ^{0} CA				Combustion duration (90% MFB), ^{0} CA				% MFB at TDC (360 ^{0} CA)			
	SP1	SP2	SP3	SP4	SP1	SP2	SP3	SP4	SP1	SP2	SP3	SP4
10	344	342	345	351	31	**25**	29	29	33.65	**54.94**	32.08	13.78
9	349	349	350	354	27	**25**	31	28	33.328	**44.33**	25.92	14.28
8	358	351	353	358	22	**21**	25	24	14.99	**47.22**	25.13	15.16

Thus time required for 10 % mass fraction burned is lowest for position SP2 than other spark plug locations. Further, 90 % of mass is seen to be burned at 375 ^{0} CA, 367 ^{0} CA, 374 ^{0} CA and 380 ^{0} CA for SP1, SP2, SP3 and SP4 respectively.

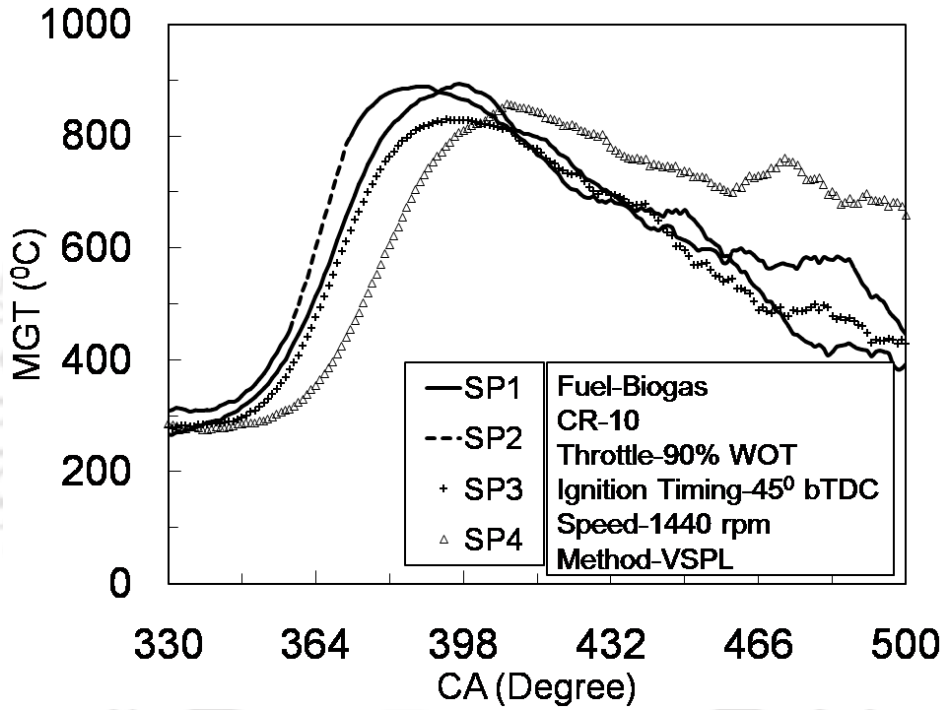

Fig.7.8 Variation of MGT with crank angle for different spark plug location

Thus the combustion duration which is between 10 % to 90 % mass burnt is 31 ^{0} CA, 25 ^{0} CA, 29 ^{0} CA and 29 ^{0} CA for those spark plug locations respectively. Thus it is evident that combustion is faster in case of SP2.

The percentage MFB for different compression ratio with various spark plug position is given in Table 7.2. The MFB for SP2 is 47.22 %, 25.13 % for SP3 whereas 14.99 % for SP1 and 15.16 % for SP4 at CR 8. At CR 9, the percentage MFB is 44.33% for SP2 where as for other spark plug positions the MFB is either found increased or remains steady. At CR10, the percent MFB was 54.94 %, 32.08 %, 33.65 % and 13.78 % for SP2, SP3, SP1 and SP4 respectively.

Variation of MGT calculated [Eq.C-15 (APPENDIX-C)] as a function of crank angle is shown in Fig.7.8. It is known that, MGT depends upon the combustion process. Higher MGT is recorded at SP2 where spark plug will be 2 mm extruded inside the chamber. However the

MGT is equally high at SP1 with delayed combustion than that of SP2 from TDC. Therefore MGT variation also suggests that the SP2 location is most appropriate for the engine. This observation is in phase with the conclusion made from Fig.7.6 since MGT depends upon the combustion process in-side the combustion chamber.

The coefficient of variance (COV) [Eq-C-16 (APPENDIX-C)] with respect to spark plug location for different compression ratio using raw biogas is as shown in Fig 7.9. The COV can be found to be reduced with change in spark plug location from SP1 to SP2 for all the compression ratios. This decrement in cycle-by-cycle variations shows that the combustion of raw biogas is smoother when spark plug is at SP2 (Han et al., 2000).

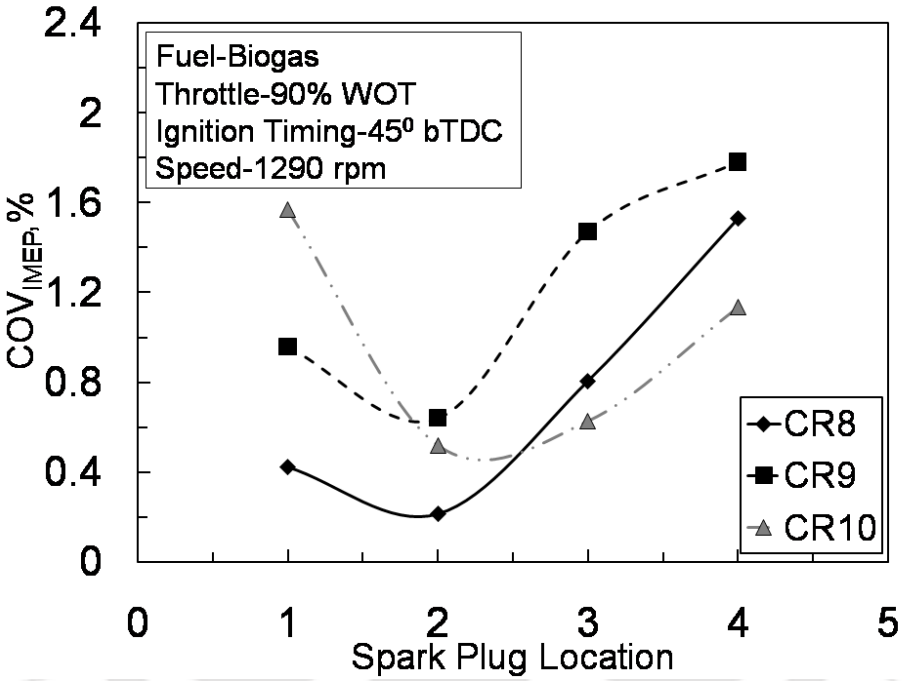

Fig.7.9 Percent COV $_{IMEP}$ variation with spark plug location for different compression ratio

But thereafter at SP3 and SP4 the variations is found more and COV increases with positive slope for all CRs. At position SP2, the cycle-by-cycle variations are 0.215 %, 0.64 % and 0.52 % while these variations at SP4 are 1.53 %, 1.78 %, 1.135 % for CR 8, CR 9 and CR 10 respectively.

Thus the combustion analysis from combustion chamber pressure, NHHR, MFB, MGT and COV clearly indicate that the combustion in the combustion chamber gets largely influenced with axial location of the spark plug. Further SP2 location is seen to be effective in making combustion faster with maximum mass burned, high energy release rate and high mean gas temperature. It has also been noticed that the cycle-by- cycle variation is also less for this spark plug location.

7.2.1.3 Emission analysis for spark plug location

Exhaust gas analysis is performed to understand the alterations in emission due to change in spark plug location. The effect of spark location on variable compression ratio biogas engine

has been demonstrated in terms of carbon monoxide (CO) emission as shown in Fig. 7.10. CO emission decreases with increase in compression ratio for any spark plug location. Further, it is found that the CO emission decreases by 18 %, 31 % and 25 % for change in spark plug location from SP1 to SP2 for compression ratios CR 8, CR 9 and CR 10 respectively. But thereafter it increases for further change in position to SP3 and SP4.

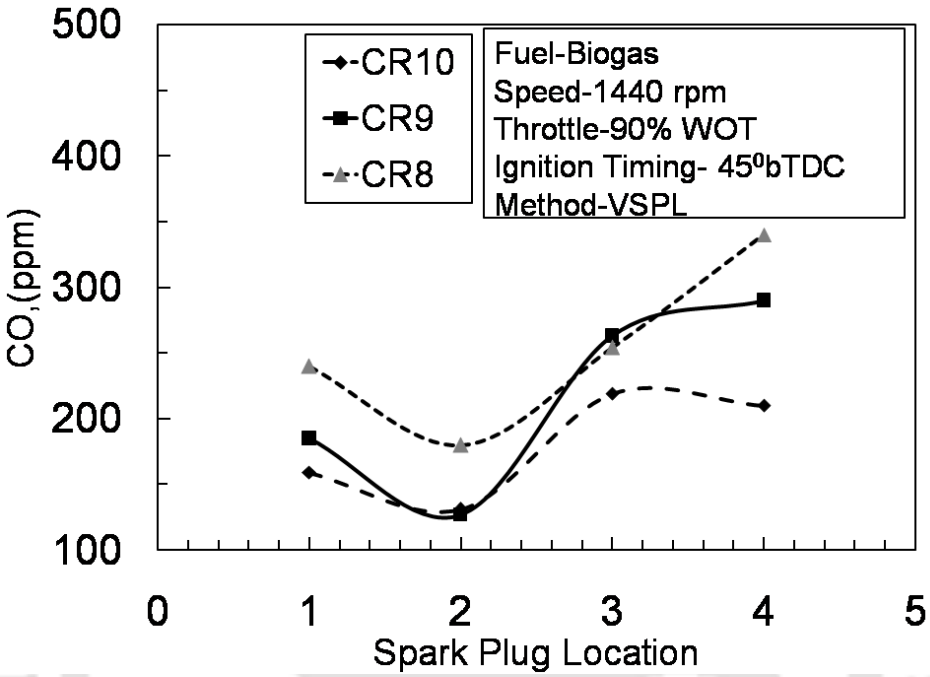

Fig.7.10 CO emission for different spark plug locations compression ratios.

The increment reported is 38 %, 56 % and 47 % for CR 8, CR 9 and CR 10 respectively. Mean gas temperature remains high for SP2 location due to higher heat release rate associated with it.

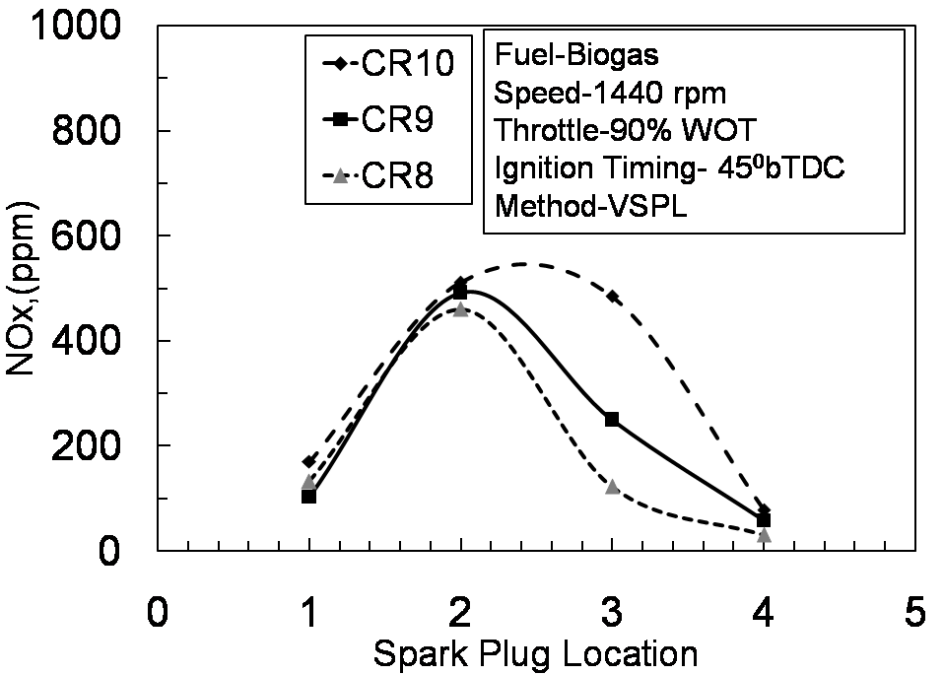

Fig.7.11 NO_x emission for different spark plug locations compression ratios.

In view of these facts emission of CO remains lower for SP2 location as it decreases with compression ratio. Nitrogen oxide (NO_x) emission from the biogas fuelled engine is plotted for variable spark location along with variation in compression ratio. It has been found that the NO_x emissions are increased with change in spark plug location from SP1 to SP2.

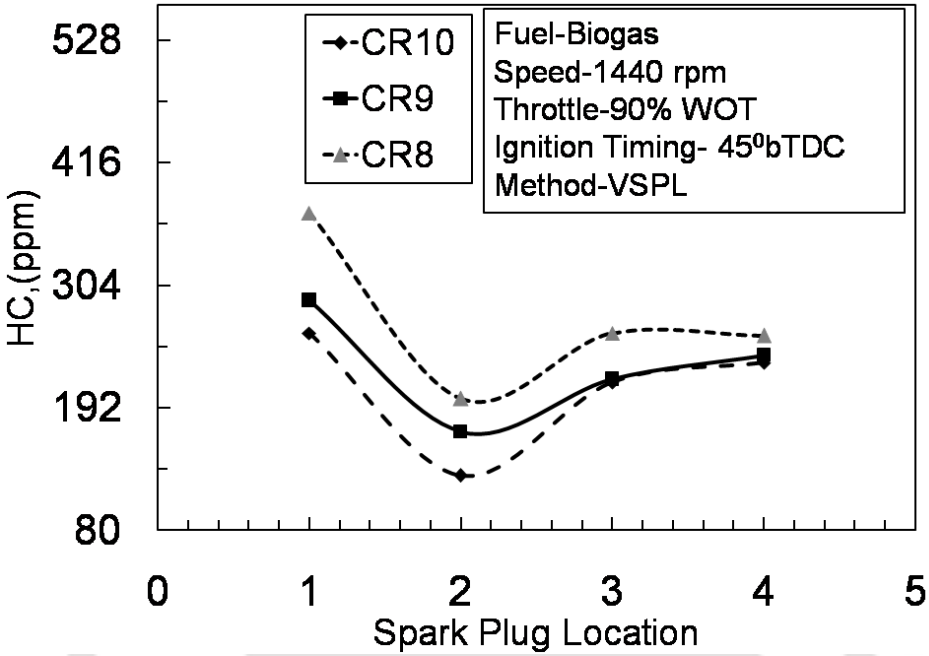

Fig.7.12 HC emission variation with spark plug location for variable compression ratio.

This increment was 63 %, 76 % and 74 % respectively for CR 8, CR 9 and CR 10 with respect to SP1(Fig.7.11). The rise in NO_x is due to more complete combustion which causes the increase in combustion temperature. However further change in spark plug location from SP2 to SP3 and further SP4 is shown to decrease the NO_x emission. Thus, increase in NO_x emission with change in spark plug location has same reason for its increment with compression ratio for same spark plug location. Higher combustion temperature is leading to high NO_x emission for either cases.

The effect of variable spark location on unburnt hydrocarbon (HC) emissions is explained in Fig.7.12 for different compression ratios. As shown in figure, the HC emission found minimum at SP2 as compared to that of SP1, SP3 and SP4 for all CR. The compression ratio effect is clearly visible from the figure where at higher CR10; the HC is lower as compared to other CR9 and 8. This is a outcome of maximum fuel combustion in presence of higher compression pressure. So there is lower the chance that fuel remains unburnt in the crevices of piston ring or around the secondary piston. This is called flame quenching which depends upon cylinder piston geometry (Heywood,1998). But with lowering the CR these effect influence the fuel combustion and leaves the fuel unburnt which ultimately rises HC in exhaust. At SP2, the HC is found to be 130, 170 and 200 ppm for CR10, 9 and 8 respectively. The percentage increment of 44 to 50 % for SP1, 22 to 40 % for SP3 and 22 to 45 % for SP4 with respect to SP2 for all CR10, 9 and 8.

The green house gas CO_2 emission with spark plug location is as explained in Fig.7.13 for different crank angles. As shown in figure, the lowest CO_2 percentage in exhaust is found at

SP_2 location for all CR under consideration. However, higher CR10 shows 3.63% CO_2 at SP2. The CO emission (Fig.7.10) is lowest for CR10 at SP2.

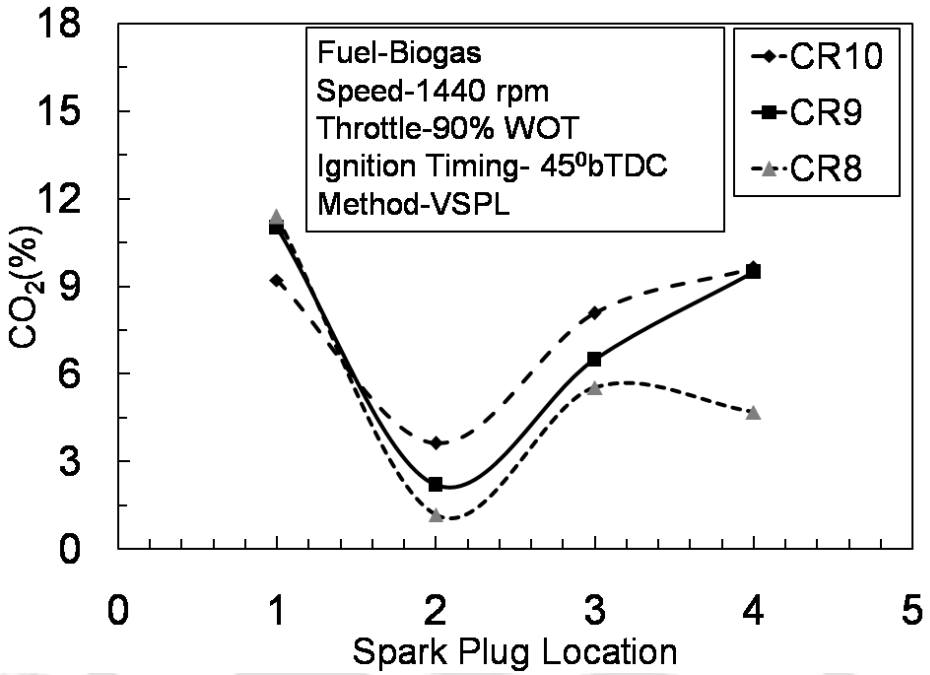

Fig.7.13 CO_2 emission variation with spark plug location for variable compression ratio.

This reflects the oxidation of hydrocarbon to be maximum. So CO gets converted into CO_2 emissions at CR10 and SP2 location. Whereas at CR 9 and 8, CO_2 emissions are lower 2.21 % and 1.18 %. This clearly reflects in rising of CO emission at SP2 location. In terms of magnitude, the percentage CO_2 at SP2 is 3.63% which is 9.21 %, 8.08 % and 9.64 % at SP1, SP3 and SP4 respectively for biogas at CR10.

7.2.2 LPG fuel for variable spark plug location

The major difference between LPG and raw biogas fuel selected for experimentation is their heat capacity. LPG is high heat value gaseous fuel and raw biogas is very poor heat value gaseous fuel. It's not only enough to burn these fuels in spark ignition engine to produce power, but to identify the dominating engine parameters which restrict those fuels to burn with maximum efficiency possible. Some of the important engine structural changes are identified and variations in those engine parameters or components, the studies are performed. The identified structural changes are variable compression ratio and variable spark plug location. Every individual parameter has influence on the performance of the engine as reported by literature (Crookes, 2007; Mustafi et al., 2001). Even both the parameters combined together have the effect on the performance of the engine using gaseous fuels. In this section, the variable spark plug location technique is being applied to LPG fueled spark ignition engine. The analysis is done in the form of performance, combustion and emission study as follows.

7.2.2.1 Performance Analysis using LPG fuel for different spark locations

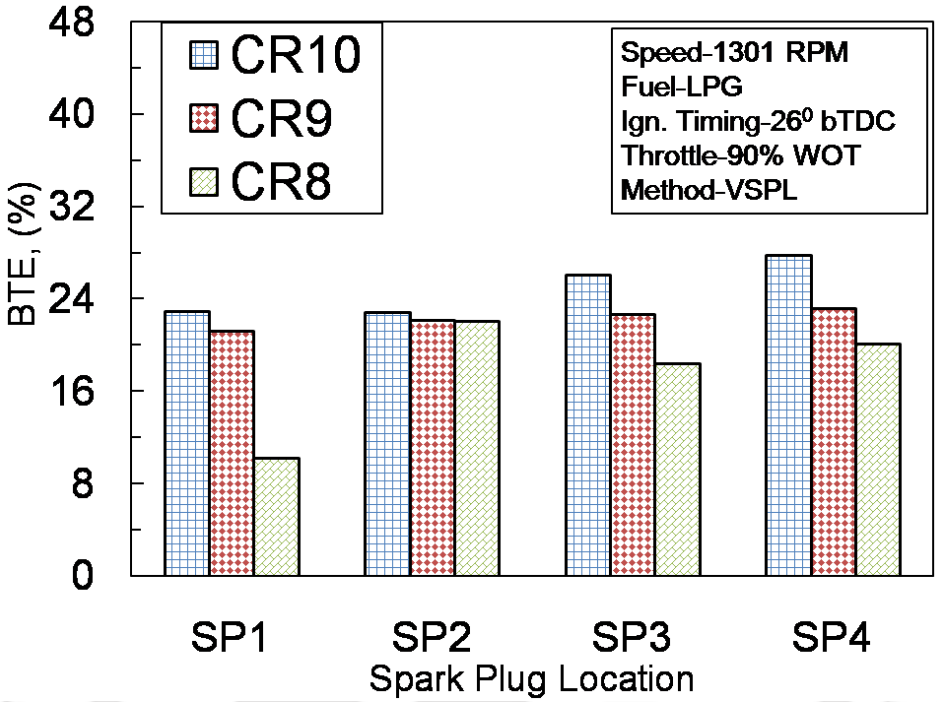

Fig.7.14 BTE variation with spark plug location for variable compression ratio.

For different spark locations the Fig.7.14 and Fig.7.15 show variation of BTE and BSFC for CR 10, 9 and 8. As discussed previously, pure LPG has been supplied to the engine. The variation of BTE for all SP location shows the rise in BTE with rise in CR from 8 to 10 (Akansu and Bayraktar, 2011). More especially it was seen that for SP4 location i.e. maximum protruded length (10 mm) of secondary piston shows maximum efficiency for LPG fuel engine is noted. With optimizing the spark location at SP4, the maximum efficiency achieved is 27.83 % which is 4.27 % higher than that of conventional spark location at conventional CR 10. When the compression ratio is shifted to CR 9, it is also seen that the spark location SP4 shows maximum efficiency. Finally for CR8, the optimum location is changed to SP2.The increase in cylinder volume with decrease in CR, affects the performance while spark plug is at SP4. This may occur due to lower velocity and charge turbulence around the 10 mm protruded length of secondary piston. In addition to this, the compression pressure reduces with decrement in CR. The combined effect of this is the delayed combustion. The flame speed also reduces with decrease in compression ratio causing incomplete or as said delayed combustion of charge. For the stoichiometric air fuel ratio, constant CR, constant spark timing supplied to the engine , change in SP location from original to 10 mm protrusion inside coaxially causes the central combustion where burn rate may be maximum, increased flame velocity and complete combustion.

Also another important point here is that as the protrusion length is higher enhances the swirl rate of fuel air charge for homogeneous mixing and initiate combustion faster provided the compression ratio to be higher.

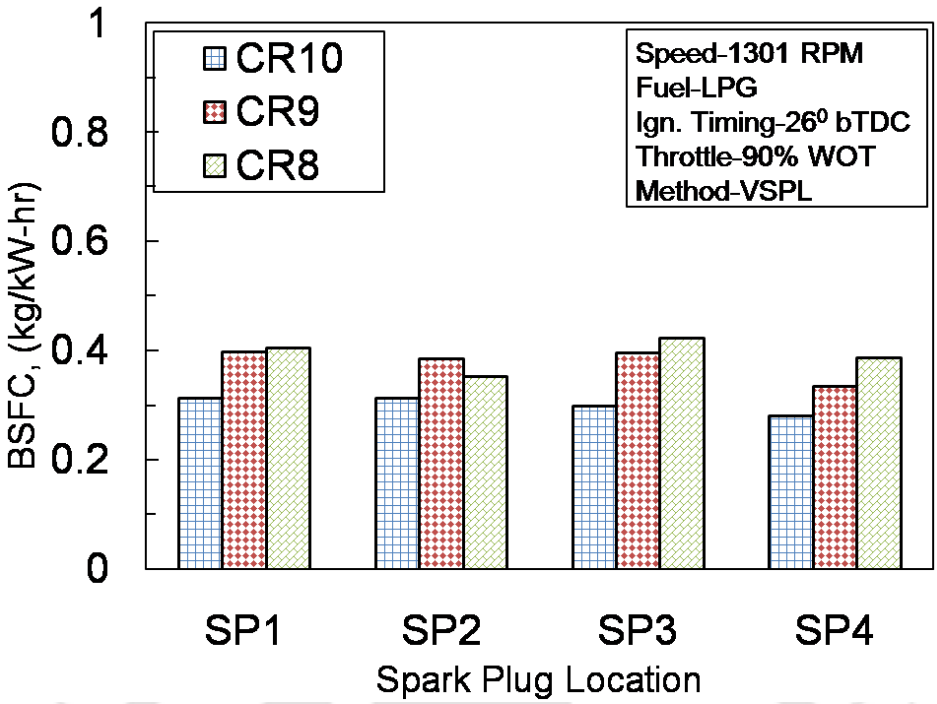

Fig.7.15 BSFC variation with spark plug location for variable compression ratio.

Due to higher heating value of fuel the flame spread faster in all corners of the cylinder and causes combustion. This causes the improvement in performance of engine. The homogeneous and complete combustion of charge increases the brake power per kg of fuel. That is how the fuel consumption shows decrement in BSFC.

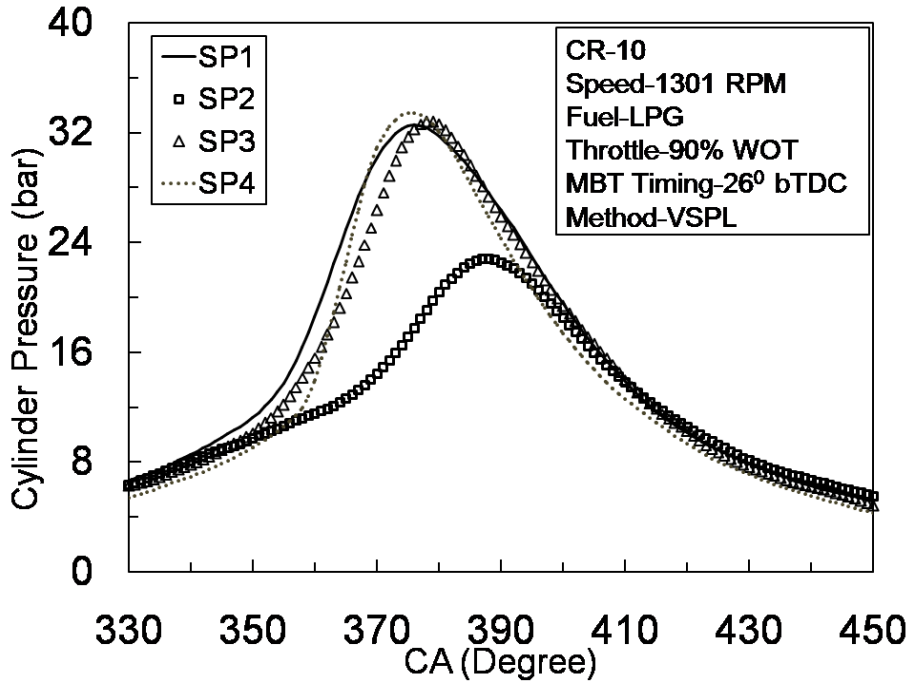

Fig.7.16 Cylinder pressure variation with CA for different spark plug location

As shown in Fig.7.15, the BSFC is 0.281 kg/kW-hr showing decrement by 10.22% with respect to SP1 for CR10. Similarly the corresponding decrement of 15.57 % and 13.05 % is recorded at optimum locations SP4 and SP2 for CR9 and CR8 respectively.

7.2.2.2 Combustion Analysis of LPG fuel for different spark locations

The cylinder pressure variation with crank angle for different spark plug location has been plotted as shown in Fig. 7.16. It is found that for the constant ignition timing of 26^0 bTDC, CR 10 having constant speed of 1301 rpm with the change in spark plug location, the maximum pressure varies both in magnitude as well as crank angle attaining maximum pressure. The SP location, SP4 achieves maximum pressure of 34 bar at 371 ^{0} CA ignition advance. Thereafter SP3, SP1 and finally SP2 shows the pressure curve with reduced peak pressure of 32bar, 32 bar and 23 bar and CA beyond TDC by 373 ^{0} CA, 375 ^{0} CA and 390 ^{0} CA respectively. The position SP4 is 10 mm protrusion length inside combustion chamber in coaxial direction (Fig 4.22 of chapter 4). So the position of spark plug is at combustion centre and higher heating value of fuel develops the flame kernel with minimum time. Witze (1982) presented effect of swirl level and spark location on combustion duration in homogeneous charge engine. For lower swirl level ignition point should be located towards center of the chamber while for higher swirl the same should be moved towards wall of the chamber.

This may cause the central combustion of fuel –air charge and flame produced spreads radially outward in all directions. This causes the combustion faster and hence peak achieved close to TDC at 371 ^{0} CA. However, if the included angle increases causing increment in offset position of spark plug with respect to original position say for position SP3, SP2 and SP1, the performance is found to be reduced.

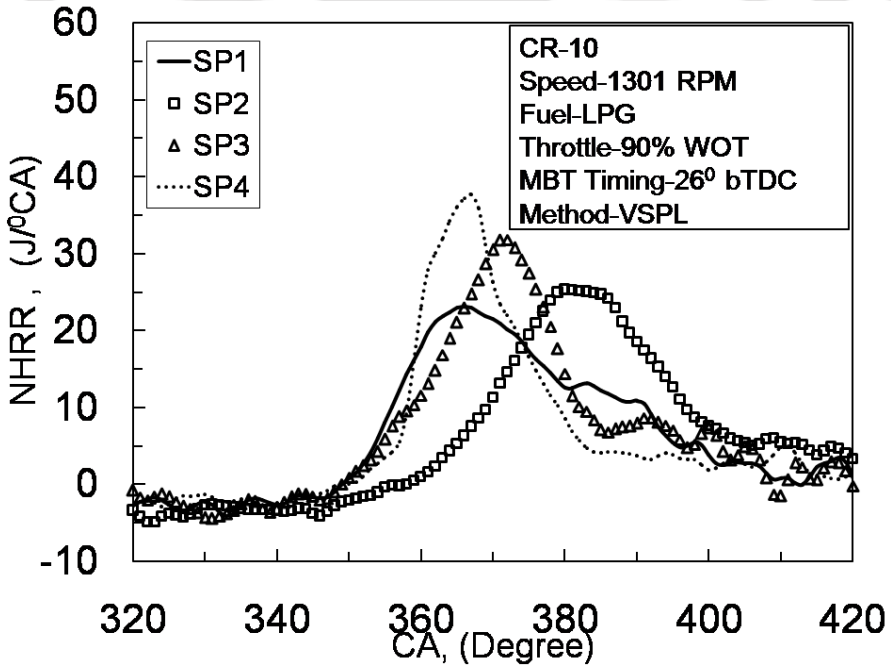

Fig.7.17 NHRR variation with CA for different spark plug location

This may be due to shift of spark from central combustion causing uneven flame travel in radial direction. Also flame takes more time to reach opposite corner of the chamber to initiate combustion (shrivastava and Agarwal, 2014).The Net Heat Release Rate (NHRR) variation with crank angle for different SP location has been plotted in Fig.7.17 The figure

shows that NHRR for SP4 remains constant upto 357 ^{0} CA thereafter causes combustion accelerated, raising the NHRR showing peak at 367 ^{0} CA.

This shows that the combustion is very fast and also complete as the peak NHRR reaches to 38 J/ ^{0} CA. This could be happened due to homogeneous mixing of fuel-air charge added with turbulence due to protrusion length of secondary piston causing the central combustion (Ebrahimi, 2011). As LPG is high octane fuel under high compression pressure, the combustion of gases takes place faster producing heat and high combustion pressure results in maximum work. However at SP1, the NHRR is lower as compared to SP4. The reason for this is the spark produced takes longer time to reach to the combustible mixture, hence the peak NHRR is lowed to 22 J/ ^{0} CA. This causes increase in combustion duration and lowered peak pressure which affects the efficiency. The curve of SP3 from the Fig.7.17 shows that NHRR is 30 J/ ^{0} CA which is higher than SP1 but lower than SP4 where the advantage is only the turbulence of fuel-air charge causes homogeneous combustion. But the spark plug angular location has been shifted away from original position causing delay in flame travel. This ultimately affects the combustion duration. The nature of SP2 itself shows that the delayed combustion causing incomplete combustion and hence reduced efficiency.

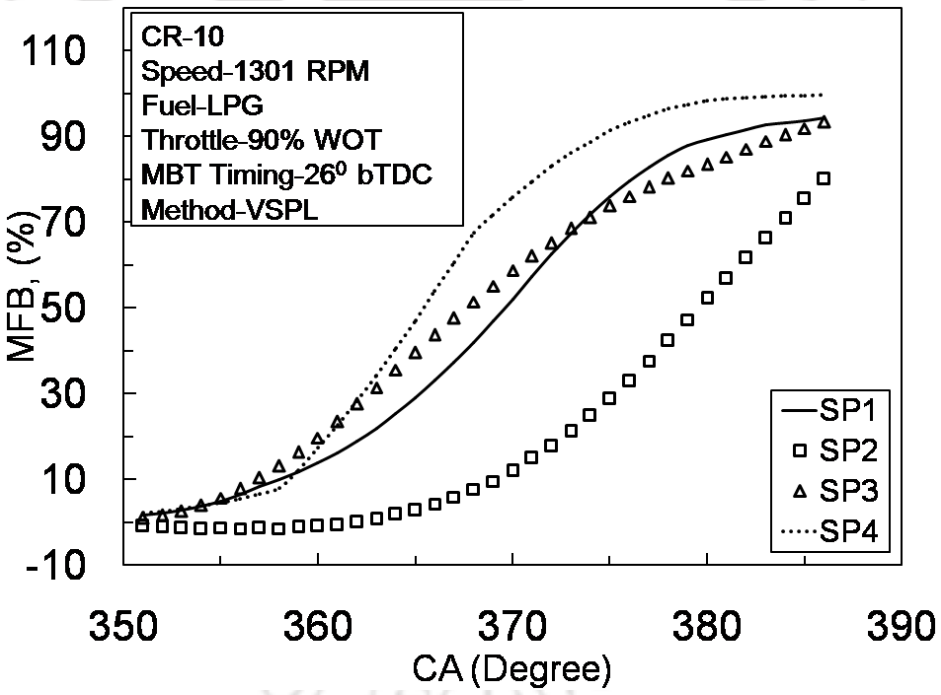

Fig.7.18 % MFB variation with CA for different spark plug location

The percentage mass fraction burned (MFB) variation with crank angle for different spark plug position at CR10 and speed 1301 rpm has been plotted in Fig.7.18. The figure shows that MFB for SP3 at TDC (360 ^{0} CA) is maximum followed by SP4 and SP1. The percent MFB at SP2 is quite poor as compared to previous SP locations.

The MFB is the representation of percentage mass that has been burned per degree of crank angle seems to remain unaffected upto 350 ^{0} CA but thereafter it shows rise in the percent MFB. The 10% MFB has been found at 360 ^{0} CA , 363 ^{0} CA, 357 ^{0} CA and 355 ^{0} CA whereas the 90% MFB was found at 375 ^{0} CA, 384 ^{0} CA ,380 ^{0} CA, 370 ^{0} CA for SP1, SP2, SP3 and SP4 respectively.

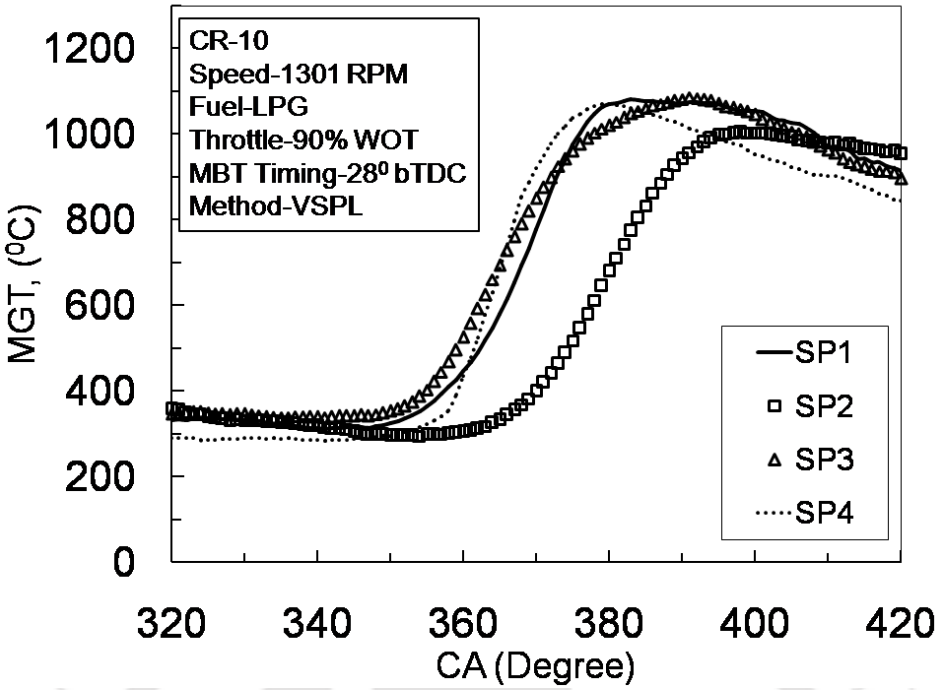

Fig.7.19 MGT variation with CA for different spark plug location

From the results it is seen that the ignition delay is higher for SP4 but the combustion duration is found lower as compared to other spark locations. When spark plug is close to the combustion centre, the mass of fuel air charge takes time to reach towards centre in vicinity of spark plug and this increases ignition delay. However once spark produced, higher flame speed may cause the faster combustion and reduced the combustion duration. As the plug position shifted away with increase in included angle from vertical centroidal axis of combustion chamber, the combustion duration found increased which clearly defined the combustion phenomenon inside combustion chamber.

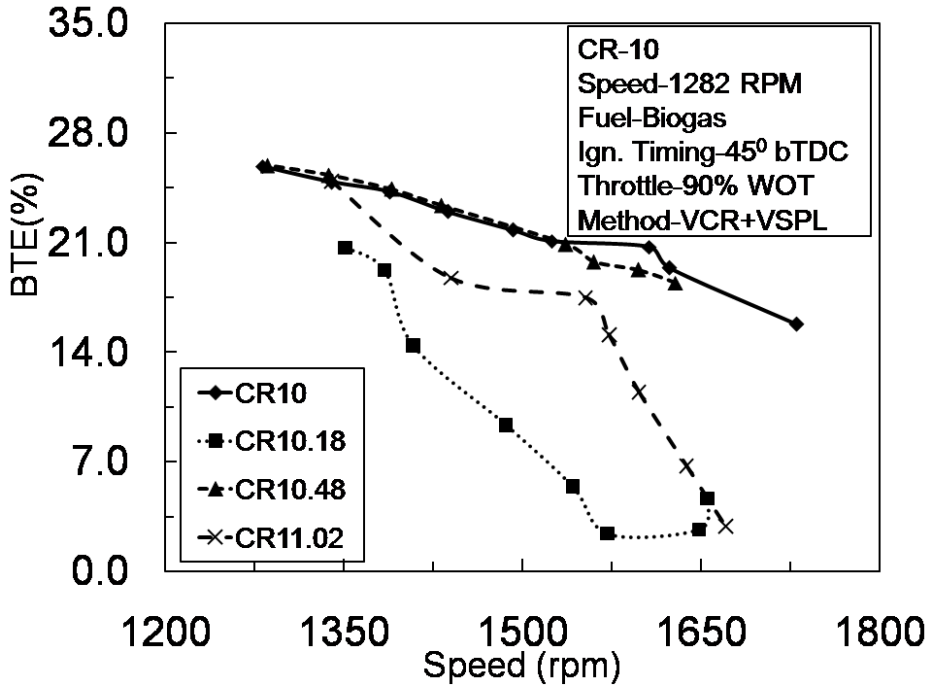

Fig. 7.20 BTE variation with speed for different CR accompanied with spark plug location

The mean gas temperature for LPG fueled engine at CR10 and speed 1301 rpm is as plotted in Fig.7.19. From the figure it is seen that MGT is maximum at SP4 (10 mm protrusion length of piston) inside the combustion chamber. The maximum temperature recorded is 1070.83 ^{0} C at 370 ^{0} CA for SP4 and CR10. The temperature at other spark locations is also seems to be close to that maximum temperature. However there is shift of peak temperature aTDC. This is having adverse effect on the performance of the engine as the heat generated couldnot been utilized for converting in power, but lost to the jacket cooling water or engine exhaust gases.

7.3 COMBINED EFFECT OF NOVEL VCR AND VSPL MECHANISM

7.3.1 Biogas fuel performance under novel VCR and VSPL

The raw biogas as fuel being explored in spark ignition engine for optimum spark plug location individually using the novel Top-up Mechanism. However, this mechanism is very much efficient to operate the engine based on combined impact of optimum VCR and VSP. In this situation , it becomes important to study the performance of the engine with simultaneous variation of compression ratio along with variation of spark plug location.

7.3.1.1 Performance Analysis

The performance of the biogas fueled spark ignition engine under effect of VCR and VSPL is evaluated. The Fig.7.20 shows the BTE variaion with speed for varaible CR accompained with VSPL. From the figure, it is seen that the BTE is higher for CR10.48 upto 1540 rpm speed, but thereafter it is found to be reduced for the higher speed.

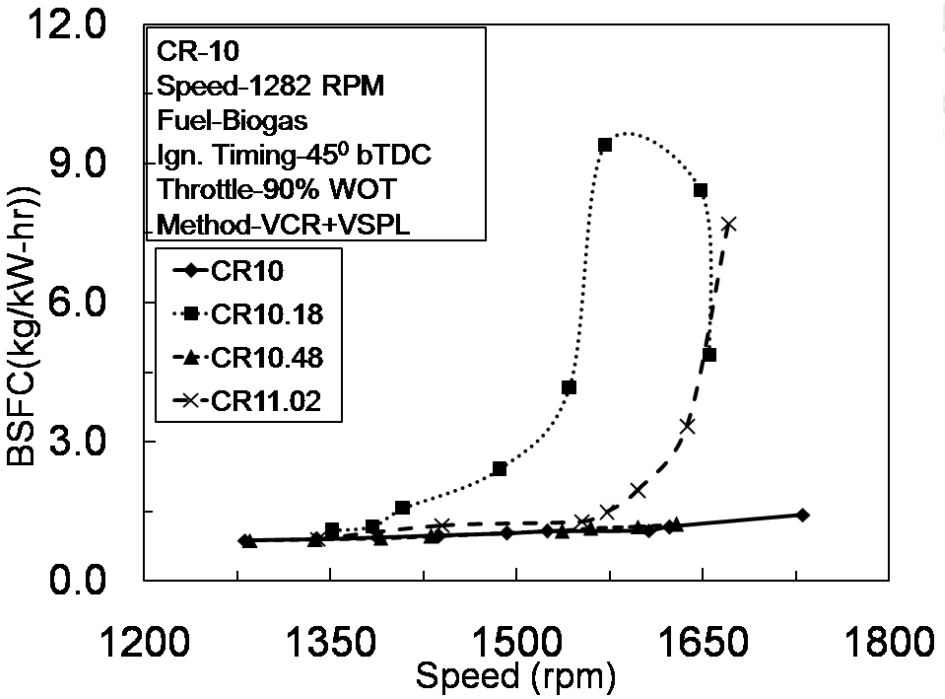

Fig.7.21 BSFC variation with speed for different CR accompanied with spark plug location

The BTE at CR 11.02 is approacing the maximum with increase in load or reduction of speed, still it is found lower than that of original CR10 and CR10.48. Simlar the situation for

CR10.18 is observed. Aftr spark ignition, the flame kernel developed plays an impoprtant role in the development of that flame throughout combustion chamber.

This kernel formation and development has two processs, one being the mass and energy transfer process that are controlled by pressure wave. The second process is quite longer and causes diffusion and thereby transport of mass and conduction of energy transfer (Hill and Kapil,1989). In this regards, the combined VCR and VSPL maintaining CR10.48 by protrusion length of 5 mm is found optimum over speed range 1290-1540 rpm. Individually the CR11.02 was optimum with VCR only where as CR10.18 is optimum for VSPL only.

The ultimate effect of variation in BTE is only because of BSFC. The BSFC variation with speed for different CR is as plotted in Fig.7.21. It is observed that the BSFC for CR 10.48 shows decrement of 1.65 % with respect to CR10 at speed 1340 rpm. At other locations, the decrement of 0.2% and increment of 20% respectively at CR 11.02 and CR10.18 is recorded. During higher speed, BSFC found increased substantially reducing the BTE. With the increase in speed load on the engine decreases, reducing the power produced for the same mass of fuel consumed, that is why the BSFC is found increased. Here CR10.48 with spark location SP3 are optimum as far as possible for raw biogas fuel.

7.3.1.2 Combustion Analysis

The combustion analysis of VCR combined with VSPL is important to justify the outcomes of performance of the engine. The important parameters here are cylinder pressure, NHRR, MFB, MGT and cumulative heat release rate. The Fig.7.22 represents the variation of cylinder pressure with CA for different CR combined with VSPL. From the figure, for constant ignition timing 45^0 bTDC, constant speed, equivalence ratio (1 ± 0.2), the cylinder pressure is shooting high for

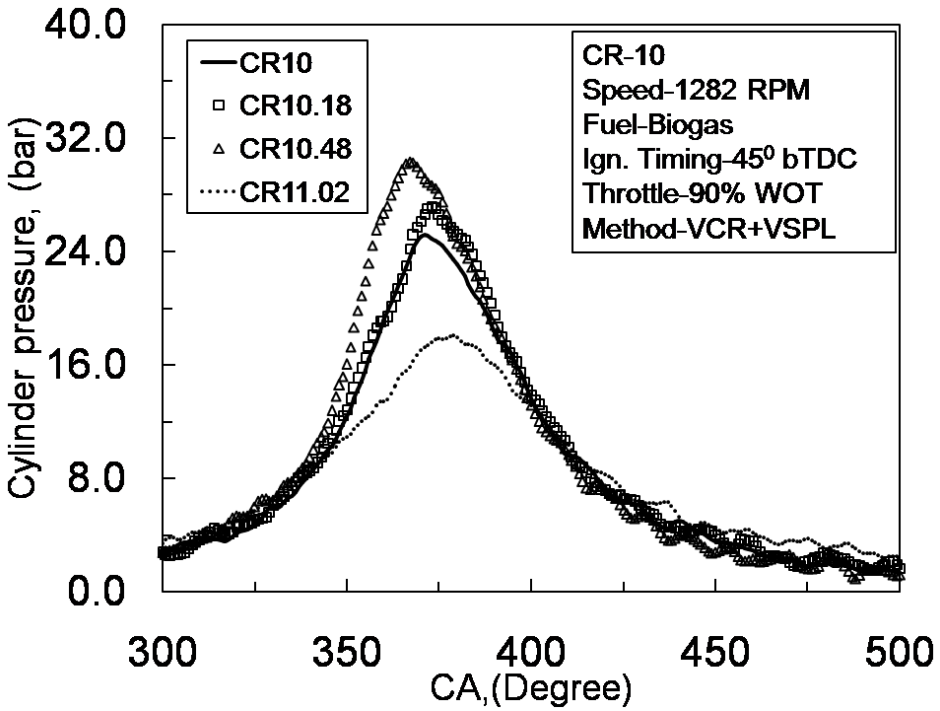

Fig.7.22 Cylinder pressure variation with CA for different CR accompanied with spark plug location

CR10.48 with respect to all other CRs. This may be happened due to the combustion behavior inside combustion chamber.

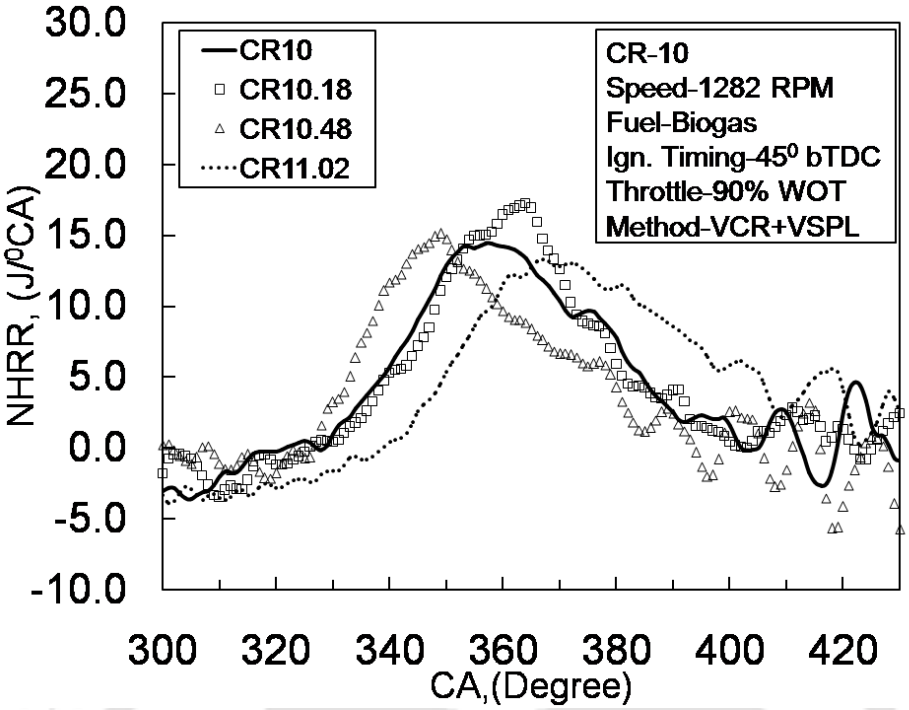

Fig.7.23 NHRR variation with CA for different spark plug location

The charge composed if fuel-air mixture gets in contact with spark plug instantly and hence at the desired CA (45^0 bTDC), the ignition takes place. The peak cylinder pressure is 25.156 bar at 371^0 CA at speed 1290 rpm where CR is 10. This peak pressure shows increment of 20.55% while working at CR 10.48 observing peak at 367^0CA.

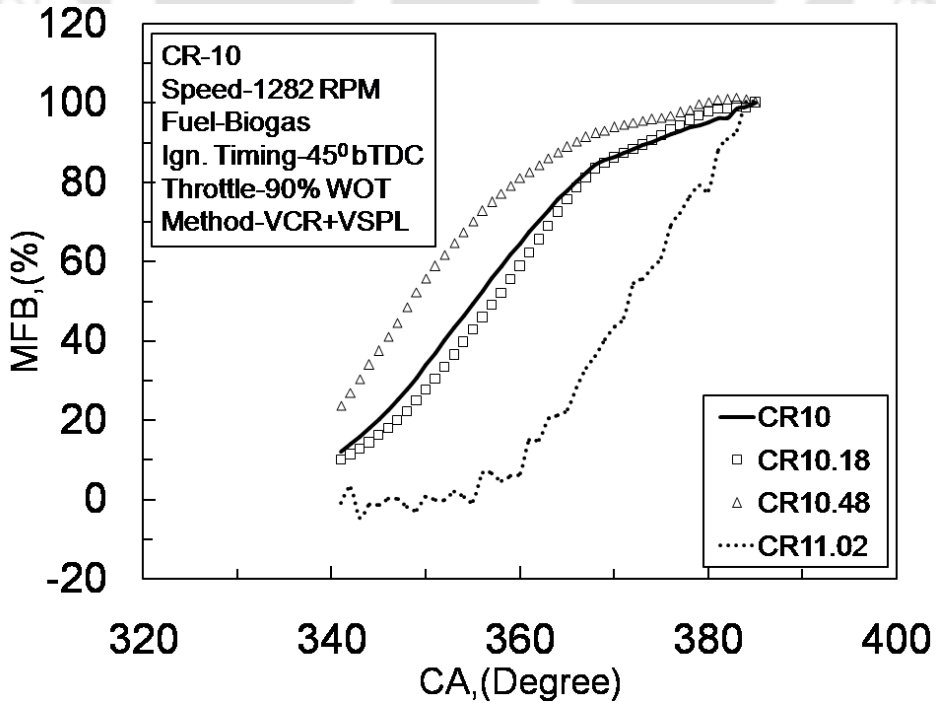

Fig.7.24 Percent MFB variation with CA for different spark plug location

Similarly, the increment of 8.05% and decrement of 28.33% is observed at CR 10.18 and CR 11.02 respectively. Even though there is increment in peak cylinder pressure at CR10.18, the peak observed at 373^0 CA provides only 167^0CA effective expansion work in a cycle. That is the reason the brake power found reduced and efficiency falls down at CR10.18.

The NHRR is the another factor which clearly justifies the performance of the engine at a particular combination of VCR and VSPL. As shown in Fig. 7.23, the peak NHRR is seen for CR10.48 combined with SP3. The magnitude of peak NHRR is 15.082 J/ ^{0} CA at 350 ^{0} CA for CR10.48 which is 14.412 J/ ^{0} CA at 358 ^{0} CA, 17.230 J/ ^{0} CA at 365 ^{0} CA and 13.259 J/ ^{0} CA at 368 ^{0} CA for CR10, CR 10.18 and CR11.02 respectively. However, the higher NHRR at CR10.18 is responsible for reduction in power output because of delay in combustion. For the fuel like raw biogas, the CR11.02 is found unsuitable as far as engine efficiency is considered.

The spark advance for raw biogas fuel is 45^0 bTDC (315 ^{0} CA). As seen in Fig.7.24, the flame travels at maximum velocity when engine operated at CR10.48. This is because, at CR10.48, the % MFB is 55.43% which is maximum at TDC. The % MFB of 33.65%, 22.09% and 5.86% are recorded at CR10, CR10.18 and CR11.02 respectively at TDC. The start of combustion takes place where 10 % MFB recorded at 354 ^{0} CA, 354 ^{0} CA, 350 ^{0} CA and 365 ^{0} CA for CR10, CR10.18, CR10.48 and CR11.02. While 90% MFB is at 384 ^{0} CA, 383 ^{0} CA, 376 ^{0} CA and 386 ^{0}

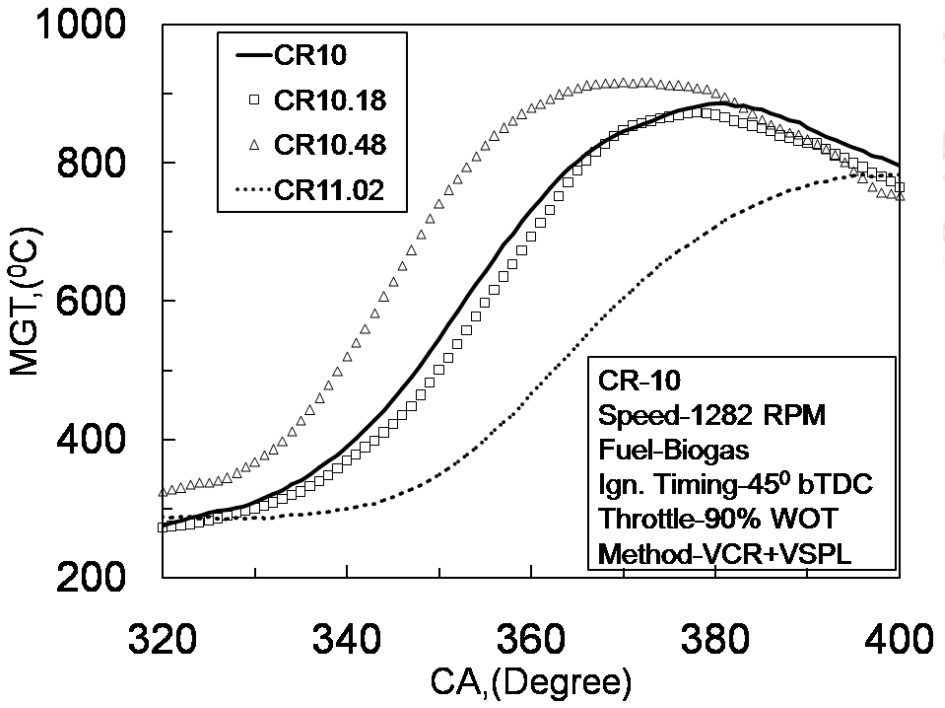

Fig.7.25 MGT variation with CA for different compression ratio accompanied with VSPL

CA for corresponding CRs respectively. The combustion duration is found minimum for CR10.48.The mean gas temperature (MGT) for raw biogas fuel combustion in SI engine is as plotted in Fig.7.25.

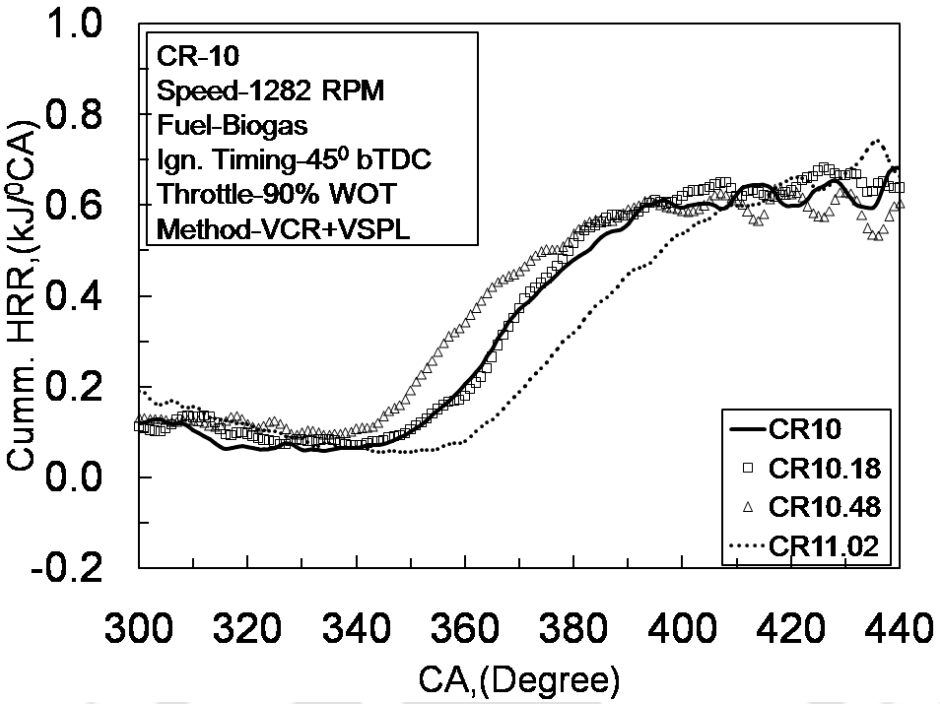

Fig.7.26 CHRR variation with CA for different compression ratio accompanied with VSPL

From the figure, it is seen that the MGT is 937.49 ^{0}C which is maximum in all the CRs. This shows that the combustion is smooth and faster so as to get rise in temperature to the maximum value at the end of combustion. The MGT is found lower and recorded to be 916.5 ^{0}C, 904.6 ^{0}C and 814.43 ^{0}C respectively at CR10, CR10.18 and CR11.02.

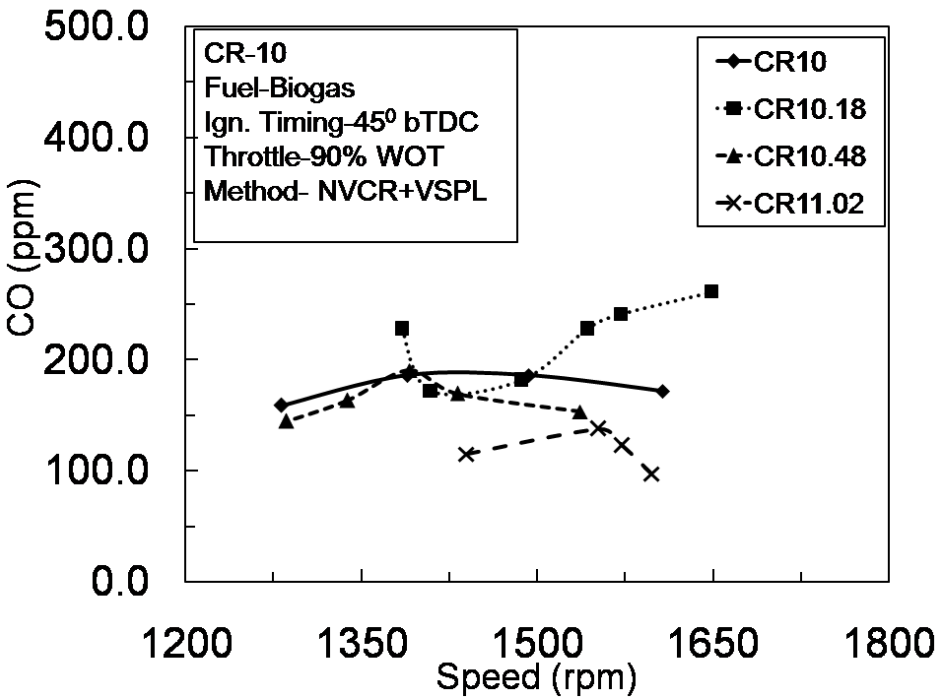

Fig.7.27 CO emission variation with CA for different compression ratio accompanied with VSPL

Cumulative heat release rate is the parameter defined from the mass fraction burned. Rather Mass fraction burned is the ratio of cumulative heat release rate to the total heat release rate (Ebrahimi , 2011). So, the effect of VCR accompanied with VSPL on biogas fueled SI engine

is important and as plotted in Fig.7.26. As shown in figure, $CHRR_{max}$ is observed at CR10.48 followed by CR10, CR10.18 and CR11.02. The specific heat ratio remains fixed during the analysis of the combustion parameters at 1.3.

7.3.1.3 Emission Analysis

The CO emission from the engine for variable CR accompanied with variable spark plug location is plotted in Fig.7.27. It is seen that the CO emission at original CR10 is maximum and thereafter found reduced with increase in CR during high load condition. The CO emission for CR10.48 is in range of 153 ppm reaches to 145 ppm over speed range of 1280 to 1740 rpm. The CO emission found lowest at CR11.02.

Accordingly higher the CR lower will be the CO emission from the engine. The observations at CR10.18 are not consistent with the others.

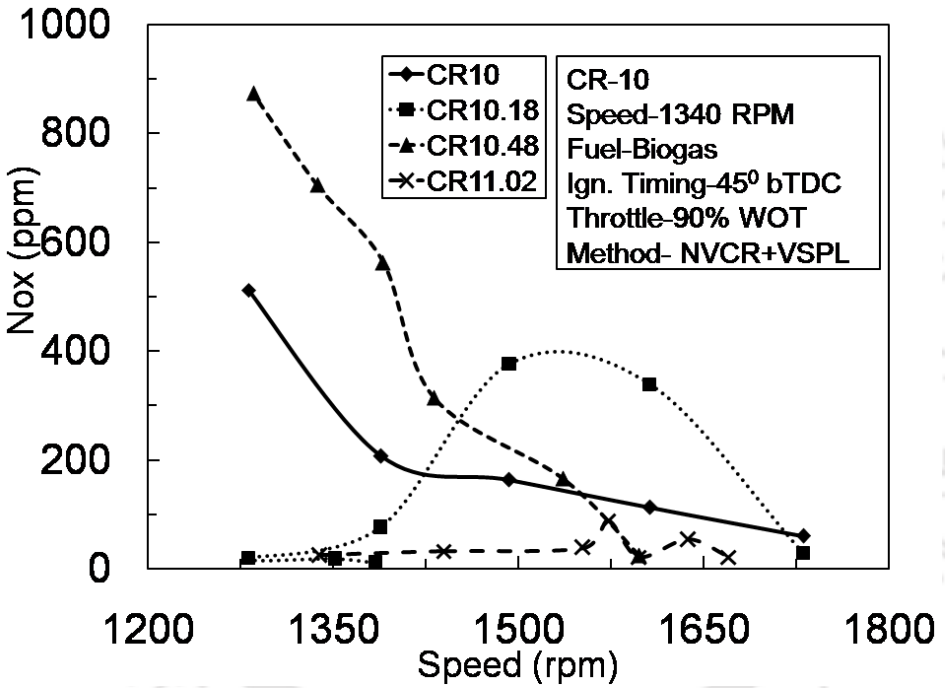

Fig.7.28 NOx emission variation with CA for different compression ratio accompanied with VSPL

The NO_x from the engine exhaust is plotted as shown in Fig.7.38 for variable CR and VSPL. As shown in figure, the nature of NO_x is of decreasing order with speed over the complete speed range. It is falling in range of 60-152 ppm, 11-376 ppm, 24-873 ppm and 21-24 ppm for CR10, CR10.18, CR10.48 and CR11.02 respectively. The cylinder combustion temperature is the major cause of NO_x increment. As the temperature is maximum at higher load, the NO_x will be more and reduces as load decreases on the engine.

7.3.2 LPG fuel performance with Novel VCR added with VSPL

7.3.2.1 Performance Analysis

The combined impact of VCR and VSPL on the performance of the LPG fueled SI engine can be seen from Fig.7.29 and Fig 7.30. As shown in figure, the BTE is found decreasing with speed for the complete speed range. However BTE for CR 10.48 with SP3 location is

seen maximum from all the CRs considered here. Maximum BTE obtained is 28.357% at CR10.48 with SP3 which is decreased to 26.69% at CR10 with SP1, 23.58% at CR10.18 with SP2 and 22.12% at CR11.02 with SP4.

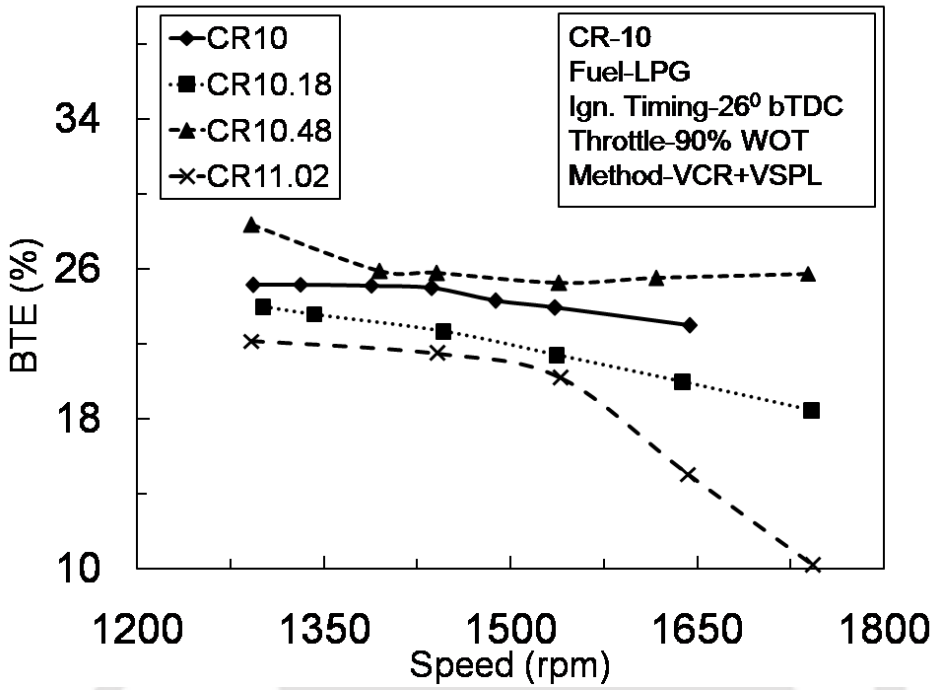

Fig.7.29 BTE variation with speed for different CR accompanied with SPL

The cylinder pressure is found maximum at CR10.48 from Fig.7.21. This figure also represent the combustion tobe smooth and absence of knock.

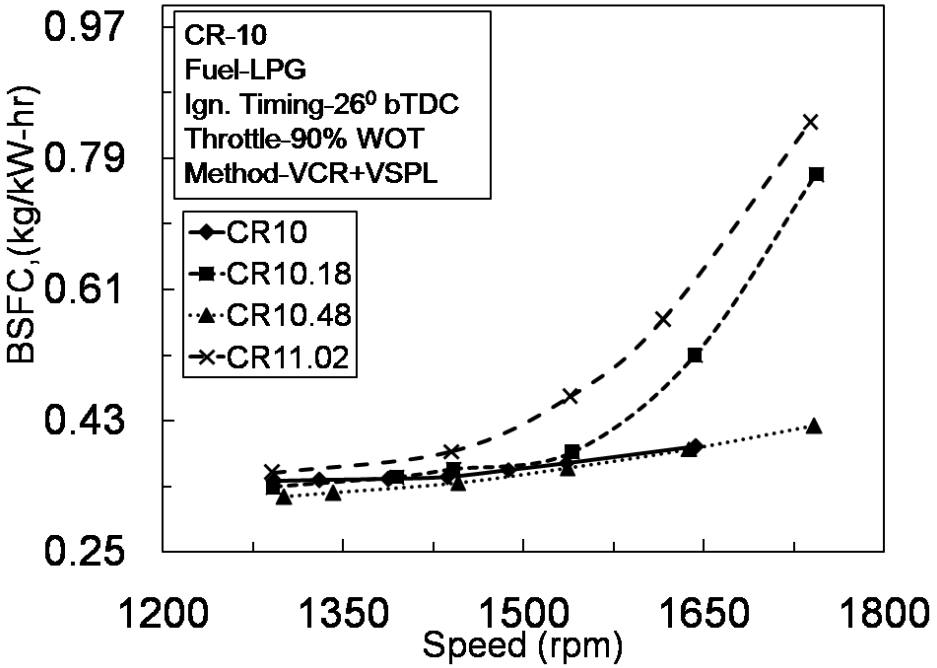

Fig.7.30 BTE variation with speed for different CR accompanied with SPL

The efficiency at CR10.48 is 3.88% higher than that of original CR with original location of spark plug. The deciding parameter for the efficiency of the engine is the fuel consumption as per load and speed of the engine. From Fig.7.27, the BSFC recorded for LPG fueled engine increases with increase in speed.This is obvious because with increase in speed brake power reduces and if the mass of fuel consumed remains constant then BSFC will rise (Chaudhari et al.,2015).

The BSFC of 0.325 kg/ kW-hr at CR10.48 running at 1301 rpm and spark location SP3 is recorded. However 0.348 kg/ kW-hr, 0.339 kg/ kW-hr and 0.359 kg/kWhr are recorded for CR10, CR10.18 and CR11.02 respectively.

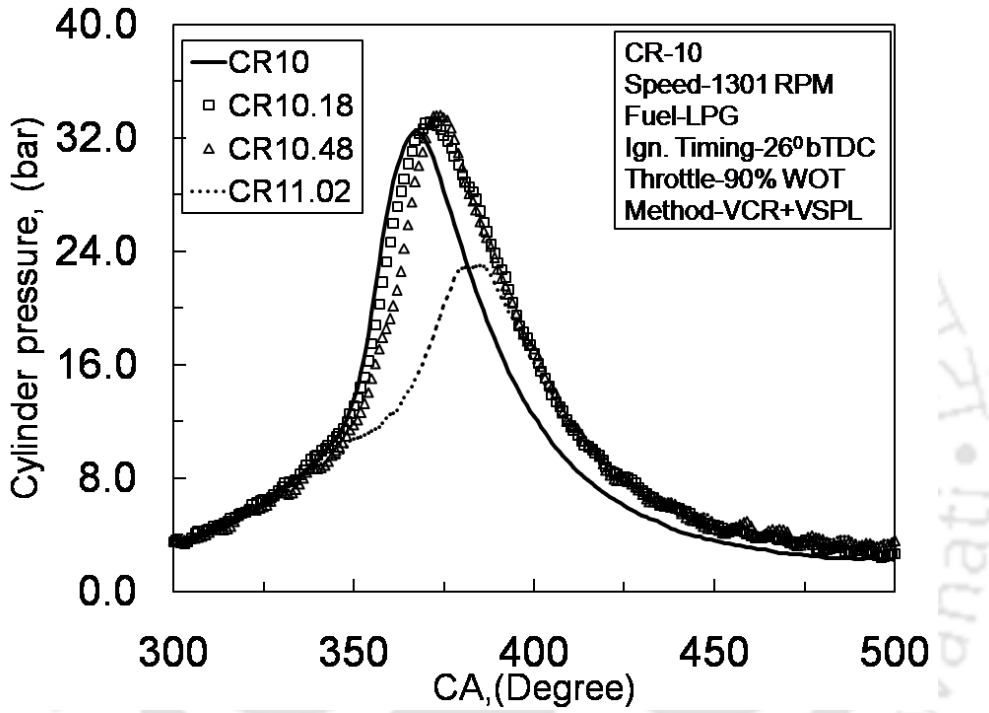

Fig. 7.31 Cylinder Pressure variation with CA for different CR attained by novel Top up mechanism combined with novel VSPL

It is seen that the BSFC is lower at CR10.48. This is the outcome of efficient and homogeneous combustion of charge at CR10.48 and spark plug location SP3.

7.3.2.2 Combustion Analysis

The variation of cylinder pressure with CA for different CR with CR10 as base CR is plotted in Fig.7.31. The CR10.18 is obtained with displacement of secondary piston containing spark plug by 2mm inside combustion chamber or locating piston at SP2. Similarly, CR10.48 and CR11.02 by corresponding 5mm (SP3) and 10mm (SP4) displacement inside combustion chamber could be attained. The performance of the engine under this structural manipulation in terms of cylinder pressure shows that with increase in CR, the cylinder pressure increases and this continues till CR10.48. Thereafter there is substantial decrement in pressure. The operating parameters such as ignition timing, load on the engine, air/fuel ratio are maintained constant for all studies. From the graph, at CR10.18, the increment in peak pressure is 1.71 % above base CR10. Similarly the increment of 3.59 % at CR10.48 is being reported with

respect to CR10. With further rise in CR to 11.02, the peak pressure shows decrement of 29.22 % with respect to CR10. This represent CR10.48 is most optimum CR at this condition of speed and load.

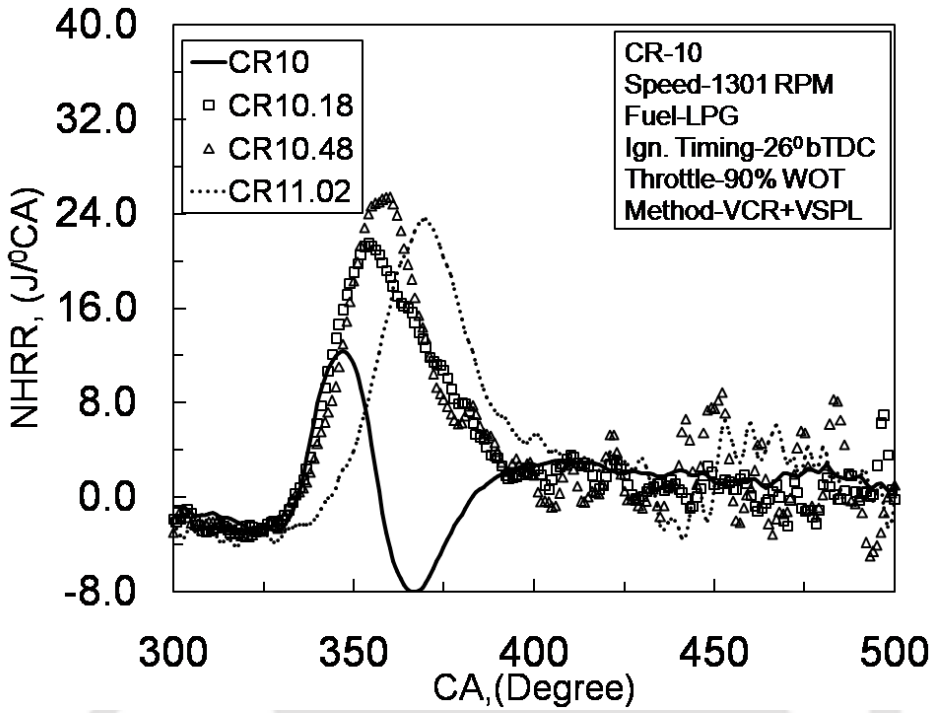

Fig. 7.32 NHRR variation with CA for different CR attained by novel Top up mechanism combined with novel VSPL

The combination of VCR and VSPL relocate optimum working conditions for the fuel LPG. The work done by engine largly depends upon the heat released during combustion of charge.

The NHRR variation with CA for different CR is as plotted in Fig.7.32. From the Fig. 7.32, it is seen that with the increase in CR the peak NHRR is found increasing, but the CA also found retarding at maximum NHRR. The peak NHRR of 12.318 J/ ^{0} CA at 347 ^{0} CA, 20.501 J/ ^{0} CA at 357 ^{0} CA, 25.365 J/ ^{0} CA at 359 ^{0} CA and 23.476 J/ ^{0} CA at 370 ^{0} CA at CR10, CR10.18, CR10.48 and CR11.02 respectively. The combustion gets accelerated after 343 ^{0} CA. It is seen that CR10.48 with spark plug location 5 mm inside the combustion chamber cause the homogeneous combustion, thereby raising the NHRR. At CR 11.02 also, NHRR is higher than base CR, but the combustion is much delayed and hence reduces peak cylinder pressure (Fig.7.31) and looses effective expansion stroke. The speed of combustion is more clearly understood by the study of percent mass fraction burned as shown in Fig.7.33.

The percent MFB based on VCR combined with VSPL shows that the 10 % MFB takes place at 356 ^{0} CA, 347 ^{0} CA, 345 ^{0} CA and 355 ^{0} CA for CR 10, CR 10.18, CR 10.48 and CR 11.02 respectively. Also the 90% charge burned at 381 ^{0} CA, 373 ^{0} CA, 370 ^{0} CA and 382 ^{0} CA for CR 10, CR 10.18, CR 10.48 and CR 11.02 respectively. As compared to base CR 10 with conventional spark location, the flame speed is high for the 5mm location inside combustion chamber. The location of spark plug is optimum according to centre of combustion and as spark plug is not wetted with fuel air charge, the flame developed can spread through the combustion chamber.

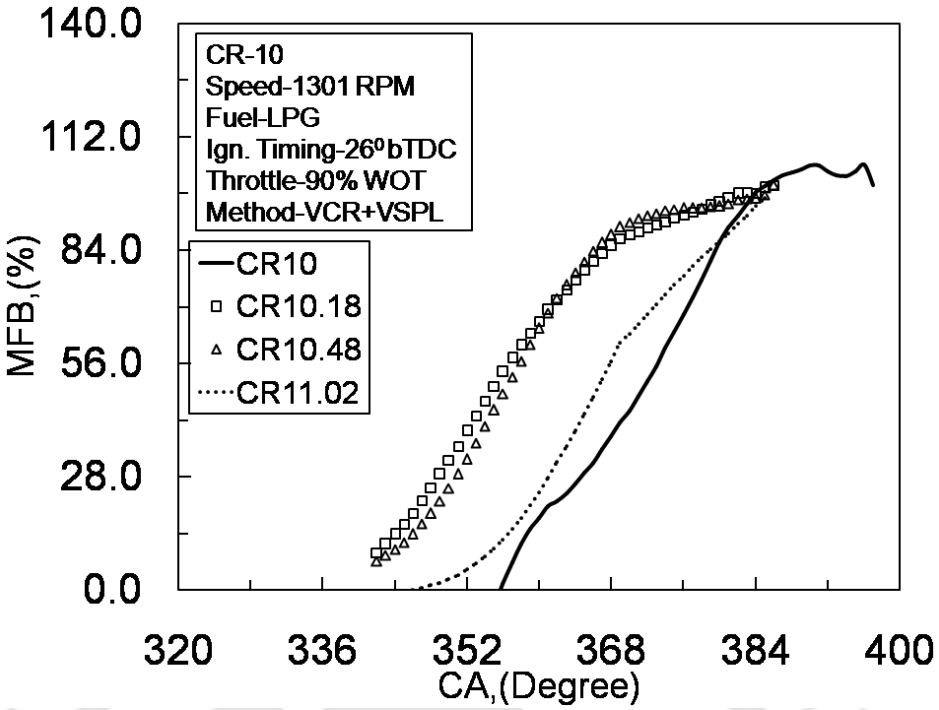

Fig. 7.33 Cylinder Pressure variation with CA for different CR attained by novel Top up mechanism combined with novel VSPL

The location 2mm and 10 mm may be offsetting the centre of combustion inside cylinder on account of reduction of cylinder volume with increase in CR.

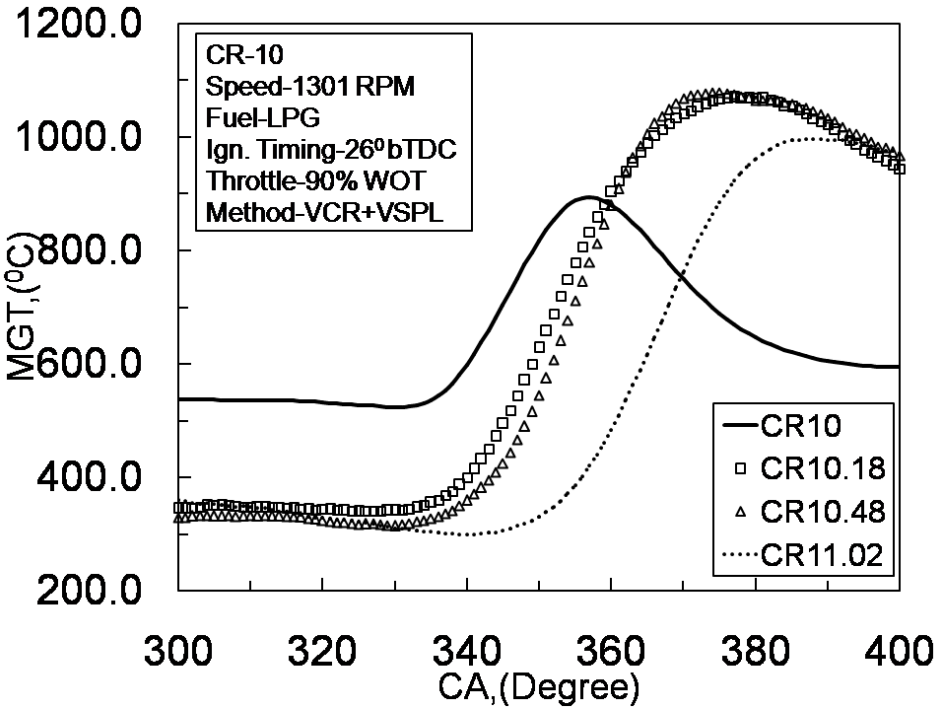

Fig. 7.34 MGT variation with CA for different CR attained by novel Top up mechanism combined with novel VSPL

Hence spark produced can't reach towards fuel air charge causing delayed combustion and lowered the power output.

The mean gas temperature is the outcome of how efficiently the combustion happened inside the engine cylinder. The MGT variation with CA for different compression ratio is as represented in Fig.7.34. It is observed that maximum MGT is 893 ^{0}C, 1070 ^{0}C, 1078 ^{0}C and 996 ^{0}C respectively at CR 10, CR 10.18, CR 10.48 and CR 11.02. It is obvious that MGT is higher at CR 10.148 with SP3 location.

7.3.2.3 Emission Analysis

The emission from the SI engine under the influence of VCR and VSPL is important. In this regards, the harmful emission such as CO as shown in Fig.7.35 for different CR combined with VSPL. The CO emission is found increasing with speed for all the CR under consideration. However with increase in CR, the CO emission found higher in this case. At high load condition say speed 1440 rpm, the CO emission is 92 ppm, 194 ppm, 185 ppm and 158 ppm for CR 10, CR 10.18, CR 10.48 and CR 11.02 respectively. The CO emission is found to be higher at CR 10.18 followed by CR 10.48. As LPG is a gaseous fuel, the volumetric efficiency will be reduced reducing the supply of fresh air required for combustion. So, with increase in CR, the volume of cylinder is reduced, therefore percentage volume of air in intake charge reduces and causes the partial combustion raising the CO in exhaust.

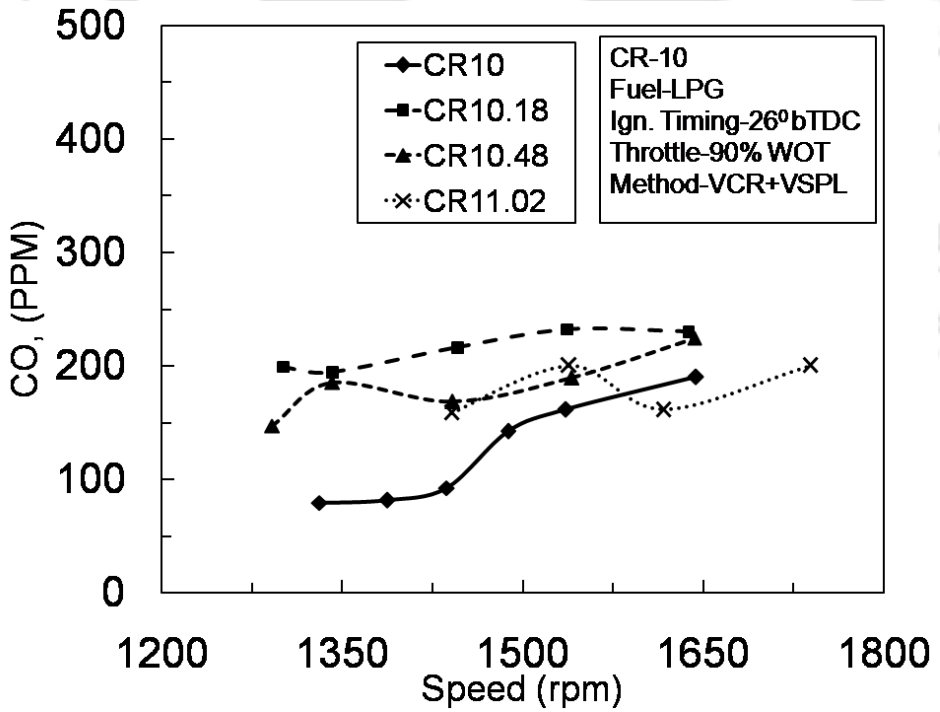

Fig. 7.35 CO emission variation with speed for different CR attained by novel Top up mechanism combined with novel VSPL

In the similar way other harmful emissions which cause damage to environment is NO_x are plotted in Fig.7.36. As shown in this figure, the NO_x reduces with increase in speed of the engine.

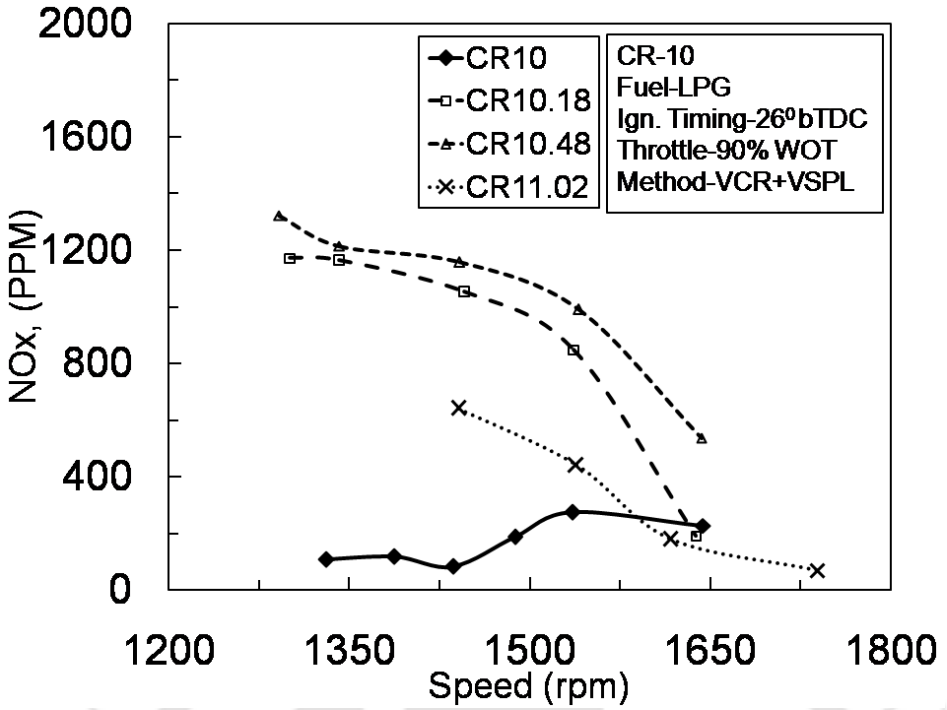

Table 7.36 NO_x variation with speed for LPG fuel run Engine

The combustion temperature increases with increase in load on the engine or decrease in speed of the engine. This may be the reason for reduced NO_x with increase in speed. From the figure the overall variation of 53.09 %, 89.35 %, 59.24 % and 89.35 % for CR 10,CR 10.18,CR 10.48 and CR 11.02 have been recorded over the speed range of 1290-1740 rpm.

Table 7.4 The optimum combination for LPG fuel run Engine

CR	**BTE**	**% Increment w.r.t. original CR**	**CR**	**BTE**	**% Increment w.r.t. original CR**	**CR**	**BTE**	**% Increment w.r.t. original CR**
10	26.79	--	**9**	21.237	--	**8**	22.459	--
10_SP4	27.83	3.88	**9_SP2**	22.714	6.95	**8_SP2**	19.257	**14.25(D)**
10.48_SP3	28.357	5.84	**9.14_SP2**	23.437	10.35	**8.11_SP2**	23.452	4.42

At 1440 rpm, the NO_x emission is found to be 81 ppm, 1163 ppm, 1212 ppm and 639 ppm for CR 10, CR 10.18, CR 10.48 and CR 11.02. The maximum NO_x is seen at CR 10.48 and again falls when CR is increased to 11.02. The increment in CR is accompanied with VSPL in our case, which has seen to be having impact over the reduction in NO_x for higher CR.

Table. 7.4 represents the optimum composition for the LPG fuel in conventional spark ignition engine. From the figure, if engine is operated at CR10, which is maximum compression ratio possible on SI engine in our case, then maximum thermal efficiency achieved is 26.79 % where as 25.52 % and 19.28 % are the values of the same for CR 9 and CR 8 respectively.

However the performance is possibly upgraded with optimizing spark plug location inside combustion chamber. If the engine structure is manipulated and optimized at 10 mm distance coaxial (SP4) to the cylinder vertical centroidal axis, then the brake thermal efficiency found increased to 27.83 % showing rise of 3.88 %. There is some more scope for rise in efficiency by minutely increasing the CR to 10.48 and simultaneously relocating spark plug at 5mm from original position. Under this configuration, the thermal efficiency obtained is 28.357 % which is 5.84 % higher than original CR and 1.89 % more over 10 mm spark plug location.

7.4 GASEOUS FUEL PERFORMANCE WITH EGR UNDER INFLUENCE OF VCR AND VSPL.

As seen from the analysis of raw biogas and LPG fuel with novel VCR combined with VSPL, the performance is found improved. But the exhaust gas emissions are also found raised with rise of CR and adjusting spark location. In order to trace this issue, the technique of exhaust gas recirculation as studied and analyzed in chapter- 6 for conventional VCR SI engine using similar fuels can possibly been implemented. Under such situation, if EGR rate of different magnitudes are utilized in the biogas or LPG run SI engine, then the effect of novel VCR and VSPL on the performance of the engine in presence of EGR becomes utmost importance to select the optimum configuration at each situation.

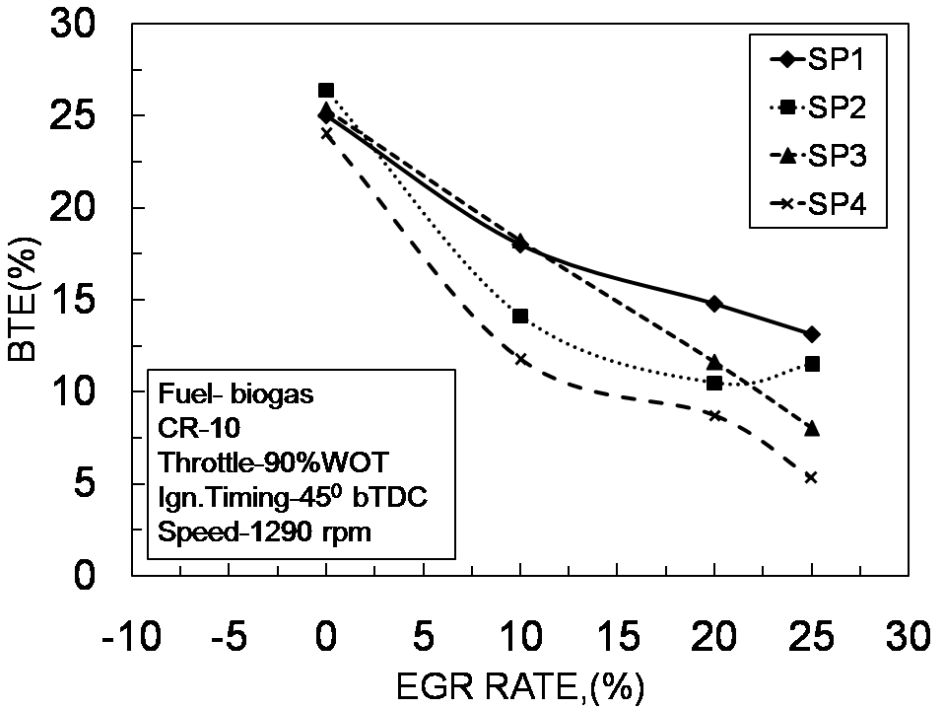

Fig.7.37 BTE variation with EGR rate for different spark location at CR10

7.4.1 Biogas run SI engine performance with EGR under influence of VCR and VSPL.

Upon the successful operation of the biogas fueled SI engine using novel VCR combined with VSPL mechanism, it is possible to improve the performance of the engine. However the emissions which grows rapidly, needs to be controlled by some technique. To control these emissions, the effective system called as exhaust gas recirculation can be adopted. So the EGR rate 10%, 20% and 25% can be used based on the analysis reported in chapter 6. The

lower heating value fuel raw biogas mixed with EGR supplied to the engine. It is interesting to see the selection of optimum configuration of the engine such as CR and SP location to achieve maximum output with minimum exhaust emission.

7.4.1.1 Performance Analysis

The performance of the engine can be measured in terms of BTE . The BTE variation with EGR rate for different spark location maintaining constant CR10 is as plotted in Fig.7.37. As shown in figure, the BTE keeps on reducing with increase in EGR rate from 0% towards 25%. This is because of the non combustable recirculated exhaust gas when mixed with the fresh charge of fuel and air, makes the charge dilute and hence reduces its heating value. The outcome of this is the reduction in BTE. The corrosponding decrement of 47.56 %, 56.51 %, 68.33 % and 78 % respectively at SP1, SP2, SP3 and SP4 when operated at base CR 10 and speed 1290 rpm. At a particular EGR rate say EGR 0, SP2 shows maximum BTE of 26.4%.

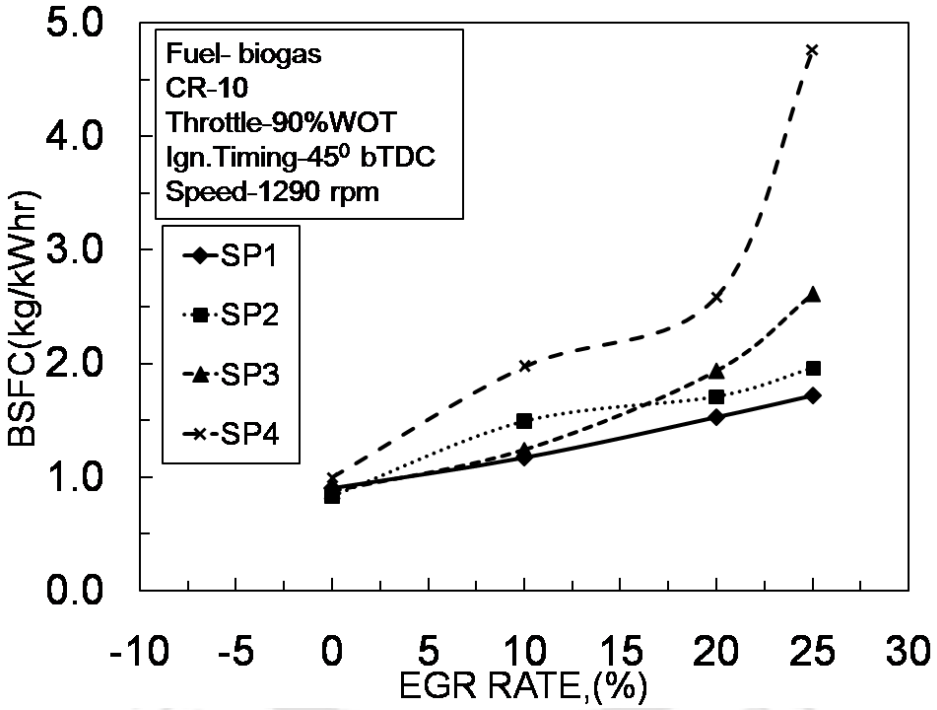

Fig.7.38 BSFC variation with EGR rate for different spark location at CR10.

Other spark locations are having decrement of 5.30 %, 4.17 % and 9.09 % for SP1, SP3 and SP4 with respect to SP2. But this trend doesnot remains same for other EGR rate. At EGR 10, SP3 shows maximum BTE of 18.203 % showing decrement of 1.11 %, 22.37 % and 35.50 % for SP1, SP2 and SP4 respectively with respect to SP3. With the increase of EGR rate, the temperature of recirculated exhaust gas inreases which intern preheat the intake charge of fuel and air. This causes the combustion earlier with lesser compression pressure as compared to previous case of EGR 0. That may be the reason due to which the protrusion of 5mm (SP3) attains homogeneous combustion and increased efficiency. When EGR rate is increased further to 20 % or 25 %, it diluted the mixture to a great extent and hence the optimum location is found to be SP1 followed by SP3, SP2 and SP4. The overall decrement of 47.56 % ,56.15 %, 69.16 % and 77.95 % is recorded for SP1, SP2, SP3 and SP4 respectively with EGR 0 to EGR 25.

The effect of BTE variation is appeaed on the brake specific fuel consumption. Rather, if BTE found decreased with EGR rate, then BSFC gets increased with increse of EGR rate. This can be seen in Fig.7.38 showing BSFC variation with EGR rate for different SP locations. For EGR 0, the SP2 shows 0.832 kg/ kW-hr BSFC which increases by 78.60 % at EGR 10, 105.52 % at EGR 20 and 135.58 % for EGR 25. Whith increase in EGR rate, brake power reduces which ultimately shows rise in BSFC. For EGR 10 showing optimum location to be SP3, EGR 20 shows SP1 and EGR 25 shows SP1 being maximum BTE or lowest BSFC settings.

7.4.1.2 Combustion Analysis

The combustion analysis is the only tool by which one can justify the engine performance at a particular compression ratio, spark location and EGR rate. To understand further the BTE (Fig.7.37) and BSFC (Fig.7.38) variations for the particular EGR rate, variable spark location for varying CR , the analysis has been carried out for cylinder pressure, NHRR, MFB and MGT.

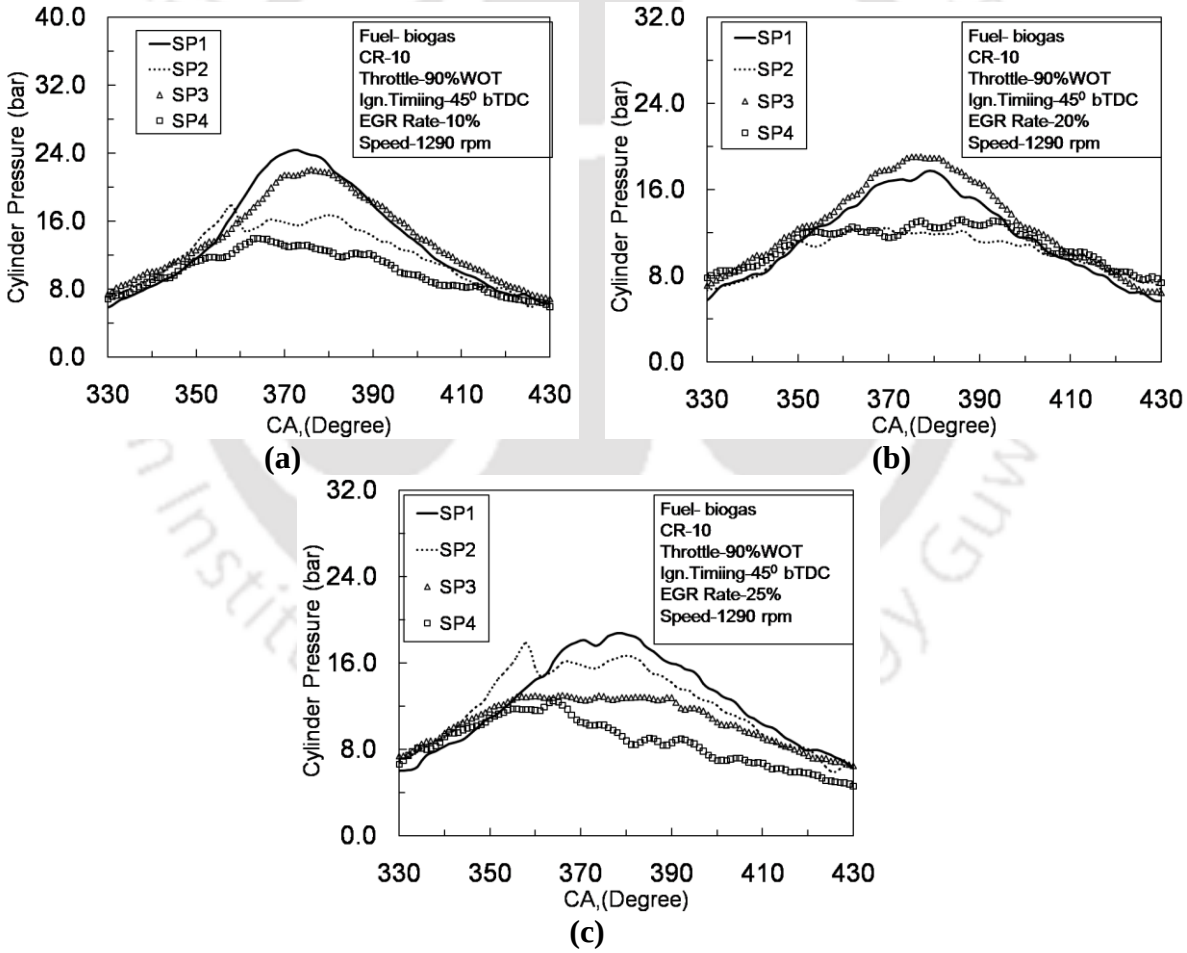

Fig.7.39 Cylinder pressure variation with CA for different spark location at CR10 with (a) EGR 10; (b) EGR 20 and (c) EGR 25.

The combustion parameter such as cylinder pressure is as plotted in Fig.7.39(a-c) with CA for different SP locations and EGR rate. For EGR0 the cylinder pressure variation shows that SP2 was the optimum location. For EGR 0, peak cylinder pressure is 25.156 bar at 371 ^{0} CA

increases to 29.160 bar at 371 ^{0} CA for SP2. Further to SP3 and SP4, it is 23.556 bar and 18.642 bar occurred at 370 ^{0} CA and 378 ^{0} CA respectively. If EGR rate increased to 10%, the peak pressure is at SP1 followed by SP3 showing a decrement of 9.40 %.

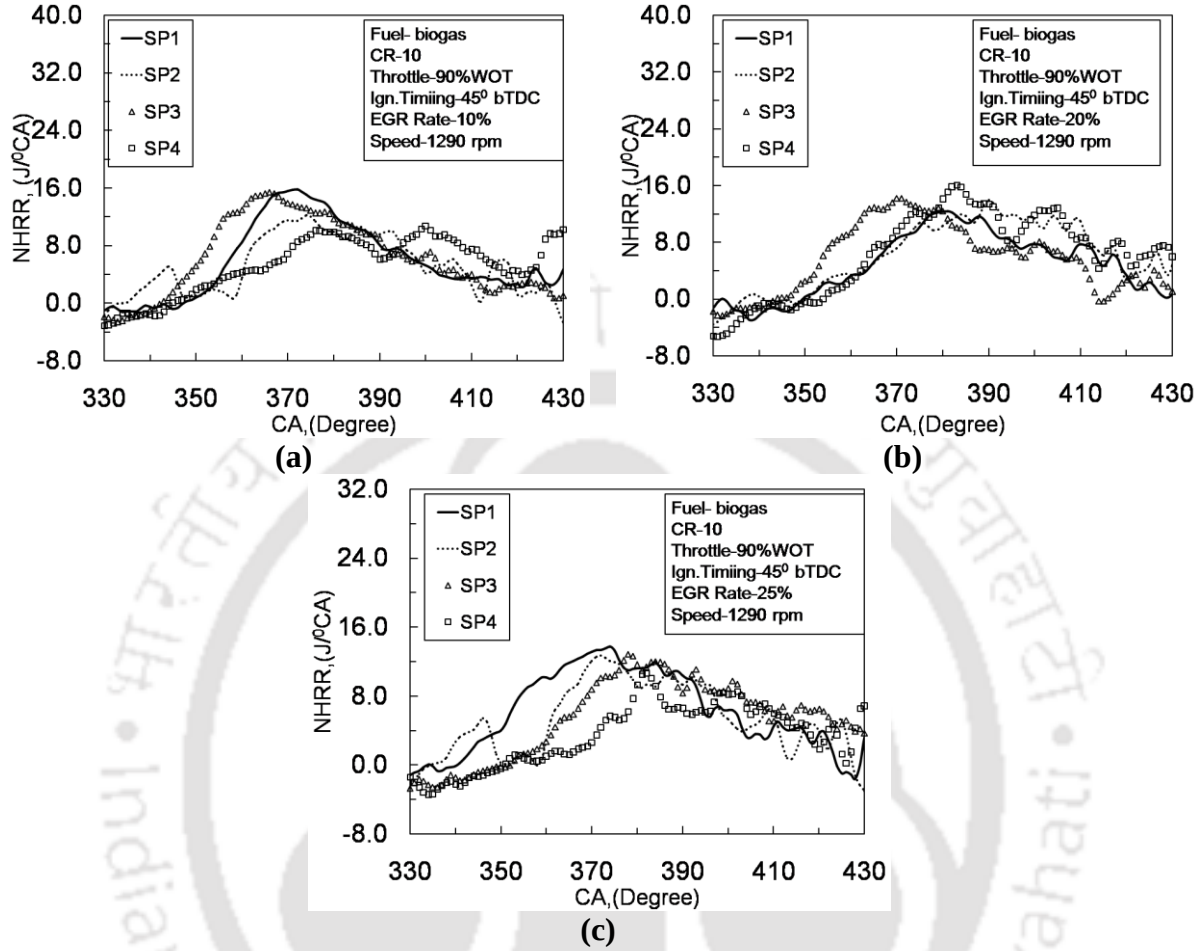

Fig.7.40 NHRR variation with CA for different spark location at CR10 with (a) EGR 10; (b) EGR 20 and (c) EGR 25.

However at EGR 20, the peak pressure located at SP3 having magnitude 19.033 bar with decrement of 6.81 %, 12.42 % and 31.53 % respectively for SP1,SP2 and SP4 with respect to SP3. Highest EGR rate carried by biogas is EGR 25 in our case showing maximum pressure at SP1 location. As biogas is a poor heating value, it needs more time for combustion to occur and hence the peak pressure observed is quite far ahead of TDC.

The NHRR is the parameter directly depending upon the fuel being used and the working condition of the engine such as load, speed, ignition advance, compression ratio and spark location. The NHRR for biogas fueled SI engine varying with CA is as plotted in Fig. 7.40 (a-c) for different EGR rate with SP location at CR10 and speed 1290 rpm. From the diagram it is seen that the peak NHRR doesnot remain fixed at one CR and signifies the combustion behavior in engine with varying EGR rate. Peak NHRR at EGR 0 is 15.649 J/ ^{0} CA for SP1 raises further when engine is operated to SP2 having magnitude 19.187 J/ ^{0} CA. At other SP location the decrement of 22.74 %, 21.66 % is recorded respectively for SP3 and SP4 with respect to SP2. If the EGR rate is increased to 10 %, then SP3 is comparable with SP1

showing maximum NHRR in all locations considered. In terms of CA, SP3 reaches peak at 366 ^{0} CA where as SP1 reaches at 372 ^{0} CA and shows delayed combustion.

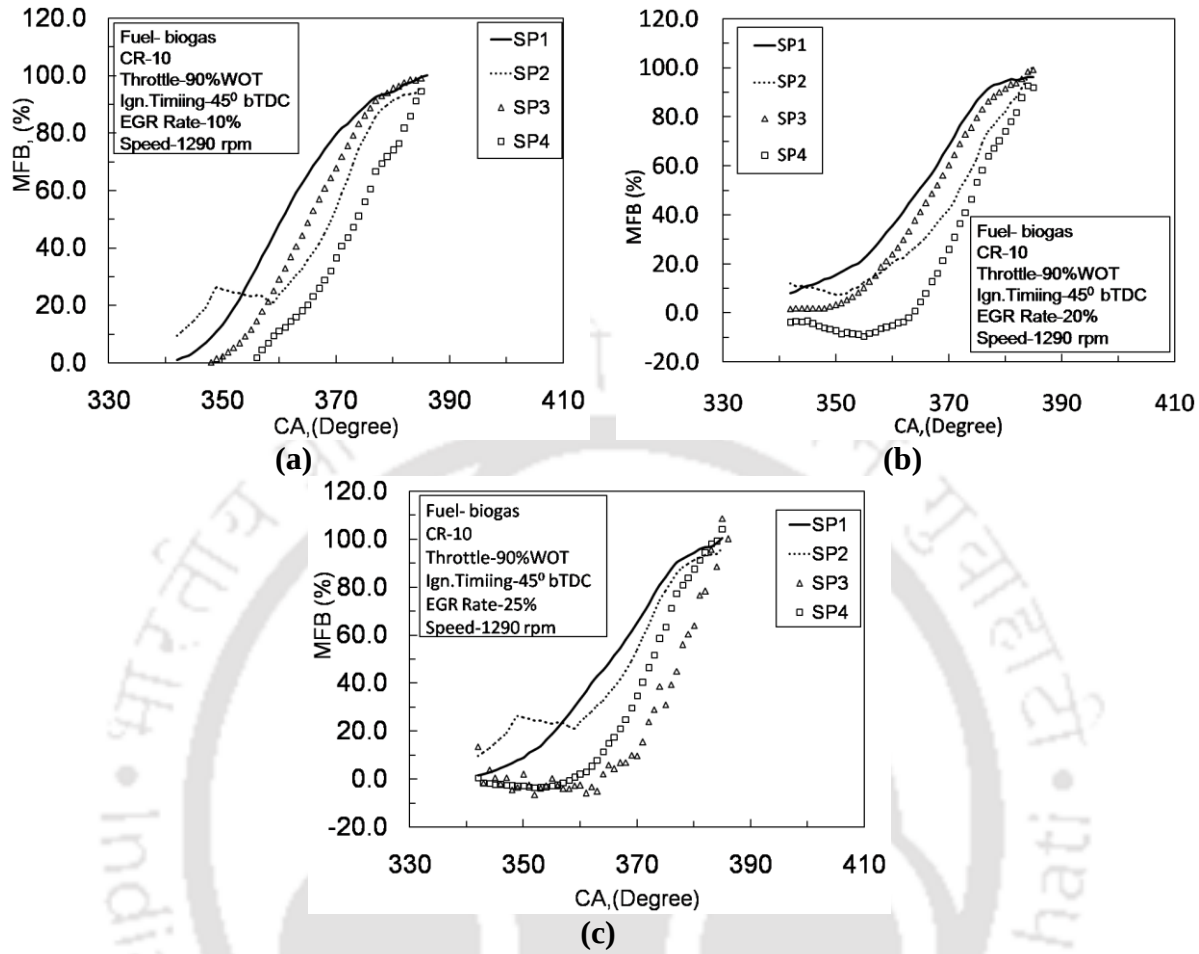

Fig.7.41 Percent MFB variation with CA for different spark location at CR10 with (a)EGR 10; (b)EGR 20 and (c)EGR 25.

This shows that the protrusion of 5 mm inside combustion chamber can be optimally used in case of 10 % EGR rate.

Table 7.5 Percent MFB variation with CA for different spark location at CR10 with (a) EGR 10; (b) EGR 20 and (c) EGR 25.

EGR RATE	SP1			SP2			SP3			SP4		
	10% MFB	90% MFB	MFB @ TDC	10% MFB	90% MFB	MFB @ TDC	10% MFB	90% MFB	MFB @ TDC	10% MFB	90% MFB	MFB @ TDC
0	344	375	54.45	**342**	**367**	**75.24**	345	374	53.81	351	380	30.04
10	349	375	48.36	343	379	23.71	**354**	**377**	**29.00**	360	384	11.08
20	344	377	35.57	354	383	20.57	**355**	**379**	**23.92**	367	384	0
25	**351**	**377**	**33.14**	342	379	23.71	364	381	18.30	374	384	0

If the EGR rate increases further then it shows SP3 be the optimum location attaining peak NHRR of 14.162 J/ ^{0} CA at 371 ^{0} CA. The heavy EGR rate 25 % is carried optimally by

SP1 location only. As combustion is a complex phenomenon, it is difficult to judge the influencing parameter for achieving the best performance especially for fuels like raw biogas. However it is very clear from the above discussion that the spark plug location is a matter of fact for enhancing the performance of the engine.

The percent MFB for biogas fuelled SI engine added with EGR rate from 0 % - 25 % is plotted in Fig. 7.41 (a-c) for variable spark location running at CR10 with speed 1290 rpm. The 10% MFB for EGR0 which is lowest at SP2, represents the combustion initiation at 342 ^{0} CA. This shows the faster flame development and higher flame velocity causing maximum MFB of 75.24% at TDC in all locations.

Alongside, the 90% MFB occurs at 367 ^{0} CA when combustion takes place at SP2 location, noting lowest combustion duration of 25 ^{0} CA. If the EGR rate increases to EGR10, then it is seen that at 354 ^{0} CA, the combustion initiates and continues up to 377 ^{0} CA where 10% to 90% MFB located respectively.

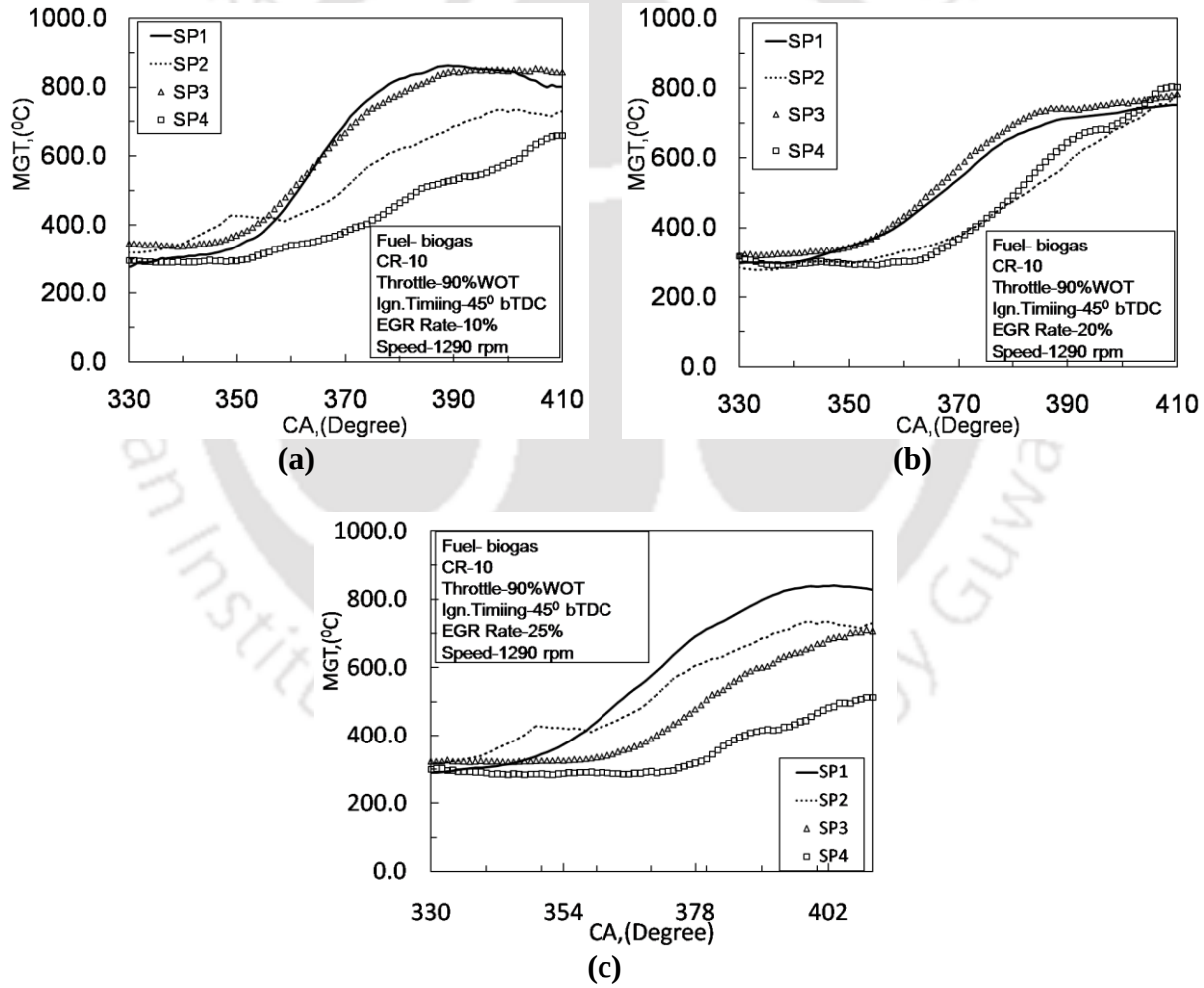

Fig.7.42 Mean Gas Temperature variation with CA for different spark location at CR10.

Thus lowest combustion duration of 23 ^{0} CA for SP3 is recorded for consuming 29.005 % MFB at TDC as compared with other locations. Further EGR rate 20 % shows combustion duration of 24 ^{0} CA at SP3 which is minimum in all SP locations consuming 23.92 % MFB at TDC.

However at EGR25, the combustion duration is 26 ^{0} CA, 37 ^{0} CA, 17 ^{0} CA and 10 ^{0} CA at SP1, SP2, SP3 and SP4 respectively.

In all, SP4 is having minimum combustion duration but the crank angle at which combustion initiated is much delayed beyond TDC (374 ^{0} CA) so could not be a possible optimum spark location. Next to it is the SP3 showing 17 ^{0} CA, but the combustion initiates at 364 ^{0} CA reduces the effective expansion stroke so cannot be a optimum SP location. So finally SP1 is most optimum SP location for EGR 25 with biogas fuel (Table 7.5).

Mean gas temperature as generated due to combustion of fuel air charge inside combustion chamber is plotted in Fig. 7.42 (a-c). MGT for EGR 0 is 888.35 ^{0} C for SP2 occurred at 384 ^{0} CA utilizes for 157 ^{0} CA during power stroke.

The peak cylinder pressure variation with SP location under influence of EGR is as plotted in Fig.7.43. As seen from the figure, peak cylinder pressure at CR 10 is SP2 for EGR 0. Similarly for EGR 10, the peak pressure occurred at SP1. In the similar way the peak pressure observed at SP3 and SP1 for EGR 20 and EGR 25 respectively. The scenario is little different when the engine operated at lower CR9. For EGR 0, SP2 being the optimum spark location as shown in Fig. 7.43.

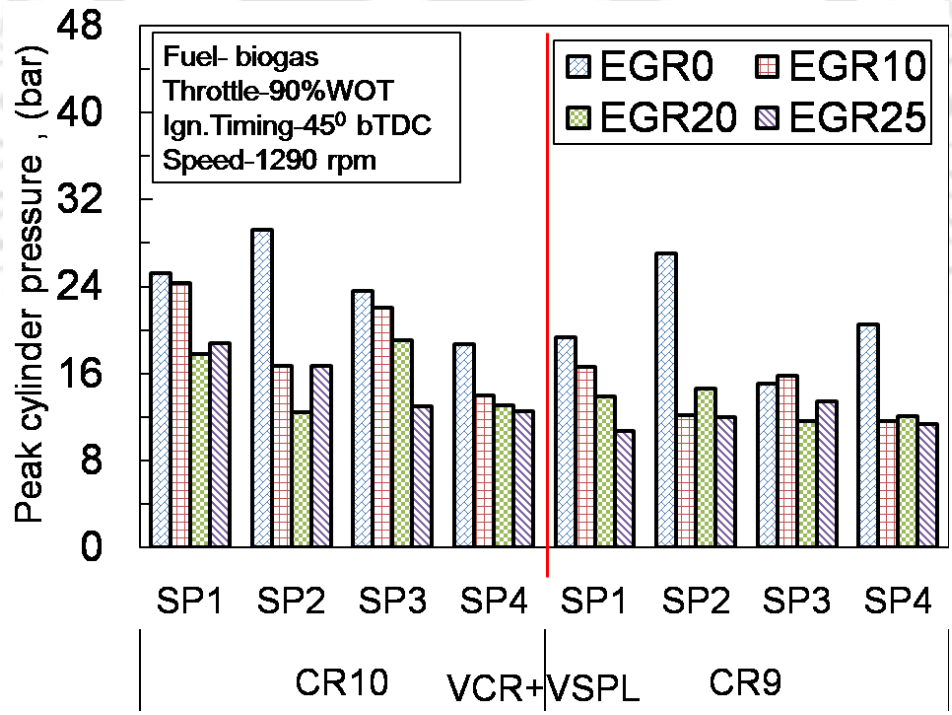

Fig.7.43 Peak cylinder pressure variation under effect of EGR for VCR combined with VSPL

In the similar way peak pressure of 16.579 J/ ^{0} CA is found at SP1 while 15.74% has been obtained at SP3 location.

However the crank angle at which these peaks are observed are 384 ^{0} CA and 374 ^{0} CA respectively for SP1 and SP3. The effective expansion stroke for SP1 remains to 156 ^{0} CA whereas for SP3 it is 166 ^{0} CA. This justifies the optimum location for spark plug at 5 mm (SP3) when EGR 10 is being supplied to the engine. For EGR 20 and EGR2 5, the maximum

cylinder pressure occurred at SP2 and SP3 respectively. The combustion is very poor and misfire is observed especially when EGR 25 is used during the engine operating on CR 9

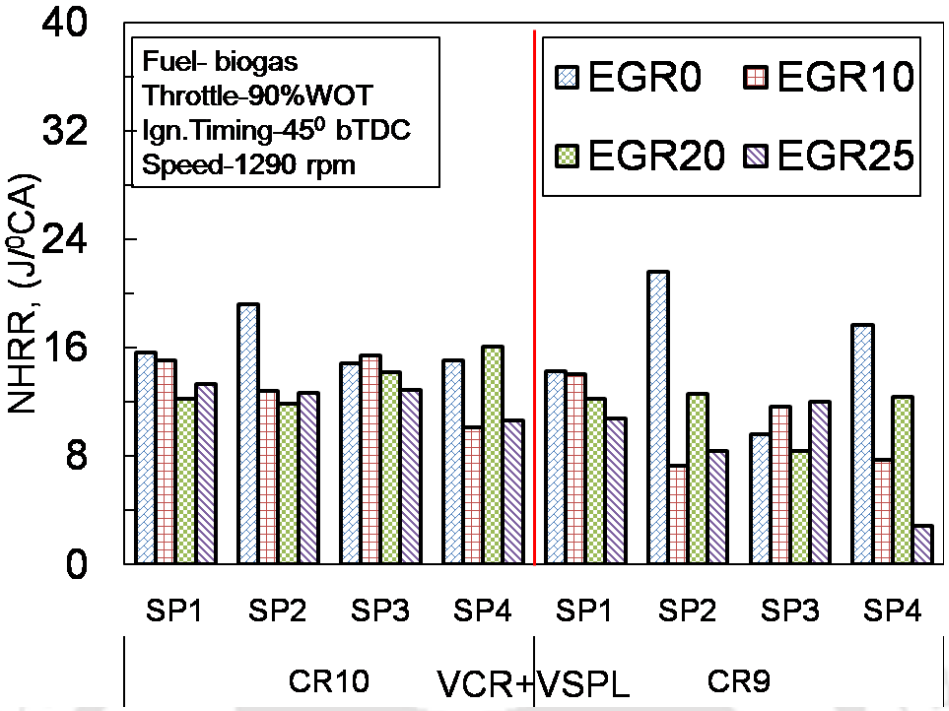

Fig.7.44 NHRR variation under effect of EGR for VCR combined with VSPL

The NHRR variation with SP location for different EGR rates is as plotted in Fig.7.44. The NHRR for CR10 as elaborated in section 7.5 shows the optimum spark locations. From the figure, SP2 is optimum for EGR0 showing maximum NHRR at CR10.

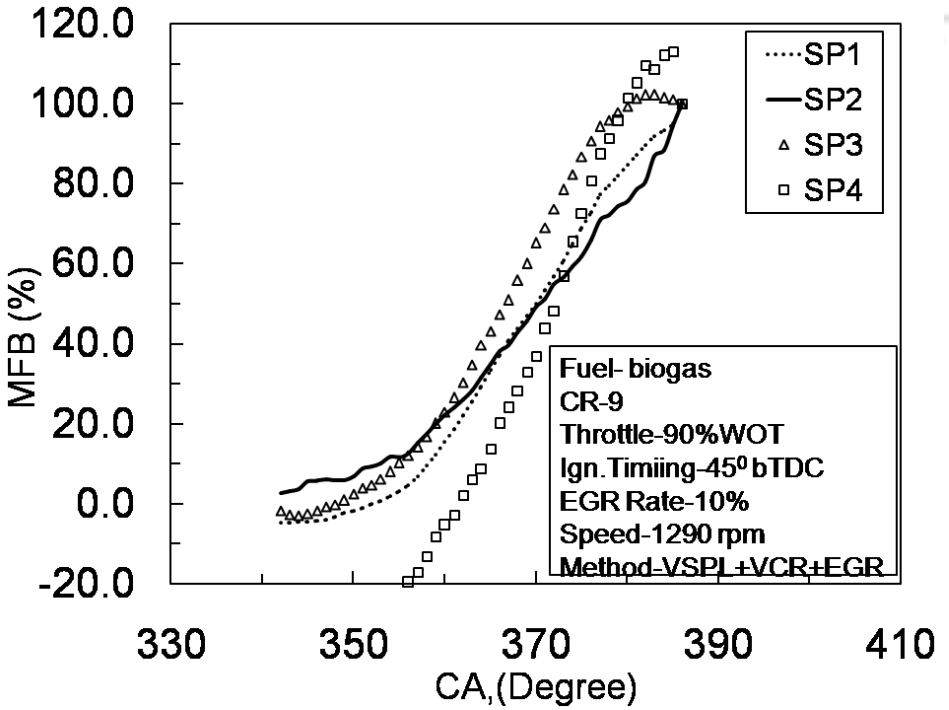

Fig.7.45 Percent MFB variation under effect of EGR for CR9 combined with VSPL

Actually, SP1 and SP3 are close in magnitude having 15.76 J /^{0} CA obtained at 372 ^{0} CA and 15.337 J/ ^{0} CA at 366 ^{0} CA when EGR rate is increased to 10 %. The optimum location is SP3 based on the crank angle close to TDC which attained maximum efficiency from the engine. For the higher EGR rate SP3 for EGR 20 and SP1 for EGR 25 are found optimum at CR 10. Although, the EGR rate and protrusion length 2 mm, 5 mm and 10 mm remains same, if the compression ratio is changed, it affects the performance of raw biogas fueled engine. From the figure, it is observed that SP2, SP3, SP2 and SP3 show maximum NHRR for EGR 0, EGR 10, EGR 20 and EGR 25 respectively. However, the combustion issue such as speed fluctuations, misfire etc during working on CR9 shows variation in performance.

The combination of compression ratio and spark plug location for varying CR using EGR rate can be optimized with greater accuracy by knowing the percent MFB for each case. For this, Fig.7.45 shows the percent MFB variation with CA for different SP location, CR9 and EGR 10. The magnitudes of percent MFB for all cases are tabulated in Table 7.5 as well. From Fig.7.45 combustion initiates at angle 345 ^{0} CA for SP1, SP2 and SP3 but delayed slightly if EGR 25 is supplied. The 10% MFB is noted at 358 ^{0} CA for SP1, 353 ^{0} CA for SP2, 355 ^{0} CA for SP3 and 364 ^{0} CA for SP4 when running at CR 9 and speed 1290 rpm. However the SP3 location shows smooth rise in MFB with greater slope as compared to other cases. This represents the flame kernel developed faster and cause combustion.

Fig.7.6 Percent MFB variation with CA for different spark location at CR9.

EGR RATE	SP1			SP2			SP3			SP4		
	10% MFB	90% MFB	MFB @ TDC	10% MFB	90% MFB	MFB @ TDC	10% MFB	90% MFB	MFB @ TDC	10% MFB	90% MFB	MFB @ TDC
0	353	373	17.76	**351**	**370**	**54.29**	352	383	27.34	354	381	14.28
10	358	382	15.47	353	377	22.14	**355**	**376**	**22.82**	364	377	0
20	361	389	8.92	**356**	**380**	**20.53**	362	387	4.70	361	381	9.50
25	353	378	29.86	359	385	15.0	**362**	**380**	**4.93**	363	369	0

The 90% MFB obtained at 382 ^{0} CA, 377 ^{0} CA, 376 ^{0} CA and 377 ^{0} CA for SP1, SP2, SP3 and SP4 respectively. The important measurement called as combustion duration evaluated from Fig.7.46, will give good indication of combustion rate inside combustion chamber.

From the Table 7.6, the rate of combustion can be identified for each EGR rate with the multiple spark locations for biogas run engine. The highlighted set of combustion duration (time of combustion from 10% to 90% mass of fuel in degree CA) along with % mass burned at TDC arrives at the optimum location of spark plug for the particular EGR rate. As discussed previously, the combustion duration for SP2 is lowest in case of EGR 0 with maximum MFB at TDC. Similarly, SP3, SP2 for EGR 10 and EGR 20.

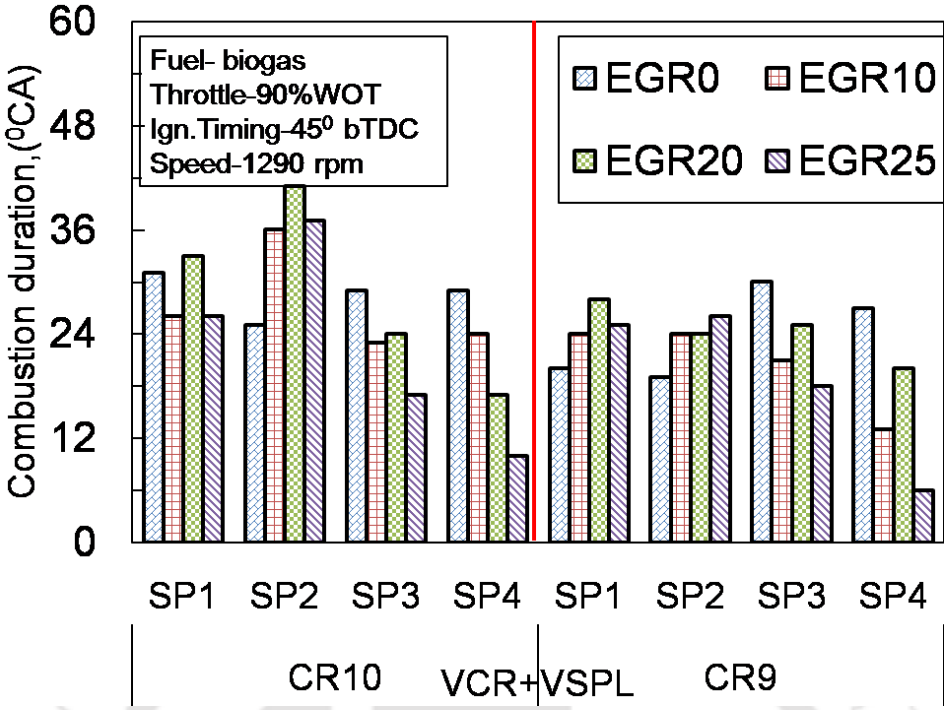

Fig.7.46 Combustion Duration variation under effect of EGR for VCR combined with VSPL

However, the combustion at EGR 25 with low CR 9 causes improper combustion so, the optimum spark location according to % MFB@ TDC found to be SP1. But as per peak pressure (Fig.7.46) and peak NHRR (Fig.7.46), SP3 is optimum. It is advised hereby that, the EGR rate 25 % is not suitable for the biogas fueled SI engine .

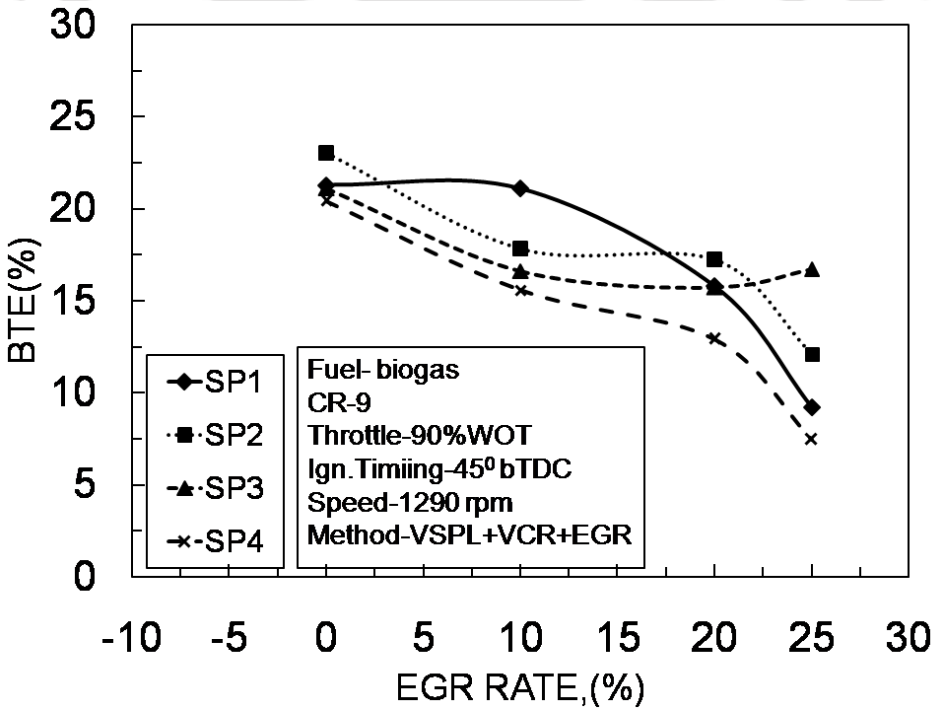

Fig.7.47 BTE variation under effect of EGR for VCR combined with VSPL

The combustion duration for variable CR is plotted (Fig.7.46) in the form of column with respect to SP location for different EGR rates. The minimum the column height represent the optimum spark location for the particular EGR rate. Accordingly, SP2, SP3, SP3, SP3 are the

optimum spark locations for EGR 0, EGR 10, EGR 20 and EGR 25 under working conditions of CR 10 and speed 1290 rpm. Along the same format, there are SP2, SP3, SP2 and SP3 find minimum combustion time and possibly attains maximum efficiency when running at CR 9 and speed 1290 rpm.

The performance of the biogas fuelled engine at CR 9 with speed 1290 rpm in terms of BTE is plotted with EGR rate. As seen from figure, the maximum BTE at EGR 0 is 23% for SP2 showing results are concordant with combustion outcomes.

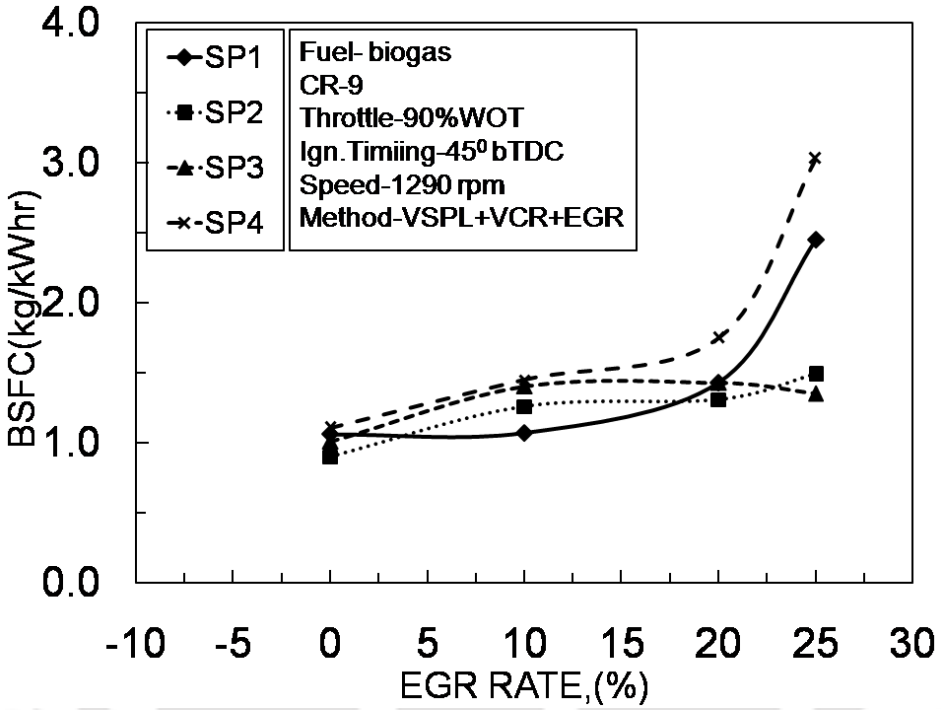

Fig.7.48 BSFC variation under effect of EGR for VCR combined with VSPL

However there is decrement of 7.52 %, 8.26 % and 11.28 % in BTE for SP1, SP3 and SP4 respectively with respect to BTE at SP2. If EGR rate is increased to 10%, then SP1 shows 21.07 % BTE which is maximum in all cases. The result of BTE (Fig.7.47) is contradicting with the combustion outcomes where the peak pressure, NHRR and combustion duration show that SP3 is the optimum location. If EGR rate increased to 20 %, then BTE 17.2 % could be achieved for biogas locating spark plug at SP2. This gives rise of 9.06% with respect to original spark location. At EGR 25, the SP3 location is found to be optimum showing BTE 16.7 % which is 81 % higher than that attained at original SP location SP1.

The BSFC variation with EGR rate for different spark location working under CR9 and speed 1290 rpm is as plotted in Fig.7.48. Here, BSFC is found increasing with increase in EGR rate following nature exactly opposite to that of BTE variation. The BSFC reported to be 0.9kg/ kW-hr decreased by 14.93 % with respect to original location SP1 when spark plug located at SP2 and EGR 0. If the EGR rate increases to 10 %, the lowest BSFC 1.068 kg/ kW-hr is observed at SP1. Further increment in EGR rate to 20 % shows 1.307 kg/ kW-hr at SP2 found decreased by 8.40 % with respect to original SP1 location. Again increment of EGR rate to 25 % settled BSFC at SP3 showing 1.35 kg kW-hr which is much lesser than that of original SP1 location. This justifies the relocation of spark plug over original position

in case of raw biogas fuel definitely improves the performance even with addition of EGR upto 25 %.

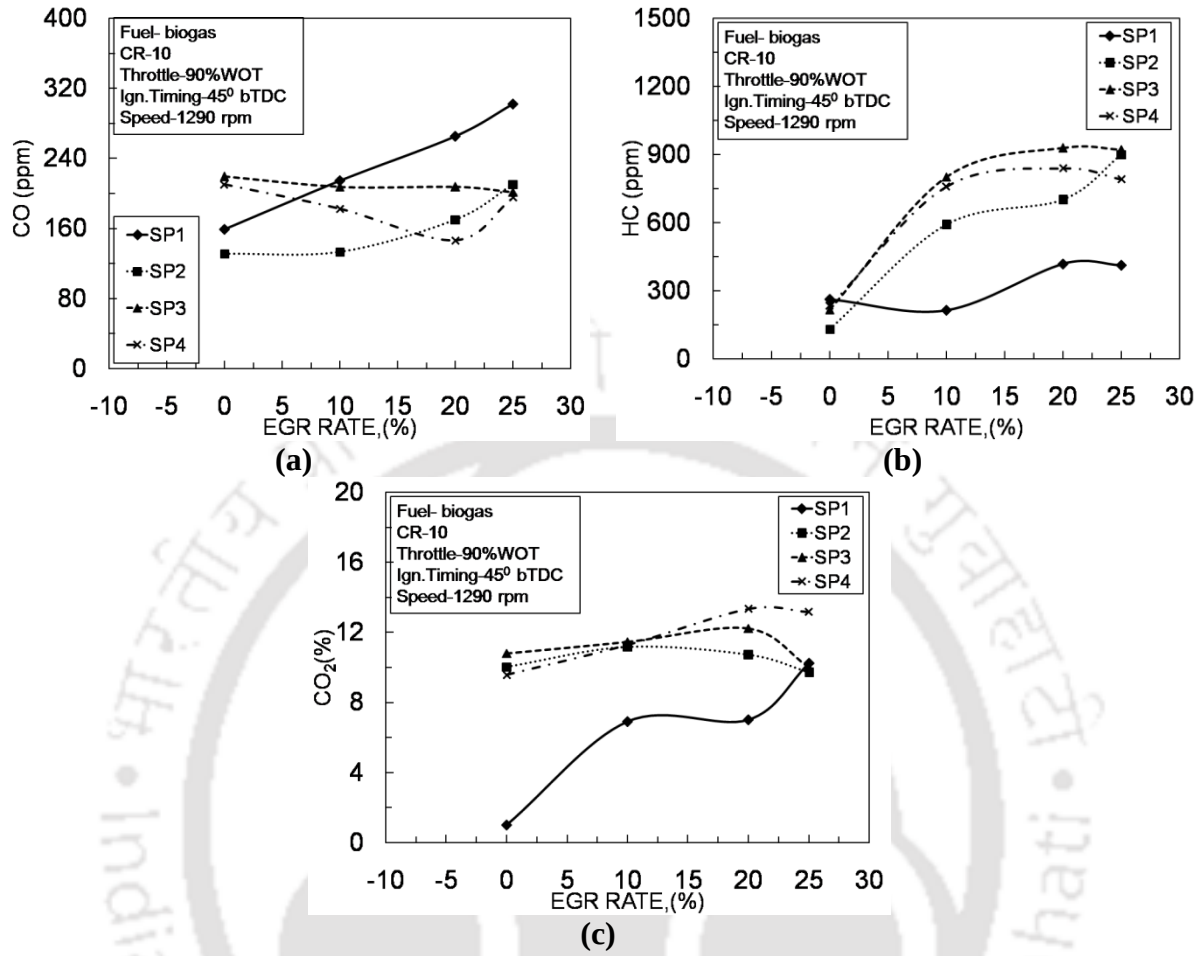

Fig.7.49 Exhaust gas emission variation with EGR rate for different spark location at CR10.
(a) CO variation with EGR rate;(b)HC variation with EGR rate;(c)CO_2 variation with EGR rate

7.4.1.3 Emission Analysis.

The emissions are unavoidable with any type of fuel combustion. The only chance of having higher or lower percentage of exhaust gases emissions with variety of fuels. Here the raw biogas combustion in presence of EGR for variable spark plug location is shown in Fig.7.49 (a-c). The CO emissions distribution with EGR rate is plotted in Fig.7.49 (a).

With increase in EGR rate CO found increasing for all spark plug locations. This is certainly happened due to incomplete combustion in absence of fresh oxygen in intake charge. The SP2 location is showing lowest CO emission at EGR 0 and EGR 10. Similarly for EGR 20, optimum SP location is SP4 and SP3 for EGR 25 where the CO is found lower. Under the fixed operating conditions for all SP locations at a particular EGR rate shows variation in CO, this may be because of combustion initiation from close to the combustion centre causes rich fuel charge to burn first. So the combustion accelerates outward as kernel developed and complete combustion takes place. Accordingly Co found lowered. Unburnt HC found higher in case of novel VCR mechanism attachment as shown in Fig.7.49 (b). With SP1 location, the HC is found lowest for all EGR rates and found higher with SP2, SP3 and SP4 locations. The

major reason of this may be the protrusion length of secondary piston with a very narrow gap between cylinder wall and secondary piston. This forms the crevices and fuel charge may not burn completely and flows outside with exhaust.

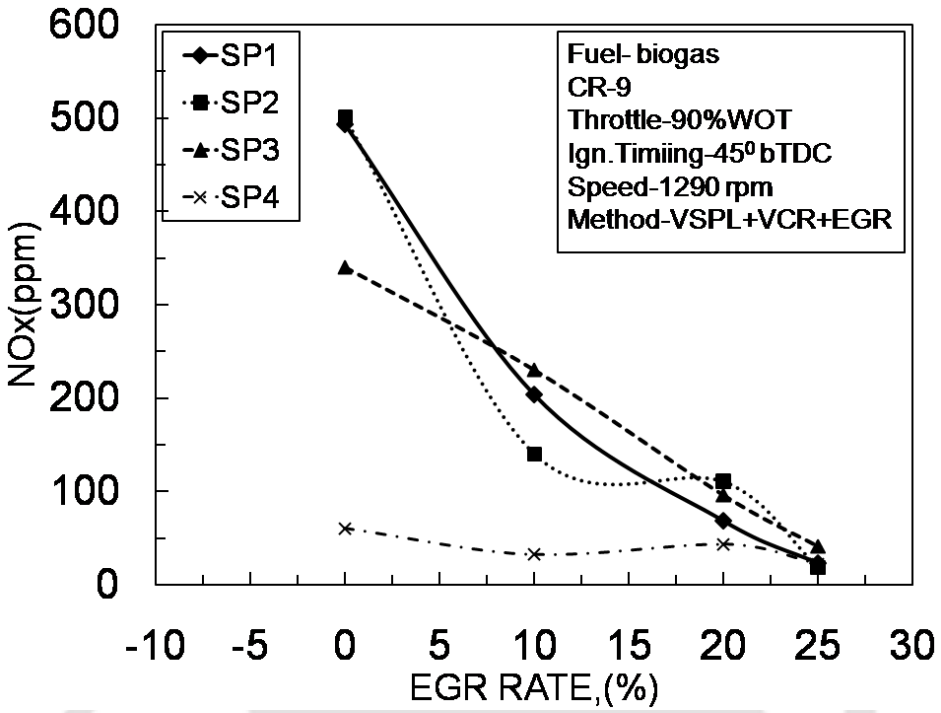

Fig.7.50 NO_x variation under effect of EGR for VCR combined with VSPL

Green house gas CO_2 emission with EGR rate for various SP location is plotted in Fig.7.49(c) where the CO_2 emission is higher in case of SP2, SP3 and SP4 in comparison to that of SP1. This is a positive implication of variable spark plug location.

The important effect of EGR rate on exhaust gas emission is NO_x control. The NO_x variation with EGR rate is as plotted in Fig.7.50. Here the NO_x keeps on reducing with greater slope for all the curves formed by spark location at SP1, SP2, SP3 and SP4. In terms of magnitude the maximum NO_x is released during the SP2 location while engine working at CR 9 and speed 1290 rpm. This is obvious as seen in the combustion analysis; if the cylinder peak pressure is higher at SP2 represent higher NHRR.

So the mean gas temperature will definitely be higher at same location. The temperature dependent exhaust emission component called as NO_x will be recorded higher. If the EGR rate is increased to 10 %, then there is decrement in NO_x by 58.82 %, 72 %, 32.35 % and 47 % for SP1, SP2, SP3 and SP4 with respect to EGR 0 emissions. Further rise in EGR rate to 20 % , reduces the emissions by 86 %, 78 %, 72 % and 28 % for SP1, SP2, SP3 and SP4 with respect to EGR 0 emissions. If the EGR 25 is mixed with intake charge then the same are 95 %, 96 %, 88 % and 63 % for SP1, SP2, SP3 and SP4 with respect to EGR 0 emissions.

7.4.2 LPG fuel combustion with EGR, varying CR and SPL coalesce.

The effect of EGR in LPG fueled engine becomes important from the point of view of maximum performance and lowest emission from the engine. Although, both the terms used

here are not possible unless until there are certain engine structural modifications to improve performance and most suitable adulteration with fuel for reducing the emissions.

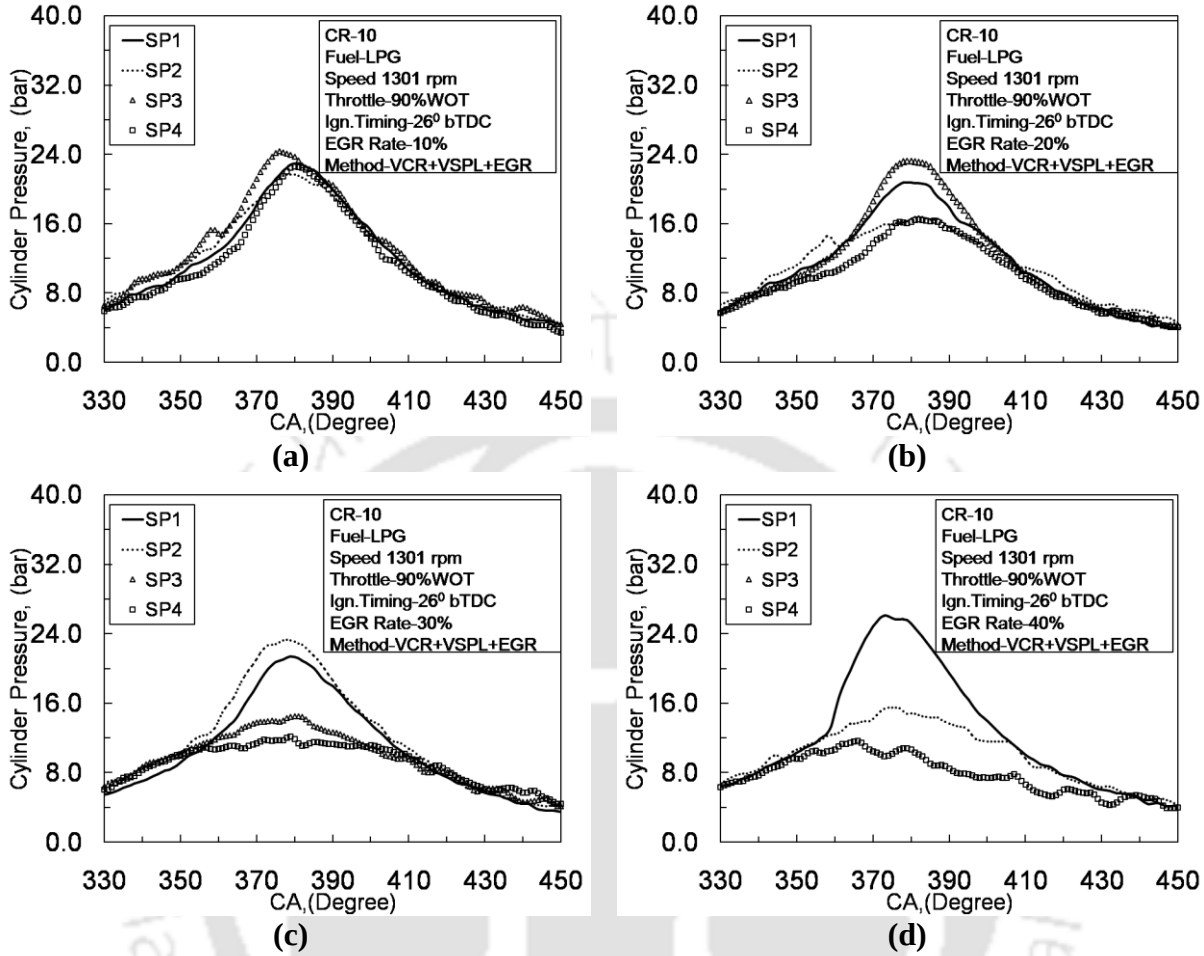

Fig.7.51 Cylinder pressure variation with CA for different spark location at CR 10 added with (a) EGR 10; (b) EGR 20; (c) EGR 30 and (d) EGR 40

During discussion of LPG fuel in SI engine, the performance could definitely be improved if compression ratio and spark plug location are optimized. However, with adulteration of EGR for reducing emission, there becomes the need to optimize the CR and spark plug location again. The discussion in this regards is presented as follows

7.4.2.1 Combustion Analysis

The combustion analysis of LPG fueled engine under effect of novel VCR accompanied with VSPL is presented in presence of EGR rate. The cylinder pressure variation with CA for different EGR rate is as plotted in Fig. 7.51 (a-d). From the figure, the maximum pressure 24.351 bar is recorded at CR10.48 with SP3 while EGR rate is 10 %. The peak pressure at other locations are 22.946 bar, 21.67 bar and 22.58 bar respectively at CR 10 with SP1, CR 10.18 associated with SP2 and CR 11.02 accompanied with SP4. However, there is decrement of 30.78 %, 35.49 %, 28.71 % and 1.61 % when EGR is increased from 0 to 10 %. As the fuel gets diluted with exhaust gas, the heating value gets affected causing change of spark location when working on CR 10 at speed 1301 rpm. This change of spark location is decreased to 5 mm which was 10 mm for EGR 0 as discussed before. If the EGR rate is

increased further then SP3 is found optimum showing peak pressure 23.239 bar. However, the decrement of 4.57 % with respect to EGR 10 is noted for SP3 location. Similar trend is followed for other SP locations as well. Further for EGR rate 30 % and 40 %, the peak pressure 23.214 bar at SP2 and 26.016 bar at SP1 location has been recorded respectively. EGR 40 is heavy for the engine to produce power from the constant air-fuel supply. This causes non uniform combustion as well as misfiring during working at CR10.

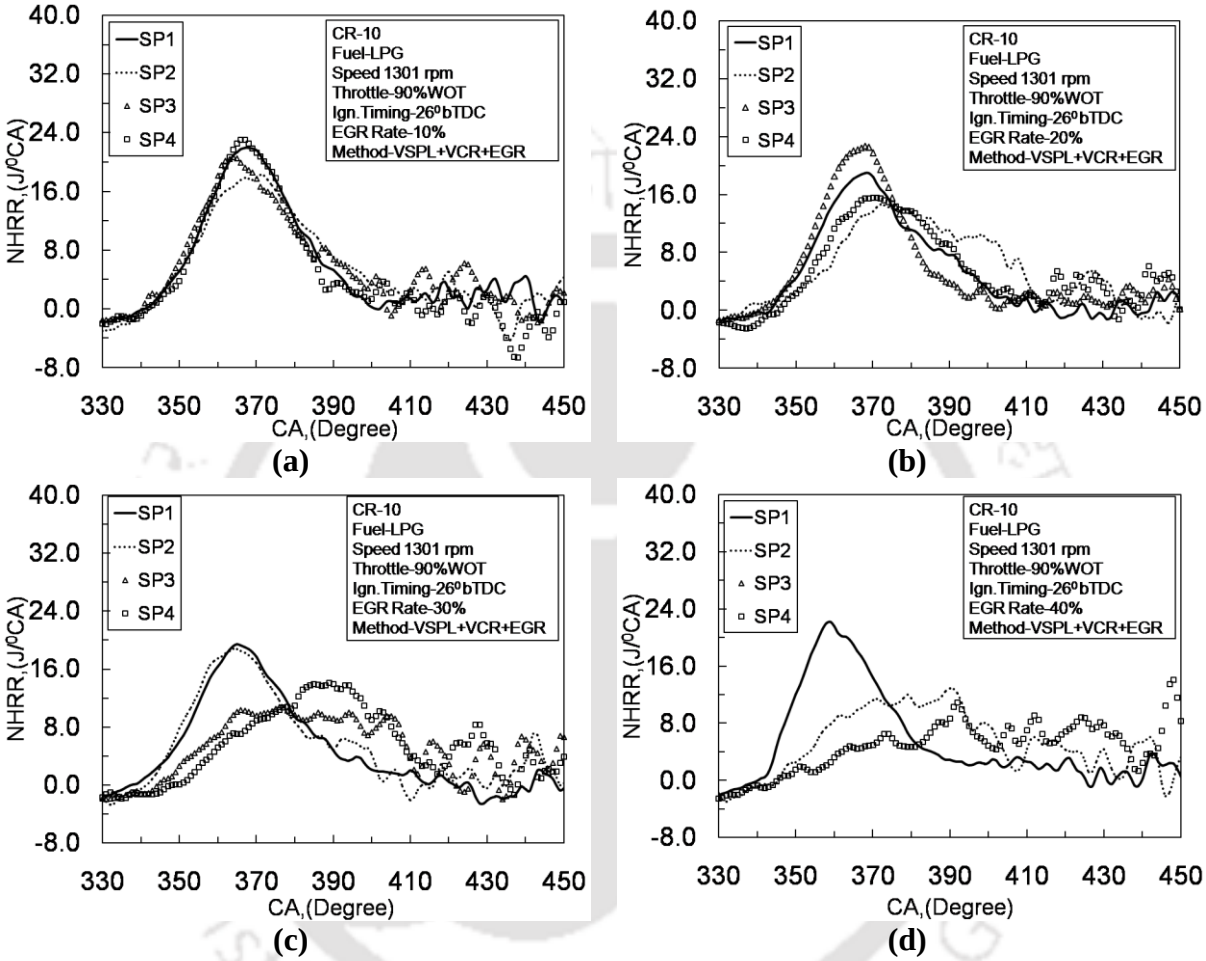

Fig.7.52 NHRR variation with CA for different spark location at CR10 added with (a) EGR 10; (b) EGR 20; (c) EGR 30 and (d) EGR 40.

The NHRR variation with CA for LPG fueled engine when working at CR10 and speed 1301 rpm is as plotted in Fig.7.52 (a-d). The maximum NHRR reported here are for SP4, SP3, SP3, SP2 and SP1 with EGR 0, EGR 10, EGR 20, EGR 30 and EGR 40 respectively. The decrement is unavoidable when EGR rate increased from 0% to 10%. The maximum NHRR at SP4 is 30.54 J/ ^{0} CA during EGR 0 shows decrement of 32.31 % for SP1, 41.61 % for SP2, 28.16 % for SP3 and 24.44 % at SP4 for higher EGR rate 10 %. The minimum decrement reported at SP4 showing peak NHRR at 366 ^{0} CA causing delayed combustion. So even though there is peak NHRR at SP4, the power output will be minimum. On the other side SP3 is the location where decrement is lower with respect to EGR 0. So this location is most optimum for maximum power and hence efficiency. On the similar track the spark location could be optimized for EGR 20, EGR 30 and EGR 40.

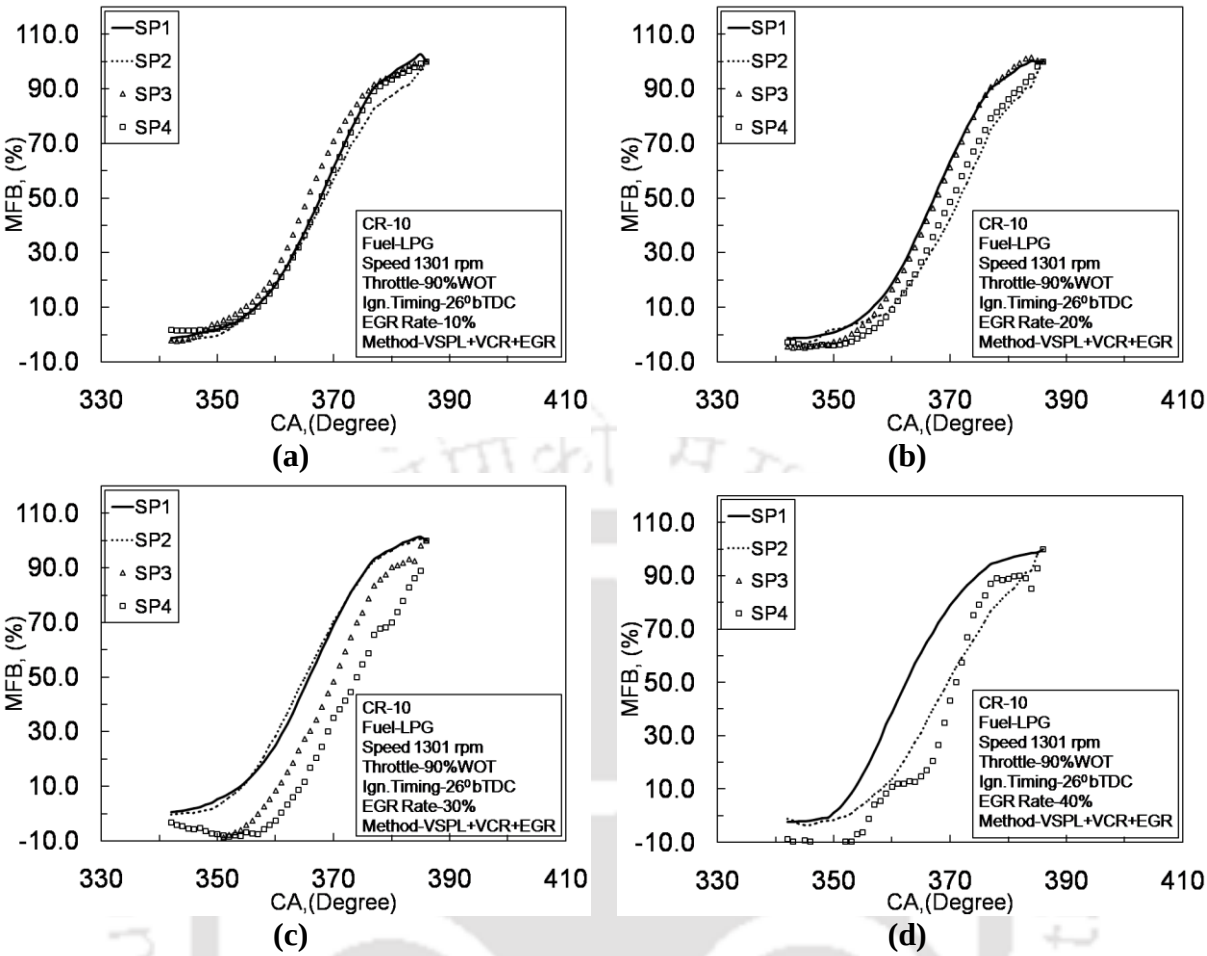

Fig.7.53 Percent MFB variation with CA for different spark location at CR10 added with (a) EGR 10; (b) EGR 20; (c) EGR 30 and (d) EGR 40.

The percent MFB variation with CA for spark location 0 mm (SP1), 2 mm (SP2),5 mm (SP3) and 10 mm (SP4) is plotted in Fig. 7.53 (a-d) for different EGR rate (0 - 40) %. For the spark timing of 26^0 bTDC, the percent MFB shows variation with change in spark location for a particular EGR rate.

Table 7.7 Percent MFB variation with CA for different spark location at CR10 using LPG fuel.

EGR RATE	SP1			SP2			SP3			SP4		
	10% MFB	90% MFB	MFB@ TDC	10% MFB	90% MFB	MFB@ TDC	10% MFB	90% MFB	MFB@ TDC	10% MFB	90% MFB	MFB@ TDC
0	349	372	46.93	360	382	9.58	348	375	55.09	**350**	**366**	**71.80**
10	356	377	18.38	357	382	18.96	**356**	**377**	**23.03**	357	378	17.76
20	357	377	16.53	360	383	10.18	**358**	**377**	**18.78**	360	382	9.14
30	354	376	25.01	**354**	**376**	**28.57**	361	380	8.45	365	385	0
40	**354**	**375**	**38.89**	358	383	13.89	-	-	-	360	382	10.79

From Table 7.7, the crank angle at which the 10% and 90% percent MFB observed are tabulated based on the Fig.7.53 (a-d). Analyzing the magnitudes in each block, it is quite easier to understand the optimum spark location for various EGR rates attaining maximum efficiency during working at CR10. According to this, the SP4, SP3, SP3, SP2 and SP1 spark locations are considered to be the optimum spark location based on two criteria.

The first criteria is the period in terms of degree CA between start of combustion (10 % MFB) to the end of it (90 % MFB) called as combustion duration.

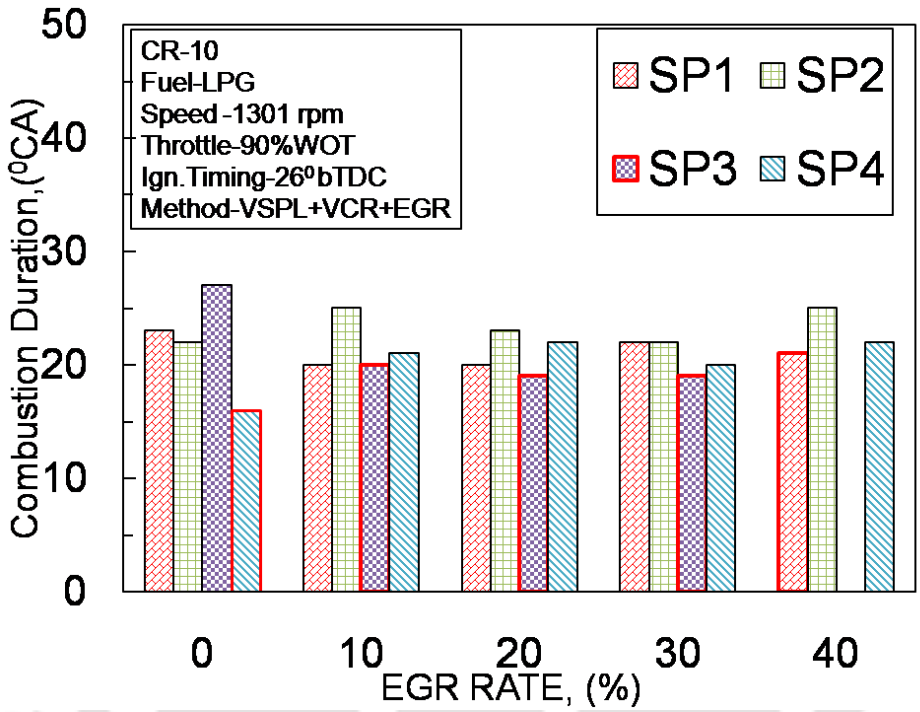

Fig.7.54 Combustion duration variation with EGR rate for different spark location at CR10

The second criteria will be the mass of fuel burnt at TDC. The percent MFB at TDC is found reducing with increase in EGR rate. This is for the reason of dilution of EGR with fuel-air mixture and reduces the flame velocity and in turn reduces the percent mass fraction burned.

The mean gas temperature (MGT) in the presence of EGR for LPG fueled engine is drawn in Fig. 7.55 (a-d) for various spark locations keeping CR10 fixed for the analysis. The peak temperature recorded is 1070.83^{0}C at 370 ^{0} CA for EGR 0 when working at SP 4 location inside combustion chamber. The same are 987.3 ^{0} C at 387 ^{0} CA for SP3, 945.79 ^{0} C at 396 ^{0} CA for SP3, 848.49 ^{0} C at 393 ^{0} CA for SP2 and 940.84 ^{0} C at 380 ^{0} CA for SP1 respectively when working at EGR 10, EGR 20, EGR 30 and EGR 40. Higher MGT is the outcome of homogeneous combustion at the prevailing conditions of speed, load and fuel consumption.

7.4.2.2 Performance Analysis

The Fig.7.56 and Fig.7.57 shows variation of BTE and BSFC for CR10, 9 and 8 with variable parameters such as EGR Rate and VSP location. The variation of BTE for all SP location shows the decrement obtaining maximum BTE at EGR 0 and lowest at EGR 40. This could be happened due to decrement of heating value of intake charge with increase of EGR rate

also reduction in mass of fresh air required for combustion causing the incomplete combustion inside cylinder and lowers the power produced intern decrement in efficiency.

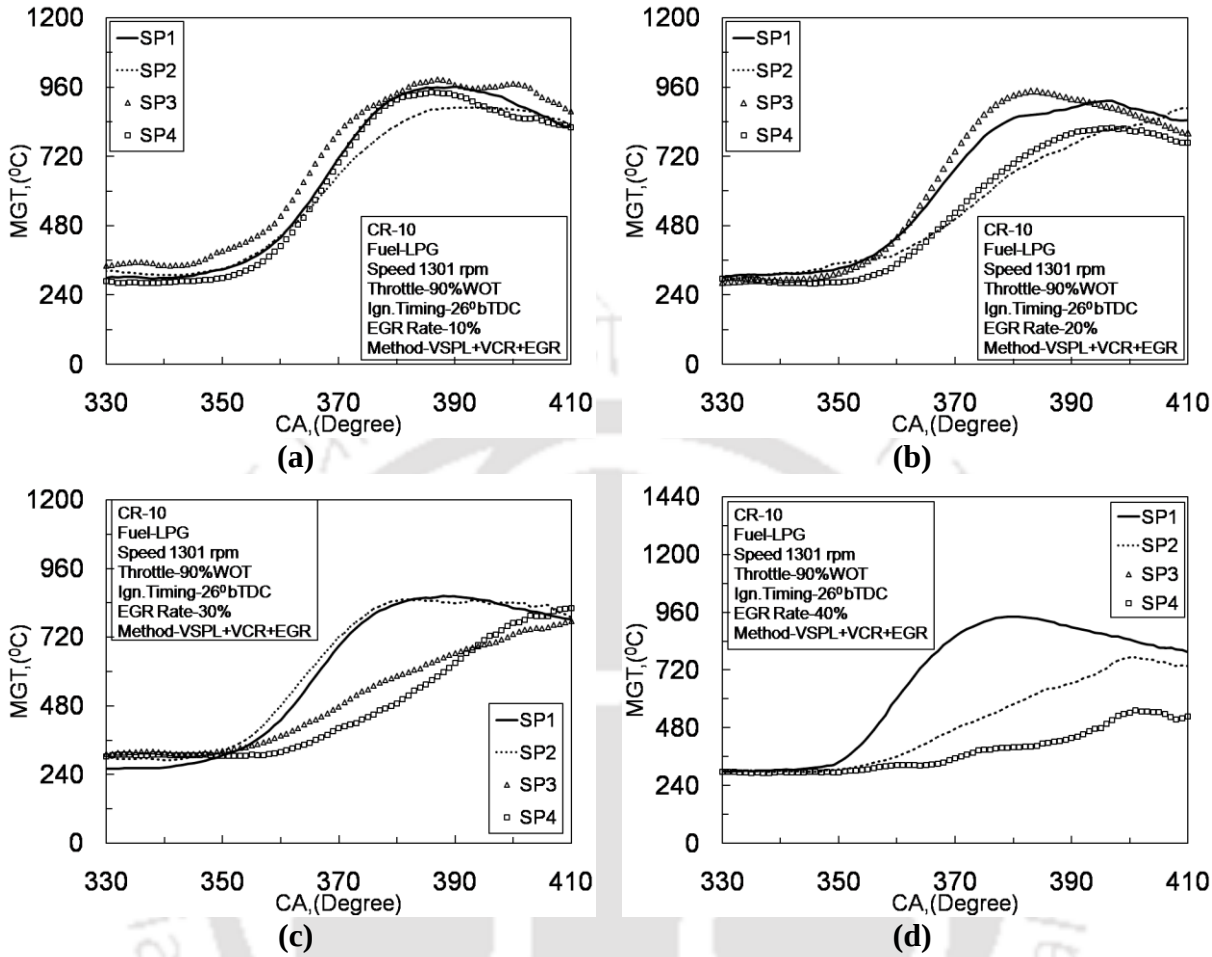

Fig.7.55 Mean Gas temperature variation with CA for different spark location at CR10 added with (a) EGR 10; (b) EGR 20; (c) EGR 30 and (d) EGR 40.

Moreover it is seen that for SP4 location shows maximum efficiency 27.83 % for SP4. The original spark location (SP1) at EGR 0 shows 24.9 % which is 10.53 % lower than that attained with shift of spark plug at new location 10 mm (SP4) inside combustion chamber. If EGR rate is increased to 10 %, then SP3 is showing maximum efficiency of 26.22 % which is still 5.03 % higher than that attained by engine with original SP location at EGR 0. Similarly if EGR rate increased to 20 %, then SP3 shows 23.099 % efficiency which is lower by 7.26 % with respect to BTE at EGR 0 with SP1 location. However efficiency is 12.77 % higher when EGR 10 is supplied to engine at SP1 location. On the similar track, there is SP2 and SP1 recorded higher efficiency with EGR 30 and EGR 40 respectively. If compression ratio is changed to CR 9 then SP4, SP3, SP3, SP1 and SP1 are the optimum locations attaining maximum efficiency while working at EGR 0, EGR 10, EGR 20, EGR 30 and EGR 40 respectively. With the decrease in compression ratio engine volume increased so the spark location needs to be optimized with respect to original spark location. Further decrement in CR from 9 to 8, the SP2 is found optimum for all EGR rates as shown in Fig. 7.56(c)

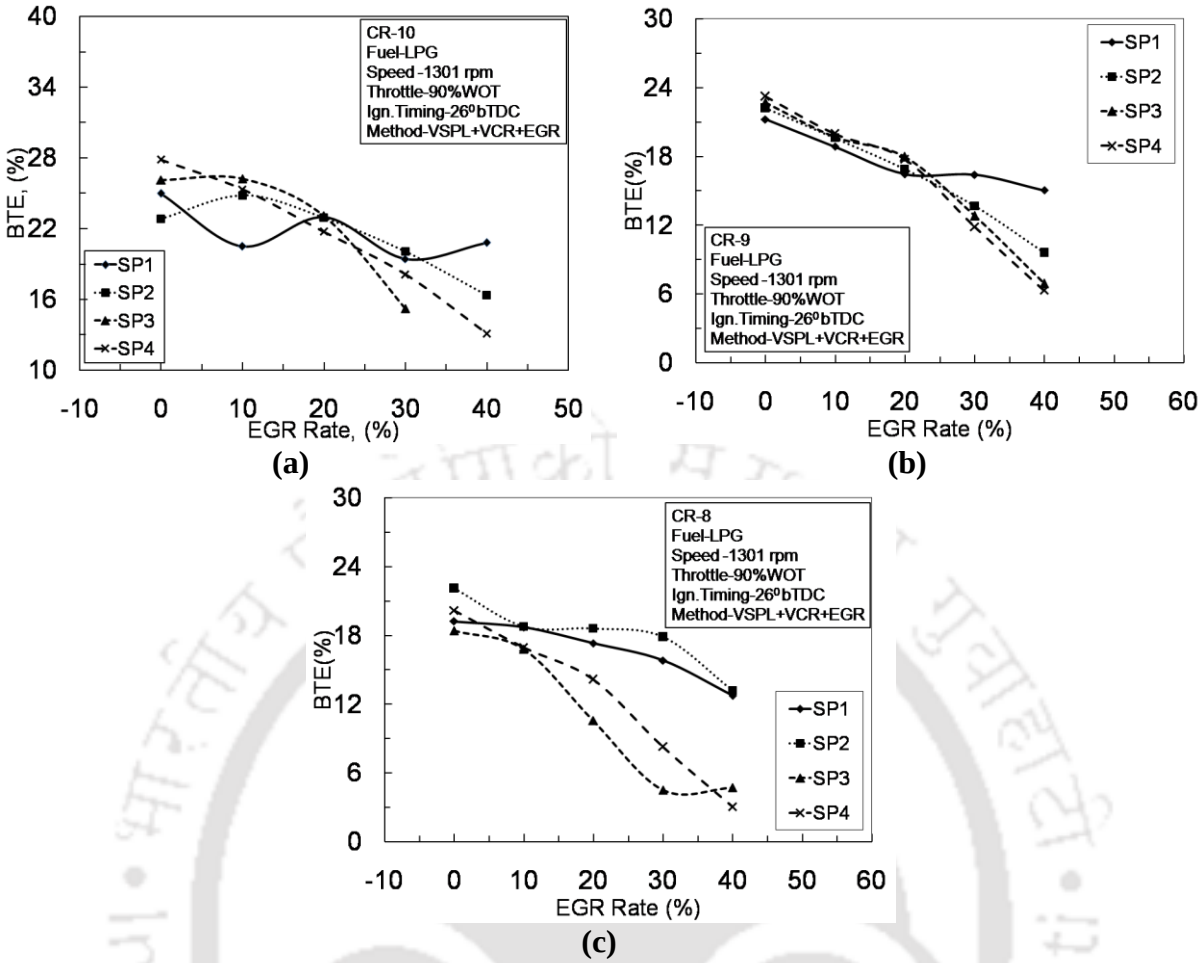

Fig. 7.56 BTE variation with EGR Rate for different spark location at (a) CR 10; (b) CR 9 and (c) CR 8

The Fig.7.57 (a-c) represent the fuel consumption per unit brake power in terms of BSFC for varying CR, SP location and EGR rate. At CR10 and running at speed 1301 rpm, the spark locations SP4, SP3, SP3, SP2 and SP1 is found optimum having minimum fuel consumption for same unit of brake power using EGR rate 0, 10, 20, 30 and 40 % respectively.

If CR 9 is used for LPG fuel engine, then fuel consumption is increased due to decrement of CR. However engine can run optimally when spark plug is maintained at SP4, SP3, SP3, SP1 and SP1 for EGR 0, EGR 10, EGR 20, EGR 30 and EGR 40 respectively. Further decrement of CR reduces the efficiency of the engine with respect to that of CR 10 or CR 9. However sometimes due to constraints of engine, CR cannot be increased above 8. In this situation, with optimizing spark plug location, the performance could be improved as shown in Fig.7.56 (c). With application of EGR rate (0-40%), the corresponding optimized SP locations are found to be SP2 for all EGR rates.

7.4.2.3 Emission Analysis

The important issue with use of high hydrocarbon fuels such as LPG is of exhaust gas emissions. There is clear influence of the parameters such as compression ratio, spark location and variable EGR rate.

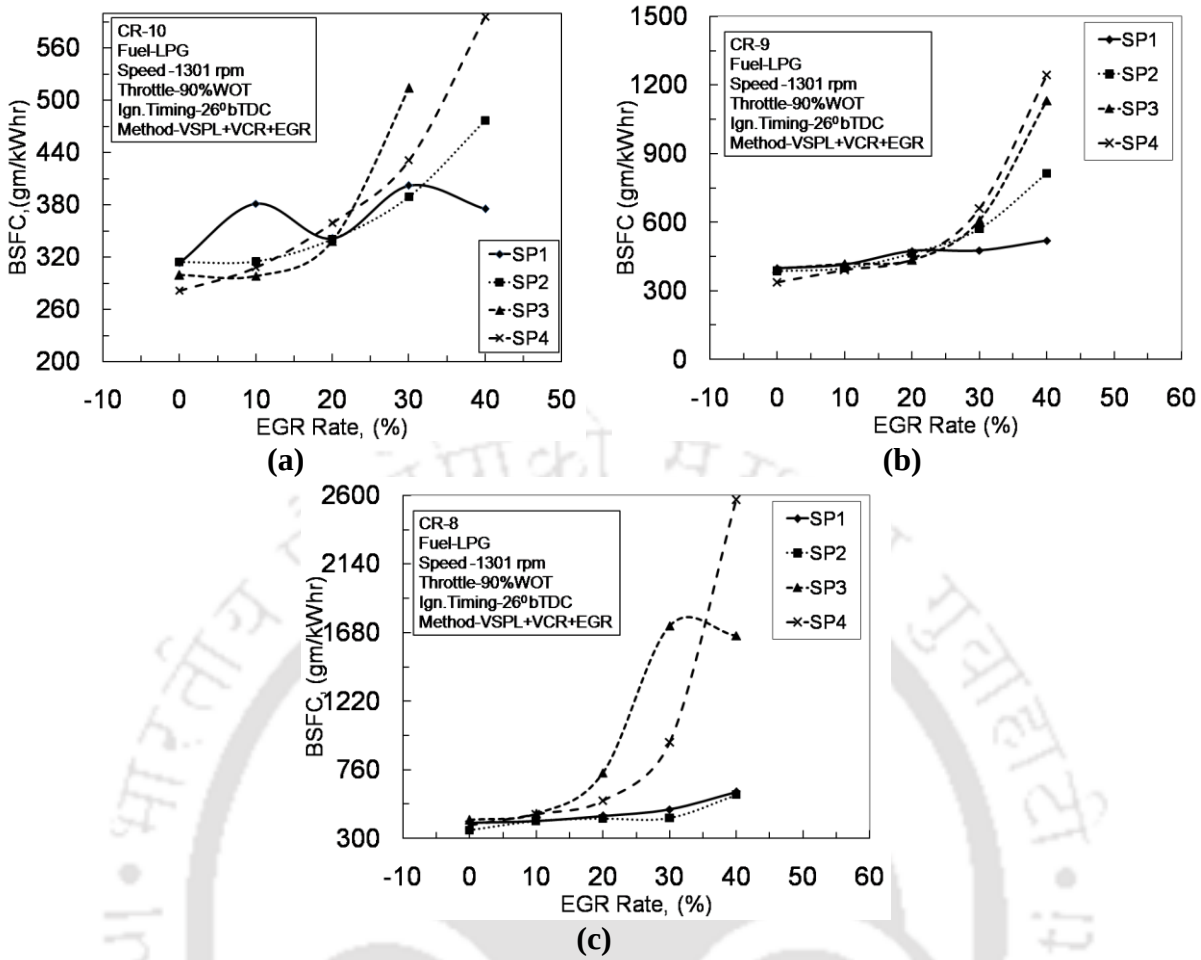

Fig.7.57 BSFC variation with EGR Rate for different spark location at (a) CR 10; (b) CR 9 and (c) CR 8

The CO emission is plotted with EGR rate for different spark locations as shown in Fig. 7.58 (a) while engine operates at CR 10 and maintained at speed 1301 rpm. It is seen that CO emission keeps on rising with increase in EGR rate.

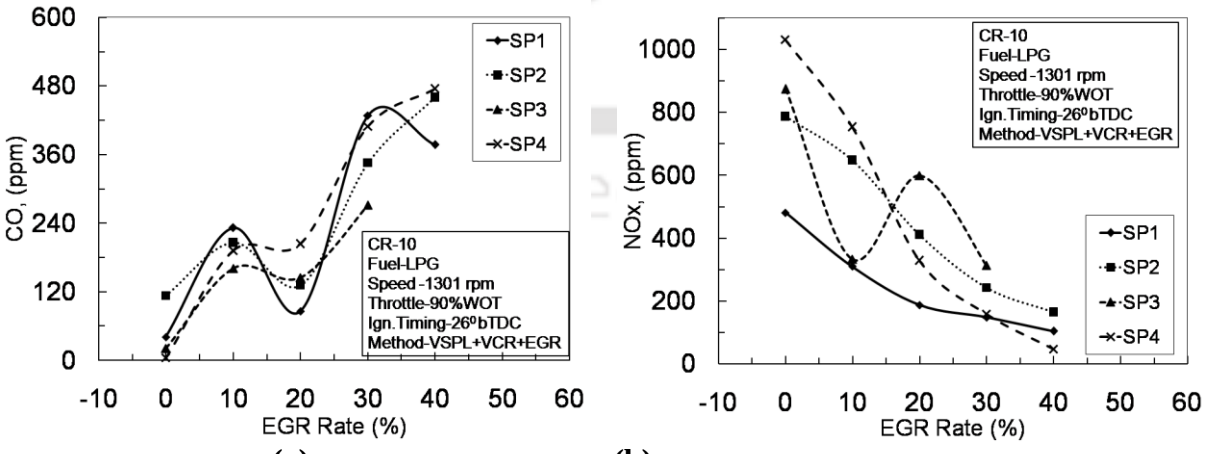

Fig.7.58 (a) CO emission variation with EGR Rate for different spark locations ; (b) NO_x emission variation with EGR Rate for different spark locations.

As seen from figure, at EGR 0, the maximum CO is at SP2 for EGR 0 and minimum at SP4. Likewise, SP1 and SP3 show maximum and minimum CO respectively at EGR 10. Further rise in EGR rate shows SP1 and SP3 while at EGR 40, it is SP4 and SP1 to be maximum and minimum CO emission. At optimum spark locations identified from combustion and performance analysis, the CO emission is found lesser compared to the other SP locations.

Table 7.8 (a) Summary of performance of NVCR engine with LPG and raw biogas

Method	Test	Performance parameter	LPG	Raw biogas
Conventional VCR	CR 8,9 and 10 over speed range 1290-1740 rpm with ignition timing from 24^0 bTDC-47^0 bTDC	Ignition timing, ^{0}bTDC	26	45^0
		Optimum CR	10	10
		BTE,%	26.79	25.86
		BSFC, gm/kWhr	299	968
		Pressure, bar	39 @365^0CA	25.2@371^0CA
		NOx, ppm	490	60-512
Conventional VCR+EGR	CR 8,9 and 10 over speed range 1290-1740 rpm with optimum ignition timing and EGR rate 10 to 40% in case of LPG and 10-25%in case of raw biogas	Ignition timing, ^{0}bTDC	26^0	45^0
		Optimum CR	10	10
		Optimum EGR	EGR10	EGR10
		BTE,%	25.05	19.5
		BSFC, gm/kWhr	307.16	1300
		Pressure, bar	32.98 @370^0CA	17.5 @380^0CA
		NOx, ppm	99-201	110
Novel VSPL	Maintaining fixed CR8, 9 and 10 combining conventional VCR mechanism and novel VCR mechanism. The spark location 2mm ,5mm and 10mm inside chamber	Optimum CR	10	10
		Optimum SP location,mm	10(SP4)	2(SP2)
		BTE,%	27.8	26.4
		BSFC, gm/kWhr	290	832
		Pressure, bar	34 @370^0CA	29 @373^0CA
		%MFB@TDC	20	54.94
		NOx, ppm	--	900

NO_x is a targeted component which needs to be controlled by application of EGR rate from 0-40 % to the engine. In doing so, there is direct effect on the performance parameters such as thermal efficiency and fuel efficiency. However with implementation of performance improvement techniques such as variable compression ratio and variable spark plug location, the decrement in performance can be controlled to certain extent. In this regards, the variation of NO_x with EGR rate for different spark location is as plotted in Fig. 7.58 (b). With application of EGR 10, there is decrement of 35.55 %, 17.66 %, 62 % and 26 % for SP1, SP2, SP3 and SP4 respectively. With further increase in EGR rate shows decrement of 61.12 %, 47.78 %, 31.46 % and 68.05 % for SP1, SP2, SP3 and SP4 respectively. At EGR 20, the nature of EGR 20 is showing higher NO_x than that at EGR 10. This may occur due to

measurement errors and uncertainty of the measuring instruments. With further increment in EGR rate to 30%, there is decrement of 69.23 %, 69.25 %, 64.18 % and 85.43 % has been recorded. Finally at EGR 40, the decrement of 70.89 %, 80.30 %, 95.53 % is found for SP2, SP1 and SP4 respectively.

7.5 Comparative performance analysis of gaseous fuels under different methods of operation.

The fuels used in this study are from far poor heating value to very good heating value category. If the performance of both the fuels are compared with same operating conditions and method as described in chapter 6 and sections in this chapter 7.1,7.2,7.3,7.4, then the properties of the fuels are the deciding parameter for best performance in the engine.

Table 7.8 (b) Summary of performance of NVCR engines with LPG and raw biogas

Method	Test	Performance parameter	LPG	Raw biogas
Novel VCR+VSPL	Maintain fixed CR say 10. Using novel VCR mechanism and protruding secondary piston 2mm, 5mm and 10mm causing increase in CR above 10 as well attains VSPL	Optimum CR	10.48	10.48
		Optimum SP location,mm	5	5
		BTE,%	28.358	27.04
		BSFC, gm/kWhr	325	1230
		Pressure, bar	35 @363^{0}CA	31 @367^{0}CA
		%MFB@TDC	69	55.4
		NOx,ppm	1212	873
VCR+VSPL +EGR	Maintain fixed CR say 10. Using novel VCR mechanism and protruding secondary piston 2mm, 5mm and 10mm VSPL. Add EGR from 10-40% for LPG and 10-25% for raw biogas.	Optimum CR EGR10,20	10	10
		Optimum SP location EGR10,20	5(SP3)	5(SP3)
		Optimum EGR rate,%	10	10
		BTE,%	26.22	23.556
		BSFC,gm/kW hr	290	1480
		Pressure,bar	24 .351@373^{0}CA	15.74@374^{0}CA
		%MFB@TDC	23.03	29
		NOx,ppm	360	350

In order to compare the performance, combustion and emission , it could be possible to attain best operating condition under a particular situation while engine is in operation.

7.6 SUMMARY

The novel variable compression ratio mechanism is successfully installed on the conventional SI engine with modification in the engine head and then used for the renewable as well as non-renewable gaseous fuels. These studies help to overcome the structural limitations of an

SI engine where compression ratio and spark plug locations are fixed. Initially experiments are carried out for the effect of only variable spark plug location on the performance of the engine using 100% raw biogas and LPG fuels. The spark location SP2 is found optimum for raw biogas and SP4 for LPG fuel. Investigations are further extended for various CRs and spark plug locations. Here the results are interesting where the advantage of higher compression ratio as well as optimum spark location could be identified for the fuels under study. Following this, it is noted that CR10.48 is optimum for raw biogas as well as for LPG fuel with corresponding spark plug location. But, the concept of variation of compression ratio and spark plug location could not able to control the exhaust emissions from the engine. In such situation, if the EGR rate is introduced with intake charge, then the optimum engine performance with novel VCR and VSPL can be further altered. Based on the study, it is found that the percentage EGR rate is a matter of importance to set the VCR mechanism. The optimum conditions for raw bio gas are noted to be CR 10.48 with SP3 for EGR 10 and EGR 20. For EGR 25 with raw biogas, optimum condition is CR 10 with SP1. Similarly for the LPG fuel, optimum conditions are CR 10.48 with SP3, for EGR 10 and EGR 20. Other alternatives for LPG fuels are CR 10.18 with SP 2 for EGR 30 and CR 10 with SP1 for EGR 40 where the performance of the engine is highest in terms of efficiency, fuel consumption. This study will definitely help to design the SI engine with the novel VCR mechanism which can accommodate different octane rating fuels.

CHAPTER 8

Computational Analysis of Combustion Parameters

OVERVIEW

A single-zone zero-dimensional model for hydrocarbon fuel based on Wiebe heat release function has been implemented in Simulink to test the performance of spark ignition engine. Annand's model for convective heat losses is taken for modelling of engine cycle. The Simulink results are validated with experimental results from literature. Two dimensional Computational Fluid Dynamic model using FLUENT of experimental test engine was made for axi-symmetric flow in the combustion chamber. It is a setup for closed cycle simulation that can predict pressure, mass burn fraction. CFD Simulation was carried out on an experimental engine set up at rated rpm of engine (1.8 HP @3600 rpm). The CFD results will be tested with results of Simulink model for this engine configuration.

8.1 SIMULINK MODEL DEVELOPMENT

A single-zone thermodynamic model is chosen for computer simulation for a four stroke SI engine. The model is divided into parts (subsystems) with different processes (compression, combustion, expansion, exhaust and intake) during 720º crank angle (CA) of one-thermodynamic cycle in the following sequence: intake valve closing (IVC), spark timing, end of combustion (EOC), exhaust valve opening (EVO), exhaust process (from EVO to EVC/IVO) and intake process (from IVO to IVC).

During the entire cycle of combustion process, the gases in cylinder are assumed to form a homogeneous mixture. Spatial homogeneity of pressure and temperature for the whole cylinder are considered for each zone. From IVC to EOC, the specific heats are calculated by considering only fresh gases to be present in the mixture while the properties from EOC to EVC are calculated considering only burned gases. The gaseous mixture follows ideal gas law. It is assumed that exhaust valve closes at the instant the intake valve opens. Heat transfer is considered to happen only during the closed cycle operation i.e. IVC to EVO. The exhaust and intake process are assumed to be isentropic through a converging-diverging nozzle. The Simulink model has following computation methodologies derived for determination of various parameters.

8.1.1 Modelling of heat release during combustion

If we are using single-zone thermodynamic model then we can use wiebe function for calculating heat release during combustion.

Heat release during combustion: The experimental investigation of combustion process in engines is very difficult. So, the combustion investigation in engines has been carried out by analyzing cylinder pressure data in single-zone thermodynamic model using Wiebe function for calculating mass fraction burned (Perini et al., 2010). The heat release rate from combustion is obtained from Eq. 8.1. A functional form (Eq. 8.2) is often used to represent the mass fraction burned versus crank angle curve (Gunter et al.,2006;Sarkar,1990).

$$\frac{dQ_{ch}}{d\theta} = \frac{\gamma}{\gamma-1} p \frac{dV}{d\theta} + \frac{1}{\gamma-1} V \frac{dP}{d\theta} + \frac{dQ_{ht}}{d\theta} \quad \text{(Eq.8.1)}$$

$$\frac{dx_b}{d\theta} = \frac{1}{Q_{\max}} \frac{dQ_{ch}}{d\theta} \text{ where fuel mass burned fraction } x_b = \frac{m_b}{m} \quad \text{(Eq.8.2)}$$

A functional form to represent the mass fraction burned is the Wiebe function

$$x_b = 1 - \exp\left[-a \left(\frac{a - a_0}{\Delta\theta} \right)^{m+1} \right] \quad \text{(Eq.8.3)}$$

If δQ_{ch} is the heat released from combustion, then the following relation;

$$\frac{dQ_{ch}}{d\theta} = \begin{cases} 0, & \theta_{ivc} < \theta \le \theta_0 \text{ and } \theta > \theta_{eoc} \\ Q_{\max} \dfrac{dx_b}{d\theta}, & \text{for } \theta_0 < \theta \le \theta_{eoc} \end{cases} \quad \text{(Eq.8.4)}$$

Here, $\frac{dx_b}{d\theta}$ is the fuel mass burn rate which can be calculated from Wiebe function (Eq. 8.4). So the equation of mass burn fraction takes the following form;

$$\frac{dx_b}{d\theta} = \frac{a(m+1)}{\Delta\theta} \left(\frac{\theta - \theta_0}{\Delta\theta} \right)^m \exp\left[-a \left(\frac{\theta - \theta_0}{\Delta\theta} \right)^{m+1} \right] \quad \text{(Eq.8.5)}$$

where, ' a ' is combustion completeness factor and tells about the efficiency of combustion; It depends upon the intensity of charge motion, engine design (Sarkar, 1990) and falls in the range of $2 \le a \le 6$, $\Delta\theta$ is the combustion duration and m is the form factor that affects the shape of mass burned profile. These parameters determine the shape of Wiebe function and hence its accuracy to predict the actual heat release during combustion(Eq.8.5). As per Stone,1999, mass fraction burned curves were plotted for range $2 \le a \le 10$ as well as $0 \le m \le 3$ represent the change of shape of MFB and ultimately the effect on rate of combustion.

Combustion duration: The total mass burnt during combustion process and the heat release are independent of the combustion duration ($\Delta\theta$). However, if same heat is released in small combustion duration, the rate of heat release will be more and pressure peak would be higher as compared to the large combustion duration (Jerzembecka et al., 2009).

$$\Delta\theta(r,N,\varphi,\theta_0) = f_1(r)\, f_2(N)\, f_3(\varphi)\, f_4(\theta_0)\Delta\theta_1$$

$$f_1(r) = 3.2989 - 3.3612\left(\frac{r}{r_1}\right) + 1.0800\left(\frac{r}{r_1}\right)^2;\quad f_2(N) = 0.1222 + 0.9717\left(\frac{N}{N_1}\right) + 5.0510\times10^{-2}\left(\frac{N}{N_1}\right)^2 \qquad \text{(Eq.8.6)}$$

$$f_3(\varphi) = 4.3111 - 5.6393\left(\frac{\varphi}{\varphi_1}\right) + 2.3040\left(\frac{\varphi}{\varphi_1}\right)^2;\quad f_4(\theta_0) = 1.0685 - 0.2902\left(\frac{\theta_0}{\theta_{01}}\right) + 0.2545\left(\frac{\theta_0}{\theta_{01}}\right)^2$$

Thus, the combustion duration at any operating conditions for a particular engine can be estimated from Eq.8.6.

Table 8.1 The SIMULINK input data

Sr No	**Input data**	**Parameter**	**Only Simulink Validation** (Ganesan,1996)	**Only CFD Validation**	**Combined Simulink and CFD Validation**
01	Geometric parameters	Bore	79.4	52	52
		Stroke	111.2	46	46
		Connecting rod length	233.4	81	81
		Compression ratio	7.4	4.8	4.8
02	Intake conditions	Intake pressure	1 bar	1 bar	1 bar
		Intake temperature	300 K	300 K	300 K
03	Charge properties	Air/fuel ratio	1.1	1.1	1.1
		Residual gas fraction	0.05	0.05	0.05
04	Fuel data	Molecular formula	Gasoline- C_8H_{18}	Gasoline- C_8H_{18}	Gasoline- C_8H_{18}
		Lower heating value	Gasoline-44 MJ	Gasoline-44 MJ	Gasoline-44 MJ
05	Operating conditions	Engine speed	4000 rpm	3600	1000,2000,3000
		Ignition timing	Gasoline:25^0bT DC	Gasoline:20^0 bTDC	Gasoline:20^0 bTDC
07	Valve timings	IVC	-160	-160	-160
		EVO	160	160	160
		EVC/IVO	360	360	360
08	Rated Power		5 HP	1.8 HP	1.8 HP

Convective heat transfer rate: Using the Annand's correlation (Heywood,1988; Perini et al., 2010) for convective heat transfer coefficient is obtained (Eq.8.7).

$$\frac{h_c B}{k} = a\left(\frac{\rho \bar{S}_p B}{\mu}\right)^b ;\ b = 0.7;\ \bar{S}_p = \frac{2aN}{60}\ (Mean\ Piston\ Speed) \qquad \text{(Eq.8.7)}$$

$$\mu = \frac{\mu_{air}}{1+0.027\varphi} = \frac{3.3\times10^{-7}\times T^{0.7}}{1+0.027\varphi};\ k = \frac{9\gamma-5}{4}\mu Cv$$

Here value of a changes with intensity of charge motion and engine design and falls in the range $0.35 \le a \le 0.8$.

8.1.2 Single-zone zero-dimensional thermodynamic model

The cylinder pressure as a variation of crank angle($P-\theta$), Volume variation with crank angle($V-\theta$) and temperature variation with crank angle($T-\theta$) are the possible outcome of this model.

Volume: Using the geometry parameters of the engines, the cylinder volume at any crank angle by following relation;

$$V(\theta) = V_c + \left(\frac{\pi B^2}{4}\right)\left[1+a(1-\cos\theta)-\sqrt{l^2-(a\sin\theta)^2}\right] \qquad \text{(Eq.8.8)}$$

Since the volume is known function of crank angle from Eq.8.8, the cylinder pressure can be evaluated. However the mathematical model or differential equation of pressure would be different during closed cycle and gas exchange process.

A- For the closed cycle (IVC to EVO)

The first law of thermodynamics as applied to closed volume of combustion chamber is

$$dQ_{ch} = dU_s + \delta Q_{ht} + \delta W \qquad \text{(Eq.8.9)}$$

$$\frac{dQ_{ch}}{d\theta} = mCv\frac{dT}{d\theta} + \frac{dQ_{ht}}{d\theta} + P\frac{dV}{d\theta} \qquad \text{(Eq.8.10)}$$

The thermodynamic properties are known functions of temperature which are calculated as

$$Cp = \frac{1}{m_{RP}}\sum\nolimits_i n_i Cp_i \qquad \text{(Eq. 8.11)}$$

$$M_b = \frac{m_{RP}}{n_b} \text{ and } M_u = \frac{m_{RP}}{n_u} \qquad \text{(Eq.8.12)}$$

From Eq.8.10

$$\frac{dT}{d\theta} = \frac{1}{mC_v(T)}\left[\frac{dQ_{ch}}{d\theta} - \frac{dQ_{ht}}{d\theta} - P\frac{dV}{d\theta}\right] \quad \text{(Eq 8.13)}$$

This is a non linear differential equation in terms of temperature. Using ideal gas law for closed cycle operation

$$PV = m_0 RT \quad \text{(Eq.8.14)}$$

Differentiating the above equation

$$\frac{dP}{d\theta} = \frac{1}{V}\left[m_0 R\frac{dT}{d\theta} - P\frac{dV}{d\theta}\right] \quad \text{(Eq. 8.15)}$$

Both the above Eq. 8.13 and Eq.8.15 are mutually dependent. The initial conditions at time of IVC ($\theta = \theta_{ivc}$) in terms of P_0 and T_0 are needed. If those equations are combined replacing pressure in Eq. 8.15 by ideal gas equation (Eq.8.14), a single non linear differential equation in terms of T could be solved with m_0 is input rather than P_0.

This set of differential equations can be systematically modelled in Matlab Simulink having built in solver for ordinary differential equation.

B- During the gas exchange process ,

The system (consisting of control volume surrounding the chamber gases) is open where gas may leave or come inside chamber. During exhaust process the differential equation of pressure is

$$\frac{dP}{d\theta} = \gamma_1 P\left(\frac{1}{m}\frac{dm}{d\theta} - \frac{1}{V}\frac{dV}{d\theta}\right)_{exhaust} \quad \text{(Eq.8.16)}$$

While during intake process

$$\frac{dP}{d\theta} = \gamma_2 P\left(\frac{1}{m}\frac{T_m}{T}\frac{dm}{d\theta} - \frac{1}{V}\frac{dV}{d\theta}\right)_{intake} \quad \text{(Eq.8.17)}$$

$$\frac{dP}{d\theta} = \gamma_2\left(\frac{RT_m}{V}\frac{dm}{d\theta} - \frac{P}{V}\frac{dV}{d\theta}\right)_{intakest} \quad \text{(Eq.8.18)}$$

Where, T_m is the intake manifold temperature. γ_1 and γ_2 can be assumed constant and taken as 1.28 and 1.30 respectively during gas exchange process for the reason of lower variation in temperature.

When gas at P, V with specific heat ratio γ_1 flows through an opening of effective area A into a region P_0, the flow must be composed of subsonic and supersonic regimes. The critical

pressure ratio defines the nature of flow. If the pressure ratio between two regions is less than critical pressure ratio, the flow is subsonic and else it is supersonic.

The critical pressure ratio, $P_{cr} = \left(\frac{\gamma+1}{2}\right)^{\left(\frac{\gamma}{\gamma-1}\right)}$ (Eq.8.19)

i. For exhaust process

If, $\frac{P}{Pe_x} < P_{cr}$

$$\frac{dm}{d\theta} = -\frac{A_{ex}P_{ex}}{6N}\sqrt{\frac{2\gamma}{RT(\gamma-1)}\left(\frac{P}{Pe_x}\right)^{\frac{\gamma+1}{2}}\left[\left(\frac{P}{P_{ex}}\right)^{\frac{\gamma-1}{\gamma}}-1\right]} \quad \text{(Eq.8.20)}$$

If $\frac{P}{Pe_x} > P_{cr}$

$$\frac{dm}{d\theta} = -\frac{AP}{6N}\sqrt{\frac{\gamma}{RT}\left(\frac{2}{\gamma+1}\right)^{\frac{\gamma+1}{\gamma-1}}} \quad \text{(Eq.8.21)}$$

ii. For intake process

If , $\frac{P_{in}}{P} < P_{cr}$

$$\frac{dm}{d\theta} = -\frac{A_{in}P}{6N}\sqrt{\frac{2\gamma}{RT(\gamma-1)}\left(\frac{P_{in}}{P}\right)^{\frac{\gamma+1}{2}}\left[\left(\frac{P_{in}}{P}\right)^{\frac{\gamma-1}{\gamma}}-1\right]} \quad \text{(Eq.8.22)}$$

If $\frac{P_{in}}{P} > P_{cr}$

$$\frac{dm}{d\theta} = -\frac{Ai_nP_{in}}{6N}\sqrt{\frac{\gamma}{RT}\left(\frac{2}{\gamma+1}\right)^{\frac{\gamma+1}{\gamma-1}}} \quad \text{(Eq.8.23)}$$

The valve opening area evaluated from

$$A_{ex} = A_{exo}\left|\left\{\sin\left(\frac{180(\theta-\theta_{evo})}{\theta_{evc}-\theta_{evo}}\right)\right\}^{1/2}\right| \quad \text{(Eq.8.24)}$$

$$A_{in} = A_{ino}\left|\left\{\sin\left(\frac{180(\theta-\theta_{ivo})}{720+\theta_{ivc}-\theta_{ivo}}\right)\right\}^{1/2}\right| \qquad \text{(Eq.8.25)}$$

The Eq.8.24 and Eq.8.25 are the variable area as cam rotates which is supplied as input to the model.

Indicated torque: Indicated torque $T(\theta)$ as a function of crank angle (Jerzembecka et al., 2009) is obtained from the piston force (F_P) by neglecting inertia of various components and friction.

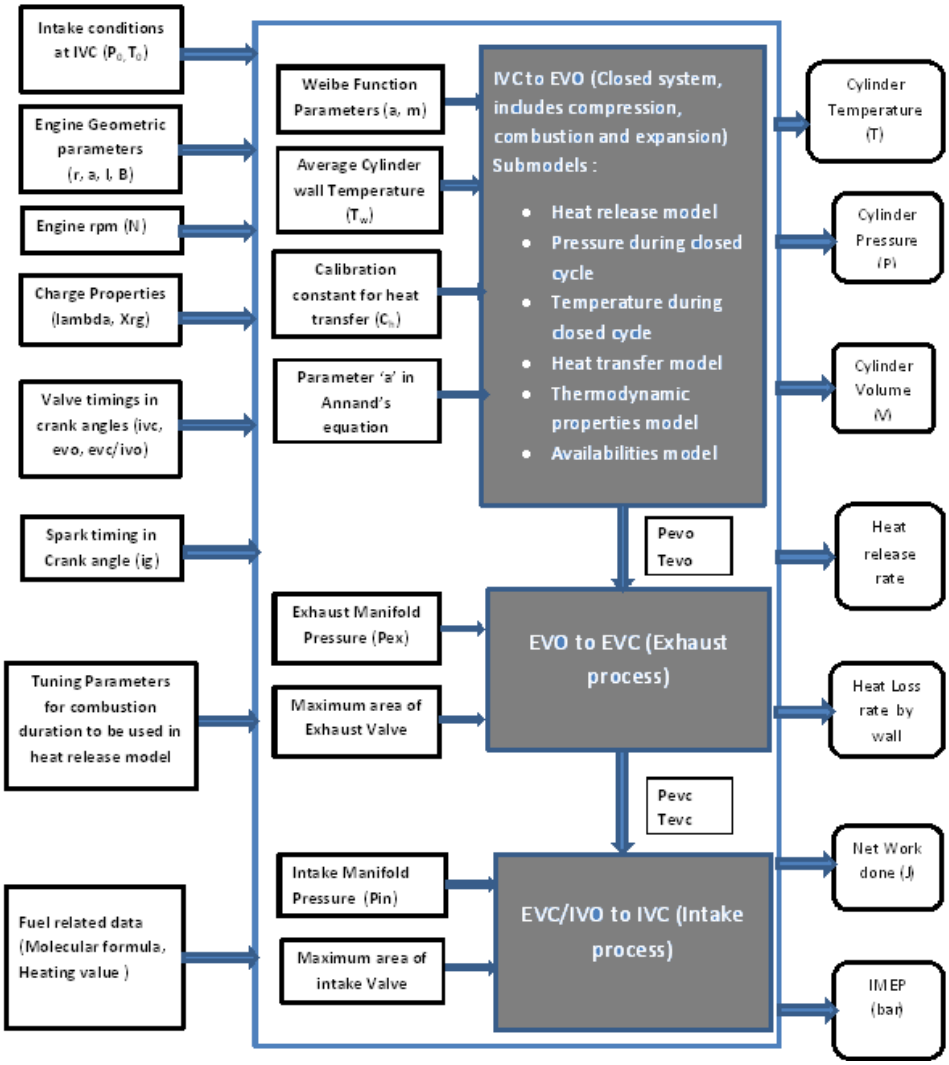

Fig. 8.1. Flowchart of Simulink model.

Piston force, $F_p = (P - P_{atm})A_p$; $T(\theta) = F_p\, a\left(\sin\theta + \frac{\sin 2\theta}{2\sqrt{\left(l/a\right)^2 - \sin 2\theta}}\right)$ (Eq.8.26)

Indicated work done, $$W_d = \int_{IVC}^{IVC+720} \left(P(\theta) \frac{dV}{d\theta} \right) d\theta \quad \text{(Eq.8.27)}$$

Indicated Power, $$I.P. = \frac{W_d}{120} \times N \quad \text{(Eq.8.28)}$$

Indicated Efficiency, $$\eta_{th} = \frac{I.P.}{m \times cv} \times 100 \quad \text{(Eq.8.29)}$$

Based on the above formulation for the zero-dimensional and single zone thermodynamic model simulation, the Simulink model being introduced for a four-stroke SI engine. This model has been built in solvers for ordinary differential equation, when the model is formulated in appropriate logical manner. The flow chart of Simulink model is shown in Fig.8.1.

8.2 CFD MODEL DEVELOPMENT

IC engines while analyzed computationally using the CFD, then the domain consist of combustion chamber where it needs to solve the continuity equation, momentum equation, and energy equations. The combustion process is highly dependent on flow field and turbulence level. Turbulence increases the flame velocity and enhances the combustion.

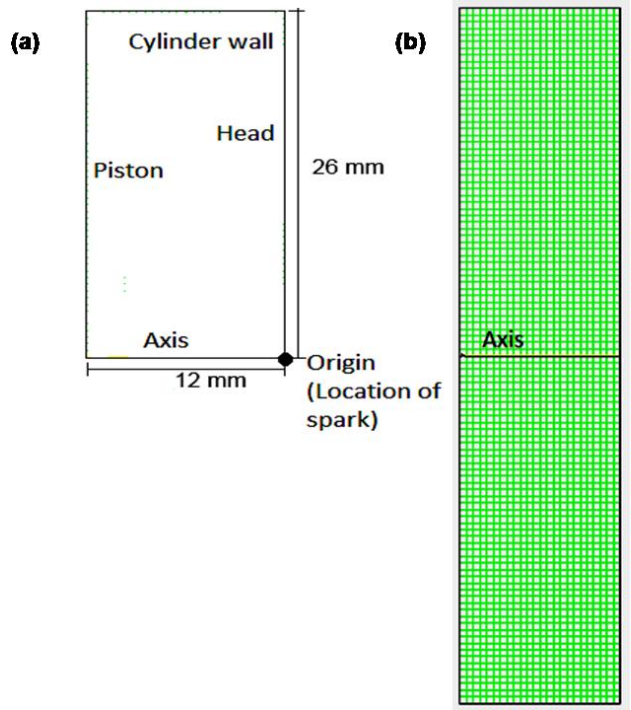

Fig. 8.2 (a) Two dimensional geometry of combustion chamber (Only half section above the axis) at TDC; (b) Dynamic mesh used for CFD simulation.

In CFD models, combustion is predicted by using the flow field data obtained from conservation equations. For predicting performance of an engine from CFD models, one should be able to do transient simulation in it and for that dynamic mesh or moving mesh is required. Fluent 'in-cylinder' module is incorporated for creating dynamic mesh with

premixed combustion model required for simulating engine combustion. However flame speed data needs to be given as input to fluent via UDF. 2D simulation of engine with axi-symmetric swirl on Fluent has been performed.

CFD model has been developed for the combustion chamber of a test engine available in laboratory to predict its performance (Fig. 8.2-a). It is a Honda Make (Model- GK100) four-strokes, 97 cc, air cooled, 1.8HP (HONDA make) engine with rated speed of 3600 rpm (Table 8.1).

8.2.1 Setting up CFD Model in Fluent

2D CFD model of the engine for closed cycle (i.e. from IVC to EVO) consist of domain to be axisymmetric with mesh on only half portion in 2D and specifying the swirl ratio. This will reduce numbers of cells- making the simulation to happen faster as compared to creating entire domain in 2D.

8.2.2 Creating the Mesh

In engine the domain consist of combustion chamber keeps on changing its volume with crank angle. So it needs to create moving mesh in the domain. The steps involved are first to create the combustion chamber geometry at TDC (crank angle 360 deg.) using the geometrical data of engine (compression ratio, bore, stroke, bowl shape if known).

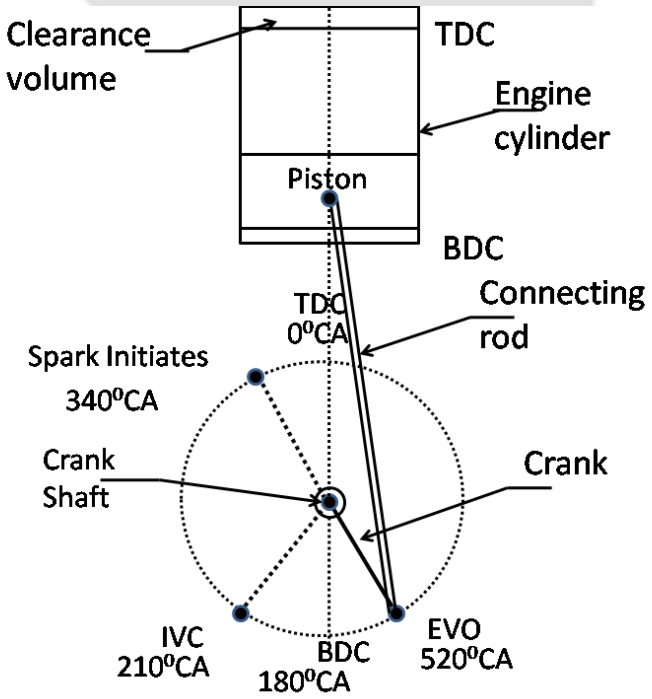

Fig. 8.3 The schematic diagram of valve positions and ignition timings for the CFD analysis

With the engine specifications shown in Table 8.1 and corresponding evaluation using standard compression ratio, the clearance volume can be found to be 25.52 cc. Now as the piston surface is observed to be nearly flat, and assuming the cylinder head to be flat as well the combustion chamber at TDC has disc type shape. The clearance distance of piston from

the head can be then found. As bore diameter is 5.2 cm the clearance height would become 1.2 cm (Fig. 8.2-b). Using these data while drawing the geometry of combustion chamber at TDC in Gambit. The combustion chamber is now meshed via structured quad mesh in Gambit. After meshing, the boundaries are specified. Once the mesh is created in gambit it is exported to fluent. In Fluent the mesh is scaled and checked (Fig 8.2-b). Then mirror image about axis is taken to show full chamber in 2D.

8.2.3 Solving the Mesh Motion.

After importing the mesh Unsteady and Axisymmetric swirl models are turned on. Then the engine geometric parameters are specified in dynamic mesh section and rpm of 3600 is specified for solving the case because rated power could be specified with this speed. The mesh motion is then set-up with beginning of suction stroke from 0^0 CA to 210^0 CA (30^0 aBDC) where inlet/suction valve closes (Fig.8.3). The computations are begin from 210^0 CA (IVC position) and continued till the exhaust valve opens at 520^0 CA. This would be a closed cycle simulation involving no exchange of mass with surrounding. When the mesh motion is solved deforming mesh can be viewed in graphic window and can be saved.

8.2.4 Setting up the Physics of the problem

In creating the physical setup for IC engines three user defined functions (UDFs) are needed which were available at the time of modelling the problem. These are *initialize.cLaminar flame*

velocity.c and *work.c.* These UDFs are provided in appendix. Initialize.c has functions to initialize the flow field. Only swirl ratio (default value 2.0) and axis directions have to be specified in the UDF. Laminar flame velocity.c has functions to give the fluent laminar flame velocity data of the fuel. Different fuels are available in the UDF which the user can specify by editing. By default the fuel is octane (for simulating gasoline). Work.c has functions which compute average cylinder pressure, temperature, volume, burned mass fraction as function of crank angle and save it onto a work.txt file.

These UDFs have to be first built and loaded in fluent. Apart from using these UDFs several models have to be used which are.

- *Define>Models>Energy equation*:- On

- *Define>Models>Viscous:*- k-epsilon as the turbulence model.(default values)

- *Define>Models>Transport and reaction*:-Premixed combustion. Non-adiabatic under *species model* panel.

- *Define>Materials:-ideal gas* for density, *user-defined* laminar flame speed, and input the heat of combustion (4.4e+07 for gasoline) and unburned mass fraction (0.0625 for stoichiometric gasoline-air mixture).

• *Define>Models>Species>Spark Ignition*: Define the location of sparking (0,0) , 2mm as *initial radius*, Select *Fixed spark size* and Circle as *shapes*. Timing of sparking (340^0CA), 0.001sec as *spark duration*, 0.01 sec as *diffusion time.*

The basic general equations governing the flow model along with the equation of mass conservation, momentum and energy were summarized in the conservative form of the Navier-Stokes equations suggested by Stewar et al., (2007)(Eq-8.30,8.31 and 8.32). In the present, the flow is steady and incompressible density (ρ) is assumed to be constant and time variation of any property is zero. Where 'S_i' is the external force per unit mass, 'h' is the thermal enthalpy, 'Q_H' is the heat source or sink per unit volume, 'S_{ij}' is the viscous shear stress tensor, 'q_i' is the diffusive heat flux. The subscripts are used to denote summation over the three coordinate direction.

$$\frac{\partial \rho}{\partial t}+\frac{\partial}{\partial x_i}\left(\rho U_i\right)=0 \qquad \text{(Eq-8.30)}$$

$$\frac{\partial}{\partial t}\left(\rho U_i\right)+\frac{\partial}{\partial x_i}\left(\rho U_i U_j\right)=-\frac{\partial P}{\partial x_i}+\frac{\partial}{\partial x_j}\left[\tau_{ij}+\tau_{ji}\right]+S_{ij},i \qquad \text{(Eq-8.31)}$$

$$\frac{\partial \rho}{\partial t}\left(\rho H\right)+\frac{\partial}{\partial x_i}\left(\rho U_i H\right)=\frac{\partial}{\partial x_j}\left(U_j\left(\tau_{ij}+\tau_{ji}\right)+q_i\right)+\frac{\partial P}{\partial t}-\tau_{ij}\frac{\partial U_i}{\partial x_j}+\rho\varepsilon+S_i U_j+Q_H \qquad \text{(Eq-8.32)}$$

Boundary conditions: Specify the wall temperatures and set axis to have boundary type axis.

• *Initialize* the flow. Set up the progress variable to be zero to show that all fuel is unburnt.

• *Solve>controls>solution*: PRESTO! For pressure and PISO for pressure-velocity coupling. Change *Under-relaxation factor* for pressure from 0.3 to 0.5. Set the convergence criteria to be 0.001 for all the parameters.

• Time-step duration is setup to be same as time taken to rotate crank rod by 0.5 deg.

After setting up the problem iterations are carried out and the plots for progress variable are saved. Progress variable is a quantity that keeps track of fuel quantity at a location. In an unburned mixture its value is zero and in a burned mixture its value is one. After the solution is converged result can be plotted from work.txt file obtained.

8.3 RESULTS AND DISCUSSION

The Simulink model is developed by considering mathematical formulation given in section 8.2 and the flow chart (Fig. 8.1). First, the model simulation results are validated with the experiments performed on the engine by the researchers (Soylu and Gerpen, 2004). The specifications of this engine are given in Table 8.1(Column 1). Subsequently, the same Simulink model is used for another engine with specifications as mentioned in Table 8.1 (Column 4). Then, the performance of the model is compared with that CFD results. In this way, the suitability of the Simulink model is justified for its application to spark ignition engine.

8.3.1 Validation of Simulink model

Using the heat release rate obtained from experimental data (Soylu and Gerpen, 2004), the combustion duration for those operating conditions of experimental engine were found after tuning combustion model. At crank angles 25^{o} before top dead centre (bTDC), the heat release rate starts and ends at around 50^{0}CA aTDC sometimes taken as end of combustion(EOC) so that the combustion duration remains as 75^{o}.The following reference parameters are obtained as below;

$$r_1 = 7.4, \quad N_1 = 4000rpm,\ \phi_1 = 1.1,\ \theta_{01} = 25^{0}bTDC \text{ and } \Delta\theta_1 = 75^{0}CA$$

These values were taken as input to the main model for simulating the cycle for any operating condition.

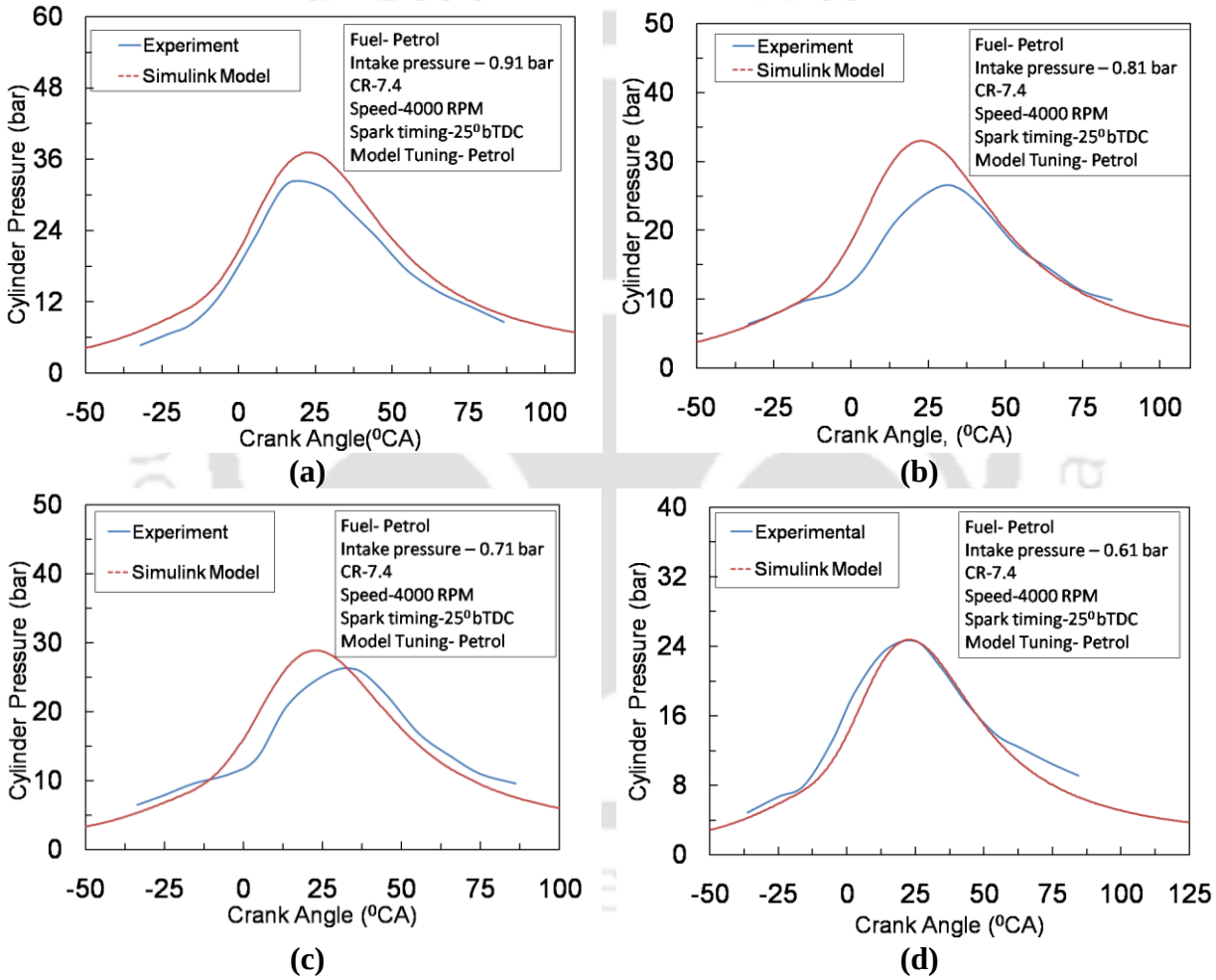

Fig. 8.4 Pressure variation in the cylinder with crank angle at different intake pressures.

The parametric studies are done and results are compared with experimental data. The simulation results follow the experimental trend of decrease of peak pressure as intake pressure *(P_0)* is reduced. (Figs. 8.4 a-d). Also, they are able to follow the trend of pressure rise at the start of combustion and its decrease during expansion. Assuming the experiments were performed with care and that experimental data (Soylu and Gerpen, 2004) are good, there is some mismatch in terms of peak pressure. The deviation in peak pressure found to be 6%, which reduces to 1% between Simulink and experimental results with decrease in intake

pressure. This anomaly is always lies between simulation and experiments in case of complex system like IC engines especially when higher intake pressure.

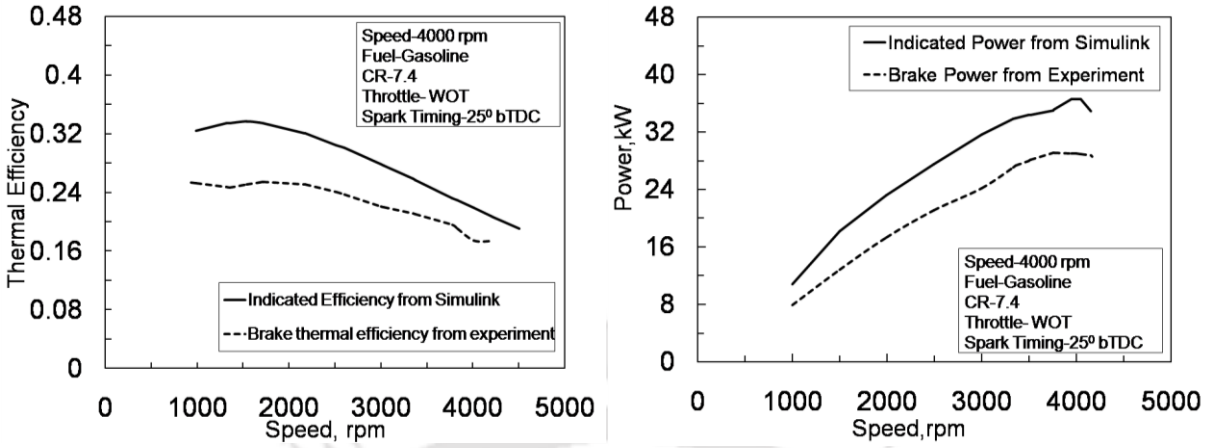

Fig. 8.5 Performance parameter variation with speed (a) Thermal efficiency variation with speed; (b) Power Vs speed

It is mainly because of the fact that combustion is a very complex phenomenon and the simple Wiebe function based model is not sophisticated enough to take into account many factors that affects the combustion process. However, the prediction of heat release during combustion from the model can be considered as an accurate estimate. It does its job well enough to emulate heat released during combustion and produce meaningful results. The operating experimental condition consist of the experiments with a 4-stroke, single cylinder, 5HP @ 4000 rpm petrol engine (Table 8.1). The engine runs at wide open throttle (WOT) condition with stoichiometric air-fuel ratio and the spark timing is maintained constant. Even at wide open throttle operation, the manifold pressure would not reach atmospheric value due to various restrictions in flow passage.

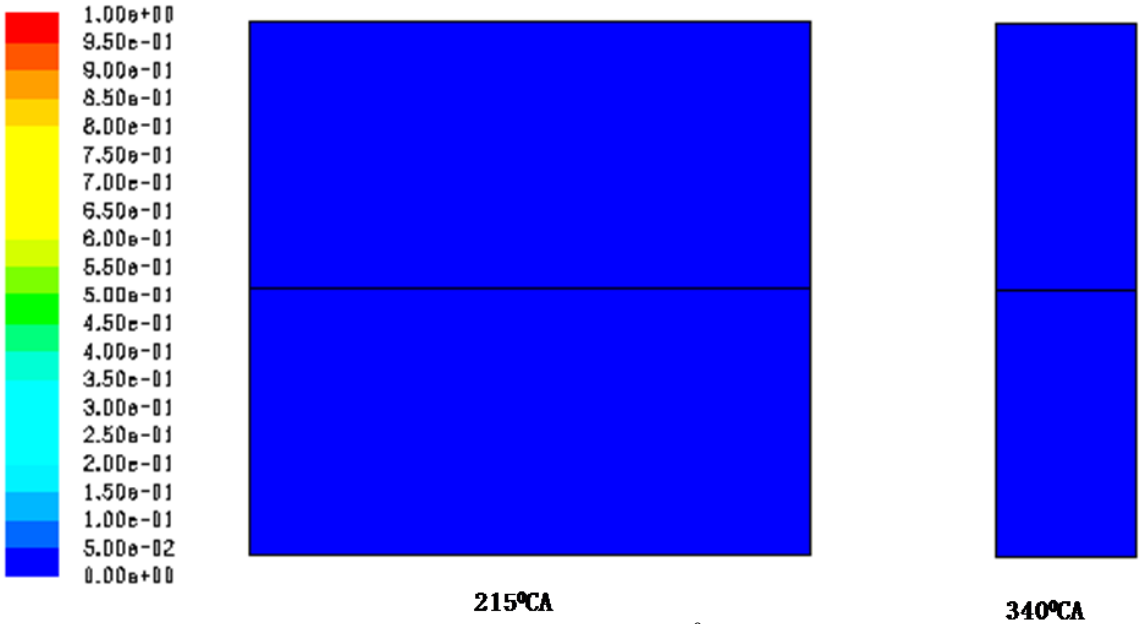

Fig. 8.6 Contour plots Progress variable at 215 ^{0}CA. IVC(just after start of Simulation) and at 340 ^{0}CA (20 ^{0}bTDC) when combustion is not initiated.

The effect of efficiency variation is observed with the increase in speed from experiment with simulation result. The indicated efficiency is again higher.

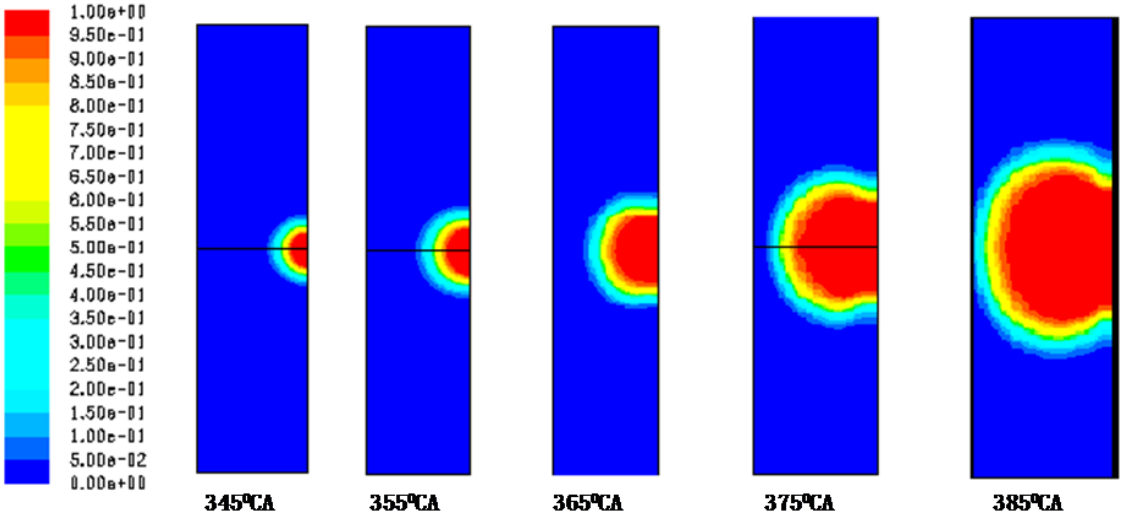

Fig. 8.7 (a) Contour plots progress variable at start after spark initiation and progress of flame over 345 ^{0} CA to 385 ^{0} CA.

However, the simulation curve follows the trend of decreasing efficiency as the rpm is increased (Fig. 8.5-a). It can be explained from the fact that as speed of the engine (rpm) increases the piston speed also increases while the flame speed increases only marginally. It is mainly due to the increase in turbulence resulting from increased piston speed. The indicated power and brake power variation with speed is shown in Fig. 8.5 (b). The maximum indicated power for the Simulink model is 36 kW while the experiments had the brake power of about 29 kW for same operating conditions. The indicated power is higher than brake power and also follows the trend. It should be noted that the brake power obtained from experiment is lower due to the friction power lost.

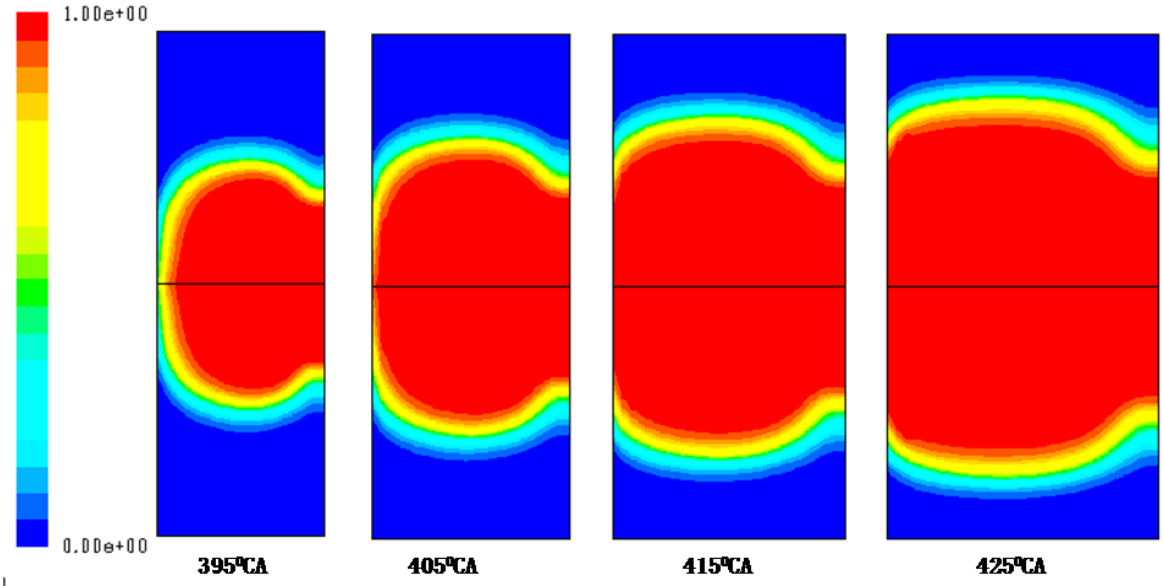

Fig. 8.7 (b) contour plots Progress variable at CA 395^{0}CA (just after start of simulation) and at 425^{0} CA

8.3.2 CFD Results Analysis

As per the procedure discussed in section 8.3, the model is being simulated with the boundary conditions for the close cycle of combustion chamber (IVC to EVO).

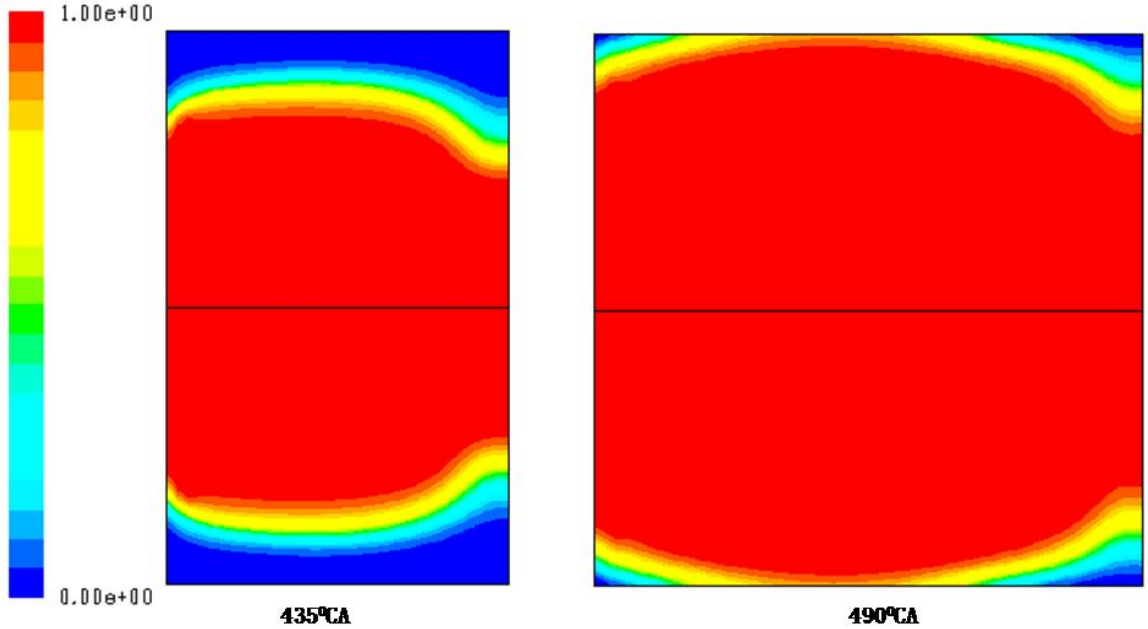

Fig. 8.7 (c) contour plots Progress variable at CA 435^0 CA (just after start of simulation) and at 490^0 CA.

Figure 8.7(a), (b) and (c) are the contour plots of progress variable after initiation of spark. A spherical flame front is formed at origin a 345^0 CA. This is the completion of compression stroke at 360^{0}CA.

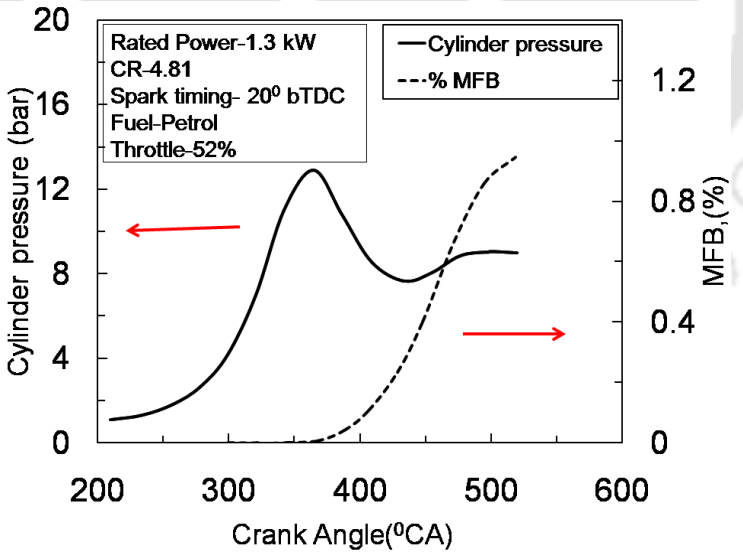

Fig. 8.8 The cylinder pressure and Percent MFB variation with CA

Flame simulation (Fig.8.6 and Fig 8.7-a,b and c) effectively define the position of the front or leading edge of the turbulent engine flame. At the beginning of compression stroke as shown in Fig. 8.6, the charge available inside closed volume consist of fuel air mixture shown by blue colour at 215^{0}CA.The charge is compressed till 340^{0}C just before spark initiate so there is no heat addition. But at 18^0 BTDC when the spark initiate by spark plug shown by orange

colour of flame which is developed at 345^{0}CA and ahead of flame is unburnt mixture shown by sky blue colour. This flame moves outward in early stage of development as a spherical surface at 355^{0}CA, 365^{0}CA,375^{0}CA and 385^{0}CA during power stroke.

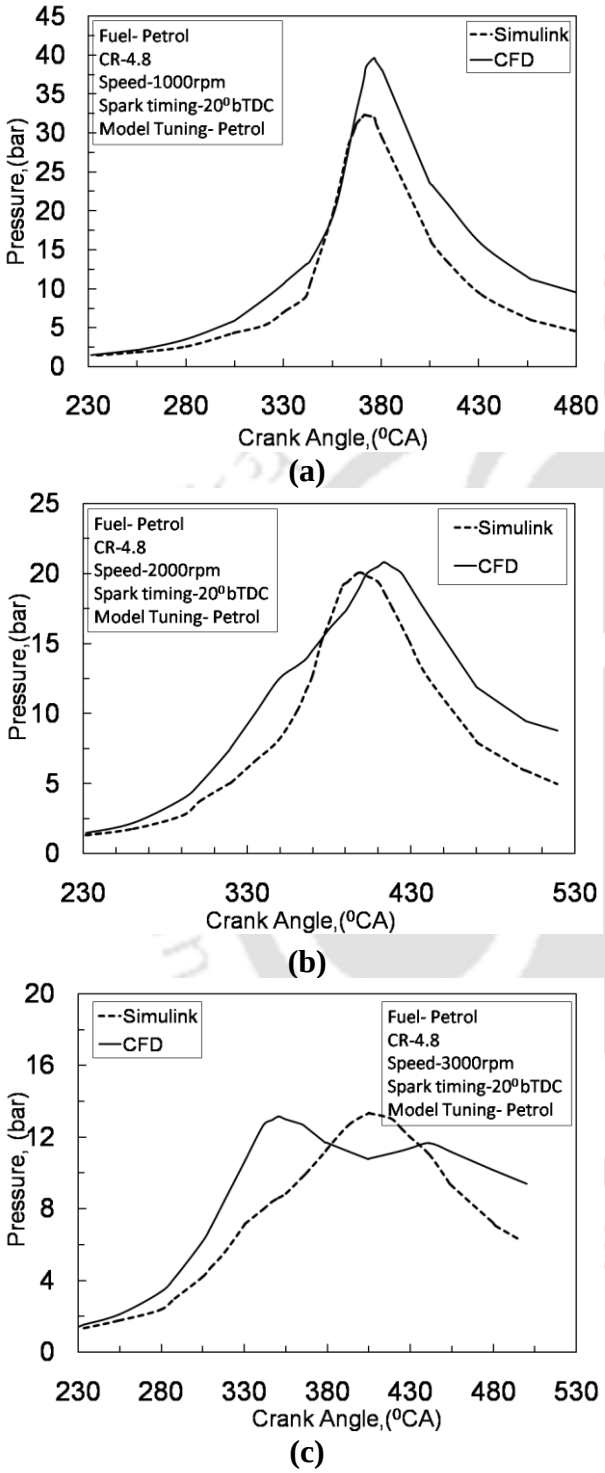

Fig.8.9 cylinder pressure variation with crank angle for Simulink and CFD maintaining speed (a)1000 rpm; (b) 2000 rpm; (c) 3000 rpm.

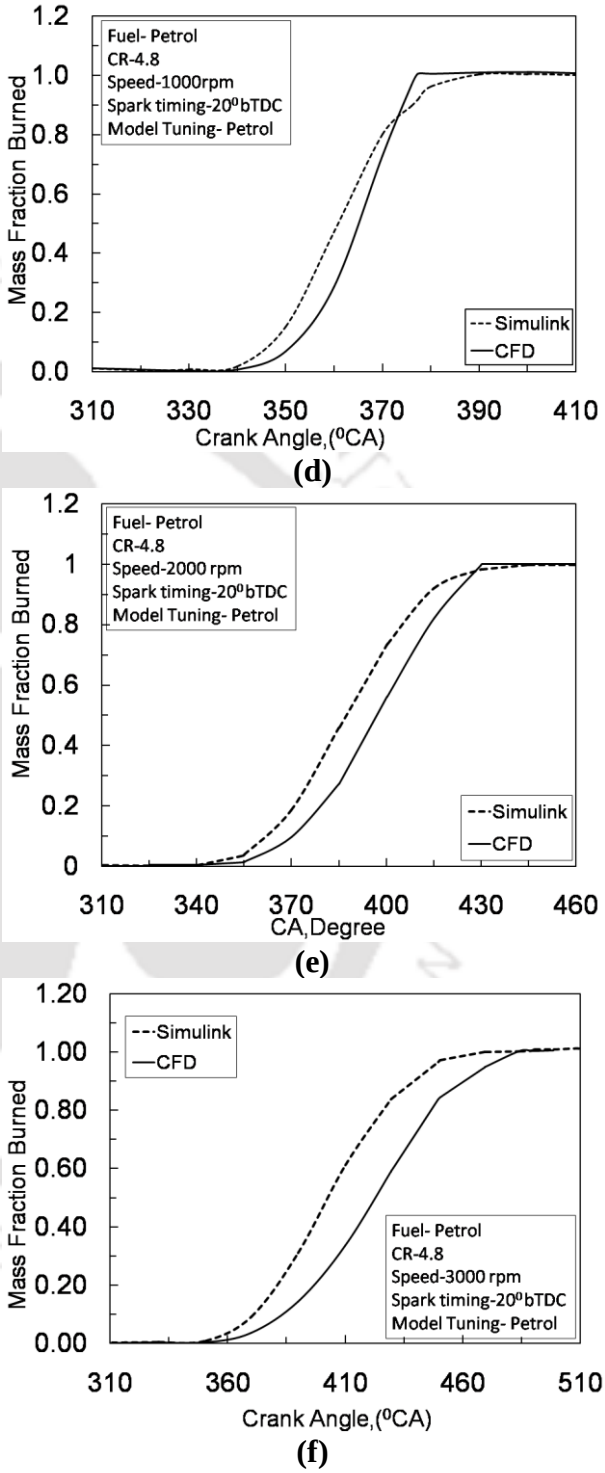

Fig.8.10 Mass fraction burned variation with crank angle for Simulink and CFD maintaining speed (a)1000 rpm; (b)2000 rpm; (c) 3000rpm.

As the crank angle increases flame moves further towards piston consuming more and more charge during power stroke. At 435^{0}CA and 490^{0}CA the maximum charge gets burned just

before completing power stroke at 540^0CA. It can be observed that percent mass fraction burned at 490^0 CA is 95% representing end of combustion. From Fig. 8.8 The ignition timing was set at 340^0CA. Thus combustion duration is 150^0CA.

Work done obtained from simulation is 48.1 J (Eq.8.27). So the power generated is 1.934 HP (Eq.8.28). This power value is higher that rated brake power at this rpm (Table 8.1) that is 1.8 HP yet very close to it. Thus the CFD model setup in Fluent is good enough to be used for analysis.

8.3.3 Combustion Analysis of Honda Engine with combination of Simulink and CFD.

In Simulink model it needs to know the combustion duration $(\Delta\theta_1)$ for one operating condition. From CFD simulation, it could be possible to evaluate the combustion duration as shown in Fig.8.8. The magnitude could be found out for one operating condition. With this data, it is then possible to carry out combustion analysis successfully in Simulink. The Simulink model is tuned using result from fluent model to have a good estimate for combustion duration.

$$r_1 = 4.8, \quad N_1 = 3600rpm,\ \phi_1 = 1,\ \theta_{01} = 20^0\, bTDC \text{ and } \Delta\theta_1 = 150^0 CA$$

This Simulink model can further used for other operating conditions as well as speed variation of the engine. Using those reference values, parametric studies are performed with Simulink model and the results are compared with that from Fluent model.

In Fig. 8.9, it can be observed that the pressure curves of the Simulink and Fluent model do not match very well. With the increase in speed the peak pressure recorded are 40 bar, 20 bar and 12 bar at 380^0CA, 410^0CA and 430^0CA using Simulink model respectively. Whereas the pressure of 33bar, 20 bar and 12 bar at 350^0CA, 390^0CA and 410^0CA respectively using CFD model. This is obvious because the load on the engine is reduced result in increase of speed. This causes reduction in compression pressure and ultimately delayed the combustion of charge. Similarly from Fig 8.10, the mass fraction burned of the two models shows increment in combustion duration with increase in speed of the engine. The magnitude of 32^0CA , 75^0CA and 130^0CA be the combustion duration for speed 1000,2000 and 3000 rpm of the engine using Simulink model. Whereas 35^0CA, 80^0CA and 140^0CA be the combustion duration for speed 1000,2000 and 3000 rpm. In the absence of experimental pressure curve these computational tool can successfully been used to understand the combustion behaviour of the engine as demonstrated in this article.

8.4 SUMMARY

CFD model of given engine was built using Fluent 6.3 using premixed combustion model. The model was then used to carry out parametric studies. The effect of rpm on performance was analyzed and predicted. Using the result from the CFD model, the thermodynamics based Simulink model was then tuned for combustion. It is found that, it produced reasonably good approximations with CFD model. However, since the experimental data for cylinder pressure was not available, the simulation models could not be validated.

CHAPTER 9

Conclusions and Future Scope

OVERVIEW

The developments in SI engine with variable compression ratio technique are dedicated towards the fuel dependence, as well as running conditions. In order to incorporate this technique, the sophisticated mechanism needs to be developed followed by its lab testing. As the octane fuels in case of SI engines are of different varieties and variable calorific values and when such different octane fuels are combusted in SI engine, the proper tuning of structural components such as compression ratio, spark plug location and dependent parameters such as ignition timing need alteration for better engine performance for the available fuel.

9.1 CONTRIBUTION OF THE PRESENT WORK

For the above mentioned objectives, the novel VCR mechanism is designed and developed separately for both HONDA and Large VCR APEX engine. Large SI Engine is also tested with the tilting block type VCR mechanism. Following are the results obtained from those experiments.

9.1.1 HONDA ENGINE with novel VCR

- Novel VCR mechanism has been successfully implemented in the Honda engine (Model: GK100).
- The engine working using this new novel mechanism is so smooth that there are no vibrations, no misfire and uneven combustion inside combustion chamber.
- The novel mechanism is found as an appropriate and viable alternative among the present available ones mainly due to possibility of change in compression ratio in the running condition of the engine.
- Two fuels viz. petrol and kerosene are used during the experiments for torque and power measurement in a specially designed experimental set-up at 52% throttle position. With fixed original CR 4.8, the maximum brake thermal efficiency (BTE) recorded to be 8.3% and 9% for petrol and kerosene fuel.
- It has been noted that the optimum compression ratio is CR 5.02 for petrol where efficiency increment reported to be 19% higher and CR 5.27 for kerosene with 37% increment in efficiency over fixed CR 4.8.

- Even specific fuel consumption is found decreased by 17.64% and 37% with that of original CR4.8 for petrol and kerosene fuels.
- Thus, it has been revealed that the commercial engine was underutilized without the variable compression mechanism attachment. Thus, possibility of performance enhancement of the engine for a fuel by altering working compression ratio and also accommodation of different fuels in the same engine have been demonstrated from current investigations.
- MATLAB Simulink simulation package is found useful for computational analysis of the combustion parameters of engine.

9.1.2 Large VCR engine with gaseous fuels

Based on the successful experimentations using novel VCR mechanism over small HONDA engine, the objective is to assess the feasibility of the mechanism over large commercial engine. Before installation of novel VCR mechanism, baseline study has been performed on new octane fuels LPG and raw biogas. The outcomes are as follows

- The engine has been tested with CR8, CR9 and CR10 for constant speed 1430 rpm with ignition timing 24^0, 26^0, 28^0,33^0,38^0,43^0, 45^0,46^0 and 47^0 bTDC for LPG and raw biogas. The maximum brake torque is recorded at 26^0 bTDC for LPG and 45^0 bTDC for raw biogas. The trend remains same for all CR 8,9 and 10.

- Accordingly the BTE found is 26.69% for LPG at 26^0 bTDC where as for raw biogas the same is 23.258% at 45^0 bTDC while running at CR10 at 1430 rpm. The trend remains same for lower CR9 and CR8 as well where maximum BTE recorded to be 26% and 23.9% for LPG and 22.77% and 17.25% for raw biogas respectively.

- With speed 1290 rpm and MBT spark timing, the maximum BTE is found to be 26.79% at CR10 with lowest BSFC of 299 gm/kW-hr. If the CR is lowered the same are 23.94% at CR8 with BSFC of 326 gm/kW-hr. Even at CR9, the maximum BTE is recorded to be 26.04% with BSFC 303 gm/kW-hr. This clearly depicts that with increase in compression ratio the performance of the engine improved. With speed 1290 rpm BTE found increased for raw biogas to 25.86% while operating at CR10 and MBT spark timing as compared to that attained at CR8 and CR9. With raising speed, the efficiency found decreases at rate of 53%, 36% and 40% for CR10, CR9 and CR8 respectively. The BSFC at speed 1430 rpm recorded is 1.304 kg/kW-hr, 0.988 kg//kW-hr and 0.968 kg/kW-hr for CR8, CR9 and CR10 respectively.

- The CO emission from biogas run spark ignition engine are found to be in rage of 44 - 159 ppm, 7-186 ppm and 154-216 ppm for CR10, CR9 and CR8 respectively. The HC emission is found to be higher with decrease in CR at a particular speed. The NOx is one of the harmful emission which is found in range of 60 - 512 ppm, 66 - 493 ppm and 50 - 460 ppm for CR10, CR9 and CR8 respectively.

- In order to control the NO_x, the method of EGR in different percentage are supplied with the intake charge and performance of LPG fuel and raw biogas fuel with variable CR, IT, EGR rate and throttle position are analyzed.

- With addition of EGR rate with LPG fuel, the spark timing relocated for maximum MBT are 26^0 bTDC for EGR0, EGR10 and EGR20. Thereafter the MBT timing is found advanced to 38^0 bTDC and 46^0 bTDC for EGR30 and EGR40 respectively. In case of raw biogas as EGR rate is small (10%-25%) there is not much variation in ignition timing was observed.

- BTE using LPG fuel and in presence of 10% EGR rate is 25.05% at CR10 showing decrement of 1.64% with respect to EGR0 whereas NO_x is found to be reduced and fallen in range of 99-201 ppm with EGR10 at intake. At maximum EGR40, the decrement of 4.78% is observed. This explains the suitability of EGR rate with intake charge upto 10% with little compromise in BTE.

- In case of raw biogas the BTE is noted to be 19.5% at EGR10 while working at CR10. This shows decrement of 24%. Even further increment of EGR rate causes the uneven combustion with misfire of substantial magnitude and accordingly performance degraded. The NO_x emission results are promising with EGR10 showing 110 ppm at CR10 causing decrement of 78%. Here the results are promising for emission but for the performance parameter view point, need more rich fuel air charge.

9.1.3 Large VCR engine with novel VCR mechanism

According to the results obtained in baseline test performed on large VCR engine, the novel VCR mechanism has been designed and developed for 73.44 cc clearance volume. The novel VCR mechanism accompanied with spark plug may travel axially up to 10 mm inside the combustion chamber. This cause rise in CR up to 11.02 if original CR is 10. Similar to this for original CR9, there is increase in CR upto 9.8 and with CR8, it raises to 8.6.

- The trials are performed on biogas for only VSP location with fixed CR. This explains the effect of variation in spark plug location in conventional vehicles. Using biogas fuel, the BTE is found to be increased at spark location of 2 mm (SP2) showing magnitude of 26.4% which was 24.9% at original CR10 while running at 1301 rpm. Similarly at lower CR 9 and 8 also the SP2 location is noted as optimum showing rise in BTE by 9% and 16% respectively. At SP2 location combustion behavior is improved substantially showing faster combustion and almost 45% MFB at TDC position. Pressure pulsation data in form of cycle by cycle variation is found minimum at SP2 with compared to other locations SP1, SP3 and SP4. The harmful emissions have adverse effect showing rise in NO_x emission by 76%, 74% and 74% increment for CR8, CR9 and CR10 with respect to that of original CR.

- The higher octane fuel LPG also been tested for the optimum spark plug location at constant CR. There also the results suggested that it must be necessary to relocate

spark plug as and when it needs to change the fuel in conventional spark ignition engine. For LPG fuel, the efficiency increases to 27.83 % with relocating of spark plug to SP4 location in our study while original CR at 10. For other CR as well the optimum locations are SP3 for CR9 and SP2 for CR8 showing maximum efficiency 23.9% and 23.3% respectively. With these optimum locations at corresponding CRs, the BSFC reduced to 13.05%, 15.57% and 10.22% respectively for CR10, CR9 and CR8 with new SP locations.

- When engine attains optimum compression ratio along with relocated spark plug position, it will guarantee that the engine will run to its maximum possible output. Looking this angle of view, the biogas is tested for the optimum CR along with optimum SP location by installing the novel VCR mechanism on the large VCR engine. Here the optimum CR and optimum SP location can be highlighted such as CR10.48 with SP3 is found optimum at basic CR10. The maximum BTE reported to be 27.04% over speed range 1290-1540 rpm. But beyond this range the combination phenomenon changed and new settings again possibly attain maximum efficiency.

- Similarly the LPG fuel also can be utilized optimally in SI engine with novel VCR and SP locations. Based on the experiments, it was found that, BTE shows increment if CR10.48 with SP3 location approaching to 28.358% BTE. This shows remarkable rise of 3.88% over original CR and SP location. Similarly for lower CR9, the optimum combination is CR9.15 with SP2. Ahead for CR8 also the optimum set of CR8.11 with SP2 location shows higher BTE. BSFC shows notable decrement of 6.6% with respect to original CR. Similar outcomes are also observed for CR9 and CR8 as well. This performance improvement is based on the combustion phenomenon only. This shows that the combustion gets accelerated with optimizing CR and SP location showing increment in peak pressure to be 3.59%. Mean gas temperature also raises to a high vale 1078 ^{0}C which was 893 ^{0}C for original CR and SP location. The effect of efficient combustion is on exhaust gas emission where maximum NO_x found to be 1212 ppm at maximum load on the engine while working at CR10.48 with SP3 location.

- If the EGR rate is added with the fuel such as raw biogas and in this situation, if the CR and SP location is optimized, it would be possible to harness maximum possible energy from the fuel to produce work. However EGR rates are different, so for EGR10 and EGR 20, the optimum configuration is CR10.48 with SP location SP3. If EGR rate is increased further then, optimum configuration will be CR10 with SP1 only. Similarly for around CR9, the optimum configuration is CR9.15@SP2, CR9.38@SP3, CR9.15@SP2 and CR9.38@SP3 found for EGR0, EGR10, EGR20 and EGR25 respectively while engine is running at maximum load or lowest speed. This could be well justified with combustion parameters such as mass fraction burned and combustion duration. The positive effect can be seen with harmful emission NO_x which decreases to 32.35% at optimum combination of CR and SP location.

- For LPG fuel in presence of EGR for optimizing CR and SP location, the experiments are carried out. The outcomes are for EGR10, the optimum combination is CR10.48 with SP3, If EGR increased to EGR20, then also CR10.48 with SP3 location is found optimum. Similarly CR10.18@SP2, CR10@SP1 are optimum for EGR30 and EGR40 respectively. The major pollutant NO_x are found reduced to maximum 95% with implementation of EGR in the system.

- Based on the outcomes listed above, the novality of research finding suggest for continuous variation of CR accompanied with spark location for attaining best performance from multifuels available easily. As well as for mitigating the harmful emissions, the technique of EGR upto the percentage of acceptable limit for the particular fuel is suitable. In this situation the optimum combination of VCR, VSP and EGR avail the best performance.

9.2 SCOPE OF FUTURE WORK

The present investigations focus the prospects of online variation of compression ratio(CR) by developing the novel variable compression ratio mechanism. The importance of the variable compression ratio and especially the suitability of the mechanism developed can be demonstrated on different engines and with different fuels from liquid to gases. The exhaustive experiments on novel mechanism with multifuels show that the mechanism could increase or decrease CR in a small range. The results obtained reveled that thus obtained variation in CR itself is enough to improve the performance of the engine while engine is running on road. Further study could be extended as

- The improvements in novel VCR mechanism, in the sense that the engine head equal to cylinder bore diameter could become the secondary piston and displacement of that will vary the compression ratio as per load, speed and type of fuel used. Regarding the suction and exhaust valves, they will be fixed in this secondary piston and complete assembly will displace up or down inside combustion chamber as per users need. The advantage of this will be the large variation in CR suitably carried by the engine under consideration.

- As secondary piston travels in and out of combustion chamber, there may be some crevices formed around the axial length of secondary piston where fuel air mixture may left unburnt and performance may dropped. In such situation the shape of secondary piston becomes a parameter of optimization. Different shapes having different surface volume could be tried in the engine. But it may take a long time to design followed by manufacturing of the mechanism and incorporating it in engine. Also chance of failure are more while experimentations. To bypass exhaustive experimentation, the computation study using CFD could be helpful to simulate the engine combustion behavior

with such different shape and surface volume secondary piston. This will provide us the information about the turbulence level, high and low pressure zones, combustion centre, fuel rich/lean area which is out of scope with experimentations.

- The novel technique of installation of spark plug inside of secondary piston, makes the engine to vary its spark plug location. The optimization of spark plug location will be more precise if, the study carried out using optical window combustion chamber with high speed photography. This will explain the combustion phenomenon with axial travel of spark plug inside combustion chamber, the behavior of flame after initiation and corresponding flame kernel development at each location. Based on the analysis and combustion duration, the spark plug location could be optimized in laboratory for multi fuels.
- Along the same track, computation study of variable spark plug location accompanied with variable compression ratio is important to provide a wide information such as swirl rate, pressure distribution along axis of spark plug, flame velocity, combustion duration etc which even out of scope with optical window engine study. This makes the commercial viability of the novel VCR mechanism for multifuels also.

References

Arroyo, J., Moreno, F., Mun, M., and Monne, C. (2013), " Efficiency and emissions of a spark ignition engine fueled with synthetic gases obtained from catalytic decomposition of biogas," *International Journal of Hydrogen Energy*, Vol.38, pp.3784-3792

Abdel, R. and Osman, (1997), "Experimental investigation of varying the compression ratio of SI engine under different ethanol gasoline fuel blends," *International Journal of Energy Research*, Vol.21, pp.31-40.

Al-Bagdadi, Maher A.R.S. (2006), "A simulation model for a single cylinder four-stroke spark ignition engine fueled with alternative fuels," *Turkish J. Eng. Env. Sci.*, Vol. 30, pp. 331 – 350.

Alasfour, F.N. (1996), " Butanol- A single-cylinder engine study: Availability analysis," *Applied Thermal Engineering*, Vol. 17(6), pp. 537-549.

Alger, T., Gingrich, J., Roberts, C. and Mangold, B. (2012), "Cooled exhaust-gas recirculation for fuel economy and emissions improvement in gasoline engines," *International Journal of Engine Research*, Vol. 12(3), pp.252–64.

Alger, T. and Mangold, B. (2009), " Dedicated EGR: A new concept in high efficiency engines, " SAE International Journal of Engines, Vol.2(1), pp.620-631.

Aina, F. and Pam (2012), "Influence of compression ratio on the performance characteristics of SI engine," *Advances in Science applied resarch*,Vol.4(3), pp. 1915-1922.

Arbab, M.I., Masjuki, H.H., Varman, M., Kalam, M.A., Imtenan, S. and Sajjad, H. (2013), "Fuel properties, engine performance and emission characteristic of common biodiesels as a renewable and sustainable source of fuel," *Renewable and Sustainable Energy Reviews*, Vol. 22 , pp.133–147

Assanis, D.C., Wooheum, C., Choi, I., Ickes, A., Jung, D., Martz, J., Nelson, R., Sanko, J., Thompson, S., Brevick, J. and Inwood, B. (2005), "Pressure reactive piston technology," Investigation and development for spark ignition engines'. SAE Paper 2005-01-1648.

Bhandari, V. B. (2010), "Design of machine elements," Tata-McGraw Hill Publications, 4th edition.

Bayraktar, H. and Durgun, O., 2005, "Investigating the effects of LPG on spark ignition engine combustion and performance," Energy Conversion and Management, Vol. 46, pp. 2317–2333.

Borjesson, P., and Mattiasson, B. (2008), "Biogas as a resource-efficient vehicle fuel," *Trends in Biotechnology* , Vol. 26(1), pp.7-13.

Brevick, J., "Design and development of a pressure reactive piston (PRP) to achieve variable compression ratio," *Department of Energy Contract FC02-99EE50576 Final Technical Report.*

British Petroleum statistical combustion process Report 2014.

Boretti, A. (2013), " Conversion of a heavy duty truck diesel engine with an innovative power turbine connected to the crankshaft through a continuously variable transmission to operate compression ignition dual fuel diesel-LPG," *Fuel Processing Technology*,Vol.113, pp.97-108.

Caris and Nelson, (1959), "A new look at high compression engines," *SAE trans.*, Vol. 67, pp. 112-124.

Chaudhari, A., Kulkarni, V., and Sahoo, N. (2013), "A simulation models for spark ignition engine: a comparative performance study," *Energy Procedia*, Vol. 54, pp.330-341.

Chandra, R., Vijay, V.K., Subbarao, P.M.V. and Khura, T.K. (2011), "Performance evaluation of a constant speed IC engine on CNG, methane enriched biogas and biogas," *Applied Energy*, Vol.88,

pp.3969–3977

Cerri, T., D'Errico, G. and Onorati, A. (2013), "Experimental investigations on high octane number gasoline formulations for internal combustion engines," Fuel, Vol.111, pp.305–315.

Chanchaowna, S. (1999), "The effect of gasoline octane number on engine performance," Research *Report of King Mongkut's University of Technology*, Thailand, pp. 1–8.

Ceviz, M.A. and Yuksel, F. (2005), "Cyclic variations on LPG and gasoline-fuelled lean burn SI engine," *Renewable Energy* , Vol. 31, pp. 1950–1960.

Chicurel, R. (1993), "Dual-fuel system to provide a variable octane mixture to an engine," *Energy*, Vol. 18(6), pp. 611-614.

Choi, G.H., Han, S.B., and Chung, Y.J. (2003), "The effect of hydrogen enrichment on exhaust emissions and thermal efficiency in a LPG fuelled engine," *KSME International Journal*, Vol. 17(8), pp. 1196-1202

Cowans, K.W.(2002), " High efficiency engine with variable compression ratio and charge,"US Patent No-0104492 A1

Crookes, R.J. (2006), "Comparative Bio-Fuel Performance in Internal Combustion Engines," *Biomass and Bioenergy* , Vol. 30, pp. 461–468.

Debnath, B.K., Sahoo, N. and Saha U.K. (2013), "Adjusting the operating characteristics to improve the performance of an emulsified palm oil methyl ester run diesel engine," *Energy Conversion and Management*, Vol. 69, pp.191–198.

Demesoukas, S, Caillol, C, Higelin, P, Boiarciuc, A. and Floch, A. (2015), "Near wall combustion modeling in spark ignition engines. Part A: Flame–wall interaction," *Energy Conversion and Management*, Vol.106, pp.1426–1438.

Duclos, J, Bruneaux, G. and Baritaud, T. (1996), "3D modeling of combustion and pollutants in a 4-valve SI engine; effect of fuel and residuals distribution and spark location," SAE Technical Paper 961964 , doi:10.4271/961964.

Emission Standards. Obtained through the Internet:http://www.dieselnet.com/standards.

Erkus, B., Surmen, A. and Karamangil, M.I. (2013), "A comparative study of carburetion and injection fuel supply methods in an LPG-fuelled SI engine," Fuel, Vol.107, pp.511-517.

Folayan, A., and Pam (2012) , "Influence of compression ratio on the performance characteristics of SI engine," *Advances iin Science applied resarch*, Vol. 4(3), pp.1915-1922.

Fontana G and Galloni E.(2010), " Experimental analysis of a spark-ignition engine using exhaust gas recycle at WOT operation," Applied Energy, Vol.87(7), pp.2187-2193.

Filipi, Z.S. and Assanis, D.N.(2000), "The effect of the stroke-to-bore ratio on combustion, heat ransfer and efficiency of a homogeneous charge spark ignition engine of given displacement," International Journal of Engine Research, Vol. 2(1), pp. 191–208

Freudenstein, F. and Maki, E.R.(1983), "Development of an optimum variable-stroke internal-combustion engine mechanism from the viewpoint of kinematic structure," *Journal of Mechanisms, Transmissions, and Automation in Design*, Vol.105, pp.259-266.

Ganesan, V. (1996), " Computer simulation of spark-ignited engine process," Universities press (India) Limited. 1996.

Gumus, M. (2011), "Effects of volumetric efficiency on the performance and emissions characteristics of a dual fuelled gasoline and LPG spark ignition engine," *Fuel Processing Technology*, Vol. 92, pp.

1862-1867.

Hanipah, M., R., Michelson, R. and Roskilly, A.P. (2015), "Recent commercial free-piston engine developments for automotive applications," *Applied Thermal Engineering*, Vol. 75, pp. 493-503.

Heywood, J.B. (1988), "Internal combustion engine fundamentals," *McGraw Hill international editions*, New York.

Heffel, J.W. (2003), "NO_x emission reduction in a hydrogen fueled internal combustion engine at 3000 rpm using exhaust gas recirculation," *International Journal of Hydrogen Energy*, Vol. 28, pp.1285 – 1292

Hiyoshi, R.(2013), " Variable compression ratio engine," US patent number-US2013/0327302 A1, Nissan Motor company.

Hook, M., Tang, X. (2006), " Depletion of fossil fuels and anthropogenic climate change—A review," Energy Policy, Vol.52, pp. 797–809.

Hu, E., Huang, Z., Liu, B., Zheng, J., Gu, X. and Huang, B. (2009), "Experimental investigation on performance and emission of a spark-ignition engine fueled with natural gas-hydrogen blends combined with EGR," *International Journal of Hydrogen Energy*, Vol. 34, pp.528 – 539

Huang, J. and Crookes, R.J. (1998), "Spark ignition engine performance with simulated biogas- a comparison with gasoline and natural gas," *Journal of Institute of Energy*, Vol.71, pp.197-203

Han, S.B.(2000), "Cycle-by-cycle variations under cylinder pressure-based combustion analysis in spark igntion engines," *KSME International journal*, Vol.14(10), pp.1151-1158.

Ibrahim, A. and Bari, S. (2009), "A comparison between EGR and lean-burn strategies employed in a natural gas SI engine using a two-zone combustion model," *Energy Conversion and Management* , Vol. 50, pp. 3129–3139

Indian Standard, 1980, "Methods of tests for internal combustion engines- declaration of power, efficiency, fuel consumption and lubricating oil consumption," *IS: 10000 (Part IV) Edition 1.1.*

International Energy Agency "World Energy outlook Report,2014".

Ismail, S. and Mehta, P.S. (2011), "Second law analysis of hydrogen-air combustion in a spark ignition engine," *International Journal of Hydrogen Energy*, Vol. 36, pp.931 – 946

Jeong, C., Kim, T., Lee, K., Song, S., and Chun, K. M. (2009), "Generating efficiency and emissions of a spark-ignition gas engine generator fuelled with biogas–hydrogen blends," *International Journal of hydrogen energy*, Vol. 34, pp.9620-9627.

Jerzembecka, S., Peters, N., Pepiot-Desjardins, P. and Pitsch, H. (2009), " Laminar burning velocities at high pressure for primary terence fuels and gasoline: Experimental and numerical investigation," Combustion and Flame, Vol.156, pp.292–301.

Kerley and Thurston. (1962), " The indicated performance of otto cycle engines," *SAE Trans.*, Vol.70, pp. 5-30.

Korakianitis, T., Namasivayam, A.M. and Crookes, R.J. (2011), "Natural-gas fueled spark-ignition (SI) and compression-ignition (CI) engine performance and emissions," *Progress in Energy and Combustion Science*, Vol. 37 ,pp. 89-112.

Kline, S.J. and McClintock, F.A. (1953), "Describing uncertainties in single-sample experiments," Mechanical Engineering, Vol.75, pp. 3-12.

Klein, S. A. (1991), "An explanation for observed compression ratios in internal combustion engines,"

Journal of Engineering for Gas Turbines and Power , Vol. 113 , pp.511-513.

Kuang, Z., Lyon, E, Cheng, H., Page V., Shenton T. and, Dearden, G. (2017), " Multi-location laser ignition using a spatial light modulator towards improving automotive gasoline engine performance," Optics and Lasers in Engineering, Vol. 90,pp. 275–283.

Larsen, G. J. (1991), "Reciprocating piston engine with a varying compression ratio," US5025757 (A), pp.1-10.

Lee, K., Kim, T., Cha, H., Song, S. and Min, C.K. (2010), "Generating efficiency and NO_x emissions of a gas engine generator fueled with a biogas hydrogen blend and using an exhaust gas recirculation system," *International Journal of Hydrogen Energy*, Vol. 35, pp.5723-5730

Li, H. and Karim, G.A. (2005), "Exhaust emissions from an SI engine operating on gaseous fuel mixtures containing hydrogen," *International Journal of Hydrogen Energy*, Vol. 30, pp.715 – 720

Li, T., Wu, D. and Xu, M. (2013), "Thermodynamic analysis of EGR effects on the first and second law efficiencies of a boosted spark-ignited direct- injection gasoline engine," *Energy Conversion and Management*, Vol. 70, pp.130–138.

Li, J., Gong, C.M., Su, Y., Dou, H.L. and Liu, X.J. (2010), "Effect of injection and ignition timings on performance and emissions from a spark-ignition engine fuelled with methanol," *Fuel*, Vol. 89 , pp. 3919–3925

Massi, M. (2012), " Experimental analysis of spark ignition petrol engine fuelled with LPG (Liquefied Petroleum Gas)," *Energy*, Vol.41, pp.252-260.

Midkiff, K.C., Bell, S.R., Rathnam, S. and Bhargava, S. (2001), "Fuel composition effects on emissions from a spark-ignited engine operated on simulated biogases," ASME Journal of Engineering for Gas Turbines and Power, Vol. 123, pp. 132-138.

Morganti, K.J., Foong, T.M., Brear, M.J., DeSilva, G., Yang, Y. and Dryer, F.L.(2013)," The Research and Motor Octane Numbers of Liquefied Petroleum Gas (LPG*)," Fuel* , Vol.108,pp. 797–811.

Nagalingam, B., Duebel, F. and Schmillen, K. (1983), "Performance study using natural gas, hydrogen supplemented natural gas and hydrogen in AVL research engine," *International Journal of Hydrogen Energy*, Vol. 8(9), pp.715 – 720.

Ma,T.T. (1992), "Engine with variable compression ratio," US Patent ,no-5101776

Masi, M. (2012), "Experimental analysis on a spark ignition petrol engine fuelled with LPG (liquefied petroleum gas),"*Energy*, Vol.41, pp.252-260

Martyn, R. (2002), "Benefits and challenges in variable compression ratio (VCR)," *SAE Technical Paper*, 03-227. doi:10.4271/2003-01-0398.

Merker, G.P., Schwarz, C., Stiesch, G. and Otto, F. (2006), "Simulating combustion- simulation of combustion and pollutant formation for engine development," Springer Publications. ISBN 10 3-540-25161-8

Mital , K.M. (1996), " Biogas system: principles and application. India," *New Age International (P) Limited.*

Moffat, R. J. (1982),"Contributions to the theory of single-sample uncertainty analysis," *ASME Journal of Fluids Engineering*, Vol.104(2), pp. 250–260.

Mustafi, N.N., Miragli, Y.C., Raine, R.R., Bansal, P.K. and Elder, S.T. (2006), "Spark-ignition engine performance with 'Powergas' fuel (mixture of CO/H_2): a comparison with gasoline and natural gas,"

Fuel, Vol. 85, pp.1605–1612.

Murillo,S., Mıguez, J.L., Porteiro, J., Lopez, L.M, Gonzalez, Granada, E. and Moran, J.C.(2005), " LPG: Pollutant emission and performance enhancement for spark-ignition four strokes outboard engines," *Applied Thermal Engineering* , Vol.25,pp.1882–1893

Neame, G.R., Gardiner, D.P., Mallory, R.W., Rao, V.K.M., Bardon, F. and Battista, V. (1995), " Improving the fuel economy of stoichiometrically fuelled S.I. engines by means of EGR and enhanced ignition- a comparison of gasoline, methanol and natural gas," SAE Tech. Pap. Ser. 952376.

Nagalingam, B., Duebel, F. and Schmillen, K. (1983), "Performance study using natural gas, hydrogen supplemented natural gas and hydrogen in AVL research engine," *International Journal of Hydrogen Energy*, Vol. 8, No. 9, pp.715 – 720.

Orhan A. S., Kahraman, N. and Ceper, B. (2007) , "Experimental study on a spark ignition engine fuelled by methane–hydrogen mixtures," *International Journal of Hydrogen Energy*, Vol 32, pp. 4279-4284

Ozcan, H. and Jehad, A.A.Y. (2008), " Performance and emission characteristics of LPG powered four stroke SI engine under variable stroke length and compression *ratio," Energy Conservation and Management*, Vol.49, pp. 1193-1201

Pal, A., Agarwal, A. K .(2016), "Comparative study of laser ignition and convention electric spark ignition systems in a hydrogen fuelled engine", *International Journal of Hydrogen Energy*, Vol. 41(1),pp.675-682

Pan, M., Shu, G., Wei, H., Zhu, T., Liang, Y., and Liu, C. (2014), "Effects of EGR, compression ratio and boost pressure on cyclic variation of PFI gasoline engine at WOT operation," *Applied Thermal Engineering*, Vol.64, pp. 491-498.

Park, C., Park, S., Lee, Y., Kim, C., Lee S. and Moriyoshi, Y. (2011), "Performance and emission characteristics of a SI engine fueled by low calorific biogas blended with hydrogen," *International Journal of hydrogen energy*, Vol. 36, pp.10080-10088.

Park, C., Park, Y., Oh, S., Lee, Y., Kim, T. Y., Kim, H., Choi, Y. and Kang, K.Y. (2013), " Emission characteristics of gasoline and LPG in a spray-guided-type direct injection engine," *SAE Technical Paper 2013-01-1323*, doi:10.4271/2013-01-1323,2013

Perini, F., Paltrinieri, F. and Mattarelli, E. (2010), "A quasi-dimensional combustion model for performance and emissions of SI engines running on hydrogen–methane blends," *International Journal of Hydrogen Energy*, Vol. 35, pp.4687–4701.

Pierce , J.(1914), " Variable stroke mechanisms," U.S. Patent No. 1,112,832.

Porpatham, E., Ramesh, A. and Nagalingam, B. (2007), "Effect of hydrogen addition on the performance of a biogas fuelled spark ignition engine," *International Journal of Hydrogen Energy*, Vol. 32, pp.2057 – 2065

Porpatham, E., Ramesh, A. and Nagalingam, B. (2008), " Investigation on the effect of concentration of methane in biogas when used as a fuel for a spark ignition engine," *Fuel*, Vol. 87, pp.1651–1659.

Porpatham, E., Ramesh, A. and Nagalingam, B.(2012), " Effect of compression ratio on the performance and combustion of a biogas fuelled spark ignition engine," *Fuel*, Vol.95, pp.247–256.

Pundir, B,P.(2010), " IC engines: combustion and emissions," *Narosa Publishing House.*

Pulkrabek, W. (2003), "Engineering fundamentals of internal combustion engine," Prentice hall, New Jersey , 2nd edition, Chapter 4, pp. 148.

Quader, A. (1973), "Effects of spark location and combustion duration on nitric oxide and hydrocarbon emissions," *SAE Technical Paper 730153* 1973; doi:10.4271/730153.

Rakopoulos, C.D. (1993), " Evaluation of a spark ignition engine cycle using first and second law analysis techniques," *Energy Conversion and Management*, Vol. 34(12), pp. 1299-1314

Rakopoulos, C.D. and Kyritsis, D.C. (2006), "Hydrogen enrichment effects on the second law analysis of natural and landfill gas combustion in engine cylinders," *International Journal of Hydrogen Energy*, Vol. 31, pp. 1384 – 1393.

Rakopoulos, C.D., Kosmadakis, G.M. and Pariotis, E.G. (2009), "Evaluation of a new computational fluid dynamics model for internal combustion engines using hydrogen under motoring conditions," *Energy*. Vol. 34, pp. 2158–2166.

Rakopoulos C.D., Michos C.N. and Giakoumis E.G. (2008), "Availability analysis of a syngas fueled spark ignition engine using a multi-zone combustion model," *Energy*, Vol. 33, pp.1378– 1398.

Shigley, S. S.(2014), " Mechanical engineering design," Mc-Graw Hill Publication, 10th Edition.

Sahoo, B.B., Sahoo, N. and Saha, U.K. (2009), "Effect of engine parameters and type of gaseous fuel on the performance of dual-fuel gas diesel engines—A critical review," *Renewable and Sustainable Energy Reviews*, Vol.13, pp.1151–1184

Sarkar, S. (1990), "Fuels and Combustion," *Orient Longman Ltd.* second edition.

Sayin, C. Hosoz, M., Canakci, M. and Kilicaslan, I..(2010), "Energy and exergy analysis of gasoline engine," *International journal of Energy Research*, DOI: 10.1002/er

Sayin, C., Kilicaslan, I., Canakci, M. and Ozsezen, N. (2005), "An experimental study of the effect of octane number higher than engine requirement on the engine performance and emissions," *Applied Thermal Engineering*, Vol.25, pp.1315-1324.

Shah, A, Per, T and Bengt, J. (2012), "Investigation of performance and emission characteristics of a heavy duty natural gas engine operated with pre-chamber spark plug and dilution with excess air and EGR," *SAE International Journal of Engines*, Vol. 5(4), pp. 1790-1801.

Shehata, M.S., and Razek, S.M.A. (2008), "Engine performance parameters and emissions reduction methods for spark ignition engine," Engineering Research Journal, Vol.120, pp. M32 – M57.

Srivastava, D. and Agarwal, A. (2013), "Laser ignition of single cylinder engine and effects of ignition location," SAE Technical Paper, paper no. 2013-01-1631: doi:10.4271/2013-01-1631.

Soylu, S., and Gerpen, J.V.(2004), " Development of empirically based burning rate sub-models for a natural gas engine," *Energy Conversion and Management*,Vol.45, pp.467–481

Srinivaas, V. and Reddy, P. (2010), "Some innovations in the design of low cost variable compression ratio 2 stroke petrol engine," *kadapa.*

Sridhar, G., Paul, P.J. and Mukunda, H.S. (2001), "Biomass derived producer gas as a reciprocating engine fuel—An experimental analysis," *Biomass and Bioenergy*, Vol. 21, pp. 61–72.

Subrahmanyam, J.P. and Gajendra, B.M.K. (2001), "Experimental investigations on the performance characteristics of a producer gas fuelled spark ignition engine," *SAE International Journal*, Paper Number: 2001-01-1189.

Subramanian, K.A. Mathad, VC. Vijay, V.K. and Subbarao, P.M.V. (2013), " Comparative evaluation of emission and fuel economy of an automotive spark ignition vehicle fuelled with methane enriched biogas and CNG using chassis dynamometer," Applied Energy, Vol.105, pp.17-29

Sudsanguan S, Chanchaowna S. (1999), "Using higher octane rating gasoline than engine requirement: loss or gain," *Research Report of King Mongkut's University of Technology, Thailand.*

Stone, R. (1997), "Introduction to internal combustion engines," *Society of Automotive Engineers Inc.*, Warrendale, USA.

Styron, J.,P., (2007), "Variable Compression Ratio Connecting Rod for Internal Combustion Engine," US7028647B2.

Tartakovsky,L., Amiel,R., Baibikov, V., Fieischman, R., Gutam, M., Poran, A. and Veinblat, M., (2015), "SI engine with direct injection of methanol reforming products – First experimental results, " SAE technical paper, 2015-32-0712.

Taylor, C.F. (1985), "The internal combustion engine in theory and practice," *The M.I.T.Press,* First Revised Edition

Thurnheer, T., Soltic, P. and Dimopoulos, E.P. (2009), "S.I. engine fuelled with gasoline, methane and methane/hydrogen blends: heat release and loss analysis," *International Journal of Hydrogen Energy*, Vol.34, pp.2494-2503

Turkoz, N., Erkus, B.M., Karamangil, I., Sürmen, A. and Arslanog, N. (2014), "Experimental investigation of the effect of E85 on engine performance and emissions under various ignition timings," *Fuel*, Vo.115, pp. 826-832

Wang, J., Huang, Z., Lui, B. and Wang, X. (2009), "Simulation of combustion in spark ignition engine fueled with natural gas hydrogen blends combined with EGR," *Frontier Energy Power Engineering China*, Vol. 3(2), pp.204-211.

Welsh, H.W., Riley, C.T.(1971), " The Variable Displacement Engine, An Advanced Concept Power Plant," SAE technical Paper 710830.

Wentworth, J. (1976), "Effects of combustion chamber shape and spark location on exhaust nitric oxide and hydrocarbon emissions," *SAE Technical Paper* 740529; doi:10.4271/740529.

Witze, P. (1982), "The effect of spark location on combustion in a variable-swirl engine. *SAE Technical Paper* 820044; doi:10.4271/820044.

Wittek, K., Tiemann, C., and Pischinger, S. (2009),"Two-stage variable compression ratio with eccentric piston pin and exploitation of crank train forces," *SAE Int. J. Engines,* Vol. 2(1), pp.:1304-1313.

Wirbeleit, F.G., Binder, K. and Gwinner, D. (1990), "Development of piston with variable compression height for increasing efficiency and specific power output of combustion engines," SAE technical paper no 900229.

Wu, Y.Y., Chen, B.C., Hsieh, F.C. and Ke, C.T. (2009), "Heat transfer model for small-scale spark-ignition engines," *International Journal of Heat and Mass Transfer*, Vol. 52, pp.1875–1886

Wu, Y.Y., Chen B.C. and Hsieh, F.C. (2006), "Heat transfer model for small-scale air-cooled spark-ignition four-stroke engines," *International Journal of Heat and Mass Transfer*, Vol. 49, pp.3895–3905

Xie, F.X., Li, X.P. and Wang, X.C., Su, Y. (2013), "Research on using EGR and ignition timing to control load of a spark-ignition engine fuelled with methanol," *Applied Thermal Engineering*, Vol. 50, pp.1084-1091

Yamin, J.A.A. and Dado, M. H. (2004), "Performance simulation of a four-stroke engine with variable stroke length and compression ratio," Applied *Energy*, Vol.77, pp. 447-463.

Yamin, J.A., Badran, O.O. (2002), "Analytical study to minimise the heat losses from a propane

powered 4-stroke spark ignition engine ," Renewable Energy, Vol. 27 , pp.463–478

Yingjian, Li, Qi, Qiu , Xiangzhu, He and Jiezhi, Li (2014), " Energy balance and efficiency analysis for power generation in internal combustion engine sets using biogas," Sustainable Energy Technologies and Assessments, Vol. 6,pp.25–33

Yuh and Tohru (2010), "The effect of higher compression ratio in 2 strokes engine," *Yannaha motor co Ltd.*, pp. 355-362.

Zhang, Z., Zhang, H., Wang, T. and Jia, M. (2014), "Effect of tumble combined with EGR (exhaust gas recirculation) on combustion and emission in spark ignition engines at part load," *Energy*, Vol. 65, pp.18-24.

Zheng, W. and Huang (2009), "Effect of compression ratio on the performance and combustion of natural gas direct injection engine," *Journal of automobile engineering*, Vol. 223.

APPENDIX-A

NOVEL VCR MECHANISM

I. Theoretical determination of Compression ratio for VCR mechanism

For one (360^0) complete rotation of the ball screw, the secondary piston is linearly displaced by distance equal to thread pitch inside the geometric clearance volume (Fig.4.3). Thereby reduces the actual clearance volume and help to increase the compression ratio of the engine.

With the help of VCR mechanism the secondary piston could be travelled through the clearance volume at calculated steps to the maximum distance equal to clearance volume depth . The theoretical compression ratios have been found from

$$V_C' = V_C - \Delta V \quad \text{(Eq-A-1)}$$

$$CR = \frac{V_C' + V_D}{V_C'} \quad \text{(Eq-A-2)}$$

Where, V_C' is the clearance volume of the cylinder

ΔV is the volume of secondary piston protruded inside clearance volume

V_C is the geometric clearance volume as specified by the manufacturer of the engine

V_D is the swept volume of cylinder, and

CR is the compression ratio of the engine

II. Novel VCR settings for Honda engine

As per the specifications of the Honda engine for the bore diameter 52 mm and stroke 46 mm maintained at CR 4.81, the clearance volume is 25.52 cc. The bore diameter is fixed, but owing to some oblique shape of the clearance volume, the depth of clearance volume could be 9 mm. Following this the theoretical compression ratio can be evaluated over fixed CR as provided by the manufacturer. The Table A-1 shows the variation of CR with the stepped displacement of the ball screw. The original Clearance Volume is $V_C = 25.52\ cc$

The Ball Screw that we chose for this mechanism is a 12 x 2 ball screw which implies that root diameter is 12 mm and pitch is 2mm. The Stepper Motor is rotated in steps of 180^o which implies that the ball nut moves 0.5mm downward which in turn moves the piston 1mm

inside the Clearance volume, thereby reducing the clearance volume and the compression ratio increases.

Change in clearance volume, $\Delta V = \frac{\pi \times (dia.of\ secondary\ piston)^2 \times distance\ moved\ in\ 1\ step}{4}$

In 1st step, when the stepper motor rotates for the first 180^0 the secondary piston moves 1 mm so the change in clearance volume, $\Delta V = \frac{\pi \times 30^2 \times 1 \times 10^{-3}}{4} = 0.707\ cc$

Therefore, New clearance volume, $V_C` = V_C - \Delta V = 24.813\ cc$

Therefore, New Compression ratio $r` = 1 + \frac{V_d}{V_c`} = 4.91$

Similarly other new compression ratios can be found out.

Table A-1 Theoretical values of compression ratio for Honda Engine

Distance Moved by Auxilary Piston (mm)	New Clearance Volume (cc)	Change in Clearance Volume (cc)	New Compression Ratio
0	25.52	0	4.8
1	24.813	0.707	4.91
2	24.106	1.413	5.02
3	23.399	2.120	5.14
4	22.692	2.820	5.27
5	21.985	3.530	5.40

The Fig. A-1 shows the theoretical curve for compression ratio(CR) which could be found increasing with increment of protrusion length of secondary piston. The experimental CR considering least count of ball screw and measured actual displacement for one complete rotation has been calculated with variation of 1.4%

III. Experimental determination of Compression ratio for VCR mechanism in Honda engine

The clearance volume of the new engine head along with the gaskets was measured using Wheat flour dough and was averaged out to be 28.91 cc. The original clearance volume was 25.52 cc. The clearance volume measured was $V_C = 28.91\ cc$

Similarly following above steps clearance volume, $V_C` = V_C - \Delta V = 28.203\ cc$

Experimental new Compression ratio $r` = 1 + \frac{V_d}{V_c`} = 4.36$

Similarly other compression ratios can be found.

$$\%\,error\,in\,clearance\,volume = \frac{change\ \ in\ clearance\ volume}{Original\ clearance\ volume} \times 100$$

$$\%\ error = 13.28\%$$

The percentage error in clearance volume was 13.28%. Table 4.2 shows experimentally calculated values of different compression ratios.

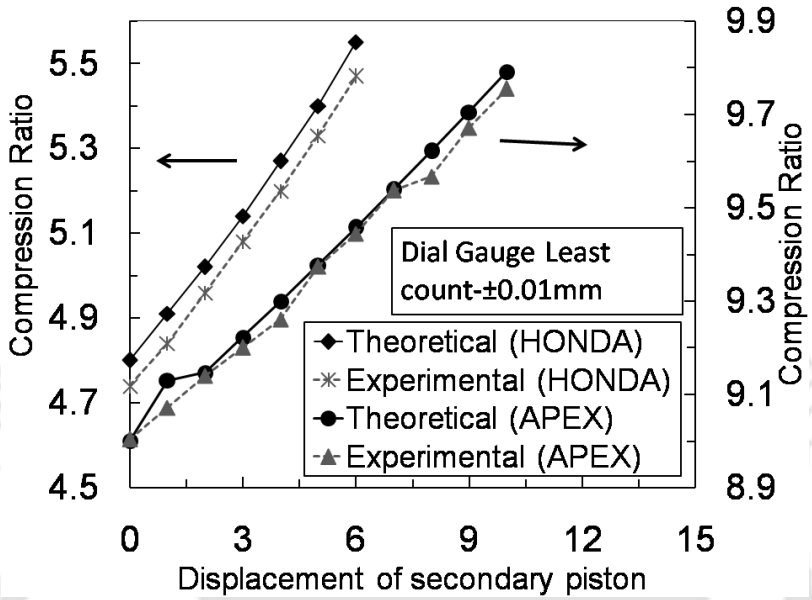

Fig.A-1 Compression ratio with theoretical and experimental method for HONDA and Large VCR engine (APEX)

Table A-2 Experimental values of compression ratio

Distance Moved by Auxilary Piston (mm)	New Clearance Volume (cc)	Change in Clearance Volume (cc)	New Compression Ratio
0	28.91	0	4.36
1	28.203	0.707	4.44
2	27.496	1.413	4.52
3	26.789	2.120	4.62
4	26.082	2.820	4.72
5	25.375	3.530	4.82
6	24.668	4.24	4.93

So with the new engine head and the VCR mechanism the engine now has the capability to vary its compression ratio from 4.36 to 4.93.

IV. Novel VCR settings for large VCR(APEX)engine

The method of CR variation followed for large VCR engine (Make:APEX) is similar to that followed for small Honda engine.

Table A-3 Compression ratio with Novel VCR mechanism for large VCR engine

CR	Cylinder bore, cm	Clearance volume, cc	auxiliary piston displacement, cm	auxiliary piston volume, cc	new clearance volume. cc	new compression ratio
10	8.75	73.46	0	0.00	73.46	10.00
10	8.75	73.46	0.1	0.75	72.71	10.09
10	8.75	73.46	0.2	1.50	71.96	10.19
10	8.75	73.46	0.3	2.25	71.21	10.28
10	8.75	73.46	0.4	3.00	70.46	10.38
10	8.75	73.46	0.5	3.75	69.71	10.48
10	8.75	73.46	0.6	4.50	68.96	10.59
10	8.75	73.46	0.7	5.25	68.21	10.69
10	8.75	73.46	0.8	6.00	67.46	10.80
10	8.75	73.46	0.9	6.75	66.71	10.91
10	8.75	73.46	1	7.50	65.96	11.02
10	8.75	73.46	1.1	8.24	65.21	11.14
10	8.75	73.46	1.2	8.99	64.46	11.26

In case of large VCR engine the bore diameter is 87.5 mm and stroke length is 111 mm. The swept volume of cylinder is 661.11 cc.

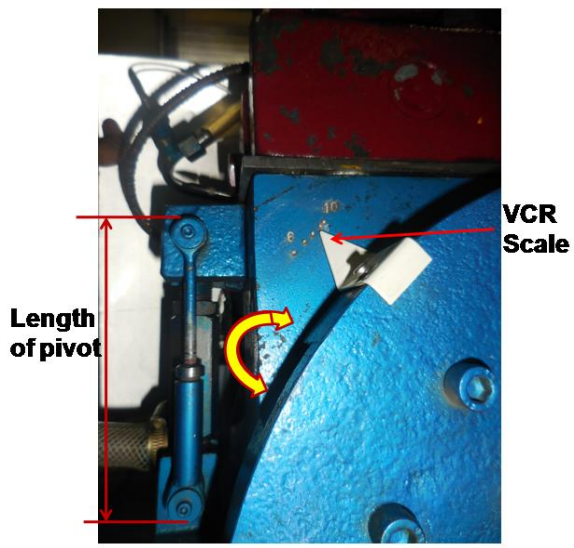

Fig. A-2(a) The linear displacement of pivot for particular CR on Tilting block set up.

If the engine is maintained at CR10 as tabulated in Table A-3, the clearance volume becomes 73.46 cc. As the clearance volume maintains a cylindrical shape, the depth of clearance volume can be calculated and is equal to 12.2 mm. So, if the novel VCR mechanism is installed over conventional engine, then secondary piston of 30.9 mm diameter have the scope to protrude up to 12 mm inside combustion chamber. Accordingly, there is possible increment in CR from CR10 to CR11.26 over fixed CR10.

V. Simultaneous VCR settings for large VCR (APEX) engine

The method of pivot displacement with CR of tilting block is followed for calculation of simultaneous coordination of CR. The Tiltimg block VCR follows the parabolic nature of pivot displacement which is plotted as shown in Fig.A-2.

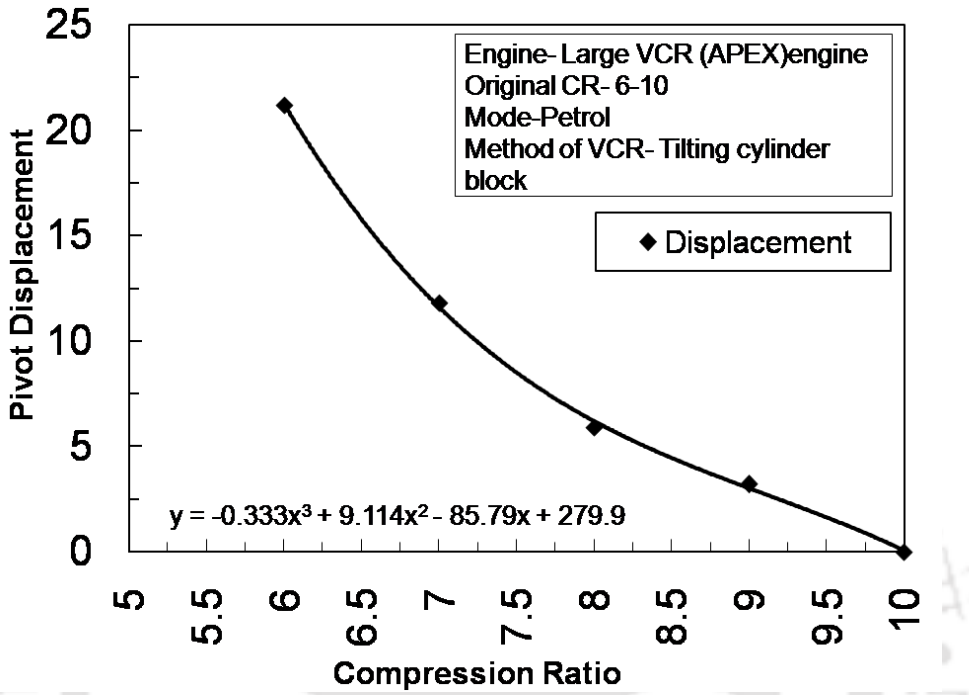

Fig. A-2 (b)The linear displacement of pivot for particular CR on Tilting block set up.

So, with the equation followed upto 3 polynomials the new CR could be attained by simultaneous adjustment of tilting as well as novel VCR mechanisms. The Table A-4 will show the displacement of pivot for particular secondary piston displacement.

Table A-4 Pivot length for particular constant CR

CR	Secondary piston displacement, mm			
	0	2	5	10
10	0	1	1.8	2.8
9	3.2	4	4.2	5.2
8	5.9	6.8	7.5	8.8
7	11.8	12.33	13.26	14.78
6	21.2	22.09	23.13	24.91

VI. Calibration of Novel VCR mechanism

The calibration of novel VCR mechanism is important from the view point of attaining the optimum CR with operating secondary piston as discussed in Fig.3.1. The displacement of secondary piston occurred due to 180^0/ 360^0/ 540^0/ 720^0 rotation of ball screw is 1mm/ 2mm/ 3mm/ 4mm respectively which is invisible inside combustion chamber. In order to confirm

about the rectilinear displacement of calculated distance, the trials are performed on the novel VCR mechanism. The calibration facility is as shown in Fig. A-3.

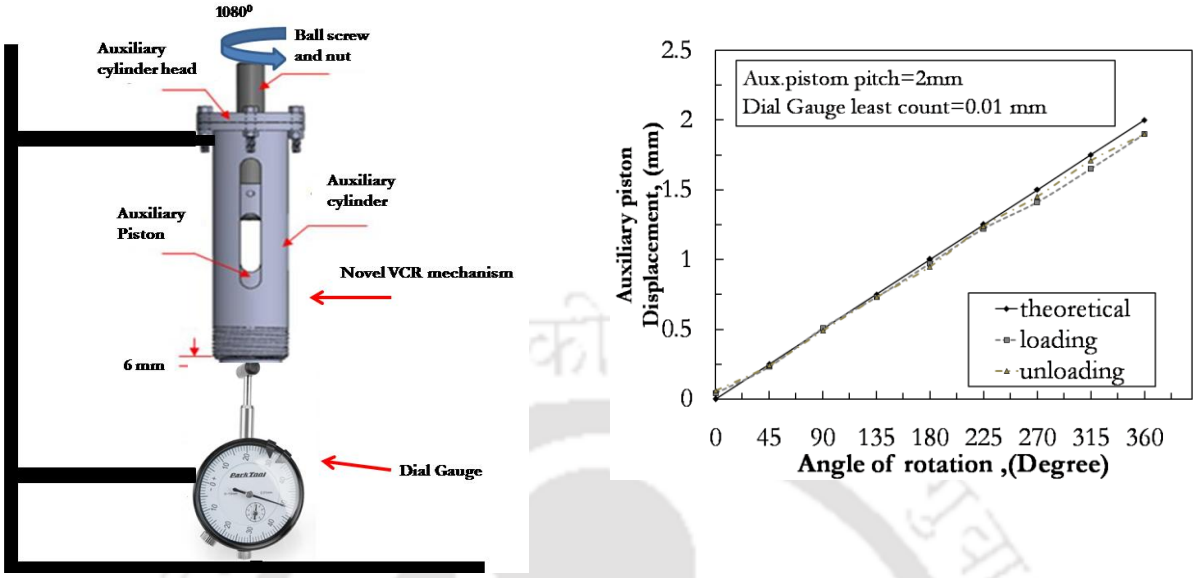

Fig. A-3 (a) Schematic diagram of calibration set up for novel VCR mechanism; (b) the calibration curve with loading and unloading

That is the reason, the magnitude by which the CR to be controlled is measured in the Fig.4.8. The dial gauge (Make: Omega) having least count 0.01 mm is used for measurement of linear travel of secondary piston caused by the controlled rotation of ball screw. For anticlockwise rotation, the set of data collected called as forward stroke and again the ball screw is rotated in clockwise direction called as return stroke to reach to original position.

VII. Technical drawings of the system

1. Ball Nut

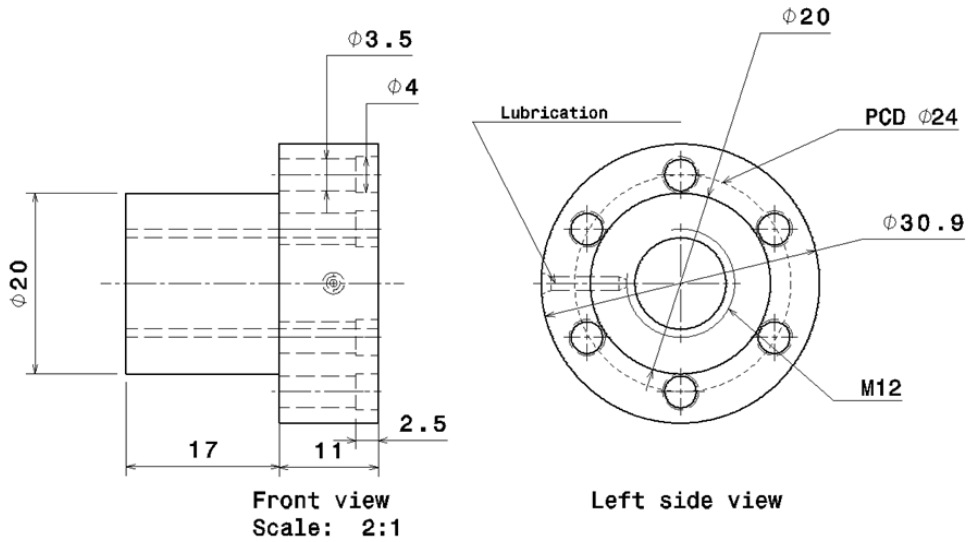

All dimensions are in 'mm'.

Fig. A-4 Ball nut of ball screw mechanism

2. secondary cylinder

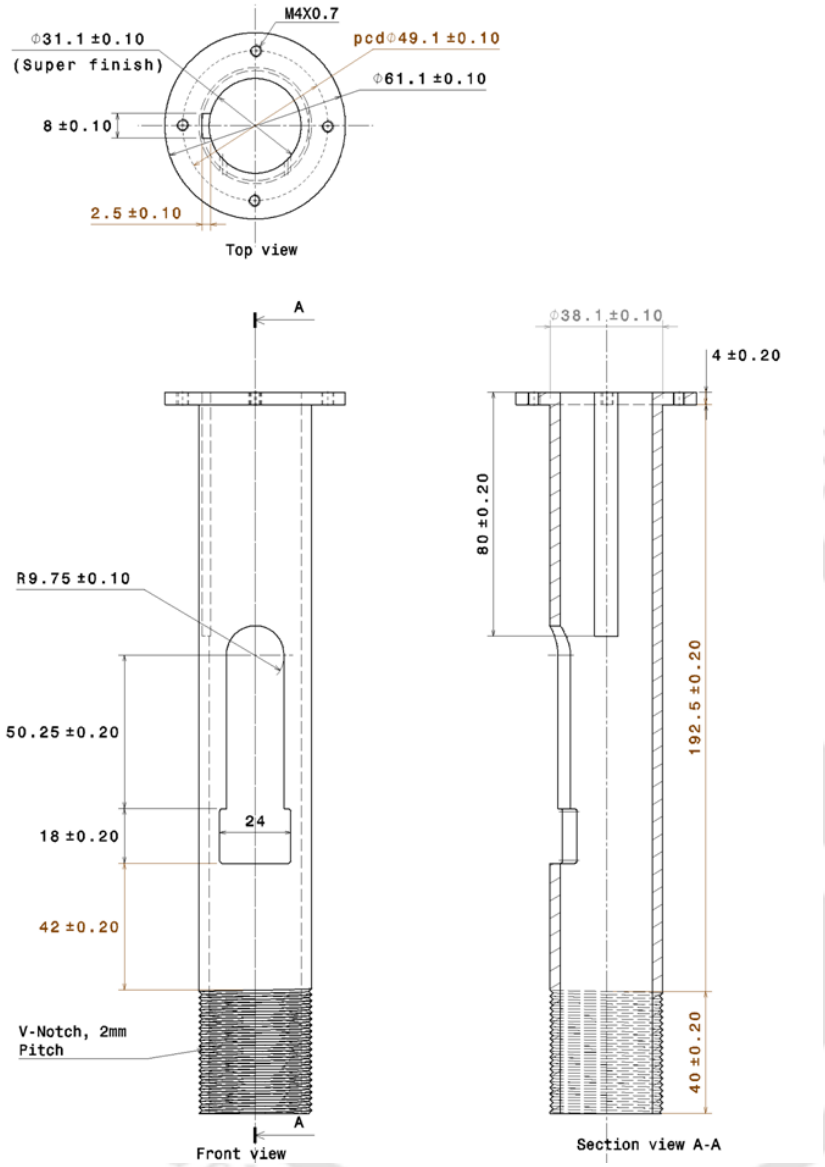

All dimensions are in 'mm'.

Fig. A-5 Secondary cylinder of novel VCR mechanism.

3. Secondary Piston

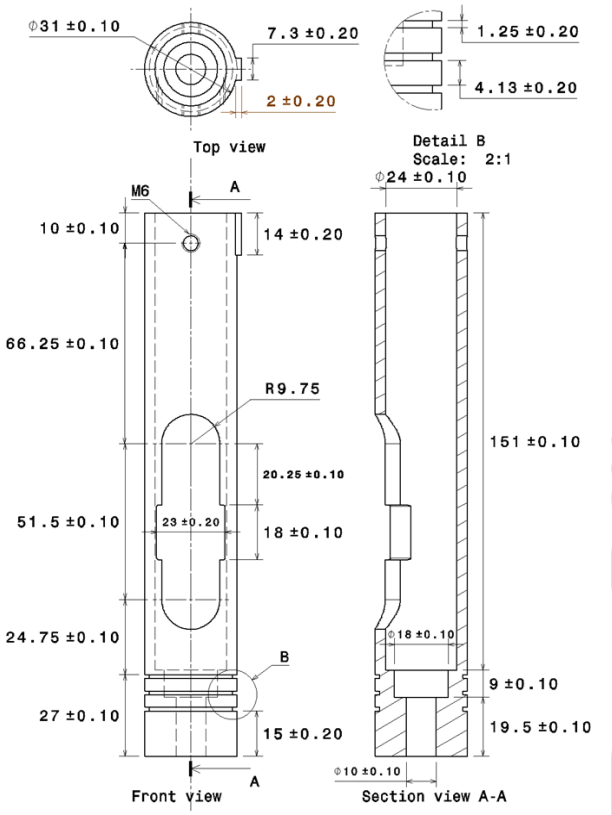

All dimensions are in 'mm'.

Fig. A-6 Secondary piston of novel VCR mechanism.

4. Secondary cylinder head

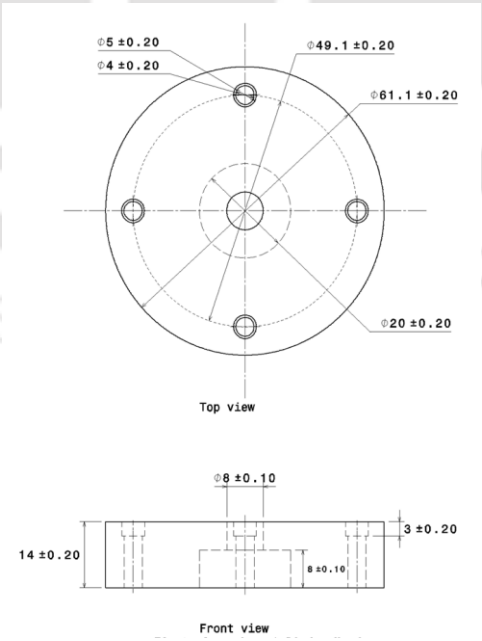

All dimensions are in 'mm'.

Fig. A-7 Secondary cylinder head of novel VCR mechanism.

5. Ball screw system

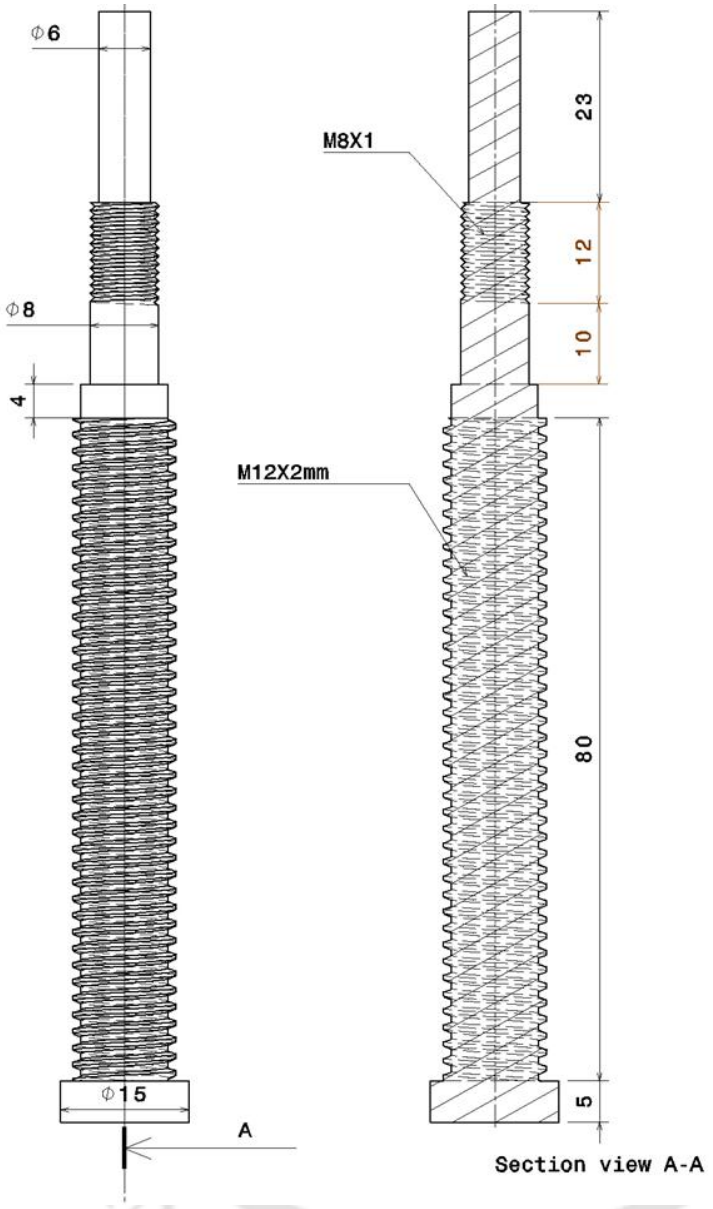

All dimensions are in 'mm'.

Fig. A-8 Ball screw of novel VCR mechanism.

6. Piston holder

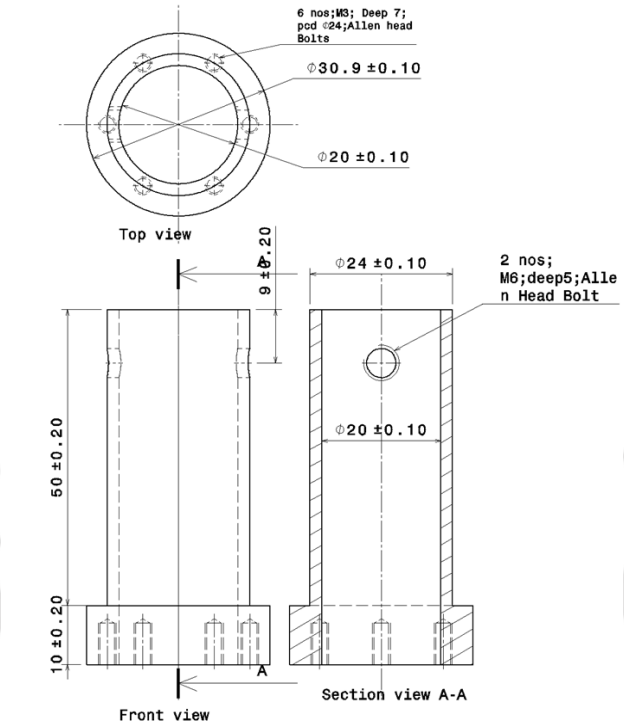

All dimensions are in 'mm'.

Fig. A-9 Secondary Piston holder of novel VCR mechanism

APPENDIX-B

Specifications of the Equipments

I. Large VCR engine experimental bench.

Table B-1. VCR engine specifications

System specifications	
Parameter	*Specification*
Product	Research engine test setup, Code 240
Type	Research Engine test setup 1 cylinder, 4 stroke, Multi-fuel VCR with open ECU for petrol mode (Computerized)
Power	4.5 KW @ 1800 rpm, Speed range 1200-1800 rpm.
Type of cooling	Water cooled
CR range	6:1-10:1
Combustion chamber	Hemispherical bowl in piston type
Dynamometer	Eddy current type, water cooled with loading unit
Air box	MS fabricated with orifice meter and manometer (100 - 0 - 100)
Fuel tank	Capacity 15 lit with measuring tube (0-450 ml)
Calorimeter	Pipe in pipe type
Rotameters	Engine cooling 40-400 lph, calorimeter 25-250 lph
Data acquisition Software	'Enginesoft' engine performance analysis software
Transmitters, sensors and indicators	
Fuel flow transmitter	DP transmitter, range 0-500 mm WC
Air flow transmitter	Pressure transmitter (-) 250 mm WC
Pressure sensors	Piezo type, range 5000 PSI, with low noise cable
Temperature sensors and transmitters	PT100 (RTD) type, range 0-100º C, output 4-20 mA (4 nos) K (ungrounded) type, range 0-1200º C, output 4-20 mA (2 nos)
Load sensor and indicator	Strain gauge type load cell with digital indicator, range 0-50 kg
Speed sensor and indicator	Resolution 1º, range (5500 rpm) with TDC pulse
Data acquisition device	NI USB-6210, 16-bit, 250 kS/s
Setup constants	
Pulse per revolution	360º
No. of cycles	10
Fuel measuring interval	60 s
Speed scanning intervals	2000 ms

System specifications	
Parameter	*Specification*
Bore × Stroke	87.5 mm × 110 mm
Capacity	661 cc
Orifice diameter	20 mm
Dynamometer arm length	185 mm
Connecting rod length	234 mm
Theoretical constants	
Orifice coefficient of discharge	0.6
Specific heat of exhaust gas	1.00 – 1.25 kJ/kg-K
Specific heat of water	4.186 kJ/kg-K
Density of Air	1.174 kg/m^3

II. Emission Analyzer Specifications

Table B-2 The specifications of Testo 350 S/M/XL flue gas analyzer

Sl. No.	Measured gas	Resolution	Accuracy	Range
1	O_2	0.1%	± 0.8%	0 – 25%
2	CO	1 ppm	± 10 ppm < 200 ppm ± 5% reading < 2000 ppm ± 10% reading > 2000 ppm	0 – 10000 ppm
3	CO_2	0.01% vol. < 25% 0.1% vol. > 25%	± 0.3% vol. < 25% ± 0.5% vol. > 25%	0 – 50%
4	NO	1 ppm	± 5 ppm < 100 ppm ± 5% reading < 2000 ppm ± 10% reading > 2000 ppm	0 – 3000 ppm
5	NO_2	0.1 ppm	± 5 ppm < 100 ppm ± 5% reading > 100 ppm	0 – 500 ppm
6	HC	1 ppm	400 ppm < 4000 ppm 10% reading > 4000 ppm	0 – 40000 ppm

III. Chromatography Analyzer Specifications

Table B-3 GFM 406 for biogas technical specification

Gas Measurement	Range(Resolution)	Typical Accuracy
Methane	0-100% v/v	0.3%@5% 1.0%@60% 2.0%@100%
Carbon Dioxide	0-100% v/v	0.3%@5% 1.0%@60% 2.0%@100%
Oxygen	0-25% v/v	0.1%
Hydrogen Sulphide	0-5000 ppm v/v	10 ppm
Differential pressure measurement	+/-30 mB	0.5 mbar
Vane anemometer	0-40 m/s(0.1)	0.5 m/s
Temperature probe	-10-100^{0}C	0.2^{0}C

IV. Novel VCR Ball Screw catalog

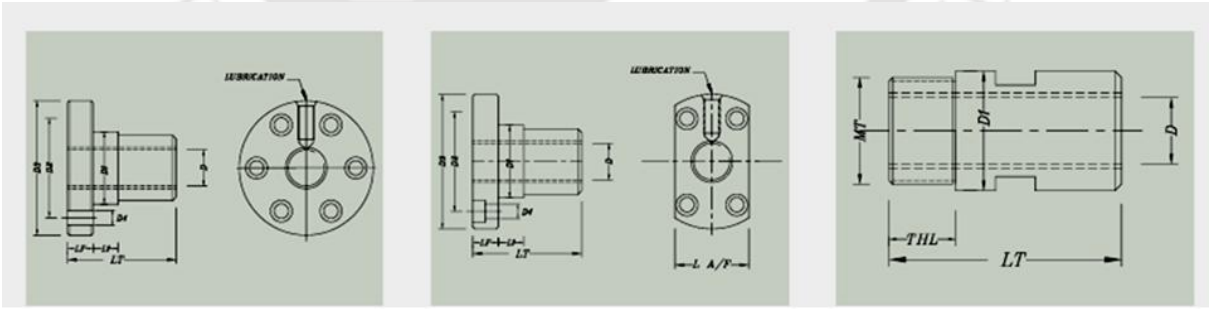

Fig.B-1 The Ball nut design

Table B-4 The Catalog for ball screw selection (IAR,Pune)

V.

IAR FLANGED NUT SERIES 1011 AND 1012 DETIALS ARE IN FOLLOWING TABLE. AND ALSO CUSTOM DESIGNS ARE ALSO AVAILABLE.

	NUT DIAMENSIONS													LOAD RATINGS N	
MODEL	NOM. DIA.	LEAD	BALL DIA	NO. OF CIRCUITS	D	D1	D2	D3	D4	L A/F	LF	L1	LT	DYNAMIC N	STATIC N
IAR 5X0.5	5	0.5	Ø0.3	3	5	12	18	24	3.3	14	8	6	25	80	130
IAR 5X1	5	1	Ø0.6	3	5	12	18	24	3.3	14	10	6	25	170	240
IAR 8X1	8	1	Ø0.6	3	8	16	22	30	4.2	18	10	6	25	400	540
IAR 10X1	10	1	Ø0.6	3	10	18	24	32	4.2	20	12	6	28	600	940
IAR 12X1	12	1	Ø0.6	3	12	20	26	34	4.2	14	12	6	30	600	1100
IAR 5X1.5	5	1.5	Ø1	3	5	12	18	24	3.3	14	10	6	25	640	860
IAR 8X1.5	8	1.5	Ø1	4	8	16	22	30	4.2	18	12	6	30	1200	1800
IAR 10X1.5	10	1.5	Ø1	3	10	18	24	32	4.2	20	12	6	30	1600	2200
IAR 12X1.5	12	1.5	Ø1	3	12	21	26	32	4.2	22	10	6	30	2000	2800
IAR 8X2	8	2	Ø1.58	4	8	20	26	32	4.2	22	10	6	35	2000	2100
IAR 10X2	10	2	Ø1.58	4	10	22	28	34	4.2	24	10	6	35	2200	2100
IAR 12X2	12	2	Ø1.58	4	12	24	29	34	4.2	24	12	6	35	2500	3400

IAR FLANGED NUT SERIES 1013 DETIALS ARE IN FOLLOWING TABLE. AND ALSO CUSTOM DESIGN IS ALSO AVAILABLE.

	NUT DIAMENSIONS								LOAD RATINGS	
MODEL	NOM. DIA.	LEAD	BALL DIA.	NO. OF CIRCUITS	D	D1	MT	TL	LT	DYNAMIC N	STATIC N
IAR 5X0.5	5	0.5	Ø0.3	3	5	15	12X1	10	36	80	130
IAR 5X1	5	1	Ø0.6	3	5	15	10x1	10	36	170	240
IAR 8X1	8	1	Ø0.6	3	8	18	15X1	12	40	400	540
IAR 10X1	10	1	Ø0.6	3	10	22	17X1	12	42	600	940
IAR 12X1	12	1	Ø0.6	3	12	25	20X1.5	15	50	600	1100
IAR 5X1.5	5	1.5	Ø1	3	5	15	10x1	10	36	640	860
IAR 8X1.5	8	1.5	Ø1	4	8	20	15X1	12	40	1200	1800
IAR 10X1.5	10	1.5	Ø1	3	10	22	17X1	12	42	1600	2200
IAR 12X1.5	12	1.5	Ø1	3	12	24	20X1.5	15	50	2000	2800
IAR 8X2	8	2	Ø1.58	4	8	20	15X1	12	40	2000	2100
IAR 10X2	10	2	Ø1.58	4	10	22	17X1	12	42	2200	2100
IAR 12X2	12	2	Ø1.58	4	12	24	20X1.5	15	50	2500	3400

All dimensions are in mm. Standard supply is RH Ball Screw. Ball Screw with LH orientation can be supplied on request.
Above dimensions may change as and when decided by Institute of Applied Research

APPENDIX-C

Equations for Performance and Combustion Analysis

I. Performance Analysis:

(i) Brake power (BP):

$$BP = \frac{2 \times 3.124 \times N \times W \times r}{60 \times 1000}, kW \qquad \text{(Eq-C-1)}$$

where N, W and r are the speed of the engine (rpm), engine load (kg-m/s^2) and dynamometer arm radius (m), respectively.

(ii) Brake thermal efficiency (BTE):

$$\eta_{bthe} = \frac{BP}{\dot{m}_{fuel} \times LHV_{fuel}} \times 100,\% \qquad \text{(Eq-C-2)}$$

where m_{fuel} (kg/s) is the fuel mass flow rate , and LHV_{fuel} (kJ/kg) is the lower heating values of fuel .

(iii) Brake specific fuel consumption (BSFC):

$$BSFC = \left[\frac{m_{fuel}}{BP} \times 3600\right]; \quad \frac{\left(kg/h\right)_{fuel}}{kW_{output}} \qquad \text{(Eq-C-3)}$$

$$m_{fuel} = \left[\rho_{fuel} \times \frac{cc}{\min} \times 10^{-6} \times 60\right]; \quad kg/hr \qquad \text{(Eq-C-4)}$$

Where, m_{fuel} and LHV_{fuel} are the mass flow rate(s) and the lower heating vale(s) of the fuel(s) used ρ_{fuel} density of the fuel.

(iv) Volumetric efficiency (VE):

$$\eta_{vol} = \frac{\dot{m}_a\,(kg/s)\times 3600}{(3.142/4)\times D^2 \times L \times N/n \times 60 \times K \times \rho_a} \times 100, \% \qquad \text{(Eq-C-5)}$$

$$\text{Where, } \dot{m}_a = C_d \times \frac{\pi}{4} \times d_o{}^2 \times \sqrt{\left(2 \times 9.81 \times h \times \frac{\rho_w}{\rho_a}\right)} \times 3600 \times \rho_a; \quad kg/hr \qquad \text{(Eq-C-6)}$$

where C_d, d_o , h, ρ_w, and ρ_a are coefficient of discharge, diameter of the orifice of air flow (m), manometer reading across orifice (m), water density (kg/m^3) and the density of ambient air (kg/m^3), respectively.

(v) Stoichiometric air-fuel ratio of LPG (λ):

The complete combustion of POME with air generates following equation

$$0.7C_3H_8 + 0.3C_4H_{10} + 5.45[O_2 + 3.76N_2] = 3.3[CO_2] + 4.3[H_2O] + 20.492[N_2] \qquad \text{(Eq-C-7)}$$

Therefore, stoichiometric air-fuel ratio (λ)

$$= \frac{mole\ of\ \ aiir}{mole\ of\ \ fuel} \times \frac{molecular\ \ weight\ \ of\ \ air}{molecular\ \ weight\ of\ \ fuel} \qquad \text{(Eq- C-8)}$$

$$= 15.52$$

II. Combustion Analysis:

(i) Pressure smoothing:

The DAC can record cylinder pressure variation with each degree of crank angle change. Differentiating the raw pressure data shows a noisy trend between successive values. Therefore after treatment of these pressure data in the form of smoothing becomes necessary (Stone 1997). For this the smoothing algorithm for (2b+1) value is used as follows:

$$P_n = \frac{1}{b^2}\left[P_{n-(b-1)} + 2P_{n-(b-2)} + 3P_{n-(b-3)} + \ldots + bP_n + \ldots + 3P_{n+(b-3)} + 2P_{n+(b-2)} + P_{n+(b-1)}\right] \qquad \text{(Eq-C-9)}$$

The terms in Eq. (A6) are only evaluated when the part of the subscript in bracket is not negative. This is illustrated by simplest case when *b = 2*

$$P_n = \frac{(P_{n-1}) + 2(P_n) + (P_{n+1})}{4} \qquad \text{(Eq-C-10)}$$

Where, '*p'* is the instantaneous pressure data. The above equation is used for smoothing the instantaneous pressure data.

(ii) Rate of pressure rise:

The rate of pressure rise calculated from the smoothened pressure data by using first order finite difference equation with fourth order accuracy (Stone 1997).

$$\frac{dP}{d\theta} = \frac{(P_{n-2}) - 8(P_{n-1}) + 8(P_{n+1}) - (P_{n+2})}{12(\Delta\theta)} \qquad \text{(Eq-C-11)}$$

Where 'p' is the instantaneous pressure data and '$\Delta\theta$' is successive change of crank angle.

(iii) Rate of change of volume

$$\frac{dV}{d\theta} = \frac{V_{n+1} - V_n}{\theta_{n+1} - \theta_n} \qquad \text{(Eq-C-12)}$$

Where, V is volume of combustion chamber at crank angle θ.

(iv) Net Heat release rate:

The equation used for net heat release rate is obtained from the first law analysis by implementing rate of pressure rise and rate of volume change, which is given below.

$$\frac{dQ_n}{d\theta} = \left(\frac{\gamma}{\gamma - 1} \times P \times \frac{dV}{d\theta}\right) + \left(\frac{1}{\gamma - 1} \times V \times \frac{dP}{d\theta}\right) \qquad \text{(Eq-C-13)}$$

Where, $\frac{dQ_n}{d\theta}$ is the net heat release rate, γ is the ratio of specific heats, P the cylinder pressure, V the instantaneous volume of the cylinder. The ranges of γ varies from 1.3 to 1.35 (Heywood, 1988; Pundir, 2010). Here required rate of change of pressure with crank angle is obtained as in Eq.C-8 (Stone 1997).

(iv) Mass fraction burned at various crank angles can be evaluated using Eq.3. (Rakopoulos et al.,2008). With the results evaluated for NHRR from pressure curve the MFB can be calculated by (Stone 1997).

$$MFB = \frac{\sum_{0}^{i} \Delta P_C'}{\sum_{0}^{N} \Delta P_C'} \qquad \text{(Eq-C-14)}$$

$$\Delta P_C = P_{i+1} - P_i \left(\frac{V_i}{V_{i+1}}\right)^k \qquad \text{(Eq-C-15)}$$

$$\text{So, } \Delta P_C' = \Delta P_C \left(\frac{V_i}{V_C} \right) \qquad \text{(Eq-C-16)}$$

Where, ΔP_C is the pressure rise due to combustion; $\Delta P_C'$ is the referenced pressure rise; k is constant of polytropic process.

(v) Mean gas temperature (MGT) is evaluated using Eq. 4 (Heywood, 1988)

$$MGT = \frac{P_\theta \times \left\{ V_c + \left[\frac{\pi D^2}{4} \times \left[l + r - r \left(\cos\theta + \frac{l}{r} \left(1 - 0.5 \times \left(\frac{r}{l} \right)^2 \times (0.5 - 0.5\cos 2\theta) \right) \right) \right] \right] \right\}}{\rho_a \times V_\theta \times R} \qquad \text{(Eq.C-17)}$$

Where, P_θ is the pressure per degree of crank angle (N/m^2), V_c the clearance volume (m^3), D is the bore diameter (m), l is the stroke length (m), r is the crank radius (m), θ is the crank angle $(\text{deg}ree)$, ρ is the density of air (kg/m^3), V_θ is the total cylinder volume at crank angle (m^3), R is the specific gas constant (kJ/kgK).

(vi) Cycle-by-cycle variation in indicated work per cycle of is known as coefficient of variance (COV) that can be calculated using (Eq.5-7)(Porpatham et al., 2012).

$$COV_{IMEP} = \frac{IMEP_{STD}}{IMEP_{mean}} \times 100 \qquad \text{(Eq-C-18)}$$

$$IMEP_{STD} = \frac{1}{m} \left(\sqrt{\left(\sum_{i=1}^{m} \left(Pi_{\max} - P_{\max} \right) \right)} \right) \qquad \text{(Eq-C-19)}$$

$$IMEP_{mean} = \frac{1}{m} \left(\sum_{i=1}^{m} Pi_{\max} \right) \qquad \text{(Eq-C-20)}$$

Where, COV_{IMEP} is the coefficient of variation of $IMEP$ for m-consecutive cycles. $IMEP_{STD}$= Standard deviation of maximum in cylinder pressure; $Pi_{\max}$ = Maximum in cylinder pressure of ith cycle; $P_{\max}$ = Average of maximum in cylinder pressure of m- cycles; m = No of cycles.

(vii) Percentage EGR can be evaluated where the exhaust gas is recirculated through the orifice for gas flow measurement. The water column manometer level difference h_{ex} across orifice meter decides the percentage of EGR using **Eqs.1-3**(Heywood,1988)

$$R_{EGR} = \frac{\dot{m}_{EGR}}{\dot{m}_i} \times 100 \quad \text{(Eq-C-21)}$$

$$\dot{m}_{EGR} = Cd \times \left(\frac{\pi}{4} \times d_{exo}{}^2 \right) \times \rho_{ex} \times \left(\sqrt{\left(2 \times 9.81 \times \left(\frac{\rho_W}{\rho_{ex}} \right) \times h_{ex} \right)} \right) \times 3600 \quad \text{(Eq-C-22)}$$

$$\dot{m}_i = m_{air} + \dot{m}_{EGR} + m_{fuel} \quad \text{(Eq-C-23)}$$

(viii) Ignition delay- It is the crank angle during which flame kernel develops after spark ignition

$$\Delta\theta_d = \left(\theta_{IT} - \theta_{10\%MFB} \right) \quad \text{(Eq-C-24)}$$

(ix) Combustion duration- The crank angle required to burn most of the mixture

$$\Delta\theta_b = \left(\theta_{90\%MFB} - \theta_{10\%MFB} \right) \quad \text{(Eq-C-25)}$$

The standard fuel IT is obtained from the PE3 monitor software. The ITs, other than the standard one are obtained from the fuel pressure data stored during data acquisition. The crank angle at which combustion starts is obtained from the $\frac{dP}{d\theta}$ diagram as it changes its concavity when combustion starts.

APPENDIX-D

APPENDIX-D

1. Uncertainty of experiment

The percent variation in experimental data are those factors that are always vague to some extent and carry some amount of uncertainty. It is important to know how uncertin a particular observation may be and to devise a consistent way of specifying the uncertanity in analytical form.The more precise method of estimating uncertainty in experimental results has been presented by Kline and McClintock as well as Moffat by sequential perturbation technique (Kline and McClintock,1953; Moffat,1982, Holman,1996). If N is a dependant measuring parameter which is a function of the independent variables x_1, x_2 , x_3 , x_4,…., x_n . Therefore,

$$N = N(x_1, x_2, ..., x_n) \qquad \text{(Eq-D-1)}$$

If ΔN is the uncertainty created due to the individual uncertainties of the independent parameters termed as ΔN_1, ΔN_2, ΔN_3, ΔN_4,….., ΔN_n. Then the uncertainty of the dependent variable can be written as,

$$\Delta N = \left[\left(\frac{\partial N}{\partial x_1} \Delta N_1 \right)^2 + \left(\frac{\partial N}{\partial x_2} \Delta N_2 \right)^2 + ... + \left(\frac{\partial N}{\partial x_n} \Delta N_n \right)^2 \right]^{\frac{1}{2}} \qquad \text{(Eq-D-2)}$$

Some observed parameter of HONDA engine experimental faciltiy uncertainties are : Engine speed(0.5%), Brake load(3%), mass flow rate of liquid fuel(1%), mass flow rate of air(1%), LHV of petrol(1%), LHV of kerosene(1%). Based on these, the computed performance parameter uncertainties are found as listed in **Table-1**.

A sample calculation provided here for measurement of uncertainty.

The BP of the engine is given by (A1)

$$BP = \frac{2 \times 3.142 \times N \times W \times R}{60 \times 1000}, kW \qquad \text{(Eq-D-3)}$$

In the above equation N and W are independent variable, because *R* has a constant value. The uncertainties of N and W are 0.5% and 0.5% respectively. Therefore

$$\%BP = \left\{ \left[\left(\frac{dBP}{dN} \right)^2 (\varepsilon_1)^2 \right] + \left[\left(\frac{dBP}{dW} \right)^2 (\varepsilon_2)^2 \right] \right\}^{1/2} \qquad \text{(Eq-D-4)}$$

$$= \left\{ \left[\left(\frac{2 \times 3.14 \times W \times R}{60000} \right)^2 \times (0.5)^2 \right] + \left[\left(\frac{2 \times 3.14 \times N \times R}{60000} \right)^2 \times (0.5)^2 \right] \right\}^{1/2}$$

=1.3

Similarly, uncertainties of other dependant parameters are calculated.

Table 1. Uncertainty associated with computed parameters for HONDA Engine

Computed parameters	**Uncertainty**
Brake power	± 17.90%
Brake thermal efficiency	± 11.25%
Brake specific fuel consumption	± 11.23%

Table D-2. Uncertainty associated with independent parameters for large VCR Engine(APX)

	Independent Variables	Relative Error, (%)
1	Engine speed	0.5
2	Engine load	0.5
3	Liquid fuel flow rate	1.0
4	Biogas flow rate	1.0
4	Water flow rate	2.0
5	LHV of liquid fuel	1.0
6	Temperature	3^0C
7	Cylinder pressure	1.6
8	Cylinder volume	0.1
9	Specific heat of exhaust gas	0.5
10	Ratio of specific heat	0.5
11	secondary piston displacement	0.5
11	CO, CO2, NO_x and HC emissions	2.3

Table D-3. Uncertainty associated with performance parameters for large VCR Engine(APEX)

Sr No	Performance Parameter	% Uncertainty
01	Air flow rate	1.1
02	Air fuel ratio	1.1
03	Gas flow rate	1.1
04	Brake Power	1.3
05	Brake thermal efficiency	1.6
06	Brake specific fuel consumption	1.3
07	Net heat release rate	1.6
08	Volumetric efficiency	1.7
09	Novel compression ratio	0.5

APPENDIX-E

FLUENT USER DEFINED FUNCTIONS

(1) Laminar Flame Velocity.c

```
# include "udf.h"
/*************** User input starts ****************************************/
/* Ydil is the mass fraction of diluent, included to account for any EGR product. */
static real Ydil = 0.05;
/* Fuel type. Supported ones are methane, methanol, isooctane, RMFD_303_indolene. . */
enum
{
methane, methanol, propane, isooctane, RMFD_303_indolene, FLAG
}fuel = isooctane;
/* Fuel mass fraction (required for partially premixed model) */
real Fuel_Mass_Fraction = 0.05;
/************ User input ends *************** ********************/
/* Fuel molecular weight for each fuel. */
static real molecular_weight[]={16.043, 32.040, 44.096, 114.23, 114.23};
/* For one mole of fuel, how many moles of air needed for stoichiometric combustion */
static real stoic_air_moles[]={2.0, 1.5, 5.0, 12.5, 12.5};
/* Unburnt gas temperature */
static real f_T_u(Thread * t)
{
/* determine the unburnt temperature as the weighted average of the unburnt temperature
in each cell ahead of the flame. If c>0.001 everywhere, then the unburnt temperature
is the lowest temperature of the cell zone */
real T_u, vol, T_u_min=1e10;
cell_t c;

T_u=0.;
vol=0.;
begin_c_loop_int (c,t)
{
if( C_PREMIXC(c,t) < 0.001 )
{
T_u += C_T(c,t)*C_VOLUME(c,t);
vol += C_VOLUME(c,t);
}
```

```
else
{
if( C_T(c,t) < T_u_min )
{
T_u_min = C_T(c,t);
}
}
}
end_c_loop_int (c,t)
T_u_min=PRF_GRLOW1(T_u_min);
PRF_GRSUM2(T_u, vol);
if(T_u>0. && vol>0.)
{
return T_u/vol;
}
else
{
return T_u_min;
}
}
/* Calculate unburnt gas temperature for laminar flame speed calculation */
DEFINE_ADJUST(my_T_u, domain)
{
#if !RP_HOST
Thread *t;
cell_t c;
real T_u;

thread_loop_c (t,domain)
{
T_u=f_T_u(t);
begin_c_loop_int(c, t)
{
C_UDMI(c, t, 0)= T_u;
}
end_c_loop_int(c, t)
}
#endif
}
/* Laminar flame speed calculation */
DEFINE_PROPERTY(laminar_flame_speed, c, t)
{
real SL, SL_ref, T_u, gama, beta, FIm[FLAG], Bm[FLAG], B2[FLAG], fi, fm;
/* Correlation from Metghalchi and Keck. */
FIm[methane]=1.08;
Bm[methane]=44e-2;
B2[methane]=-152e-2;
FIm[methanol]=1.11;
Bm[methanol]=36.92e-2;
```

```
B2[methanol]=-140.51e-2;
FIm[propane]=1.08;
Bm[propane]=34.22e-2;
B2[propane]=-138.65e-2;
FIm[isooctane]=1.13;
Bm[isooctane]=26.32e-2;
B2[isooctane]=-84.72e-2;
FIm[RMFD_303_indolene]=1.13;
Bm[RMFD_303_indolene]=27.58e-2;
B2[RMFD_303_indolene]=-78.34e-2;

if(sg_premixed)
{
fm = THREAD_PROP(t,PROP_premix_unburnt_fuel_mf,0);
}
else
{
fm = Fuel_Mass_Fraction; /* C_FMEAN(c,t) */
}
if(fm<1e-5)
fm=1e-5;
fi = (4.76*stoic_air_moles[fuel]*29/molecular_weight[fuel])/(1.0/fm-1);
SL_ref = Bm[fuel]+B2[fuel]*pow(fi-FIm[fuel],2);
gama = 2.18-0.8*(fi-1);
beta = -0.16+0.22*(fi-1);
T_u = C_UDMI(c,t,0);
SL = SL_ref*pow(T_u/298, gama)*pow((C_P(c, t)+RP_Get_Real("operatingpressure"))/
1.013e5, beta)*(1-2.1*Ydil);
if (SL>0)
return SL;
else
return 0;
}
```

(2) Initialize.c

```
#include<udf.h>
#define RPM RP_Get_Real("dynamesh/in-cyn/crank-rpm")
/************************************ User input starts ********************/
/* Initial swirl ratio and swirl axis*/
static real init_swirl_ratio = 2.0;
static real swirl_axis[ND_ND] = {1, 0};

static real swirl_origin[ND_ND] = {0, 0};
/* This variable defines whether the inialization occurs to the whole domain or just some
cell zones */
enum
{
whole_domain, defined_cell_zones
}method = whole_domain;
/* If defined_cell_zones is used in the above, then specify cell zone ID list for initialization.
```

```
-1 is a flag so please keep it. */
static int Zone_ID[]={2, -1};
/************************************ User input ends*********************/
static void initialize_cell_zone(Thread * t, real * omega)
{
cell_t c;
real xc[ND_ND], x[ND_ND];
static int counter=0;
/* loop over all cells */
begin_c_loop(c,t)
{
C_CENTROID(xc,c,t);
NV_VV(x,=,xc,-,swirl_origin);
#if RP_2D
if (rp_axi)
{
C_U(c,t)=NV_CROSS_X(omega, x);
C_V(c,t)=NV_CROSS_Y(omega, x);
C_W(c,t)=NV_CROSS_Z(omega, x);
}
else
{
if(counter == 0)
{
Message0("\nNo initialization for pure 2D. Needs to turn on 2d
axisymmetric with swirl!\n");
counter++;
}
}
#else
C_U(c,t)=NV_CROSS_X(omega, x);
C_V(c,t)=NV_CROSS_Y(omega, x);

C_W(c,t)=NV_CROSS_Z(omega, x);
#endif
}
end_c_loop(c,t)
}
DEFINE_INIT(my_init_function, domain)
{
Thread *t;
int i;
real omega[ND_ND], mag;
/* Normalize swirl axis */
mag=NV_MAG(swirl_axis);
NV_S(swirl_axis, /=, mag);
if (RP_Get_Boolean("dynamesh/models/in-cylinder?")==TRUE)
{
NV_VS(omega, =, swirl_axis, *, RPM/60.*2.*M_PI*init_swirl_ratio);
```

```
if(method == whole_domain)
{
/* loop over all cell threads in the domain */
thread_loop_c (t,domain)
{
initialize_cell_zone(t, omega);
}
}
else if (method == defined_cell_zones)
{
i=0;
while(Zone_ID[i]>=0)
{
t=Lookup_Thread(domain, Zone_ID[i]);
initialize_cell_zone(t, omega);
i++;
}
}
else
{
Message0("\n\nWrong method for initialization calculation--aborting!!\n");
exit(0);
}

Init_Face_Flux(domain);
}
else
{
Message0("\nIC not turned on. No initialization is performed.\n");
}
}
```

(3) Work.c

```
# include"udf.h"
# define RPM RP_Get_Real("dynamesh/in-cyn/crank-rpm")
/************************************ User input star*******************/
/* Cell zone ID list for pressure output (cell zone ID for combustion chamber). -1 is a
flag
so please keep it. */
static int Zone_ID[]={2, -1};
/* Face zone ID list for work output (face zone ID for the piston) */
static int Piston_ID[]={6, -1};
/************************************ User input ends ****************/
static real work=0, start_CA=0, end_CA=0;
static int counter=0;
/* Function to calculate cell volume. It takes care of 2d and 2daxisymmetric cases as well. */
static real C_MYVOLUME(cell_t c, Thread *tc)
{
float factor=1.0;
#if RP_2D
```

```
if (rp_axi) factor=2*M_PI;
#endif
return C_VOLUME(c,tc)*factor;
}
/* Function to calculate face area. It takes care of 2d and 2d axisymmetric case as well. */
static void F_MYAREA(real * x, face_t f, Thread *tf)

{
real factor=1.0;
F_AREA(x, f, tf);
#if RP_2D
if (rp_axi) factor=2*M_PI;
#endif
NV_S(x, *=, factor);
}
DEFINE_ON_DEMAND(Indicated_work)
{
if(counter==0)
{
Message0("\n\n********** IC Indicated Work Results
**********\n");
Message0("\nIndicated work calculation has not started. Please do at least one
time step.\n");
Message0("\nStart CA :%5.2f (deg) End CA :%5.2f (deg) Work : %9.3e (J)",
start_CA, end_CA, work);
Message0("\n\n**********************************************************
**********\n");
}
else
{
Message0("\n\n********** IC Indicated Work Results
**********\n");
Message0("\nIndicated work calculation started at :%7.2f (deg)", start_CA);
Message0("\nIndicated work calculation finished at :%7.2f (deg)", end_CA);
Message0("\nFor the above duration, the indicated work is :%12.4e (J)", work);
Message0("\n\n**********************************************************
**********\n");
}
}
DEFINE_ON_DEMAND(reset)
{
counter=0;
work=0;
start_CA=0;
end_CA=0;

Message0("\n\n********** WARNING
**********\n");
Message0("\nNote that this resets indicated work and the calculation start CA to zero.");
```

```
Message0("\nPlease save the data file to save the new values.");
Message0("\n\n**********************************************************
**********\n");
}
DEFINE_EXECUTE_AT_END(output_results)
{
#if !RP_HOST
int i;
real pressure,temperature, volume, fmf, mass, work_one_dt, x[ND_ND];
Thread *tc, *tf;
cell_t c;
face_t f;
FILE *fp_results;
Domain* domain;
domain=Get_Domain(1);
#if PARALLEL
if(I_AM_NODE_ZERO_P)
#endif
{
if(!(fp_results=fopen("work.txt","a")))
{
Message0("\nCan not open file-aborting!!");
exit(0);
}
}
if(counter==0)
{
start_CA = (CURRENT_TIMECURRENT_
TIMESTEP)*RPM*6.0+RP_Get_Real("dynamesh/in-cyn/crank-startangle");
#if PARALLEL
if(I_AM_NODE_ZERO_P)
#endif
{
fprintf(fp_results, " CA Volume Pressure temperature Yfb Work\n");
}

counter ++;
}
end_CA=CURRENT_TIME*RPM*6.0+RP_Get_Real("dynamesh/in-cyn/crank-startangle");
#endif
node_to_host_int_1(counter);
node_to_host_real_2(start_CA, end_CA);
#if !RP_HOST
/* Calculate volume weighted pressure and burnt fuel mass fraction */
pressure=0;
temperature=0;
volume=0;
fmf=0;
mass=0;
```

```
i=0;
while(Zone_ID[i]>=0)
{
tc=Lookup_Thread(domain, Zone_ID[i]);
begin_c_loop_int(c, tc)
{
pressure += C_P(c,tc) * C_MYVOLUME(c,tc);
temperature+=C_T(c,tc)*C_MYVOLUME(c,tc);
volume += C_MYVOLUME(c,tc);
if(sg_premixed)
{
fmf += C_PREMIXC(c,tc) * C_R(c,tc) *
C_MYVOLUME(c,tc);
}
mass += C_R(c,tc) * C_MYVOLUME(c,tc);
}
end_c_loop_int(c, tc)
i++;
}
pressure = PRF_GRSUM1(pressure);
temperature = PRF_GRSUM1(temperature);
volume = PRF_GRSUM1(volume);

fmf = PRF_GRSUM1(fmf);
mass = PRF_GRSUM1(mass);
temperature/=volume;
pressure /= volume;
fmf /= mass;
/* Calcualte work by piston. Only pressure force is accounted for and viscous force is
neglected. */
work_one_dt=0;
i=0;
while(Piston_ID[i]>=0)
{
tf=Lookup_Thread(domain, Piston_ID[i]);
begin_f_loop(f, tf)
{
F_MYAREA(x, f, tf);
work_one_dt += CURRENT_TIMESTEP * F_P(f,tf) * NVD_DOT(x,
WALL_F_GRID_VV(f, tf)[0], WALL_F_GRID_VV(f, tf)[1], WALL_F_GRID_VV(f,
tf)[2]);
}
end_f_loop(f, tf)
i++;
}
work_one_dt = PRF_GRSUM1(work_one_dt);
work += work_one_dt;
#endif
node_to_host_real_1(work);
```

```
#if !RP_HOST
/* Output volume, pressure, burnt fuel mass fraction */
#if PARALLEL
if(I_AM_NODE_ZERO_P)
#endif
{
fprintf(fp_results, "%8.2f %12.4e %12.4e %12.4e %12.4e %12.4e\n", end_CA, volume,
pressure,temperature, fmf, work);
fclose(fp_results);

}
#endif
}
DEFINE_RW_FILE(write_data, fp)
{
Message0("\nWriting user defined data to the data file...\n");
#if PARALLEL
#if RP_HOST
fprintf(fp, "\n%d", counter);
fprintf(fp, "\n%e", work);
fprintf(fp, "\n%e", start_CA);
fprintf(fp, "\n%e", end_CA);
#endif
#else
fprintf(fp, "\n%d", counter);
fprintf(fp, "\n%e", work);
fprintf(fp, "\n%e", start_CA);
fprintf(fp, "\n%e", end_CA);
#endif
}
DEFINE_RW_FILE(read_data, fp)
{
Message0("\nReading user defined data from the data file...\n");
#if PARALLEL
#if RP_HOST
fscanf(fp, "%d", &counter);
fscanf(fp, "%e", &work);
fscanf(fp, "%e", &start_CA);
fscanf(fp, "%e", &end_CA);
#endif
#else
fscanf(fp, "%d", &counter);
fscanf(fp, "%e", &work);
fscanf(fp, "%e", &start_CA);
fscanf(fp, "%e", &end_CA);
#endif
host_to_node_int_1(counter);
host_to_node_real_3(work,start_CA,end_CA);
}
```